



**This electronic thesis or dissertation has been
downloaded from Explore Bristol Research,
<http://research-information.bristol.ac.uk>**

Author:
Delisser, Peter

Title:
The effect of loading context on bone's deficient adaptive response to mechanical loading in old mice

General rights

Access to the thesis is subject to the Creative Commons Attribution - NonCommercial-No Derivatives 4.0 International Public License. A copy of this may be found at <https://creativecommons.org/licenses/by-nc-nd/4.0/legalcode> This license sets out your rights and the restrictions that apply to your access to the thesis so it is important you read this before proceeding.

Take down policy

Some pages of this thesis may have been removed for copyright restrictions prior to having it been deposited in Explore Bristol Research. However, if you have discovered material within the thesis that you consider to be unlawful e.g. breaches of copyright (either yours or that of a third party) or any other law, including but not limited to those relating to patent, trademark, confidentiality, data protection, obscenity, defamation, libel, then please contact collections-metadata@bristol.ac.uk and include the following information in your message:

- Your contact details
- Bibliographic details for the item, including a URL
- An outline nature of the complaint

Your claim will be investigated and, where appropriate, the item in question will be removed from public view as soon as possible.



**This electronic thesis or dissertation has been
downloaded from Explore Bristol Research,
<http://research-information.bristol.ac.uk>**

Author:

Delisser, Peter

Title:

The effect of loading context on bone's deficient adaptive response to mechanical loading in old mice

General rights

Access to the thesis is subject to the Creative Commons Attribution - NonCommercial-No Derivatives 4.0 International Public License. A copy of this may be found at <https://creativecommons.org/licenses/by-nc-nd/4.0/legalcode>. This license sets out your rights and the restrictions that apply to your access to the thesis so it is important you read this before proceeding.

Take down policy

Some pages of this thesis may have been removed for copyright restrictions prior to having it been deposited in Explore Bristol Research. However, if you have discovered material within the thesis that you consider to be unlawful e.g. breaches of copyright (either yours or that of a third party) or any other law, including but not limited to those relating to patent, trademark, confidentiality, data protection, obscenity, defamation, libel, then please contact collections-metadata@bristol.ac.uk and include the following information in your message:

- Your contact details
- Bibliographic details for the item, including a URL
- An outline nature of the complaint

Your claim will be investigated and, where appropriate, the item in question will be removed from public view as soon as possible.

The effect of loading context on bone's deficient adaptive response to mechanical loading in old mice

Peter James Delisser

A dissertation submitted to the University of Bristol in accordance with the
requirements for award of the degree of Doctor of Philosophy in the Faculty
of Health Sciences



79,848 words

Abstract

Normal bone maintains its ability to resist failure by adapting to the strain environment experienced by habitual activity. This adaptive process begins failing with advancing age, and subsequently bone loss occurs despite ongoing activity. This thesis reports experiments designed to investigate the effect of altering the context within which mechanical loading is applied on the adaptive loading response in old mice. These contextual changes include treatment with pharmaceuticals and changes in the level of background activity.

Although there is evidence that RANKL produced by osteocytes is essential for the bone loss associated with disuse, we were unable to identify any changes in the level of expression of RANKL in cortical bone osteocytes, using either qPCR or immunohistochemistry following either increased mechanical loading, or disuse.

Studies exploring the effect of altered context within which loading is applied found that preceding loading with a short period of disuse was sufficient to “rescue” the adaptive response to loading in old (19-months) female mice. Administration of the anti-resorptive risedronate (RIS) did not impair the loading response in old female mice, suggesting that loading, like in young mice is primarily mediated through bone modelling. Furthermore, the disuse-associated “rescue” was not affected by the concurrent administration of risedronate, suggesting that the mechanism involved is probably related to alterations in the strain environment, rather than being associated with any enhancement of bone remodelling following disuse.

Finally, the potent anabolic treatment, parathyroid hormone (PTH) was able to promote a strong anabolic response in very old (22-months) mice, which was not impaired by concurrent treatment with RIS, and resulted in additive gains in bone mass compared to vehicle treated mice. The loading response in 22-month-old mice was further impaired when compared to 19-month-old mice. This loading response was essentially unaffected by concurrent treatment with PTH and/or RIS.

Dedication

This thesis is dedicated to my unfailingly supportive and loving wife, Sarah. Without her support, and patience, it would not have been possible. I also hope my two amazing daughters, Emily and Lucy, can be proud of their daddy for “PhD-ing”.

Acknowledgements

The completion of this thesis would not have been possible without the support and assistance provided by several people throughout the nearly 6 years it has taken to complete. Firstly, I would like to thank my primary supervisor, Professor Joanna Price. With her assistance, along with the input of her husband, another world-renowned researcher in the field of bone mechanobiology, Professor Lance Lanyon, we prepared a successful application to the Wellcome Trust for a Veterinary Research Entry Fellowship, which funded the first 12 months of my research. Without the expertise, experience and unwavering support and regular critique of my work provided by Professors Price and Lanyon, this thesis would not have reached the standard it has.

I would also like to thank the other members of our laboratory for their expert technical assistance and teaching, and furthermore for their friendship and encouragement. Dr Lee Meakin provided all of the *in vivo* training required and was always available for assistance and troubleshooting in times of need. Dr Gabriel Galea provided all training in the *ex vivo* techniques in the early parts of my research, and critically, provided important support and advice on the statistical analysis of the data included in my experiments. I also wish to thank Dr Sara Windahl, Henry Todd, Sharon Holt and Xuedong Liu for their various contributions and advice.

Further thanks go to Professors Larry Suva and Dana Gaddy, formerly of the University of Arkansas for Medical Sciences (now both at Texas Agriculture and Mining University), for their advice, knowledge and friendship. Prof Suva and his laboratory technicians Frances Swain and Robert Skinner helped me undertake the immunohistochemistry protocol optimisation experiments in Chapter 4.

Lastly, I would like to thank the Wellcome Trust for providing partial funding for the work included in this thesis. Their veterinary training fellowships, although no longer available, were a valuable avenue for veterinarians to pursue world-class research.

Author's declaration

I declare that the work in this dissertation was carried out in accordance with the requirements of the University's Regulations and Code of Practice for Research Degree Programmes and that it has not been submitted for any other academic award. Except where indicated by specific reference in the text, the work is the candidate's own work. Work done in collaboration with, or with the assistance of, others, is indicated as such. Any views expressed in the dissertation are those of the author.

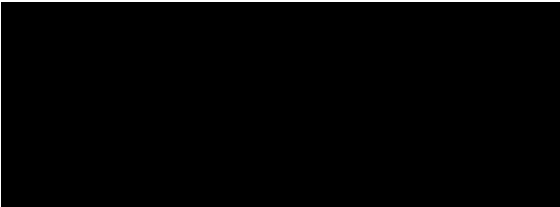
SIGNED:  DATE: ...2nd February 2019....

Table of Contents

Abstract	3
Dedication	5
Acknowledgements.....	7
Author’s declaration.....	9
Table of Contents	11
Table of Figures	20
List of Tables.....	25
List of abbreviations:.....	27
Chapter 1: General Introduction	30
1.1 The skeleton and the effects of aging.....	37
1.1.1 Diagnosis and monitoring of osteoporosis.....	41
1.1.2 Bone structure changes with age	42
1.2 Bone cells and bone (re)modelling, and the effects of aging.	44
1.2.1 Bone cell origins and function	44
1.3 Bone (re)modelling	48
1.3.1 Transcriptional control of bone cell activity during remodelling	50
1.4 The effect of aging on bone cell function	57
1.5 Aging and systemic regulators of bone remodelling	61
1.5.1 Regulation of Calcium Homeostasis	61
1.5.2 Parathyroid Hormone.....	63
1.5.3 The role of sex steroids on age-related bone loss.....	64
1.5.4 Role of oxidative stress in age-related bone loss	66

Table of Contents

1.6	Animal models of skeletal aging	67
1.6.1	Non-rodent models of skeletal aging	67
1.6.2	Rodent models of aging	68
1.7	Current treatment options for age-related osteoporosis	70
1.7.1	Calcium and Vitamin D supplementation	70
1.7.2	Antiresorptive treatments	71
1.7.3	Anabolic therapies	76
1.7.4	Combined anti-resorptive and anabolic therapies	81
1.7.5	Combining physical therapies with pharmaceutical treatments.	83
1.8	Regulation of bone mass and architecture by mechanical loading	84
1.8.1	The mechanostat	85
1.8.2	The cellular response to mechanical loading.....	87
1.8.3	The effect of aging on bone's structural response to mechanical loading ..	94
1.8.4	The effect of concurrent treatments on bone's response to mechanical loading. 96	
1.8.5	Models for studying the effect of altered mechanical loading on bone....	100
1.9	Thesis Aims	114
Chapter 2: Materials and Methods		116
2.1	<i>In vivo</i> procedures:.....	116
2.1.1	Animals	116
2.1.2	General Anaesthesia.....	116
2.1.3	Fluorochrome administration.....	117
2.1.4	Sacrifice.....	118
2.1.5	Sciatic Neurectomy.....	119
2.1.6	<i>In vivo</i> mechanical loading.....	120

2.2	<i>Ex vivo</i> procedures.....	121
2.2.1	Ex-vivo strain measurements	121
2.2.2	High resolution micro-computed tomography (μ CT) analysis.....	125
2.2.3	Site Specificity Analysis of tibial cortical bone.....	127
2.2.3	Quantitative Real-Time Reverse Transcription Polymerase Chain Reaction (qRT-PCR)	129
2.2.4	Tissue fixation and decalcification.....	137
2.2.5	Paraffin embedding and sectioning.....	138
2.2.6	Sclerostin and RANKL immunolocalization.....	139
2.2.7	Bone embedding in methylmethacrylate	139
2.2.8	MMA embedded bone sectioning and visualisation using confocal microscopy	140
Chapter 3	– Optimising <i>in vivo</i> experimental models	143
3.1	Introduction	143
3.1.1	Optimising a model of increased mechanical load.....	144
3.1.2	Optimising a model of decreased mechanical loading.....	146
3.1.3	Objectives.....	149
3.2	Materials and Methods:.....	149
3.2.1	Objective 1: Determine the temporal pattern of bone mass changes in the murine tibia using μ CT, following repeated axial loading for two, three or four weeks.	149
3.2.2	Objective 2: Determine the temporal pattern of cortical bone formation in the murine tibia following repeated axial loading for two, three or four weeks using dynamic histomorphometry.....	152
3.2.3	Objective 3: Characterise the effect of unilateral sciatic neurectomy and contralateral sham surgery on bone mass in the murine tibia using μ CT.....	153

3.2.3 Statistical analysis	153
3.3 Results:	155
3.3.1 Determine the temporal pattern of bone mass changes in the murine tibia using μ CT, following repeated axial loading for two, three or four weeks, (Objective 1).	155
3.3.2 Determine the temporal pattern of cortical bone formation in the murine tibia following repeated axial loading for two, three or four weeks using dynamic histomorphometry (DH) (Objective 2).....	161
3.3.3 Characterise the effect of unilateral sciatic neurectomy and contralateral sham surgery on bone mass in the murine tibia using μ CT (Objective 3).	167
3.3.4 Results summary	171
3.4 Discussion	172
3.4.1 The temporal pattern of bone mass changes in the murine tibia following repeated axial loading, using μ CT (Objective 1).	173
3.4.2 The temporal pattern of cortical bone formation in the murine tibia following repeated axial loading for two, three or four weeks using dynamic histomorphometry (Objective 2)	175
3.4.3 The effect of unilateral sciatic neurectomy and contralateral sham surgery on bone mass in the murine tibia using μ CT (Objective 3).....	180
3.5 Conclusions.....	183
Chapter 4 – RANKL and bone remodelling during mechanical loading	185
4.1 – Introduction	185
4.1.1 Osteocytes as mechanosensors and a source of signalling factors.	186
4.1.2 Optimising RANKL immunolocalisation in bone	191
4.1.3 Objectives	192
4.2 Materials and Methods	193
4.2.1 Optimise a protocol for immunolocalisation of RANKL in decalcified, paraffin-embedded murine cortical bone (Objective 1).....	193

4.2.2 <i>In vivo</i> procedures	196
4.2.3 <i>Ex vivo</i> procedures	197
4.2.4 Statistical analysis.....	198
4.3 Results	199
3.3.1 Objective 1: Develop a protocol for immunolocalisation of RANKL in decalcified, paraffin-embedded murine cortical bone.....	199
4.3.2 Objective 2: Describe the effect of contralateral sham surgery on the osteocytic expression of RANKL and sclerostin protein in mice following unilateral disuse engendered by SN, using IHC	206
4.3.3 Objective 3: Describe the effect of disuse, engendered by SN on the osteocytic expression of RANKL and sclerostin protein, using IHC.....	209
4.3.4 Objective 4: To establish the temporal response to disuse engendered by SN on the mRNA expression of RANKL, OPG and Sclerostin using qRT-PCR.....	209
4.3.5 Objective 5: Describe the effect of increased mechanical loading on the expression of the RANKL and sclerostin protein, using IHC	212
4.3.6 Objective 6: To establish the temporal response to a single episode of mechanical loading on the mRNA expression of RANKL, OPG and sclerostin using qRT-PCR.	212
4.4 Discussion.....	215
4.4.1 Immunolocalisation of RANKL in cortical bone.	215
4.4.2 Contralateral sham surgery does not affect the osteocytic expression of RANKL or Sclerostin.	217
4.4.3 Disuse sufficient to cause cortical bone loss and increased expression of sclerostin has no effect on RANKL expression.	218
4.4.4 Axial tibial loading sufficient to result in bone formation decreases osteocytic sclerostin expression but has no effect on RANKL expression.....	222
4.5 Conclusions	224

Chapter 5 – The effect of disuse on the osteogenic response to loading in old mice.	227
5.1 Introduction.....	227
5.2 Objectives	230
5.3 Materials and Methods	231
5.3.1 Animals and <i>in vivo</i> procedures.....	231
5.3.2 <i>Ex vivo</i> procedures.....	232
5.4 Results	234
5.4.1 Objective 1: Characterise the site-specific changes in cortical bone 3 weeks after unilateral sciatic neurectomy in old (19-month-old) female mice using SSA.	234
5.4.2 Preliminary single-site μ CT analysis from Meakin [4].....	237
5.4.3 Objective 2: Determine the effect of sciatic neurectomy on the bone mass and architecture of the contralateral non-loaded limb in old female mice using SSA. ...	238
5.4.4 Objective 3: Determine the effect of prior SN on the response to mechanical loading of cortical and trabecular bone regions of interest in old female mice, using single-site μ CT analysis.	239
5.4.5 Objective 4: Determine the effect of prior SN on the rate of bone formation in loaded tibias of old female mice, using dynamic histomorphometry	243
5.4.6 Objective 5: Determine the effect of prior SN on the response to mechanical loading of the entire cortical bone in old female mice, using SSA.	244
5.4.7 Results summary	248
5.5 Discussion	249
5.5.1 Sciatic neurectomy in old mice results in endosteal and intracortical bone loss.	250
5.5.2 A short period of prior disuse enhances the periosteal response to loading in old female mice.	251
5.6 Conclusions.....	258

Chapter 6 - The effect of risedronate and loading in old mice.....	261
6.1 Introduction	261
6.2 Objectives.....	264
6.3 Materials and Methods	265
6.3.1 Effects of risedronate and disuse on tibial loading responses in aged female mice.....	265
6.4 Results	268
6.4.1 Effect of RIS on the response to mechanical loading in old female mice.....	269
6.4.2 Effect of RIS on the disuse-mediated rescue of the impaired loading response in old mice.....	273
6.4.3 Site Specificity Analysis.....	275
6.5 Discussion.....	285
6.5.1 Response to risedronate treatment is site- and age-specific.....	285
6.5.2 Risedronate treatment does not impair the loading response in aged mice.	288
6.5.3 The SN-associated rescue of age-impaired adaptive bone formation is not affected by treatment with risedronate.....	289
6.6 Conclusions	291
Chapter 7 – RIS+PTH and the loading response in old mice.....	293
7.1 Introduction	293
7.2 Objectives:.....	297
7.2 Materials and Methods	297
7.2.1 Experiment 1: load strain relationship of old mice treated with RIS and/or PTH	298
7.2.2 Experiment 2: The effect of concurrent RIS treatment on the anabolic effect of PTH and axial tibial loading.	298
7.2.3 Statistical Analysis	300

7.4 Results	302
7.4.1 Strain gauge experiment	302
7.4.2 The effect of RIS and/or PTH on the tibial trabecular and cortical bone.....	303
7.4.3 The effect of RIS and/or PTH on the adaptive response to loading in old female mice	314
7.4.4 Results summary	327
7.5 Discussion	329
7.5.1 PTH treatment increases bone mass, but concurrently increases porosity in old mice.	329
7.5.2 RIS treatment has no effect on the anabolic effect of PTH in old mice.....	331
7.5.3 Mechanical loading is not affected by PTH and/or RIS treatment in old female mice	333
7.6 Conclusions.....	335
Chapter 8 - General Discussion.....	337
8.1 Optimising murine tibial loading models to study the effect of altering the loading context in old mice.	337
8.2 RANKL expression in unaffected in murine cortical bone following increased or decreased loading.	339
8.3 Disuse “rescues” the age-impaired osteogenic response to loading in old mice. .	341
8.4 Disuse-mediated “rescue” of the age-impaired adaptive loading response is not mediated by remodelling associated with prior disuse.....	343
8.5 The anabolic response to PTH treatment is maintained following impairment of resorption in old mice.	344
8.6 Conclusions and implications	346
Implications and further work.....	347
References.....	350

Appendix 1	403
CTAn μ CT analysis task lists	403
Table A1.4.....	406
Table A1.5.....	407
Appendix 2	408
Immunohistochemistry Protocols	408
Appendix 3	413
Experimental data tables	413
Chapter 3.....	413
Chapter 4.....	415
Appendix 4	417
Peer-reviewed papers/conference abstracts.....	417
Risedronate-loading in aged mice – ASBMR Abstract 2015	435

List of Figures

Figure 1 –Structural change in cortical bone porosity with age.	38
Figure 2 - Scanning electron micrograph (SEM) of the third lumbar vertebra of an adult 30-year-old (left) and an osteoporotic 71-year-old woman (right).	39
Figure 3 – Diagrammatic representation of cortical bone anatomy.....	40
Figure 4 – Aging is associated with cortical thinning due to medullary expansion.	42
Figure 5 - Differentiation lineage markers for osteoblastic/osteocytic lineage.	45
Figure 6 – Evolution of osteoblastic and osteoclastic lineage cells.	47
Figure 7 Schematic representation of the RANK/RANKL/OPG axis and its effect on osteoclasts.	51
Figure 8 - Schematic representation of canonical Wnt signalling.	56
Figure 9 – Schematic diagram illustrating the mechanostat theory of the control of bone mass	85
Figure 10: Schematic representation of (A) the isolated avian ulna, (B) tibial four point and (C) ulnar axial loading models	104
Figure 11: The non-invasive axial tibial loading model.....	106
Figure 12 Analysis of response of the mouse tibia to loading at each site along the bone’s length using Site Specificity Analysis software.	107
Figure 13 – Loading waveforms for application of load represent strain rate.	109
Figure 14 – Schematic diagram indicating the placement of the mouse limb into the loading cups to apply non-invasive axial loading.....	121
Figure 15 – Strain gauge used for tibial strain measurements.	122
Figure 16 – Photomicrograph of strain gauge preparation for <i>ex vivo</i> strain measurement on murine tibias.....	124
Figure 17 Representative agarose gel electrophoresis image run from young mice femoral cortical bone.....	132
Figure 18 – Experimental timeline for the loading time-course study.	150
Figure 19 – Representative image of selected posteriolateral cortex used for analysis of response to loading.....	151
Figure 20 – Schematic diagram describing calculation of the measures explored using dynamic histomorphometry.	154
Figure 21 - Representative regions of interest in the mouse tibia that were analysed using μ CT.	155

Figure 22 – The effect of different time periods of axial loading on trabecular bone of young adult female mice.	157
Figure 23 - The effect of different time periods of axial loading on trabecular bone μ CT parameters of young adult female mice.	158
Figure 24 – The effect of different time periods of repeated loading on cortical bone μ CT parameters of young adult female mice.....	159
Figure 25 – The effect of different time periods of repeated loading on cortical bone μ CT parameters of young adult female mice.....	160
Figure 26 – The effect of different time periods of repeated loading on the percentage increase in μ CT parameters.	161
Figure 27 – The effect of loading duration on dynamic histomorphometry parameters following loading in young adult female mice.....	162
Figure 28 – Confocal laser scanning micrograph images of transverse sections of the tibia of young adult female mice after 2, 3 or 4 weeks of loading.	163
Figure 29 – The effect of different time periods of loading on endosteal resorption.	165
Figure 30 – Dynamic histomorphometric indices for the weekly intervals following the start of repeated axial tibial loading in young adult female mice.	166
Figure 31 – The effect of sham surgery (left leg) and SN (right leg) on trabecular bone parameters in young adult mice.	167
Figure 32 – The effect of sham surgery (left leg) and SN (right leg) on cortical bone parameters in young adult mice.	169
Figure 33 – Comparing the effect of sham surgery (left leg) and SN (right leg) on cortical bone parameters in young adult mice.	170
Figure 34 – (A) Finite Element Model (FEM) of a murine tibia following axial tibial loading and (B) dynamic histomorphometry image following four weeks of loading.	177
Figure 35 – Simplified organogram depicting the interactions between RANKL, OPG and Sclerostin.	190
Figure 36 – Immunolocalisation of RANKL in mouse cortical bone (Protocol 1)	199
Figure 37 – RANKL immunolocalisation in mouse cortical bone according to (A, C) Protocol 1 and (B, D) Protocol 2.....	200
Figure 38 – RANKL immunolocalisation in mouse cortical bone (Protocol 3).....	201
Figure 39 – RANKL immunolocalisation in mouse cortical bone (Protocol 4).....	202
Figure 40 –RANKL immunolocalisation (Protocol 4).....	203

Figure 41 – High power representative images of selected positive control sections following RANKL immunolocalisation.....	206
Figure 42 – Effect of sham surgery and disuse (by SN) on sclerostin expression in osteocytes..	207
Figure 43 – Effect of sham surgery and disuse (by SN) on sclerostin expression in osteocytes..	207
Figure 44 - Effect of sham surgery and disuse (by SN) on RANKL expression in osteocytes.	208
Figure 45 - Effect of sham surgery and disuse (by SN) on RANKL expression in osteocytes.	208
Figure 46 – Change in mRNA expression of SOST, RANKL and OPG following disuse in young adult female mice	210
Figure 47 – Change in mRNA expression of (A) SOST, (B) RANKL and (C) OPG in young adult female mice following 2 weeks of disuse	211
Figure 48 - Effect of axial loading on RANKL and Sclerostin expression in osteocytes in young adult mice, determined by immunohistochemistry.	213
Figure 49 – Change in mRNA expression of SOST, RANKL and OPG following a single episode of mechanical loading in young adult female mice	214
Figure 50 – Time line describing the experimental protocol for SN/loading experiments in aged mice.	232
Figure 51 – Site-Specificity Analysis illustrating the effect of three weeks of disuse engendered by SN on cortical bone structure.	236
Figure 52 – Representative images of the 37% site following 3 weeks of SN.	237
Figure 53: The effect of prior disuse on loading-related changes in Ct.Ar at the proximal 37% site at different magnitudes of mechanical strain in young and aged male and female mice.....	238
Figure 54 – Site-Specificity Analysis (SSA) illustrating the effect of unilateral disuse engendered by right SN and/or loading on cortical bone structure of the left contralateral leg of mice.	239
Figure 55 – The effect of a background of disuse engendered by SN on the cortical bone response to axial tibial loading in old female mice.	241
Figure 56 – Effect of a background of disuse engendered by SN on the loading-associated periosteal and endosteal bone formation in aged mice.....	243
Figure 57 – Effect of a background of disuse engendered by SN on the adaptive response to loading in cortical bone of old female mice.	246
Figure 58 – The effect on cortical porosity of a background of disuse engendered by SN and/or mechanical loading of the tibia in old female mice.	247
Figure 59 – The effect of a background of disuse engendered by SN on the ipsilaterally loaded limb of old female mice.	248

Figure 60 – Diagrammatic representation of the strain averaging hypothesis.....	252
Figure 61 – Experimental timetable for loading/SN and Risedronate (RIS) experiment in old female mice.	266
Figure 62 – The effect of axial compressive tibial loading and Risedronate (RIS) treatment on trabecular bone parameters of old mice.	271
Figure 63 – The effect of axial compressive tibial loading and Risedronate (RIS) treatment on proximal cortical bone parameters of old mice.....	272
Figure 64 - Effect of Risedronate (RIS) and Sciatic Neurectomy (SN) on the adaptive response to axial tibial mechanical loading in cortical bone.	274
Figure 65 – The effect of risedronate (RIS) and/or loading on Tt.Ar of whole tibia in old female mice.	277
Figure 66 – The effect of risedronate (RIS) and/or loading on Ct.Ar of whole tibia in old female mice.	278
Figure 67 – The effect of risedronate (RIS) and/or loading on Ma.Ar of whole tibia in old female mice.	279
Figure 68 - The effect of risedronate (RIS) and/or loading on Ct.Th of whole tibia in old female mice.	280
Figure 69 – The effect of SN on the loading response in old female mice.	281
Figure 70 - The effect of RIS on the loading response in old female mice.....	282
Figure 71 Effect of Risedronate (RIS) on the response to loading following prior disuse in old female mice.	283
Figure 72 Effect of SN on the response to loading following Risedronate (RIS) treatment in old female mice.	284
Figure 73 – Experimental plan for the Strain gauging and RIS-PTH treatment response study. .	300
Figure 74 – The effect of 28 days of RIS and/or PTH treatment on the load:strain relationship in the tibia of old female mice.	302
Figure 75 – The effect of 6 weeks of RIS and/or PTH treatment on bone mass μ CT parameters of the proximal trabecular region of the tibia of old female mice.....	304
Figure 76 – The effect of RIS on the anabolic response to PTH treatment on tibial trabecular bone microarchitectural parameters in old female mice.	305
Figure 77 – The effect of 6 weeks of RIS and/or PTH treatment on bone mass μ CT parameters of the 37% site cortical bone of the tibia of old female mice.	306

Figure 78 – The effect of 6 weeks of RIS and/or PTH treatment on micro-architectural μ CT parameters of the 37% site cortical bone of the tibia of old female mice. 307

Figure 79 – Effect of RIS treatment on the anabolic response to PTH treatment in old female mice. 312

Figure 80 - Effect of RIS treatment on the anabolic response to PTH treatment in old female mice. 312

Figure 81 – Effect of two weeks of axial tibial loading on the tibia of old female mice using SSA. 316

Figure 82 - Effect of two weeks of axial tibial loading on the tibia of old female mice using SSA. 317

Figure 83 – The effect of RIS and PTH on the response to axial tibial loading in cortical bone of old female mice using single-site analysis at the 37% site. 318

Figure 84 - The effect of RIS and PTH on the response to axial tibial loading in trabecular bone of old female mice using single-site analysis. 319

Figure 85 –The effect of PTH and combined RIS+PTH on the osteogenic response to loading in old female mice. 324

Figure 86 – The effect of PTH and combined RIS+PTH on the osteogenic response to loading in old female mice. 324

Figure 87 – The effect of RIS and/or PTH on the loading response in the distal tibia of 22-month-old female mice. 326

List of Tables

Table 1 – Fluorochromes used for sequential injections and subsequent dynamic histomorphometry experiments.....	118
Table 2 - Primer Sequences and amplicon length for genes of interest	135
Table 3 – Mouse weights and tibial lengths following axial tibial loading for 2, 3 or 4 weeks. ...	156
Table 4 – Effect of a background of disuse engendered by SN and/or right tibial loading on bodyweight, tibial length and muscle area.....	240
Table 5 – Effect of a background of disuse engendered by SN on the osteogenic response to loading in old female mice using conventional μ CT analysis.....	242
Table 6 - The effect of a background of disuse engendered by SN on the response to loading in old female mice.	245
Table 7 – Effect of RIS treatment, loading and/or sciatic neurectomy on tibial length, bodyweight and muscle area in aged mice.	269
Table 8 - Trabecular and cortical μ CT parameters in the left (non-loaded) and right (loaded) tibiae of old mice.	270
Table 9 - Load:Strain relationship from tibiae of old female mice treated with RIS, PTH or both.	303
Table 10 – Effect of RIS and PTH treatment on the trabecular bone of old female mice.....	305
Table 11 – Effect of RIS and PTH treatment on the cortical bone of old female mice.....	307
Table 12 – Effect of RIS and PTH and their interactions on the cortical bone of old female mice.	308
Table 13 – The effect of two weeks of axial tibial loading on bone in vehicle (control) 22-month-old female mice using single-site μ CT analysis.	314
Table 14 – The effect of RIS and/or PTH treatment on the osteogenic response to loading in 22-month-old female mice.	320
Table 15 - The effect of RIS and/or PTH treatment on the response to axial tibial loading in 22-month-old female mice.	320
Table 16 – The effect of PTH and RIS on the loading response of 22-month-old female mice by SSA.	321
Table A1. 1 - CTAn tasklist for analysis of cortical bone parameters in young mice tibiae	403
Table A1. 2 - CTAn tasklist for analysis of cortical bone parameters in old mice tibiae	404

List of Tables

Table A1. 3 – CTAn tasklist for analysis of cortical bone porosity	405
Table A1. 4 – CTAn tasklist for analysis of trabecular and cortical bone porosity in proximal tibial metaphyseal bone of mice	406
Table A1. 5 – CTAn tasklist for analysis of trabecular bone parameters in old mice tibias	407
Table A2. 1 – Immunostaining protocol for RANKL	410
Table A2. 2 – Immunostaining protocol for Sclerostin	412

List of abbreviations:

• 3D	three dimensional
• μ CT	Micro-computed Tomography
• ABC	Avidin-Biotin Complex
• ALP	Alkaline Phosphatase
• ANOVA	Analysis of Variance
• ASBMR	American Society of Bone and Mineral Research
• β 2MG	β -2 Microglobulin
• BMD	Bone Mineral Density
• BMP	Bone morphogenetic protein
• BMU	Bone multicellular unit
• BP	Bisphosphonate
• BV/TV	Bone volume fraction
• cDNA	complementary DNA
• CO ₂	carbon dioxide
• Ct.Ar	Cortical bone area (mm ²)
• Ct.Po	Cortical Porosity
• Ct.Th	Cortical bone thickness (mm)
• DAB	3, 3'-diaminobenzidine
• DEXA	Dual energy x-ray absorptiometry
• DH	Dynamic histomorphometry
• DMP-1	Dentin matrix acidic phosphoprotein 1
• DNA	Deoxyribonucleic acid
• EDTA	ethylenediaminetetraacetic acid
• EtOH	Ethanol
• ER	Oestrogen receptor
• FEM	Finite element modelling
• H&E	Haematoxylin and Eosin
• H ₂ O ₂	Hydrogen peroxide
• HCl	Hydrochloric acid
• HR-pQCT	High resolution pQCT
• IHC	Immunohistochemistry
• LRP	low density lipoprotein receptor protein
• Ma.Ar	medullary area (mm ²)
• MES	Minimum Effective Strain
• mm	millimetres

List of abbreviations:

- MMA Methyl Methacrylate
- mRNA messenger Ribonucleic Acid
- Mu.Ar Muscle area
- NFκB Nuclear factor-κB
- OPG Osteoprotegerin
- PBS Phosphate buffered saline
- PCR Polymerase chain reaction
- PFA Paraformaldehyde
- PG Prostaglandin
- pQCT peripheral quantitative computed tomography
- PTH Parathyroid Hormone
- PTHrP PTH-related peptide
- qRT-PCR quantitative Reverse Transcriptase PCR
- RANK Receptor Activator of NFκB
- RANKL - RANK Ligand
- RNA Ribonucleic acid
- Runx2 Runt-related transcription factor 2
- SEM Standard Error of the Mean
- SERM Selective oestrogen receptor modulator
- SMI Structure Model Index
- SN Sciatic Neurectomy
- *Sost* The gene encoding for Sclerostin
- Tb.Ct.Po Trabecular region cortical porosity
- Tb.N Trabecular number
- Tb.Pf Trabecular Pattern Factor
- Tb.Sp Trabecular separation
- Tb. Th Trabecular thickness
- TGF Transforming growth factor
- TNF Tumour necrosis factor
- TRAP Tartrate resistant acid phosphatase
- Tt.Ar Periosteally enclosed area (mm²)
- Wnt Wingless homology

Chapter 1

General Introduction

Chapter 1: General Introduction

A prerequisite for the active life lived by most vertebrates is that they have a skeleton sufficiently rigid to provide the struts and levers for muscles to work against and sufficiently strong to withstand the loads involved without either monotonic failure or irreparable degrees of microdamage, yet light enough to allow ease of movement. The evolutionary solution to this problem in large animals appears to be that the overall form of each skeletal element, femur, tibia etc., is genetically determined but that the detailed structure, on which load bearing competence depends, is achieved through local adaptation to the effects of loading itself. Thus mechanical loading is the principal functional determinant of bone mass and architecture; an influence that is achieved through functional strains in bone tissue influencing, and potentially controlling, the bone forming and resorbing activity of populations of osteoblasts and osteoclasts [10] to achieve “target” levels of functional strain and strain distributions. Higher than target strain magnitudes, or novel strain distributions, result in osteogenesis which increases bone mass and this subsequently reduces strain to re-establish the target. Sub-target strain results in bone loss and a consequent increase in the strain experienced at a given site to restore the target [11]. This negative feedback homeostatic mechanism of bone structure, engendered through response to changes in strain within the bone, has been called the “mechanostat” [12-14].

In humans the commonest failure of the mechanostat is osteoporosis, a disorder characterised by a loss of bone mass most commonly associated with aging and loss of oestrogen following menopause [15]. Bone mass in people peaks as early as 20 years old, from which time it gradually decreases, with the fastest loss following menopause in women, associated with loss of oestrogen [16]. Most fractures in people with osteoporosis occur in the vertebrae, the femoral neck, the distal radius and less commonly the distal tibia. The lifetime risk of a fragility fracture past 50 years of age in women is 53.2% and in men is 20.7% [17].

Generally, the primary goal of most osteoporosis therapies is to reduce the risk/incidence of fragility fracture, and they are generally classed as either anti-resorptive, or anabolic. However, most medications are often administered long after significant bone loss has occurred, and as such, anti-resorptives, such as bisphosphonates, tend to only achieve maintenance of, or at best modest increases in bone mass. Available anabolic therapies are at present limited, with the only currently licensed treatments based on parathyroid hormone (PTH) or truncated analogues of the hormone, such as teriparatide and abaloparatide. These have all been demonstrated to have a significant positive effect on bone mass when given, although treatment is expensive and is often used only as a second-choice treatment, reserved for the most severe cases of low bone mass, or those at greatest risk of fracture. Combined treatment with anti-resorptive drugs and anabolic drugs appears a logical approach to simultaneously increase formation and decrease resorption of bone. There is, however, some evidence that following treatment by anti-resorptive bisphosphonates with the anabolic drug PTH may inhibit the magnitude of the anabolic response of PTH. This may be in part because a proportion of the bone formation stimulated by PTH treatment is a result of bone remodelling.

Bone is the end result of many pathways including those of growth and development in addition to mechanical loading. In adults these include systemic changes in parathyroid hormone and sex hormone levels as well as local control of coupling of resorption and formation associated with homeostasis. Bone remodelling involves the coordinated activity of both osteoclasts and osteoblasts in a sequence which initially removes old or damaged bone through osteoclasts, then subsequently replaces the removed bone through activity of osteoblasts. Hence if osteoclast activity is reduced, then the subsequent bone formation response can also be affected. This spatially and temporally linked activity of osteoblasts with osteoclasts is referred to as bone cell coupling. The coupling of resorption and formation is essential for the maintenance of skeletal integrity and health in the adult. Without continual renewal of old/damaged skeletal tissue through bone remodelling, the accumulation of microdamage and senescent cells results in greater risk of bone failure and fractures. Bone modelling, on the other hand, is the primary activity of osteoblasts which does not require the prior activity of osteoclasts to mediate

formation activity and is primarily associated with the growth of the skeleton in youth and the adaptive response seen following mechanical loading.

The precise mechanisms associated with adaptive modelling and remodelling (henceforward referred to as (re)modelling) are still frustratingly obscure but must involve certain components. For a strain-related feedback control to operate strains must initially be “measured” by some strain-related response in a population of cells. This response leads eventually to structurally appropriate adjustment of bone mass and architecture. The current appreciation is that the cells involved in strain “measurement” are the osteocytes [18, 19]. These cells transduce strain change into a cascade of stimuli to promote or suppress bone formation or resorption, by altering the activity of osteoblasts and/or osteoclasts respectively.

The cellular pathways controlling these methods of bone adaptation are complex and at present remain undefined. However, there are several key molecules which have been identified in the past two decades which have been shown to be particularly important, especially with regards to the response to loading. For example, the expression of the Wnt antagonist, sclerostin, has been demonstrated to decrease with increased loading, and increase with decreased loading [8, 20], consequently altering the activity of the downstream Wnt targets, including osteoblasts. The control of osteoclasts has also recently been demonstrated to be mediated by signalling molecules produced by osteocytes. Receptor Activator of Nuclear Factor κ B ligand (RANKL) is a key differentiation and activation signal for osteoclasts. Two paradigm-shifting studies published at the time the experiments for this thesis were being conceived demonstrated for the first time that it is osteocytes, and not only osteoblasts as once thought, that produce the RANKL essential for bone loss associated with disuse [21, 22]. At the time the first experiments for this thesis were undertaken, although the expression of sclerostin had previously been linked to changes in mechanical loading [8], to the author’s knowledge, no studies had ever linked changes in RANKL expression with alterations in the mechanical loading environment, and particularly if RANKL was involved in the age-related impairment of the adaptive loading response.

When the skeleton ages, the ability of the body to maintain appropriate bone mass becomes impaired after an imbalance occurs between bone formation and bone resorption, subsequently resulting in osteoporosis. This systemic failure of the remodelling process due to aging effectively uncouples the resorptive and formative processes of remodelling with many remodelling events not being followed by adequate amounts of bone formation. This bone loss results in decreased bone mass, and subsequent strength, which generally results in an increase in the strain experienced in affected bone. Despite this systemic failure of remodelling, if the mechanostat were still fully functional in the elderly, then any stimulus which resulted in a reduction in bone mass, would cause a subsequent decrease in stiffness and increase in strain, which should stimulate an anabolic response, mostly via bone modelling, to correct the bone mass lost. It has been hypothesised this age-related osteoporosis is due to a primary and inherent failure of the mechanostat in the elderly [23].

There are many studies demonstrating that the adaptive response to mechanical loading in humans and animal models is impaired with age [24-31], however, there is little known about the specific mechanisms which underlie this deterioration. Meakin *et al* [29] in our laboratory were able to demonstrate that old mice do not appear to have a deficiency in their ability to “sense” strain and produce appropriate early responses to loading, but did demonstrate an impaired ability of osteoblasts to proliferate in response to loading. The molecular pathways affected in old mice with deficiencies in the mechanostat are yet to be fully delineated.

Most of the currently licensed pharmaceutical options in common use for treatment of osteoporosis have a systemic effect which is not necessarily selective for the “at risk” sites commonly affected by fragility fracture, although there is some evidence that their use may affect the magnitude of the adaptive response to loading [32, 33]. Mechanical loading normally involves a structurally appropriate adaptive response with bone formed at the areas where it is most needed. Finding treatments or management strategies which improve the adaptive response to mechanical loading should permit a structurally appropriate adaptive response to help “rescue” a deficient loading response and allow a

more selective improvement in bone mass in sites that are at greater risk of injury. The potential for changing the site-specific adaptive loading response through alteration of the context within which mechanical loading is applied provides an intriguing and potentially useful strategy with which to treat conditions of low bone mass in people.

Although osteoporosis is primarily a disease associated with old age, most experimental work exploring the effect on the response to increased loading of altering the context within which loading is applied is reported in young animals. The bisphosphonate, risedronate had no effect on the anabolic response to loading in young mice, suggesting that increases in mechanical loading stimulate an increase in bone formation, primarily via bone modelling, as impairment of osteoclast activity did not affect adaptive loading response [34]. Parathyroid hormone (PTH) generates an increase in both bone modelling and remodelling. In young mice, the loading response was actually synergistically improved following treatment with PTH, suggesting that PTH may actually improve the response to mechanical loading in young mice [32]. The magnitude of the loading response was also increased following loading preceded by a short period of disuse in young mice, suggesting that altering the mechanical context on which loading is applied to bone is sufficient to modulate the response to applied loads [35].

Interestingly, pilot work performed by our laboratory has suggested that the impaired response to mechanical loading in old female mice can be “rescued” by preceding the loading with a short period of disuse [4]. Meakin hypothesised that the habitual strain environment modulates the subsequent cellular response to contemporaneous loads experienced. Therefore, in the situation of decreased habitual loading, that modulatory effect on the cells responsible for adaptive bone formation is reduced, and subsequently, the magnitude of the formation response stimulated by loading is greater. A simple analogy to this is the apparent intensity/brightness of a camera flash when seen in daylight compared with the same flash seen at night.

Establishing the mechanisms involved in the impairment of the mechanostat has the potential to better direct the development of treatments for disorders involving inappropriate, usually insufficient, bone mass. Increased mechanical loading alone,

through exercise or resistance training is typically not as efficient at improving bone mass and architecture in old people as it is in young people [36]. As the normally functioning mechanostat directs bone formation to areas where it is most needed (ie. areas under the greatest load), identification of mechanisms which modulate the mechanostat's activity should provide avenues to identify and direct "smart" treatments which could help the skeleton respond with structurally appropriate bone mass changes in regions of high strain and high risk of fragility fracture. Improvement of the mechanostat function prior to significant bone loss could even abrogate the onset of low bone mass seen with age-related osteoporosis in the first place.

The aim of the experiments included in this thesis is to use the external bone loading *in vivo* model in mice to characterise the response to altered mechanical loading and how detrimental changes in the response to loading seen with aging are affected by altering the context within which mechanical loading is applied. This aims to inform the hypothesis that altering the context within which mechanical loading is applied, either physically or pharmacologically, may affect the magnitude of the adaptive response to mechanical loading in the aged skeleton, to provide a site-specific and structurally appropriate effect on bone mass in old animals.

The objectives of the experiments described in this thesis were to establish a number of parameters in the regulatory pathways between functional loading and changes in bone architecture. Specifically, these experiments, were designed to establish:-

- 1. The optimal loading duration to elicit a measurable osteogenic response for use in subsequent experiments and the effect of contralateral sham surgery on the pattern of bone loss in the tibia following unilateral sciatic neurectomy. (Chapter 3)**
- 2. Is RANKL involved in bone (re)modelling associated with altered mechanical loading? (Chapter 4)**
- 3. The effect of disuse on the adaptive response of bone in old mice. (Chapter 5)**

- 4. The effect of the antiresorptive bisphosphonate risedronate on the osteogenic response to loading in ambulatory and sciatic neurectomised old mice (Chapter 6)**
- 5. The effect of risedronate on the anabolic effect of PTH and loading on bone in old mice. (Chapter 7)**

1.1 The skeleton and the effects of aging

The normal skeleton provides a myriad of functions. It aids mechanical transduction of forces to allow locomotion. It acts as protection for vital organs. It acts as a store for essential minerals, such as calcium and phosphorus and it acts as a haematopoietic centre in the marrow cavities [13, 37, 38].

Bone is primarily comprised of dense lamellar sheets of hydroxyapatite crystals and type I collagen fibres, which provide majority of the strength, and the essential material properties of bone [39]. The collagen molecules provide the bone's key resistance to tensile forces, whilst the mineralised components of the bone provide the key resistance to compressive forces [40]. It is reported that, of the factors that are associated with bone strength, bone mass, measured as bone mineral density (BMD) contributes approximately 70% [41]. Bone mass is the amount of bone per unit area or volume and is reported as either areal BMD (bone mass per unit area, (g/cm^2)) or volumetric BMD (bone mass per unit volume (g/cm^3)). Loss of bone mass is problematic, as the structural functions of the skeleton are impaired and the risk of failure through fracture is increased. Bone mass reduces and fracture risk increases with age in both men and women, but most severely in post-menopausal women [15].

The resultant condition of low bone mass is generally referred to as osteoporosis. Osteoporosis is a significant public health concern, becoming even more clinically important with the aging population of many developing countries. Osteoporosis is generally defined by a low bone mass. Clinically, BMD is generally reported in relation to the number of standard deviations from a young healthy adult and is referred to as the T-score [42]. Because peak bone mass is reached in young adulthood, most T-scores are negative. A T-score of -1 or higher is considered normal, a patient with a score between -1 and -2.5 is considered osteopenic, and those with a score lower than -2.5 are considered osteoporotic [43]. Suffering a fragility (low-impact) fracture in a site usually associated with osteoporosis (spine/hip/wrist) also generally qualifies a patient for a diagnosis of osteoporosis. Treatment for osteoporosis is generally instigated in elderly patients with a T-score lower than -2.5 or a fragility fracture and can range from dietary management of

calcium intake and increased mechanical loading, to pharmaceutical inhibition of bone resorption and/or anabolic stimulation of bone formation in more severe cases. These potential treatments are discussed in more detail in section 1.6 of this chapter.

In the normal adult skeleton, cortical bone comprises 80% of the bone mass and trabecular bone the remaining 20% [39]. The cortical and trabecular compartments of bone both experience loss of bone mass with advancing age (Figure 1 and Figure 2). This gradual reduction in bone mass and strength results in marked increases in the incidence of fractures from low-impact falls, typically referred to as fragility fractures. Fragility

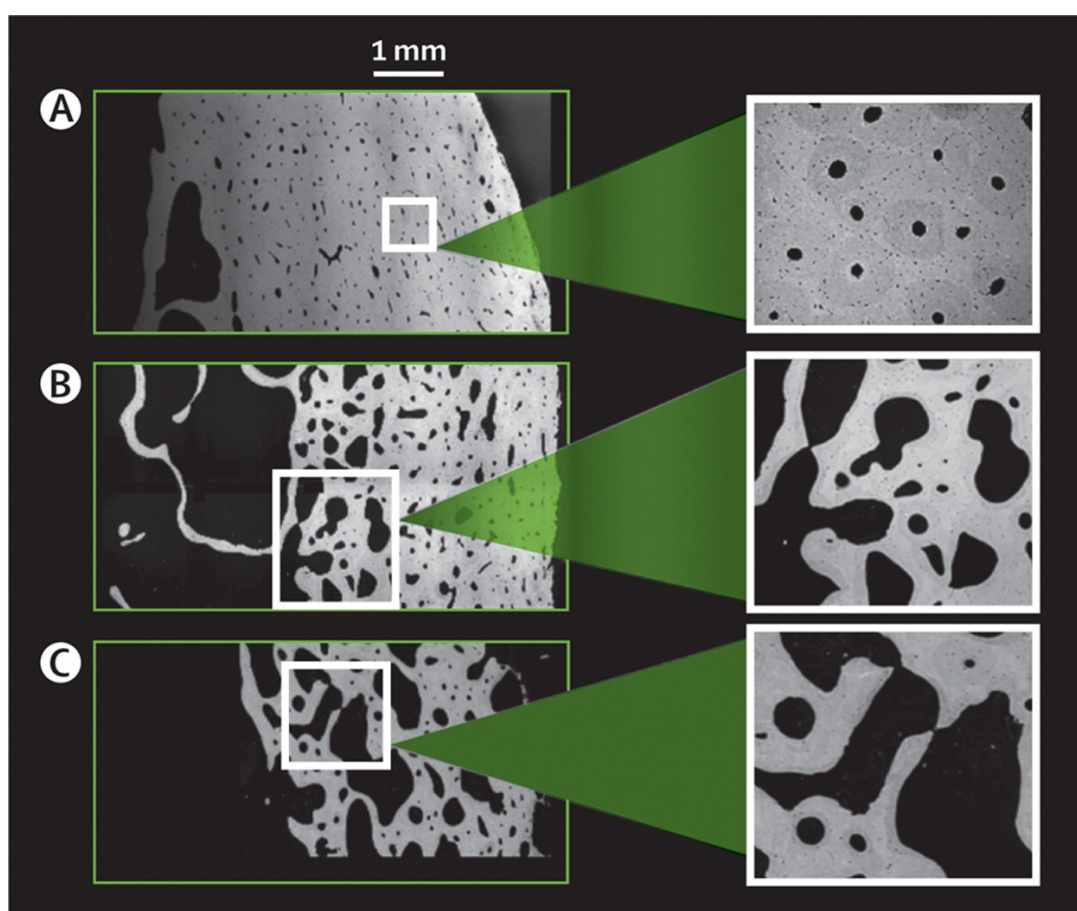


Figure 1 –Structural change in cortical bone porosity with age.

(A) Micrograph of a specimen from a 29-year-old woman. Pores are regular in shape and evenly distributed in the cortex. (B) Micrograph of a specimen from a 67-year-old woman. Pores are large, irregularly shaped, and have coalesced in cortex adjacent to the marrow producing cortical remnants. (C) Micrograph of a specimen from a 90-year-old woman. Most of the cortex is trabecularised by large and coalesced pores. Micrographs are of anterior subtrochanteric specimens. Figure and legend reproduced with permission [3].

fractures are one of the hallmarks of osteoporosis. Van Staa *et al* [17] showed women have a greater chance than men of experiencing a fragility fracture after the age of 50. The predominance of women experiencing osteoporosis and fragility fractures led to the long-held view that the primary cause of osteoporosis was due to the acute reduction in oestrogen following menopause [15]. Longitudinal studies of bone mass in women and men have demonstrated that bone mass starts to decline with aging well before the onset of menopause, suggesting there are additional factors which contribute to the age-associated decline in bone mass and subsequent increase in fragility fracture incidence [44-48]. Additional potential systemic and age-related factors affecting bone mass will be discussed in more detail in Section 1.4.

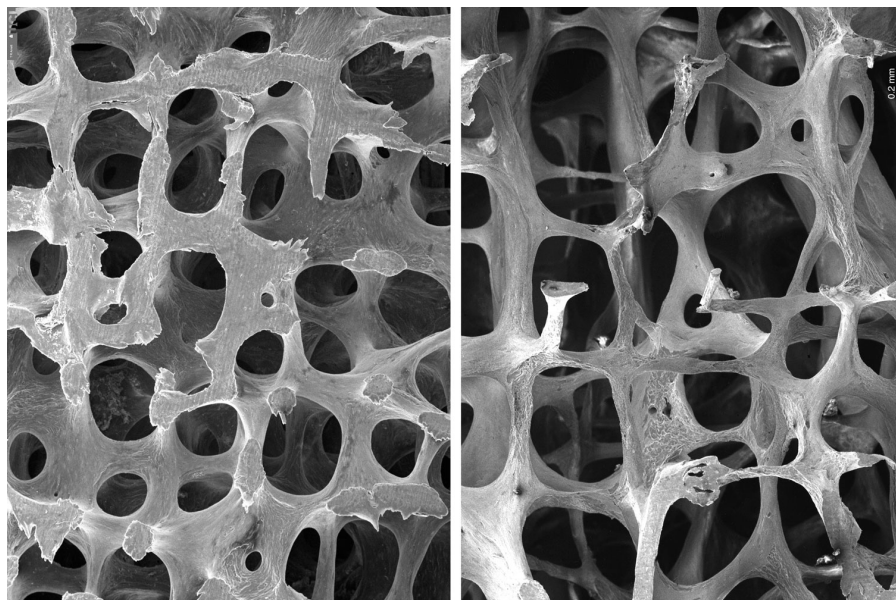


Figure 2 - Scanning electron micrograph (SEM) of the third lumbar vertebra of an adult 30-year-old (left) and an osteoporotic 71-year-old woman (right).

Images produced by Tim Arnett, University College London, made freely available via the European Calcified Tissue Society (ECTS) educational resources.

Bone resorption results in loss of both bone mineral and also the organic components of bone, such as Type I collagen. Type I collagen molecules comprise approximately 90% of the organic component of bone [49], formed into a triple-helix configuration which then are combined into collagen fibres. These collagen fibres are then modified in the post-translational setting to form covalent crosslinks between adjacent collagen fibres,

subsequently increasing tissue strength. These crosslinks, which are biochemically distinct from those formed in other forms of connective tissue in the body, are broken down during bone resorption by osteoclasts, with the breakdown products providing systemically measurable markers of bone resorption, via serum or urine [50].

The arrangement of collagen fibres and subsequently the arrangement of hydroxyapatite crystal orientation governs bone's relative strength and resistance of bone to damage from increased mechanical forces. Lamellar bone consists of concentric sheets of dense, compact bone laid down in an orientation which is best suited to resist the primary strain directions and magnitudes experienced at that site. In humans (and other larger mammals) with thick cortical bone, this lamellar arrangement of the cortical bone is arranged into osteons, which are tubular structures generally aligned with the longitudinal axis of the bone. The central canal of these osteons, called Haversian canals, carry the neurovascular supply to the cortical bone. The transverse communicating channels between neighbouring Haversian canals are termed Volkmann's canals (Figure 3). These vascular channels provide access for resorptive cells to access the cortical bone and permit intracortical resorption and subsequent porosity and bone loss associated with osteoporosis.

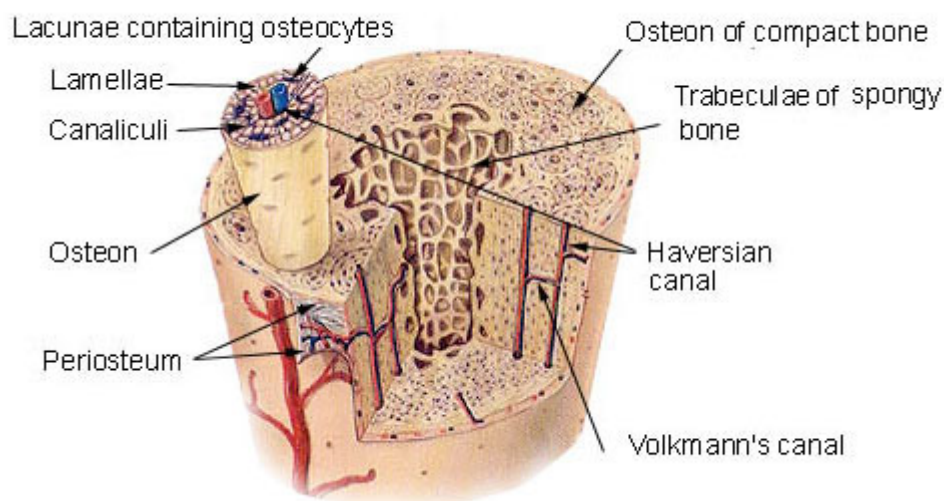


Figure 3 – Diagrammatic representation of cortical bone anatomy

Reproduced from U.S. National Cancer Institute's Surveillance, Epidemiology and End Results (SEER) Program (<http://training.seer.cancer.gov/anatomy/skeletal/tissue.html>) (Accessed 05/12/2017)

1.1.1 Diagnosis and monitoring of osteoporosis

The deterioration in bone mass seen with age is made more difficult to diagnose early in the disease course because it is a clinically “silent” deterioration which is likely only to show clinical signs once a resultant fragility fracture has occurred. At this point, bone mass is frequently deteriorated to a point where intervention is less successful at restoring bone mass.

Evaluation of bone mass can be performed using several techniques. Clinical evaluation of bone mineral density (BMD) using dual-energy x-ray absorptiometry (DEXA) is currently the standard of care for monitoring of bone mass in people, primarily due to the rapid test times, low radiation dose and non-invasive nature. Initial studies demonstrating the age-related loss in bone mass were performed using DEXA [44, 48, 51]. Although DEXA is used commonly for monitoring of treatment efficacy in clinical trials [52-56], and most osteoporosis clinical guidelines use DEXA-derived BMD values for diagnosis and treatment decision making [42, 57-59], it is not able to easily separate cortical from trabecular bone compartments due to relatively low scan resolution and the two-dimensional nature of the images generated [45, 47].

Advances in computed tomography (CT) imaging technology have led to the wider adoption of quantitative CT (QCT) for assessment of bone density, which is able to resolve bone structure in 3D and achieve separate quantitative measures of both trabecular and cortical bone mass and architecture. QCT is also able to overcome sources of artefactual error seen using DEXA, associated with factors such as variable body mass or patient positioning [57, 60]. QCT is able to assess additional parameters which are shown to correlate to fracture risk and/or bone strength that aren't possible with DEXA, such as trabecular plate/rod architecture [61-63] and intracortical porosity [64-67]. Both in clinical trials and in research animal models, CT-based imaging is becoming the gold standard for assessment of bone mass and architecture changes seen with aging and also in response to pharmacological and other treatments. A recent systematic review of studies evaluating the effects of osteoporosis treatments using high resolution peripheral QCT (HR-pQCT) identified treatment-specific differences between trabecular and cortical bone and also

between anti-resorptive and anabolic agents [64], although these authors reiterated the valid point that, as with any new technology which may improve diagnostic sensitivity, a degree of standardisation of the measures collected between and within studies needs to be agreed to permit more meaningful comparisons between studies evaluating age- or treatment-related changes in volumetric BMD (vBMD).

1.1.2 Bone structure changes with age

Age-related changes in bone mass are compartment specific with clear age- and sex-specific differences in the cortical versus the trabecular compartments. As humans age, typically the cortical shell expands, increasing the periosteal area, but it becomes thinner due to endosteal resorption; between the ages 20- 90 years of age, periosteal apposition increases bone total cross-sectional area by ~15%, but endosteal resorption concurrently increases by 25-40%, resulting in thinner cortical shell [45] (Figure 4). The age-related periosteal expansion does result in improvements in the biomechanical performance of cortical bone. The greater distance of the cortical bone from the centroid of the bone results in increases in the area moment of inertia which improves resistance to bending

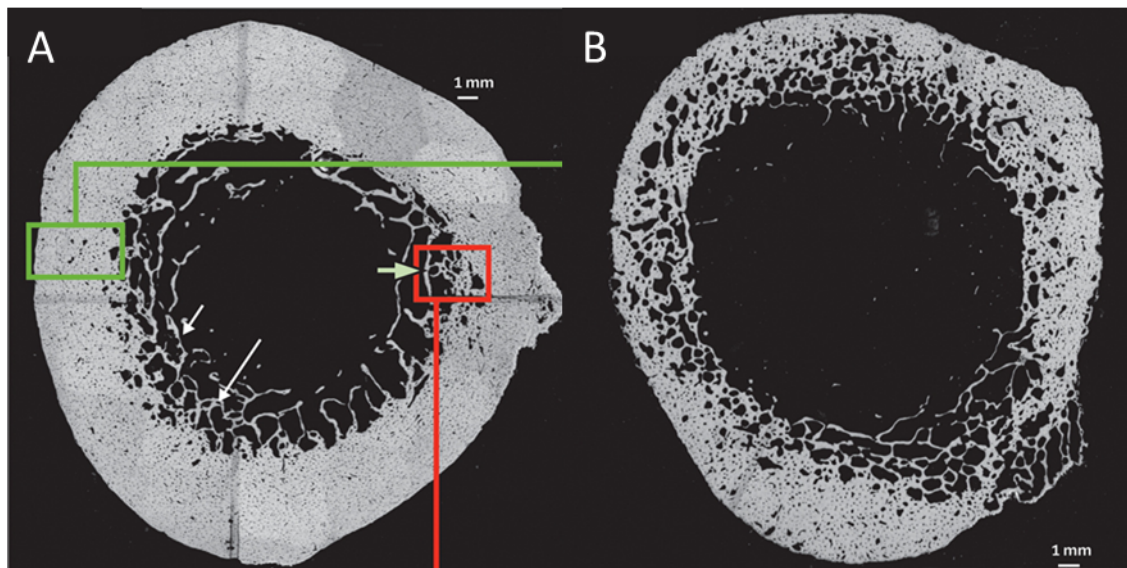


Figure 4 – Aging is associated with cortical thinning due to medullary expansion.

Aging results in medullary expansion and intracortical resorption. (A) Micrograph of a specimen from a 78-year-old woman. (B) Micrograph of a specimen from a 90-year-old woman. Micrographs are from anterior subtrochanteric specimens. Cracks are preparation artifacts. Figure adapted and used with permission from [3].

[45, 68]. Men have larger bones, on average, at all ages, compared to women, and this factor is one of the main determinants of the sex-dependant differences in whole-bone strength [68].

In women, substantial cortical bone loss does not occur until midlife, associated with menopause, with a significant correlation to the serum levels of biologically active sex-steroids, and it is well established that sex-steroid deficiency contributes to osteoporosis [47]. Cortical bone loss in men is slightly different, with a small, but significant loss seen in young adulthood, which remains consistent until 75 years of age [47] and lower overall cortical bone losses compared to women (-8% vs -17% respectively, for cortical area at the distal radius [45]).

A further advantage of the increased usage of HR-pQCT has been its ability to evaluate trabecular bone mass and architecture, independent of the overlying cortical shell, whilst being able to avoid the use of bone biopsies. Bone biopsies are invasive and are typically taken from regions of the skeleton which are not representative of common fracture sites (biopsies are most commonly taken from the ilium, an uncommon site for fragility fractures resulting from osteoporosis).

Trabecular bone mass, like cortical bone mass, also declines with age, in both men and women [46]. The axial skeleton trabecular bone appears to be more severely affected with aging in women, with a 55% loss of bone mass compared to 46% in men between the ages of 20 and 90 [45]. This sex-specific reduction in trabecular bone mass is less clear when peripheral trabecular bone sites are analysed. Distal radial trabecular bone mass is less affected by aging in men and women, and there was no sex-specific differences in the trabecular microarchitecture [45, 66]. These clinical studies help demonstrate site- and sex-specific differences in the response of bone to aging in people, however, a thorough understanding of the mechanisms underlying the site- and sex-specific differences remains unclear. The use of *in vitro* and *in vivo* animal models has helped further our knowledge of the cellular mechanisms underpinning the processes of bone (re)modelling and bone's biological response to aging.

1.2 Bone cells and bone (re)modelling, and the effects of aging.

1.2.1 Bone cell origins and function

Osteoblasts

Osteoblasts are derived from marrow stromal cells (MSC). MSCs can also develop into other cell lineages such as adipocytes, myocytes, chondrocytes and possibly neuronal cells [69]. Understanding of the molecular triggers/transcription factors that help differentiate these cells from their ancestral cell lines has greatly increased in recent years with the proliferation of molecular genetics techniques. The differentiation of MSCs into osteoblasts is promoted by key transcription factors including the principal osteogenic master gene, runt-related transcription factor 2 (Runx-2) [70], and osterix [71]. Cells then differentiate into mature, matrix-synthesising osteoblasts, actively forming bone matrix and promoting mineralisation. Other transcription factors which regulate osteoblast differentiation and activity have been identified, but detailed discussion of these is beyond the scope of this thesis, and they are reviewed elsewhere [72-74]. Developing knowledge of this transcriptional cascade has led to the identification of several key genes primarily expressed at certain stages of the MSC lineage development, which have been utilised in the generation of cell-line specific mutants using Cre-recombinase techniques to permit expression of a given gene mutation of interest only in the given cell type of interest (and all subsequent stages in the lineage). Figure 5 demonstrates the common Cre-recombinase variants used in the investigation of MSC lineage cells. Comprehensive discussion of the use of cell-specific transgenic mice in the study of bone biology is well reviewed elsewhere [75-77].

After osteoblasts have completed the necessary amount of bone formation, some of them are committed to differentiate further into osteocytes, which become embedded in the deposited matrix, and others appear to change into seemingly quiescent bone lining cells. This is illustrated in Figure 6. Most osteoblasts, however, undergo apoptosis [78].

Osteocytes

Osteocytes are cells encased in the mineral matrix of bone following terminal differentiation of osteoblasts along the osteoprogenitor lineage of cells. They are embedded within the mineral matrix by the bone formed by osteoblasts. This process was initially thought to be a passive process following bone mineralisation [79], but further evidence implicates a more active process in which they actively migrate into the osteoid being deposited by their osteoblast counterparts through the use of collagenase and Matrix Metalloproteinases (MMPs) [80] resulting in the invasive development of dendritic processes and canaliculi between the newly embedded cells and existing, deeper osteocytes [18]. Further evidence that osteocytes are not just “passive prisoners” in the matrix includes the finding that aging promotes an increase in the number of dendritic connections between osteocytes in adult versus juvenile rats, although aged rats

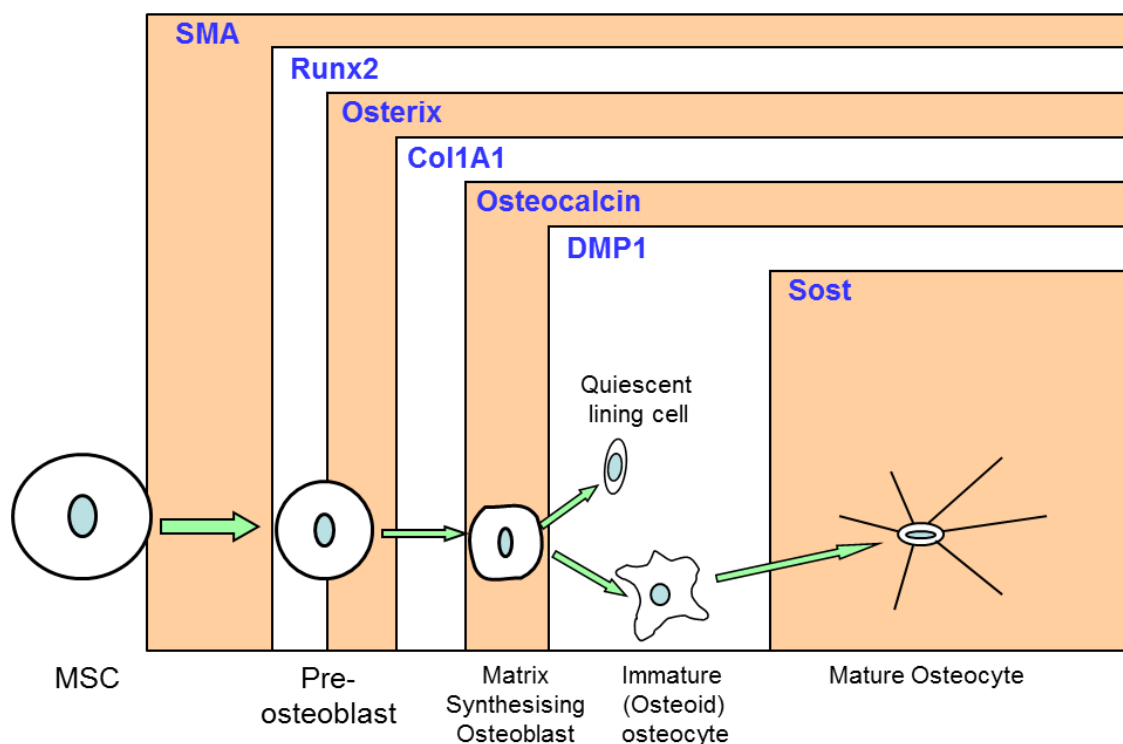


Figure 5 - Differentiation lineage markers for osteoblastic/osteocytic lineage.

Cre-recombinase is bound to the above genes to breed mice with other genes of interest expressed only in the cell type above, and their descendants. SMA – Smooth muscle actin, Runx2 – Runt-related transcription factor 2; Col1A1 - Collagen 1 A1; DMP1 – Dentin Matrix Protein 1, Sost – Sclerostin.

demonstrated a reduction in canalicular number compared with adults [80, 81]. Another study using acid etching and back-scattered electron microscopy also demonstrated that osteocyte lacunae showed decreasing canalicular connections with neighbouring lacunae with advancing age [82]. Furthermore, lactation stimulates a reversible increase in the size of the osteocytic lacunae [83, 84], suggesting ongoing cellular activity that alters bone structure is present, even in osteocytes imprisoned within mineral matrix.

Osteocytes are also now widely accepted to be the primary mechanosensory cells of bone. They sense changes in mechanical strain and transduce externally applied strain stimuli into a signal to promote or suppress bone formation or resorption as required. Since it was first established [85] that osteocytes respond to strains in their surrounding matrix, evidence has accumulated that their responses are diverse [18, 22, 38, 86-88] and potentially significant in controlling subsequent bone formation by osteoblasts [38] and bone resorption by osteoclasts [21, 22, 89]. More discussion on strain sensing by osteocytes is included in section 1.8. The imbalance between bone formation and bone resorption and poorly regulated bone remodelling and modelling is one of the underlying defects in bone metabolism which precipitates age-related osteoporosis [30, 31]. Bone (re)modelling is discussed in more detail in the next section (1.3) of this chapter.

Osteoclasts

Osteoclasts are cells descendant from haematopoietic (myeloid) cells, related to the macrophage lineage [90, 91]. They mature from these precursors to form multinucleate giant cells whose primary role is to resorb bone (Figure 6). The majority of osteoclast precursors reside in the bone marrow, and for this reason, endosteal bone resorption is greater than periosteal bone resorption. The key regulators of osteoclast activity are Macrophage Colony Stimulating Factor (M-CSF) and Receptor Activator of Nuclear Factor κ B (RANK) ligand (RANKL). M-CSF binds the CSF1R receptor, which in turn generates a cascade of reactions which includes, among other targets, synthesis of the RANK receptor in osteoclasts [90]. Impairment of the gene encoding for CSF1R receptor results in severe osteopetrotic phenotype, and treatment with M-CSF in these animals results in abrogation of this effect [92-94]. RANKL, discussed in more detail in the next section, has been shown

to be a key osteoclastogenic factor [95, 96] which aids in the maturation and differentiation of osteoclasts and promotes bone resorption.

Once formed, osteoclasts spread across the bone surface that is to be resorbed and form a seal over the area, allowing the secretion of osteolytic substances (proteases, tartrate-resistant acid phosphatase (TRAP) and cathepsin K) to combine with the acidic environment provided by the osteoclast through secretion of HCl. These substances, combined with the low pH environment at the brush border of the osteoclast allows digestion of the bone mineral matrix and subsequent release of other factors, such as Transforming Growth Factor β (TGF- β) [97] and bone morphogenetic proteins (BMPs) from the mineral matrix. The ability of molecules such as TGF- β to simultaneously increase osteoclast and osteoblast activity may begin to explain why bone formation and resorption appear closely coupled during bone (re)modelling [98]. The control of activity of osteoblasts and osteoclasts is primarily mediated by osteocytes.

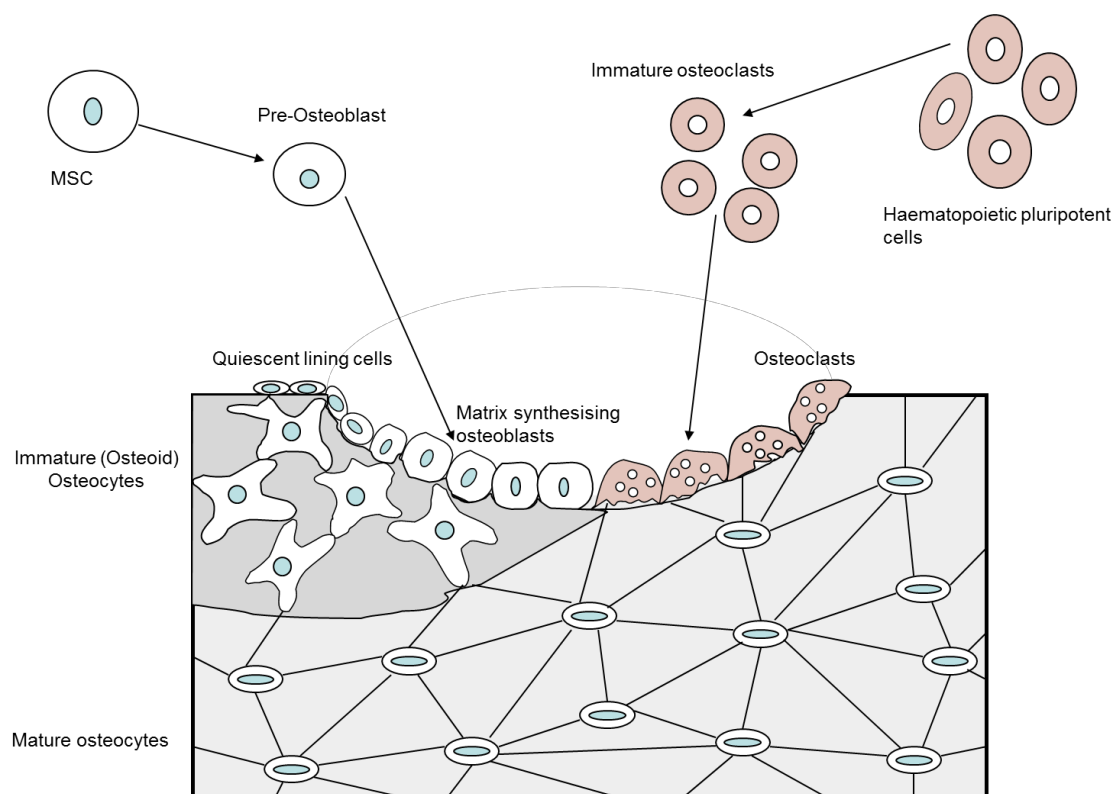


Figure 6 – Evolution of osteoblastic and osteoclastic lineage cells.

Mesenchymal stem cells (MSC) develop into matrix embedded osteocytes.
Haematopoietic pluripotent stem cells develop into multinucleate osteoclasts.

1.3 Bone (re)modelling

Bone modelling describes the situation where bone formation occurs without the necessity for prior resorption. Bone *remodelling*, on the other hand, is the coordinated activity of osteoclasts removing old/damaged bone and osteoblasts subsequently forming new bone in the same site, typically in efforts to maintain bone mass. In young animals, with growing bone, modelling dominates over remodelling, however, once most growth is complete in the adult skeleton, maintenance of bone mass is needed, so the primary process involved in bone mass management is bone remodelling. Remodelling occurs to help repair areas of microdamage, which would otherwise accumulate and could lead to eventual fatigue failure/fracture. The processes of remodelling involve three main sequential phases: resorption, reversal and then formation, which are primarily mediated by the activity of osteoclasts and osteoblasts and their progenitors. The initial resorption phase is conducted by osteoclasts, which remove old, unnecessary, or damaged bone. The reversal phase is the transition phase where the activity of osteoclasts starts to decrease and the activity of osteoprogenitors increases and the development/recruitment of osteoblasts increases to eventually transition into an active site of bone formation [99].

As described previously, remodelling activity is primarily orchestrated through the controlling influences of the neighbouring osteocytes, although some osteoblastic activity is through the effect of cross-talk with osteoclasts and the processes of bone resorption. The closely associated niche formed by the presence of these major bone cell types has been referred to as the basic multicellular unit (BMU) and all phases of the remodelling cycle occur within the BMU. The cellular niche of the BMU may also have an integral role to play in the close coupling of the remodelling functions of bone. Osteoclasts may control the pH of the extracellular environment in the BMU thus regulating osteoblast function [100, 101]. These compartments have also been shown to be covered by modified lining “canopy” cells which show markers of osteoblast differentiation [102]. Reduced bone formation and increased resorption was shown after disruption of these lining cells [103]. The proposed signalling mechanism for this remains to be proven experimentally.

Osteocytes are now widely thought of as the “master regulator” of adaptive bone remodelling, subsequently signalling to nearby osteoclasts to initiate the resorptive phase and then in turn to osteoblasts to promote the formation phase, thus modulating their development and activity [18, 19, 104].

The recruitment of osteoclasts and initiation of a remodelling event can be controlled by multiple factors. Strain has been hypothesised to mediate the direction of osteoclasts tunnelling in BMUs, with principal strain direction dictating the direction of travel of osteons [105], which should increase the tensile strength of bone. In contrast, reduced mechanical loading results in increased osteoclast numbers and bone resorption [106], although the bone loss associated with unloading is not necessarily coupled to formation, so may not represent a true bone *remodelling* situation. It could alternately represent a remodelling event that is aborted prior to the formation phase. The effect of mechanical loading on bone cell activity is discussed in further detail in section 1.8.2 of this chapter.

In addition to the direction of principle strain, bone microdamage has also been repeatedly shown to mediate remodelling activity. In adult bone with fatigue damage, remodelling osteons were 7 times more likely to be situated adjacent to a microcrack, than elsewhere. In the normal adult situation; 2-10% of the skeleton is estimated to be replaced annually through bone remodelling [107, 108]. An earlier study also demonstrated increased bone remodelling associated with fatigue micro-damage to bone, with 44 times more microcracks in association with resorption spaces than expected by chance alone [109]. The development of the BMUs was later confirmed to be a result of microdamage, suggesting that the remodelling is directed by site of microdamage, and not that the microdamage occurs in sites of already remodelling bone due to inherent weakness [110]. The direction of travel of osteons was also demonstrated to be guided by the location of microcracks and the subsequent osteocyte apoptosis surrounding these areas of injury [111]. More recent work has localised osteocytic expression of RANKL to those cells surrounding areas of micro-damage, and the related apoptotic cells [112]. It is quite likely that this RANKL expressed at the cells adjacent to microdamage and apoptosis promotes the differentiation and activity of osteoclasts to initiate or direct a remodelling event.

1.3.1 Transcriptional control of bone cell activity during remodelling

The control of bone cell activity is complex and multifactorial. A detailed review of the current state of understanding of molecular control of bone remodelling is outside the scope of this thesis. Notwithstanding, it is important to discuss several key signalling molecules and pathways with key involvement in the control of both osteoclastic resorption, and also osteoblastic formation. RANKL and osteoprotegerin (OPG) are essential for the normal differentiation and activity of osteoclasts, and the Wnt pathway, and its inhibitor, sclerostin are key regulators of osteoblast activity.

RANKL and OPG and the resorptive phase of bone remodelling

Initiation of the remodelling cycle must be stimulated initially by a resorptive event. Therefore, recruitment and activation of osteoclasts is essential for remodelling to begin. As mentioned earlier, M-CSF and RANKL are integral signalling factors necessary for osteoclast activity. RANKL is a primarily membrane-bound protein involved in recruitment and differentiation of bone marrow macrophage cells into osteoclasts.

RANKL is competitively inhibited by OPG, a competitive decoy receptor of RANKL, thus preventing the activation of the RANK receptor. OPG is also important in intracellular trafficking of RANKL [113]. Hence, increase in the concentration of OPG also decreases the degree of bone resorption. See Figure 7 for a diagram summarising the function of the RANK/RANKL/OPG pathway.

RANKL was originally believed to be produced primarily by osteoblasts, as co-culture with osteoblast progenitors was able to stimulate osteoclast differentiation [114, 115]. However, two paradigm-shifting studies [21, 22] have shown, using DMP1-Cre RANKL knockout mice, that in growing mice at least, it is osteocytes (and possibly late osteoblasts and bone lining cells), and not, as was previously thought, osteoblasts or their progenitors, that are the predominant source of RANKL necessary for bone remodelling. Genetically-

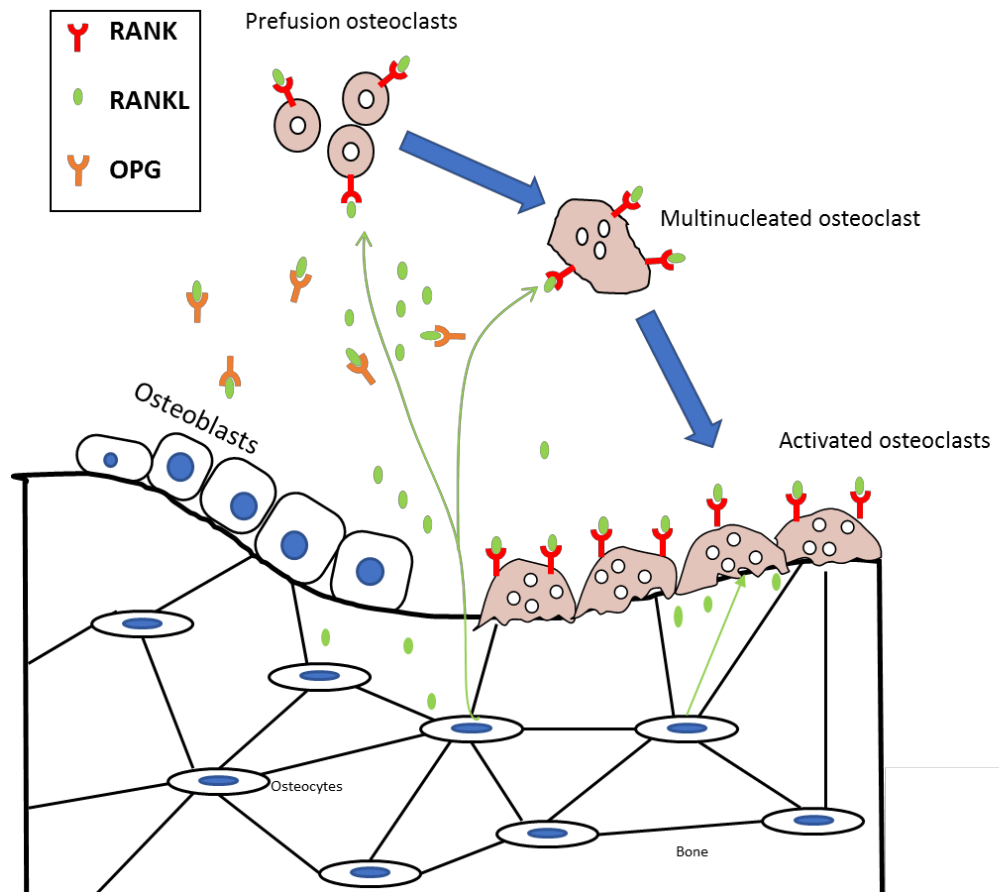


Figure 7 Schematic representation of the RANK/RANKL/OPG axis and its effect on osteoclasts.

RANKL, produced primarily in osteocytes, binds RANK, which stimulates the differentiation of immature osteoclasts, and the activation of mature osteoclasts to stimulate active bone resorption. OPG, produced by osteoblasts and osteocytes, is a competitive decoy receptor molecule which blocks RANKL from activating the RANK receptor. Decreased RANKL:OPG ratios decrease osteoclast activity.

modified mice lacking RANKL in osteocytes alone did not lose bone when loading was reduced by tail suspension [21]. In a follow-up [116] to the initial study [21], Sost-Cre transgenic mice, with knockout of RANKL in osteocytes only (and not bone-lining cells) still demonstrated a marked decrease in osteoclast number and also increase in cancellous bone mass. These publications demonstrating a shift in understanding of RANKL regulation were published concurrently, around the time that the author's PhD experiments were being conceived. Whilst these studies demonstrated RANKL is produced by osteocytes, the temporal and spatial relationships between changes in strain, RANKL expression and osteoclast activity had never been established. One of the aims of one of

the experiments described in Chapter 4 of this thesis was to better characterise the temporal and spatial patterns of expression of RANKL in cortical bone osteocytes following alterations in the mechanical loading environment, particularly following disuse.

With respect to bone phenotypes, genetic studies deleting the genes responsible for the production of RANKL and RANK (the *Tnfrsf11* gene and *Tnfrsf11a* gene, respectively) resulted in severe osteopetrotic phenotype and failed tooth eruption in mice [117, 118]. Deletion of the gene expressing OPG (*Tnfrsf11b*), conversely resulted in osteoporosis and increased osteoclastic activity [119, 120]. Over expression of RANKL in transgenic mice shows an osteoporotic phenotype [121] and over expression of OPG results in osteopetrosis but normal tooth eruption [122]. Based on these findings, RANKL/RANK/OPG interaction is essential for control of osteoclastogenesis *in vivo*. RANKL remains membrane bound unless cleaved proteolytically by enzymes such as matrix metalloproteinases (MMPs) like MMP-14. In primary neonatal calvarial osteoblasts, addition of MMP-14 increased RANKL cleavage and suppression of MMP-14 increased membrane-bound RANKL and promoted osteoclastogenesis [123]. MMP-14 deficient mice also showed an increase in osteoclastogenesis *in vivo* [123]. Hence, the membrane-bound form of RANKL is more effective than serum RANKL at stimulation of osteoclastogenesis [22, 123-126]. The membrane-bound nature of RANKL involved in bone resorption also suggests that its activity is through primarily localised paracrine pathways, rather than systemic increases in serum levels. This allows the resorptive response to be controlled in a localised and site-specific manner, as is necessary for effective adaptive bone remodelling.

There appear to be many factors which can upregulate RANKL expression. These include PTH, prostaglandin E₂, Vitamin D₃, TNF- α and various interleukins (IL-1, IL-6, IL-11 and IL-17) [126, 127]. TGF- β can down regulate RANKL mRNA expression [127, 128] however one study demonstrated that RANKL protein expression was unaffected by TGF- β administration *in vitro* [126]. There is evidence that mechanical load regulates the expression of RANKL in a load dependant manner, although studies have demonstrated conflicting results when load is applied using *in vitro* loading systems, and *in vivo* in

rodents. *In vitro* cell culture experiments have shown variable results when applying load to cells. These vary from increased RANKL expression with load to decreased expression [129-135]. Unfortunately, the techniques of load application were not the same in these studies, so comparison is difficult, and additionally, the *in vitro* response to load may not necessarily correlate with the *in vivo* situation as the three-dimensional orientation and lacunocanalicular arrangement of osteocytes in bone may confer additional and/or different responses to mechanical load. The quantification of RANKL expression in situations of altered mechanical load *in vivo* has not been extensively investigated, however RANKL is increased in osteocytes following disuse [21, 22, 136] induced by tail suspension. RANKL was also increased in tibial bone marrow following disuse from sciatic neurectomy in mice, although this increase was mitigated by parathyroidectomy indicating the modulatory effect that PTH can have on bone remodelling [137].

In addition to expression in osteocytes and osteoblasts, RANKL expression is widespread throughout the mouse and human body with lymphocytes (B and T cells)[118, 138], thymus [139], developing mammary tissue [140], brain, skeletal muscle, skin, spleen, kidney [141] and neoplastic tissues including mammary carcinoma and metastatic bone neoplasia [142] all displaying expression of the mRNA and/or protein. The effect of these extraskeletal sources of RANKL on bone remodelling is debatable. Activating T cells was shown to stimulate RANKL production *in vitro* and *in vivo* and this resulted in an osteoporotic phenotype in mice [118]. However, crossing the *Lck-Cre* mice with RANKL deficient transgenic mice, to create mice deficient in RANKL specifically in T cells, did not result in a noticeably osteopetrotic phenotype [22].

Although osteoclastic control appears to be primarily controlled by RANKL produced within the skeletal tissue, isolation of pure osteocyte or osteoblast fractions has been met with technical difficulty. RANKL mRNA expression has been detected in both osteocyte rich fractions and osteoblast rich fractions in mice [21, 22, 136]. As described previously, the use of transgenic mice, however, has enabled the identification of the cellular origin of RANKL involved in osteoclastic differentiation and activity. *In situ* localisation of RANKL expression, however has been met with more difficulty. Immunohistochemistry (IHC)

techniques have been hampered by the poor affinity of commercially available anti-mouse RANKL antibodies. An early study, using *in situ* hybridization (ISH) to localise RANKL mRNA and IHC to identify RANKL protein found both RANKL mRNA and protein expressed in most tissue examined, including extraskeletal sites. Interestingly, the mature osteocytes examined in this study did not appear to express much RANKL [141]. Chapter 4 reports the optimisation of a protocol for the immunolocalisation of RANKL in cortical bone.

Antibodies developed against human RANKL (Denosumab) have been used therapeutically to control the osteoclastogenesis often implicated in bone fragility disorders, mainly osteoporosis, but also resorptive conditions such as breast or prostate neoplasia metastasis to bone [143-146]. Discussion of RANKL inhibition as a therapeutic treatment option is further detailed in section 1.7.2 of this chapter and in Chapter 4.

The reversal phase of bone remodelling

Once the resorptive phase of remodelling is complete, a reversal phase ensues, where mononuclear cells are recruited to the eroded surface to help prepare it for future bone formation by osteoblasts. Recent work has confirmed these “reversal” cells are part of the osteoprogenitor lineage [147-149]. Additionally, very recent work has proposed an overlapping transitional phase of the remodelling cycle, called the “reversal-resorption” phase. By examining longitudinal sections of Haversian canals undergoing remodelling, the authors identified a region immediately behind the cutting cone of the remodelling front, where osteoclasts and reversal osteoprogenitors alternated on the bone surface and canal diameter further widened, suggesting that a section of the remodelling process is still undergoing resorption whilst the reversal cells are beginning to prepare the region for the subsequent formation phase [99].

Although the process of bone cell coupling is incompletely understood, the reversal phase is integral in coupling the subsequent bone formation to the preceding bone resorption. Several potential coupling factors originating from osteoclasts and the activity of resorption have been identified [99, 150] and inhibition of osteoclasts impairs the formation phase of the remodelling cycle [151]. Furthermore, although coupling factors

are important to promote recruitment and differentiation of osteoprogenitors, proximity and viability of sufficient numbers of these cells is also critical to allow effective reversal of the remodelling cycle [152]. Andersen *et al* [147] demonstrated a significantly reduced “reversal” cell density on the eroded surface of post-menopausal iliac biopsy samples with greater distances between osteoclast and osteoblast cell clusters, suggesting a greater number of aborted reversal events. This may go part-way to explaining the increase in intracortical porosity seen in cortical bone of old people. Impairment of the activity of osteoclasts to impair the initiation of the formation phase of the remodelling cycle is, in part, the basis for the use of the anti-resorptive, Risedronate, in chapters 6 and 7.

Recruitment and differentiation of osteoblasts in the BMU is essential for the effective completion of the bone remodelling cycle. The coupling of bone formation to the preceding bone resorption is, as mentioned earlier, incompletely understood, with several physical and biochemical factors proposed to modulate the rate of osteoclast:osteoblast coupling. The origin of the osteoblasts located in the BMU is also incompletely understood. Cell division has not been observed within the BMU, so osteoblasts must be recruited from other sites, or potentially differentiate from other related cell types, such as bone lining cells [153], or possibly the osteoblastic “reversal” cells discussed earlier in this section [152]. As both bone lining cells and reversal cells have been shown to express gene markers suggestive of the osteoblast lineage, and bone lining cells typically cover the bone surface prior to bone resorption and separate to make way for osteoclasts, these cells are a likely source of the matrix-synthesising osteoblasts present in the formation phase of the bone remodelling cycle. Recruitment from the MSC cell pool may also be a source of these cells. Lineage tracing techniques have recently allowed better characterisation of the source of osteoblasts [153-155], and ongoing work, in collaboration with our laboratory, aims to further elucidate the physical origins of these proliferating cells.

Wnt/ β -Catenin Pathway, sclerostin and the formation phase of bone remodelling

Once the reversal phase is complete, recruited matrix synthesising osteoblasts proceed with the formation phase of the remodelling cycle. As described earlier, osteoblasts are influenced by several different signalling factors. One of the key transcriptional regulators of differentiation into osteoblasts is provided by the Wingless Homology (Wnt) signalling pathway [156]. There are several Wnt genes which have been implicated in the control of bone mass, both through action on osteoblasts, and also through action on osteoclasts [157]. Synthesis of bone matrix is facilitated through activation of target genes through both the canonical (Wnt/ β -catenin) pathway, and other non-canonical pathways. The canonical Wnt pathway is illustrated diagrammatically in Figure 8. In the canonical Wnt

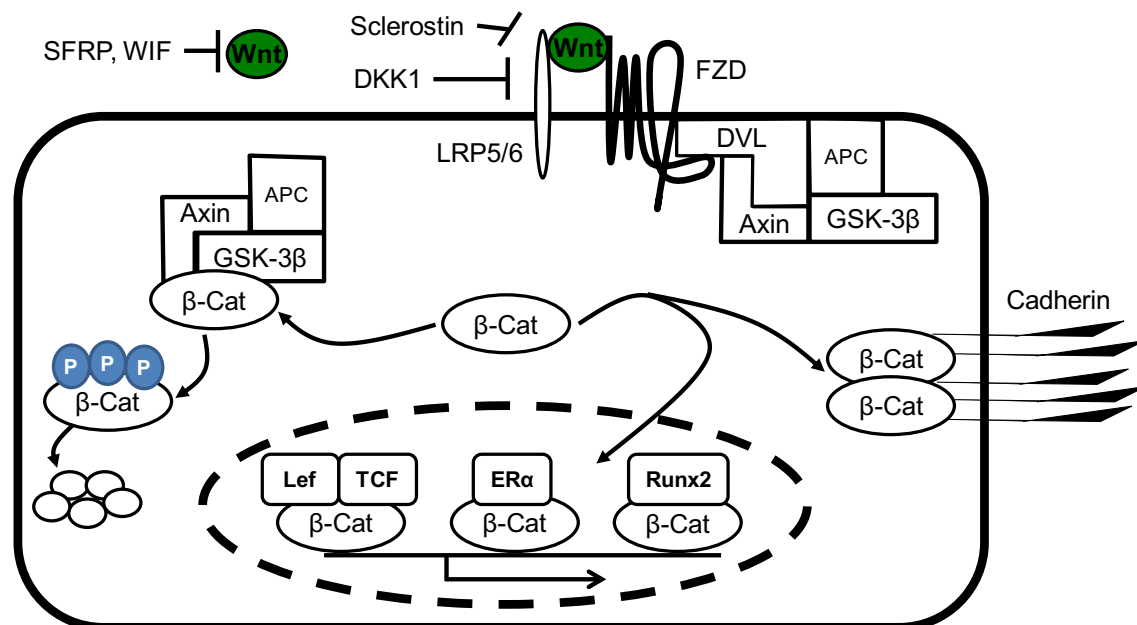


Figure 8 - Schematic representation of canonical Wnt signalling.

The central molecule required for canonical Wnt signalling is β -catenin, which is normally degraded following poly-phosphorylation by a protein complex including GSK-3 β , thereby limiting its levels in cytoplasmic pools. Wnts binding to their co-receptors LRP and FZD results in inhibition of the GSK-3 β complex, permitting β -catenin cytoplasmic accumulation. Cytoplasmic β -catenin can either translocate to cadherin junctions at the cell membrane, or into the nucleus where it is able to alter gene expression in conjunction with other transcription factors. This pathway is also regulated through extracellular inhibitors including sclerostin, dickkopf (DKK)1, secreted frizzled-related proteins (SFRPs) and Wnt inhibitory factors (WIFs). Reproduced with permission [6]

pathway, Wnt proteins bind to the Frizzled (Fzd)/Lipoprotein-related receptor (LRP)5, activating it and blocking the phosphorylation and subsequent degradation of intracellular β -catenin. Consequently, intracellular β -catenin concentration increases, resulting in its translocation to the nucleus, and binding with other transcription factors, resulting in the transcription of osteogenic target genes [158]. Wnt proteins have a multitude of functions which depend quite heavily on context, so the exact role of the varied pathways affected by individual Wnt proteins still remains somewhat unclear. Detailed reviews of the current state of knowledge is provided elsewhere [157, 158].

Sclerostin, produced almost exclusively by osteocytes, acts as an antagonist to the Wnt pathway [159]. We, and others, have shown that, in osteocytes, sclerostin is up-regulated *in vivo* following unloading and down-regulated following loading [8, 20, 160]. Sclerostin also may have a role in controlling osteoclastogenesis through the potential down regulation of OPG expression in osteocytes and osteoblasts [96, 161]. Osteocytes, in addition to being the major source of sclerostin, also produce several BMPs shown to modulate bone formation [73, 162-164].

Antibodies against sclerostin are in the final regulatory stages for approval for treatment to reduce fracture risk and increase bone mass in osteoporotic patients. Sclerostin antibody (Scl-Ab) treatment resulted in reactivation of quiescent bone lining cells, but no increase in proliferation or change in rate of apoptosis, suggesting the anabolic effect of Scl-Ab may be due to activation of quiescent cells [165]. Sclerostin blocking antibodies have demonstrated significant increases in hip and spine BMD and strength following treatment [166, 167], although bone mass did return to baseline following discontinuation after 12 months [168]. Further discussion of therapeutic treatment with sclerostin blocking antibodies for management of osteoporosis is detailed in section 1.7.3 of this chapter.

1.4 The effect of aging on bone cell function

As bone ages, resorption increases, with a concurrent decrease in the rate of bone formation. This results in net bone loss in people [169]. This impairment of the processes

involved in maintenance of bone mass and architecture is probably due to derangement of normal cellular activity of the cells involved in bone homeostasis and the subsequent imbalance in the rates of resorption and formation. In this section, the potential contribution of age-related changes in cell number and function to the age-related failure in regulation of bone mass will be discussed.

Osteocytes

The number of osteocytes has been demonstrated to decrease with aging in humans [170] and mice [29, 171]. The reduction in osteocyte number, primarily through apoptosis, has been hypothesised to increase bone fragility [172]. Osteocyte apoptosis is also associated with other bone catabolic situations. Glucocorticoid treatment-associated fragility fractures of the femoral neck were correlated to the degree of osteocyte apoptosis [173]. Disuse [174, 175] and withdrawal of oestrogen following ovariectomy [176-178] have both also been shown to reduce osteocyte number through apoptosis. Reduced osteocyte viability and subsequent reduction in numbers has been hypothesised to result in an increase in bone fragility as the bone effectively has lost its ability to sense damage and direct remodelling appropriately [18]. Although osteocyte apoptosis following disuse and mechanical overload and microdamage [109, 111, 179] has in itself been associated with triggering bone remodelling [180], the overall decrease in cell numbers once cells have died is likely to eventually result in a decreased mechanosensory capacity.

However, although osteocyte number is decreased with aging, the activity of surviving osteocytes may not necessarily be impaired. RANKL and sclerostin concentration in bone marrow serum was decreased with aging in mice [181], although this study did not quantify osteocytic concentration. Conversely, Meakin *et al* [29] have demonstrated that despite a significant decrease in the percentage of viable osteocytes with aging, the proportionate response to loading was maintained in old mice, compared to young mice, evaluated through decreased osteocytic expression of sclerostin. This suggests that surviving osteocytes in old mice are still able to respond to exogenous signals with similar efficacy to young mice.

Osteoclasts

The amount of bone resorption increases with age, but little evidence exists exploring the direct effect of aging on the cellular activity and number of osteoclasts. Cultured human osteoclasts demonstrated significantly greater proliferation and resorptive activity when cultured on cortical bone chips from old (8y) versus young (9-month) cattle femoral diaphyseal bone [182], suggesting that the control of osteoclast-mediated resorption is dependent on the age of the bone itself. Aged rat bone also demonstrated an increased osteoclast number on periosteal bone compared with young animals *in vivo* [183]. This study also demonstrated a greater increase in osteoclast number in aged bone at the metaphyseal periosteum, compared with the diaphyseal periosteum, which may explain the significantly greater increase in cortical porosity noted with aging in metaphyseal bone compared with mid-diaphyseal bone [184].

Osteoclasts from old bone may also impair osteoblast function more than those from young bone. Conditioned media from osteoclasts cultured from old mice suppressed mineralisation of osteoblasts *in vitro* more than media from young mice [185]. Furthermore, these authors were also able to demonstrate that this inhibition of osteoblast function was mediated by sclerostin production from the old mice osteoclasts, a cell type previously believed to be incapable of producing sclerostin. Age-specific inhibition of osteoblast function mediated by osteoclastic expression of sclerostin may, at least in part, contribute to an age-related impairment of bone formation.

Osteoblasts

There are numerous studies exploring the effects of aging on the differentiation, activity and number of osteoblasts described in reviews on the effect of aging on the differentiation of mesenchymal stem cells into the osteoblastic lineage [186] and the effect of aging on osteoblast number and activity [187, 188].

There are several key points to note when considering the effect of age on osteoblast function. A greater proportion of MSCs differentiates into adipocytes instead of osteoblasts in old compared with young animals and people and this consequently impairs

the regenerative potential of bone [186, 189-191]. The reduction in osteoblast cell numbers and differentiation seen with aging subsequently reduces the number of colony forming units in bone marrow samples cultured *in vitro* in old mice, compared with young mice [192]. The inverse relationship of age with osteoblast differentiation versus adipocytogenesis is proposed to be heavily dependent on the transcription factor peroxisome proliferator-activated receptor (PPAR) γ [193] which is expressed in higher concentrations in old mice compared with young mice [194]. The later stages of osteoblast differentiation are also inhibited with aging, with one early study demonstrating an age-related increase in the number of pre-osteoblasts and a decreased number of mature osteoblasts in rats [195]. In addition to the age-related changes in differentiation of MSCs, there is also an age-related alteration of both the TGF- β and BMP signalling pathways [194] which suggests that aging also affects both of these pathways, which are key bone formation signalling pathways.

As well as reduced numbers of osteoblasts in old mice and people, there is also some evidence that their lifespan is also decreased through more prevalent apoptosis associated with an increase in oxidative stress [196]. Another study demonstrated an increase in the number of apoptotic cells in MSC culture from old animals compared with young animals [197]. Conversely, in a study of human bone marrow samples, there was no effect of age on the expression of apoptosis markers, BCL-2 and DRAK1 in whole bone marrow aspirates suggesting that apoptosis in human marrow is not affected by aging. However, this study was performed on the mixed population of cells retrieved from a bone marrow aspirate, rather than a pure culture of MSCs [198]. There are also studies suggesting that the speed of proliferation of osteoblasts is decreased [197] and that the potential number of population doublings *in vitro* is decreased with age [199, 200], probably due to rapid decrease in telomere length (an indicator of cellular senescence) following *in vitro* expansion. As osteoblasts experience a decrease in differentiation, cell life-span and increased apoptosis, this ultimately leads to a decrease in the overall osteoblast number with aging, which, in turn, results in decreased bone formation.

There is also strong evidence that osteoblast activity in response to mechanical loading is reduced in old versus young cells in both *in vitro* and *in vivo* experimental models. Of importance, it appears that the ability of osteoblasts to proliferate in response to loading appears reduced when compared to young animals [29]. This and other relevant studies will be discussed in more detail in Section 1.8.2.

1.5 Aging and systemic regulators of bone remodelling

Although bone remodelling is locally regulated, there are numerous systemic regulators of bone cell activity involved in growth and demand for increased serum calcium, such as pregnancy and lactation. These include parathyroid hormone (PTH), calcitonin, sex steroids, growth hormone, insulin-like growth factor (IGF), fibroblast-like growth factor (FGF)23, osteocalcin and Vitamin D. Consideration of the effect of aging on these systemic pathways is, therefore, important. The key mechanisms for physiological control of bone mass to adapt to periods of physiological demands such as. These regulators have all been reviewed extensively elsewhere [37, 201-209] and apart from PTH, and sex steroids will not be discussed in detail in this thesis.

1.5.1 Regulation of Calcium Homeostasis

One of the most significant systemic metabolic demands placed on the skeleton in a normal physiological situation occurs during pregnancy and subsequent lactation. During pregnancy, and even more so during lactation, the demand for calcium is increased [210-212]. To facilitate the required increase in calcium demand for both foetal growth and milk production, Vitamin D synthesis is increased, which, in turn results in increased intestinal absorption of calcium. Once lactation begins, and the calcium loss through milk production increases, the increase in intestinal absorption of calcium facilitated by Vitamin D is insufficient to maintain physiological levels of serum calcium. Lactation also stimulates a hormone called prolactin, which further improves the efficiency of calcium uptake from the intestine and improves calcium and phosphate conservation in the kidney [213]. Although prolactin helps provides some improvement in serum calcium levels, the major source of calcium for the lactating animal comes from the maternal skeleton [211].

This demand for calcium is so great that a typical 6-month lactation period in humans results in a 5-8% decrease in BMD – equivalent to the yearly loss seen in post-menopausal women [212].

It appears that much of the lactation-associated bone loss occurs through osteocytic osteolysis, where the peri-lacunar bone mineral is resorbed to mobilise the calcium stores. Interestingly, as it is not possible for osteoclasts to access the osteocyte lacunae in majority of instances, it must be the osteocytes themselves that are enacting the resorption process [83, 214]. Osteocytes have been shown, during lactation, to express genes typically associated with osteoclastic resorption of bone, such as tartrate-resistant acid phosphatase (TRAP), Cathepsin K, carbonic anhydrase, and matrix metalloproteinase (MMP) 13 [84, 214, 215]. The key mediators of active bone loss during lactation are PTH-related protein (PTHrP) and suppression of oestrogen seen with suckling. PTHrP is typically produced in the mammary tissues in response to lactation and serum levels correlate inversely to the bone mass in mice and women [216, 217]. Mice with osteocytes in which the PTH receptor has been knocked out, do not demonstrate the lactation-related enlargement of the osteocyte lacunae or increase in osteocytic TRAP activity seen in control mice [214]. The bone loss seen in relation to the suckling-dependant decrease in oestrogen is probably mediated by similar mechanisms to that seen following menopause. These mechanisms will be discussed more in the later section (1.8.4) on age-related effects on sex-hormones in bone remodelling.

Furthermore, as the lacunar size returns to normal within 1 week of weaning, osteocytes must also possess the ability to form bone mineral as well as resorb it [214]. Although the increase in bone resorption results in a sudden increase in serum concentration of calcium and phosphate and acute bone loss, typically, following weaning, bone mass can return to normal levels relatively quickly. This is probably due to the acute surge in PTH following weaning resulting in a formation response by osteoblasts, although recent work suggests that PTH is not necessary to achieve the post-lactational replenishment of the bone mineral content [218].

1.5.2 Parathyroid Hormone

As it remains, for the time being, the only licenced anabolic treatment for management of low bone mass, PTH is probably the most studied and well-understood hormone involved in regulating bone mass. The parathyroid gland chief cells produce PTH in response to changing levels of circulating serum calcium. PTH's primary purpose is to maintain serum calcium within a very narrow physiological range. It achieves this by modulating renal calcium secretion and Vitamin D production and, most importantly, regulating the resorption of calcium from bone mineral. Although the primary physiological role of PTH on bone is to promote bone resorption through osteoclasts, the pattern of PTH administration can affect the balance of bone resorption and bone formation. Intermittent daily administration of PTH results in a primarily formative response, which is likely due to the differential effects on the key osteoclast activator, RANKL seen between continuous versus intermittent administration [219, 220].

PTH and PTHrP bind to the PTH/PTHrP receptor to exert their effects. The receptor is found on many cells, including osteoblasts, osteocytes and renal tubule cells [221]. Whilst several of the individual pathways affected by PTH/PTHrP have been investigated, one of the specific details of great clinical importance is what proportion of the hormone's anabolic effect on bone is mediated through the mechanisms of bone modelling, where prior resorption is not necessary, and what proportion is due to stimulation of a remodelling response associated with the activation of osteoclastic bone resorption [222]. The dual effect of PTH both allows its positive clinical effect, but ultimately limits its long term use, as prolonged treatment with PTH results in time-dependent increases in cortical bone porosity [223, 224]. Regardless of the balance of these two modes of action, PTH and its analogues have been repeatedly demonstrated to increase bone mass at trabecular sites and increase cortical thickness and porosity in cortical bone, resulting in a decreased risk of fracture [222]. The effects of PTH on aged bone are described in more detail in chapter 7 of this thesis, which describes a series of experiments evaluating the effect of combining PTH with the bisphosphonate, risedronate, to inhibit osteoclast function and reduce

resorption, to evaluate the contribution of remodelling and modelling to the anabolic response following intermittent PTH treatment.

1.5.3 The role of sex steroids on age-related bone loss

Oestrogens

The importance of sex steroids, particularly oestrogen, in the maintenance of appropriate bone mass and architecture is powerfully demonstrated by the prevalence of osteoporosis and increased risk of fragility fractures noted in postmenopausal women, compared with men and eumenorrhic women. Lifetime risk of any fracture was 53.2% at 50 years of age for women and 20.7% for men, and overall prevalence of vertebral fractures alone in Europe was 18-26% dependent on the country of origin [17, 225]. The effect of oestrogens and androgens on skeletal physiology and pathophysiology has been very recently reviewed [226] and the effects of sex hormones is not the focus of this thesis, so only a summary overview of the effects will be provided in this section.

Oestrogen is primarily produced in the ovary and acts primarily at the oestrogen receptors (ER) α and β . Osteoblasts, osteocytes and osteoclasts have all been demonstrated to express ER α and ER β [227]. ER's roles in bone have also been extensively reviewed elsewhere [228-230]. At puberty, the increase in circulating oestrogens result in increased long-bone growth and diaphyseal expansion in females. Following the completion of puberty, the surge in serum oestrogen concentration leads to apoptosis of the hypertrophic chondrocytes, resulting in cessation of longitudinal bone growth [231]. ER α has also been demonstrated to be involved in the response to mechanical loading [232], but involvement of ERs in the response to loading will be discussed in some more detail later in section 1.8.

Oestrogen's main role in the adult skeleton is to maintain bone mass. In the normal situation oestrogen suppresses bone turnover to help match it with formation to maintain a stable bone mass [107]. Oestrogen has multiple effects on bone cells. Its anti-resorptive mechanism of action is to suppress osteoclastogenesis and activity of osteoclasts. It also

increases apoptosis of osteoclasts. In contrast, its effects on osteoblasts are generally positive, with increased formation, differentiation, proliferation and activity [226].

As discussed earlier, cessation of menstrual activity, or menopause, results in a precipitous drop in serum oestrogens, which subsequently leads to accelerated bone loss with aging [233]. 20-30% of trabecular bone mass is lost in the 4-8 years following menopause onset, with smaller, but still significant losses of cortical bone of around 5-10% [234]. Ovariectomy in rats and mice results in similar deterioration in bone mass [235, 236]. Following the decline in serum oestrogen, bone resorption markers increase by more than formation markers, but both are increased following menopause, suggesting the primary determinant in these women may be increased bone turnover, with an imbalance toward more resorption, thus causing the bone mass loss [237]. Osteoclasts number is also increased in ovariectomised mice [238].

Although the most rapid bone loss is seen in the 5-10 years following menopause onset in women, there is a continued loss of bone mass that progresses at a similar rate in both women and men. This continued age-associated bone loss has been ascribed most recently to increased oxidative stress with increases in reactive oxygen species (ROS) and possibly changes in growth hormones [16]. The effects of oxidative stress will be discussed briefly in section 1.5.4 of this chapter.

Androgens

Androgens have been demonstrated to have similar effects to those of oestrogens in females; decreased osteoclast formation and activity and increased osteoblast formation and activity [226]. However, the major androgen hormone, testosterone, is aromatised to produce oestrogen, which makes separation of the distinct effects of these two hormones in men difficult [239]. In men with an aberrant aromatase enzyme, and consequently minimal circulating oestrogen, persistent linear growth due to delayed physal closure, and osteopaenia are seen [240, 241] illustrating the importance of the conversion of testosterone to oestrogen. Testosterone itself does also have effects on the skeleton. This is demonstrated by the positive effects that dihydrotestosterone (DHT), a non-

aromatisable analogue, has on bone – the impaired skeletal growth seen in growth hormone knockout mice during puberty was rescued following treatment with DHT, highlighting the importance of androgens on skeletal growth [242].

Unlike in women, there is no clear decrease in circulating sex hormones in men, which results in only steady decline in bone mass with aging, rather than the precipitous drop in trabecular bone mass seen in menopausal women. Acute loss of sex hormones in men, demonstrated by castration of male sex offenders, mimicked the loss of bone seen in post-menopausal women [243]. As most men do not experience the acute loss of sex hormone and subsequent severe bone loss, their risk of osteoporosis and fragility fracture is reduced compared with women [244]. Furthermore, as only 7% of osteoporotic men were testosterone deficient [245], it is likely that the age-related bone loss seen in men is primarily due to other mechanisms, such as increased oxidative stress, or other age-related impairment of bone cell function.

1.5.4 Role of oxidative stress in age-related bone loss

Although the age-related bone loss seen in humans and mice is certainly multifactorial, a growing body of evidence implicates the deleterious effects of oxidative stress in bone as a major contributing factor to the reduced osteoblast activity seen in the elderly [187]. The concentration of reactive oxygen species (ROS) is elevated in bone of old mice [196] and these changes can be recreated by administration of glucocorticoids. [246]. The increase in ROS may be partly to do with the fact that serum levels of endogenous glucocorticoids are elevated in old mice [171].

Age-related increase in ROS in bone has several negative effects on bone mass and bone turnover. Osteoclastogenesis is promoted by ROS [247, 248] and osteoblast number and rate of bone formation is reduced, subsequently reducing bone mass [249]. This impairment appears to be related to inhibition of Wnt signalling in osteoblasts [250]. There also appears to be an association with increased ROS and increased apoptosis of osteocytes and osteoblasts, further reducing bone formation activity [196, 251]. This

multifactorial nature of the effect of ROS on bone metabolism adds another underlying factor which can influence age-related bone loss.

Whilst this section has described some of the mechanisms which may contribute to the bone loss seen with advancing age, there are certainly other effects which may contribute, yet are not discussed in detail within this literature review, as they fall outside the scope of this thesis. These include the immune system [252, 253], growth hormone [254, 255], advanced glycation end products and their receptors [256], telomere shortening [257, 258], and increased endogenous glucocorticoids [171].

1.6 Animal models of skeletal aging

1.6.1 Non-rodent models of skeletal aging

An ideal experimental model to study age-related responses to mechanical and pharmaceutical stimuli should mimic the age-related changes described earlier whilst being cost-effective and reproducible. Whilst non-human primates are commonly used as experimental models due to their biological similarities to humans, their use in studies of age-related changes is limited. Although they display similarities to humans following aging and ovariectomy, including intracortical remodelling, an aspect of bone remodelling usually absent in old rodents [259-263], there are some limitations to their use in experimental studies. Female rhesus monkeys do not reach menopause until 24 years of age [264]. Furthermore, they do not appear to experience post-menopausal bone loss from the vertebrae; a hallmark of human post-menopausal osteoporosis [265, 266]. Hence, due to their long life-span, associated increased costs, availability, and importantly, the welfare and emotive issues surrounding their use in scientific research, non-human primates are not a feasible model for routine studies of skeletal aging.

Aged sheep have been used to study skeletal response to glucocorticoid treatment [267], hip replacement implants [268] and implants coated with the bone signalling factor, BMP-2 [269]. Young sheep have also been used to study the osteogenic response to loading [270], although this will be discussed in more detail later in this literature review.

However, similar to primates, sheep's high cost as experimental animals, genetic diversity, lack of a true menopause and housing limitations limit their usefulness for study of age-related osteoporosis. Similar limitations exist for use of pigs, cattle and dogs, although they have been used in occasional studies of the effect of age on bone [271-273].

1.6.2 Rodent models of aging

Compared to the large mammals discussed in the previous section, rodents are cheaper, easier to house and show very small amounts of phenotypic variation between animals due to their highly-inbred nature [274]. Genetic manipulation of mice is also now routine and allows generation of strains of mice with genetically accelerated aging and early senescence. This helps reduce the time required to generate an "aged" animal. Takeda *et al* [275] developed the senescence accelerated mouse (SAM) model which remains the most comprehensively studied model of early senescence. A further refinement of this model, the SAMP6 mouse, was established as a model of age-related osteoporosis, which demonstrates low bone mass and spontaneous fractures at skeletal maturity [276]. An antagonistic refinement of the SAM mouse is the SAMR model which is resistant to aging. This mouse has been used as a control mouse in aging studies [277, 278]. Although these mice show similarities related to normal aging, use of these models has been criticised because the molecular mechanisms involved in the accelerated senescence is unknown, and the mechanisms associated with normal aging are certainly multifactorial and cannot be accurately mimicked by single genetic mutations. Furthermore, and very importantly, SAMP6 mice did not demonstrate a reduced responsiveness to mechanical loading compared with SAMR controls [278], despite several studies demonstrating a reduced responsiveness to mechanical loading in naturally aged animals. This is of particular relevance to studies examining the response to mechanical loading in aging animals, discussed further in Section 1.8 of this chapter, and such as those planned for the experiments described within this thesis.

Although the reduced time-scale required to generate early senescence mice models is convenient, wild-type mice still have relatively short lifespans, which makes them still a reasonable, and feasible choice for use as an experimental model for investigating the

effect of aging on the skeleton and for investigating the response to mechanical loading. Rats and mice both demonstrate age-related changes in bone mass and architecture. Bone loss is detectable after approximately 12 months of age in Wistar rats, in both their cortical and trabecular compartments [279]. Although rats are commonly used in studies exploring age-related changes in bone, the majority of the studies exploring the effect of aging on bone biology are now performed in mice, in particular the C57BL/6 strain of mouse. C57BL/6 mice do not undergo a true menopause. Uterine weight, a sensitive indicator of sex-steroid status, remains normal until at least 31 months of age [196]. Therefore, loss of bone mass seen in old mice is predominantly due to age-related factors, and not sex-steroid deficiency. This makes them an ideal model for studying the effects of aging on the skeleton and the diseases associated with aging [280].

The effect of aging on the skeleton has been characterised more comprehensively in the C57BL/6 strain than in any other [260]. Periosteal expansion and endosteal resorption occur in mice older than 12 months [281, 282], although both of these studies explored cortical changes within the femur. Until recently, no studies had characterised the pattern of bone mass changes seen with aging in the tibia of mice. Our laboratory has recently demonstrated that the tibia experiences marked trabecular and moderate cortical bone loss associated with aging [4] and that the cortical response is site specific, with the proximal tibia failing to demonstrate the cortical expansion (increase in periosteally enclosed area) evident in the distal tibia of the same mice (despite an increase in medullary area), and in the femur of mice [281, 282].

In addition to their well characterised skeletal response to aging, C57BL/6 strains form the background for the majority of genetically modified mice used for research [283]. Also, the C57BL/6 strain demonstrates a more robust response to mechanical loading than other strains of mouse or rats [284]. It is for these reasons that we chose to use the C57BL/6 aged mouse for the experiments described in this thesis. Our laboratory also has extensive experience of applying axial compressive loads to the tibia of C57BL/6 mice [1, 2, 8, 11, 29, 32, 34, 285-287]. Finally, and a significant factor, the C57BL/6 mouse strain was, at the time of experimenting, the only strain of mouse that had readily available

populations of aged mice in the UK (Charles River Ltd, UK). Therefore, all experiments described in this thesis utilised young adult (17-19-week-old) and old (19-22-month-old) female C57BL/6 mice.

1.7 Current treatment options for age-related osteoporosis

Despite the increased understanding of the regulation of bone mass in health and in the contribution of different regulators to disease processes such as age-related osteoporosis, a comprehensive understanding of the complex interactions between certain key pathways remains elusive. A multitude of mechanisms have been implicated in control of aspects of bone mass and architecture, but it is becoming increasingly clear that there is no single pathway which is responsible for maintenance of bone mass, nor is there a single pathway associated with the deterioration in bone mass seen with aging in people or animals. For this reason, it is unlikely there will be a single “magic bullet” treatment which will treat all clinical signs of age-related osteoporosis. Regardless, several treatments have been developed to slow/stop the bone loss, and even improve bone mass, all with the aim to reduce fracture risk in osteoporotic patients. In this section, current and potential future therapeutic targets for management of age-related osteoporosis are discussed. Broadly, management options for osteoporosis include those which can maintain bone mass by reducing the degree of bone resorption, and those which can increase bone mass, by increasing bone formation.

1.7.1 Calcium and Vitamin D supplementation

The role of calcium and vitamin D in the regulation of bone mass was briefly discussed earlier in this chapter in section 1.5.1. Reduced levels of circulating calcium in the serum stimulate bone resorption due to endogenous PTH secretion. Reduced serum calcium can be due to reduced dietary intake. It can also be due to poor bioavailability of oral calcium due to decreased vitamin D levels reducing intestinal absorption and slowing renal conservation of calcium. As vitamin D is produced following UV light (sun) exposure of the skin, women with low sun exposure are more prone to low circulating Vit D levels and lower bone mass than women in climates with greater sun exposure. Northern European

countries have a slightly higher incidence of osteoporosis than in southern European countries, proposed to be due to the short day length in winter in high latitudes [225]. Furthermore, vitamin D production through sun exposure tends to reduce with age, due to reduced activity levels and changes in the dermis seen with aging [288, 289]. Low vitamin D reduces calcium availability, with over 30% of post-menopausal females showing insufficient vitamin D serum levels to maintain PTH levels sufficiently low enough to reduce bone resorption. For this reason, vitamin D supplementation has been widely used to reduce risk of fracture in post-menopausal osteoporotic women and is often recommended as the first line of treatment in patients with osteoporosis. Combination of oral calcium supplementation with Vitamin D helps further increase calcium intestinal absorption and bioavailability thus reducing the catabolic draw on bone mineral and the consequent bone loss seen with aging. One study demonstrated a 25% reduction in hip fracture risk when calcium supplementation was added to vitamin D treatment [290]. A more recent meta-analysis demonstrated a 15% reduction in all fractures and a 30% reduction in hip fractures when combined vitamin D and Calcium supplementation is compared with no treatment [291]. However, use of dietary calcium supplements has been associated with some adverse cardiovascular events in some studies, so the continued use of calcium supplements for management of osteoporosis requires further evaluation of the safety profile [292].

1.7.2 Antiresorptive treatments

Hormone replacement therapy and selective oestrogen receptor modulators

As discussed earlier, the acute drop in circulating oestrogen following the onset of menopause contributes to the prevalence of osteoporosis and fractures seen in post-menopausal women [293]. The use of oestrogen to manage post-menopausal osteoporosis was successful at avoiding bone loss in multiple studies [294-296]. Despite these promising results with respect to rescue of bone mass loss in elderly women, a publication by Rossouw *et al* [297] demonstrated unacceptably high rates of secondary side-effects with use of hormone therapy, including breast cancer, cardiovascular disease

and dementia. Subsequently, the treatment was withdrawn from general use, and the search for alternate targets to manage bone loss was continued.

In place of supplemental oestrogen, modifying the effect of the endogenous oestrogen by modifying the function of the oestrogen receptors provides one such alternative target that avoids the side effects associated with supraphysiological levels of oestrogen. These selective oestrogen receptor modulators (SERMs) modify the activity of the ERs by inducing a conformational change to the receptor. Raloxifene is the only SERM licenced for use in the treatment of osteoporosis, as it has been demonstrated to reduce vertebral fracture incidence by 30-50%, although hip fracture incidence was unaffected [298]. Raloxifene does not increase the risk of breast cancer like oestrogen does, in fact there is a slight reduction in risk following raloxifene treatment. Another SERM, tamoxifen is licenced for treatment of breast cancer, which demonstrated an increase in ER signalling. Furthermore, although not licenced for treatment of osteoporosis [299], tamoxifen also has beneficial effects on bone mass [287].

Third generation SERMs (arsoxifene and lasoxifene) have also been investigated and been trialled in clinical trials where they resulted in similar fracture risk reduction results to currently available SERMs with a similar, but possibly slightly worse safety profile [300, 301]. The manufacturers did not pursue further development of either of these drugs.

Bisphosphonates

Bisphosphonates (BPs) are a frontline treatment for the pharmaceutical management of low bone mass seen in osteoporosis, as well as several other diseases which are characterised by increased levels of bone resorption, such as metastatic neoplastic disease and Paget's disease of bone [302-304]. BPs are all analogues of inorganic pyrophosphate; all variants have two phosphonate groups that share a common carbon atom. Modification of one or both phosphonate groups can greatly affect the affinity of binding to bone mineral. Factors affecting the binding affinity include the molecular arrangement of phosphonate side-chains – the N-H-O bond angle has been demonstrated to affect the affinity of binding to hydroxyapatite, the primary bone mineral matrix ingredient [302,

305]. Zoledronate has also been shown to form a dual bond to both hydroxyapatite crystals and a second type of calcium molecule [302]. The affinity with which a BP binds to mineral will help govern its biological availability during resorption and also its duration of action [306, 307]. For example, zoledronate only requires yearly injections to maintain its biological activity, whilst other BPs require much more frequent injections or oral medications.

As BPs are preferentially adsorbed to bone minerals, they are consequently brought into direct contact with bone cells, particularly osteoclasts. They are generally dissociated from the bone mineral by the acidic environment in the resorption lacunae and then internalised through a process of endocytosis via vesicular movement into the cytosol [308]. They are then transported within the cell to the organelles, where they exert their ultimate cellular actions.

The most widely used subclass of BPs in a clinical setting are the nitrogen-containing BPs (N-BPs). These include pamidronate, alendronate, ibandronate, risedronate and zoledronate. Their primary action is through interference with the mevalonate pathway by inhibiting the enzyme farnesyl pyrophosphate synthase (FPPS) [309, 310]. The mevalonate pathway is involved in prenylation of small GTPases essential for the function and survival of osteoclasts. Use of N-BPs results in a build-up of unprenylated GTPases, which thus results in reduced activation of downstream cellular processes related to osteoclast activity and survival. The initial cellular effect of N-BPs is to impair osteoclast function and reduce resorption, and in some cases result in osteoclast apoptosis, although apoptosis does not appear to be a mandatory requirement for inhibition by N-BPs [302].

There is also building evidence that some of these N-BPs also have anti-apoptotic effects on osteoblasts and osteocytes, which are likely independent of their action on osteoclasts [311-314]. Even in the absence of any measurable anti-resorptive effect, the anti-apoptotic effect of BPs can subsequently prevent the loss of bone strength [315]. The variable efficacy of different BPs is related not only to their binding affinity to the mineral matrix, but also to their variable effects on certain cellular mechanisms.

BPs have been, and still are, a very commonly prescribed treatment for diseases associated with low bone mass, and have been demonstrated to reduce the incidence of fragility fractures commonly seen in patients with osteoporosis [55, 316, 317]. However, use of BPs reduced by around 50% between 2008 and 2012 [318, 319], due in large part to publicity surrounding adverse events such as osteonecrosis of the jaw [320-322] and atypical femoral fractures [323-325].

Chapters 6 and 7 in this thesis describe a series of experiments which utilise the ability of the BP risedronate to impair osteoclast activity and bone resorption to help determine its effect on the loading response following unilateral sciatic neurectomy to engender limb disuse, a resorptive stimulus (Chapter 6) or following PTH treatment (another potent stimulus of resorption/remodelling). The literature surrounding bisphosphonates, particularly risedronate, is reviewed further in the introductions of these chapters, and also in several comprehensive review articles [302, 326, 327].

RANKL antibodies (Denosumab)

Since identifying the biological effects of RANKL in the mammalian skeleton, utilising RANKL as a therapeutic target to protect against bone loss has been of interest to researchers and clinicians alike. Whilst administration of exogenous OPG has been investigated [328], for its antagonistic properties against RANKL, its clinical use was not pursued due to concerns over its potential immunogenicity and subsequent risk of impairing other systemic functions of this important osteoregulatory protein.

Antibodies targeting RANKL have been preferentially pursued due to their reduced likelihood of immunogenicity. Initial animal studies in wild-type mice using Denosumab, an anti-human RANKL antibody did not demonstrate any effect on bone mass, however, transgenic mice with knock-in of a human/murine chimeric RANKL gene, denosumab demonstrated decreased bone resorption and increased cortical and trabecular bone mass and architecture [329]. The same group administered Denosumab to ovariectomised cynomolgus monkeys which resulted in prevention of cancellous bone loss and prevented deterioration of bone strength indices [330]. In addition to laboratory animal studies,

clinical trials were pursued to investigate the clinical safety and utility of denosumab. Bekker *et al* [331] demonstrated rapid decreases (within 12 hrs after administration) in urinary cross-linked n-telopeptide of collagen (NTX), a biomarker of active bone resorption, suggesting denosumab can have a rapid and significant effect on bone resorption in humans. Further phase II studies exploring the effect on post-menopausal women with low bone mass have shown significant increases in bone mass [332, 333], and one study demonstrated reversibility of the bone turnover changes following discontinuation, and subsequent restoration following re-treatment [334]. Furthermore, patients that had received 2 years of denosumab still maintained a higher BMD than placebo patient 2 years after discontinuing treatment [335]. Fracture risk is also reduced following denosumab treatment in the vertebrae (68%), hip (40%) and non-vertebral sites (20%) [336]. When considering histomorphometry indices based on iliac bone biopsies, bone turnover markers were lower in denosumab-treated patients than in alendronate patients [337], and discontinuing treatment resulted in a complete return to baseline levels of bone turnover seen in placebo patients [338], confirming the effects of denosumab on bone remodelling are reversible.

Long term treatment with denosumab has demonstrated a fairly low risk of adverse events, comparable with existing treatments [336] and that continued treatment demonstrated a progressive and substantial increase in BMD over the 8 years of the study in post-menopausal women with low bone mass [339].

Although phase II and III clinical trials have demonstrated a good safety profile, the concern remains that inhibiting the function of RANKL systemically could result in impaired immune function due to RANKL's almost ubiquitous presence in many tissues. Meta-analysis of trials using denosumab for osteoporosis treatment have identified a borderline increased risk of serious infection [340]. Furthermore, given the recent identification of bisphosphonate-associated adverse events such as osteonecrosis of the jaw (ONJ) and atypical femoral fractures (see section on BPs above), surveillance of treated patients for these particular complications should be continued. A very recent

report describes 7 cases of ONJ and two of atypical femoral fractures within the cohort of 4550 women eligible for the extension trial of the FREEDOM study [341].

Denosumab is licenced for use in the USA and Europe for osteoporosis [342] and to protect against metastatic and primary bone neoplasia-associated bone loss [343]. The increasing clinical usage and the recent demonstration that RANKL produced by osteocytes is essential for the bone loss associated with disuse led us to investigate the relationship of osteocytic RANKL expression following both disuse and increased loading (Chapter 4).

Cathepsin K antibodies

Cathepsin K is an enzyme that the osteoclast uses to digest bone mineral matrix proteins, such as collagen. Odanacatib inhibits cathepsin K. Therefore, odanacatib treatment actually spares osteoclasts, but still inhibits resorption [344].

Treatment of adult rhesus monkeys with odanacatib resulted in improved bone strength and BMD at the lumbar spine and the hip [345, 346]. Histomorphometry demonstrated that trabecular bone remodeling was reduced in the lumbar spine and hip, yet periosteal modeling-based formation was increased [345, 346]. The effect of odanacatib on cortical bone was also investigated at the central femur. Improved formation and reduced resorption following odanacatib treatment led to increased cortical thickness and volume [347]. Human trials have demonstrated a robust improvement in cortical bone parameters and similar reduction in fracture risk compared to denosumab (Relative risk reduction for vertebral, hip and non-vertebral fractures of 72%, 47% and 23% respectively – $p < 0.001$) [348]. Unfortunately, further analysis of the data from this trial, including an extension arm identified an unacceptably high risk of adverse cardiovascular events, including stroke and atrial fibrillation (RR 1.37; 95% CI 1.10–1.71; $p = 0.005$) [349], which subsequently led to the discontinuation of development of odanacatib by Merck in September 2016.

1.7.3 Anabolic therapies

Beyond maintenance of bone mass through impairing bone resorption, anabolic therapies provide promise for replacing lost bone. Currently the only licenced anabolic treatments

for management of osteoporosis are analogues of PTH. These treatments have been shown with high degrees of confidence to reduce fracture risk compared with no treatment [52, 350], however, a recent economic review from the Institute for Clinical and Economic Review has voiced concerns over the cost-effectiveness of using these novel treatments in management of low bone mass, given there is currently no clear evidence that they perform better than existing anti-resorptive treatments such as zoledronic acid [351].

Teriparatide and Abaloparatide

The anabolic drugs, Teriparatide (PTH 1-34) and Abaloparatide (PTHrP 1-34) are now both licenced for treatment of post-menopausal osteoporosis by the Food and Drug Administration (FDA) in the USA.

Although the physiological effect of PTH excretion in the body normally is to promote mobilisation of calcium from the skeleton through bone resorption, intermittent administration of PTH (or its analogues) demonstrates a potent anabolic effect on bone formation with elevation in bone formation markers exceeding bone resorption markers for at least 2 years [352]. Improvement in histomorphometric parameters following teriparatide treatment mirrors the changes in bone turnover markers, with increases in %MS/BS in all bone compartments for all time-points measured up to 2 years [353].

Abaloparatide has only recently been approved by the FDA (April 2017) so longer-term information on its effects is more limited than for teriparatide. The most recent phase III clinical trials demonstrated robust improvements in risk of both vertebral and non-vertebral fractures compared to placebo and equivalent risk reduction to teriparatide treatment [52].

Treatment duration is limited to only 2 years for teriparatide due to concerns over increased incidence of osteosarcoma development following lifelong treatment in rats. [354, 355]. The incidence of osteosarcoma was also increased in rodents treated with abaloparatide in a dose and duration dependent fashion, and this incidence was no different to the positive control group treated with teriparatide [356]. Despite these

concerns, the incidence of primary bone tumours in humans treated with teriparatide is very low [357], and apparently no greater than the incidence in the untreated population [358].

Currently, anabolic therapies are mostly used as a second-tier treatment, reserved for cases with higher risk of fragility fracture, a decision based partly on their greater expense, and necessity for daily subcutaneous injections. When considering combination therapies, the sequence with which multiple drugs are administered does appear to affect the magnitude of the response to treatment. This is discussed in more detail in the later section in this chapter on combination therapies, and in Chapter 7.

Calcium Sensing Receptor Antagonists

It was hypothesised that antagonising calcium sensing receptors would stimulate a consequent surge in PTH production, resulting in anabolic effects – clinical trials of two separate drugs (roncalceret, MK-5442) demonstrated inferior results when exploring BMD compared to alendronate, and also teriparatide, with roncalceret *also* resulting in a reduction in hip BMD [359, 360]. Further development of these two medications was not pursued by their manufacturers.

Strontium ranelate

Strontium ranelate treatment showed decreased risk of both vertebral and non-vertebral fracture in women and men [361-364]. Strontium ranelate never achieved FDA approval for the USA, but it was licensed for use in Europe for management of osteoporosis but had its licence conditions restricted once evidence of increased risks of myocardial infarction became evident. Subsequent to these restrictions, its manufacturer in Europe has discontinued supply due to reduced/limited market demand and concerns over cardiovascular adverse events [365].

Sclerostin antibodies

Sclerostin inhibits the Wnt pathway, subsequently impairing osteocyte proliferation and bone formation. Romosozumab is a monoclonal sclerostin antibody (Scl-Ab). Blocking

sclerostin's activity results in improved bone formation, so Romosozumab is an anabolic medication which is reaching the final stages of regulatory approval with the FDA. The anabolism is effected by enhanced osteoblast and chondroblast differentiation and maturation, and inhibition of apoptosis of osteoblasts and osteocytes [366].

The major phase 3 trial of romosozumab in 7180 postmenopausal women with osteoporosis administered romosozumab 210 mg monthly or a placebo and showed new vertebral fractures reduced by 73% compared to placebo after 1 year (incidence 0.5% vs. 1.8%, $p < 0.001$) [367]. There was also a 36% decrease in clinical fractures ($p = 0.008$). In the second year of this trial all participants were switched to denosumab. After 2 years, romosozumab/denosumab treated patients had 75% lower fracture rate than placebo/denosumab treated patients (0.6% vs. 2.5%, $p < 0.001$). In this trial, the incidence of adverse events adverse events between groups was roughly equivalent.

A second active comparator trial comparing the efficacy of romosozumab to alendronate has recently been reported [368]. This study enrolled 4093 postmenopausal women and randomised their treatment into 12-months treatment with either romosozumab followed by a further 12-months treatment with alendronate, or 12 months of alendronate, followed by continued alendronate for a further 12 months. The study demonstrated improved fracture risk in both new vertebral fracture (48% risk reduction) and clinical fracture, defined as clinical vertebral fracture or non-vertebral fracture (27% risk reduction) in the romosozumab:alendronate group compared to alendronate;alendronate group. However, this study did report an increased incidence of adjudicated serious cardiovascular adverse events compared to the alendronate-treated group. Sixteen patients (0.8%) in the romosozumab group and 6 (0.3%) in the alendronate group reported cardiac ischemic events (odds ratio, 2.65; 95% CI, 1.03 to 6.77). Sixteen patients (0.8%) in the romosozumab group and 7 (0.3%) in the alendronate group reported cerebrovascular events (odds ratio, 2.27; 95% CI, 0.93 to 5.22). This finding could be explained by the finding that use of bisphosphonates has been shown to reduce the incidence of myocardial infarction [369].

Initially it was hoped that the FDA would approve Romosozumab for use in treatment of post-menopausal osteoporosis and reduction of fracture risk in July 2017, providing an additional anabolic treatment for management of osteoporosis. However, due to the report by Saag *et al* [368] reporting increased incidence of cardiovascular serious adverse events, the approval was deferred until the drug's developers, Amgen/UCB, can provide further evidence of the safety of Romosozumab with regards to its risk of precipitating cardiovascular adverse events. The larger, placebo-controlled phase III study by [367] did not demonstrate any increase in risk of serious cardiovascular adverse events. The resubmission analysis is likely to pool all data between all phase III studies, to evaluate the safety profile of the drug [370].

Another anti-sclerostin antibody, blosozumab is also being developed by Eli Lilly and phase II trials have demonstrated similar changes in BMD to those seen with romosozumab [167]. Although BMD declined slowly following discontinuation of blosozumab, BMD for the hip and spine remained greater than placebo treated women and no adverse events were reported in these studies related to the blosozumab [168]. No phase III trials have been reported yet for blosozumab.

An interesting observation in both studies is that treatment with sclerostin antibodies was not associated with any increase in the BMD of the distal radius. Sugiyama *et al* [371] hypothesise that the lack of response in this area when other regions do respond occurs because the radius is typically a low strain area, and thus sclerostin antibody sensitises the bone to responding better to mechanical strains to which it is normally incapable of in an elderly patient. This is supported by recently published preclinical data which demonstrates that the loading response is augmented following treatment with sclerostin antibody [372] or following genetic deletion of the sclerostin gene in mice [33]. This suggests that Scl-Ab could help improve the deficient mechanostat in the elderly and provide, in conjunction with relevant mechanical loading exercises; a "Smart" therapy that provides bone at areas of greatest need.

Additionally, with regards to preclinical safety data, in contrast to PTH/PTHrP treatments, romosozumab was not associated with any treatment effect associated with tumour

development in a rodent life-long treatment study [373], which suggests that romosozumab is unlikely to pose an increased carcinogenic risk to humans.

1.7.4 Combined anti-resorptive and anabolic therapies

Management of osteoporosis is most commonly facilitated by treatment with anti-resorptive medications, such as bisphosphonates, and more recently denosumab, an anti-RANKL antibody. Yet, in many cases of more severe osteoporosis, particularly those at imminent risk of fracture, it is prudent to consider combining therapies to maximise improvements in bone mass and strength and subsequently reduce risk of fracture. As described in more detail in section 1.3, bone formation can occur without prior bone resorption (modelling), or via bone remodelling, which must be preceded by resorption at the same site. Therefore, impairment of bone resorption with medication may limit the amount of bone formation possible following treatment with a typically anabolic drug by limiting the contribution of bone remodelling to the formative response.

The clinical interest in combined therapies has been increasing in recent years due to the availability of anabolic treatments beyond PTH/teriparatide. Several authors have comprehensively reviewed the literature relating to the combined or sequential use of antiresorptives and PTH [374-376]. Generally, the most consistent effect noted between studies for combined PTH and antiresorptives is an increase in the BMD outcome in the hip compared to monotherapy with PTH. In contrast, the effect of combination therapy on spine BMD, compared to monotherapy in majority of studies is not significantly different. However, when teriparatide was combined with denosumab, spine and hip BMD was increased [377] compared with either monotherapy. In peripheral sites, using HR-qCT, combined treatment was superior to teriparatide monotherapy but only marginally better than denosumab alone [378].

The effects following sequential use of the drugs appears to be dependent on the order the drugs are delivered. Initial concerns over the efficacy of combining anti-resorptives and anabolic drugs were raised by early studies of sequential treatment. Some studies identified inhibitory effects of alendronate on the anabolic actions of PTH/teriparatide in

postmenopausal women, thus limiting the benefit of therapy to bone mass [379, 380], but generally these studies were not sufficiently powered to detect differences in fracture risk between combined and monotherapy. Using histomorphometry, trabecular bone from iliac crest biopsies in women pre-treated with alendronate showed less tetracycline labelled surface at baseline than treatment naïve patients [381]. In this same study, most indices of bone formation following teriparatide treatment were lower in alendronate treated women than in untreated women.

However, there is relatively robust evidence of a benefit of sequential combined therapy over monotherapy to bone mass if the teriparatide treatment is used initially, then followed by an anti-resorptive drug [382]. It is proposed that this discrepancy is because use of initial anti-resorptive drugs may impair the anabolic effect of subsequent teriparatide by limiting remodelling. Starting with anabolic drugs allows their anabolic effects to proceed unhindered, and then, once their effects are realised, an anti-resorptive drug can be used to maintain bone mass and strength by limiting the subsequent resorption. The combination of bisphosphonates and PTH analogues is discussed further in Chapter 7.

Combining other antiresorptives with teriparatide may result in different outcomes. For example, following denosumab treatment with teriparatide treatment resulted in a transient reduction of the hip BMD [350]. This finding has lead authors to recommend continuing denosumab to overlap treatment for at least 6 months after the implementation of teriparatide treatment [382, 383]. Some antiresorptives, such as the cathepsin K inhibitor odanacatib, reduce osteoclast activity, but not number [344, 384]. Presence of osteoclasts, and not necessarily activity of osteoclasts may be sufficient to allow better bone formation by teriparatide than with bisphosphonates. There are no clinical trials, to the author's knowledge, that compare the efficacy of combined teriparatide, or other anabolic with inhibition of cathepsin K. A preclinical trial in rats demonstrated an additive effect on BFR and BMD when PTH was combined with ONO-KK1-300-01, a cathepsin K inhibitor, which was not present when alendronate was combined with PTH, confirming that the anabolic effect of PTH is maintained with

inhibition of Cathepsin K, but is slightly impaired following treatment with alendronate [385]. Unfortunately, as the development of odanacatib has been discontinued, it is unlikely that further clinical trials will be pursued.

Treatment with the PTHrP analogue, abaloparatide followed by 6 months of alendronate resulted in significant risk reductions for vertebral and non-vertebral fractures in post-menopausal women, and also significant increases in BMD at all sites measured, when compared with alendronate treatment alone [386]. Similarly, the active comparator trial for romosozumab also reported significantly improved BMD and fracture risk outcomes in the hip and spine [368].

1.7.5 Combining physical therapies with pharmaceutical treatments.

Combining traditional pharmaceutical treatments with non-pharmaceutical treatments is also an area of clinical interest to our research group. Mechanical loading provides a stimulus that results in an adaptive response that is both structurally appropriate and effective at resisting the strains to which it is normally exposed. By discovering treatments which work in addition to, and ideally synergistically with mechanical loading, systemic treatments are then able to promote and improve the structurally appropriate adaptive response achieved by mechanical loading. As a failure in the mechanisms associated with the normal adaptive response to mechanical loading is hypothesised to underlie the onset of age-associated osteoporosis [23], discovering mechanisms and strategies to augment this deficient response to mechanical loading could provide clinicians another avenue to improve bone mass and hopefully reduce fracture risk in clinically important areas by directing appropriate mechanical loading activities to improve these “at-risk” sites. The effect on bone of altering the mechanical loading environment and the effect that aging has on these normal responses is discussed in detail in the next section of this literature review and in each individual chapter introductions. In this thesis, in an effort to identify strategies which may improve the age-impaired loading response, we investigate the effect, in old female mice, of altering the habitual loading environment prior to exogenous loading (Chapter 5), the effect of blocking resorption with the bisphosphonate risedronate, on the loading response in ambulatory and sciatic neurectomised mice

(Chapter 6), and the effect of blocking resorption with risedronate on the anabolic responses to parathyroid hormone and/or loading (Chapter 7). Current literature discussing the specific effects of certain pharmaceuticals on the response to mechanical loading in the aged skeleton is discussed in more detail later in this chapter, in section 1.8.4.

1.8 Regulation of bone mass and architecture by mechanical loading

Whilst pharmaceutical therapies can both limit bone resorption and increase formation, these therapies mostly act in a systemic manner with effects in all bones rather than as a targeted treatment affecting bone sites that most need it. In contrast, mechanical loading acts locally by increasing bone mass and strength in sites that need it and reducing it in sites that do not. This adaptive change in bone mass and architecture provided by appropriate mechanical loading provides a “Smart” stimulus which provides bone where it is most needed. Augmentation of this structurally appropriate modification of bone mass provides an ideal strategy to improve bone mass in situations of low bone mass, and thus potentially reduce the risk of fracture in at-risk sites which typically suffer from reduced bone mass, yet high stress. The response to mechanical loading is particularly impaired in older people, so treatment strategies which may augment the structurally appropriate formation of bone imbued by mechanical loading provides an intriguing and potentially very important avenue for improving the bone mass in at-risk bone sites in osteoporotic patients, such as the hip, and distal antebrachium.

Altering the habitual loading context within which loading is administered through disuse can improve the response to mechanical loading in young mice [35], as can treatment with a range of therapeutic agents including parathyroid hormone [32, 387, 388], Cyclosporin [389], tamoxifen [287] or sclerostin antibody [372]. These experiments demonstrate that pharmaceutical and physical manipulation of the context within which loading is performed can affect the magnitude of the response to loading. The later chapters of this thesis (chapters 5-7) explore the effects of manipulating the context within which loading is applied in old mice with an impaired osteogenic response to loading.

1.8.1 The mechanostat

Mechanical strain is widely accepted as the principal factor controlling bone mass and architecture. Whether the loading stimulus induces adaptive changes in bone effectively can be affected by many systemic and local factors [5]. The mechanostat theory was originally postulated by Harold Frost [12, 13, 390]. The theory states that control of resorption and formation is tightly regulated based on the local strain environment to keep the density and architecture of bone at a level where the forces experienced are met by a subsequent reduction or increase in the strength of the bone to maintain a certain “optimal” strain [13]. This homeostatic mechanism is supposed to reduce the chances of mechanical failure of the bone by ensuring sufficient strength, whilst at the same time minimising excessive weight and metabolic wastage inherent with excessive bone mass. The mechanostat is summarised in Figure 9.

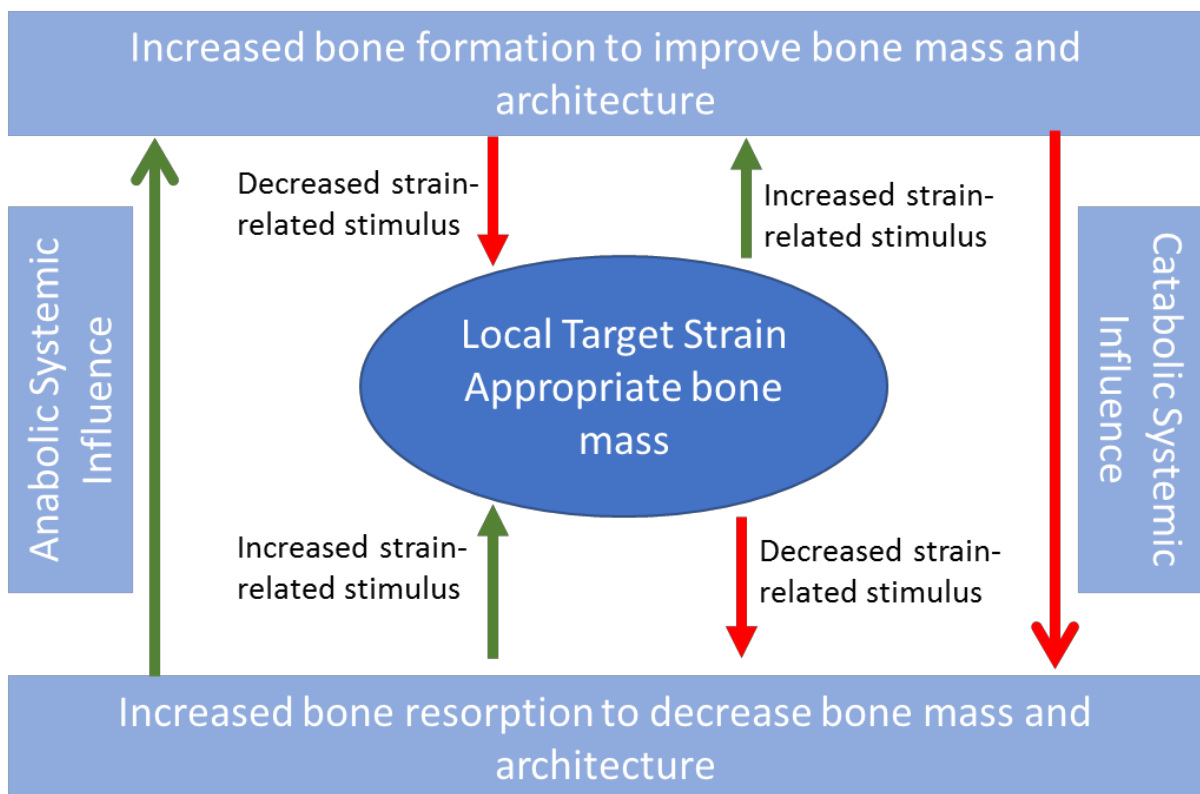


Figure 9 – Schematic diagram illustrating the mechanostat theory of the control of bone mass

Figure adapted from Lanyon *et al* [5].

Demonstrations of altered environmental loading modifying the human skeleton have been widely investigated and reported. The overall anabolic effect of loading is well recognised. The earliest studies to demonstrate the effect of loading and the site-specific nature of the adaptive response to increased loading showed increased cortical thickness and/or BMD in the bones of tennis players' racquet arms compared to their contralateral arm [391, 392]. Further demonstration of the anabolic effect of increased mechanical loading and the varied effects of the character of the loading activity was reported by Heinonen *et al* [393] where weight lifters and squash players demonstrated greater tibial BMD than sedentary controls, but cyclists did not demonstrate a difference in BMD compared to the sedentary controls. In professional footballers undergoing intensive training, bone mineral content is greater than age- and weight-matched controls [394].

Although strain is the primary effector of the cellular response to mechanical loading in bone, changes in mechanical loading are typically also associated with activity-related changes in the degree of muscle mass and local blood flow, together with potential changes in cardiorespiratory health. These factors may also influence bone mass independently [207, 395], although we have recently demonstrated that concurrent exercise did not affect the magnitude of the response to exogenous axial tibial loading in mice [396].

Decreased loading results in a rapid reduction in skeletal mass through an increase in bone resorption and a decrease in bone formation. This uncoupling of formation from resorption is a hallmark of all forms of disuse [397]. An excellent example of the bone loss promoted by reduced mechanical loading is in healthy adult astronauts; unloading of the entire skeleton results in a reduction in bone formation and an increase in bone resorption and bone loss in the order of 1-1.6% per month is observed [398, 399]. Earlier studies demonstrated most bone parameters are able to return to normal in astronauts following resumption of earthly weight-bearing, although vBMD measures were not able to recover fully [400]. A more recent study reported that majority of parameters measured using qCT were not fully recovered within 12 months after return to earth [401]. Reduction of mechanical loading in humans, and a reduction in bone mass is observed in several other

situations, such as patients requiring prolonged bed rest, limb immobilisation to allow fracture repair, or those with spinal/nerve injury [402-405].

The degree of bone loss seen following onset of disuse appears to be site-specific rather than generalised to the whole skeleton. The areas with greatest loss seem to be focused around those areas where the loading was previously applied – a further demonstration of the efficacy of the mechanostat. For example, the bone loss is greatest around the knees in patients following spinal cord injury, whilst vertebral bone mass actually increased compared to age-matched ambulatory controls [406] suggesting that the bones primarily affected are those which developed under the influence of mechanical stimuli that are subsequently unloaded due to spinal cord injury. Further evidence supporting the site-specificity of the response to unloading includes a demonstration in astronauts that weight-bearing bones demonstrated a greater loss in bone mass than non-weight-bearing bones following microgravity [407]

1.8.2 The cellular response to mechanical loading

1.8.2.1 *Osteocytes*

Increasing evidence is mounting to show that the osteocyte is the cell type primarily responsible as the mechanosensor for bone. The unique biology of the orientation and distribution of the dendritic projections through the very narrow canalicular spaces allows the osteocyte to have an intimate association with the physical structure of the mineralised portions of the bone, and additionally to be able to communicate directly with adjacent osteocytes via cell:cell junctions and also with osteoclasts and osteoblasts on the lamellar and trabecular surface and within BMUs. Early work by our laboratory demonstrated a rapid increase in osteocyte staining for glucose 6-phosphate dehydrogenase (G6PD) within 6 minutes of mechanical loading in turkey ulnas [85] demonstrating osteocytes very quickly respond to changes in the mechanical loading environment. Several recent reviews have comprehensively summarised the evidence supporting the role of osteocytes as the chief mechanosensor [18, 38, 104].

The specific mechanosensory mechanisms of osteocytes have still not been fully identified. The lacunocanalicular network (LCN) throughout bone and its extracellular fluid matrix are likely to be involved in the mechanism of transmitting whole bone stresses into fluid flow shear stress which can be sensed by the osteocyte to appropriately respond to strain and/or shear forces. A very recent review has postulated that the shape of the osteocytic lacunae and canaliculi can affect the mechanosensitivity of osteocytes [19]. The specific mechanisms for osteocyte mechanosensation are, however, only partially understood. This is in part because it is difficult to study the physiological context of the osteocyte's role in mechanical loading in cortical bone *ex vivo* and *in vivo* models cannot easily study the physiological activity of the osteocyte given its location within the LCN. Likewise, *in vitro* models of osteocyte loading are limited by the inability to provide an appropriate 3-dimensional matrix which completely mimics the *in vivo* LCN.

Multiple different mechanisms have been postulated as mechanosensory pathways. The primary cilium present on osteocyte-like cells has been shown to deform in cells subjected to pulsatile fluid flow, and the cellular response shown to be mediated via a calcium-independent mechanism [408]. Inhibition of the primary cilia resulted in reduced expression of COX-2 and reduced OPG/RANKL ratio following pulsatile fluid flow *in vitro* [408]. Actin-rich cytoskeletal projections which are associated with the extracellular matrix are also thought to contribute to pathways for sensation of mechanical deformation through deformation of stretch-activated cation (Ca^{2+}) gated channels. It is thought these microfilaments may attach to the canalicular walls to provide deformation of the stretch-activated ion channels during increased fluid shear stresses generated during bone loading [409]. Connexin 43 (Cx43) is a membrane-bound receptor which has been demonstrated to be important in osteocyte response to mechanical loading, both *in vitro* and *in vivo* [410-412]. In two separate studies from our laboratory, using a microarray approach, we were able to demonstrate that, in an osteocyte-rich cortical bone sample from young mice, there were many pathways that were differentially regulated following increased mechanical loading [413], particularly upregulation of genes associated with proliferation, and that the basal and loading-related gene expression were substantially modified by context, such as oestrogen deficiency and disuse [86]. Ultimately, there is still

not a definitive single pathway that can be implicated for osteocyte mechanosensation, and instead, there is not one, but many mechanisms/pathways for mechanosensation.

Although many cellular pathways are affected by changes in mechanical loading, there are several key proteins/pathways related to mechanosensation and subsequent bone formation/resorption that are affected by mechanical loading that are of interest to our group. For example, osteocytes have been identified as the primary source of RANKL necessary for the resorption of bone seen following disuse induced by tail suspension [21, 22], suggesting this molecule is not only important in regulation of osteoclast activity associated with disuse, but that the source of this RANKL is primarily from osteocytes, and not osteoblasts as originally believed. The role of RANKL in bone is discussed earlier in section 1.4.1 and in more detail in Chapter 4, which reports a series of experiments exploring the change in expression of RANKL and other related molecules following both induction of disuse with sciatic neurectomy, and increased loading via axial tibial loading to determine the temporal and spatial pattern of expression following these stimuli. We, and others have studied the Wnt pathway in the context of loading and demonstrated that the protein, sclerostin, discussed earlier in section 1.4.1, is strongly regulated by mechanical loading [8, 20, 227, 414]. It is down-regulated following application of mechanical strain *in vitro* [414, 415], and *in vivo* its expression in osteocytes is reduced following application of increased strain [8, 20], and it is increased following disuse/decreased mechanical loading [8]. These strain-related changes in sclerostin expression subsequently modulate osteoblast activity through sclerostin's selective inhibition of the Wnt pathway [159].

Circulating levels of oestrogen are known to affect the responsiveness of osteocytes (and osteoblasts) to mechanical loading, and this action is likely mediated through regulation of the expression of ER α ; administration of oestrogen results in upregulation of osteoblastic ER α *in vitro* [416, 417]. There is abundant evidence that oestrogen receptors (ER) are involved in signalling associated with loading-related bone formation. Early studies demonstrated that ER α is necessary for the normal anabolic response to increased mechanical loading [232]. Knockout of ER α resulted in a diminished response to

mechanical loading and knockout of ER β resulted in an increased response to mechanical loading [418]. *In vitro* work has demonstrated that while ER α is essential for the proliferative response of osteoblastic cells mediated by Wnt/ β -Catenin signalling, this is via a LRP5/Wnt receptor independent pathway [415, 419, 420]. ER β mediates the acute sclerostin downregulation seen following loading [419]. Taken together, these results suggest that signalling through ER α increases the bones' response to mechanical strain (increases cell number) while ER β suppresses it. Interestingly, osteocyte specific deletion of ER α did not effect the magnitude of the response to axial tibial loading in 3 month-old mice [421]. There are several detailed reviews discussing the role of oestrogen and its receptors on the adaptive response to loading in bone and further detailed discussion is outside the scope of this literature review [228, 229, 422].

Whilst many other biochemical signalling pathways have been demonstrated to be mediated by altered mechanical loading, their pathways are typically dependant on other biochemical changes for their activation, rather than being directly mediated by the changes in strain within the cell. For example, increases in intracellular calcium mediate various secondary biochemical pathways involved in the remodelling response, such as Protein Kinase C and Prostaglandin E2 [423] and Insulin-like Growth Factor-1R [424]. Although osteocytes are the primary cell involved in sensing the mechanical stimulus associated with loading, they are not the cells that affect the primary responses to changes in mechanical load. Osteoblasts and osteoclasts are the cells that mediate bone formation and resorption respectively, typically in response to cues from signalling molecules produced by osteocytes.

Effect of aging on osteocytes

There is considerable data to support the theory that osteocyte number and/or function is reduced with aging [19, 280, 425]. Lacunar density in cortical bone is reduced with aging [426, 427] and the number of empty osteocyte lacunae is increased in old murine bone [29]. The number of dendritic connections between osteocytes increases in adult versus juvenile rats, then decreases again with advancing age [81]. Another study using acid etching and back-scattered electron microscopy also demonstrated that osteocyte

lacunae in showed decreasing canalicular connections with neighbouring lacunae with advancing age [82]. A recent review looking at osteocyte lacunocanicular architecture and adaptation with aging has hypothesised that the changes in lacunar shape and density and number of canaliculi associated with aging may be related to decreases in mechanosensation by osteocytes, although definitive data is still lacking [19].

Although the response to mechanical loading is impaired in aged animals, [25, 27, 29], whether osteocytes are the rate-limiting factor is still uncertain. We have shown that osteocytes, although reduced in number compared with young animals are still able to respond appropriately to a loading stimulus. The suppression of osteocytic expression of sclerostin following loading was equivalent to that seen in young mice, when only viable osteocytes were evaluated [29]. However, when exploring the response to repeated loading episodes, a more recent study has demonstrated that the sustained suppression of sclerostin is impaired in old mice (22 months), compared to young adult mice (5 months) [428], suggesting that osteocyte response to increased mechanical stimulus in old mice, although adequate after initial stimulation, cannot be sustained following repeated stimuli, and appears to involve the Wnt pathway. Several factors probably contribute to the reduced cellular activity of osteocytes in old bone, including cellular senescence, increased osteocyte apoptosis, and altered intercellular signalling, however, extended discussion of these factors is outside the scope of this literature review and is covered in review articles [280, 429].

1.8.2.2 *Osteoblasts*

Osteoblast numbers typically increase following increased mechanical loading. Early studies confirmed their proliferation was an important step on the road to bone formation in response to mechanical loading in turkeys and rats [430, 431]. Using bromodeoxyuridine (BrdU) to label proliferating cells, Turner *et al* [431] demonstrated that the endosteum incorporated 6 times more BrdU positive cells 96hrs after loading. Additionally, the thickness of the periosteum has also been shown to increase within 5 days of loading the turkey ulna [430] and within 24 hours in mice [4]. These proliferative responses are promoted by several of the mechanosensory pathways discussed in the

previous paragraphs, and although the degree of response to mechanical stimulus dictates the magnitude of the proliferative response, there are several other external and systemic factors which can limit the response to mechanical loading. Of particular relevance to this thesis, aging [25, 27, 29, 389] and increased habitual physical activity levels (eg fighting) [285] have been demonstrated to impair the osteogenic response to loading. Furthermore, reducing the intensity of habitual loading by prior denervation of the loaded limb has also been demonstrated to increase the magnitude of the loading response in young mice [35], further supporting the suggestion that existing mechanical loading environment can affect the magnitude of the osteoblastic response to loading. Chapter 5 explores the effect of reducing habitual loading on the deficient loading response in old mice.

As discussed in Section 1.8.2, ER α and ER β are important regulators of the adaptive response to mechanical loading. This response is mediated via regulation of osteoblastic, as well as osteocytic expression of the receptor. Much of the advancement of the understanding of the roles of ERs in bone biology has been achieved through the use of genetically modified mice lacking either ER α or ER β . Initial experiments explored the effect of global deletion of the gene on the loading response [232]. Whilst the phenotype of several bone cell-specific ER α knockout strains has been relatively well described and summarised well in the review by Rooney *et al* [432], the response of these bone-cell specific strains of mice to mechanical loading has not been as well investigated. However, one study deleting ER α from osteoblastic lineage cells demonstrated an increased responsiveness to mechanical loading, but this effect was only evident in the cancellous bone and not in the cortical bone [433]. Taken together, the differential responses of bone to loading following ER α global deletion vs osteoblast/osteocyte-specific deletion suggests that ER α expression in mature bone cells may not be necessary for the control of functional adaptation and that further investigation is required to gain a clearer understanding of the role of ER α in skeletal adaptation [432].

Effect of aging on osteoblasts

In the study from our lab which demonstrated initial mechanosensation by osteocytes was unaffected, we also demonstrated that it appears to be a failure of proliferation of osteoblasts in aged mice that underlies the age-impaired response to mechanical loading [29]. In a follow-up microarray study, we also demonstrated that genes associated with proliferation were down-regulated in old mice and that loading regulated similar signalling cascades in old and young mice, but the responses were not sustained in old mice, compared to young mice [413]. This study also concluded that bone cells' ability to translate acute responses into functionally relevant outcomes is impaired. This finding is consistent with the findings from Holguin *et al* [428] showing the suppression of sclerostin was not sustained in old mice following repeated loading. These and other studies relevant to the individual chapters will be discussed in more detail in the introduction of chapters 5, 6 and 7. Furthermore, there are review articles discussing the effect of aging on bone cell responses to loading [19, 434].

1.8.2.3 Osteoclasts

It is proposed by Skerry [435] that the response of bone to unloading is simply one end of a spectrum of response to mechanical stimuli, where increased mechanical loading causes the other end of the response spectrum. It is likely that habitual loading represents a middle ground on this spectrum and that unloading causes the opposite effect to increased loading, but that these responses are mediated by common pathways. However, although bone formation following disuse is reduced compared to normal ambulatory animals, the amount of osteoblast surface was not decreased until an extended period of disuse had occurred [106]. In the same study, osteoclast numbers increased following disuse [106]. Osteoclasts are most important for bone resorption, so osteoclast activity tends to increase when the magnitude of mechanical loading is decreased. Additionally, expression of pro-osteoclastic markers such as tartrate-resistant acid phosphatase (TRAP) and cathepsin K decrease when mechanical load is applied [436] *in vitro*. Several comprehensive reviews discussing the cellular responses to changes in

mechanical loading are published, and should be consulted for further information [38, 104, 435, 437].

Effect of aging on osteoclasts

The effect of aging on the response of osteoclast activity is not well reported. Although osteoclast number and activity is typically increased with aging [183, 185], there is little reported that examines the effect of mechanical loading on osteoclast activity in aged mice. In aged mice, the rate of resorption is reduced following loading, however, the degree of suppression of resorption is not as great as that seen following loading in young mice, which suggests that the ability of osteoclasts to respond to loading in aged mice is diminished compared to that in young adult mice [30, 31]. Further studies are needed to further define the effect of aging on the response to mechanical loading in osteoclasts.

1.8.3 The effect of aging on bone's structural response to mechanical loading

It is postulated that reduction in bone mass seen in age-related osteoporosis is primarily mediated through a failure of the mechanostat [23]. Loss of bone mass associated with aging results in weaker bone and subsequently increased deformation of bone and increased strain. In the elderly, bone mass can reduce to the extent that minimal trauma can result in fracture, despite no appreciable changes in the levels of functional loading. As the normal physiological response to mechanical loading is impaired in elderly humans [26, 438, 439] a greatly increased risk of vertebral and non-vertebral fractures in elderly people is encountered, especially in women [17, 440-442]. Hence, if the mechanostat were functioning normally, this increase in strain seen due to decreased bone mass should promote an anabolic response and restore bone mass to a suitably robust state. Therefore, the failure of mechanical loading to stimulate a sufficient formative response in the elderly indicates a failure of the mechanostat.

Studies comparing exercise interventions in people have supported the hypothesis that the mechanostat fails with aging; Srinivasan *et al* [443] have recently reviewed the age-related effect on the response to exercise. In young children, exercise programmes resulted in significant increases in bone mass [444, 445], whereas in post-menopausal

women, most studies generally find that the bone is less responsive to loading, with no response or a limited magnitude of response compared to non-exercised controls [446-448] suggesting the response to exercise in the elderly is impaired.

There are, unfortunately very few studies directly comparing young and old people's response to the same stimulus. Bassey *et al* [438] compared the osteogenic response to a vertical jumping programme of pre- and post-menopausal women and identified no difference in their response, although the ground reaction force measured between groups demonstrated higher forces in the post-menopausal women, who are likely to have weaker bone. This suggests that this group of women experienced greater strain magnitudes than their younger control groups. Although impaired in the elderly, mechanical loading of bone through exercise and resistance training has been demonstrated to lead to a higher bone mass in some studies in older humans [26, 449, 450]. A single episode of exercise was sufficient to increase formation markers and decrease resorption markers in one study of postmenopausal women [451]. Furthermore, a metaanalysis of studies examining bone's response to exercise concluded that it is still possible to increase lumbar and femoral neck bone density in older patients using physical therapies [452].

Several experimental animal studies have confirmed a reduced sensitivity of bone to mechanical loading in rodents. Rubin *et al* [24] used an invasive model of loading using the turkey ulna and demonstrated a decreased mechanoresponsiveness in the old turkey, compared with the young turkeys – that the level of loading that generated bone formation in the young animal was insufficient to generate similar levels of bone formation in the old animals. This provided the first experimental evidence of an age-related impairment of the mechanostat. Following on from that study, Turner *et al* [25] demonstrated in rat tibiae, using four-point bending, that old animals had a higher threshold to strain before bone formation was stimulated, and a lower bone formation rate once formation was stimulated, compared to young controls. However, invasive loading models and four-point bending models result in excessive periosteal woven bone

formation, and as such limit the region of bone that can be analysed to the endosteal surface only.

Using non-invasive loading, loads which were osteogenic in 10w old mice were ineffective in 26 week old mice when strains were matched between groups [453]. A more recent *in vivo* μ CT study yielded similar findings and came to similar conclusions [454]. Although these studies demonstrate bone is less sensitive to loading in older animals, the mice used in these studies were only 26 weeks old. It is not until mice are 16 months (59-60w) old that age-related cortical bone loss becomes evident [196], although trabecular bone loss can be evident as early as 26 weeks [282]. Recent studies by our laboratory and others have repeatedly shown a decreased sensitivity to loading stimuli in truly aged mice compared with young animals [27, 29-31, 389]. [428, 455].

1.8.4 The effect of concurrent treatments on bone's response to mechanical loading.

Whilst many different treatments are used to help preserve adequate bone mass and reduce fracture risk in clinically affected patients, as described in Section 1.7 of this chapter, their effects on the response of the mechanostat are less well reported. Of particular importance to the experiments reported in this thesis, are anti-resorptive bisphosphonates, and the anabolic treatment, PTH. Whilst reports detailing the effect of bisphosphonates and PTH treatment following disuse are relatively frequent, there are fewer reports describing their effects on the adaptive response to increased mechanical loading following treatment with bisphosphonates or PTH. This section describes literature exploring these interactions.

1.8.4.1 Bisphosphonates

BPs can attenuate the bone loss seen with reduced loading in humans and experimental animals. Pamidronate reduced bone loss following extended bed rest in young men [456] and alendronate administration abrogated bone loss in astronauts treated with alendronate and exercise, compared to exercise-only controls [457]. Several rodent

studies have demonstrated that BPs are able to completely abrogate deterioration of bone parameters in disuse back to levels seen in ambulatory animals [303, 458-461].

Several studies have previously investigated the combined use of BPs and anabolic levels of loading in young adult rodents. We have shown in young adult female mice (17-weeks-old) that risedronate (RIS) has no effect on the magnitude of the osteogenic response to mechanical loading [34]. This suggests that the loading response primarily involves osteogenic modelling without requiring “coupling” of osteoblast and osteoclast activity in mice [34]. This study showed strong positive effects of RIS on trabecular bone, which were additive to the anabolic effects of loading. However, RIS had no independent effect on cortical bone parameters. In a similar study in young rats, Feher *et al* [462] showed the periosteal bone modelling response seen following axial ulnar loading was unaffected by treatment with a variety of BPs, including RIS. In the study by Feher *et al* [462], bisphosphonate treatment following concurrent ovariectomy, an additional resorptive stimulus, also had no effect on the degree of the loading-related response. Furthermore, whole body vibration-related changes in bone mass were unaffected by alendronate treatment [463]. Some human clinical trials have also shown that the response to exercise in humans is unaffected by BPs. While two studies from the same author have found additive increases in bone mass with exercise and BPs [464, 465], others have found no additional effect of exercise/loading on BMD above the effect of BPs [446, 466]. The section modulus, a surrogate measure of bone strength, increased with jumping exercises in one study and this was unaffected by treatment with BPs [446].

Overall, in humans and rodents, it does not appear that the loading response is affected following concurrent treatment with bisphosphonates. Studies including old rodents have not, to the authors knowledge, combined mechanical loading and treatment with bisphosphonates. As bone resorption is increased with aging, we wanted to determine if the response to mechanical loading in old mice following treatment with risedronate was like that reported in young mice. Chapter 6 contains further discussion of the literature surrounding bisphosphonates and altered mechanical loading and then describes

experiments aimed at determining if bisphosphonates affect the loading response in old mice, both in situations of habitual loading and following prior disuse.

1.8.4.2 *Parathyroid Hormone*

PTH treatment is reported to abrogate the bone loss experienced with disuse in rats [467-470]. Interestingly, combination of PTH with growth hormone had additive effects on both skeletal and muscle mass following disuse induced by Botox, although PTH generally prevented all skeletal deterioration seen following disuse [470]. PTH treatment also shows a dose responsive effect following hindlimb unloading, with low doses abrogating the trabecular bone loss and higher doses promoting an anabolic response that resulted in further bone mass accrual beyond that of vehicle treated ambulatory rats [468].

Significantly, the anabolic response to loading in young mice was synergistically improved following pre-treatment with PTH [32], suggesting that PTH treatment sensitises the mechanostat to respond with a greater formation response to the same loading stimulus. An earlier study supported these findings, by demonstrating a synergistic effect of PTH with reloading following limb immobilisation with an elastic bandage; PTH promoted an enhanced response to re-loading of the immobilised limb compared to vehicle treated animals [471]. A recent paper demonstrated that the PTH receptor 1 in osteocytes (DMP1-Cre) was essential for the anabolic effect of mechanical loading, supporting the inference from these two earlier studies that PTH signalling is involved in the response to mechanical loading [472]. However, a separate study looking at combined loading and PTH treatment on periprosthetic bone demonstrated additive, but not synergistic effects on bone mass [473]. Similarly, a study combining four-point bending and PTH demonstrated additive effects of loading and PTH, but no synergism [387].

Although the response to combined PTH and mechanical loading was reported to be synergistic, or at least additive, there is only one report, to the author's knowledge, that has explored the response to loading following PTH treatment in old mice. In a study published recently by our laboratory exploring the effects of PTH treatment on the loading response in old (19-month) mice, the anabolic effects of both mechanical loading and PTH

were additive, but not synergistic, highlighting the difference in response between young [32] and old mice [388]. Chapter 7 of this thesis explores the effect of PTH treatment in very old (22m) mice on the mechanical loading response.

1.8.4.3 Other treatments

The effect of other osteoporosis therapies on the response to altered mechanical loading has been sporadically reported. In one study, post-menopausal women, the skeletal response to exercise training is significantly increased following oestrogen (17 β -oestradiol) treatment [474]. Conversely, another study compared women under treatment with the hormone replacement therapy tibolone, and compared women with high levels of activity with those with low activity levels, and found no difference in BMD between the groups [475]. In fact this study demonstrated a greater initial increase in BMD in the low activity group, supposedly due to the slightly higher baseline BMD and probably lower resorption activity at baseline in the high activity group. Evidence from animal models where oestrogen was replaced have showed oestrogen treatment typically had no effect or reduced the magnitude of the response to mechanical loading [476]. The SERM, tamoxifen demonstrated partial abrogation of the trabecular bone loss seen following SN, but no effect on the cortical bone loss [477]. Tamoxifen also had only partial sparing effects on bone loss seen in dogs following cast-immobilisation [478]. Another SERM, Raloxifene demonstrated a more robust inhibition of the bone loss associated with tail suspension with trabecular architecture similar to control -non-suspended rats [303]. The effect of SERMs on the response to increased mechanical loading is only reported in one study, where loading in young mice was combined with tamoxifen [287]. In this study, tamoxifen treatment was associated with a synergistic response when combined with mechanical loading when examining the trabecular bone volume, suggesting that SERMs may be able to enhance the adaptive response to loading in trabecular bone.

Sclerostin antibody has been intensively researched in the last decade. Its protective effect against disuse has been repeatedly demonstrated [479-483]. The anabolic response to increased mechanical loading has also been recently reported to be improved following treatment with sclerostin antibody [372], suggesting that sclerostin is involved in the

modulation of the adaptive response to loading in mice. Further discussion of the promise of combining Scl-Ab with loading is included in the general discussion chapter of this thesis (Chapter 8).

1.8.4.4 *Combination therapies*

Whilst the effect of combination therapy using different osteoporosis drugs on bone mass has been investigated in many reports, and described in more detail in Section 1.7.4, fewer studies have explored the effect of combining therapies on the response to altered mechanical loading. The response to disuse following combined treatment with PTH and zoledronate demonstrated additive effects on bone mass, and more than abrogated the bone loss associated with disuse in vehicle treated animals [467]. In a related study by the same group, combining PTH and Strontium Ranelate was no different to PTH treatment alone, with rescue of the bone loss seen following disuse [469]. Strontium ranelate alone had no protective effect against the bone loss associated with disuse [469].

To the author's knowledge, there are no reports exploring the effects of combination therapy on the response to increased mechanical loading. Chapter 7 of this thesis describes an experiment which explores the effect of combined Risedronate and PTH therapy on the adaptive response to mechanical loading in very old mice. Furthermore, as the response to PTH stimulates a primarily remodelling response, with significant increases in bone resorption and subsequent cortical porosity [388], we sought to investigate whether impairment of resorption with bisphosphonates would affect the anabolic response of combined loading and PTH in old mice.

1.8.5 *Models for studying the effect of altered mechanical loading on bone*

In addition to clinical and environmental situations of altered mechanical loading in humans, many research/experimental models have been used to investigate the response to alterations in mechanical loading of bone.

In order to explore bone's response to changes in the mechanical loading environment *in vivo*, several models have been designed to alter the amount of strain experienced by

bone. These models include intrinsic loading models, utilising physiological movement of the skeleton using muscles of the skeleton to increase strains, and extrinsic loading models, utilising external forces to apply additional loading forces and increase strains in bone. The majority of these models are well summarised in a review by Meakin *et al* [484], but are discussed in brief below.

1.8.5.1 Exercise models of increased mechanical loading

Increased exercise has been used to increase the level of strain experienced in bone. The most simplistic of these is to train animals to exercise on a treadmill [485, 486]. Treadmill exercise is non-invasive and the mechanical forces derived from muscle contraction and ground force reaction are transmitted along the length of the entire bone, leading to adaptive changes in all compartments of the long bone [487]. Exercise-induced mechanical strains can be measured [488], but controlling these between individuals and treatment groups is difficult [489].

Swimming, wearing a weighted backpack, and jumping up to or down from platforms have also been used to increase mechanical loading [490-497]. These other forms of exercise have similar advantages to those of treadmill exercise, although it is more difficult to control the nature of the exercise regimen such as speed and angle of inclination. Furthermore, the effects of exercise are not isolated to the bone itself. Exercise initiates several other physiological responses which can affect bone mass. However, although treadmill exercise resulted in increased muscle mass and systemic changes in serum IGF1, it did not affect the adaptive response of bone to extrinsic mechanical loading in young or old mice [396].

1.8.5.2 Invasive models of artificial mechanical loading

One of the earliest experimental models of increasing the mechanical loads transmitted through a bone was to remove a segment of a paired appendicular bone, such as the ulna, which increases loads transmitted through the radius. Several species including rats, rabbits, guinea pigs, dogs, sheep and pigs have been utilised for this model [498-503]. These models do not control the magnitude of the strain stimulus as it is dependent on

the activity levels and bodyweight of the individual and postoperative pain may also limit weight-bearing in the limb, thus limiting the desired effect of overloading.

To circumvent these difficulties, invasive models of mechanical loading were developed, which allowed the direct application of precise amounts of mechanical load to a bone that did not rely on habitual weight-bearing. The first invasive loading models involved insertion of two transcortical metal pins to permit application of mechanical loads to the intervening bone. Heřt and colleagues originally devised these techniques in the 1970s using the rabbit tibia [504, 505] and later the technique was adapted for use in sheep and dogs by others [498, 506, 507]. This model includes the ability to control parameters such as peak mechanical strain, strain rate and number of loading cycles, and differences in bone mass and architecture between groups are controlled for by delivering different forces to each group, based on preliminary experiments using strain gauges to characterise the strain experienced in each group. However, when using this experimental model, an animal's episodes of exogenously applied mechanical loading are superimposed on normal ambulation, so strains engendered by habitual activity could potentially mask some of the responses to loading. Additionally, as with the osteotomy model discussed in the last paragraph, disuse of the limb may occur due to surgical pain.

Rubin and Lanyon modified this model further in the 1980s [508-511] by isolating the mid-shaft of the turkey ulna with proximal and distal osteotomies in an effort to isolate the effect of habitual loading on the studied bone. Surgical pins were placed at the extremities of the isolated bone to permit compressive loads to be applied to the isolated bone. A schematic representation of this model is shown in Figure 10A. By isolating the ulna, strains engendered by normal activity are negligible. The wing in turkeys is not weight bearing and is not used for flying, so the contralateral limb is unlikely to be affected by changes in the loaded limb, thus serving as a suitable internal control. However, placement of the metal pins in bone stimulates an inflammatory reaction in the surrounding bone, resulting in bone formation separate to that elicited from the mechanical loading. To overcome this limitation, the area of bone which can be studied is restricted to the central diaphyseal region, away from the pins. Therefore, only cortical

bone, and not trabecular bone, usually situated at the epiphyses, can be studied using this model.

To overcome this limitation, a model utilising application of mechanical loads to the vertebrae of the tail, which contain abundant trabecular bone, was devised [512]. The pins were placed through vertebrae adjacent to the studied bone to lessen the inflammatory reaction in the region of interest and permit the study of trabecular bone's response to mechanical loading. Rodent tail vertebrae are not normally weight bearing bones, unlike human vertebrae, however, so this represents a potential disadvantage to this loading model. It still represents the only feasible model with which to mechanically load vertebrae to recreate vertebral loading in humans, so the vertebral loading model is still in use today [513-516], whereas invasive loading of long bones is not.

1.8.5.3 Non-invasive models of artificial mechanical loading

To overcome the limitations of invasive models of loading, non-invasive methods of loading limb bones have been developed. These models do not require surgical procedures for the placement of surgical pins and there is no recovery period following surgery which means the length of the experiments can be reduced. This has animal welfare benefits and reduces experimental costs.

Four-point bending

Turner and colleagues first developed a four-point bending model for use in rodents [517, 518]. In this model, depicted schematically in Figure 10B, two contact points are placed eccentrically on the downward surface of a bone, usually the tibia. Two centrally placed contact points apply a downward force to the uppermost surface, resulting in a bending force. To generate a sham loading model, the contact points can be moved so they directly oppose each other, thus applying a similar squeeze to the bone, but not bending the central region of interest. Unfortunately, the contact points cause a woven bone formation response, preventing study of the periosteal surface of the bone and restricting any investigations to the endosteal bone surface. Again, similar to the invasive cortical bone models, this model is limited to the study of only cortical bone adaptive responses.

Cantilever bending

A variation on the four-point bending model was developed by the Gross *et al* [519]. The proximal tibia is immobilised in a custom jig, whilst a laterally applied force is applied to the tibiotarsal joint, resulting in a cantilever bending mechanism. Since the only contact points on the bone are in the proximal and distal tibia, this model allows study of both endocortical and periosteal surfaces. Again, the cantilever bending model also precludes evaluation of trabecular bone. Both bending models do not apply load in a physiological direction (axially) meaning lower load magnitudes are required. However, the relevance of non-physiological loading directions is unknown.

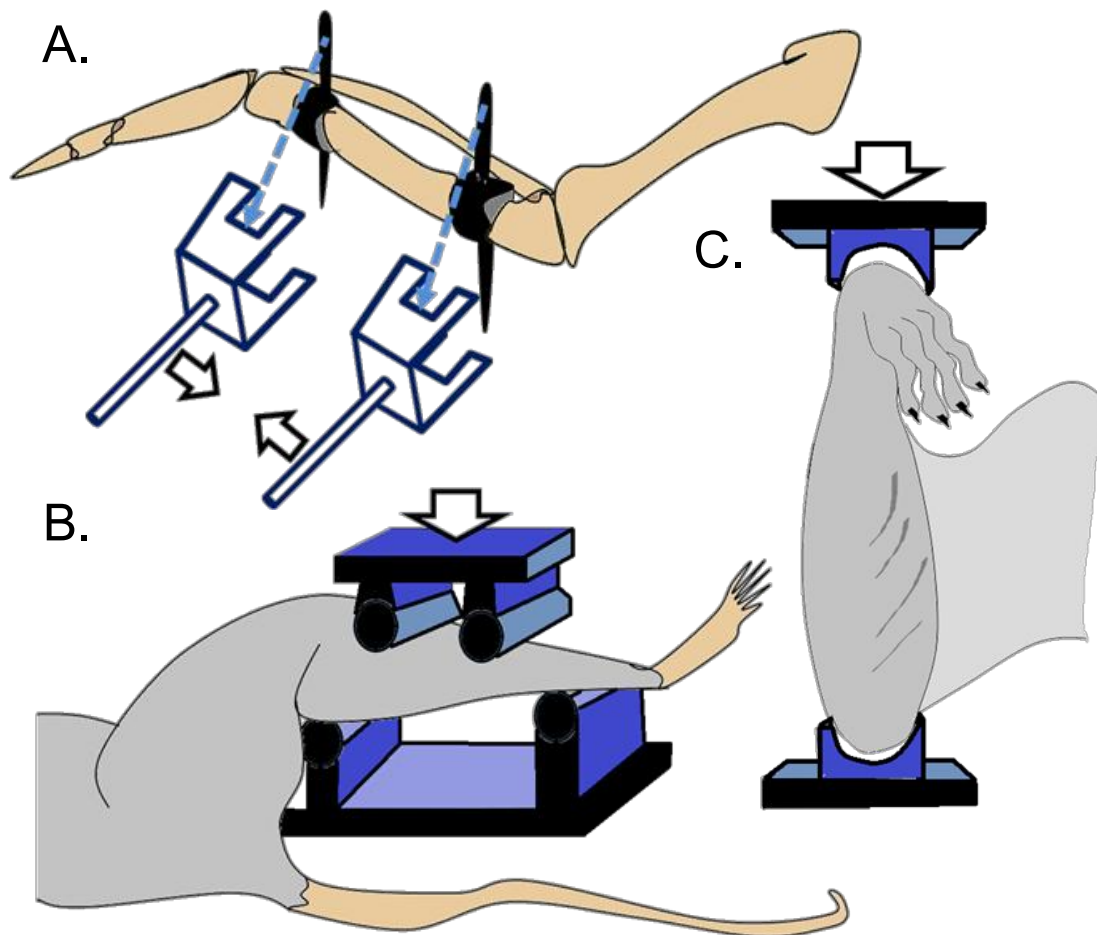


Figure 10: Schematic representation of (A) the isolated avian ulna, (B) tibial four point and (C) ulnar axial loading models

Figure reproduced here with permission [4].

Axial compression models of mechanical loading

To address the issue of non-physiological directions of applied mechanical loads, our laboratory developed a non-invasive axial ulnar loading model to study the adaptive response of bone to exogenously applied mechanical loading similar to those experienced by normal ambulation in rodents *in vivo* [520, 521]. As shown in Figure 10C, the carpus and elbow are placed in cups from a materials-testing machine and an axial compressive load is applied. Although this model generally requires greater forces to elicit bone formation than the bending models, likely because the bone is already adapted to forces applied in the axial direction, the loads applied do not result in evidence of bone damage, such as woven bone formation and/or microcrack formation. The length of the loaded bone has been reported to be shorter due to premature closure of the growth plate [522, 523]. Furthermore, the amount of trabecular bone in the rat ulna is limited, still limiting the ability to evaluate the adaptive response of trabecular bone to mechanical loading in long bones.

Because the tibia contains more trabecular bone in its proximal epiphysis than the ulna, our laboratory subsequently developed an axial loading model for the tibia [2], compressing the knee/stifle joint and the ankle/hock joint in custom-made loading cups (Figure 11A). Unexpectedly, significant trabecular bone loss with loading was demonstrated despite a significant gain in cortical bone mass [2]. However, later studies using a tenfold higher strain rate have demonstrated that both cortical and trabecular masses increase substantially with mechanical loading as shown in Figure 11B [1, 32, 34, 285, 287], suggesting it is the strain rate, and not loading direction that resulted in the trabecular bone loss. The next section of this chapter will discuss optimising the strain stimulus.

Another advantage of the axial tibial loading model is that the attached fibula also demonstrates a significant bone formation response to mechanical loading [160] and can be easily dissected from the tibia after mice are sacrificed to provide a second bone to study bone's adaptation to mechanical loading. The response to mechanical loading is site-specific along the length of the tibial cortex. The mid-proximal region of the tibia (around

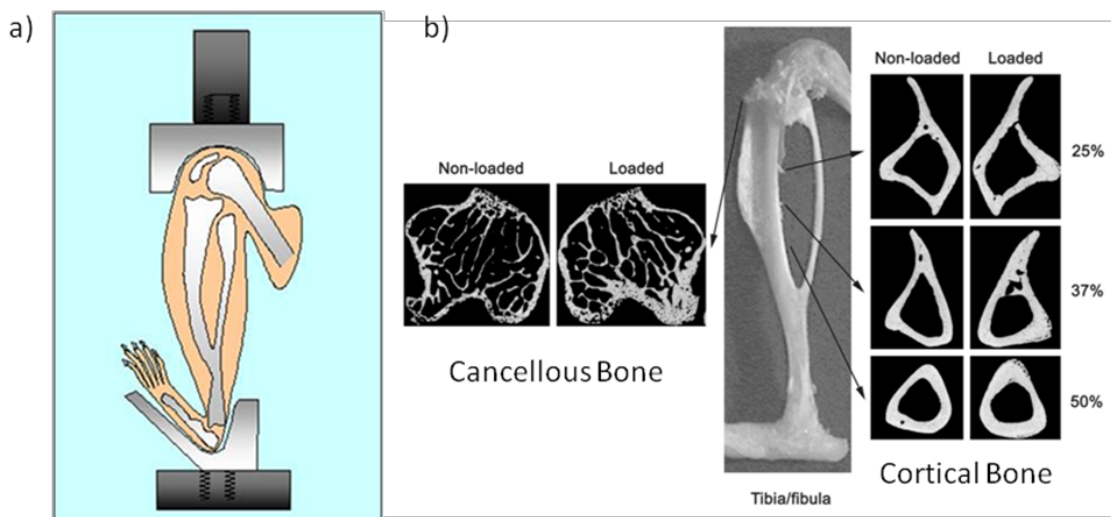


Figure 11: The non-invasive axial tibial loading model

a) Schematic diagram showing the non-invasive axial tibial loading apparatus and b) a photograph of a murine tibia/fibula after dissection with corresponding micro-computed tomography images demonstrating the different sites (measured from the proximal end) which respond to mechanical loading. Figure adapted from and reproduced with permission (Sugiyama *et al.*, 2008).

the 37% mark) appears most responsive to axial tibial loading according to early studies [11, 32]. The distal tibia does not demonstrate a significant increase in bone formation even though the applied strains are estimated to be of similar magnitude using finite element modelling (FEM) [8]. These findings are supported by a more recent study published by our laboratory using site-specificity software to more closely interrogate the relative changes over the length of the cortical bone of the tibia (Figure 12) [7], a technique utilised in chapters 4-7 of this thesis.

Some researchers have argued that applying mechanical load to one limb may result in systemic effects altering the adaptive response in bones adjacent and even distant to the loaded bone [524], and that this effect is neuronally mediated. The systemic effects were abrogated by perineural local anaesthetic application prior to loading. However, further studies by ourselves and others have since determined that the response is confined to the loaded bone [1, 525] validating the use of the contralateral tibia as an internal control, increasing statistical power and reducing the number of experimental animals. It is, therefore the loading model we chose for the experiments described within this thesis.

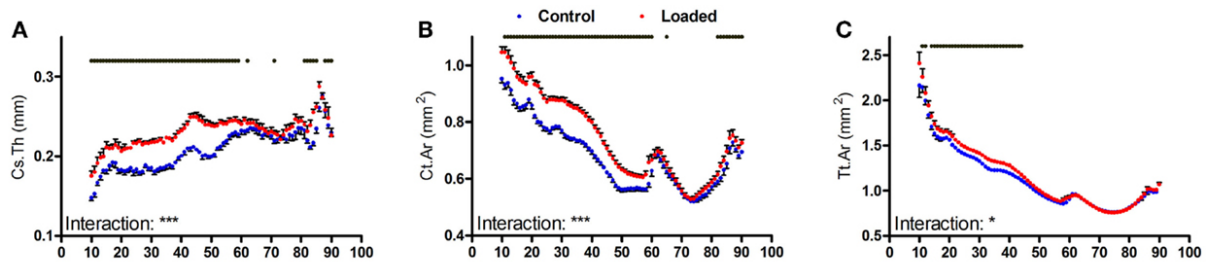


Figure 12 Analysis of response of the mouse tibia to loading at each site along the bone's length using Site Specificity Analysis software.

Site specificity analysis of (A) Cross sectional cortical thickness (Ct.Th), (B) Cortical bone area (Ct.Ar), and (C) periosteally enclosed area (Tt.Ar), calculated from control left tibiae and loaded right tibiae from the same mice, $n = 15$. The x axis indicates percentile length along the tibia measured from the proximal end. Dots/bars above the graphs indicate sites of significant difference, $p < 0.05$ following Bonferroni correction. Interactions are the site by loading interactions calculated by mixed models; * $p < 0.05$, *** $p < 0.001$. Note that the sites between 60-80% are not affected by loading. Figure adapted from and reproduced with permission [7]

Unfortunately, application of sufficient loading force to result in bone formation in rats also resulted in skin necrosis and pressure sores over the contact points on the knee and ankle [526], so the model's use in larger rodents is limited. Despite its limited utility in rats, the tibial loading model has been widely accepted and duplicated in many other labs throughout the world wishing to investigate trabecular and cortical bone's adaptation to its mechanical environment [453, 454, 527-531].

1.8.5.4 *Optimising the mechanical strain stimulus to elicit bone formation*

Application of an externally applied mechanical load permits precise control over the load stimulus and several previous studies have determined characteristics of the loading stimulus which affect the bone formation response to loading. This section will briefly discuss those relevant to designing the loading regimen for use in the experiments described within this thesis.

Static versus dynamic loading

Continuous static loading of bone does not stimulate an adaptive response whereas cyclical dynamic loading of the same bones at the same peak strain magnitudes does elicit an osteogenic response [505, 511]. Hence, most studies using exogenously applied loads

use a cyclic loading waveform, of either triangular, sinusoidal, or trapezoidal shape [2, 29, 232, 529, 532].

Peak strain magnitude

The peak magnitude of the stimulus is clearly the most important component of the strain stimulus to stimulate an osteogenic response to mechanical loading. Several studies have demonstrated that increasing the peak strain magnitude yet keeping all other loading characteristics the same, results in a bone formation dose response [11, 29, 509, 517, 522, 532]. Interestingly, evidence suggests that within the strain magnitudes which cause lamellar bone formation, the relationship is linear, although this varies once bone experiences strains sufficiently large to generate woven bone formation [11].

Strain distribution/orientation

In the ulnar osteotomy study by Lanyon, described earlier, rosette strain gauges were affixed to the surface of the radius following ulnar osteotomy to record strain magnitudes [500]. Increases of strain on the cranial surface of the radius in the osteotomised limb were around 20%, which was more than double the recording on the caudal surface of just 8%. However, over the duration of the study (50 weeks), the caudal radial cortex, where less strain is typically experienced in intact bones, was the predominant site for formation. The amount of newly formed bone was equivalent to that removed by ulnar osteotomy. This sudden occurrence of strain in a site which doesn't normally experience much strain resulted in an exaggerated formation response to restore baseline strains. This suggests the distribution, rather than just the magnitude, of the applied strain is an important osteogenic stimulus. Indeed, strains of similar peak magnitude as those engendered by wing flapping to the osteotomised turkey ulna, applied in a novel direction, were sufficient to stimulate bone formation [533]. Likewise, the strains necessary to elicit bone formation in the bending models of non-invasive loading are much lower than the strain necessary to cause bone formation when loading is applied in a physiologically similar direction to that experienced during normal physiological loading (i.e. axially) [29, 519].

Strain rate

The rate of change of strain magnitude is also important in designing an osteogenic stimulus. Using the rat ulnar loading model, it has been demonstrated using various strain rates but the same peak magnitude, number of loading cycles etc. that increasing the strain rate by approximately five-fold was able to increase the osteogenic bone formation response by 67% [534]. Results from a separate study yielded similar results and led the authors to conclude that new bone formation was directly proportional to the rate of strain in bone tissue [535].

Our standard loading protocol applies an axial force in a cyclic trapezoidal wave-form to reach the desired peak strain, measured by strain gauges placed on the periosteal surface of the medial tibia. The linear loading and unloading phases of the trapezoidal loading wave-form allow calculation and application of a strain rate of $30\,000\mu\epsilon\text{s}^{-1}$, shown to be equal to the physiological strain rate in mammals [488, 536]. The short (0.05s) pause at the peak load with a trapezoidal wave form permits a more consistent achievement of the desired peak load than with use of a triangular wave form. The use of a sinusoidal waveform limits the ability to reach the desired peak strain rate to a single time point

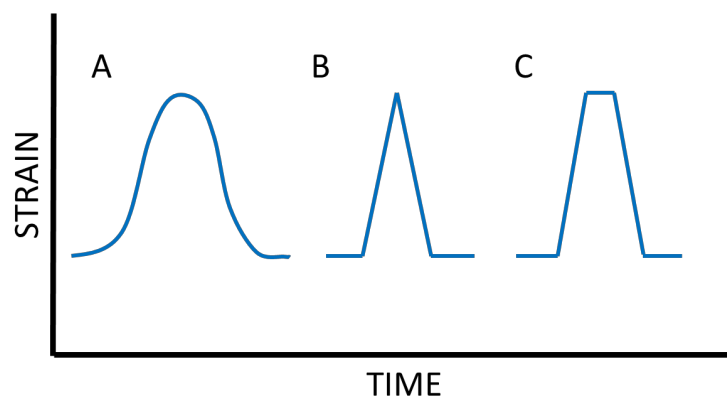


Figure 13 – Loading waveforms for application of load represent strain rate.

The slope of the strain vs time curves represents the strain rate. (A) Sinusoidal loading waveforms only achieve the maximum strain rate a single timepoint throughout the loading and unloading phases. (B) Triangular and (C) trapezoidal waveforms have a linear loading and unloading phase, thus maintaining the peak strain rate for the duration of the loading and unloading phases of the loading cycle.

throughout the loading wave-form. At all other time-points, the strain rate will be lower than that desired. See Figure 13 for a graphical representation of the wave-forms.

Optimum number of cycles

Evidence that the osteogenic response to loading is not related to the number of cycles of loading applied was first published several decades ago. Rubin and Lanyon [533] first demonstrated in the isolated turkey ulna, that 4 cycles per day was sufficient to abrogate bone loss associated with disuse, and that increasing from 36 cycles to 1800 did not result in any further increase in the osteogenic response. Supporting this finding, a study in rats trained to jump a 40cm height demonstrated little further effect of increasing the number of jumps from 5 up to 40 per day [497]. Despite this evidence that relatively few cycles are required to generate a maximal osteogenic response, many researchers still frequently use several thousand loading cycles which are more likely to result in woven bone formation and inflammation [525]. Our laboratory routinely uses 40 cycles per loading bout when using the axial tibial loading model [1, 8, 11, 29, 32, 34, 160, 285, 286, 388]

Rest insertion

Inserting a short period of rest in between loading cycles has been shown to improve the osteogenic response to loading. A study by Robling *et al* [537] demonstrated that portioning 360 loading cycles into 4 bouts of 90 cycles or 6 bouts of 60 cycles per day enhanced the osteogenic response to loading suggesting there may be some saturation of the mechanical loading stimulus with increasing numbers of cycles. A subsequent study by the same group demonstrated that a recovery period of 8 hours between loading sessions was sufficient to allow complete restoration of bone's mechanosensitivity, and that a 14s rest period between individual loading stimuli allowed a greater osteogenic response than a shorter rest-insertion [538]. A further study by Gross' group observed that inserting a 10 or 15 second rest period between each loading cycle enhanced the osteogenic stimulus in both young and aged mice [27, 539, 540]. The standard loading protocol in our laboratory inserts a 10 second rest period between individual loading cycles.

1.8.5.5 *Models of reduced bone loading (disuse)*

As described previously, reduced mechanical loading is a clinically important cause of bone loss seen in people in a variety of situations. Patients immobilised through bed-rest, or as a result of spinal injuries experience significant bone loss, and astronauts who experience microgravity and reduced bone loading also undergo rapid bone loss. While pathological and environmental causes of reduced bone loading in humans provide a useful source of information and data for investigation of disuse-associated bone remodelling, controlling the loading stimulus is difficult, and/or the population of participants (astronauts) is very small. For this reason, researchers have sought experimental models which can provide a more controlled unloading stimulus.

Ideally, reducing strain on the bone surface to zero would allow determination of the effects of a full range of strain stimuli. Perhaps the closest to achieving this would be experiencing zero gravity during space flight and multiple animal studies have been performed in space [541-547]. However, this is, for obvious reasons, not practically possible for most researchers. Furthermore, the effects of endogenous muscle-induced strains are not eliminated. Indeed, increased activity during space flight from group housing animals has been shown to prevent bone loss [548]. Further complicating the use of spaceflight as a model for reduced mechanical loading is the increase in ionising radiation exposure inherent with being outside our protective magnetosphere. Ionising radiation has been shown to reduce bone mass and increase osteoclast number [549, 550], and also reduce the osteogenic potential of cortical but not trabecular bone in response to loading [551].

Several terrestrial (and far more practical!) experimental models of reducing the magnitude of mechanical loading have been described. These include cast application to a limb, Achilles tenotomy to unload the calcaneus and tibia, tenotomy of the patella tendons to unload the tibia and bandaging a limb to the abdomen [106, 552-557]. The techniques mentioned above are not suitable for the experiments involved in this experiments for a number of reasons. Cast application and bandaging of the abdomen to the limb is prone to slipping and as such, difficult to control the amount of strain

experienced in small murine legs. Furthermore, once a cast is applied, it is difficult to apply additional exogenous loading stimuli. When considering tenotomy, the position of the skin incision necessary for the section of the patella ligaments is in close proximity to the position of the proximal loading cup in the tibial loading apparatus, this encouraging wound healing problems. Achilles tenotomy was attempted by the author in aged mice, and a high proportion of the operated mice experienced pressure sores on the plantar surface of their ankles, due to the plantigrade stance engendered by tenotomy, therefore, this model is also unsuitable for use in aged mice with thin skin predisposed to pressure sores.

Probably the most commonly used model for exploring disuse of the bone is that of tail suspension which eliminates ground reaction forces on the hindlimbs [558, 559]. This model is extensively reported in the literature and reliably demonstrates bone loss in the femur and tibia [21, 543, 560-562]. However, we did not select this model for several reasons. Firstly, there is a redistribution of blood to the cranial aspect of the animal with some stress response observed [563]. Additionally, this model causes bilateral bone loss, losing the ability to compare one limb with its contralateral control. Lastly, there will still be strains experienced on the bone surface from muscle contractions. Critically, in the UK, use of this model is not permitted on welfare grounds. This is in part because tail suspension is stressful – it has been utilised as an experimental model of inducing behavioural stress/depression [564].

Two further methods of inducing unloading have been reported. These induce paralysis of the hindlimb and therefore bone loss. This is achieved either by sciatic denervation via sciatic neurectomy (SN) or by the injection of botulinum toxin (Botox) to particular muscle groups [11, 35, 565, 566]. Following paralysis, tibial bone surface strains are reduced to around $300\mu\epsilon$ (compared with $600\mu\epsilon$ in ambulatory animals) and the tibia can be subsequently reloaded using the axial tibial loading model to prevent bone loss [11, 35]. Interestingly, a recent paper reported the effects of combining tail suspension and Botox [567]. This study reported an additive effect of the two treatments on the degree of bone loss, and that individually each model resulted in similar degrees of bone loss.

Interestingly, in mice treated with unilateral Botox, some muscle and skeletal mass was lost in the contralateral limb – suggesting that although primarily a local effect, Botox can have systemic effects, which could limit the contralateral limb’s utility as an internal control limb.

SN and Botox both have different advantages and disadvantages. For the studies reported within this thesis we chose to use SN to induce bone loss in the tibia because the paralysis is permanent (Botox only lasts 1-2 weeks) and it is generally more complete (Botox injection has to be performed in each muscle group). Botox is more difficult to obtain due to its status as a prescription only medicine and, as mentioned above, may not permit use of the contralateral limb as a valid internal control limb. Lastly, our laboratory has prior experience with using the SN model [8, 11]. Further discussion of disuse models, specific to those chapters is included in the introductions of Chapters 3 and 5.

1.9 Thesis Aims

The aim of the experiments included in this thesis is to use the external bone loading *in vivo* model in mice to characterise the response to altered mechanical loading and how detrimental changes in the response to loading seen with aging are affected by altering the context within which mechanical loading is applied. This aims to inform the hypothesis that altering the context within which mechanical loading is applied, either physically or pharmacologically, will affect the magnitude of the adaptive response to mechanical loading in the aged skeleton, to provide a site-specific and structurally appropriate effect on bone mass in old animals.

The objectives of the experiments described in this thesis were to establish a number of parameters in the regulatory pathways between functional loading and changes in bone architecture. Specifically, these experiments, were designed to establish:-

- 1. The optimal loading duration to elicit a measurable osteogenic response for use in subsequent experiments and the effect of contralateral sham surgery on the pattern of bone loss in the tibia following unilateral sciatic neurectomy. (Chapter 3)**
- 2. Is RANKL involved in bone (re)modelling associated with altered mechanical loading? (Chapter 4)**
- 3. The effect of disuse on the adaptive response of bone in old mice. (Chapter 5)**
- 4. The effect of the antiresorptive bisphosphonate risedronate on the osteogenic response to loading in ambulatory and sciatic neurectomised old mice (Chapter 6)**
- 5. The effect of risedronate on the anabolic effect of PTH and loading on bone in old mice. (Chapter 7)**

Chapter 2

Materials and Methods

Chapter 2: Materials and Methods

All general materials and methods are described within this chapter. Specific materials and methods relating to individual chapters are described later, in corresponding chapters.

2.1 *In vivo* procedures:

2.1.1 Animals

All *in vivo* experiments were performed using female C57Bl/6J wild-type mice purchased from Charles River Laboratories, Margate, UK. Young adult mice were 16 weeks old at the time of delivery to the University of Bristol (UoB). Old mice were at least 19-months old on delivery. Mice were sorted into weight-matched groups after arrival to achieve a similar weight average amongst each group. These mice were then housed in groups of 4-5 for at least one week prior to experiment start to allow acclimatisation to the new environment and cage-mates. Housing was provided in polypropylene cages with sterile wood shavings, a cardboard tube for environmental enrichment and paper bedding. All mice were allowed free access to water and a maintenance diet containing 0.75% calcium (EURodent Diet 22%; PMI Nutrition International, LLC, Brentwood, MO, USA) in a 12-hour light/dark cycle, with room temperature at $21\pm 2^{\circ}\text{C}$. All procedures complied with the UK Animals (Scientific Procedures) Act 1986 and were approved by the ethics committee at the UoB. The principal investigator was the holder of a home office personal license, number PIL 30/9965 working within project license PPL 30/2829.

2.1.2 General Anaesthesia

Materials

- Isoflurane (Isoflo, Abbott Animal Health, Maidenhead, UK)

Equipment

- Anaesthesia induction chamber and anaesthetic machine with oxygen flow regulator and isoflurane vaporizer.

Method

After initial priming of the anaesthetic induction chamber with 100% oxygen at approximately 2L/Min, the induction chamber was infused with isoflurane, initially at 6% vapor. The mice were placed inside the anaesthetic chamber until they were rendered unconscious and laying in recumbent position. Mice were then retrieved from the chamber carefully and then prepared for their given procedure (either surgical procedure or non-invasive loading of the tibia). Mice were maintained under anaesthesia using inhaled isoflurane in 100% oxygen altered to effect (typically around 2%) administered via a mask.

2.1.3 Fluorochrome administration

Materials

- Calcein, alizarin, xylene orange, doxycycline (Sigma chemical company, Dorset, UK)
- 0.9% saline (Hameln pharmaceuticals Ltd, Gloucester, UK)
- 0.22µm bacterial filter (Minisart plus, Sartorius, VivaScience, Hannover, Germany)
- Insulin syringes (BD Micro-fine+ 100IU/ml syringes 1ml, B-D Ltd, Oxford, UK)
- 5ml polypropylene round-bottomed Falcon tubes (B-D Ltd UK, Oxford, UK)
- Aluminium Foil (Sainsbury's Kitchen Foil, Sainsbury's, UK)

Solutions

Calcein, alizarin and doxycycline solutions were made to 10mg/ml. 500mg of powder was mixed with approximately 48ml 0.9% saline continuously until dissolved completely. Sodium bicarbonate powder was added until the pH was at physiological levels (7.3 – 7.4) and saline added to total 50ml solution volume.

Xylene orange was made up to 20mg/ml. 1g of powder was added to 48ml 0.9% saline. The remainder of the mixing process was identical to that for the other fluorochromes.

Once dissolved, solutions were passed through a bacterial filter and aliquots stored in sterile 5ml polypropylene Falcon tubes.

All stages of the process were protected from light with aluminium foil and solutions were immediately stored at -20°C for later use. After defrosting, solutions were thoroughly mixed and passed again through a bacterial filter prior to injection.

Method

Calcein, alizarin, doxycycline (50mg/kg) or xylenol orange (90mg/kg) were injected subcutaneously on the allotted day of the loading/treatment protocol using insulin syringes. The schedule of treatment varied between experiments and will be described in each specific chapter.

Table 1 demonstrates the excitation and emission maxima and the laser type and wavelength used to permit confocal imaging of the bone cross-sections.

Fluoro-chrome	Manufacturer (Product code)	Peak excitation wavelength (nm)*	Peak emission wavelength * (colour)	Laser type/ wavelength (nm)	Concentration (mg/ml)	Dose rate (mg/kg)
Calcein	Sigma (C0875)	494	517 (green)	Argon (488)	10	50
Doxycycline HCl	Sigma (D9891)	390-425	520-560 (yellow)	Diode (405)	10	50
Xylenol Orange	Sigma (227854)	440/570	610 (orange)	HeNe (564)	20	90
Alizarin complexone	Sigma (A3882)	530-580	624-645 (red)	HeNe (564)	10	50

Table 1 – Fluorochromes used for sequential injections and subsequent dynamic histomorphometry experiments.

Data on wavelengths and dose rates from Pautke *et al* [568]

2.1.4 Sacrifice

Materials

- Medetomidine 1mg/ml (Domitor, Vetoquinol, Great Slade, UK)
- Ketamine 100mg/ml (Anesketin, Dechra, Bladel, Netherlands)
- 1ml hypodermic syringe (BD plastipak, Oxford, UK)
- 21G 1 ½" hypodermic needle (Terumo Neolus, Leuven Belgium).

At the end of the scientific procedure, mice were killed humanely in accordance with the UK Animals (Scientific Procedures) Act 1986. Mice were anaesthetised using intraperitoneal injection of medetomidine (1mg/kg) and ketamine (100mg/kg), then, following blood sampling via cardiac puncture, were killed via cervical dislocation.

Following sacrifice and blood collection, both pelvic limbs were dissected from the body via coxofemoral disarticulation. After removal from the pelvis, the distal limb was dissected by femorotibial disarticulation. The common calcaneal tendon was transected and the musculature elevated proximally to allow transection of the muscle origins proximally and tibio-tarsal disarticulation then performed with care not to damage the tibial bone. Following this dissection, management of the isolated tibia and periosteal musculature varied depending on the subsequent experimental techniques planned. Further processing will be described in each relevant section later in this chapter.

2.1.5 Sciatic Neurectomy

Materials

- 0.7 metric EP Polyglactin 910 (Vicryl Rapide, Ethicon, Livingston, UK)
- 0.9% saline (Hameln Pharmaceuticals Ltd, Gloucester, UK)
- Insulin syringes (BD Micro-fine + 100iu/ml 0.5ml 29G insulin syringes, Becton-Dickinson Ltd., Oxford, UK)
- Buprenorphine 0.3mg/ml (Vetergesic, Multidose vial, Alstoe Limited, Sheriff Hutton, UK)
- 2% povidone iodine solution (Vetasept, Animalcare UK, York, UK)

Equipment

- Surgical instruments
- Electric hair clippers

Methods

Following induction of anaesthesia, buprenorphine was diluted 1 in 10 with sterile saline and administered subcutaneously preoperatively at 45-50µg/kg.

The dorsal lumbar spine region from the tail base to the thoracolumbar region and laterally to the level of the stifle joints was clipped bilaterally using electric clippers and then prepared for aseptic surgery using 2% povidone iodine solution. A small skin incision of approximately 5-7mm was made in a craniomedial to caudolateral direction caudodorsal to the right coxofemoral joint. Blunt dissection between the superficial gluteal and biceps femoris muscle was made to expose the sciatic nerve. The nerve was grasped and transected and a 5-7mm segment was excised. The muscles were manually reapposed then the skin wound sutured with one buried simple interrupted suture. In the groups with a sham surgery performed, the skin incision and exposure and visualisation of the sciatic nerve was undertaken but care was taken not to manipulate or traumatise the nerve. The skin wound was closed in the same manner. Following surgery and recovery, mice were returned to their previously determined cage groups until required for killing and sample collection. The exception were groups scheduled for killing at zero hours, which had surgery performed and then prior to anaesthesia recovery, were killed and samples collected, as described later in this chapter. Mice were administered additional buprenorphine subcutaneously if welfare scores were judged to be excessive.

2.1.6 *In vivo* mechanical loading

Equipment

- Electromagnetic materials testing machine (ElectroForce 3100; Bose Co., Eden Prairie, MN, USA).

Method

The *in vivo* non-invasive axial tibial mechanical loading protocol has been previously described [1, 2, 11, 285]. Right tibiae were subjected to external mechanical loading under isoflurane-induced anaesthesia using an electromagnetic materials testing machine. Left limbs were used as internal controls, as validated in previous studies [1, 525].

To apply one episode of mechanical loading, mice were anaesthetised and the flexed knee and ankle joints placed in concave custom-designed cups; the knee was placed in the

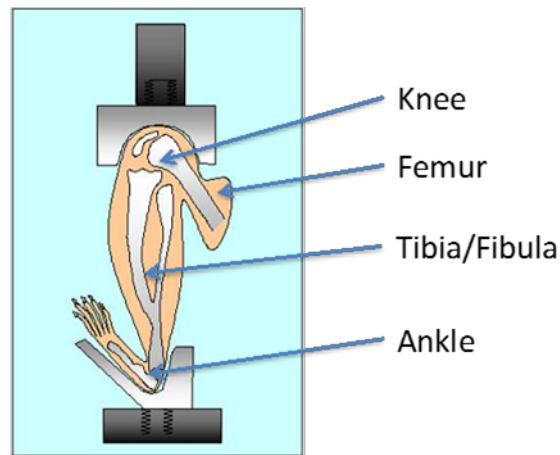


Figure 14 – Schematic diagram indicating the placement of the mouse limb into the loading cups to apply non-invasive axial loading.

The electromagnetic actuator acts on the upper, knee cup and the lower hock cup is positioned over a Load cell which measures the load applied to the limb

upper cup and attached to the actuator arm of the electromagnetic materials testing machine and the ankle in the lower cup attached to a 22N dynamic load cell as shown in Figure 14. The limb is held in place by a continuous static preload of 0.5N upon which the dynamic load is superimposed in a series of 40 trapezoidal shaped pulses; each with a dwell time of 0.05s and a 10s rest period between pulses. The load rates also required variation between groups in order to apply an average strain rate of $30,000\mu\epsilon/s$. This has been previously shown to be equivalent to physiological strain rates [488, 536]. Load rates for individual treatment groups are calculated based on *ex vivo* strain gauging and are detailed in each individual results chapter.

2.2 *Ex vivo* procedures

2.2.1 Ex-vivo strain measurements

Materials

- Ultra-Flexible PVC Lead Wire (NUF36-2550, Cooner Wire Co., Chatsworth, CA, USA).
- Single element strain gauges (EA-06-015DJ-120, Vishay Measurement Group, NC, USA).

- Cyanoacrylate adhesive, catalyst, soldering flux and solder (M-bond 200, Vishay Measurement Group, NC, USA).
- Isopropanol (Sigma, Poole, UK).
- Small self-seal LDPE plastic bags 60x80mm (HK-Pack Krautscheid GMBH, Gelsdorf, Germany)

Equipment

- Materials testing machine (ElectroForce 3100; Bose Co., Eden Prairie, MN, USA).
- Soldering iron (Vishay Measurement Group, NC, USA).
- Ohmmeter (Digital Multimeter, Clarke International, Essex, UK).

Method

In order to apply similar magnitudes of peak strain to bones of mice of different treatment groups, we first established the strain:load relationship *ex vivo* in a sub-sample of 5-6 mice from each treatment group as previously described [11, 285, 418, 569].

Before gauges could be attached to the tibiae, wires had to be attached to the solder points of the strain gauge indicated by the red arrows in Figure 15. Appropriate lengths of

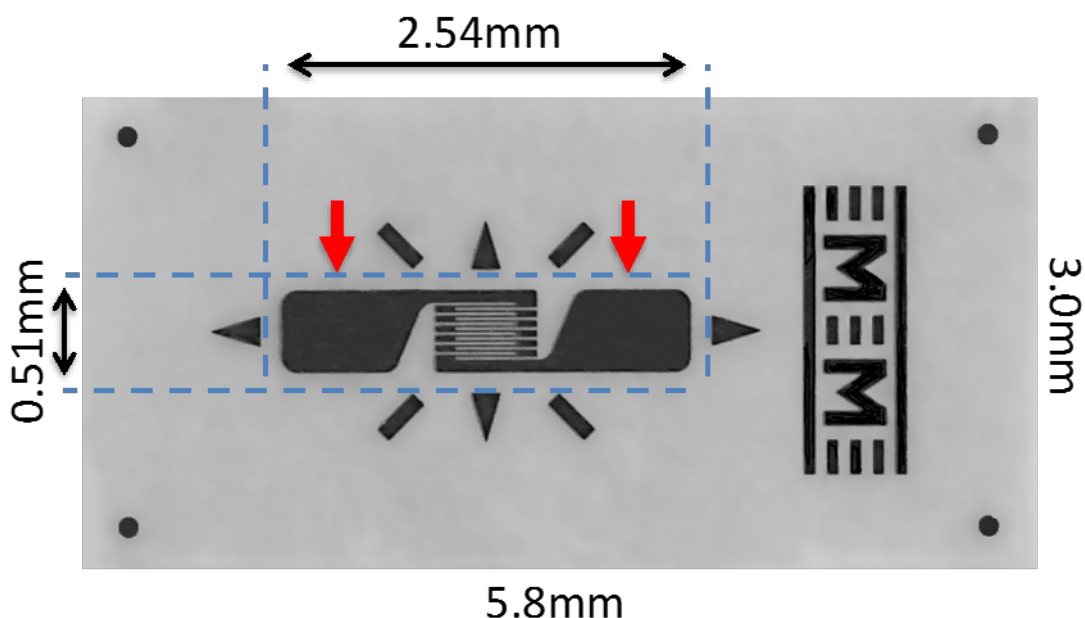


Figure 15 – Strain gauge used for tibial strain measurements.

Red arrows indicate solder points for wire attachment. Dotted lines indicate final gauge size after trimming

wire were cut from the reel and the PVC insulation carefully removed from both ends of the wire using a No.11 scalpel blade under the dissecting microscope, taking care not to damage the internal strands of wire. Next the wires were dipped into soldering flux and then solder was applied using a soldering iron. The excess plastic was then trimmed from the left side of the gauge using the base of the arrowhead as a cutting guide. The plastic film over the soldering points was then scratched off using a needle, flux applied using a trimmed down toothpick and then solder attached. Next, the solder on the gauge solder points was heated with the soldering iron and the wire inserted. Finally, the remaining three sides of the gauge were trimmed down using the bases of the arrowheads as cutting guides Figure 15. Figure 16 shows the finished gauge prior to application to the tibia. After completion, the resistance of the gauge was tested using an ohmmeter. A reading of $120\pm 0.3\Omega$ indicated no damage to the gauge element had occurred during soldering of wires. If the reading was outside of this range then the gauge was discarded, as there would be a concern that the strain reading would not be accurate.

Following appropriate experimental treatment, all mice were killed via a recognised Schedule 1 killing method (see section 2.1.5) and entire right hindlimbs were collected by disarticulating the hip joint, whilst preserving as much proximal skin and soft tissue as possible to allow normal skin coverage of the limb when loading into the materials testing machine. Limbs were stored at -20°C in labelled self-seal plastic bags. 30 minutes prior to use, limbs were brought up to body temperature in a water bath set to 37°C . The limb was positioned under a dissecting microscope with the medial aspect facing upwards and pinned into position. The skin was incised with a No.11 scalpel blade from the proximal end of the tibia to approximately the mid-shaft and the fascia covering the periosteum divided. The periosteum was then elevated to expose the tibial surface. The area was “de-greased” using isopropanol to aid adherence of the strain gauge. In each mouse, the previously prepared strain gauge was then attached using cyanoacrylate adhesive in longitudinal alignment to the medial aspect of the tibia at 37% of its length measured from the proximal end following manufacturer’s recommendations. The plastic backing of the strain gauge was dipped in the catalyst, excess blotted off and then dipped in the adhesive. The gauge was then placed on the bone and held in place for 60 seconds by applying direct

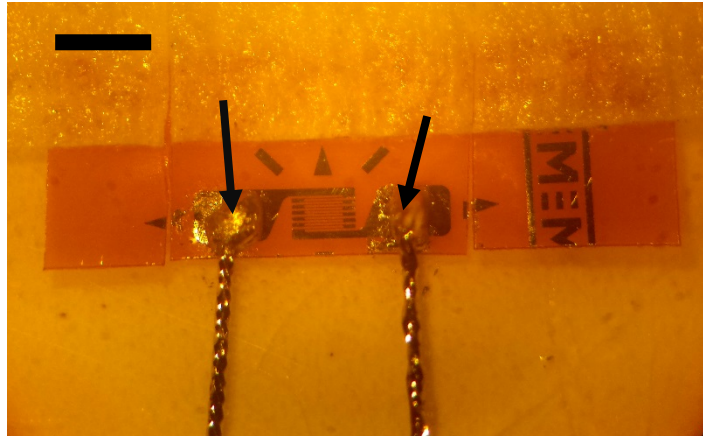


Figure 16 – Photomicrograph of strain gauge preparation for *ex vivo* strain measurement on murine tibias.

Solder points (arrows) with wire attached. The side cuts have been made and the top cut is all that remains to be made. The top edge of the gauge is immobilised by masking tape. The scale bar indicates 0.5mm.

pressure to the solder points of the gauge to avoid damage to the element. Adhesion was confirmed by applying gentle lateral pressure to the solder points.

Previous studies have shown that the 37% site corresponds to the site of greatest osteogenic response to similar loading in young adult female C57Bl/6 mice [1]. Strains were measured at a static preload of 0.5N and across a range of peak compressive loads between 5 and 19N, at a load rate of 500N/s. Using the strain gauging data, the appropriate peak loads were selected for use in the later experiments. Due to slight variability in achieving the exact requested peak loads, the actual peak load achieved for each repeat was plotted as a scatter plot against the strains achieved and linear regression calculations were made for each treatment group to determine the average strain achieved for a given load/force. The formula for each regression line was used to generate the load required for the desired strain. These peak loads were applied using the same electromagnetic materials testing machine used for *in vivo* loading later. The strain rate was also altered to achieve a strain rate of $30000\mu\text{E}s^{-1}$.

2.2.2 High resolution micro-computed tomography (μ CT) analysis

Materials

- PVC-free cling film (Sainsbury's, UK).
- Drinking straw
- 1ml hypodermic syringe (BD plastipak, Oxford, UK)
- 70% Ethanol (EOH) solution.

Equipment

- μ CT scanner and software (SkyScan 1172, Bruker, Kontich, Belgium).
 - Skyscan programmes used: NRecon, CTAn.

Method

Because mouse bones are small and the axial loading-related osteogenesis is site-specific [1, 7], high-resolution μ CT was the primary technique used to quantify three-dimensional bone architecture at precisely comparable sites of the loaded and contra-lateral control limbs, as previously described (Sugiyama *et al.*, 2010b; 2011; 2012a; Meakin *et al.*, 2013). The lower legs were stored in 70% EOH and mounted in a plastic tube wrapped in plastic film to prevent drying during scanning. During later experiments in this thesis, the bones were held within 1ml polypropylene syringes filled with 70% ethanol and held in position with the rubber stoppers from the syringe. The whole tibiae and surrounding muscles were imaged in the SkyScan 1172 (SkyScan, Kontich, Belgium) with a voxel size of $4.8\mu\text{m}$ ($110\mu\text{m}^3$). The applied x-ray voltage was 50 kV, current of 200mA, with 0.5mm aluminium filtration. The scans were over 180 degrees with a 0.6-degree rotation step. The images were reconstructed and binarised with global thresholding (Values: 1.000-1.160) using the NRecon SkyScan software.

Following a camera upgrade in the μ CT scanner in 2014, prior to the experiments performed for experiments in chapter 6 and 7, from a 1.3megapixel (MP) sensor to an 11MP sensor, images scanned had a slightly different voxel size of $4.78\mu\text{m}$ and applied voltage of 49kV, but still with a current of 200mA and using a 0.5mm aluminium filter. The scans were still performed over 180 degrees with a 0.6-degree rotation step, however

scanning did benefit from 2 x frame averaging to reduce the noise experienced due to the newer, more sensitive camera sensor. Otherwise, all remaining processing steps were the same.

Structural parameters were calculated using the SkyScan software for cortical bone (0.5mm long section at the desired site of the tibia's longitudinal length from its proximal end) and trabecular bone (secondary spongiosa; 0.25 – 0.75mm distal to the proximal tibial growth plate). Cortical sites examined included 25%, 37%, 50% and the 75%, although due to development of Site Specificity Analysis (SSA)[7] during the latter parts of the experimental periods for this thesis, only the 37% site and trabecular site was examined using the traditional single-site technique and the remainder of the cortical bone was assessed using SSA (see section 2.2.3).

Selection of the trabecular region of interest (ROI) was selected by hand and consisted of an irregular, anatomic region of interest adjacent to the endocortical boundary. All other ROIs were selected using automated task lists generated in the CTAn programme. The details of the task lists used in trabecular bone, young mouse cortical bone, old mouse cortical bone (larger transcortical perforations), and specific tasks lists to calculate cortical bone porosity (excluding the medullary cavity from the ROI for calculation of pores), and trabecular region cortical porosity and included in Appendix 1.

According to the ASBMR guidelines for assessment of bone microstructure in rodents using μ CT [570], we evaluated bone mass and architecture and changes due to loading [(right – left) / left] in cortical bone area (Ct.Ar), total cross-sectional area inside the periosteal envelope (Tt.Ar), marrow area (Ma.Ar), cortical thickness (Ct.Th), polar moment of inertia (PMI) and cortical area fraction (Ct.Ar/Tt.Ar) at the cortical sites. The additional task lists were generated to create a specific ROIs to isolate the cortical bone without the medullary cavity to enable the calculation of cortical bone porosity (Ct.Po) and the trabecular region cortical/trabecular porosity (Tb.Ct.Po) following exclusion of the medullary space. Bone volume fraction (BV/TV), trabecular number (Tb.N), trabecular thickness (Tb.Th), trabecular separation (Tb.Sp), structure model index (SMI) and

trabecular pattern factor (Tb.Pf) were calculated for the hand-selected trabecular bone ROI.

In experiments where sciatic neurectomy was performed, muscle area (Mu.Ar) was also assessed at the 50% site. Mu.Ar was drawn manually around the perimeter of the soft tissue envelope for one slice, and each group averaged. This was used in chapters 4, 5 and 6 to document muscle atrophy to confirm that neurectomy had been successful, as previously described [11].

2.2.3 Site Specificity Analysis of tibial cortical bone

Materials

- Site Specificity Analysis programme [7]

Methods

The full technique is taken from and described in detail in [7]. Briefly, mouse tibiae were scanned with high resolution μ CT and reconstructed as above. The sequentially labelled cross-sectional images from a single bone were placed in a folder called the “in path” for site specificity analysis. The “output” folder is created inside each “in path” folder. MatLab (R2015a) was then used to open the site specificity program script [available freely online at the journal page for [7]]. This program was then run as a standard script in MatLab to select and analyze the cross-sectional μ CT slices of the tibia corresponding to each 1% of the bone’s length.

After bone thresholding to binarise the image into “bone” and “non-bone”, site specificity isolates the tibia, excludes the fibula, then calculates Ct.Ar and the enclosed non-bone area (Ma.Ar). Initial output from the MATLAB script includes Ct.Ar and Ma.Ar and areas are presented in pixel area. Therefore, our scans are performed so isotropic pixels dimensions represent 4.78 μ m. By adding the values for Ct.Ar and Ma.Ar, a value for Tt.Ar is achieved. If the cortex is incomplete in a given section, the Ma.Ar calculation is unreliable and thus Tt.Ar cannot be calculated for that individual slice. Ct.Ar is still reliable, however. When examining normal young adult mice, there are rarely defects in the cortex which penetrate the whole cortex in a single given slice, as nutrient vessels and cortical defects usually enter oblique to

the cortex. Cortical defects are more frequent in the trabecular bone and distal tibia such that we can only reliably calculate the 76 slices between 15 and 90th percentile length. In addition, these errors become more frequent following aging and also following treatment with certain pharmaceuticals, and following disuse, due to the decreased bone mass, reduced Ct.Th and/or increase in cortical porosity.

After generation of the initial Ct.Ar and Ma.Ar data, saved *.bmp images are then imported into the freely available BoneJ programme [571, 572] for generation of cross-sectional thickness for each slice. BoneJ also generates several other morphometric parameters, which can be of pertinence in given situations, but we were primarily interested in basic morphometric parameters which can detail evidence of bone formation or loss at a given site.

Where necessary, the saved binarised images were also analysed using the CtAn programme as above. This can also generate slice by slice measures as detailed in the standard μ CT image analysis section in 2.2.2 for each image, corresponding to a certain percentile length, except for Cortical Thickness calculations, which are calculated based on a 3D model reconstruction in Ct.An, so therefore are not generated for each slice as output from CTAn.

All data were then imported into a custom Excel spreadsheet as described in the Galea *et al* [7] publication to permit generation of treatment group data and subsequent relevant analysis.

Statistical analysis was performed using SPSS (Version 23, IBM Corp, Armonk, NY). The data were analysed using a Mixed-model approach considering the relevant treatments as a fixed effect and the bone site as fixed categorical parameter. Mouse ID was also included as a random effect to account for the left and right limbs coming from the same animal. Sidak post-hoc adjustments were carried out if any of the effects were significant at $p < 0.05$.

2.2.3 Quantitative Real-Time Reverse Transcription Polymerase Chain Reaction (qRT-PCR)

2.2.3.1 Dissection

Materials

- RWT buffer (RWT Buffer, Qiagen, Crawley, UK) with β -Mercaptoethanol (Sigma Chemical Company, Dorset, UK) added at 10 μ L/ml
- Liquid nitrogen (BOC, Bristol, UK)
- Dry Ice (VWR, Lutterworth, UK)
- Sterile serum-gel 1.3ml blood collection tubes (Idexx laboratories, Wetherbridge, UK)
- Molecular Grade Ethanol (Sigma Chemical Company, Dorset, UK)
- 1.5ml microcentrifuge tubes (Crystal Clear, E1415-1500, Starlab, Milton Keynes, UK)
- NUNC Cryotubes vials 1.8ml #340711 (Thermo Scientific, Roskilde, Denmark)
- Sterile, RNase-free filtered pipette tips; 200 and 1250 μ L (Elkay laboratory equipment, UK)

Equipment

- Microcentrifuge (Heraeus Fresco 17, Thermo Scientific, Waltham, MA, USA)
- Manual pipette (ErgoOne, Starlab, Milton Keynes, UK)

Methods

Following sacrifice and leg dissection as described in section 2.1.4, the tibia was sectioned through all bone and other soft tissue just proximal to the distal physis, then muscles and tendons were removed in a disto-proximal direction to expose the proximal tibial and fibular region. The proximal tibia/fibula was then cut just distal to the proximal physis. A dry lint-free tissue was used to remove the periosteal tissue as much as possible. Following this, the tibia bone was placed in a sterile pipette tip trimmed to fit the distal bone end in it and placed with the bone uppermost in a 1.5ml microcentrifuge tube. The bone and tube were then centrifuged at 8000g at 4°C for 15-20 seconds. This process aimed to displace the bone marrow and blood from the marrow cavity and leave just a cortical bone sample containing predominantly osteocytes, but with some osteoclasts and osteoblasts present on the bone surface. Following centrifugation, the tibial bone sample was placed in a cryo-tube and snap

frozen by placement into liquid nitrogen. Following this, the bones were stored at -80°C until further needed. The tissue pellet of bone marrow collected in the centrifuge tube was resuspended in 600µL of RWT buffer with 10µL/ml β-mercaptoethanol. The resuspended tissue pellet was snap frozen by immersion of the tube in liquid nitrogen then stored at -80°C. Tibial cortical bone tissue and marrow collection was adapted from that previously reported in our laboratory and elsewhere [86, 419, 573]. In some instances, the left femur was also prepared in a similar manner as a control cortical bone sample – the right femur was not collected as the loading process would inevitably exert some force on the distal femur as the axial loading through the knee requires compression of the distal femur.

2.2.3.2 RNA extraction from tibia

Materials

- RNeasy™ Plus Universal Mini kit; QIAzol Lysis reagent (Qiagen, Crawley, UK)
- Molecular Grade chloroform and ethanol (Sigma Chemical Company, Dorset, UK)
- Ultrapure DNase/RNase free distilled water (Invitrogen, Paisley, UK)
- 2.0ml low-bind safety lock tubes (Eppendorf, Fisher, Loughborough, UK)
- 7mm RNase-free, DNase free stainless steel balls (Qiagen, Crawley, UK)

Equipment

- Manual pipette (ErgoOne, Starlab, Milton Keynes, UK)
- Microcentrifuge (Heraeus Fresco 17, Thermo Scientific, Waltham, MA, USA)
- Tissuelyser LT (Qiagen, Crawley, UK)
- Spectrophotometer (Nanodrop 1000 Thermo Scientific, Waltham, MA, USA)

Methods

RNA extraction and purification was performed using a commercially available kit. Bones were removed from -80°C and placed in a 2ml Safety-lock microcentrifuge tube with a 7mm stainless steel ball-bearing which had been pre-cooled to -80°C. The tube was left to stand for 2 minutes before addition of 900µL of QIAzol tissue lysis reagent. The tubes were then placed directly into the Tissuelyser LT and agitated at 50Hz for 5 minutes each to homogenise the bone. In groups where there were more samples than would fit in the Tissuelyser LT at once, half of the treated (right) tibial samples and half of the control (left) tibial samples were

homogenised consecutively. Following the homogenisation, the samples were checked for adequate homogenisation of the bone, and in cases where this was not sufficient, a further 2 minutes of agitation in the TissueLyser LT was performed. Following this step, all samples were processed together. After aspiration of the homogenised bone/lysis buffer mix into a new tube, tubes were allowed to stand for 5 minutes to allow dissociation of nucleoprotein complexes. Following this, 100µL of gDNA Eliminator Solution was added to each sample and the sample vigorously shaken for 15s then 180µL chloroform was added to each sample and the sample vigorously shaken for another 15s to precipitate protein. After allowing to stand at room temperature for 2-3 minutes, the sample was then centrifuged at 12,000g at 4°C for 15 minutes and the upper aqueous phase was carefully transferred to a new tube to ensure protein and mineral contamination was minimised. The supernatant was placed in an equal volume of 70% ethanol, diluted using RNase/DNase free water.

Half of the sample was added onto the spin column and placed in a centrifuge at 13,000rpm for 15s. The flow through was discarded and this step repeated so the entire sample had been passed through the spin column. Next, 700µL of buffer RWT was added onto the spin column and centrifuged for 15s. The flow through was discarded then 500µL buffer RPE added onto the column. This was centrifuged for 15s and the flow through discarded. This step was repeated but the second spin was extended to 2mins. Next, the spin column was placed in a new collection tube and centrifuged for 1min to completely dry the spin column and ensure removal of all ethanol contained in the RPE buffer. Finally, the spin column was placed in a new collection tube and 35µL of RNase/DNase free water placed directly onto the spin column before centrifugation for 1 min to elute the RNA.

The concentration of purified RNA was then directly quantified on the spectrophotometer using RNase/DNase free water as the control. In addition to recording the concentration of RNA in the elute, the 260/280 wavelength ratio and absorbance curve were also assessed to determine the degree of protein or DNA contamination of the sample.

2.2.3.3 Agarose gel electrophoresis to assess RNA quality

Materials

- Ethidium bromide; gel loading dye; 50 base-pair ladder (Sigma Chemical Company, Dorset, UK).

- Low melting point agarose (Invitrogen, Paisley, UK).
- 50x TAE buffer (AppliChem, Darmstadt, Germany).

Equipment

- Manual pipette (ErgoOne, Starlab, Milton Keynes, UK)
- UV transilluminator and camera (UVP Lab Product, Cambridge, UK).
- Gel electrophoresis tank (Bio-rad, Hemel Hempstead, UK)

Solution

TAE buffer: 50x TAE buffer stock solution was diluted to 1x by the addition of 4ml 50x TAE to 196ml distilled water.

1% agarose gel: 1g agarose powder was added to 100ml 1x TAE buffer. The mixture was dissolved by heating for 1min on full power in the microwave, stirring intermittently. 2 μ L of 10mg/ml ethidium bromide was then added to complete the solution.

Methods

The hot agarose solution was poured into a gel tray and left to cool with the appropriate number of lanes. Once set, the gel in the tray was placed in the electrophoresis tank and topped up with 1x TAE buffer to ensure the gel was fully submerged. 5 μ L of the RNA sample was added to 1 μ L loading dye which was mixed and loaded into each lane. Bands were

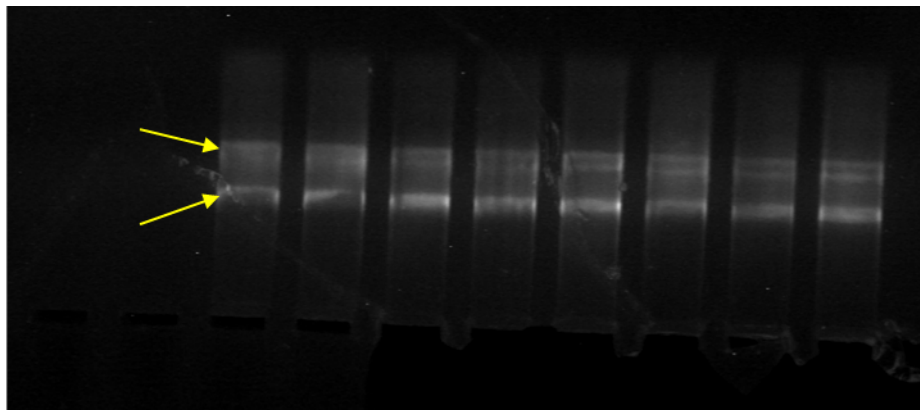


Figure 17 Representative agarose gel electrophoresis image run from young mice femoral cortical bone.

The loading wells are at the bottom of the image and the bands visible represent the 18s (lower band) and 28s (upper band).

separated by applying 200V for approximately 25mins until the dye had run half way across the gel. The bands were visualised by placing the gel on the UV transilluminator and a greyscale image captured of the gel (Figure 17). Two distinct bands were identified corresponding to the 18S and 28S RNA strands to ensure no significant amount of RNA degradation had occurred during specimen processing and RNA extraction.

2.2.3.4 cDNA synthesis

Materials

- Quantitect Reverse Transcription Kit (Qiagen, Crawley, UK)

Equipment

- DNA Thermal Cycler (Mastercycler Eppendorf Gradient, Eppendorf UK Ltd., Cambridge, UK)
- Electronic pipette (Starpet E, Starlab, Milton Keynes, UK)

Method

Synthesis was performed using a commercially available kit following the included instructions. Template RNA samples were thawed on ice and gDNA wipeout buffer, Quantiscript reverse transcriptase, Quantiscript RT Buffer, RT primer mix and RNase-free water were thawed at room temperature then tubes were briefly centrifuged to collect residual liquid from the tube sides. The genomic DNA elimination reaction was prepared on ice by adding up to 0.75µg (up to a maximum of 12µL) RNA to 2µL gDNA wipeout buffer before adding RNase/DNase free water to make a final volume of 14µL. This initial mixture was heated to 42°C for 2 minutes to eliminate any genomic DNA contamination. The reverse transcription master mix was prepared to include 1µL Quantiscript Reverse Transcriptase, 4µL Quantiscript RT buffer and 1µL RT Primer mix per reaction. Following the gDNA elimination step, the tubes were immediately removed from the heating block and cooled quickly on ice. Each tube then had 6µL of master mix added to it and then was incubated at 42°C for 15 minutes and heated further to 95°C for 3 minutes to inactivate the Reverse Transcriptase enzyme. The cDNA was stored at -80°C and thawed out for RT-PCR as required.

2.2.3.5 qRT-PCR

Gene specific standards

Materials

- Sybr Green JumpStart Taq ReadyMix (Sigma Chemical Company, Dorset, UK)
- Gene specific primers, as listed in table 1 (Eurofins-MWG, Ebersberg, Germany)
- QIA quick gel extraction kit (Qiagen, Crawley, UK)

Equipment

- DNA Thermal Cycler (Mastercycle Eppendorf Gradient, Eppendorf UK Ltd., Cambridge, UK).
- UV transilluminator (UVP Lab Product, Cambridge, UK)
- Nanodrop ND1000 (Labtech International, Ringmer, East Sussex, UK)
- Manual pipette (ErgoOne, Starlab, Milton Keynes, UK)
- Electronic pipette (Starpet E, Starlab, Milton Keynes, UK)

Methods

Lyophilised specific forward and reverse primers were dissolved in RNase/DNase free water to obtain a 100pM stock solution for each primer. The primer mix was then prepared by adding equal volumes of forward and reverse primer and diluting tenfold with RNase/DNase free water to make a final specific primer mix containing 10pM each forward and reverse primer. The primer stocks and primer mixes were stored at -20°C. Following RNA extraction and cDNA synthesis, 3µL of template cDNA was added to 2µL gene specific primer mix, 20µL RNase/DNase free water and 25µL Sybr Green.

The thermal cycler was programmed to perform an initial enzyme activation step of heating to 95°C for 2 minutes, followed by 40 cycles of 15s incubation at 95°C, 25s at the specific primer annealing temperature (shown in Table 1) followed by a 30s extension time at 72°C. Following the 40 cycles, the samples were chilled to 4°C.

Gene	Primer sequence (F then R)	Amplicon Length	T _M (°C)
RANKL (<i>Tnfsf11</i>)	CAGCATCGCTCTGTTCTGTA	107	60
	CTGCGTTTTTCATGGAGTCTCA		
SOST (<i>Sost</i>)	TGCCGCGAGCTGCACTACAC	81	60
	CACCACTTCACGCGCCCGAT		
β2-MG	ATGGCTCGCTCGGTGACCCT	110	60
	TTCTCCGGTGGGTGGCGTGA		
OPG (<i>Tnfsfr11b</i>)	TGTGTGTCCCTTGCCCTGACCA	132	60
	ACACTCGGTTGTGGGTGCGG		

Table 2 - Primer Sequences and amplicon length for genes of interest

Following PCR, the samples were checked for quality by running through a 2% agarose gel (prepared as described in section 2.2.3.3, but with twice the amount of agarose) to confirm a single band at the appropriate position in the agarose gel. Under UV light assisted visualisation and the band was excised from the gel using a sterile number 22 scalpel blade.

The product could then be extracted from the gel using the commercially available kit following manufacturer's instructions. The sample was weighed and placed in a microfuge tube with three times the volume of Buffer QG (from QIA quick gel extraction kit). This was incubated at 50°C for 10 minutes in a water bath, mixing every 2-3mins until the sample was completely dissolved. 1 gel volume of isopropanol was then added and 800µL of the solution placed on the provided spin column, centrifuged for 1min at 13,000rpm and the flow through discarded. This was repeated until the entire sample had been passed through the spin column. 500µL buffer QG was then passed through the column by centrifuging for 1min to remove all traces of agarose gel. The sample was washed by passing 750µL buffer PE through the column by centrifuging for 1min. After discarding the flow through, the column was spun for an additional minute to remove all traces of ethanol which is contained in buffer PE. Finally, the column was placed in a new microcentrifuge tube and the DNA eluted using 50µL RNase/DNase free water. The concentration of DNA was quantified using a spectrophotometer. The following website: <http://www.uri.edu/research/gsc/resources/cndna.html>, was then used to calculate total copy number based on the amplicon length (reported in the relevant primer paperwork) and the quantity of RNA in ng/µL. From this

website, the following equation was used to calculate the number of copies per μL based on the concentration and amplicon length;

$$\text{number of copies} = (\text{amount} * 6.022 \times 10^{23}) / (\text{length} * 1 \times 10^9 * 650)$$

This calculation is based on Avogadro's constant and the assumption that the average base pair weighs 650Da. This was then diluted to the nearest ten-fold dilution e.g. 1×10^{11} or 1×10^{10} copies/ μL . Ten-fold serial dilutions were then obtained from the highest concentration down to 1×10^1 copies/ μL . The serial dilutions of the primers were then used as control samples to determine a standard curve for each gene – this permitted quantification of the amount of gene product in the experimental samples.

qRT-PCR

Materials

- Sybr Green JumpStart Taq ReadyMix (Sigma Chemical Company, Dorset, UK)
- 384 well PCR plates (Life Technologies, Paisley, UK)
- PCR adhesive plate covers (Life Technologies, Paisley, UK)
- RNase/DNase free water (Qiagen, Crawley, UK)

Equipment

- 7900HT Fast 384-well qPCR machine (Applied Biosystems, Abingdon, UK)
- Chromo4 Real time PCR detection system (Bio-Rad Laboratories Ltd., Hertfordshire, UK).
- 2-20 μL and 10-200 μL electronic multipipettes (Starlab, Milton Keynes, UK).

Methods

A 10 μL reaction volume was used containing 5 μL Sybr Green ReadyMix, 3 μL RNase/DNase free water, 1 μL sample or standard and 1 μL primer mix. A standard curve was produced for each gene using the serial dilutions from section 2.2.3.5 to enable quantification of the samples. The protocol consisted of an initial enzyme activation incubation step of 2min at 95°C. There were then 40 cycles each consisting of a 15s incubation at 95°C, 15s at the specific primer annealing temperature listed in table 1, and then 35s extension at 72°C. The fluorescence was detected after each extension cycle. Finally, a melting curve was performed, to ensure only a

single product had been amplified, from 60 to 95°C reading the fluorescence every 0.5°C. Samples were analysed in triplicate and the standard curve in duplicate. The threshold was determined manually for each gene in the linear range of amplification. Using the formula derived by the line of best fit for the exponential results of the standard curve, the copy number per sample was calculated for the house-keeping gene and the genes of interest. A relative gene expression value, calculated as a ratio of the amount of $\beta 2$ Microglobulin in the sample, gave a representative value to help normalise and account for variance in amount of starting material.

2.2.4 Tissue fixation and decalcification

Materials

- Paraformaldehyde (PFA), phosphate buffered saline (PBS) tablets, sodium hydroxide pellets (NaOH), hydrochloric acid (HCl) (Sigma, Poole, UK).
- Ethylenediaminetetraacetic acid (EDTA, Fisher Scientific, Loughborough, UK).
- Whatman 2V filter (Whatman International Ltd., Maidstone, UK).

Solutions

4% PFA – 20g of PFA powder was added to ~450ml PBS and heated to 56°C to dissolve the powder with continuous stirring. 2-3 pellets of NaOH were added to clarify the solution and cooled. The pH was adjusted to 7.4 using concentrated HCl as necessary. Finally the volume of the solution adjusted to make 500ml using dH₂O and was filtered using a Whatman (2V) filter before storage at -20°C.

14% EDTA – 250g of EDTA powder was added to ~1.5l of dH₂O. The solution was heated to 75°C with continuous stirring for approximately one hour to dissolve the powder. Approximately 25g of NaOH was added to adjust the pH to 6.8-7.0 and the solution cooled. The final volume was adjusted to make 1.75l EDTA.

Method

Dissected limbs were fixed in 4% PFA for 48hrs at 4°C before further dissection. Bones were then washed thoroughly for one hour under running tap water before decalcification in 14% EDTA for 28 days at 4°C. The EDTA solution was changed three times per week.

Satisfactory decalcification was confirmed by scanning the limbs using μ CT and comparing the radio-density of the bone with surrounding muscle. If no difference was observed then paired bones were washed thoroughly under running tap water for 12 hours then processed for embedding.

2.2.5 Paraffin embedding and sectioning

Materials

- Silane coated slides (Histobond Plus – Marienfeld, Lauda-Königshofen, Germany)
- Paraffin

Equipment

- Automated histology processor (Leica Histokinette[®], Leica Microsystems, Milton Keynes, UK)
- Microtome (MICROM HM 355 S, Microm, Thermo Fischer Scientific, Loughborough, UK)
- Nikon 50i microscope (Nikon instruments, Surrey, UK).
- DP72 digital camera (Olympus, Center Valley, PA, USA).

Method

After washing under running tap water, bones were dehydrated using increasing concentrations of EOH; 30%, 50% and 70% for one hour in each concentration. Bones were then processed for wax embedding using an automated processor using a standard 24hr histology protocol.

6 μ m transverse sections were cut on a rotary microtome in the region corresponding to the 37% site of maximal osteogenic response to loading, as determined by μ CT [1]. Sagittal longitudinal 6 μ m thick sections of the proximal tibial epiphysis were also made after the proximal bone transverse sections had been collected. Sections were floated onto silane-coated slides and then heated on a block at 65°C for 20 minutes to aid adherence of bone sections.

2.2.6 Sclerostin and RANKL immunolocalization

Immunolocalisation techniques were only performed studies described in Chapter 4, and as such are described in detail in that chapter. Furthermore, a tabulated version of the immunostaining protocols for both Sclerostin and RANKL are included in Appendix 2.

2.2.7 Bone embedding in methylmethacrylate

Materials

- Analytical grade Ethanol, xylene (Fisher Scientific, Loughborough, UK)
- Methylmethacrylate, dibutyl phthalate (Fischer Scientific, Loughborough, UK)
- Benzoyl Peroxide (Millipore, Nottingham, UK)
- Polypropylene 1000ml containers (VWR, Lutterworth, UK)
- 20ml polypropylene specimen container (Securtainer III, Simport, Biloeil, QC, Canada)

Solutions

- MM I – 80% MMA, 20% dibutyl phthalate
- MM II – 100ml MM I plus 2g benzoyl peroxide as polymerisation accelerant
- MM III – 100ml MM I plus 3g benzoyl peroxide as polymerisation accelerant

Each solution was created on the morning of the day before it would be used then allowed to mix for the whole day on a magnetic stirrer whilst sealed in an airtight container. In the evening it was taken off the stirrer and placed in the sealed, air-tight polypropylene container in a spark-free refrigerator. On the morning it was to be used, it was removed from the refrigerator and allowed to come to room temperature, so as to avoid moisture condensation to contaminate the solution. The new solution was then exchanged with the previous solution.

Method

After sacrifice and μ CT scanning, bones were placed in histology cages and stored in a 1000ml clear polypropylene airtight container. They were sequentially placed in incrementally increasing concentrations of ethanol solution (80, 95, 100, 100, 100%) for 24 hrs at each concentration. The bones were then placed in 100% xylene for 24hr and 50:50 xylene:methylmethacrylate solution for 24 hr. These steps were performed at 4°C. Following

this, the bones were infiltrated with MM I, MM II and MM III for two days each, with daily changes of solution. All steps involving MM solutions were performed at room temperature during the day and then refrigerated to 4°C overnight. All stages were conducted with containers placed on an orbital shaker platform oscillating at 60-70Hz, both in the refrigerator and outside. When outside, the container was protected from light by positioning a cardboard box over the top of the container. Following this infiltration protocol, the bones were prepared for embedding. This involved placing the bones in individually labelled 20ml glass scintillation vials with a pre-polymerised bed of approx. 5-7mm of MM III in the bottom of the vial. The bones were then covered with MM III and positioned centrally on the bed. The caps on the vials were tightly shut to ensure airtightness, and then they were placed in a warm water bath at 37-39°C to promote polymerisation and then act as a heat sink to draw off the thermal energy created by the exothermic reaction and prevent boiling of the solution and bubble formation.

All steps were protected from light to minimise photobleaching of the fluorochrome labelling within the bones.

2.2.8 MMA embedded bone sectioning and visualisation using confocal microscopy

Materials

- Silane coated slides (Histobond Plus – Marienfeld, Lauda-Königshofen, Germany)
- Dental wax
- Double sided, adhesive tape (Staples Office Supplies, UK)
- Slide mounting medium (Permount, Fisher Scientific, Loughborough, UK)

Equipment

- Band-saw (Makita, Milton Keynes, UK)
- Leica SP5-AOBS confocal laser scanning microscope attached to a Leica DM I6000 inverted epifluorescence microscope. (Leica Microsystems, Milton Keynes, UK)
- Microslice II annular diamond saw (Cambridge Instruments, Cambridge, UK)
- Osteomeasure histomorphometry programme (Osteometrics, Decatur, GA, USA)

- ImageJ image analysis programme (US National Institute of Health, Bethesda, MD, USA)

Method

Plastic embedded bones were trimmed to rectangular blocks using a small band saw, then mounted on the rotary arm of the annular diamond saw. Blocks were fixed in position using melted dental wax and ensuring the bone axis was perpendicular to the cutting plane of the saw.

Sections were cut every 250µm from 45% of the bone length to 30%, measured from the proximal end. This was performed to include the load responsive region (37%) of the bone following loading. These bone sections were then mounted on glass slides using a double-sided adhesive strip. Permount embedding media and a glass cover-slip was then used to generate a clear medium for later laser confocal imaging. Images of fluorochrome labels were then acquired using the confocal microscope and 10x objective lens.

Images were captured using three different excitation laser wavelengths; Argon (488nm) for Calcein, Diode (405nm) for Doxycycline and HeNe (564nm) for Alizarin and xylenol orange.

A sequential image scan was performed of the entire transverse section of the bone at 37% of the length of the bone measured from the proximal end. These individual tiles were then fused in a mosaic to form one image of the entire bone cross section, with a pixel size of 378.8nm. Images were captured as 3 separate wavelengths and then merged in the proprietary Leica imaging programme. Files were then exported and saved as *.tif RGB format files in intel byte order without data compression using the ImageJ computer programme. This was to allow importing and measurement in the Osteomeasure programme. Identification and tracing of the fluorescent bone labels allowed automated calculation of single and double labelled perimeter, interlabel distance, marrow apposition rate and bone formation rate as necessary. This was performed for the endocortical and periosteal surface in each specimen.

Chapter 3

Optimising *in vivo* experimental models
for changing the mechanical
environment of the mouse tibia

Chapter 3 – Optimising *in vivo* experimental models

3.1 Introduction

The murine tibia provides, within a single bone, the opportunity to thoroughly interrogate the effects of altered mechanical loading. Non-invasive application of load to the tibia has been described using several models, including four-point and cantilever bending models, and axial compression [2, 517, 519]. These models are described in more detail in the general introduction of this thesis. The tibial axial compressive loading model was developed to enable study of both trabecular and cortical bone adaptation to mechanical loading in the same bone [2]. The model also permits genetic [232, 574], surgical [11, 286, 287] and pharmacological interventions [32, 34, 287, 575]. This model is now considered the gold-standard for study of bone's adaptive response to mechanical loading in rodents. Since it was first described by our laboratory [2], we have used the non-invasive axial tibial loading model extensively to study the adaptive loading response in mice [8, 11, 29, 285, 418, 574, 576, 577].

One advantage of the tibial model is that it can be used in both use and disuse situations. Disuse induced by unilateral sciatic neurectomy (SN) permits assessment of disuse-associated bone loss in trabecular and cortical bone concurrent to additional genetic [578], surgical [137] or pharmacological interventions [460]. SN in mice is also useful because it allows tibial loading to be applied [11, 35] on a unilaterally neurectomised limb. As we have shown previously, this model allows for investigation of the effects of altered strains ranging from low strains associated with disuse up to the supraphysiological strains possible following axial tibial loading [11]. The tibial axial compression model has also been shown to induce adaptive changes in the fibula as well, which provides an additional bone in which the adaptive response to loading can be investigated in mice [160].

The studies described in this chapter were undertaken to optimise the *in vivo* models to be used for subsequent studies in this thesis. The overall aim being to characterise the response to altered mechanical loading in mice and how detrimental changes in the

response to loading seen with aging are affected by altering the context on which mechanical loading is applied. However, before doing this we set out to establish the appropriate time course of loading to use to accurately explore the ‘complete’ adaptive response to loading. We also set out to evaluate the effects of a revised surgical procedure for unilateral sciatic neurectomy (SN) on bone mass and architecture.

3.1.1 Optimising a model of increased mechanical load

When examining the response to mechanical loading in murine bones, consideration of the desired endpoints is crucial. Recognising when certain processes are at their peak, or nadir, following mechanical loading has important ramifications both for planning of *in vivo* experimental procedures, to optimise the chances of identifying the changes of interest, and for interpretation of existing studies – e.g. has a given intervention delayed the full adaptive response, or has it caused a change in the magnitude of the adaptive response? It is, therefore important to identify the times following loading that various parts of the adaptive remodelling process are occurring: eg. when measurable formation begins, when peak formation is occurring, and when bone has “habituated” or fully adapted to a given loading force.

Bone cells can very quickly sense and respond to mechanical loading [18, 38]. Time course experiments, both *in vivo* and *in vitro*, following loading have demonstrated rapid changes in expression of signalling factors; for example, Skerry *et al* [85] detected strain-related changes in enzyme activity in periosteal osteocytes within 6 minutes of load application. Also, upregulation of EGR2 occurs as soon as 1-hour post loading [86, 413, 577]. Osteocytes in an isolated avian ulna model were demonstrated to incorporate H₃-Uridine within 24 hours following loading and the spatial arrangement of this increased activity of osteocytes correlated with areas of increased bone formation seen with repeated loading [509, 533, 579]. This suggests that osteocytes are associated with the cellular response to loading by strain-specific gene upregulation.

The resultant adaptive osteogenic response to mechanical loading is also relatively well characterised in the short-term. There are measurable increases in bone formation within

4 days of a single period of mechanical loading. Using four-point bending, Forwood *et al* [580] demonstrated that the rate of bone formation following one single loading bout peaked between 5-8 days after loading and was already declining by 12 days after the loading stimulus. Repeated mechanical loading likely extends the duration until complete adaptation, but should still eventually reach a state where the bone is adapted or “habituated” to the new, increased magnitude of load being applied.

Most studies examining changes in bone mass and architecture in mice in response to axial tibial loading provide intermittent loading episodes for two weeks [1, 34, 160, 287, 484, 531, 575, 581, 582] as there is typically significant bone formation detectable by μ CT at this time point. Some studies have used later time points to examine the adaptive response to loading; eg. 4 weeks [583-585], but few studies have examined the length of time it takes cortical bone to fully adapt to externally applied loads in mice, and thus the optimal duration of loading to explore certain adaptive responses. Hence, herein we describe a pilot loading time-course experiment to assess the microarchitectural changes in bone mass using μ CT and the changes in bone formation using sequentially administered fluorochromes for mice loaded for 2, 3 or 4 weeks.

There are no studies, to the author’s knowledge, which examine the temporal adaptive response to tibial axial compressive loading in mice. Lambers *et al* [586] demonstrated in trabecular bone of tail vertebrae, using *in vivo* μ CT, that adaptation to a repeated load applied to tail vertebrae is static following 10 weeks of cyclic axial compressive loading, with bone formation and resorption rates equal. They also demonstrated that calculated stiffness increased and plateaued at this point. Another study looked at the effects on tail vertebral trabecular bone in the early weeks following mechanical loading. This study demonstrated that increases in bone formation rate seen at 1-2 weeks after loading, assessed by dynamic histomorphometry, had returned to baseline following 4 weeks of loading [587].

When considering cortical bone adaptation to loading stimuli, earlier studies examined the temporal process of mineralisation following four-point bending of the tibia. Turner *et al* [588] found that woven bone formation stopped after 3 weeks of loading and then fully

mineralised by 14 weeks, however, no time points were examined between 3 and 14 weeks. [588]. Another study applied load to achieve a low strain (1200 $\mu\epsilon$) in rat tibiae for up to 18 weeks [589]. This study demonstrated that periosteal formation had plateaued by 12 weeks, but endosteal formation was still elevated compared to the control limb after 18 weeks. However, the 4-point bending loading protocol does not apply a physiological direction of loading, so adaptation to increased loads is likely to continue for longer as the bone shape is not adapted to withstand these bending loads. As bone is already adapted to forces applied in an axial direction through normal habitual loading, adaptive bone formation seen with the axial compression loading models is likely to demonstrate a different time course to that demonstrated with exogenously applied four-point/cantilever bending models, where the direction of strain is significantly different to that experienced in habitual loading.

Only one study, to the author's knowledge, has explored the temporal adaptive response to axial loading in the ulna model; Schriefer *et al* [590] demonstrated that axial loading resulted in increased bone formation initially which then plateaued within the first 5 weeks after loading onset. They hypothesised the majority of bone formation was likely to have occurred as early as 2-3 weeks. As axial tibial loading is now considered the gold standard for study of the adaptive response to bone loading, by allowing investigation of trabecular and cortical bone adaptation, we planned to characterise the temporal response to repeated loading using μ CT and dynamic histomorphometry (DH) following repeated loading of the tibia for up to four weeks. The use of DH enables identification of specific areas of formation and resorption in a given cross-section, which allows evaluation of responses which cannot be quantified with *ex vivo* μ CT alone. **The first aim of experiments described in this chapter was to establish the temporal pattern and spatial distribution of cortical bone formation to determine the optimal loading duration to use for subsequent experiments in this thesis.**

3.1.2 Optimising a model of decreased mechanical loading

In people, bone mass has been shown to be rapidly lost following disuse induced by spinal cord injury [591], bed rest [456] and cast immobilisation [592]. Experimentally induced

bone loss by SN or tail suspension in rodents parallels much of this clinical bone loss seen in human bone in situations of disuse [7, 35, 558, 559, 593] with marked trabecular bone loss and moderate endosteal resorption in cortical bone, and minimal periosteal effects. Tail suspension is one of the most commonly used experimental models for inducing disuse in rodents. We did not, however, select this model for many reasons. Primarily, the procedure is not approved for experimental use under the Animals (Scientific Procedures) Act (1986) in the United Kingdom due to welfare/ethical concerns. There is an observed stress response associated with immobilisation and restraint and redistribution of blood to the cranial aspect of the animal [563]. Endogenous glucocorticoid excess reduces bone formation rate and bone mineral density [594] and corticosteroid administration is shown to reduce bone mass [595], possibly as a result of an increase in RANKL enhancing osteoclast formation [596, 597]. The physiological stress response is a recognised limitation of the tail suspension technique; in fact, tail suspension is used as a research model for inducing psychological stress in rodents [563, 564]. Considering this, the bone loss associated with disuse engendered by tail suspension may be confounded by physiological changes associated with stress. These “stress” effects are likely to be smaller following SN as the animal is untethered and freely able to ambulate around the cage at all times, although no direct comparison of the stress response between the two procedures exists.

One of the other benefits of SN is that it can provide a background of diminished habitual loading which enables the effects of exogenous axial tibial loading to be separated from the effects of habitual loading and thus studied across a wider spectrum of strain magnitudes, as demonstrated in the paper by Sugiyama *et al* [11]. This paper demonstrated a linear relationship between bone formation and the low strains associated with disuse and the high strains associated with bone formation, thus arguing against the “Lazy Zone” hypothesis postulated by Frost [13] which states that there is a range of normal strains to which bone remains unresponsive, with only extremes of disuse or vigorous loading resulting in adaptive changes in the bone mass and/or architecture. Unilateral disuse allows comparison of changes with intervention to the contralateral normally loaded limb, thus increasing experimental power and reducing required

experimental numbers. Following SN, weight bearing in the contralateral limb has been demonstrated to remain unchanged [593]. This study did, however, document a small but significant reduction in BMD in the femoral and tibial epiphyses of the contralateral hindlimb, although the diaphyseal BMD remained unchanged [593]. Brouwers *et al* [598] have also reported “substantial” contralateral proximal tibial epiphyseal bone loss in rats in the contralateral sham operated leg following unilateral SN, however, do not report quantitative results. This suggests a systemic effect on the control of bone mass following neurectomy, which may involve the systemic release of vaso-active neuropeptides, such as Substance P [593]. Previous studies from our laboratory, and from others, have demonstrated that systemic blockade of the sympathetic nervous system and neurectomy does not impair the adaptive response to loading [35, 599, 600]. Furthermore, the osteogenic response to loading was significantly improved in young adult mice if preceded by prior SN [35], which further suggests that the involvement of any neuronally mediated influence on control of bone mass is small compared to the effect of mechanical loading. Considering these studies, our group has concluded that right unilateral SN (RUSN) provides the most effective method for engendering unilateral disuse.

When performing SN, a small surgical approach must be made to the nerve to achieve nerve transection. Neurectomy, through the pure traumatic nature of surgery results in some degree of tissue trauma, and thus an inflammatory response as part of the normal wound healing process. Several inflammatory mediators have been linked with increased bone resorption, or decreased formation; most significantly, prostaglandin E₂ (PGE₂), a variety of interleukins (IL-1, IL-6, IL-17), and tumour necrosis factor alpha (TNF α) [601-605]. It is possible that a localised inflammatory reaction associated with surgical trauma alone could stimulate a reduction in bone mass, so to control for a local effect of an inflammatory stimulus created by surgical trauma alone, we proposed a revised surgical model for unilateral SN where a left-sided sham (LSH) surgery was undertaken in addition to RUSN (RUSN+LSH). This revised model provides similar surgical wounds bilaterally, but only denervation to the right leg. Future experiments planned for this thesis examined the effect of disuse on RANKL protein expression in cortical bone. Inflammatory cytokines, such as PGE₂ and certain interleukins, are known to be associated with bone loss through

increased expression of, or synergism with RANKL [601]. Prior to establishing bone's expression of RANKL in situations of disuse and loading in the following chapter of this thesis, we first needed to confirm that RUSN+LSH resulted in similar degrees of bone loss to that previously reported following RUSN [4, 11]. **The second aim of experiments described in this chapter was to characterise the effect of contralateral sham surgery on the pattern of bone loss in the tibia following unilateral SN.**

3.1.3 Objectives

1. *Determine the temporal pattern of bone mass changes in the murine tibia following repeated axial loading for two, three or four weeks, using μ CT.*
2. *Determine the temporal pattern of cortical bone formation in the murine tibia following repeated axial loading for two, three or four weeks, using dynamic histomorphometry.*
3. *Characterise the effect of unilateral sciatic neurectomy and contralateral sham surgery on bone mass in the murine tibia using μ CT.*

3.2 Materials and Methods:

3.2.1 Objective 1: Determine the temporal pattern of bone mass changes in the murine tibia using μ CT, following repeated axial loading for two, three or four weeks.

This study was performed as an initial pilot study to provide preliminary data on the optimal duration of loading for later experiments in this thesis and also to provide the author with an introduction to axial tibial loading of the murine tibia. To establish the time-course for bone mass changes and the loading-related changes in bone formation over 4 weeks of loading, 17-week-old female C57BL/6 mice were divided into three groups. The right tibia was loaded three times weekly (Monday, Wednesday, Friday) to a peak strain of $2500\mu\epsilon$ on the medial surface of the cortex (14.97N) [29] then killed on the final Monday. Group 1 (n=3) was loaded for 2 weeks, group 2 (n=4) for 3 weeks and group 3

(n=4) for 4 weeks. Unfortunately, due to an animal death under anaesthesia, the 2 week group only included 3 animals for analysis, reducing the statistical power required to identify changes in this group. Figure 18 illustrates the experimental timeline for loading and fluorochrome administration. Fluorochrome labels were injected to allow assessment of bone formation rates throughout the experiment using DH. Fluorochrome solution preparation and injection is described fully in Chapter 2. Table 1 in Chapter 2 demonstrates the dosage, and excitation and emission wavelength maxima for each fluorochrome compound. These values were adapted from [568] and were used to establish the best wavelength to use for confocal image acquisition.

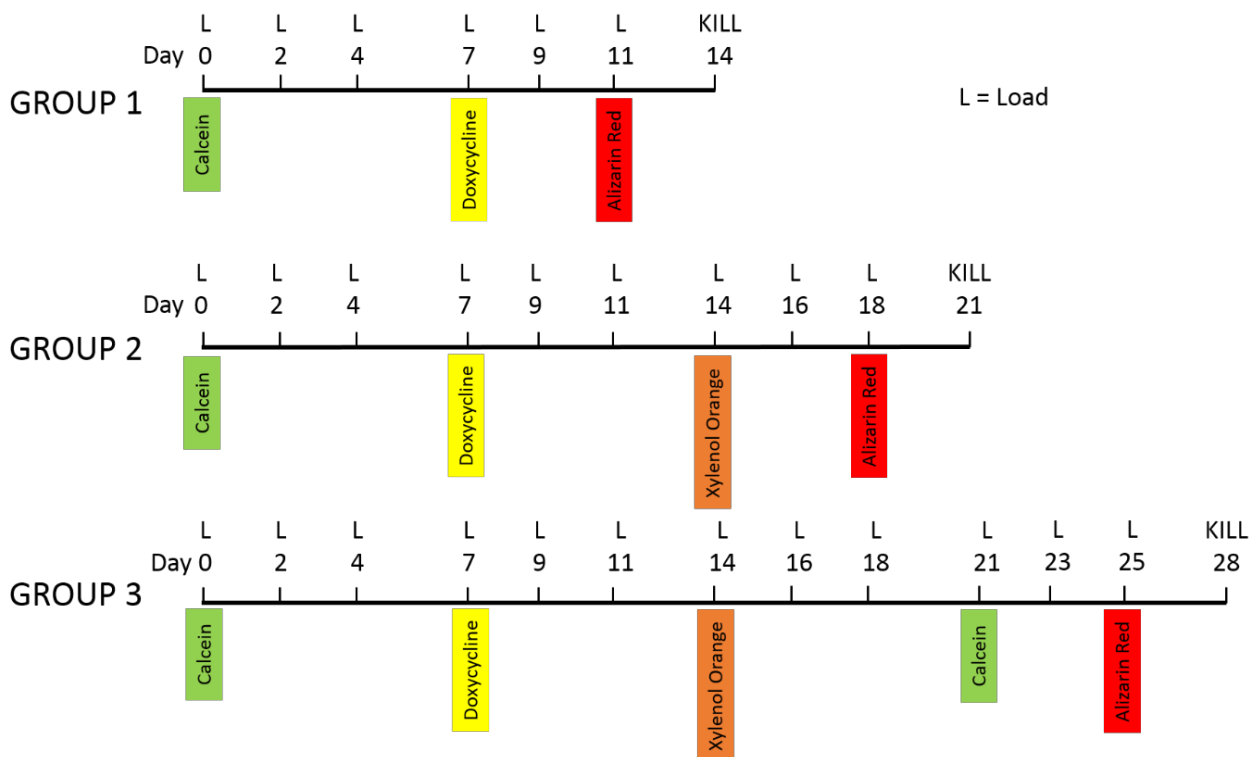


Figure 18 – Experimental timeline for the loading time-course study.

Female 17-week-old C57BL/6 mice received right axial tibial loading three times weekly for either 2, 3 or 4 weeks. Fluorochrome administration according to the schedule shown was performed to allow dynamic histomorphometry in each group. Confocal laser scanning microscopy was performed on methylmethacrylate embedded, non-decalcified transverse sections of the 37% site of the tibia using Argon (488nm), Diode (405nm) and HeNe (564nm) lasers.

Following sacrifice, mice tibias were processed for μ CT scanning as described in chapter 2. A μ CT region of interest at the 37% site, measured from the proximal end, was analysed because it is the most load-responsive site [1, 8]. Tt.Ar, Ct.Ar, Ma.Ar, Ct.Th, PMI and Ct.Ar/Tt.Ar were calculated.

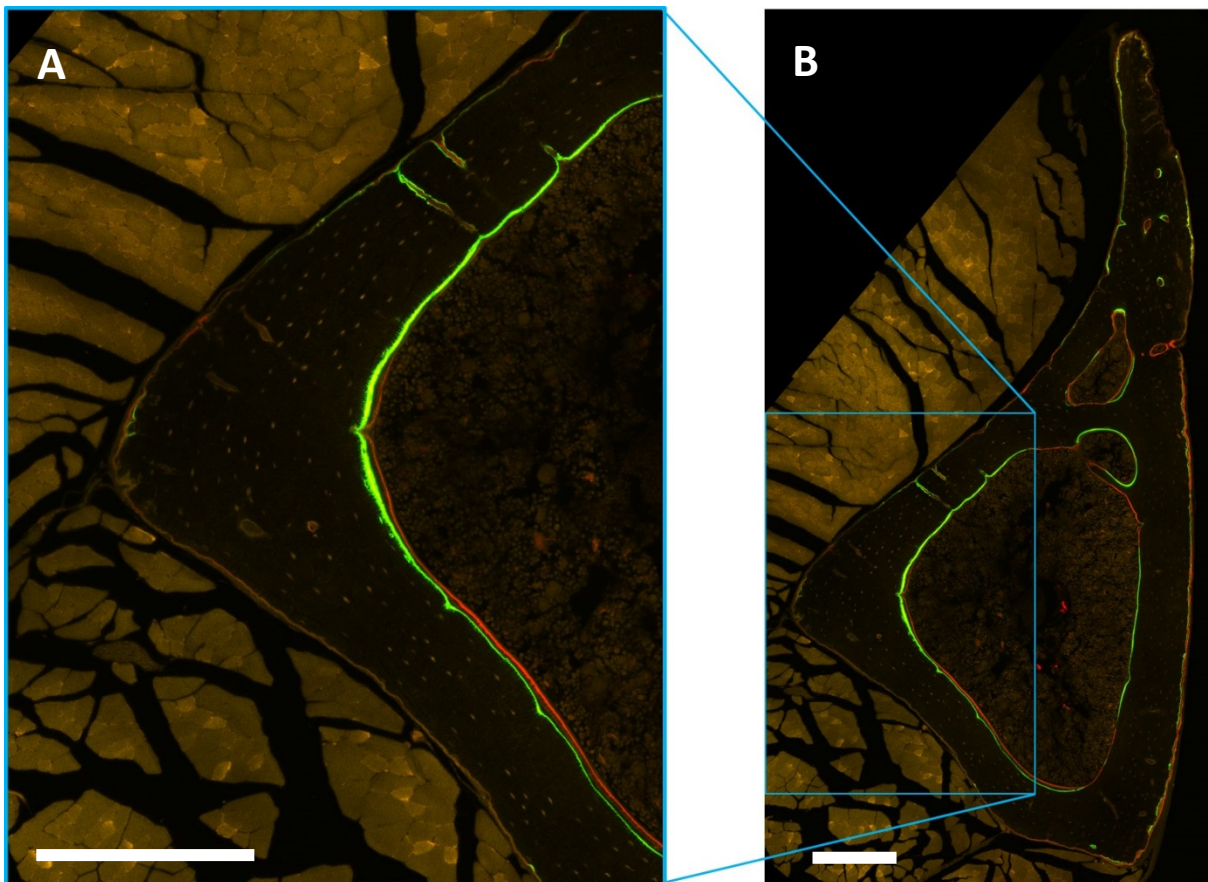


Figure 19 – Representative image of selected posteriolateral cortex used for analysis of response to loading.

The pictured image is from a control (unloaded) left limb following 2 weeks of loading and administration of calcein (green) on day 1, doxycycline (yellow) on day 7 and alizarin red (red) on day 11. Mice were killed on day 14 and bones embedded in methylmethacrylate then sectioned for imaging using confocal microscopy. Scale bar = 250 μ m

3.2.2 Objective 2: Determine the temporal pattern of cortical bone formation in the murine tibia following repeated axial loading for two, three or four weeks using dynamic histomorphometry

Following completion of μ CT scanning, embedding in methylnmethacrylate and transverse sectioning at the mid-proximal cortical site (37% of the length of the bone measured from the proximal end), confocal laser scanning microscopy was performed as described in chapter 2 to visualise the fluorochrome labels. Briefly, Argon (488nm), Diode (405nm) and HeNe (564nm) wavelength lasers were used to excite the fluorochromes and then acquire images of the four different fluorochromes used. A mosaic of the sub-scans was generated to form the entire bone cross section. Images were captured using a pixel size of 378nm. Because the posteriolateral cortex at the 37% site shows the most significant osteogenic response to loading [1, 8], sections at this level were imaged and a standard rectangular region of interest 1000x750 μ m (2640x1980 pixels) was selected of the posteriolateral cortex, centred on the mid-cortex (see Figure 19 for a representative section and box outlining the region of interest selected).

Figure 20 is a schematic diagram describing the calculation of the different dynamic histomorphometric indices. As each specimen had multiple labels administered, a separate bone formation rate and inter-label distance could be calculated for the entire experiment (first and last bone label) for each group (Total DH values) (Figure 20A-C) and, additionally, each weekly inter-label interval (0-7 days (Figure 20D), n=11; 7-14 days (Figure 20E), n=8; 14-21 days, (Figure 20F) n=4) (Weekly interval DH values). The Osteomeasure™ histomorphometry programme (Osteometrics, Decatur, GA, USA) was used to calculate the Ct.Ar, Ct.Th, interlabel thickness (Ir.L.Th), bone formation rate per bone surface (BFR.Bs) and marrow apposition rate (MAR). These parameters were calculated for both endocortical (Ec) and periosteal (Ps) surfaces, as described in Chapter 2.

3.2.3 Objective 3: Characterise the effect of unilateral sciatic neurectomy and contralateral sham surgery on bone mass in the murine tibia using μ CT.

To determine if sham surgery on the contralateral limb, in addition to right unilateral SN (RUSN+LSH) resulted in similar alterations in bone mass and architecture to those seen in the tibias of mice following right unilateral SN alone (RUSN), we proposed a revised surgical model for SN. The revised surgical model involved right SN and left sham surgery in 17-week-old female C57BL/6 mice (n=6). Mice were killed 3 weeks following surgery then bones were analysed using μ CT. Dissection, fixation and μ CT scanning was performed as described in chapter 2.

Following image reconstruction, cortical bone at 25%, 37%, 50% and 75% of the length of the bone, measured from the proximal end, was analysed for Tt.Ar, Ct.Ar, Ma.Ar, Ct.Th and PMI. The trabecular region, from 0.25-0.75mm distal to the proximal growth plate, was analysed to assess BV/TV, Tb.Th, Tb.N, Tb.Sp, Tb.Pf and SMI. Figure 21 is a representation of the location of each region analysed. Additionally, the muscle area (Mu.Ar.) at mid-shaft (50%) tibia was assessed to determine efficacy of neurectomy.

3.2.3 Statistical analysis

Any two related parameters measured within the same animal (eg. control left and neurectomised right limbs) were compared using a paired Student's T-Test or a repeated measures ANOVA for analyses with multivariate effects including a paired variable. Two-way ANOVA was used to compare analyses with >2 treatment variables, and LSD or Bonferroni post-hoc comparisons were used where appropriate. Significance was set at $p < 0.05$. All analyses were performed with SPSS Version 23 (IBM Corp, Armonk, NY).

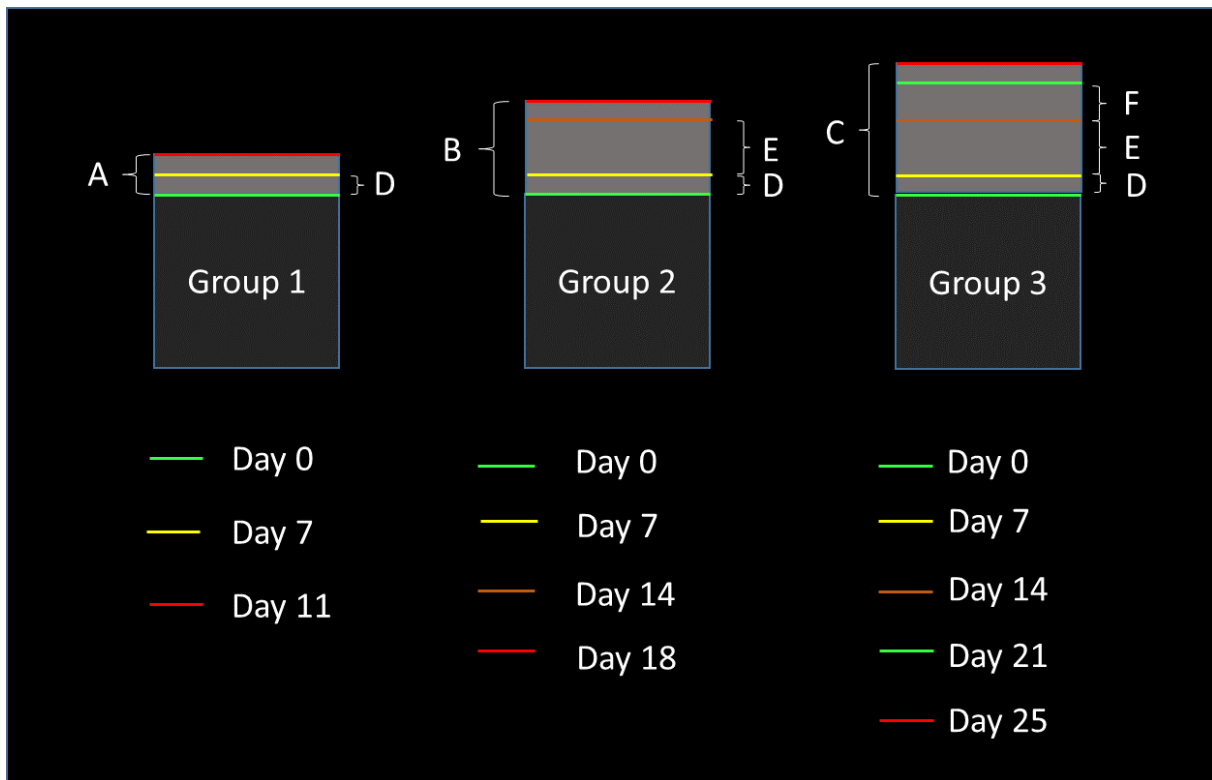


Figure 20 – Schematic diagram describing calculation of the measures explored using dynamic histomorphometry.

17w-old female C57BL/6 mice had their right tibia loaded 3 times weekly (M, W, F) for 2 weeks (Group 1), 3 weeks (Group 2) or 4 weeks (Group 3). Fluorochromes were administered to each mouse as described above. Calcein (green line), Doxycycline (yellow line), Xylenol orange (Orange/brown line), and alizarin red (Red line) were administered and interlabel thickness (Ir.L.Th), Marrow Apposition Rate (MAR) and Bone formation rate per bone surface (BFR.Bs) calculated for both periosteal and endosteal surfaces. Total formation response (between first and last fluorochrome) was calculated for (A) group 1, (B) Group 2 and (C) group 3. Formation indices for weekly intervals were also calculated for all mice. Values were calculated for (D) 0-7 days formation (n=11), (E) 7-14 days (n=8) and (F) 14-21 days (n=4) intervals to determine changes in bone formation rates throughout the experimental loading duration. Weekly interval data was calculated using values from all mice.

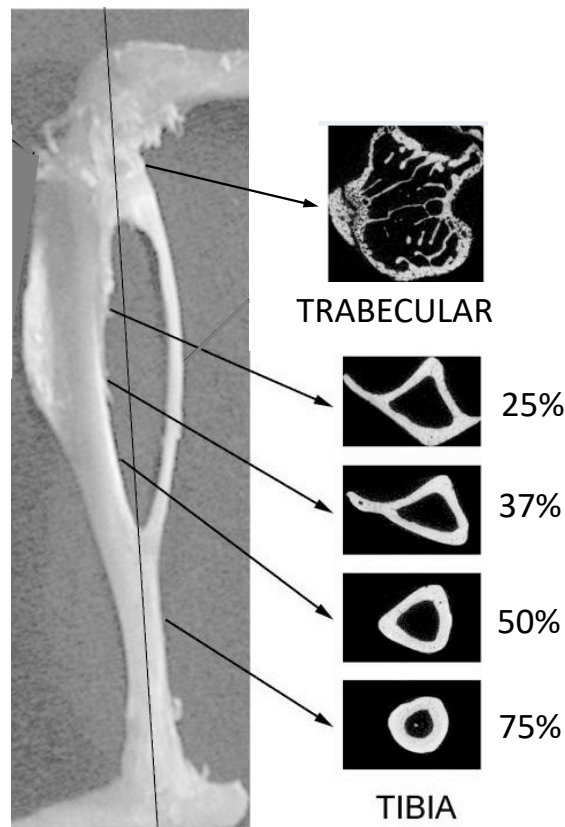


Figure 21 - Representative regions of interest in the mouse tibia that were analysed using μ CT.

Adapted from [1, 2].

3.3 Results:

3.3.1 Determine the temporal pattern of bone mass changes in the murine tibia using μ CT, following repeated axial loading for two, three or four weeks, (Objective 1).

As described in the introduction, our first aim was to determine the temporal pattern of bone formation following repeated mechanical loading using μ CT and dynamic histomorphometry with multiple sequentially administered fluorochromes. There was no significant difference identified in the average mouse weight between groups nor the tibial length between groups or between loaded and control bones (Table 3).

Loading group		2 weeks	3 weeks	4 weeks
Mouse weight (g)		22.4 ± 0.93	21.92 ± 0.67	22 ± 0.45
Tibial length (mm)	Control	17.86 ± 0.17	17.62 ± 0.25	17.95 ± 0.11
	Loaded	17.98 ± 0.22	17.67 ± 0.3	18.1 ± 0.1

Table 3 – Mouse weights and tibial lengths following axial tibial loading for 2, 3 or 4 weeks.

Groups were compared with either one-way ANOVA (Weight) or mixed-design two-way ANOVA (tibial length). There were no significant differences for any comparison. Values represent mean ± SEM

Trabecular bone

Trabecular bone mass was significantly increased following loading at each time point. Tabulated data for the trabecular analysis is presented in Appendix 3. Loading had no effect on the control limb for any parameter. BV/TV and Tb.N were significantly greater following loading after all time points. Tb.Th was only significantly greater following loading after 3 and 4 weeks of loading (Figure 23A-C). Tb.Sp was significantly reduced with loading after 3 and 4 weeks of loading (Figure 23D). Tb.Pf was reduced with loading at all three time points, indicating an increase in trabecular connectivity with loading (Figure 23E). SMI was unaffected by loading (Figure 23F). Figure 22 illustrates representative three-dimensional reconstructions of the trabecular bone regions of interest demonstrating increased bone mass and changes in Tb.Th.

Cortical Bone

Loading three times-a-week resulted in an increase in bone mass after 2, 3 and 4 weeks of loading. Tabulated data from the cortical bone analysis is presented in Appendix 3. There was no difference in any of the measured parameters between the control limbs for any group, following contralateral loading. Compared to the control limb, Tt.Ar was not significantly increased after two weeks of loading but was after 3 and 4 weeks. Ct.Ar was increased with loading at all three time points. Ma.Ar was reduced in the mice loaded for

2 weeks ($p < 0.05$), but this decrease was no longer evident in mice after 3 or 4 weeks of loading. Ct.Th was increased with loading after 4 weeks of loading only. PMI was increased with loading after all durations of loading. When considering the effect of the duration of loading, Tt.Ar and Ct.Ar both showed a not statistically significant tendency to be greater with longer durations of loading ($p = 0.077$ and $p = 0.078$ respectively). Ma.Ar and PMI were not significantly affected by loading duration, however, there was a loading*group interaction for Ma.Ar, demonstrating that the duration of loading affects the endosteal response to loading consistent with the finding that Ma.Ar reduced after 2 weeks, this response was absent again after 3 weeks of loading. The right loaded limb had significantly greater Ct.Th after 4 weeks of loading than after 2 weeks of loading ($p < 0.05$) (Figure 24 & Figure 25).

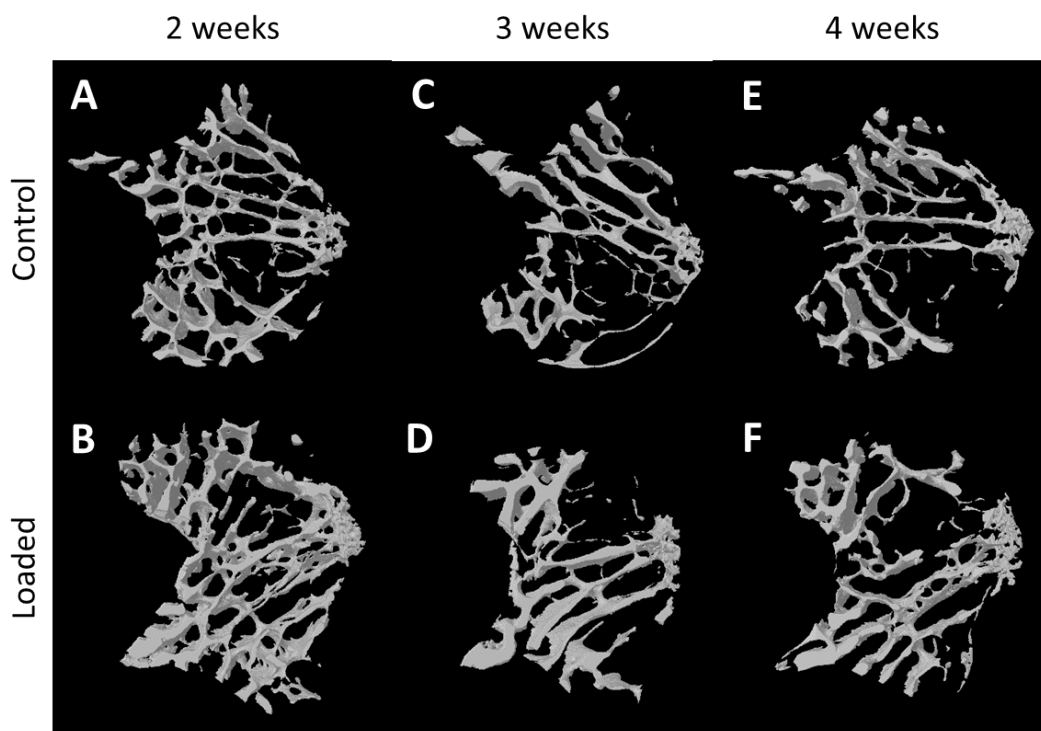


Figure 22 – The effect of different time periods of axial loading on trabecular bone of young adult female mice.

Right limbs of 17w female mice were loaded three times weekly for (A, B) 2, (C, D) 3 or (E, F) 4 weeks then killed for analysis with μ CT of the proximal tibial trabecular bone site. Representative 3-dimensional reconstructions of the tibial trabecular region of interest of control (A, C, E) and loaded (B, D, F) limbs are illustrated.

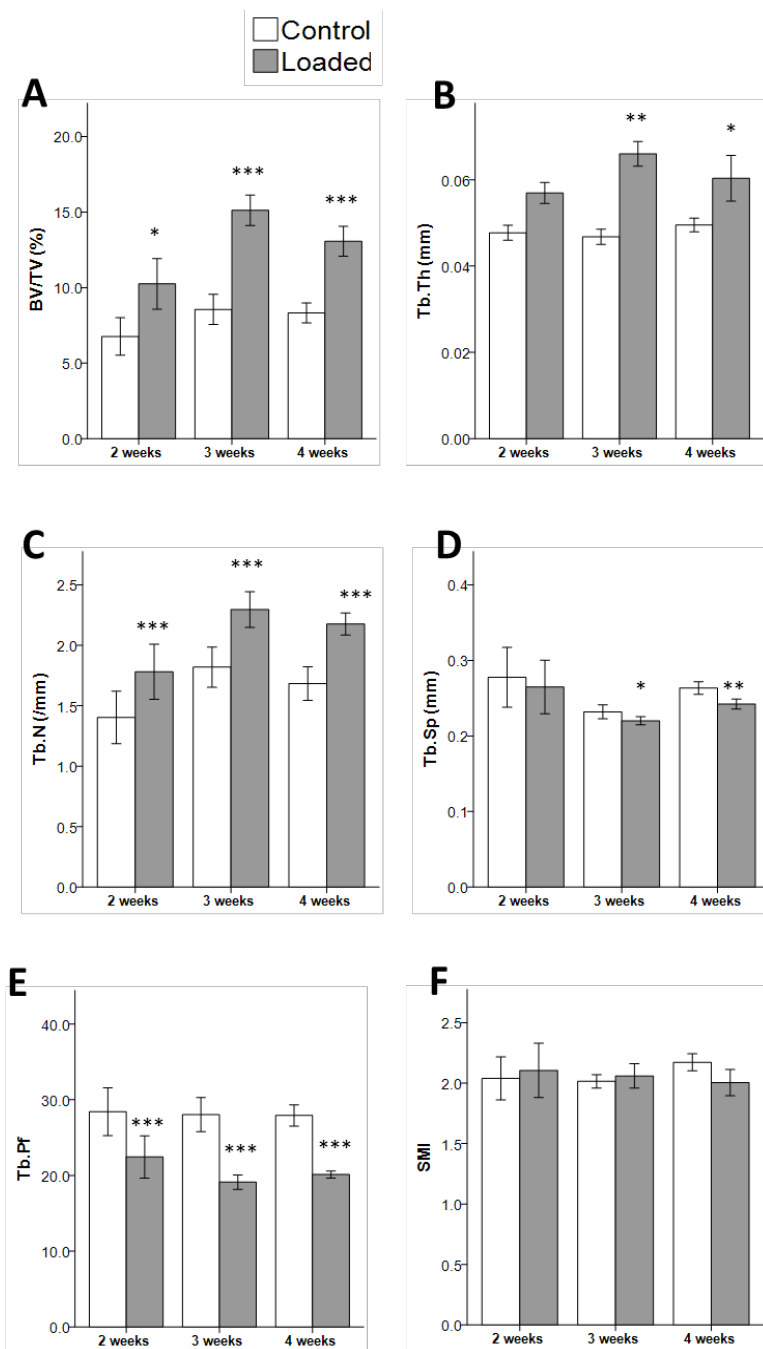


Figure 23 - The effect of different time periods of axial loading on trabecular bone μ CT parameters of young adult female mice.

17w female mice were loaded for three times weekly for 2, 3 or 4 weeks then killed for analysis with μ CT of the proximal tibial trabecular bone region of interest. (A) BV/TV, (B) Tb.Th, (C) Tb.Sp, (D) Tb.N, (E) Tb.Pf and (F) SMI were calculated. * = $p < 0.05$, ** = $p < 0.01$, *** = $p < 0.001$ vs control limb. Comparisons were performed using a mixed design ANOVA with Sidak post-hoc corrections for multiple comparisons. Bars represent mean \pm SEM, $n = 3-4$ /group

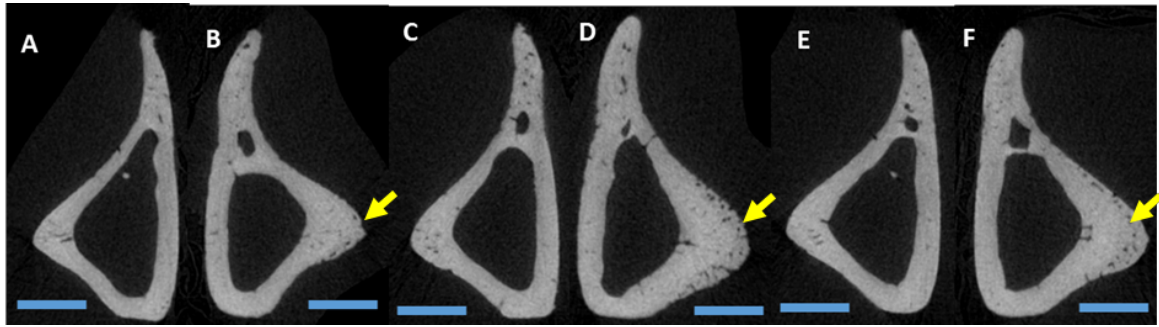


Figure 24 – The effect of different time periods of repeated loading on cortical bone μ CT parameters of young adult female mice.

Right limbs of 17w female mice were loaded three times weekly for (A, B) 2, (C, D) 3 or (E, F) 4 weeks then killed for analysis with μ CT of the 37% cortical bone site (measured from proximally). Representative axial sections of the tibia of left control (A, C, E) and right loaded (B, D, F) limbs are illustrated. The yellow arrows indicate the region of bone with greatest loading-related bone gain (at the posteriolateral cortex). The scale bars indicate 500 μ m

The percentage increase in Tt.Ar in response to loading tended toward a significantly greater increase at 3 weeks (+8.5%) compared with 2 weeks (+19.6%, $p=0.09$) (Figure 26). Ct.Ar showed a marginally greater increase due to loading at 3 weeks (29.2%) than at 2 weeks (20.9%), however this difference was not significantly different to the increase seen at 2 weeks or the increase at 4 weeks (26.2%) ($p=0.35$).

Ma.Ar significantly reduced with loading after 2 weeks (-18.2%). This reduction was significantly different to the change in Ma.Ar with loading at 4 weeks (+0.5%, $p<0.05$) and tended to be significantly different to the change with loading seen after 3 weeks of loading (-1.7%, $p=0.06$).

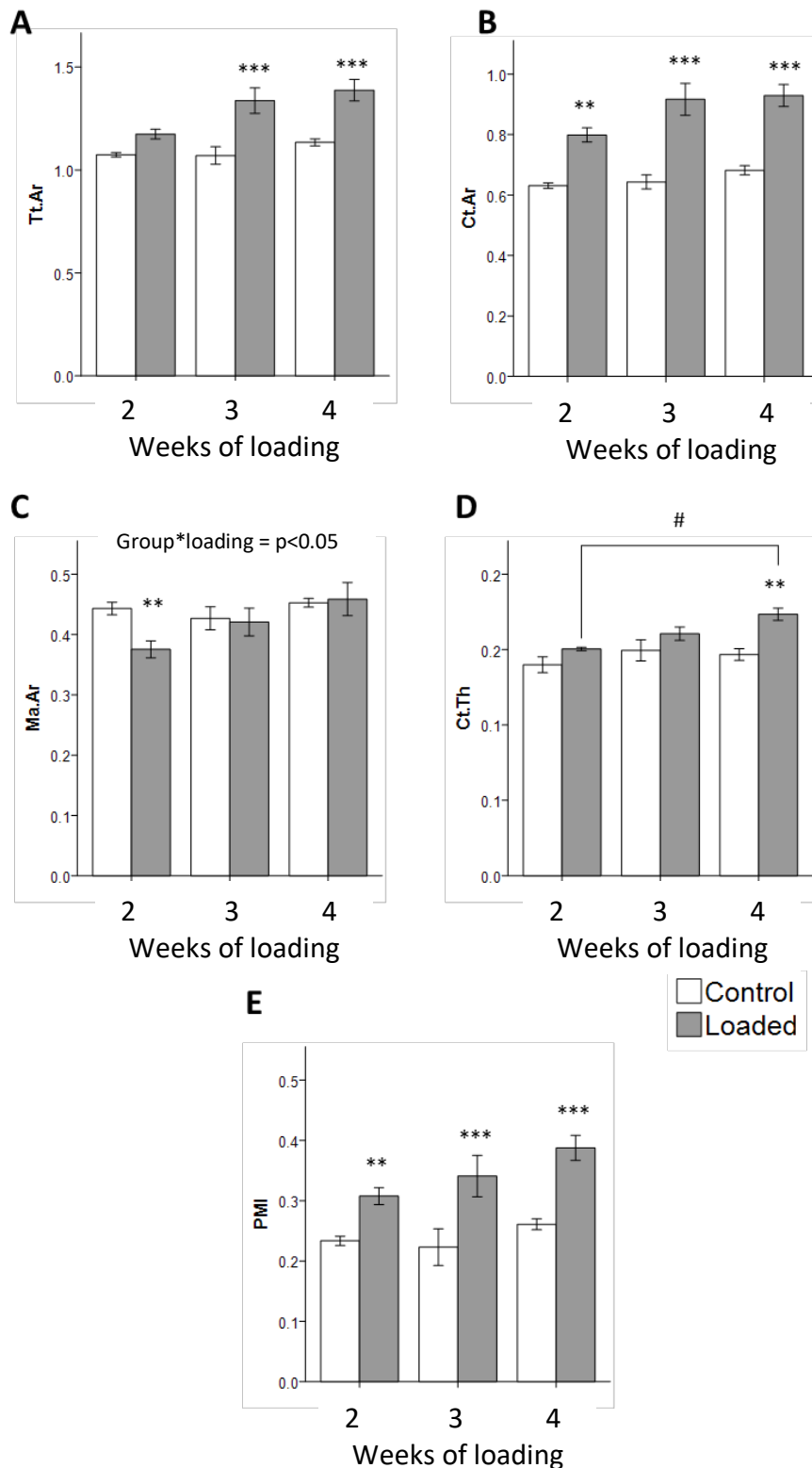


Figure 25 – The effect of different time periods of repeated loading on cortical bone μ CT parameters of young adult female mice.

17w female mice were loaded three times weekly for 2, 3 or 4 weeks then killed for analysis with μ CT of the 37% cortical bone site (measured from proximally). (A) Tt.Ar, (B) Ct.Ar, (C) Ma.Ar, (D) Ct.Th and (E) PMI were analysed. ** = $p < 0.01$, *** = $p < 0.001$ vs control limb. # = $p < 0.05$ vs loaded limb of 2 week group. Comparisons were performed using a mixed design ANOVA with Sidak post-hoc corrections for multiple comparisons. Bars represent mean \pm SEM, $n = 3-4$ /group

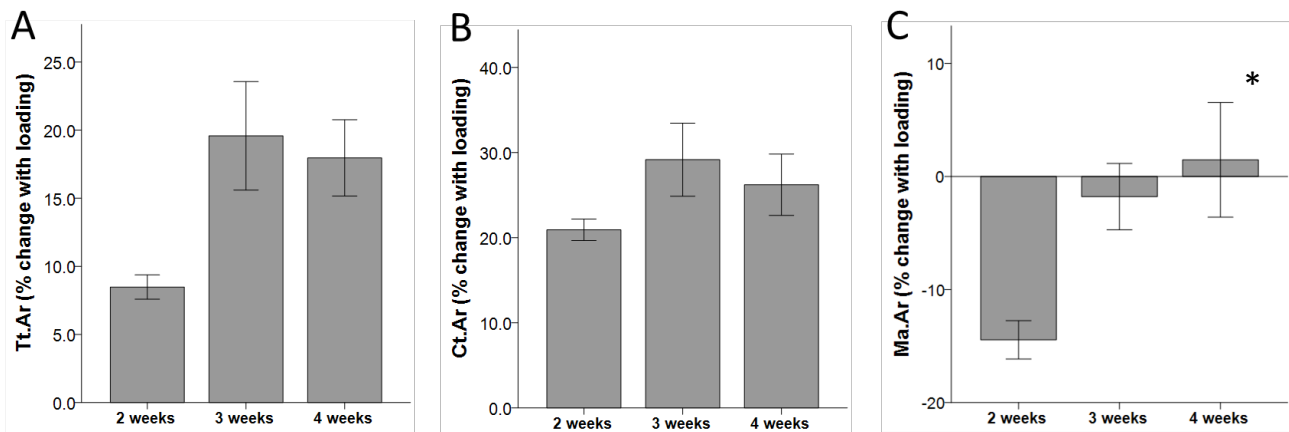


Figure 26 – The effect of different time periods of repeated loading on the percentage increase in μ CT parameters.

[[Right-left)/Left*100]] for (A) Tt.Ar, (B) Ct.Ar and (C) Ma.Ar are shown for mice following 2, 3 or 4 weeks of loading. * = $p < 0.05$ compared to 2 weeks group. Comparisons were made using One-way ANOVA with Sidak post-hoc adjustments. Bars indicate Mean \pm SEM.

3.3.2 Determine the temporal pattern of cortical bone formation in the murine tibia following repeated axial loading for two, three or four weeks using dynamic histomorphometry (DH) (Objective 2).

Total DH analysis

Dynamic histomorphometry (DH) was performed following sequential fluorochrome labelling at weekly intervals for up to four weeks. Initial evaluation, performed as described in Figure 20A-C, was completed to evaluate overall DH results from between the first and last fluorochrome measured in each group, representing 2, 3 or 4 weeks of loading. Ct.Ar in the posteriolateral cortex, assessed using DH analysis, was significantly increased after all three durations of loading, and there was no significant difference between the loading durations (Figure 27A). This change in Ct.Ar using DH is consistent with the changes seen in Ct.Ar of the whole cross-section calculated using μ CT. Ct.Th

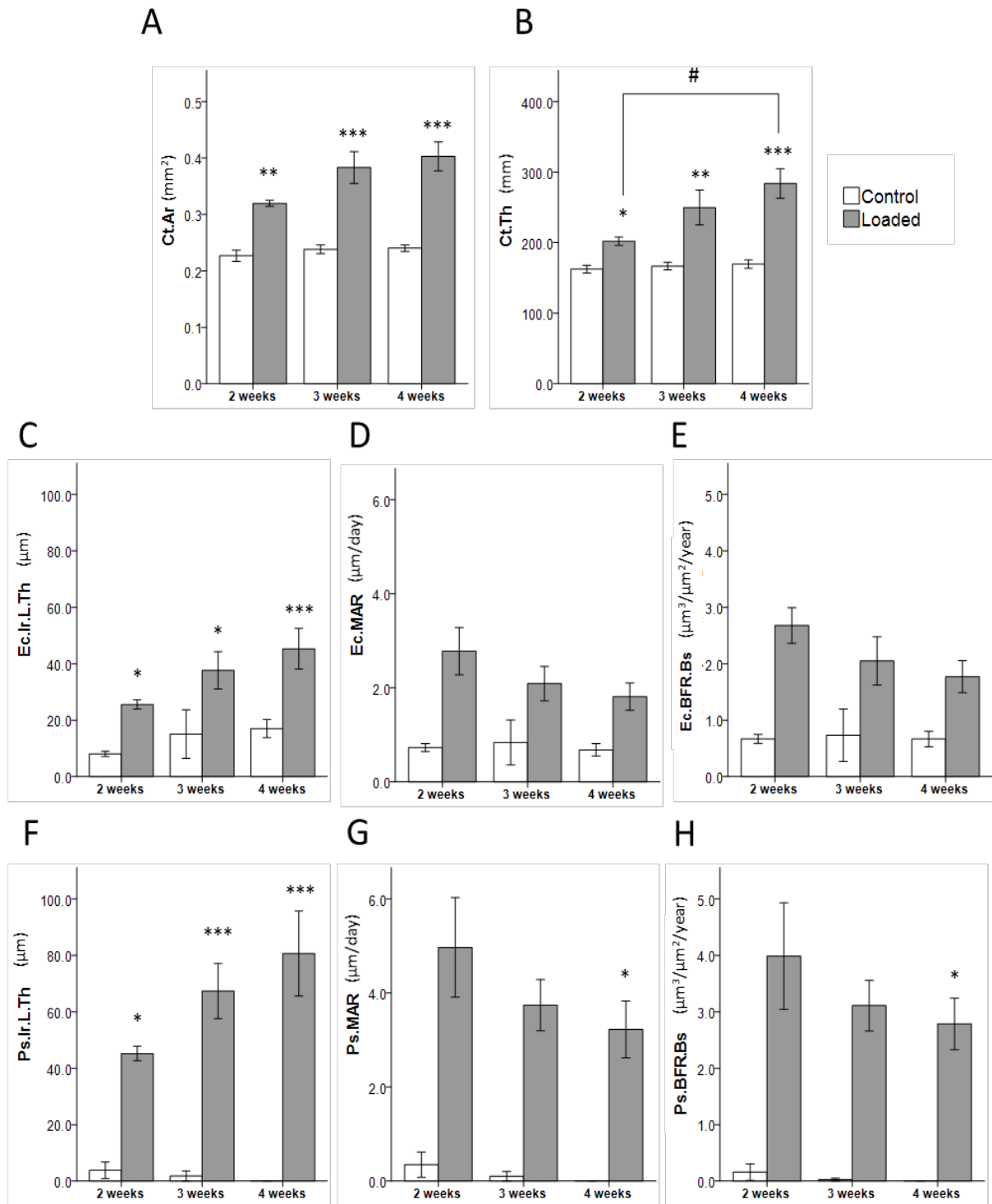


Figure 27 – The effect of loading duration on dynamic histomorphometry parameters following loading in young adult female mice.

17w female mice were loaded three times weekly for 2, 3 or 4 weeks. Fluorochromes were administered as specified in Figure 19. The first and last fluorochrome administered for each group were used to calculate the overall value for: (A) Ct.Ar, (B) Ct.Th, (C) Ec.Ir.L.Th, (D) Ec.MAR, (E) Ec.BFR.Bs, (F) Ps.Ir.L.Th, (G) Ps.MAR and (H) for each group. * = $p < 0.05$, ** = $p < 0.01$, *** = $p < 0.001$ vs control limb. # = $p < 0.05$ vs loaded limb in 2 week group. $n = 3-4$ /group. Bars represent Mean \pm SEM

increased after 2, 3 and 4 weeks of loading. The loading related change in the Ct.Th was greater after four weeks than it was after 2 weeks (Figure 27B, Figure 28). Ec.Ir.L.Th and Ps.Ir.L.Th were significantly greater following loading in all three time points. Ps.MAR and Ps.BFR.Bs were greater than control limbs after four weeks of loading (Figure 27C, F-H, Figure 28). Raw data values are presented in table form in Appendix 3.

The DH analysis was only performed on the posteriolateral tibial cortex, as we were primarily interested in the formative response and this region is the most responsive site for bone formation following loading [8]. However, when exploring the entire cross-section in the confocal images, it was evident that the endosteal cortex had undergone marked resorption at the anteriolateral and posteriomedial cortices (Figure 29C-F). Further investigation of this observation was not undertaken and was deemed beyond the scope of this project.

Weekly interval DH analysis

Next we calculated the weekly interval DH indices as described in Figure 20D-F. Endosteally, the weekly interval loading response was associated with an overall significant difference between time intervals for Ec.Ir.L.Th, Ec.MAR and Ec.BFR.Bs, however individual post-hoc comparisons between time periods did not reach significance in this pilot study. Periosteally, the period 7-14 days after initiation of loading demonstrated greatest change in Ps.Ir.L.Th, and subsequently a change in the Ps.MAR and Ps.BFR.Bs. (Figure 30).

Figure 28 – Confocal laser scanning micrograph images of transverse sections of the tibia of young adult female mice after 2, 3 or 4 weeks of loading.

IMAGE ON FOLLOWING PAGE. 17w old female C57BL/6 mice underwent three times-weekly loading for 2, 3 or 4 weeks and concurrent administration of sequential fluorochrome solutions as described in Figure 20. Bones were embedded in methacrylate then sectioned using a concentric annular diamond saw and imaged using a Confocal laser scanning microscope. Scale bars on the low power images represent 200µm. Scale bars on the high power images represent 250µm.

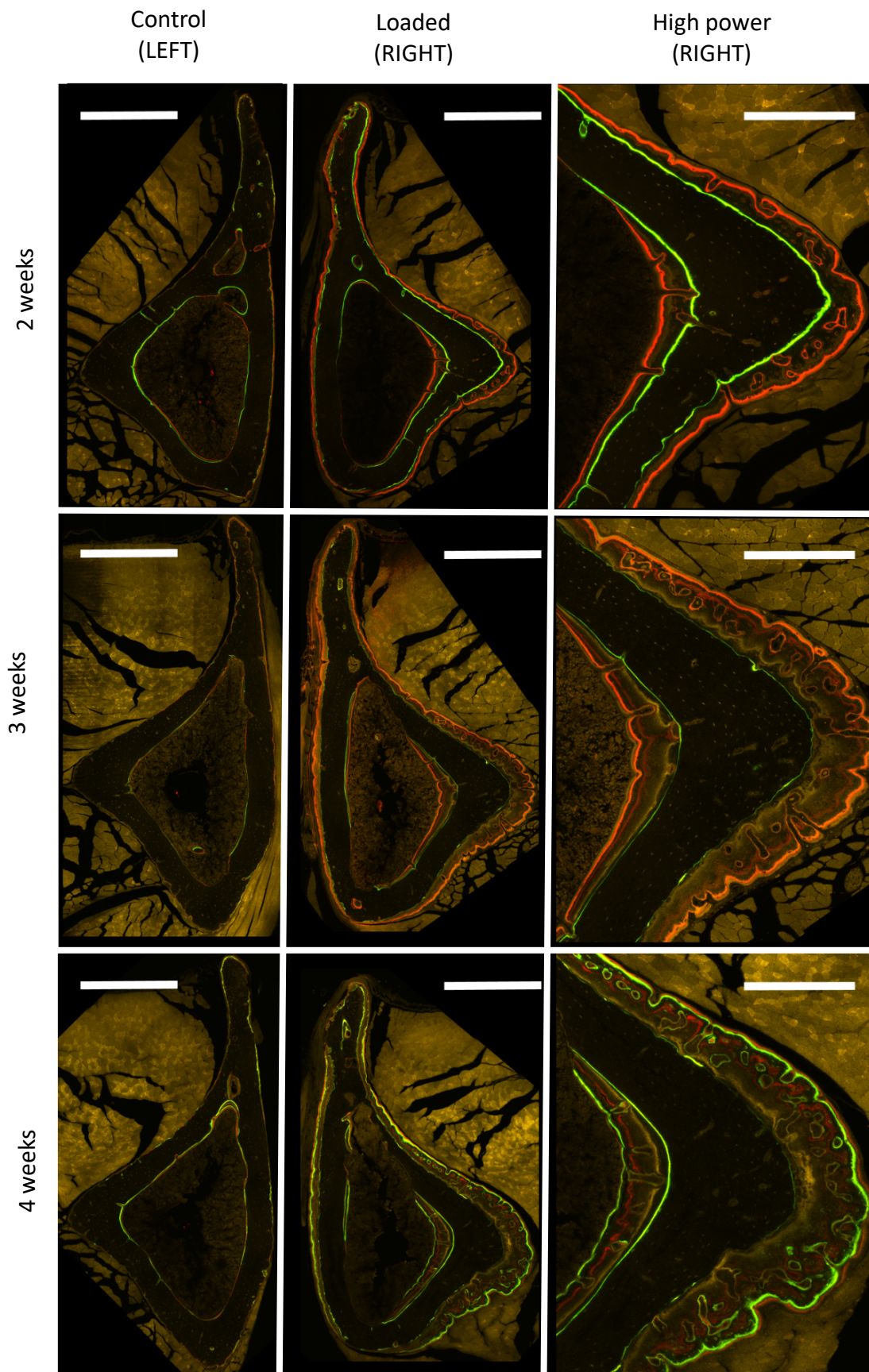


Figure 28 – legend on previous page

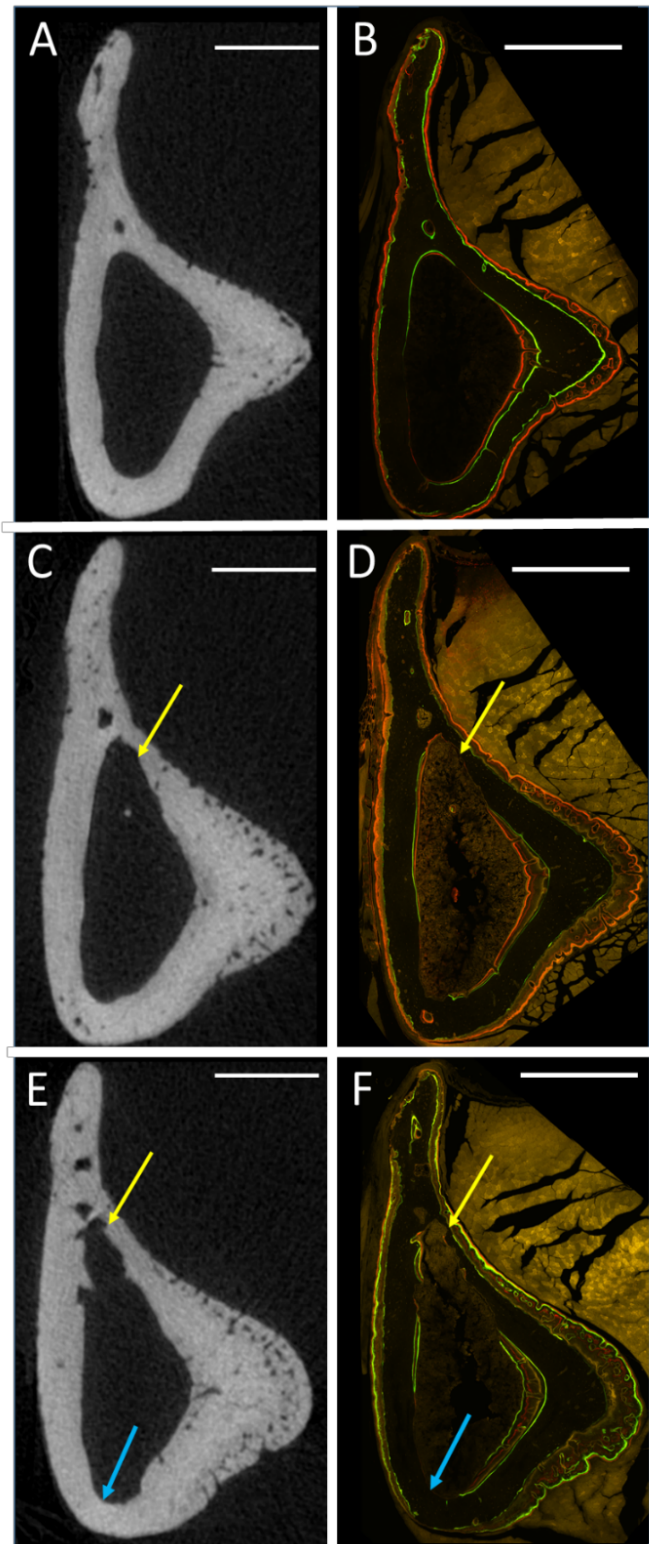


Figure 29 – The effect of different time periods of loading on endosteal resorption.

Representative images from 17-week-old Female C57BL/6 mice were loaded for 2 (A, B), 3 (C, D) or 4 weeks (E, F) and injected with serial fluorochrome solutions to allow determination of formation and resorption. Tibiae were analysed using μ CT (A, C, E) and confocal microscopy (B, D, F). Note the regions of bone resorption in the anteriolateral tibial endosteal cortex (yellow arrows) and further resorption in the posteriomedial endosteal cortex in the 4 weeks loaded mice (blue arrows). Scale bars indicate 500 μ m.

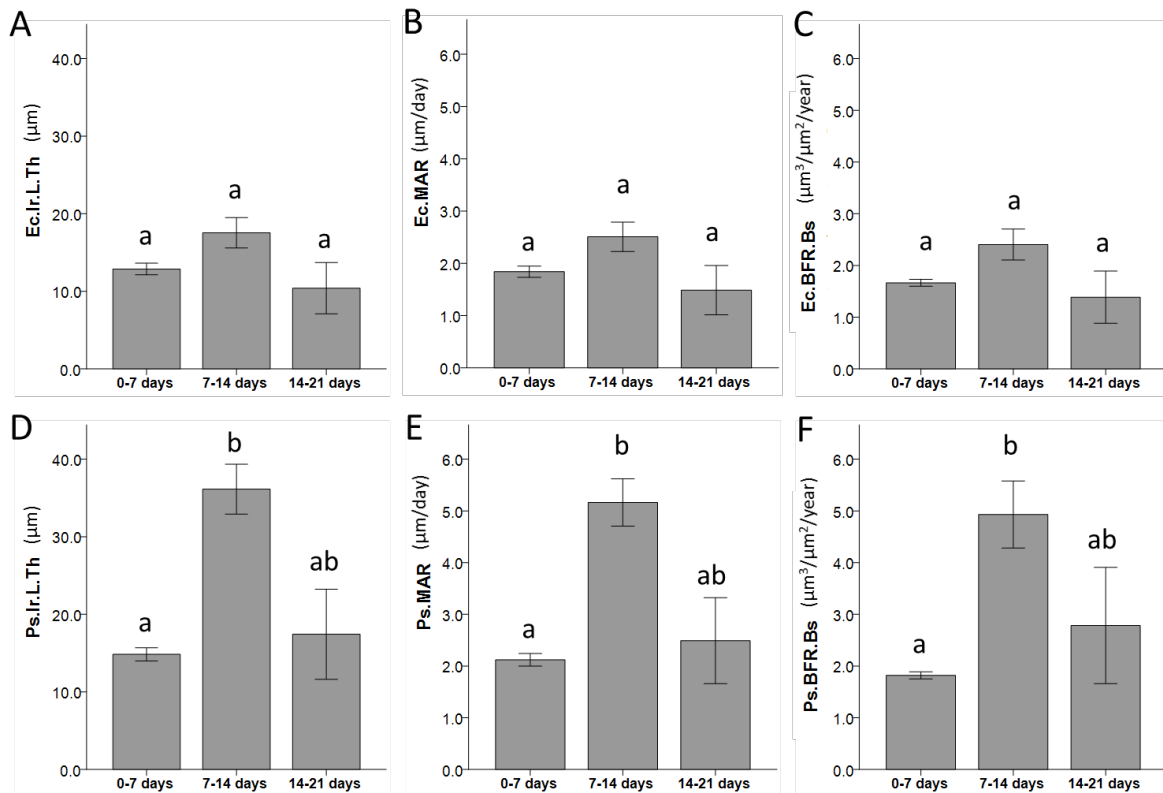


Figure 30 – Dynamic histomorphometric indices for the weekly intervals following the start of repeated axial tibial loading in young adult female mice.

17w old female C57BL/6 mice were loaded 3 times weekly for up to 28 days. Fluorochromes were administered on day 0, 7, 14, 21 and histomorphometric indices for [A-C] Endosteal (Es) and [D-F] Periosteal (Ps) [A, D] Ir.L.Th, [B, E] MAR and [C, F] BFR.Bs were calculated for each 7 day interval as described in Figure 19 and Figure 20. Bars with the labelled with the same letter are not significantly different ($p > 0.05$), based on one-way ANOVA. Scale bars represent mean \pm SEM. $n=11$ for 0-7 days, $n=8$ for 7-14 days, $n=4$ for 14-21 days.

3.3.3 Characterise the effect of unilateral SN and contralateral sham surgery on bone mass in the murine tibia using μ CT (Objective 3).

μ CT was used to confirm that the revised surgical model generated a situation of unilateral bone loss, equivalent to that previously reported in our laboratory with right neurectomy and no left sham surgery [4, 11]. The Mu.Ar was reduced significantly in the neurectomised limbs ($4.35 \pm 0.31 \text{ mm}^2$ in SN limb vs $7.16 \pm 0.42 \text{ mm}^2$ in control limbs, $p < 0.001$), indicating successful denervation. SN did not result in any significant differences

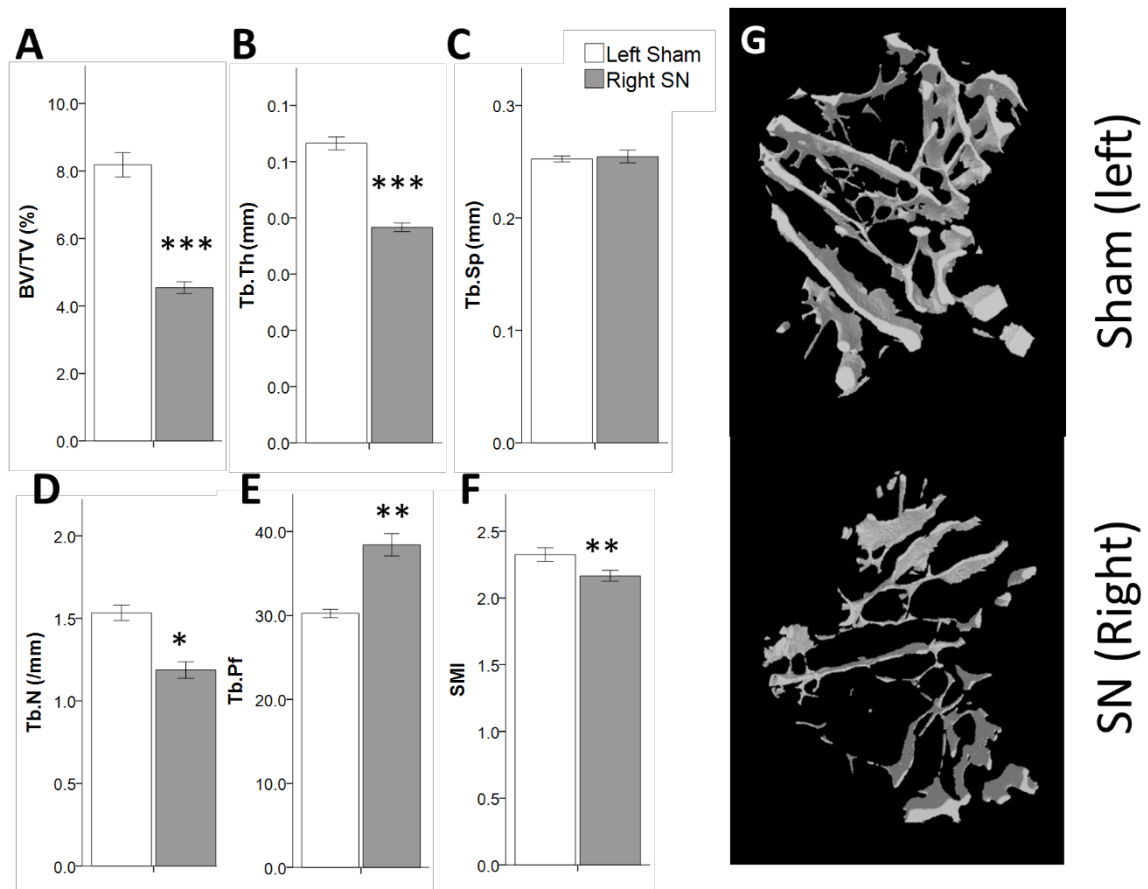


Figure 31 – The effect of sham surgery (left leg) and SN (right leg) on trabecular bone parameters in young adult mice.

17w old female C57BL/6 mice underwent SN on the right limb and were killed 3 weeks later. The proximal tibial trabecular bone 0.25-0.75mm distal to the proximal tibial physis was analysed. (A) BV/TV, (B) Tb.Th, (C) Tb.Sp, (D) Tb.N, (E) Tb.Pf and (F) SMI were calculated. * = $p < 0.05$, ** = $p < 0.01$, *** = $p < 0.001$ vs control limb. Each parameter was compared using paired t-test. $n=6$. Bars represent mean \pm SEM. (G) 3-dimensional reconstruction of the analysed trabecular bone region of interest.

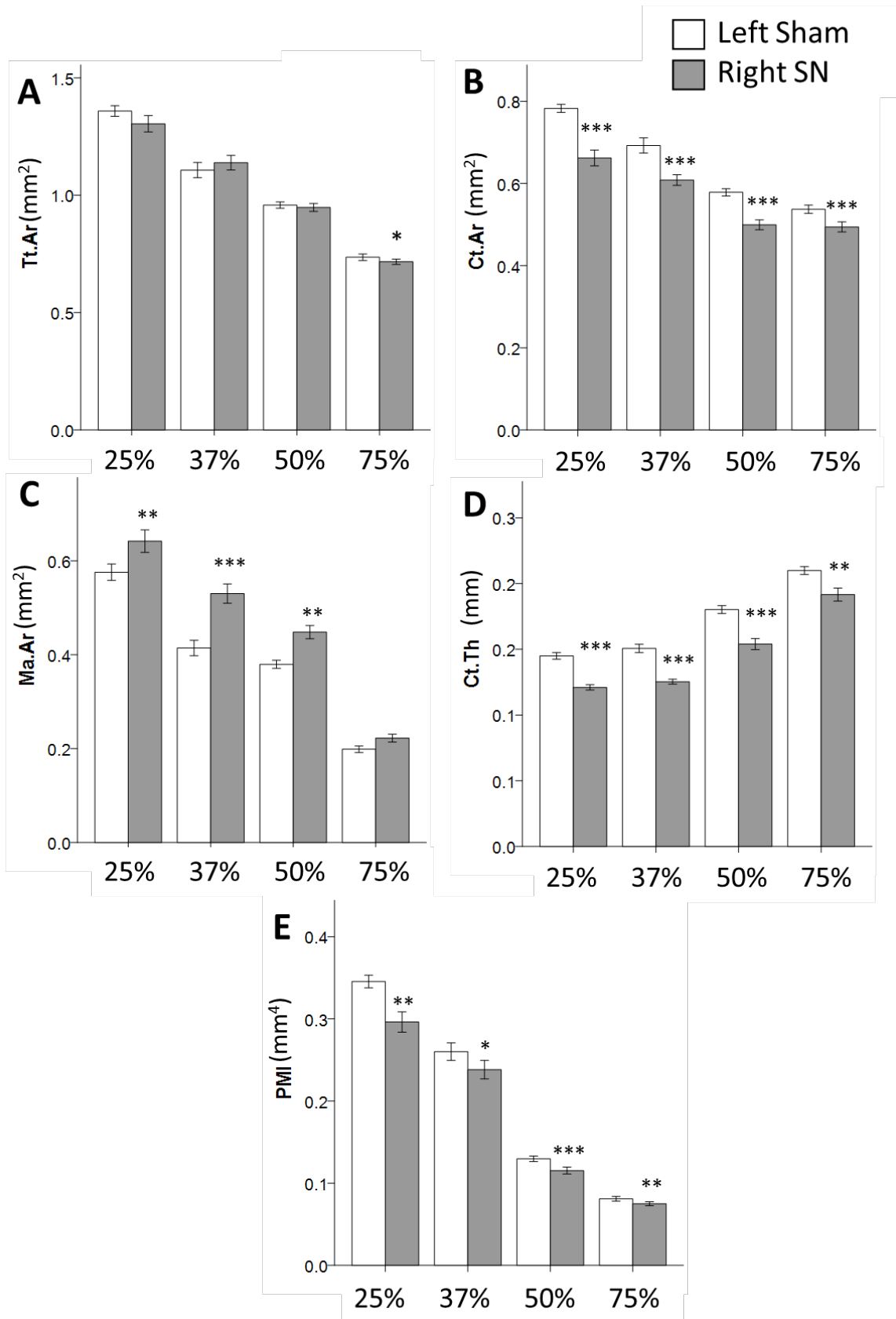


Figure 32 – Legend on following page

in tibial length (Left Sham $17.82 \pm 0.11\text{mm}$, vs Right SN = $17.81 \pm 0.12\text{mm}$). The bodyweight of the mice did not change significantly during the experiment (start weight = $22.0 \pm 0.4\text{g}$ vs end weight = $22.6 \pm 0.3\text{g}$).

Trabecular bone

As predicted, SN led to loss of trabecular bone. Figure 31 demonstrates the changes between control and neurectomised limbs. In right SN limbs, BV/TV, Tb.Th, Tb.N and SMI were significantly reduced compared with control limbs. Tb.Pf was significantly greater following SN. Tb.Sp was unchanged.

Cortical bone

Figure 32 and Figure 33 illustrate cortical bone loss at different sites between the left sham limb and right SN limb. In the SN limbs, Tt.Ar remained unchanged at all except the distal 75% site, where it decreased by a small but statistically significant amount (-2.7%). Ct.Ar significantly reduced at all sites ($p < 0.001$), indicating bone loss throughout the whole tibial length. Ma.Ar increased at all sites following SN, except the 75% site, where it remained unchanged. Ct.Th was significantly reduced at all sites following SN. PMI was also reduced at all sites following SN.

Figure 32 – The effect of sham surgery (left leg) and SN (right leg) on cortical bone parameters in young adult mice.

FIGURE ON PREVIOUS PAGE. 17w old female C57BL/6 mice underwent SN on the right limb and were killed 3 weeks later. Cortical bone was analysed at 25, 37, 50 and 75% of the length of the bone measured from the proximal end. (A) Tt.Ar, (B) Ct.Ar, (C) Ma.Ar, (D) Ct.Th and (E) PMI were calculated. * = $p < 0.05$, ** = $p < 0.01$, *** = $p < 0.001$ vs control limb. Each parameter was compared using paired t-test. $n=6$. Bars represent mean \pm SEM

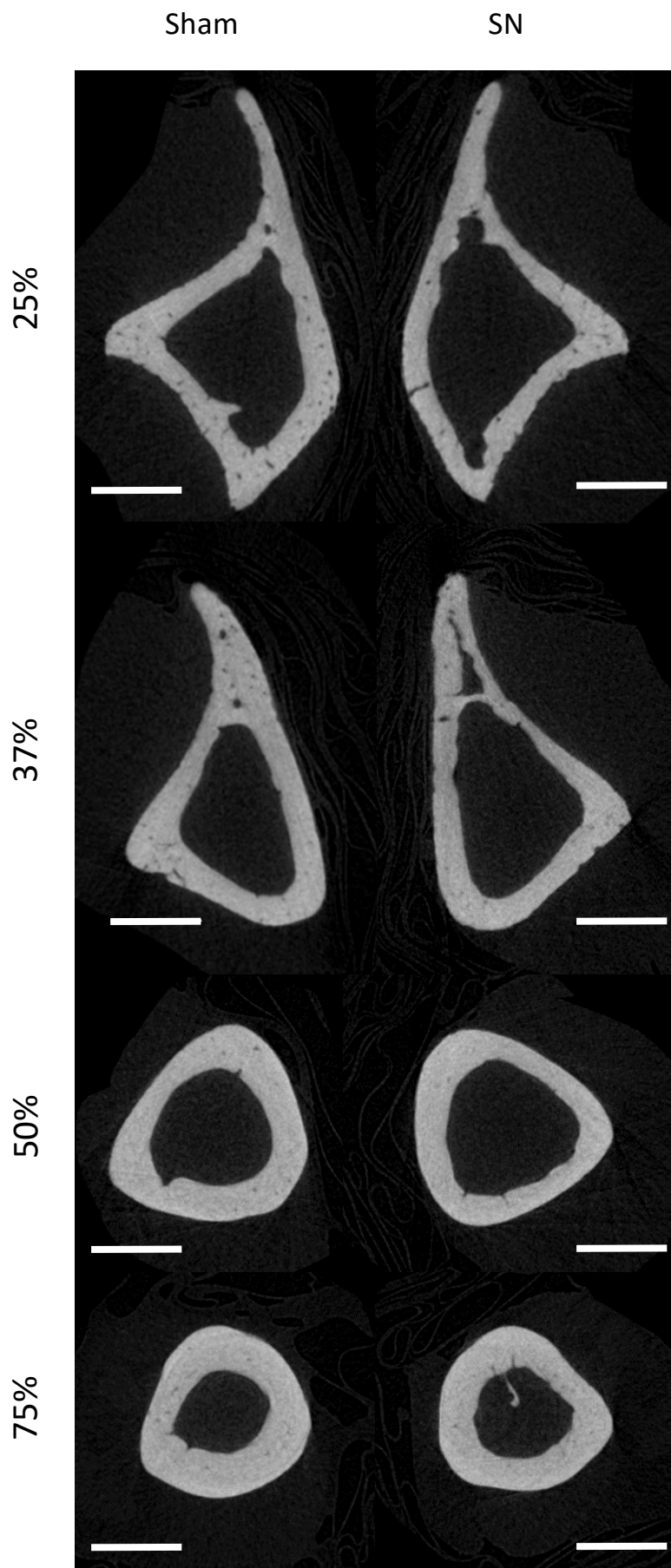


Figure 33 – Comparing the effect of sham surgery (left leg) and SN (right leg) on cortical bone parameters in young adult mice.

Axial μ CT reconstructions of the tibia of 17w old female C57BL/6 mice that underwent SN on the right limb and were killed 3 weeks later. The tibial cortical bone was analysed at 25, 37, 50 and 75% of the length of the bone measured from the proximal end. The scale bars represent 500 μ m

3.3.4 Results summary

- ***Objective 1: To determine the temporal pattern of bone mass changes in the murine tibia using μ CT, following repeated axial loading for two, three or four weeks.***
 - Loading significantly increased trabecular bone mass (BV/TV) after 2 weeks, however Tb.Th was not significantly increased until 3 weeks following loading. Trabecular connectivity was increased (decreased Tb.Pf) at all time points examined. Interpretation of data was limited by small sample size.
 - Loading significantly increased cortical bone mass (Ct.Ar) after two weeks primarily due to an decrease in Ma.Ar at two weeks, followed by periosteal expansion (increased Tt.Ar) after 3 weeks. Cortical thickness was greater after 4 weeks than after 2 weeks loading. There was no significant difference between the load-related change in any parameter after 4 weeks compared with that after 3 weeks.
- ***Objective 2: To determine the temporal pattern of cortical bone formation in the murine tibia following repeated axial loading for two, three or four weeks using dynamic histomorphometry (DH).***
 - Considering total DH values, the periosteal bone formation response at the posteriolateral cortex was greater than the endosteal formation response.
 - Load-associated endosteal bone resorption at the neutral strain axis was greater after 3 and 4 weeks of loading, compared to 2 weeks.
 - Endosteal bone formation at the posteriolateral cortex was no different when calculated for the first, second, or third week of loading. Periosteally, the MAR and BFR were greatest in the second week following loading.

- **Objective 3: To characterise the effect of unilateral sciatic neurectomy and contralateral sham surgery on bone mass in the murine tibia using μ CT.**
 - Trabecular bone mass (BV/TV) was significantly decreased following SN through reductions in trabecular thickness and number.
 - Cortical bone mass (Ct.Ar) was significantly decreased following SN, primarily through an increase in Ma.Ar resulting in decreased in Ct.Th.
 - The changes in bone mass with right SN + left sham are similar to those reported with right SN alone.

3.4 Discussion

In this chapter, we describe two studies aimed at better describing bones' adaptive response in *in vivo* models for changing the mechanical environment of the mouse tibia. Several studies by our group and others have reported that intermittent axial loading of the mouse tibia results in peak load-related increases in bone mass, and that the strain/response relationship is modulated by age and genetic modifications [232, 581, 606, 607]. What is not clear from these studies is whether this modulation is due to differences in the rate of new bone formation, the establishment of a habituated state at different strain levels, or a combination of these and other potential explanations. Timing experimental end points during the period of rapid bone formation or at later time points when functional adaptation is complete can help discriminate between these possibilities. Here, using μ CT and dynamic histomorphometry, we were able to establish, albeit in only a preliminary pilot study, that measurable bone formation happens within one week of loading, is at its peak in the second week following loading, and bone mass accrual is functionally plateaued after 3 weeks. We were also able to demonstrate that contralateral sham surgery, following unilateral SN results in no different degree of bone loss to that reported with unilateral SN alone.

3.4.1 The temporal pattern of bone mass changes in the murine tibia following repeated axial loading, using μ CT (Objective 1).

In our laboratory, and many others, it has been standard practice to use *ex vivo* μ CT examination to explore adaptive bone changes after 2 weeks of axial tibial loading [1, 8, 29, 34, 285, 287, 531, 582, 606, 608, 609]. As described in the introduction, this is because there is significant bone formation detectable at this point, however, the adaptive response to a habituated state is likely to still be incomplete, allowing potential for further interventions to have additional/synergistic effects and/or inhibit the osteogenic response.

Assessment of trabecular and cortical bone using μ CT following loading in the present study demonstrated loading-related increases in cortical and trabecular bone mass (Ct.Ar and BV/TV respectively), primarily associated with periosteal expansion in cortical bone and increased Tb.Th and Tb.N in trabecular bone. The significant increase in Ct.Ar (20.9%) after 2 weeks loading, assessed by μ CT in the present study was slightly lower than the increase in Ct.Ar seen following 2 weeks of loading in previous studies; 26.5% [34], 29% [531], and 32.7% [1]. This could be explained by different mouse ages and/or inter-operator variability in loading techniques. Interestingly, after 2 weeks loading, the primary change in Ct.Ar was actually associated with a reduction in Ma.Ar, and no significant increase in Tt.Ar, which suggests that the early loading-related osteogenic response in these mice was more endosteal in nature (Figure 25). This is not-consistent with previous studies which showed loading in young mice typically produces a periosteal response [11, 29, 34, 285, 396]. Notwithstanding, consistent with these earlier studies, periosteal bone formation was already apparent, according to DH analysis, after only 7 days, which suggests that some periosteal expansion did occur after two weeks and that reduced statistical power in the present study may have impaired the ability to detect the change; the 2-week group only had 3 animals for analysis. Post-hoc power analysis of this pilot study demonstrated that a group size of 4/group would have been sufficient to have >80% power to detect the magnitude of changes recorded suggesting that a type II error may have given a false negative result for Tt.Ar after two weeks of loading.

Interestingly, the endosteal formation response (decreased Ma.Ar) seen after two weeks of loading was no longer apparent after 3 or 4 weeks. This coincided with a subsequent tendency to more periosteal expansion. There was no significant difference in the values obtained from tibias after 3 weeks of loading, compared with tibias after 4 weeks of loading. This suggests a “plateau” in cortical bone formation after 3 weeks of axial tibial loading in mice.

This analysis focused solely on the most load-responsive region of bone following axial tibial loading, but the temporal responses to different periods of loading may be different at different sites along the cortical bone. Recently, we have developed a Site Specificity Analysis (SSA) programme [7] which permits semi-automated analysis of cortical bone responses across the length of the tibia (10-90% of the length of the bone, measured from proximally). This method allows assessment of the changes along the length of the bone, and could help determine site-specific changes beyond our single region of interest (37% site, measured from proximally). Further studies resulting from this initial pilot study should not only increase experimental numbers, but also employ SSA software to analyse the entire cortical bone response (later experiments in this thesis utilise the SSA software).

The trabecular response to loading after 2 weeks of loading in these mice is similar to that previously reported with a large increase in BV/TV (53%) due to increases in Tb.N and Tb.Th [1, 34]. However, when statistically comparing the trabecular μ CT changes with loading we were unable to find any significant differences between the loading response at two weeks compared to the loading response at 3 or 4 weeks. This is most likely because the sample size used was inadequate; post hoc power analyses performed indicated that in the present study, for BV/TV, to identify a small effect (20% change) between groups, a group size of 9 mice per group was required, a far greater number than used in the present study.

3.4.2 The temporal pattern of cortical bone formation in the murine tibia following repeated axial loading for two, three or four weeks using dynamic histomorphometry (Objective 2)

The cortical bone DH data supported the cortical bone μ CT results and conclusions, despite the low experimental numbers. Additionally, by pooling the weekly DH data from all mice for the early weeks following loading, as illustrated in Figure 20, we were also able to increase statistical power for the 0-7d and 7-14d groups. Endosteally, the rate of formation at the posteriolateral cortex was consistent over the first three weeks following onset of loading, despite the μ CT data suggesting that an endosteal formation response was present after 2 weeks but absent by 3 or 4 weeks. When examining the entire cross-sectional fluorochrome-labelled images, there are clear regions of bone resorption occurring at the anteriolateral and posteromedial endosteal cortices of the tibia in mice after 3 and 4 weeks of loading which are not apparent after only 2 weeks (Figure 29). This helps explain the apparent loss, at 3 weeks, of the endosteal formation response evident by reduced Ma.Ar after 2 weeks loading even though the DH data measured only at the posteriolateral cortex indicated a consistent endosteal formation response throughout the experiment.

These concurrent, but spatially separate formation and resorption responses suggest a cross-sectional regional specificity in the endosteal bone formation and resorption responses in response to loading. These region-specific responses are averaged out by the standard μ CT analysis methods employed here, thus appearing as a net steady state of Ma.Ar. This cross-sectional site-specificity of the response to axial tibial loading was demonstrated in a previous study that correlated the down-regulation of osteocytic sclerostin with bone formation, demonstrating new bone is formed predominantly in the posteriolateral and craniomedial regions of the tibia [8]. This suggests that the resorption response observed at the anteriolateral and posteromedial endosteal cortex in the present study (Figure 29) may be related to the low strain associated with the neutral axis experienced during axial tibial loading. Figure 34 illustrates the areas of resorption identified using DH correspond to the neutral strain axis following axial compressive

loading. Additionally, a very recent study using longitudinal *in vivo* μ CT experimental design has demonstrated that the resorptive response to loading is correlated to the calculated strain at the endosteal surface, but not the periosteal surface, whereas formation is related to strain both periosteally, and endosteally [529], further supporting our conclusion that the regions of apparent resorption are associated with the low endosteal strains on the neutral axis for axial loading. Our laboratory is currently collaborating with the laboratory of Professor Peter Pivonka at the Queensland University of Technology to develop a computed model to determine the site-specific responses to interventions in a radially site-specific manner [610]. Whilst initial studies have not examined the present dataset, we plan to expand the studies to explore the radially site-specific response to mechanical loading and correlate this to the predicted strain and strain energy density to help predict the adaptive response to loading and potentially identify if there are site-and strain specific regions of the age-related deficiency in the adaptive response to loading.

When bone formation and resorption rates are equal, bone mass does not change. There was no significant difference in the cortical bone parameters using either μ CT or overall DH indices between mice loaded for 3 weeks and mice loaded for 4 weeks, suggesting that the adaptive loading response had “plateaued”, even at the most load-responsive 37% site. This suggests that bone strains engendered during application of the fixed peak exogenous load have returned to habitual levels where the mechanostat is balancing bone formation and resorption. Whilst the response to loading typically results in bone formation in sites of high strain, and resorption in areas of low strain, as seen at the neutral axis of cortical bone undergoing bending force, as demonstrated in Figure 34, that balance should gradually return the formation and resorption to baseline levels over time after continued long term loading, once the adaptive response has returned the strain levels to normal. This effect has been demonstrated using longitudinal *in vivo* μ CT studies of trabecular bone [586]. The clear evidence of bone resorption in the fluorochrome-labelled images of mice loaded for 3+ weeks suggests that, after an initial period of significantly increased bone formation and minimal apparent resorption, the adaptive process increased the level of bone resorption to adapt the mass and architecture to best suit the

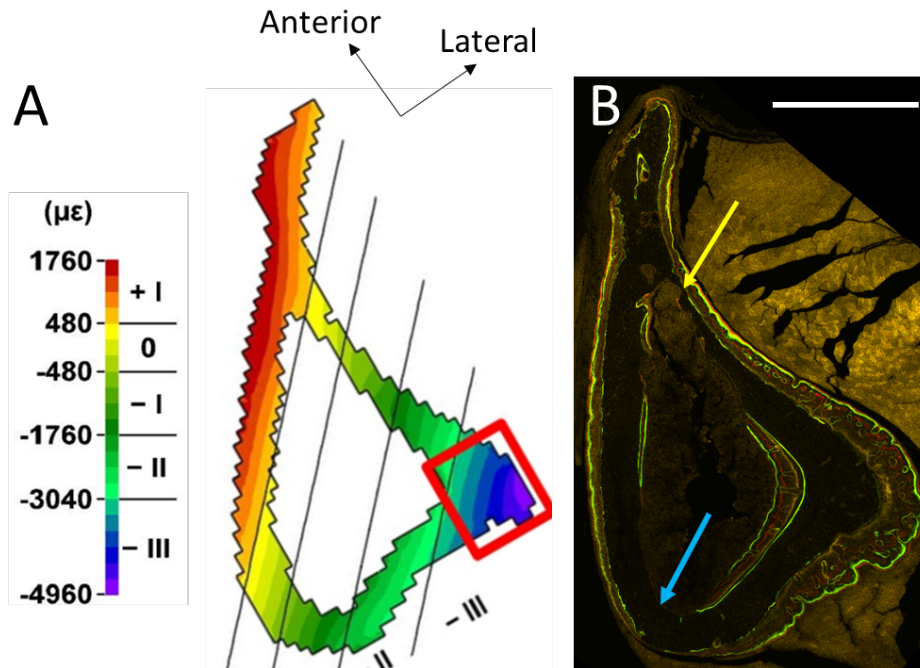


Figure 34 – (A) Finite Element Model (FEM) of a murine tibia following axial tibial loading and (B) dynamic histomorphometry image following four weeks of loading.

The yellow regions in the FEM correspond to the neutral axis where minimal strain is experienced. The yellow and blue arrows in (B) highlight the sites of clear bone resorption, with cortical bone scalloping and lack of fluorochrome labels. Scale bar in B represents 500µm. (A) adapted from Moustafa *et al* [8]

newly increased loading stresses and to maintain the “habituated state” appropriate for the loading stimulus. This is consistent with the earlier mentioned study in trabecular bone [586]. Considering the DH data collectively, when designing experiments with endpoints directly associated with bone formation rates, the most appropriate time to make measurements is within the second week after onset of loading.

Although formation and resorption appeared to be happening concurrently in the endosteal surface in this study, they appeared spatially separate in their occurrence, suggesting the anabolic response to loading was primarily a modelling response. This is consistent with an earlier study by our laboratory which demonstrated that inhibition of osteoclast activity with the bisphosphonate risedronate did not impair the osteogenic

response to loading in young adult mice, also suggesting that the osteogenic response to loading in mice is primarily a bone modelling response [34]. *In vivo* time-lapse μ CT imaging has also demonstrated that ~80% of formation occurring following loading of tail vertebrae occurred in sites where no previous resorption had occurred, suggesting a primarily modelling-based mechanism for anabolic bone gain following loading in trabecular bone of mice [586].

In this study, we have demonstrated bone formation within the first 7 days after onset of loading. Mantila-Roosa *et al* [611] demonstrated osteoid formation in loaded bones histologically, 4 days after loading and Forwood *et al* [580] have demonstrated that bone formation rate was increased compared to baseline within 4 days. Periosteally, formation was significantly greater in the second week of loading. The bone formation response was also greater periosteally than endosteally, particularly during the second week of loading. This suggests that the formation rates in the load responsive region of the tibia are consistent in the first three weeks of loading on the endosteal surface, but appear to peak in the second week for the periosteal surface. According to finite element modelling, the periosteal compressive strains at the posteriolateral cortex are generally greater than those at the endosteum in the same position during axial compressive loading [8, 30, 612]. In these young mice, the delay in peak formation is likely to reflect the time it takes for osteoblasts to proliferate and generate the formation response sufficient to quickly strengthen the loaded bone. Whether these proliferating cells are generated from activation of quiescent bone lining cells, proliferation of these resident bone cells, or migration and proliferation of a distant progenitor population is unknown. Further studies using *in vivo* cellular lineage tracing of these proliferating bone forming cells is currently underway through a collaboration between our group and another laboratory at the University of Connecticut, USA. The apparent reduction in periosteal MAR (although not significantly lower) in the third week compared with the second week after loading further supports the study by Lambers *et al* [586] that demonstrates bone formation reduces after an initial peak stimulated by continued loading once the habituated state has been reached.

The temporal changes in bone formation indices following loading demonstrated in the present study are consistent with a microarray study which explored the transcriptomic changes seen up to 32 days after a single loading episode [611]. This study demonstrated that the transcriptomic response to loading switched to genes associated with matrix production/bone formation within a few days and reached their peak expression around 12 days after loading. This 12-day time point for peak matrix production corresponds well with the apparent peak period of bone formation according to our MAR and BFR.Bs measures.

The experiments described for Objective 1 and 2 have many limitations, chiefly the low experimental power. In addition to greater experimental numbers, extending the duration of loading to confirm the “plateau” of bone formation would be necessary to more precisely identify the point where bone formation is no longer stimulated by further exposure to loading. Use of internal control limbs can help reduce experimental variance, however, longitudinal examination of a single bone can provide even greater statistical power as the same bone is directly compared before and after intervention. Currently, the best available tool to map and quantify region-specific changes is longitudinal sampling with *in vivo* μ CT. This permits direct evaluation of sites with new bone (formation sites) and sites that no longer have bone (resorptive sites) compared to the pre-intervention scan in a site-specific manner, allowing rapid and quantitative determination of both bone formation and bone resorption rates. Repeated scanning (>2 sequential images) can also help identify sites which have resulted in bone resorption followed by bone formation, helping quantify the degree of “remodelling” occurring in response to a given intervention, such as loading [586]. Other recent studies have explored the volumetric bone resorption and formation responses in response to loading [30, 31, 530]. An *in vivo* μ CT approach would have made an ideal method to approach the present experiment but was unfortunately not possible in our laboratory.

The loading response in this experiment was evaluated in young adult female mice only. Old female mice, whilst demonstrated to have a diminished magnitude of response, have not been shown have a delayed response to loading; e.g. old female mice still responded

similarly to young adult mice following a single bout of loading by down regulating their sclerostin expression [29]. The response to loading in female mice was also demonstrated to have the same minimum effective strain in young and old mice, despite the diminished osteogenic response [29]. This suggests that the response in aged mice is not necessarily delayed, despite being diminished in magnitude. The difference in response to loading in aged mice is discussed further in the general introduction (Chapter 1) of this thesis and in later chapters, particularly Chapter 5. Considering the findings from this pilot experiment, when examining processes that are likely to involve the adaptive loading response and related resorption, exploration in the second to third week after start of loading is likely to be most appropriate. Therefore, when planning later experiments in this thesis designed to explore the loading response in aged mice and following SN, we chose to undertake loading experiments for 3 weeks' duration.

3.4.3 The effect of unilateral sciatic neurectomy and contralateral sham surgery on bone mass in the murine tibia using μ CT (Objective 3)

Performing a sham surgery on the contralateral limb used as a control should minimise any surgery-related potential differences between disuse and ambulatory limbs, but this had not been previously investigated. Here we have demonstrated that SN including a contralateral sham surgery resulted in similar changes in tibial bone mass to that reported in papers utilising SN alone.

In our study, right SN with left sham surgery elicited a unilateral resorptive response, primarily via endosteal resorption, with large losses in trabecular BV/TV through reduction in Tb.Th and Tb.N and increases in Ma.Ar without concurrent increases in Tt.Ar. These losses are equivalent to that previously reported in young adult mice following SN without sham surgery [8, 11, 613]. The changes were also similar to the losses reported following tail suspension [614] and Botox injection [467], with reduction in both Tb.Th and Tb.N leading to the reduction in BV/TV.

As detailed previously, cortical bone losses were quite consistent at each site examined, with increasing Ma.Ar and unchanging Tt.Ar for most of the proximal and mid-length

diaphyseal bone. The distal bone did appear to have a small (-2.7%) but significant decrease in Tt.Ar in the SN limb with no change in Ma.Ar, compared to control limbs. This may indicate slight periosteal resorption, although active periosteal resorption is relatively uncommon. Furthermore, according to an *in vivo* μ CT and FEM study, resorption on the periosteum does not appear to be related to the strain levels experienced, unlike on the endosteal surface [529]. As the decrease identified is relative to the control limb, the apparent reduction in Tt.Ar could also indicate a possible inhibition of age-related periosteal expansion in the SN limb that continues to occur in the control limb. Periosteal expansion is a recognised process associated with aging in bone and is thought to be an adaptive response to compensate for the loss in strength seen with endosteal resorption that increases with age [615]. It is possible that the periosteal expansion normally seen with aging did not occur in the disuse limb as the bone was not undergoing as much loading and as such the adaptive response to expand the cortex to improve bending strength was not perceived as necessary.

Few other studies have explored site-specific changes along the length of the tibia following disuse. The μ CT images from mice included in this experiment were, however subsequently used in a study exploring the site specific effects of several different interventions, including disuse [7] using a novel, semi-automated Site Specificity Analysis software. The manuscript for this paper is included in Appendix 4 of this thesis. The study by Galea *et al* [7] showed consistent results with the multiple single-site analyses performed for this study, with no significant effect of SN on Tt.Ar, but a bone-wide reduction in Ct.Ar and Ct.Th. Ma.Ar was only significantly increased in the cortical bone regions proximal to the 50% site following SN. Due to the versatility and effectiveness of this new analysis tool, SSA was subsequently, where appropriate, used in subsequent experiments planned for this thesis.

This experiment has some limitations in its design. Primarily, as our goal was to determine if contralateral sham affected the response to unilateral SN, inclusion of a control group where no sham was performed on the contralateral limb would help provide a contemporaneous control group, rather than comparing to historical control values from

previous studies. Furthermore, to help determine if SN itself, and not the surgical trauma associated with it, elicits any systemic effects on bone mass, inclusion of a right sham operated group (no disuse) would help determine if limb denervation alone results in changes in the bone mass of the contralateral limb.

Although we have previously reported no apparent negative effects on the loading response of SN mice compared to sham operated mice [35], two previous studies have demonstrated reduced bone mass in the contralateral distal femur and/or proximal tibia, but not the diaphyseal femur/tibia, following denervation [593, 598]. This suggests that neurectomy of the limb may result in systemic changes which negatively affect the trabecular bone mass. Botulinum toxin has also been shown to have a negative effect on contralateral limb bone mass [616], probably due to systemic circulation of the toxin after intramuscular injection. The sympathetic nervous system has been demonstrated to have a role in control of bone mass [617-620], however, chemical sympathetic blockade of mice does not result in significant reductions in bone formation following loading [35, 599].

Decreased loading of bone without denervating the limb is possible with cast immobilisation, although this hampers the application of intermittent axial compressive loads – one of the prime reasons we preferentially use SN as a model of unilateral disuse. Section of the patellar tendon functionally reduces mechanical loading and has been used as a model for experimental tibial disuse [106, 621] and avoids the potential effects of limb denervation. However, this procedure leaves a surgical wound on the cranial aspect of the stifle, where the loading apparatus compresses the proximal end of the tibia, thus making it an unsuitable option for use in our mice.

Whilst the design of our experiment precluded direct comparison of sham operated with non-sham operated mice, due to lack of relevant control groups, our intention was to ensure that we were still able to elicit a unilateral resorptive response with the modified protocol, including a contralateral sham procedure. In achieving this aim, we were successful. Based on the results of this experiment, contralateral sham surgery performed concurrently to unilateral SN is unlikely to affect the contralateral limb's bone mass or

architecture. For subsequent experiments in this thesis we therefore included sham surgery in our experimental design.

3.5 Conclusions

1. That the appropriate time point for analysing cortical bone structure changes following axial tibial loading is not before weeks after the onset of loading
2. That the appropriate time to study the effect of loading on bone formation rate is from 7-14 days after the onset of loading.
3. There appears to be no effect of sham surgery on bone loss induced by SN, as detected by μ CT. This procedure should be incorporated in experimental protocols involving unilateral SN.

Work within this chapter contributed to a peer-reviewed publication. A copy of the published paper is included in Appendix 4 of this thesis:

Galea, G. L., Hannuna, S., Meakin, L. B., **Delisser, P. J.**, Lanyon, L. E. & Price, J. S. (2015). *Quantification of alterations in cortical bone geometry using Site Specificity Software in mouse models of aging and the responses to ovariectomy and altered loading*. *Frontiers in Endocrinology*, 6. DOI=10.3389/fendo.2015.00052

Chapter 4

Is RANKL involved in bone (re)modelling associated with altered mechanical loading?

Chapter 4 – RANKL and bone remodelling during mechanical loading

4.1 – Introduction

Bone cells adapt bones' mass and architecture to withstand the mechanical forces to which they are subjected. This tightly controlled balance of bone formation by osteoblasts and bone resorption by osteoclasts is locally controlled by a negative feedback mechanism, with loading-engendered strain as the controlling stimulus. This is known as the mechanostat [12]. Osteocytes, descendants of osteoblasts, encased in the mineralised bone matrix, are now known to play a key role in mechanosensation [18, 22, 104, 622], and the subsequent control of bone formation and resorption [8, 21, 22, 38, 89, 159, 623]. Therefore, evaluating the activity of osteocytes' expression of factors involved in bone (re)modelling provides potentially useful experimental endpoints to assess bone cells' response to mechanical stimuli in bone.

The osteogenic response to changes in mechanical loading has been quite well characterised *in vivo*, although the mechanisms involved with transducing the loading stimulus into an adaptive response are both complex and still incompletely understood. Several microarray experiments have been undertaken exploring the transcriptomic response to mechanical loading and the effect of altered loading context, such as aging, oestrogen hormone deficiency, and disuse [86, 413, 611]. We have previously identified changes in osteocyte expression of several molecules which relate to control of osteoblasts, such as sclerostin and Early Growth Response (EGR) hormone 2, and have used these markers as reliable experimental endpoints, using immunohistochemistry and/or qPCR to confirm significant *in vivo* and *in vitro* biological responses to loading and disuse [8, 29, 577].

The osteocytic control of osteoclasts in bone has been less comprehensively studied. Fairly recent work has, however, highlighted osteocytes as the key source of Receptor Activator of Nuclear Factor κ B (RANK) Ligand (RANKL) necessary for bone remodelling following

unloading. Two seminal papers, published concurrently, were the first to demonstrate that it is osteocytes, and not osteoblasts as previously believed, that are the primary source of RANKL critical for recruitment and activation of osteoclasts involved in bone remodelling [21, 22]. These papers demonstrated that the bone loss seen with disuse was abrogated and that bone remodelling was severely impaired following selective knockout of RANKL in osteocytes. This major paradigm shift in our understanding of the role of osteocytes in regulating osteoclast activity came when the experiments for this thesis were being planned. The studies described in this chapter set out to determine if osteocytic expression of RANKL could serve as a suitable experimental end-point for the evaluation of the osteocytic control of osteoclasts following alterations in the mechanical loading environment. The experiments also aimed to characterise the temporal response of osteocytic RANKL expression following changes in the mechanical environment. Our longer-term aim, at this point, was to explore the role of RANKL in age-related bone loss and how it may be influenced by loading.

4.1.1 Osteocytes as mechanosensors and a source of signalling factors.

That osteocytes are a source of signalling factors that regulate bone (re)modelling has been gaining acceptance over the past 10-15 years [18]. Osteocytes are essential for effective mechanotransduction, a point supported by the demonstration that targeted ablation of osteocytes with Diphtheria toxin resulted in diminished responsiveness to both loading and unloading in the cortical bone of mice [624]. Since it was first established that osteocytes respond to strains in their surrounding matrix [85], evidence has accumulated that their responses are complex and diverse [38, 86]. For example, we have demonstrated in two separate microarray studies that loading produces a rapid and significant increase in the number of genes both up and down-regulated by loading, and that these responses are significantly altered by context, such as oestrogen deficiency, aging and prior disuse [86, 413].

Osteocytes are a key source of signalling factors involved in controlling subsequent bone formation by osteoblasts in response to loading [8, 18, 38, 625]. Sclerostin, an inhibitor of the potentially osteogenic Wnt pathway, and expressed almost exclusively in osteocytes, has

been, using a combination of both *in vitro* and *in vivo* techniques, repeatedly demonstrated to respond to changes in mechanical loading – its expression decreases 12-24hrs following loading and increases after 3-4 days following unloading [8, 20, 159, 160, 414, 528, 623, 626]. This reliable “inverse relationship” between sclerostin and strain underlies the importance of sclerostin as a signalling molecule for the regulation of bone mass in response to changes in loading. Furthermore, this change in sclerostin expression with altered loading has been used as a reliable experimental endpoint by us to help confirm the biological response to mechanical stimulation in mice [29, 159].

Additionally, the transcription factor, EGR-2, following its initial identification as an early mechanoresponsive gene [627], was identified as another potential candidate for use as a suitable experimental endpoint to monitor immediate transcriptional responses to a mechanical stimulus (mechanosensation). In a microarray study by our laboratory, of the genes shown to be differentially regulated by disuse and loading, bioinformatics analysis revealed EGR2 as being more closely associated with more pathways and functions than any other transcription factor [86, 577]. Given we have demonstrated that EGR2 is upregulated within 30 minutes of application of mechanical strain *in vitro* and within 3h *in vivo* [577], our lab has since used EGR-2 expression as an endpoint to detect early transcriptional responses related to mechanosensation. For example, Meakin *et al* [29] used changes in the expression of EGR2 and sclerostin to confirm that the mechanosensory response to mechanical loading in aged female mice is maintained, despite the impaired formation response compared to young mice. This study concluded that it is, instead, the proliferative responses of the osteoblasts that are reduced in the age-related impairment of bone’s osteogenic response to mechanical loading.

Although there is a significant body of work exploring the control of osteoblast activity by osteocytes, less attention has been paid to their potential role in controlling and targeting the equally important activity of resorption by osteoclasts [89]. The RANK/RANKL pathway is probably the most important pathway for osteoclast recruitment, differentiation and activation [628]. More detailed discussion of the role of RANK/RANKL in the control of bone mass is included in Chapter 1 of this thesis.

Considering the recent demonstrations that mice with osteocytic knockout of RANKL did not lose bone mass following unloading of bone [21], RANKL appears to be an essential factor in the osteocytic control of bone resorption by osteoclasts. At the time of experimentation, however, there was limited evidence of changes in RANKL expression in osteocytes of wild-type mice associated with disuse. One study demonstrated that RANKL qPCR expression was increased following 3 days of tail suspension [629], however this study was performed on whole proximal tibias, including marrow and articular cartilage, and not solely the osteocyte-rich cortical bone. A more recent study has demonstrated a mild increase in RANKL expression in whole cortical bone after 3 weeks of tail suspension [21]. Moriishi *et al* [136] demonstrated increased RANKL expression following unloading after 3 days, although this unloading-related increase was specific to osteoblastic cells, and not osteocytes. Furthermore, RANKL expression was also increased in tibial bone marrow following both tail suspension [560] and sciatic neurectomy [137], although marrow samples usually contain very few osteocytes. Contrarily, Gerbaix *et al* [630] have demonstrated no effect of unloading on RANKL mRNA expression at 3 days. A microarray study performed in our laboratory, on adult mice explored the effects of disuse on the transcriptomic response, but only at one time-point (4 weeks) after unloading induced by SN [86]. RANKL expression was unaffected by SN in this study, although this delayed time point may have missed the acute cellular signalling changes associated with the onset of disuse that we were interested in. Use of *in vitro* models to simulate microgravity have met technical difficulties, although one study using a rotating centripetal force system to counter gravitational forces on a 3D osteocytic cell matrix resulted in increased RANKL expression, concurrent to upregulation of sclerostin [623]. It is worth noting that these studies only explored a single time-point following onset of unloading and as the expression of RANKL is likely to be transient following changes in the loading environment, those not demonstrating any change with disuse may have missed the peak expression time-point.

Interestingly, to the author's knowledge, only one time-course experiment exploring the temporal pattern of adaptive changes seen with disuse is reported. This study used histomorphometry and radio-isotope incorporation, and found that bone formation was

only temporarily halted for up to two weeks, but then formation indices returned to control levels, despite continued unloading with tail suspension [558]. Unfortunately, this study did not quantify resorption indices, or expression of any osteoregulatory proteins.

Since the osteogenic response to loading primarily involves modelling, RANKL's importance in disuse-associated bone resorption is likely more significant than in response to increased mechanical loading. However, control of osteoclast activity following increased mechanical loading is still important. The effect of increased mechanical loading on the expression of RANKL is less consistent than loading's effect on sclerostin expression. *In vitro* experiments have given conflicting results with application of strain to bone cell cultures. These vary from increased expression with strain to decreased expression [129-135, 631]. Unfortunately, the techniques of load application were not the same in these studies, so comparison is difficult, and additionally, the *in vitro* response to load may not necessarily correlate with the *in vivo* situation as the three-dimensional orientation and lacuno-canalicular arrangement of osteocytes in bone, together with the many added complexities of the *in vivo* environment may confer additional and/or different responses to mechanical load. The quantification of RANKL expression *in vivo* in situations of increased mechanical load has also not been extensively investigated. RANKL and IL-6 expression were elevated in rats trained to jump whilst carrying additional loads – suggesting microdamage resultant from overloading [632]. Kennedy *et al* [112] also demonstrated increased RANKL expression associated with micro-crack formation following fatigue loading. Evaluation of RANKL/OPG expression in response to non-destructive loading protocols *in vivo* is not well reported. Grosso *et al* [633] have demonstrated an increase in OPG expression following 3 days of loading, although the RANKL expression was not affected.

Microarray studies performed by our laboratory have not demonstrated a change in RANKL following loading (up to 72 hours after loading), despite changes in *Sost* [86, 413]. The more recent study did demonstrate a slight upregulation in OPG expression following loading, suggesting a possible mechanism for the down-regulation of bone resorption seen following loading. To the author's knowledge, no reports exist demonstrating the

temporal changes in RANKL expression following loading or onset of disuse. Osteoprotegerin (OPG) is a competitive decoy receptor for RANKL, and is produced by both osteocytes and osteoblasts. Increased expression of OPG can reduce activity of RANKL by altering the RANKL:OPG ratio. Hence, changes in the concentration of OPG can affect the degree of bone resorption even if RANKL expression does not change. See Figure 35 for a simplified organogram of the interactions between RANKL, Sclerostin and OPG with loading.

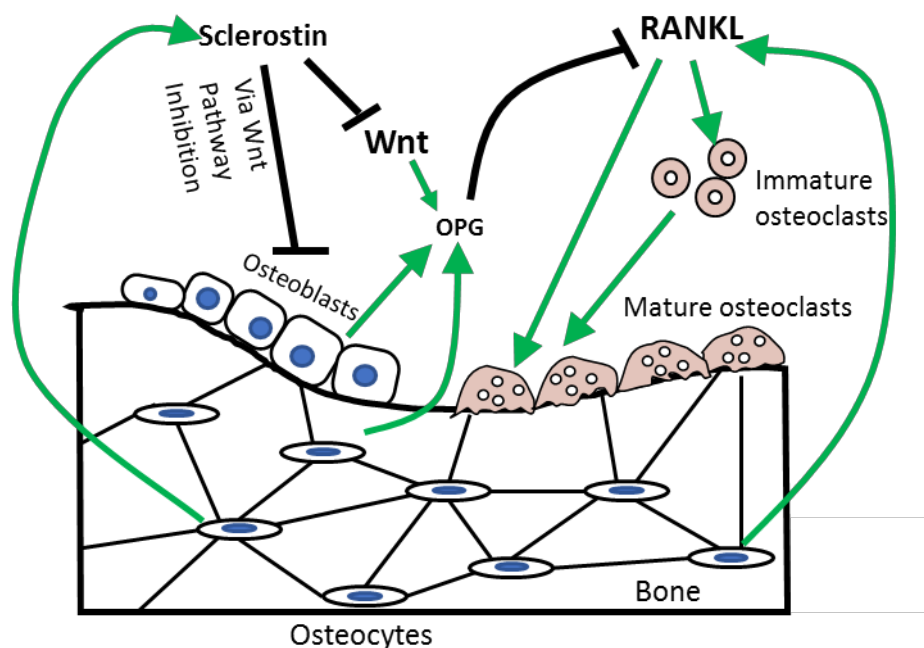


Figure 35 – Simplified organogram depicting the interactions between RANKL, OPG and Sclerostin.

RANKL, produced by osteocytes stimulates the differentiation and activation of osteoclasts. OPG, produced by osteoblasts, and osteocytes, inhibits activity of RANKL by acting as a decoy receptor. Sclerostin, produced by osteocytes, inhibits the Wnt pathway, which impairs osteogenesis, and also OPG production.

Considering the demonstrated links between RANKL, Sclerostin and OPG, our aim was to explore the temporal changes, in young adult mice, in expression of RANKL, Sclerostin and OPG following both disuse, induced by sciatic neurectomy (SN), and following increased

loading, induced by axial tibial compression. The techniques used were immunohistochemistry and qPCR.

4.1.2 Optimising RANKL immunolocalisation in bone

Whilst protocols for the immunolocalisation of sclerostin in bone are well established, one challenge of investigating RANKL regulation by strain is the paucity of commercially available antibodies with which to detect it. RANKL is membrane-bound but can be cleaved from its cell membrane to form serum RANKL. *In vitro* studies have shown that the membrane-bound form of RANKL is much more effective at stimulating osteoclastogenesis than serum soluble RANKL [22, 123-126]. Therefore, identifying cellular changes, rather than serum changes in RANKL was viewed as the most appropriate experimental endpoint for this thesis. We have previously published studies using qRT-PCR of the cortical bone shell following marrow removal to examine the transcriptomic osteocytic responses to loading and other interventions, [29, 286, 419] and also developed a reliable protocol for immunolocalisation of sclerostin in osteocytes [8], however, prior to this project being undertaken, we had not undertaken any studies to investigate osteocytic RANKL expression by IHC.

However, at the time of undertaking these studies, RANKL protein expression using IHC had been reported in other normal tissues including osteoblasts, bone marrow cells, lymphoid tissues, mammary glands, intestinal glandular cells, hair follicles, renal tubules, and also diseased tissues, including synovial fibroblasts during rheumatoid arthritis and in primary osteosarcoma and giant cell tumours of bone [95, 141, 634-640], but only in one report had RANKL been studied in cortical bone osteocytes [22]. This report did not, however, report with IHC that RANKL expression changed with decreased loading, only that it was present in osteocytes of wild-type mice and not in transgenic knockout mice.

To the author's knowledge, at the time of experimenting, there were no reports documenting the use of immunohistochemistry to study changes in expression following intervention (eg. changes in loading or OVX) in cortical bone. This probably reflects the challenges in effectively localising osteocytic RANKL using immunohistochemistry, and its

apparent low level of expression. To study changes in expression of RANKL following changes in the loading environment, we sought to optimise a protocol initially developed by Prof Larry Suva at University of Arkansas for Medical Science (UAMS) to immunolocalise RANKL in the fracture callus following experimental fracture of the tibia (unpublished data).

Our final aim was to use changes in RANKL and Sclerostin expression in osteocytes to further validate the revised surgical model for sciatic neurectomy (SN) introduced in Chapter 3 (including a contralateral sham surgery in the left leg). As described in Chapter 3, we have confirmed that unilateral SN with contralateral sham surgery resulted in equivalent bone loss to that seen with SN performed without contralateral sham.

Although the SN model is clearly effective at reducing strain-related stimuli, it is invasive (albeit minimally), requiring a small surgical incision in the proximal hindleg. Change in RANKL expression following surgical trauma was especially of concern as its expression is also affected by inflammatory cytokines, such as PGE₂ and various interleukins. These cytokines are known to be associated with bone loss through increased expression of, or synergism with RANKL [601]. When designing experiments for this thesis aimed at evaluating the effects of disuse on the expression of RANKL, we were concerned that the surgical procedure itself may be sufficient to cause an acute local inflammatory response sufficient to alter the expression of these cytokines involved in bone adaptation, separate from its effects on the mechanical environment. Inclusion of a sham surgery control group enabled us to control for the effect of surgical trauma on the acute local inflammatory response and any subsequent bone loss. As we had not included a sham surgery group in previous studies, it was important to establish whether or not the procedure itself could potentially change the expression of RANKL.

4.1.3 Objectives

4. *Optimise a protocol for immunolocalisation of RANKL in decalcified, paraffin-embedded murine cortical bone.*

5. *Describe the effect of contralateral sham surgery on the osteocytic expression of RANKL and sclerostin protein in mice following unilateral disuse engendered by SN, using IHC.*
6. *Describe the effect of disuse, engendered by SN on the osteocytic expression of RANKL and sclerostin protein, using IHC.*
7. *To establish the temporal response to disuse engendered by SN on the mRNA expression of RANKL, OPG and Sost using qRT-PCR.*
8. *Describe the effect of increased mechanical loading on the expression of the RANKL and sclerostin protein, using IHC*
9. *To establish the temporal response to a single episode of mechanical loading on the mRNA expression of RANKL, OPG and Sost using qRT-PCR.*

4.2 Materials and Methods

4.2.1 Optimise a protocol for immunolocalisation of RANKL in decalcified, paraffin-embedded murine cortical bone (Objective 1)

Tables describing solutions and the final protocols used for immunohistochemistry are included in Appendix 2. Four different methods for immunolocalisation of RANKL in mouse cortical bone were tested.

Protocol 1

8µm transverse sections of mouse tibial bone used for initial protocol assessment were provided by Dr Gabriel Galea. These had been prepared as described in Chapter 2.

Protocol 1 was essentially as described for sclerostin by Moustafa *et al* [160]. However, as work done by other members in the lab had previously found this protocol ineffective for detecting RANKL, an antigen retrieval step was included. Briefly, the protocol was as follows:

- Initial rehydration steps with graded alcohols. All steps are separated by wash in triplicate with PBS suctioned off slides and replaced – liquids retained around sections by hydrophobic pens (ImmEdge™ - Vector Labs, Peterborough, UK).
- Antigen retrieval: 10mM citrate buffer at pH 6.0 for 2 hours at room temperature
- Peroxidase blocking solution: 3% hydrogen peroxide in methanol.
- 1° polyclonal goat anti-mouse RANKL (C-20- Santa Cruz Biotechnology, Dallas, USA) 1:50 incubated overnight at 4°C.
- Biotinylated 2° antibody (rabbit, anti-goat IgG (Dako, Ely, UK) 1:50 for 30 mins.
- Apply ABC solution (Vector ABC, Vector Labs, Peterborough, UK), prepared according to manufacturer's instructions – 30 mins.
- DAB chromogen (Vector Labs, Peterborough, UK) left to develop for 5 minutes.
- Formalin fixed, paraffin-embedded (FFPE) mouse spleen sections (8µm thick) were trialled as positive control sections, due to their high concentration of T-lymphocytes, shown to express RANKL [641].
- Slides were then dehydrated and mounted.

Protocol 2

As described for protocol 1, but with shorter DAB development time of 3 minutes.

Protocol 3

For this study, we collaborated with Professor Larry Suva at the University of Arkansas for Medical Science (UAMS) who had recently developed a protocol for localisation of RANKL in decalcified cortical bone sections. The author undertook an externship at Professor Suva's laboratory at UAMS for training in IHC techniques.

- 6µm FFPE decalcified transverse sections of the tibial cortical diaphysis of 17-week-old female C57BL/6 mice were used.
- FFPE longitudinal sections from 3-4 month old wild-type mouse tibias that had undergone distraction osteogenesis for another study [642] were included as positive controls, as hypertrophic chondrocytes and the highly active regenerative

endocortical new bone formed during distraction osteogenesis stained strongly for RANKL protein (Personal communication, L. Suva – unpublished data).

- The antigen retrieval with citrate buffer was performed by heating the buffer to boiling point then placing the slides in for 60 minutes, whilst allowing the solution to cool slowly to room temperature.
- Washing was through immersion in PBS on an oscillating platform.
- 1° antibody was changed to a different batch, which had been validated for immunohistochemistry on FFPE sections. (RANKL N-19, Santa Cruz Biotechnology, Dallas, USA) and incubated overnight at 4°C.
- Proprietary ImmunoCruz™ ABC staining system (Santa Cruz Biotechnology, Dallas, USA) was used according to manufacturer's instructions
- 2° antibody was diluted to 1:200.
- The DAB was left to develop for 120 seconds.
- The sections were counterstained with haematoxylin for 10 or 30 seconds then washed and mounted.

Protocol 4: Antibody Concentration trial

- All steps were repeated as for protocol 3, except that a RANKL concentration gradient trial was performed.
- The primary antibody was made to 1:50, 1:75, 1:100 and 1:200.
- Counter-stain was changed to 1%, 0.5% or 0.25% Light green solution, and slides were stained for 45 seconds before washing, dehydrating and mounting.

Identification of a positive control cell population for RANKL IHC.

While trialling /testing the above protocols, we also sought to identify a suitable, readily available and strongly staining cell population as a positive control. The following mouse tissues were examined to evaluate RANKL staining intensity: spleen, bone fracture callus from distraction osteogenesis model mice (Courtesy of Professor Larry Suva from UAMS) and proximal tibial epiphyseal bone, including the articular cartilage and the hypertrophic

chondrocytes of the growth plate. Each of these tissues were evaluated for general stain intensity, specificity and clarity.

4.2.2 *In vivo* procedures

4.2.2.1 *Sciatic neurectomy to investigate RANKL and sclerostin expression following disuse*

Effect of disuse on RANKL/Sclerostin expression - IHC (Objectives 2 and 3)

To determine the effect of sciatic neurectomy plus sham surgery on RANKL and Sclerostin protein expression, 17-week-old female C57BL/6 mice underwent right SN alone (SN only) (n=4) or right SN and left sham (Sham+SN) (n=4) to determine if left sham surgery effected the SN-associated changes in expression of RANKL and/or sclerostin. Mice were killed 4 days after surgery and limbs dissected, fixed, decalcified and sectioned according to the protocols described in chapter 2 for IHC staining for RANKL and sclerostin.

Effect of disuse on RANKL/*Sost* expression - qRT-PCR (Objective 4)

For this temporal study of RANKL and *Sost* expression, 17-week-old female C57BL/J mice (n=48) underwent right SN and left sham surgery. Six weight-matched groups (n=8) were created and mice were killed at 0, 3, 6, 12, 24 or 72 hours following surgery. Tibiae were harvested as described in Chapter 2 and the cortical bone shells samples stored at -80°C for qRT-PCR later.

A further experiment was undertaken using the same experimental design, as an additional time point, where mice (n=8) were killed 2 weeks after Sham+SN. Sampling and specimen preparation was identical.

4.2.2.2 *Axial tibial loading to investigate RANKL and sclerostin expression following increased loading*

Effect of loading on RANKL/Sclerostin expression - IHC (Objective 5)

Female 17-week-old C57BL/6 mice underwent one single loading session to a peak strain of 2500 $\mu\epsilon$ then were sacrificed 24 hours after loading and their tibiae were prepared for

sectioning and IHC as described in Chapter 2. The mice used for this experiment were originally from an experiment performed in our lab by Dr Lee Meakin which has been published, describing the effects of loading and ageing on sclerostin expression [29]. Sections from this experiment were used for RANKL and sclerostin immunolocalisation in the present study.

Effect of loading on RANKL/*Sost* expression – qRT-PCR (Objective 6)

Female 17-week-old C57BL/6 mice (n=24) were divided into 3 weight-matched groups of n=8. All mice underwent one single loading session on the right tibia to achieve 2500 μ E on the medial tibial surface (14.97N). Mice were killed 6h, 12h or 24h after loading and tibial cortical shells prepared for qPCR as described in Chapter 2.

4.2.3 *Ex vivo* procedures

4.2.3.1 *Ex vivo* procedures

Immunohistochemistry

Immunohistochemistry to identify osteocytic RANKL and Sclerostin was performed on FFPE decalcified transverse bone according to the protocol described in section 4.2.1, and tabulated in Appendix 2.

The RANKL IHC protocol optimised in objective 1 (protocol 4) was used to examine the proportion of positive staining osteocytes in cortical bone of the posteriolateral cortex of the 37% site as this site has been demonstrated to have a high degree of load responsiveness based on previous μ CT and finite element modelling of the murine tibia in previous studies [8, 643]. RANKL and Sclerostin positive osteocytes in sections were quantified in the Sham+SN and SN only groups after blinding the author to treatment group through randomising and re-numbering the digital images to eliminate possible bias. Blinding Key assignment was performed using Microsoft Excel, and digital micrograph images were renamed by a colleague not involved in counting, and this key was then used to reassign each value to the correct animal/limb after counting was complete.

Counting of immunopositive and negative osteocytes was performed on a single high-power field (400x) of at least 6 separate cortical bone sections from the posteriolateral tibial cortex at the 37% site, measured from the proximal end, the region demonstrated to be most load-responsive [8]. After counting the percentage of positive osteocytes was calculated as: % positive cells = positive osteocytes/(positive+negative osteocytes) x 100. This value was calculated for each mouse and the mean values for each group are reported.

qRT-PCR

The cortical bone samples were prepared and analysed as described in Chapter 2 to establish the relative expression of *Sost* (Sclerostin), TNFSF11 (RANKL) and TNFSFR11B (OPG) mRNA using qRT-PCR at the above time points following induction of unilateral disuse. β 2MG was used as the house-keeping gene and the left leg was used as the internal control limb as previously reported [29, 286, 419]. Primer sequences are listed in Chapter 2.

4.2.4 Statistical analysis

For the IHC experiments, any two related parameters measured within the same animal (eg. control left and neurectomised right limbs) were compared using a paired Student's T-Test or a repeated measures ANOVA for analyses with multivariate effects including a paired variable. In the qRT-PCR timecourse experiments, comparison of expression for each gene was performed using a mixed design ANOVA with limb as a repeated measure and time-point as a fixed effect. Sidak post-hoc tests for multiple comparisons were performed where the main effect was found to be significant. Significance was set at $p < 0.05$. All analyses were performed with SPSS Version 23 (IBM Corp, Armonk, NY)

4.3 Results

3.3.1 Objective 1: Develop a protocol for immunolocalisation of RANKL in decalcified, paraffin-embedded murine cortical bone.

As seen in Figure 36, using Protocol 1, there was non-specific background staining in control IgG sections, particularly in marrow and skeletal muscle. A likely explanation for this is that the DAB exposure was too long in and/or the antibody concentration was too high. Therefore, the DAB development time was reduced in protocol 2. However, there was still visible chromogen development in the control slides, particularly around the perivascular tissues (Figure 36B), skeletal muscle and marrow where endogenous peroxidases may be at greater concentrations, and where antibodies are more likely to non-specifically bind.

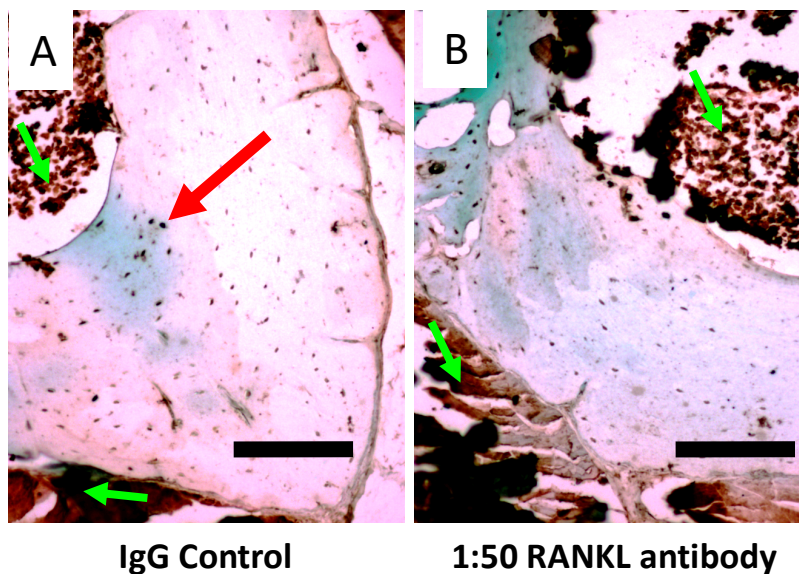


Figure 36 – Immunolocalisation of RANKL in mouse cortical bone (Protocol 1)

Low power representative images from sections of cortical bone stained using protocol 1 demonstrating high levels of non-specific staining. Note the high chromogen stain intensity particularly noted in the marrow and skeletal muscle of both (A) control IgG and (B) RANKL Ab slides (yellow arrows). Note also the positive staining osteocytes even in the control IgG sections (red arrow). Scale bars = 100µm.

For protocol 3, based on advice from Professor Larry Suva at UAMS, we changed the antibody batch and antigen retrieval steps to help expose the epitopes more effectively, which in turn enabled a reduction in the DAB development time. In addition, the counterstain was exchanged for haematoxylin. However, because it is a nuclear stain, the haematoxylin counterstain limited the ability to visualise if the osteocytes were positively stained due to high nuclear:cytoplasm ratio (Figure 38A). Even in the slides only stained with haematoxylin for 10 seconds, the cytoplasmic detail was still obscured for osteocytes. This still resulted in quite strong nuclear staining. the haematoxylin stain intensity was too great to allow effective quantification of the positive staining osteocytes, despite lowering the immersion time for slides (Figure 38A-B).

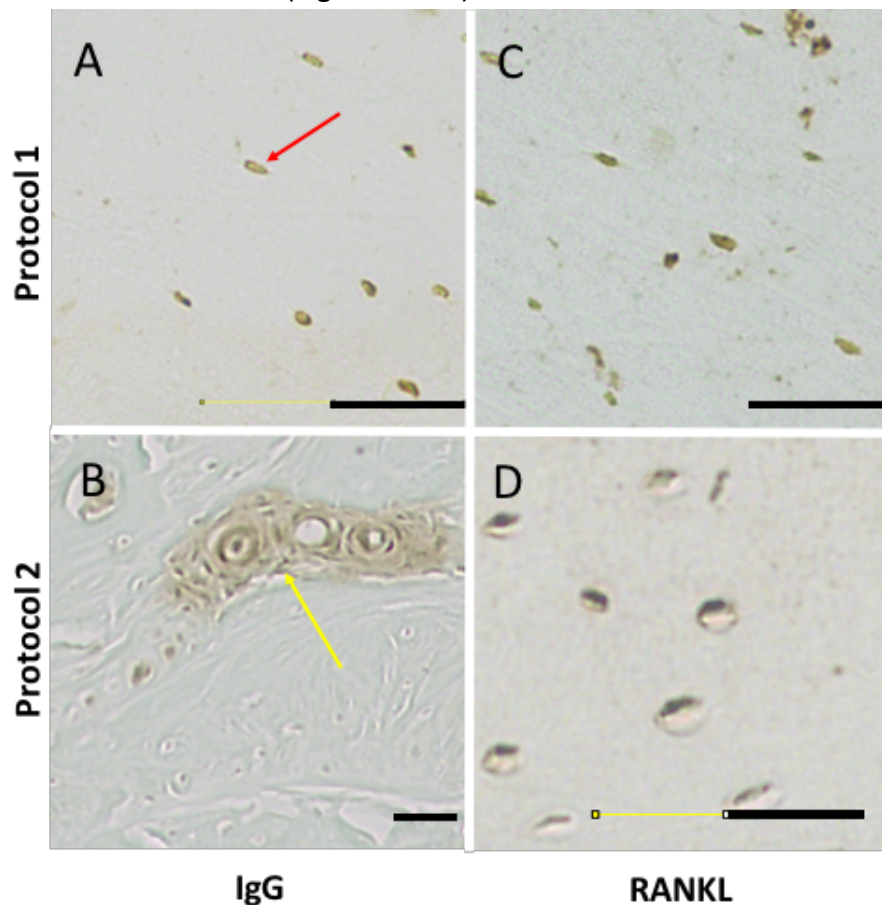


Figure 37 – RANKL immunolocalisation in mouse cortical bone according to (A, C) Protocol 1 and (B, D) Protocol 2.

These sections are representative images of osteocytes in negative IgG control sections (A, B) and RANKL stained sections (C, D). Positive staining osteocytes are visible in the negative IgG control sections in (A) (red arrow). The perivascular cells in (B) still show positive staining in the IgG control section (yellow arrow). Scale bars = 25 μ m.

As nuclear staining limited the ability to identify and count of positively staining osteocytes, in protocol 4 a concentration gradient of light green counterstain was performed as it is a general protein stain and allows better contrast between the brown colouring of the DAB chromogen. Furthermore, protocol 4 used an antibody stain dilution gradient to identify the most appropriate antibody concentration. The only dilution that resulted in sufficient osteocyte stain intensity without excessive background staining was 1:50 (Figure 39).

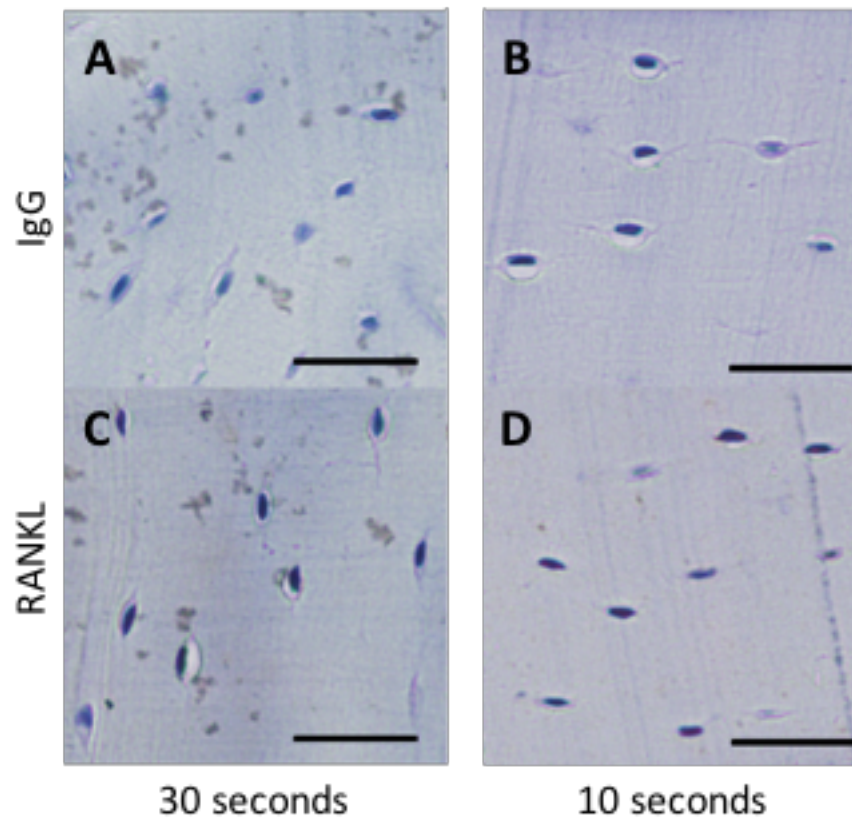


Figure 38 – RANKL immunolocalisation in mouse cortical bone (Protocol 3).

These sections are high power representative images of osteocytes in negative IgG control sections (A, B) and in RANKL labelled sections (C, D). Slides were then counterstained with haematoxylin for (A, C) 30 seconds (B, D) and 10 seconds. Note the difficulty in identifying the positive staining osteocytes due to staining of the nuclei in osteocytes. Scale bars = 25 μ m.

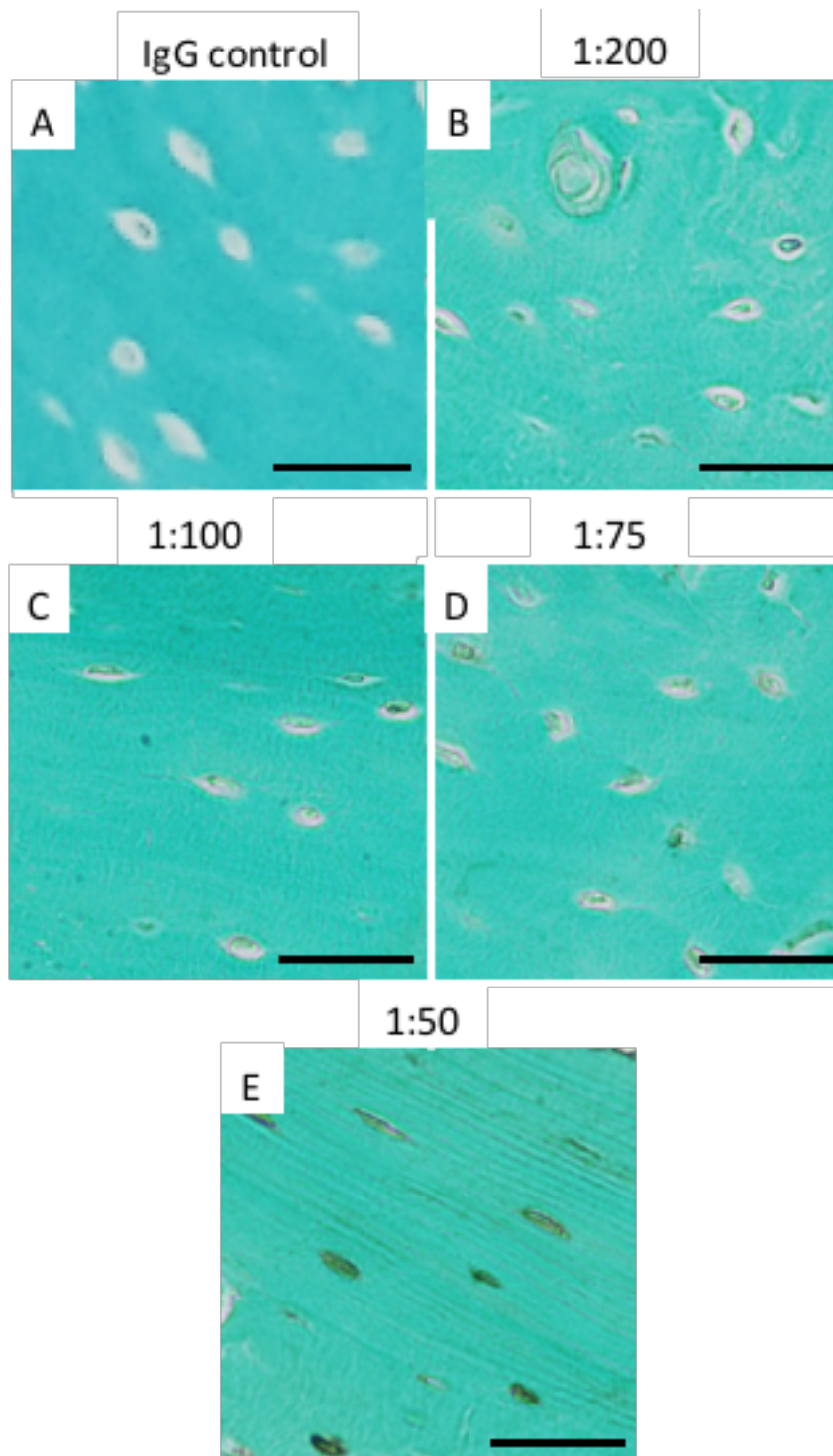


Figure 39 – RANKL immunolocalisation in mouse cortical bone (Protocol 4)

(A) 1:50 IgG negative control. (B-E) RANKL Antibody dilutions: (B) 1:200; (C) 1:100; (D) 1:75 and (E) 1:50. Note gradual increase in stain intensity in osteocyte lacunae, with 1:50 showing clearer staining than all lower dilutions. Scale bars = 50µm.

Figure 40 demonstrates the reduced concentration of Light Green (0.5% and 0.25%) at the lowest two antibody dilutions (1:100 and 1:50). Optimising this protocol demonstrated that the 1:50 antibody concentration clearly stained osteocytes better than 1:100 and that either concentration of Light Green was suitable.

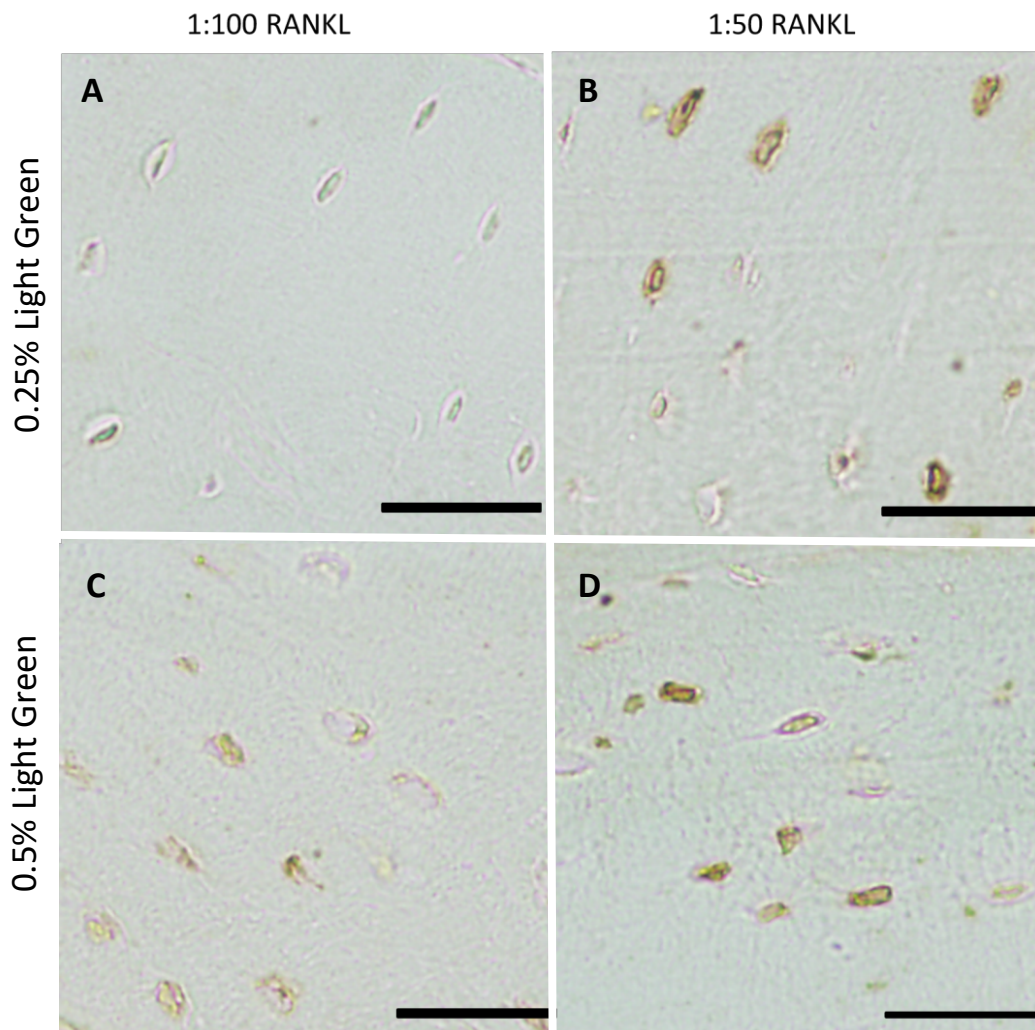


Figure 40 –RANKL immunolocalisation (Protocol 4)

Light green concentration gradient. (A,B) 0.25%, and (C,D) 0.5% Light Green Solution used as counterstain. (A, C) 1:100 and (B, D) 1:50 dilution of RANKL antibody. The staining intensity is not greatly different between 0.25% and 0.5%, and the 1:50 RANKL antibody concentration clearly provides the optimal staining intensity. Scale bars = 50 μ m.

Identification of appropriate positive control cells

The use of mouse splenic sections was unsuitable for use as a positive control, as the cellular density precluded easy identification of positive and negative cells and the endogenous peroxidase activity of the high density of red blood cells may also have enhanced DAB staining (despite blocking with hydrogen peroxide (Figure 41A,B)). Use of the epiphysis and growth plate cartilage revealed the hypertrophic chondrocytes and the articular chondrocytes as suitable and strongly staining cells for use as a positive control cell population in RANKL immunolocalisation (Figure 41C-F). Additionally, the highly active mineralising front in distraction osteogenesis also proved a strongly staining area for RANKL (Figure 41G,H). To eliminate the difficulty of haematoxylin counterstain obscuring the nucleus of the cells of interest, light green counterstain was employed and also demonstrated clear RANKL staining of the hypertrophic chondrocytes (Figure 41I,J).

Megakaryocytes within the bone marrow cell population also stained positively for RANKL and are usually within the same section as cortical bone – unlike the other cells identified in this experiment. The megakaryocytes are visible with either light green or haematoxylin counterstain, but due to their large cytoplasm, they are more easily identified with a nuclear stain, like haematoxylin, than light green (Figure 41 L, M).

Figure 40 – Legend on following page

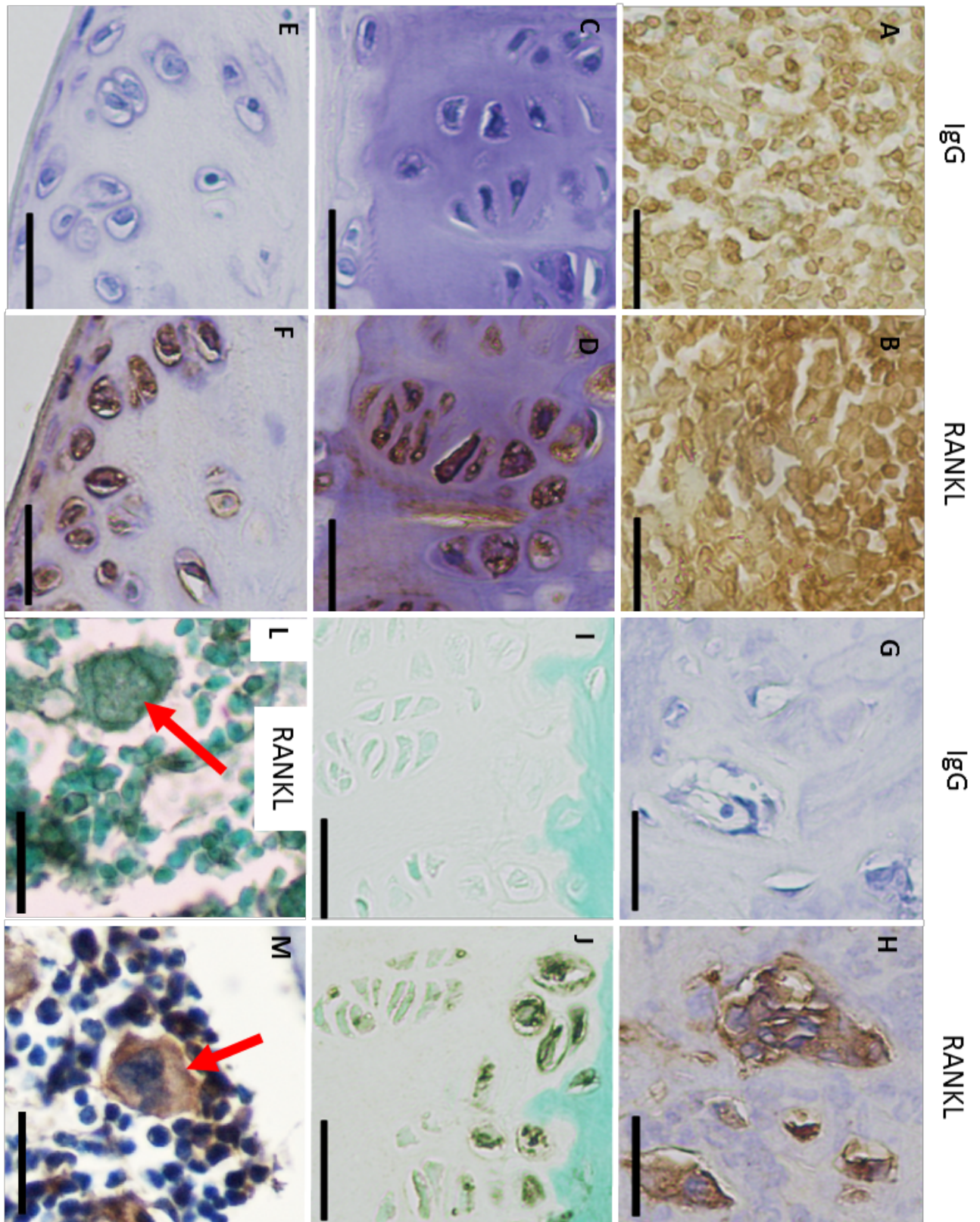


Figure 41 – High power representative images of selected positive control sections following RANKL immunolocalisation.

IMAGE ON PREVIOUS PAGE. (A-B) Mouse spleen sections; (C-D) Tibial growth plate; (E-F) Tibial articular cartilage; (G-H) Endocortical mineralising front in a distraction osteogenesis model; (I-J) Tibial growth plate; (L-M) Tibial bone marrow including megakaryocytes (arrows). A,C,E,G,I are negative control sections. A,B,I,J,L are counterstained with light green solution. All other sections are counterstained with haematoxylin. Scale bars = 25µm.

4.3.2 Objective 2: Describe the effect of contralateral sham surgery on the osteocytic expression of RANKL and sclerostin protein in mice following unilateral disuse engendered by SN, using IHC

After confirming with µCT (Chapter 3) that Sham+SN resulted in similar bone loss to that previously reported without contralateral sham surgery [11] and after optimising the RANKL IHC protocol, we next evaluated the effect of contralateral sham surgery on cortical bone osteocyte expression of sclerostin and RANKL.

There was no significant difference in the number of positive staining osteocytes between SN only and Sham+SN groups for both Sclerostin (Figure 42) and RANKL (Figure 45). Furthermore, there was no difference in the number of positive osteocytes counted between the control limbs that had not had any surgery (SN only group) and those that had undergone left sham surgery (Sham+SN group) for either Sclerostin (Figure 42) or RANKL (Figure 45). The number of positively staining osteocytes is represented in Figure 43 & Figure 44.

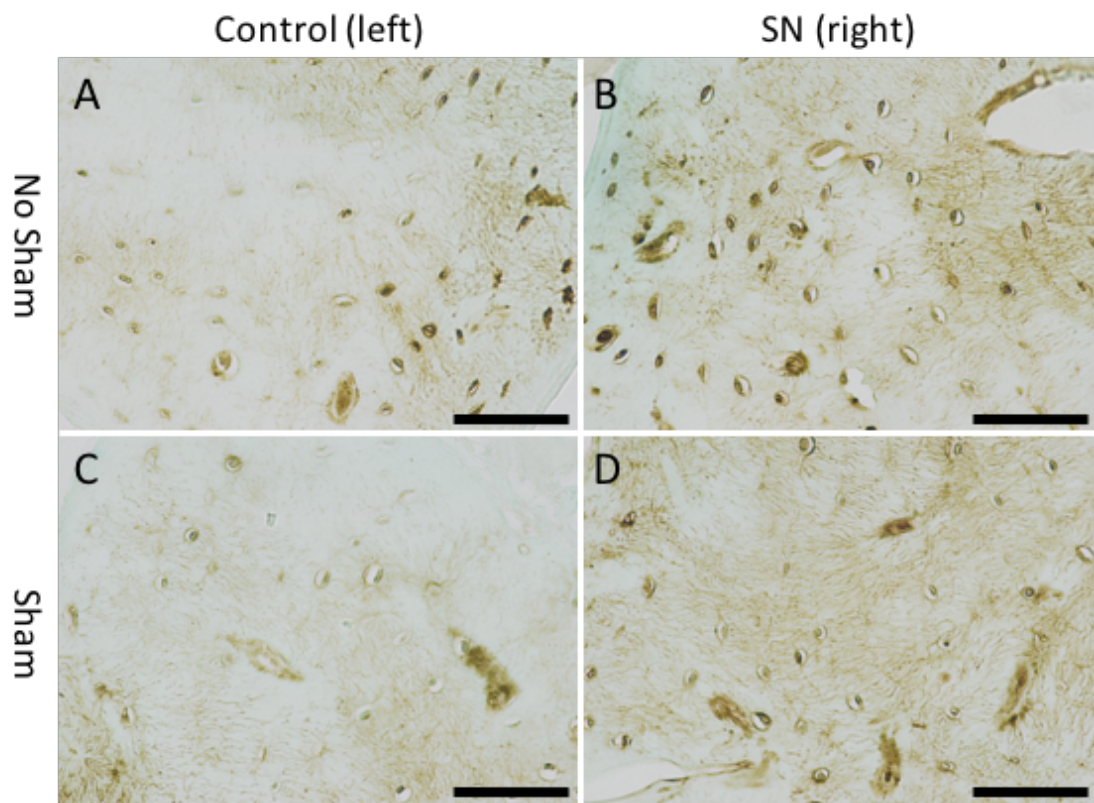


Figure 42 – Effect of sham surgery and disuse (by SN) on sclerostin expression in osteocytes.

17w old female C57BL/6 mice underwent right SN and either no surgery (n=4) or a sham surgery (n=4) on the left limb. Mice were killed 4 days later and Sclerostin IHC performed on sections of bone. Representative high power images of the posteriolateral tibial cortical bone at the 37% site, measured from the proximal end. Left Control limbs (A, C) and Right Disuse limbs (B, D) are demonstrated. Groups had either Right SN only (A, B) or left sham surgery and right SN (C, D). The number of sclerostin positive osteocytes in the control left limbs was not affected by sham surgery, but expression of sclerostin was increased following unloading by SN. Scale bars = 50µm

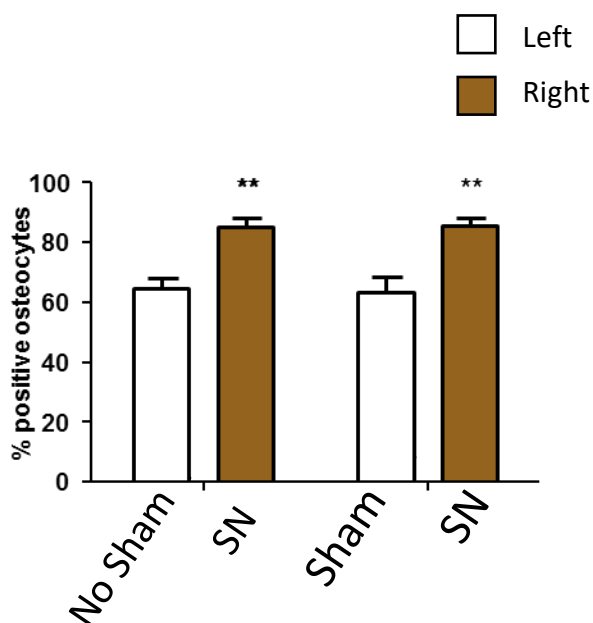


Figure 43 – Effect of sham surgery and disuse (by SN) on sclerostin expression in osteocytes

17w old female C57BL/6 mice underwent right SN and either no surgery (n=4) or a sham surgery (n=4) on the left limb. Mice were killed 4 days later. Results show % of Sclerostin immunopositive osteocytes and groups were compared using a mixed-design repeated measures ANOVA. ** = p<0.01 Right vs left limb. Means ± SEM are reported.

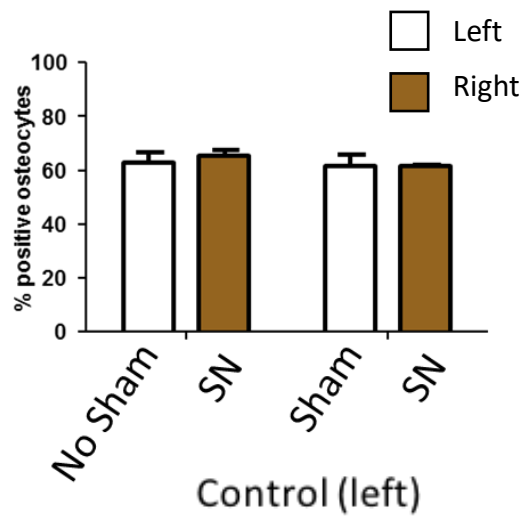


Figure 44 - Effect of sham surgery and disuse (by SN) on RANKL expression in osteocytes.

17w old female C57BL/6 mice underwent right SN and either no surgery (n=4) or a sham surgery (n=4) on the left limb. Mice were killed 4 days later. Results show % of RANKL immunopositive osteocytes and groups were compared using a mixed-design repeated measures ANOVA. Means \pm SEM are reported.

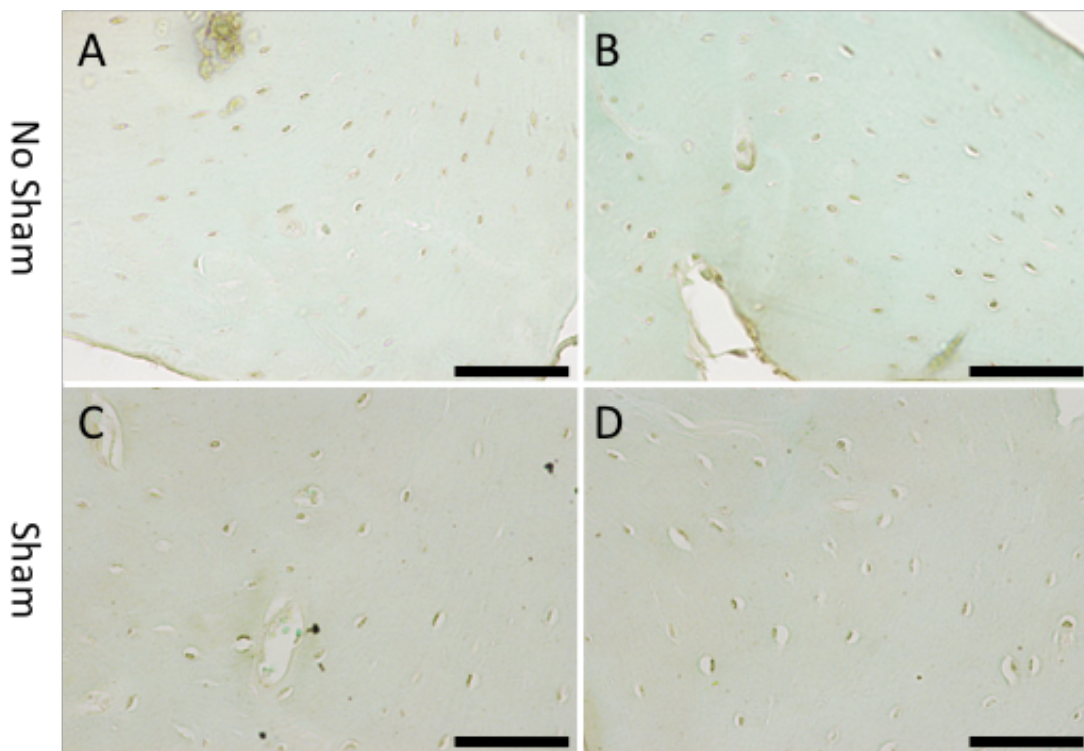


Figure 45 - Effect of sham surgery and disuse (by SN) on RANKL expression in osteocytes.

17w old female C57BL/6 mice underwent right SN and either no surgery (n=4) or a sham surgery (n=4) on the left limb. Mice were killed 4 days later and Sclerostin IHC performed on sections of bone. Representative high power images of the posteriolateral tibial cortical bone at the 37% site, measured from the proximal end. Left Control limbs (A, C) and Right Disuse limbs (B, D) are demonstrated. Groups had either Right SN only (A, B) or left sham surgery and right SN (C, D). The number of RANKL positive osteocytes was not affected by SN or sham surgery. Scale bars = 50 μ m

4.3.3 Objective 3: Describe the effect of disuse, engendered by SN on the osteocytic expression of RANKL and sclerostin protein, using IHC.

After confirming that contralateral sham appeared to have no significant effect on the expression of sclerostin or RANKL, and did not appear to affect the degree of adaptive bone changes in response to disuse engendered by SN (Chapter 3), we evaluated whether disuse resulted in significant changes in the osteocytic expression of sclerostin and RANKL. Following 4 days of disuse, sclerostin expression increased (+35.87%, $p < 0.01$) (Figure 42 & Figure 43), however, no significant change in RANKL expression was noted (-0.2%, $p > 0.05$) (Figure 44 & Figure 45, Appendix 3 - Table A4.5).

4.3.4 Objective 4: To establish the temporal response to disuse engendered by SN on the mRNA expression of RANKL, OPG and Sclerostin using qRT-PCR.

Having shown using IHC that RANKL expression was unchanged four days after SN, despite an increase in sclerostin expression, we next investigated the temporal changes in mRNA for the gene encoding for RANKL (TNFSF11) using qRT-PCR of time points earlier than 4 days. In addition, we also assessed the mRNA expression of the genes encoding for OPG (TNFSFR11B), the competitive decoy inhibitor of RANKL, and Sclerostin (*Sost*), which has been shown to affect the expression of RANKL [644].

When examining the effect of SN, there was no change in expression of *Sost*, RANKL, OPG or RANKL:OPG mRNA at any time point, at least until 3 days following surgery (Figure 46). When examining the effect of time after surgery, RANKL expression in the control limb of the 3h group was significantly higher than the expression noted in the control limb of the 12h group ($p < 0.05$), although there was no significant effect of duration after surgery for any other parameter when considering the control limbs. There was also no significant effect of time after surgery between SN limbs for any parameter (Figure 46).

Following the unexpected lack of effect of SN on expression of RANKL at the early time-points (using qPCR and also IHC), a later time point following SN was performed to

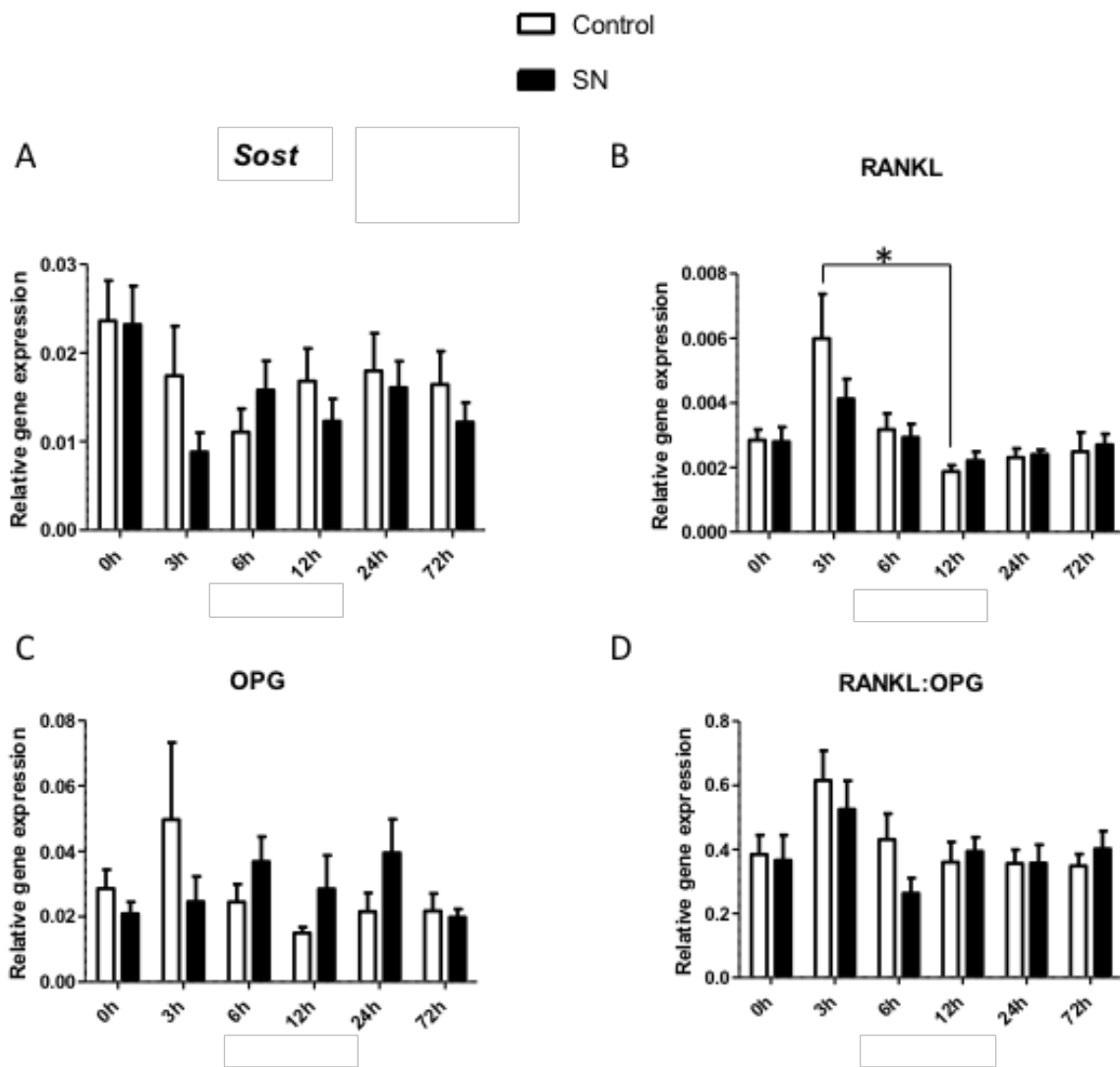


Figure 46 – Change in mRNA expression of SOST, RANKL and OPG following disuse in young adult female mice

17w old female C57BL/6 mice underwent SN and were then killed at various time points following SN and the cortical bone processed and analysed for expression of mRNA for (A) *Sost*, (B) RANKL, (C) OPG and (D) RANKL:OPG. Gene expression is reported relative to the expression of the house-keeping gene, β 2MG. * = $p < 0.05$ vs respective control limb of alternate time point. $n = 7-8$. Comparisons were performed using mixed design repeated-measures ANOVA with post hoc Bonferroni adjustments made. Error bars = mean \pm SEM.

determine if SN resulted in gene expression changes at a time point when demonstrable bone loss is typically occurring following SN, based on CT (2 weeks). *Sost* expression in tibial cortical bone was increased (+118.8% $p < 0.05$) 2 weeks after SN, however the expression of RANKL, OPG and the RANKL:OPG ratio were still unchanged following 2 weeks of disuse (Figure 47).

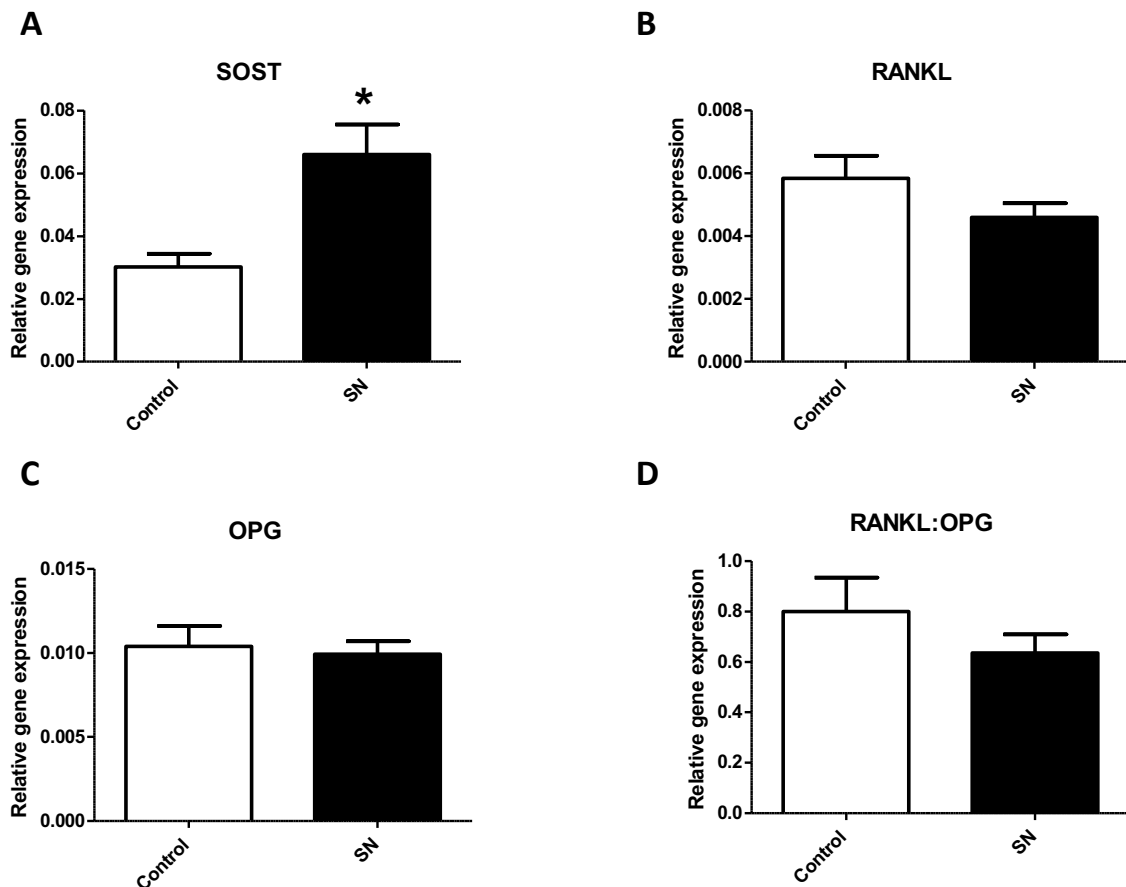


Figure 47 – Change in mRNA expression of (A) SOST, (B) RANKL and (C) OPG in young adult female mice following 2 weeks of disuse

(D) RANKL:OPG is calculated as the ratio of RANKL and OPG expression. 17w old female C57BL/6 mice underwent SN then were killed 2 weeks after surgery. Gene expression is reported relative to the expression of the house-keeping gene, $\beta 2$ MG.

* = $p < 0.05$ relative to control limb – comparisons made with paired t-test. Error bars = Mean \pm SEM (n=8).

4.3.5 Objective 5: Describe the effect of increased mechanical loading on the expression of the RANKL and sclerostin protein, using IHC

Following the unexpected lack of any apparent change in the expression of RANKL following reduced mechanical loading as a result of SN, we undertook studies to explore the effect of increased mechanical loading on the expression of RANKL and Sclerostin. Initially, immunolocalisation by immunohistochemistry of Sclerostin and RANKL expression was performed 24 hours after a single episode of loading. Expression of RANKL 24h following loading was not significantly different to that in control limbs (Figure 48A, C). This was despite a significant reduction in the expression of Sclerostin following loading, similar to that previously reported by ourselves and others [8, 20] (Figure 48B, C).

4.3.6 Objective 6: To establish the temporal response to a single episode of mechanical loading on the mRNA expression of RANKL, OPG and sclerostin using qRT-PCR.

We next sought to determine whether loading altered the RNA expression of RANKL, *Sost* or OPG. RANKL and OPG expression were unaffected by loading at any time-point tested (Figure 49 A-C). The overall expression of RANKL in mice at the 12h time-point was significantly lower than the 6h time-point, however there was no difference when paired loaded or control limbs were compared by post-hoc comparisons (Figure 49A). The RANKL:OPG ratio showed a tendency to decrease after loading ($p=0.083$) but this change was not significant.

Interestingly, loading was associated with a significant reduction in the expression of *Sost* at 6h post-loading but loading had no effect on SOST expression at 12h or 24h in this experiment (Figure 49D). The expression of *Sost* in the control limb of the 6h group was significantly greater than the expression in the control limb of the 24h group. This is difficult to explain, but as this experiment did not include a 0h control group, we could not determine whether the result was anomalous, or if the variance in the control limb at 6 hours was due to some other variable, such as diurnal variation or potentially some other

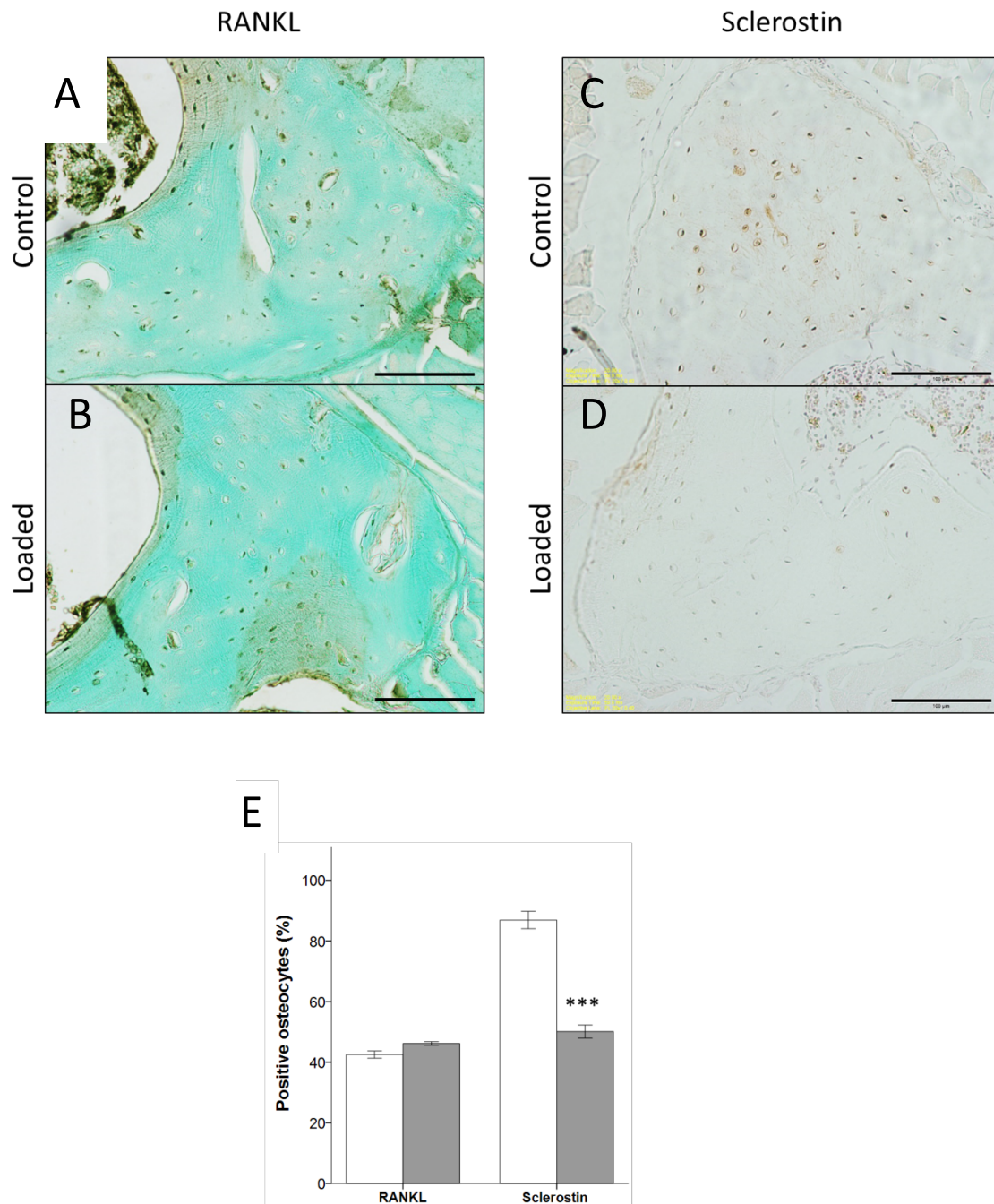


Figure 48 - Effect of axial loading on RANKL and Sclerostin expression in osteocytes in young adult mice, determined by immunohistochemistry.

Transverse sections of the tibia, 37% of the length of the bone measured from the proximal end were evaluated in the posteriolateral cortex for the percentage of positive staining osteocytes. Mice were killed 24 hours after a single session of axial tibial loading. Representative images of 200X photomicrographs of the posteriolateral cortex following (A, B) RANKL, (C, D) Sclerostin IHC. (A, C) left limbs were internal controls. (B, D) right limbs were loaded. Scale bars = 100µm. (E) percentage of positive staining osteocytes following immunolocalisation of RANKL (n=5) and Sclerostin (n=4). *** = p<0.001. Comparisons were performed with a paired Student's t-test. Error bars = Mean ± SEM.

systemic effect, such as anaesthesia related changes. On examination of the concentration of RNA in the extracted samples, there was no significant differences in RNA concentration between loaded and unloaded limbs, or between different time points (Appendix 3).

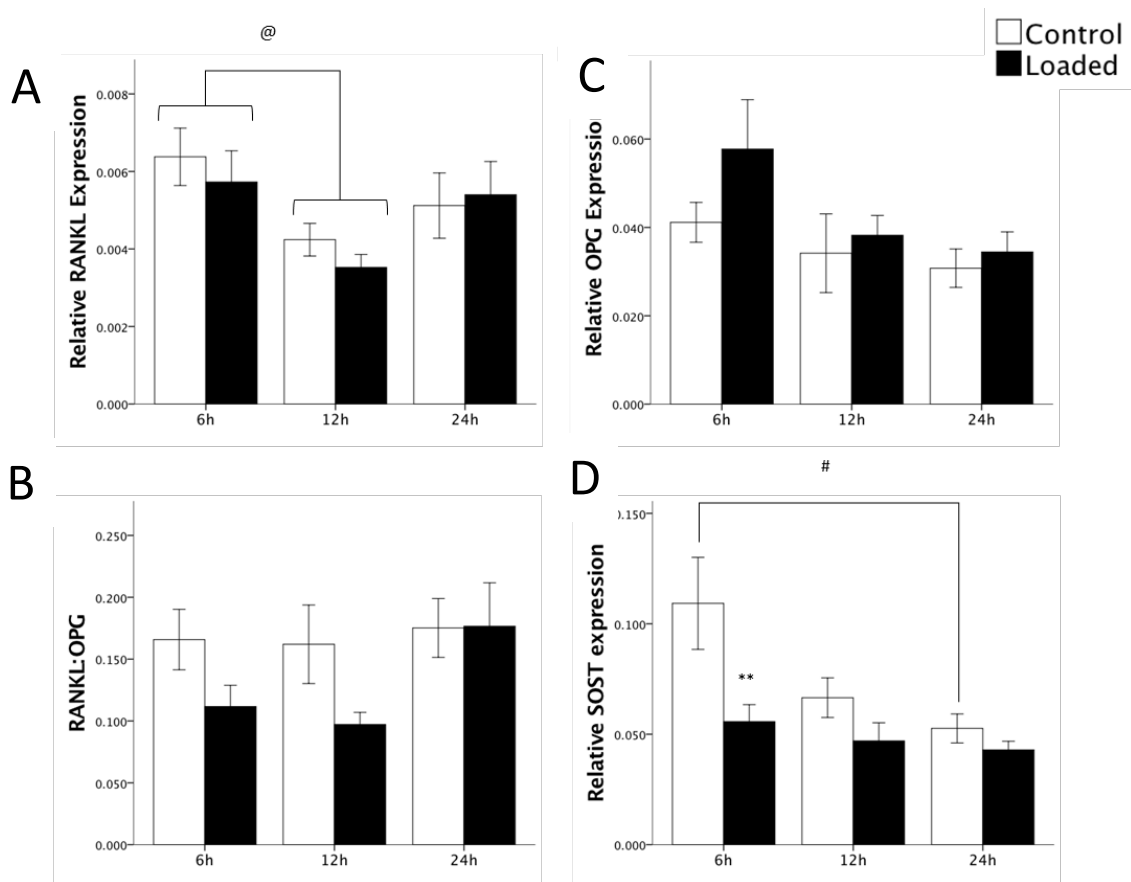


Figure 49 – Change in mRNA expression of SOST, RANKL and OPG following a single episode of mechanical loading in young adult female mice

17w old C57BL/6 female mice underwent one session of axial tibial loading and then were killed 6, 12 or 24 hours after loading. Tibial cortical bone was analysed with qRT-PCR for (A) RANKL, (B) OPG, (C) RANKL:OPG and (D) SOST. Values are expressed relative to expression of β 2MG as a house-keeping gene. Results were compared using a two-way, repeated measures, mixed design ANOVA. n=7-8. @ = p<0.05 effect of time point (including control and loaded limbs). ** = p<0.01 – effect of loading at a given timepoint. # = p<0.05 - effect of time point on control limbs only. Error bars = Mean \pm SEM.

4.4 Discussion

This chapter describes a series of experiments documenting the expression of RANKL and Sclerostin at the RNA and protein level following decreased and increased loading *in vivo*. These data replicate previous findings that sclerostin is down-regulated by increased loading and up-regulated in disuse. However, the experiments described here did not identify any concurrent changes in the expression of RANKL following unloading or loading.

4.4.1 Immunolocalisation of RANKL in cortical bone.

The first studies we described were the optimisation of a protocol to immunolocalise RANKL in cortical bone where we could illustrate moderate levels of positive staining in osteocytes. At the time of these studies, there was, to the author's knowledge, only one published report of localisation of RANKL in femoral osteocytes [22]. We interpret this to reflect low antibody affinity and, presumably, low osteocytic RANKL concentration compared with other cell populations. There have since been publications demonstrating staining within osteocytes of trabecular bone [461, 645], although the apparent staining intensity in both reports appeared similarly low when compared with that achieved using our protocol.

As RANKL produced by osteocytes is apparently essential for the activation and function of osteoclasts necessary for the bone loss seen with disuse [21, 22], the ability to visualise changes in the expression of RANKL in a site-specific manner using histologic techniques like IHC would help identify the potential site-specific nature of adaptive bone remodelling, similar to the site-specific nature of the response to loading of sclerostin expression previously demonstrated by Moustafa *et al* [8]. Hypertrophic chondrocytes were a reliable and strongly staining positive control cell population present in young adult mice. They were easily identifiable and consistently present in all mice examined. Furthermore, the articular cartilage cells, present in young and old mice, also typically stained strongly. Of note, when considering the staining of transverse tibial sections of the diaphyseal cortical bone, is that the megakaryocytes within the bone marrow were a

further population of strongly staining cells, however the marrow in general appeared to have moderate degrees of non-specific staining. Figure 41 illustrates the degree of staining in each of these populations. Having a readily available positive control cell population within the same tissue of interest is convenient and provides an internal control as the same section will have been treated identically through all processing steps, unlike a separate exogenous positive control slide, such as sections of tumour from Giant Cell Tumours of Bone, previously recommended as a suitable positive control cell population for RANKL [639].

As expected [646], RANKL immunolocalisation produces diffuse cytoplasmic staining as it is primarily a membrane bound protein. We conclude that a counterstain which does not obscure the nucleus, such as Light Green solution is more suited for IHC studies in osteocytes than nuclear stains such as haematoxylin as, due to the high nuclear:cytoplasmic ratio of osteocytes, DAB signal was obscured by the nuclear stain and made quantification difficult. Quantification of RANKL positive osteocytes was less problematic when a non-nuclear counterstain (or no counterstain at all) was used. Interestingly, images showing immunolocalisation of RANKL in cortical bone osteocytes in the study by Plotkin *et al* [461] also used a green counterstain.

In our study, a high concentration of antibody was required to help localise osteocytic RANKL. Steps to unmask the antibody and quench endogenous peroxidase activity were also essential to provide a strong enough signal in the osteocytes. As a high antibody concentration was required to generate sufficient signal, there was a degree of non-specific staining in tissues such as blood vessels, marrow and muscle. These tissues are typically quite “sticky” when high antibody concentrations are used. High levels of non-specific staining, were detected using protocols 1 and 2, particularly in muscle and bone marrow, which were improved by changing the batch of antibody and improving the washing steps in between steps of the protocol and modifying the antigen retrieval step to improve epitope exposure. Not all osteocytes appear positively-stained in each section, reinforcing the selectivity of the IHC method used. Additional negative control specimens could also have been used to demonstrate that the staining seen was not non-specific;

e.g. pre-incubating the negative control slides with a RANKL peptide would have been an alternative approach. Furthermore, sections of bone from mice with genetic global deletion of RANKL could be used. Typically, global deletion of RANKL results in severe osteopetrosis, failure of tooth eruption and failure to develop lymph nodes [21]. We did not have access to these transgenic mice for this study.

We demonstrated that immunolocalisation of RANKL in cortical bone osteocytes is possible although the antibody has low affinity and required a very high concentration of primary antibody, with appropriate antigen retrieval steps to achieve a clear enough signal. Following validation of this protocol for RANKL immunolocalisation, we next sought to use it to identify changes in RANKL expression in response to both unloading, engendered by SN, and loading, engendered by axial tibial loading.

4.4.2 Contralateral sham surgery does not affect the osteocytic expression of RANKL or Sclerostin.

One disadvantage of sciatic neurectomy as a disuse model compared with tail suspension is that it requires a surgical intervention. When planning the disuse experiments, we were concerned that the expression of RANKL locally (and thus bone mass) could be affected by the surgical trauma and subsequent inflammatory response. We therefore elected to modify the protocol for unilateral SN and perform a contralateral sham surgery on animals to control for this potential effect. Several inflammatory mediators have been linked with bone resorption, or decreased formation; most significantly, prostaglandin E₂, a variety of interleukins (IL-1, IL-6, IL-17), and tumour necrosis factor alpha (TNF α) [601-605]. These cytokines are known to be associated with bone loss through increased expression of, or synergism with RANKL [601].

As described in Chapter 3, bone loss associated with SN following a contralateral sham surgery was consistent with previous reports of unilateral SN without contralateral sham surgery [8, 11, 35]. Expression of RANKL and sclerostin using IHC was also no different in control limbs with sham surgery or no surgery. Therefore, neither bone mass, nor the expression of RANKL or sclerostin is affected when comparing sham operated and non-

operated limbs. Thus, it appears unlikely that the surgical procedure itself was sufficient to stimulate an inflammatory response significant enough to affect the remodelling response and/or bone mass.

4.4.3 Disuse sufficient to cause cortical bone loss and increased expression of sclerostin has no effect on RANKL expression.

Despite significant reductions in bone mass and the concurrent increase in the expression of sclerostin, disuse was not associated with changes in osteocytic RANKL protein expression in tibial cortical bone of young mice. However, the original hypothesis that changes in loading may alter RANKL expression is supported by other studies published after this project was started. Pichler *et al* [645] demonstrated a decrease in RANKL expression in tibial trabecular osteoblasts following whole body vibration, whilst Plotkin *et al* [461] demonstrated an increase in RANKL positive osteocytes in vertebral bone following tail suspension (disuse). Both evaluations were, however, performed in primarily trabecular bone of young mice. We evaluated changes in diaphyseal cortical bone following SN or axial tibial loading as we were interested in the cortical bone adaptive response. This shows that there can be compartment specific (trabecular vs cortical) responses to the mechanical environment.

Increased sclerostin expression after 4 days in response to SN reported in our mice was also consistent with that previously reported [8, 20, 528, 626, 647]. A recent study exploring the site-specific nature of the sclerostin response to disuse [647] demonstrated an increase in cortical bone osteocytic sclerostin protein expression after 2 and 8 weeks of disuse in rats, and a corresponding increase in mRNA *Sost* expression at both time points. Interestingly, serum concentrations of RANKL was measured in this study and *decreased* in response to disuse after 2 weeks of disuse, but had equilibrated after 8 weeks. Furthermore, change in the osteocytic expression of sclerostin in trabecular bone during unloading was not as great as that seen in cortical bone. We have previously also found that sclerostin expression in trabecular bone was site-specific [8].

Using the SN disuse model, we also did not find disuse-associated changes in the mRNA expression of RANKL or OPG at early (0-3 days) or late (2 weeks) time-points. Previous reports have demonstrated increased levels of RANKL mRNA following longer-term unloading [21, 614, 630], but these have used tail suspension rather than SN and mostly used longer periods of disuse (2 or 3 weeks) at a point where significant bone loss had already occurred. RANKL was also increased in tibial bone marrow following disuse from sciatic neurectomy in mice, although this increase was mitigated by parathyroidectomy indicating the modulatory effect that PTH can have on bone remodelling [137]. A further recent paper explored the osteocytic expression of RANKL and OPG protein using IHC and demonstrated an increase in RANKL expression and a decrease in OPG expression seen with unloading of vertebral bone, induced by tail suspension [461]. However, this same study demonstrated that inhibition of osteocyte apoptosis was insufficient to prevent bone resorption and that osteocytic RANKL is not the sole mediator of osteoclastogenesis and the bone loss induced by lack of mechanical forces [461].

Here we have demonstrated, at 3 and 14 days following unilateral SN, that RANKL mRNA expression in cortical bone was unaffected. Another report has also showed no increase in osteocyte RANKL expression at 3 and 7 days following tail suspension [136]. RANKL expression was unaffected after 7 days unloading in the study by Gerbaix *et al* [630]. In comparison, the studies discussed above demonstrating a change in RANKL expression following disuse have generally examined delayed timepoints >2 weeks, whereas we explored timepoints <2 weeks. Furthermore, studies demonstrating increased RANKL expression following disuse have mostly explored trabecular regions of the skeleton (proximal tibia and vertebrae) suggesting that osteocytic RANKL in cortical bone may not be a critical regulator of osteoclast activity.

There are several reasons why we may have been unable to demonstrate changes in the expression of RANKL using qPCR. Strain-related bone (re)modelling is well accepted to be a locally controlled process. Xiong *et al* [21] demonstrated that RANKL mRNA expression in cortical bone samples of mice with osteocyte RANKL knockout was not significantly different to that of control littermates, despite showing impaired remodelling. This

suggests that, given the expression of RANKL in cortical bone samples was unchanged, bone samples used for qPCR assessment may not contain only RANKL produced from osteocytes, subsequently overwhelming any change in the osteocytic expression. This could explain why small changes in osteocytic RANKL expression may not be detected using the cortical bone samples prepared for qPCR analysis. RNA extraction from cortical bone typically produces low yields, necessitating the analysis of the whole length of the tibial cortical bone. This may also introduce an “averaging” effect throughout the bone thus masking potential regional changes in RANKL expression. However, in comparison, sciatic neurectomy generates “uniform” increases in sclerostin expression both distally and proximally in the tibia [8] and bone loss throughout the length of the tibial cortical bone [7]. It may, in future, be possible to isolate a smaller proximal portion of the bone, where bone loss is known to be greater [7] for RNA extraction. With current technologies it is possible to detect transcriptomic changes in very small numbers of RNA transcripts/copies from cortical shell lysates.

Most other studies demonstrating increased RANKL expression in mice following unloading were performed using tail suspension. There are differences between disuse induced by SN and that engendered by tail suspension. Tail suspension results in increased serum cortisol [648]. Endogenous glucocorticoid excess reduces bone formation rate and bone mineral density [594] and corticosteroid administration is known to result in an increase in RANKL expression [596]. Stress-related increases in endogenous steroids therefore may cause increased RANKL expression, independent of, or in addition to, the effects of unloading. Endogenous cortisol has not been measured following SN, nor are there any direct comparisons between the systemic effects of SN and tail suspension, however, animals do not appear to demonstrate “stress” related behaviours following SN and continue to show normal cage behaviour such as nest-building behaviours which are not possible with tail suspension.

The data presented from cortical bone of tibias of mice following sciatic neurectomy suggest that osteocytic RANKL and OPG expression does not change, despite a significantly lower bone mass and significant upregulation in *Sost*/Sclerostin expression. This result is

not consistent with the studies of Xiong *et al* [21], which demonstrated that RANKL produced by osteocytes was essential for the trabecular bone loss associated with disuse. Furthermore, this study demonstrated that RANKL mRNA expression in cortical bone of control mice was increased following tail suspension. Osteocyte RANKL knockout mice also develop a marked increase in bone mass, primarily through gradual obliteration of the medullary cavity with bone trabeculae, even after being born with phenotypically normal skeletons, suggesting that osteocytic RANKL's role may be more important endosteally, and associated with trabecular bone, than in diaphyseal cortical bone. Even though its presence may be essential, our findings cannot support the inference that localised osteocytic RANKL up-regulation is essential for the bone resorption in cortical bone seen in situations of disuse engendered by SN.

The studies which demonstrate changes in expression of RANKL with disuse using IHC all studied the changes in trabecular bone sites [461, 645, 649], which could be consistent with a site-specific role for RANKL in bone. Apoptosis associated with disuse engendered by tail suspension was the stimulus for RANKL up-regulation and subsequent bone loss in long bones of mice. There appears to be an interaction between RANKL expression and apoptosis. Inhibition of apoptosis abrogated the RANKL increase and subsequent bone loss [649]. Conversely, Plotkin *et al* [461] showed that, in vertebral bone, following tail suspension, inhibition of osteocyte apoptosis impaired the increase in RANKL associated with disuse, but did not impair the bone loss, although this study examined vertebral bone and the study by Cabahug-Zuckerman *et al* [649] studied distal femoral trabecular bone. Previously, Kennedy *et al* [112] have shown that there was a close relationship between microcrack-associated osteocyte apoptosis and RANKL expression in cortical bone. There are no studies, to the author's knowledge, describing the degree of osteocyte apoptosis associated with sciatic neurectomy, nor are there any other studies demonstrating a change in RANKL expression following disuse in diaphyseal cortical bone. It appears likely, given our findings, that although osteoclast recruitment and activation by increased levels of osteocytic RANKL may be important in some situations of bone resorption, the requirement for its increased expression to permit resorption following disuse in cortical bone is questionable. The studies mentioned above, combined with the findings of the

experiments described in this chapter suggest that regulation of RANKL expression in trabecular bone appears more important to the remodelling response than changes in diaphyseal cortical bone. Further work exploring the effect of disuse on RANKL expression between several different sites will help elucidate any site-specificity to the changes seen following unloading.

4.4.4 Axial tibial loading sufficient to result in bone formation decreases osteocytic sclerostin expression but has no effect on RANKL expression.

Having failed to show any changes in the expression of RANKL following unloading, we next investigated if its expression had any relationship to increased loading in mice. After demonstrating the loading protocol used in the previous chapter resulted in new bone formation according to μ CT and dynamic histomorphometry analysis (Figure 24 and Figure 28 – Chapter 3), we were unable to demonstrate a reliable load-related change in the gene expression of RANKL or OPG at 6, 12 or 24 hours after loading, despite demonstrating a down-regulation in the expression of sclerostin after 6 hours. The decrease in *Sost* we identified in this loading time course experiment is consistent with previous published data suggesting that *Sost*/sclerostin decreases with loading [8, 20, 528]. The observation that RANKL expression was not significantly changed up to 24 hrs after mechanical loading in our study is also supported by microarray time course analyses of cortical bone following loading [86, 413].

In vitro studies exploring the effect of mechanical stimulation on expression of RANKL have yielded variable results. These vary from increased expression with load to decreased expression [129-135]. Comparison between these studies is challenging due to differing strain application techniques, and additionally, the *in vitro* response to load may not necessarily correlate with the *in vivo* situation as the three-dimensional orientation and lacunocanicular arrangement of osteocytes in bone may confer additional and/or different responses to mechanical load.

There are, to the author's knowledge, few other published reports exploring the response of RANKL expression in loaded cortical bone, either considering RANKL mRNA or protein

expression. Recent microarray experiments performed in our laboratory exploring the transcriptomic response of bone to mechanical loading have not detected a significant change in the expression of RANKL mRNA. However, we have demonstrated an increase in the expression of OPG mRNA up to 12h after loading [413], which, in the case of no change in RANKL expression, would result in a reduction in the RANKL:OPG ratio, thus decreasing the resorptive drive following loading. RANKL:OPG ratio did show a tendency, in the present study, to reduce at 6 and 12h after loading. This suggests that, although there was no significant change in RANKL or OPG individually, a relative reduction in the concentration of RANKL vs OPG may be sufficient to reduce the resorptive drive following loading, thus improving the osteogenic response by limiting concurrent resorption without a specific decrease in RANKL expression.

Many experimental advances in the understanding of the role of RANKL in bone remodelling have been made with genetic mutations using either whole body knock-out models, or cell-specific conditional knockouts. This approach has helped promote our understanding of the source of RANKL responsible for the bone loss seen with disuse [21, 22] and also more recently our understanding of RANKL's interaction with other molecules, such as PTH [650] and Sclerostin [651]. Further studies on the mechanical-load associated regulation of formation and resorption particularly focused on RANKL expression will be best pursued using genetically manipulated mice, and in particular, conditional knockout strains to help dissect the mechanisms involved in the regulation of the mechanostat.

In summary, this series of experiments has demonstrated that changes in sclerostin expression remain a sensitive experimental endpoint for detecting cellular responses to changes in the mechanical loading environment. Conversely, RANKL cannot be recommended as a suitable experimental endpoint to explore bone's response to changes in mechanical loading.

4.5 Conclusions

- Osteocytic RANKL expression in cortical bone does not change with mechanical unloading engendered by SN, or with mechanical loading engendered by axial compressive loading. This suggests that measurement of its expression in cortical bone is not a suitable endpoint to assess responses to loading and unloading in mice.
- The hypothesis that changes in the levels of expression of RANKL in osteocytes in cortical bone are essential for regulating osteoclast activity associated with changes in the mechanical environment cannot be supported by the results of these studies
- Regulation of RANKL expression in response to changes in the mechanical loading environment may be site specific with others reporting changes in RANKL expression in trabecular bone where none were noted in diaphyseal cortical bone. These studies suggest that while changes in osteocyte RANKL expression are clearly important for regulating adaptive bone remodelling in trabecular bone, osteocyte derived RANKL in the context of cortical bone mass remains unclear and requires further investigation.

Parts of the studies reported in this chapter were presented as a late-breaking abstract to the 2013 annual meeting of the ASBMR in Baltimore, Maryland [652]. A copy of the poster is included in Appendix 4 of this thesis.

Chapter 5

The effect of disuse on the osteogenic response to mechanical loading in old mice.

Chapter 5 – The effect of disuse on the osteogenic response to loading in old mice.

5.1 Introduction

Bones undergo functional adaptation in response to loading to ensure their structural integrity. Bone is added in areas where more stiffness/strength is required in an arrangement that best suits resistance of current forces, and bone is resorbed where bone is stiffer/stronger than is necessary, thus minimising the weight of material being used. This local homeostatic feedback mechanism aims to achieve a “target” strain as its objective through the adaptive responses that are generated once controlling “off target” strains are sensed. This mechanism has been coined the “mechanostat”[12].

As described previously in this thesis, the normal osteogenic response to mechanical loading is impaired with ageing and we have hypothesised that this is why, in old people, the incidence of fragility fractures increases [23]. It is well recognised that aging affects the osteogenic response to mechanical loading in rats and mice [25, 27, 29, 31, 453, 455, 493, 582]. In regions of cortical bone at least, despite a conserved endosteal response to loading, the periosteal osteogenic response to loading is abrogated [27, 29, 455]. It has been suggested that this may be due to impaired capability of periosteal osteoblasts to proliferate [29]. The study by Meakin *et al* (2014), undertaken in our laboratory, found evidence that cortical long bone derived osteoblasts from old mice retain their ability to initiate early transcriptional and proliferative responses to strain *in vitro*, but their progression through the cell-division cycle is delayed. Contrary to Frost’s [12] hypothesis that aging changes the “set-point” for responsiveness to increased mechanical loading in the elderly, the study by Meakin *et al* (2014) demonstrated *in vivo* that the minimum effective strain beyond which bone gain occurs was not significantly different between young and old female mice, but the amount of bone accrued over two weeks of loading was lower in the old mice [29].

Using *in vivo* longitudinal μ CT technology to investigate whether the pattern of bone gain following loading is altered by age, Razi *et al* [30] compared the number of sites where resorption or formation occurred in a site-specific manner in young (10w), adult (26w) and old (78w) mice before and after unilateral tibial loading. In this study, overall resorption was increased in adult and old mice compared with juvenile growing mice and the majority of resorption was noted endosteally. Resorption was reduced following anabolic loading in both adult and old mice, however significant ongoing resorption was still present despite loading. Loading-related bone formation was greater in young animals compared with old, and the likelihood of a given site experiencing either formation or resorption was correlated to the calculated minimum principal strains, according to finite element modelling [30]. Interestingly, a more recent study from the same group has demonstrated that the resorption probability is only correlated to calculated strains on the endosteal surface, and not the periosteal surface [529]. This suggests that additional region-specific factors, such as the local cellular context, as well as strain-related stimuli, are inherent in controlling the processes of resorption in response to loading. This is consistent with our group's suggestion that acute loading-related cellular responses are influenced by the osteogenic context in which loading acts. We have demonstrated that, in addition to aging, deletion of oestrogen receptor alpha (ER α) or oestrogen deficiency (following ovariectomy) both significantly alter the number and type of genes significantly regulated by mechanical loading [86, 413]. Furthermore, treatment with the selective oestrogen receptor modulator, tamoxifen, which is an ER agonist in bone, synergistically improved the osteogenic response to loading in trabecular bone, further supporting the suggestion that biological context affects the mechano-responsiveness of bone [287].

In addition to the altered hormonal context, we also found that changing the habitual strain environment through disuse induced by sciatic neurectomy significantly altered the number and type of genes regulated by loading [86]. A change in the osteogenic context may begin to explain the observation that, in young adult mice, axial tibial loading in limbs where normal loading is reduced by SN resulted in more new bone formation than when similar loading was superimposed upon the normal strains of habitual activity [35].

Disuse causes a reduction in bone formation and also increases in bone resorption [653]. These changes appear to have some age-dependant differences. Following tail suspension, old rats appear to lose cortical bone through intracortical resorption, causing pore formation, whereas young rats undergo endosteal resorption leaving the intracortical bone relatively intact. Conversely, trabecular bone loss seen following disuse engendered by tail suspension in young rats is not evident in old rats [184]. The response to disuse in the tibia of young adult mice was evaluated using μ CT in Chapter 3 of this thesis and demonstrated that, 3 weeks following SN, cortical bone mass was reduced primarily through endosteal resorption causing increased Ma.Ar. Periosteal apposition was mostly unaffected. Trabecular bone loss was primarily through decreases in trabecular thickness and number. The response to disuse induced through SN in old mice has not, however, to the author's knowledge, been reported, although resorption rates are generally higher and formation rates lower in old animals [31]. **The first aim of this chapter was to describe the effects of unilateral SN alone on cortical bone mass and architecture in old female mice.** To enable evaluation of the cortical bone changes over a wider selection of sites in the tibia, our group has developed a software programme called Site Specificity Analysis (SSA) which is a semi-automated programme that allows calculation of standard μ CT parameters at each centile site along the bone from 10-90% of the bone, measured from the proximal end [7]. Prior to investigating the effect of prior disuse on the loading response in old mice. We used SSA to analyse μ CT data for the present study.

As described previously, an earlier study from our lab demonstrated that the osteogenic response to loading could be augmented following a short period of prior disuse in young mice [35]. Another study in young adult mice demonstrated the osteogenic response of bone was lower in mice that received an incrementally increasing load up to a normally highly osteogenic load when compared with those that were loaded initially with the highly osteogenic peak load, then had loads reduced decrementally over the same duration [590]. This provides further evidence that load responsiveness in mice is loading history/context dependent. Although these studies were all conducted in young adult mice, a recent pilot study in our laboratory suggested that the osteogenic response to

loading in old mice could be improved by a short period of disuse prior to loading [4]. In follow up to these initial observations, **the second aim of this chapter was to determine, in old mice, whether altering the mechanical loading history through prior and concurrent disuse affects the osteogenic response to loading.** Given the loading response in mice appears to be loading history/context dependent, we hypothesised that in old, as in young mice, the adaptive response to loading would be greater if preceded by a period of reduced loading engendered by SN.

5.2 Objectives

1. Characterise the site-specific changes in cortical bone 3 weeks after unilateral SN in old (19-month-old) female mice using Site Specificity Analysis (SSA).
2. Determine the effect of SN on the bone mass and architecture of the contralateral limb without induced loading in old female mice using SSA.
3. Determine the effect of prior SN on the response to mechanical loading of cortical and trabecular bone regions of interest in old female mice, using single-site μ CT analysis.
4. Determine the effect of prior SN on the rate of bone formation in loaded tibias of old female mice, using dynamic histomorphometry.
5. Determine the effect of prior SN on the response to mechanical loading of the entire cortical bone in old female mice, using SSA.

5.3 Materials and Methods

5.3.1 Animals and *in vivo* procedures

Experiment 1: Characterise the site-specific changes in cortical bone 3 weeks after unilateral sciatic neurectomy in old (19-month-old) female mice using Site Specificity Analysis (SSA).

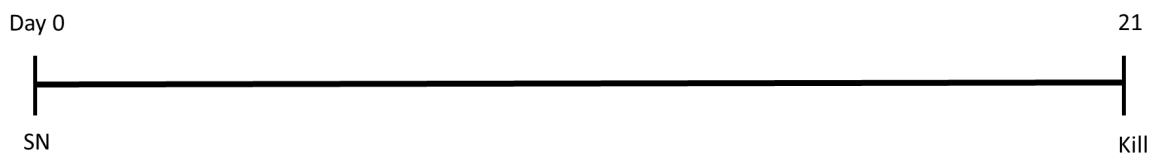
To assess the site specific response to SN in old mice using SSA software [7], nine 19-month-old female C57BL/6 mice were obtained from Charles River Laboratories (Margate, UK). All mice underwent unilateral right SN as described in Chapter 2 and the left limb was used as an internal control. Mice were confined to their standard cage and allowed free movement. μ CT data from old female mice used for this experiment were part of an earlier experiment conducted by Meakin [4] where conventional, single-site μ CT analysis of the proximal cortical bone region of interest was performed. Some of the initial results from this experiment will also be reported for reference.

Experiment 2: Determine the effect of prior disuse on the osteogenic response to loading in old female mice using single-site μ CT, SSA and dynamic histomorphometry.

Twenty 19-month-old female C57BL/6 mice were used for this study. This experiment was undertaken to achieve Objectives 2-5. The strains produced by loading were calibrated in aged mice (n=5) by strain gauges attached *ex vivo* according to the technique described in Chapter 2. The strain gauging data used for this study was performed in mice of identical age for an earlier published study [29]. Mice were divided into two weight-matched groups and after 1 week of environmental acclimatisation, SN was performed on the right limb (n=10) as described in Chapter 2. Sham surgery (n=10) was performed on the right limb of control group animals. Sham surgery was performed on the left limb of all mice, as validated in Chapter 3 and 4 of this thesis. Analgesia was provided by subcutaneous buprenorphine (0.05mg/kg), as required.

Four days following right SN/Sham surgery, right tibiae were loaded under anaesthesia on alternate days for eight sessions. The experimental time line is illustrated in Figure 50. Left limbs were used as internal controls as previously validated [1]. The protocol for non-

EXPERIMENT 1



EXPERIMENT 2

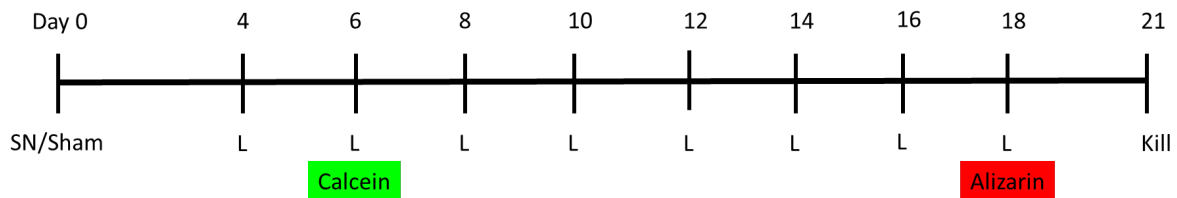


Figure 50 – Time line describing the experimental protocol for SN/loading experiments in aged mice.

Mice had surgery on day 0 and killed on day 21. In experiment 2 and 3 loading started on day 4. Calcein and Alizarin complexone were injected subcutaneously on day 6 and 18 respectively. Mice were killed on day 21. The day number is listed across the top of the figure. L = Loading. SN = Sciatic Neurectomy.

invasively loading the mouse tibia is described in Chapter 2. Mice were loaded to achieve $2500\mu\epsilon$ on the medial surface of the tibia at the 37% site. The strain rates during the application and release of load were $30,000\mu\epsilon s^{-1}$. This corresponded to a compressive load of 11.77N (+0.5N preload = 12.27N total load) with a load ramp rate of $393Ns^{-1}$. Mouse losses occurred due to death under general anaesthesia (n=2) and tibial fracture during loading (n=2), subsequently reducing experimental numbers to n=9 for the sham group and n=7 for the SN group.

5.3.2 Ex vivo procedures

High-resolution μ CT single-site analysis

Single-site analysis was performed for Objective 3. Mice were sacrificed on day 21. After dissection and fixation in 4% paraformaldehyde at 4°C for 48 hours, tibia were then washed in graded alcohol and stored in 70% ethanol. Tibial μ CT was performed as described in Chapter 2. We evaluated the effect of SN and age on changes $[(right - left) / left] * 100$ due to loading in the trabecular region (0.25-0.75mm distal to the proximal physis) and at the cortical site (37% from the proximal end), according to ASBMR

guidelines [570]. The parameters measured included; trabecular bone volume fraction (BV/TV), trabecular thickness (Tb.Th), trabecular number (Tb.N), trabecular pattern factor (Tb.Pf), cortical bone area (Ct.Ar), total cross-sectional area inside the periosteal envelope (Tt.Ar), medullary area (Ma.Ar), cortical thickness (Ct.Th) and bone area fraction (Ct.Ar/Tt.Ar). Muscle Area (Mu.Ar) was also assessed to confirm efficacy of SN.

Site Specificity Analysis

Following assessment of the osteogenic response to loading at the 37% site using our conventional, single-site analysis, we determined the SN or loading associated changes for Ct.Ar, Tt.Ar, Ma.Ar and PMI over the length of the tibial diaphysis (10% - 90% site) using SSA [7]. The procedure for performing SSA is detailed in Chapter 2. Briefly, bone site was set as a fixed categorical parameter, with the intervention (loading, surgery) included as fixed effects, the loading*surgery interaction to determine if SN affected the response to loading. The intervention*site interaction was evaluated to determine whether the main effect was site-specific (i.e. if the response to loading or SN was significantly different at different sites). The analysis undertaken for Objectives 1 and 5 included mouse ID as a random effect to account for the left and right limbs belonging to the same mouse. Sidak post-hoc correction was performed if a main effect was significant ($p < 0.05$). Each percentile site was compared between control and SN limbs of mice in experiment 1 (Objective 1). The left control limbs of the mice from the Sham group and the SN group in experiment 2 were compared to assess the effect of SN on the contralateral limb (Objective 2). The data from all mice in experiment 2 was compared to assess the effect of SN on the response to loading (Objective 5).

Dynamic histomorphometry

Mice were injected with calcein (50mg/kg) and alizarin (50mg/kg) subcutaneously on day 6 and day 18 of the loading period respectively (Figure 50). Following sacrifice, fixation and μ CT scanning, tibiae were embedded in methylmethacrylate as described in Chapter 2. Transverse sections were taken from the region in the tibia where we have previously demonstrated the response to axial loading is maximal (37% of the length measured from the proximal end) [1]. Images were captured using a confocal microscope with HeNe

(563nm) and diode (494nm) lasers with an isotropic pixel size of 378nm. Mineral apposition rate between the two labels on the endosteal and periosteal surfaces were measured in the postero-lateral aspect of the right loaded tibiae only, where strains and bone formation engendered by loading have previously been shown to be maximal [8].

Statistical analysis

Analysis of SSA data was performed using a linear mixed model approach, with bone site as a fixed categorical parameter and intervention (surgery, loading) as a fixed effect. Intervention by site interaction was also assessed to identify any site-specific responses. Mouse ID was included as a random effect. If effects were significant, post-hoc Sidak correction was applied to identify individual sites where the effect was significant ($p < 0.05$). Repeated-measures ANOVA, with post-hoc least-squares difference testing, was used to evaluate the effect of loading between left control and right loaded samples (loading effect) and between sham and SN groups (surgery effect) in the single-site μ CT analysis experiments. The interaction “loading*surgery” was also established. The effect of SN on the inter-label distance and marrow apposition rate (MAR) due to loading in aged mice of experiment 2 was evaluated using an unpaired t-test on right loaded limbs only since insufficient double label was present on left control limbs of aged mice due to their high rates of resorption and low rate of baseline formation. Values are reported as mean \pm standard error of the mean (SEM).

5.4 Results

5.4.1 Objective 1: Characterise the site-specific changes in cortical bone 3 weeks after unilateral sciatic neurectomy in old (19-month-old) female mice using SSA.

Preliminary single-site μ CT analysis from Meakin [4].

As detailed earlier, the data analysed for Objective 1 was obtained from mice used from an earlier experiment [4]. Here, for convenience, we re-report the single-site μ CT data obtained for trabecular bone and the proximal (37%) cortical site with permission from

the author (Lee Meakin). In trabecular bone, BV/TV ($-39.6 \pm 12.5\%$ $p=0.027$) and Tb.Th ($-23.3 \pm 4.7\%$ $p=0.002$) were significantly reduced following SN. Tb.N ($p=0.191$) and Tb.Pf ($p=0.785$) were not significantly affected by SN. In proximal cortical bone, Ct.Ar ($-10.47 \pm 3.1\%$ $p=0.021$) was significantly reduced following SN, but Ma.Ar ($p=0.08$) and Tt.Ar ($p=0.651$) were not affected following SN.

SSA analysis

Following three weeks of SN, SSA demonstrated Tt.Ar was significantly lower in SN limbs compared with control limbs, although following post-hoc corrections, this significant difference was only significant at a single site. Significant reductions in Ct.Ar and increased Ma.Ar were evident. Ct.Ar, but not Ma.Ar demonstrated a site-specific effect (SN*site interaction) with significantly greater loss of Ct.Ar proximally (Figure 51). Changes due to SN were more variable in the proximal tibia (Figure 51), particularly with Tt.Ar and Ma.Ar, although Ct.Ar still demonstrated a significant loss of bone following SN in the proximal region.

Interestingly, SN alone in old mice resulted in significant increases in bone porosity and complete transcortical breaches in several of the mice in this experiment, although not all. These changes occurred primarily in the cortical bone proximal to the mid-point of the bone (approximately 45-50%). Due to these changes, the SSA program experienced some difficulty in performing the boundary marking operation which isolates the overall bone periosteal perimeter in each cross section, then subsequently calculates Tt.Ar and Ma.Ar for the remaining image. Furthermore, when there were multiple complete cortical breaches, the SSA programme separated the cortex into multiple separate objects, which then, as part of the remaining programming removed all but the largest object from the image (Figure 52). This resulted in the binarised image that was eventually analysed being reduced to a fragment of the entire cortical cross section and thus resulting in erroneously reduced Ct.Ar, Ma.Ar and Tt.Ar in some individual images. This increased variability between animals resulted in an increased SEM in the mean values reported for the proximal bone sites. This limitation of the SSA programme was recognised in the initial publication by its authors [7].

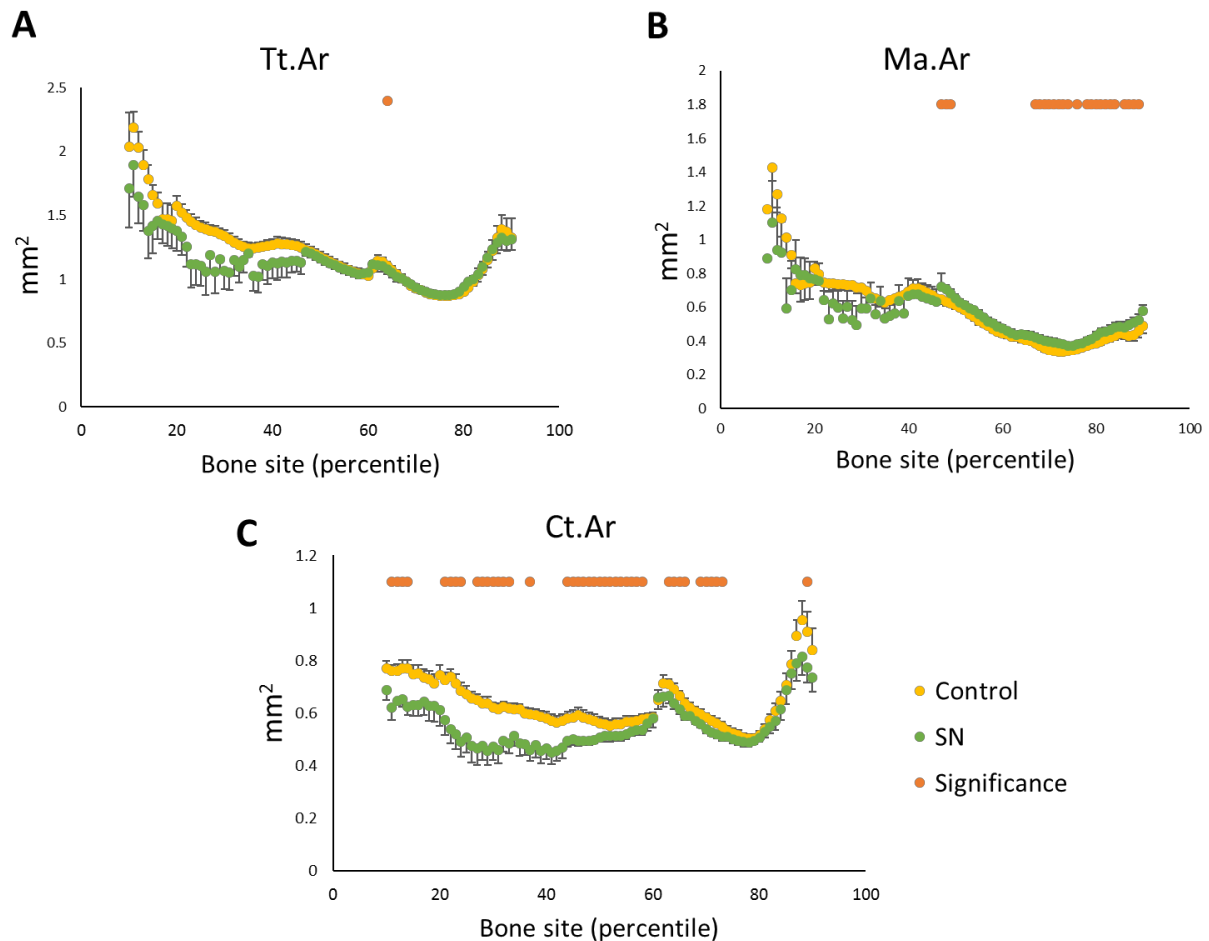


Figure 51 – Site-Specificity Analysis illustrating the effect of three weeks of disuse engendered by SN on cortical bone structure.

SSA was performed in 19-month-old female mice that were killed 21 days after SN in the right limb. (A) Tt.Ar, (B) Ct.Ar and (C) Ma.Ar were evaluated. The orange spots indicate a significant difference between control and SN limbs at that given bone site. Values represent Mean \pm SEM (n=9).

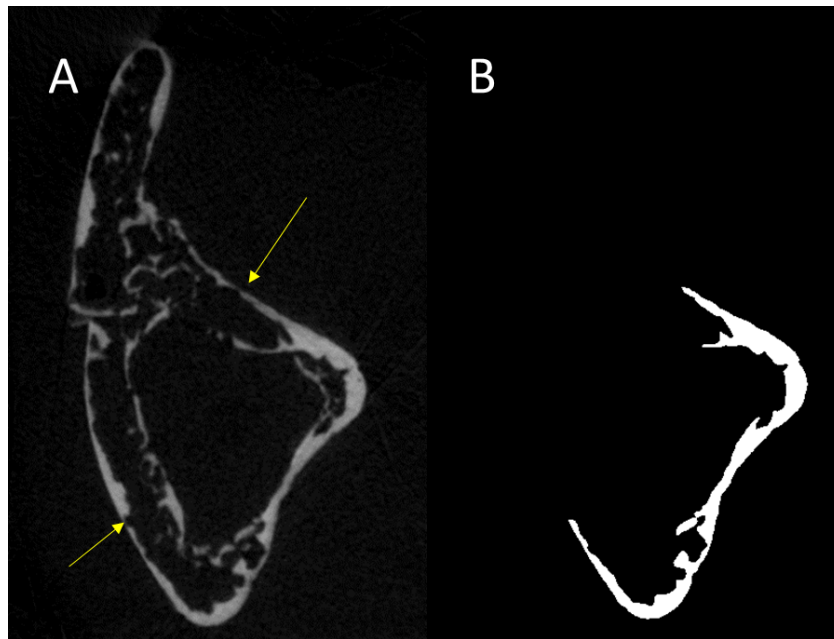


Figure 52 – Representative images of the 37% site following 3 weeks of SN.

Images represent (A) initial μ CT reconstruction of axial slices demonstrating increased intracortical porosity, and (B) output image following processing with SSA programme. The yellow arrows demonstrate cortical defects which resulted in segmentation of the cortical bone into separate objects and subsequent reduction in the calculated Ct.Ar, and Ma.Ar – The Tt.Ar used in the SSA programme is a derived sum of the Ct.Ar and Ma.Ar. In this particular image, the Ma.Ar would have been calculated as zero, as there is no enclosed space.

5.4.2 Preliminary single-site μ CT analysis from Meakin [4]

Preliminary data has suggested that the deficient response to loading in old mice can be restored following a short period of prior and concurrent disuse [4]. We reproduce this data here for ease of reference. In the Meakin (2013) study, with an identical experimental loading and SN protocol to Experiment 2 in the present study, the impaired loading response in old female mice undergoing axial tibial loading was rescued to a level of bone acquisition that was similar to that seen in young mice when loading was preceded by prior disuse engendered by SN. Figure 53 demonstrates the strain-dependent loading response is diminished in aged female mice, but following a short period of disuse (4 days), the loading response was improved such that the percentage increase in bone mass (Ct.Ar) was restored to levels similar to those seen in young mice.

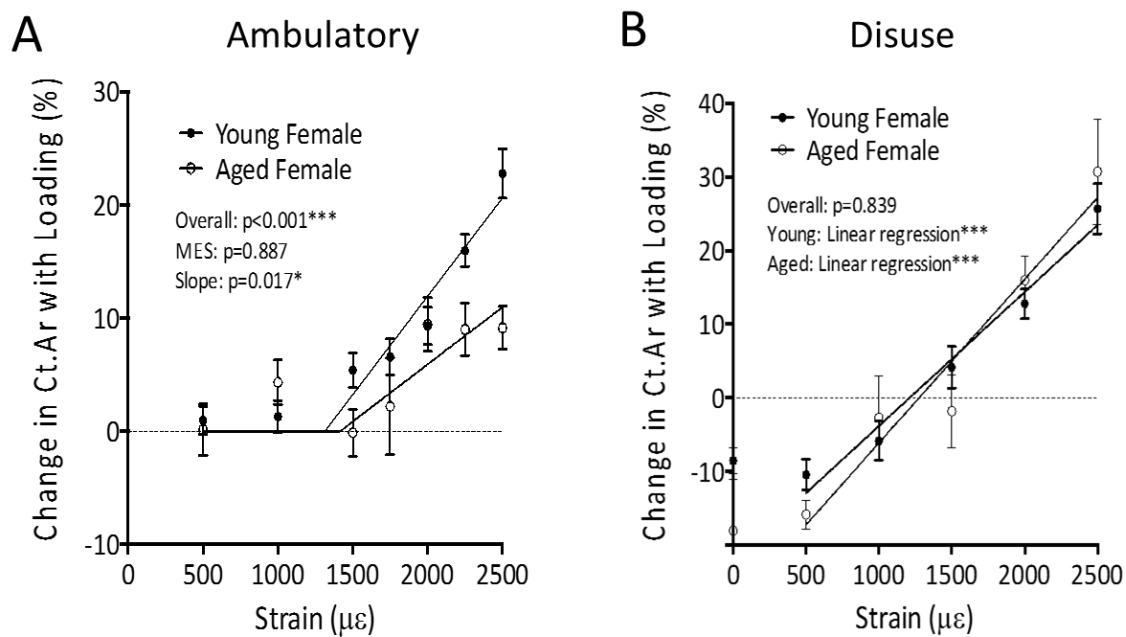


Figure 53: The effect of prior disuse on loading-related changes in Ct.Ar at the proximal 37% site at different magnitudes of mechanical strain in young and aged male and female mice.

The right tibia of (A) ambulatory and (B) right sciatic neurectomised mice was loaded and μ CT used to analyse the cortical morphology in each limb. Data represented as mean \pm SEM. Young and aged mice were compared using two-stage linear regression. Post-hoc t-tests were used to compare the MES and slope for both males and females since overall significance was detected. * $p < 0.05$, ** $p < 0.01$, *** $p < 0.001$. Figure adapted and reproduced with permission from [4].

5.4.3 Objective 2: Determine the effect of sciatic neurectomy on the bone mass and architecture of the contralateral limb without induced loading in old female mice using SSA.

To ensure that the demonstrated difference in the response to loading was not due to unintended changes in the control left limb due to right SN, a direct comparison of the left control limbs was performed using SSA. This demonstrated that Tt.Ar, Ct.Ar and Ma.Ar in the control limb of the SN group mice were not significantly different from that in the Sham group in the sites assessed by SSA (Figure 54).

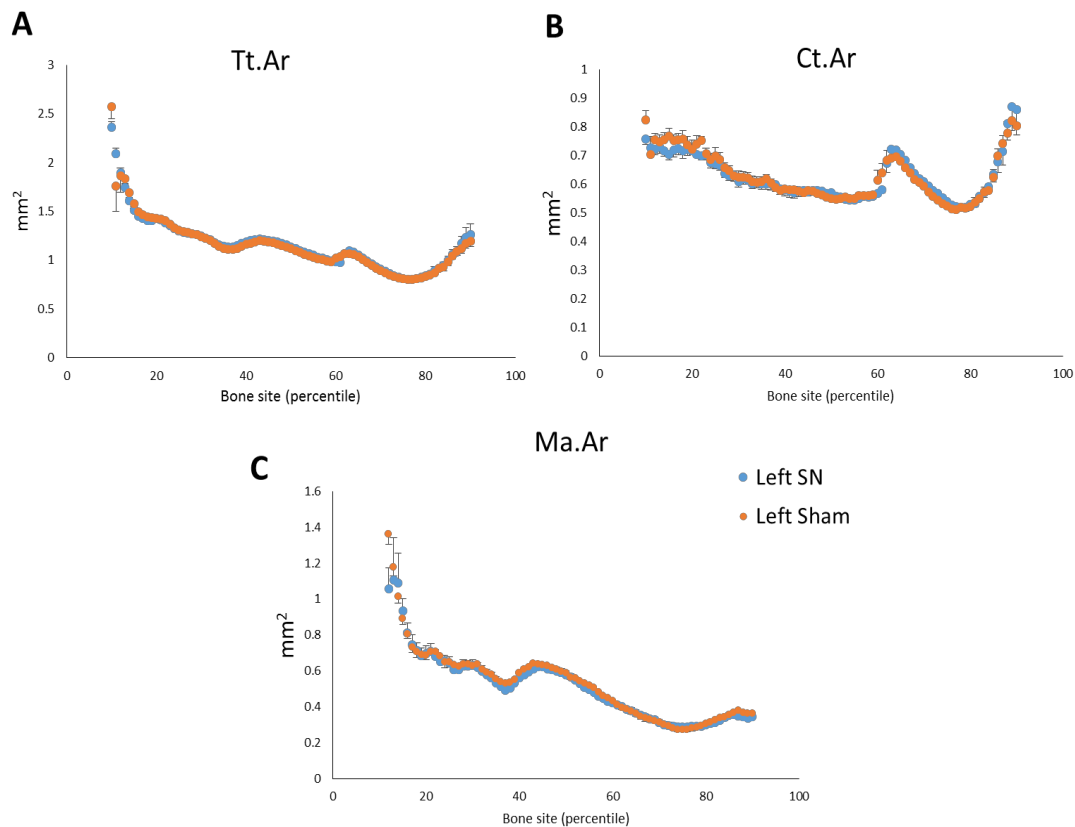


Figure 54 – Site-Specificity Analysis (SSA) illustrating the effect of unilateral disuse engendered by right SN and/or loading on cortical bone structure of the left contralateral leg of mice.

SSA of (A) Tt.Ar, (B) Ct.Ar and (C) Ma.Ar calculated from the control left tibia of mice 3 weeks after right sham or SN and right tibial loading for 8 alternate day loading episodes, n=7-9. Data points represent mean and error bars represent SEM. There was no significant difference between the left tibias of right sham or right SN mice using mixed-model analysis ($p > 0.05$).

5.4.4 Objective 3: Determine the effect of prior SN on the response to mechanical loading of cortical and trabecular bone regions of interest in old female mice, using single-site μ CT analysis.

The effect of SN (n=7) or sham surgery (n=9) on the response to loading was established using μ CT. Muscle area in SN limbs was significantly lower than in sham limbs, confirming the efficacy of SN. Tibial length and body weight were not significantly different between groups (Table 4).

		Sham operated (n=9)	Sciatic neurectomy (n=7)
Bodyweight (g)		30.22 ± 4.14	30.28 ± 2.01
Tibial length (mm)	Left Control	18.51 ± 0.09	18.56 ± 0.09
	Right Loaded	18.43 ± 0.07	18.59 ± 0.10
Mu.Ar (mm²)	Left Control	7.35 ± 0.14	7.35 ± 0.27
	Right Loaded	7.48 ± 0.13	5.36 ± 0.23 *** †††

Table 4 – Effect of a background of disuse engendered by SN and/or right tibial loading on bodyweight, tibial length and muscle area.

Bodyweight, tibial length and cross-sectional muscle area (Mu.Ar) measured at the mid diaphyseal (50% site) tibia. Data shown as mean ± SEM. ††† = $p < 0.001$ for the loading*surgery interaction; compared using mixed design ANOVA. *** = $p < 0.001$; compared with control limb using a post-hoc pairwise comparisons.

The data collected from experiment 2 for the single-site μ CT analysis of the trabecular and 37% cortical sites were examined using a mixed-design repeated measures ANOVA with loading as the within subject effect and surgery (SN) as the between subjects effect. All results reported in this section pertain to this experiment. All neurectomised limbs were also concurrently loaded. As expected, we demonstrated no apparent effect of SN on the contralateral limb for any measure (Table 5). This mirrors the findings of the SSA from Objective 2.

No measure of trabecular bone examined was affected by SN alone. Loading resulted in a 20.5% increase in Tb.Th in sham operated mice. No other trabecular parameter was significantly affected by loading. Prior SN did not affect the magnitude of the loading response in any trabecular parameter measured.

When considering the cortical bone site, SN alone had no effect on any parameter measured. Loading significantly increased Tt.Ar, Ct.Ar, Ct.Ar/Tt.Ar, Ct.Th and PMI ($p < 0.01$ for loading as a main effect by repeated measures ANOVA), but had no effect on Ma.Ar (Table 5, Figure 55).

Prior SN significantly altered the effect of loading for Tt.Ar and Ma.Ar ($p < 0.05$ for the loading*surgery interaction by repeated measures ANOVA). The increase in Tt.Ar

associated with loading was significantly higher in mice subjected to prior SN ($7.98 \pm 1.7\%$) than in the sham group ($1.02 \pm 2.2\%$, $p < 0.05$). The change in Ma.Ar was also significantly greater in the SN group (6.02 ± 3.69) than in the sham group (-5.76 ± 3.30 , $p < 0.05$) (Figure 55). Ct.Ar, Ct.Th, PMI and Ct.Ar/Tt.Ar did not show significantly different responses to loading between surgery groups (Table 5). This indicates that SN was associated with greater overall endosteal resorption, but concurrently greater periosteal bone formation, following loading.

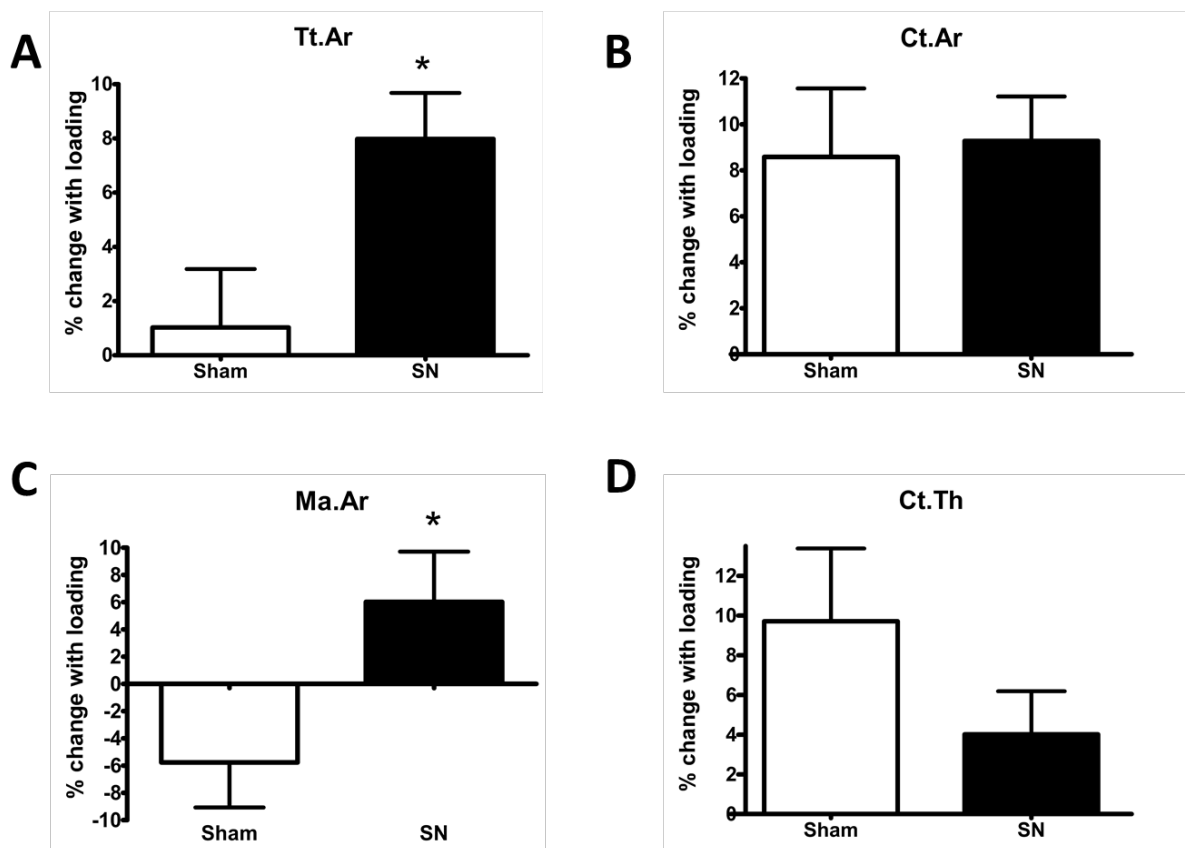


Figure 55 – The effect of a background of disuse engendered by SN on the cortical bone response to axial tibial loading in old female mice.

19m old C57BL/6 female mice underwent SN (n=7) or Sham surgery (n=9) on day 0 then 8 alternate-day episodes of right axial tibial loading sufficient to generate a strain magnitude of $2500\mu\epsilon$ starting on day 4. Mice were killed on day 21. μ CT analysis showing the percentage change between left control and right loaded limbs ($(\text{Right}-\text{Left})/\text{Left} * 100$). Data represented as mean \pm SEM. (A) Total area within the periosteal envelope (Tt.Ar); (B) Cortical bone area (Ct.Ar); (C) Medullary area (Ma.Ar); (D) Average Cortical Thickness (Ct.Th). Data were compared using a repeated measures ANOVA. * = $p < 0.05$ versus response to loading in sham. This figure is modified from the figure published in [9]

Trabecular bone		Sham operated (n=9)	Sciatic neurectomy (n=7)
BV/TV (%)	Left Control	1.714 ± 0.273	1.572 ± 0.179
	Right Loaded	2.166 ± 0.315	1.298 ± 0.281
Tb.Th (mm)	Left Control	0.044 ± 0.002	0.050 ± 0.001
	Right Loaded	0.053 ± 0.003*	0.054 ± 0.002
Tb.Sp (mm)	Left Control	0.414 ± 0.009	0.407 ± 0.007
	Right Loaded	0.413 ± 0.007	0.438 ± 0.007*
Tb.N (mm ⁻¹)	Left Control	0.411 ± 0.080	0.315 ± 0.037
	Right Loaded	0.435 ± 0.072	0.234 ± 0.046
Cortical Bone (37% site)			
Ct.Ar (mm ²)	Left Control	0.573 ± 0.020	0.574 ± 0.013
	Right Loaded ^{††}	0.620 ± 0.021 **	0.628 ± 0.019 **
Tt.Ar (mm ²)	Left Control	1.125 ± 0.022	1.083 ± 0.016
	Right Loaded ^{††}	1.137 ± 0.030	1.169 ± 0.022 ‡ ***
Ma.Ar (mm ²)	Left Control	0.552 ± 0.019	0.509 ± 0.013
	Right Loaded	0.516 ± 0.011	0.541 ± 0.020 ‡
Ct.Ar/Tt.Ar (%)	Left Control	0.509 ± 0.014	0.530 ± 0.009
	Right Loaded ^{††}	0.545 ± 0.006 **	0.537 ± 0.014
Ct.Th (mm)	Left Control	0.117 ± 0.004	0.123 ± 0.003
	Right Loaded ^{††}	0.128 ± 0.005 **	0.128 ± 0.003
PMI (mm ⁴)	Left Control	0.240 ± 0.011	0.238 ± 0.006
	Right Loaded ^{††}	0.256 ± 0.012	0.263 ± 0.010
MAR (µm/day)	Endosteal	2.22 ± 0.19	3.34 ± 0.32 ##
	Periosteal	1.49 ± 0.14	3.15 ± 0.53 ##

Table 5 – Effect of a background of disuse engendered by SN on the osteogenic response to loading in old female mice using conventional µCT analysis.

Parameters of bone mass and architecture were measured in trabecular bone of the proximal tibia (0.25-0.75mm distal to the proximal physis) and cortical bone (37% site measured from the proximal end) using µCT. Mineral apposition rate (MAR) was measured using dynamic histomorphometry. Data shown as mean ± SEM. †† = p<0.01 as a main effect for loading and ‡ = p<0.05, ‡‡‡ = p<0.001 for the loading*surgery interaction; compared using mixed design ANOVA. * = p<0.05, ** = p<0.01, *** = p<0.001; compared with control limb using a post-hoc pairwise comparisons. ## = p<0.01; compared with sham group using an unpaired t-test.

5.4.5 Objective 4: Determine the effect of prior SN on the rate of bone formation in loaded tibias of old female mice, using dynamic histomorphometry

Dynamic histomorphometry of the posteriolateral tibial cortex revealed a load-related increase in the mineral apposition rate in SN compared to Sham loaded mice on both the endosteal (+50.4%, $p < 0.01$) and periosteal (+112.2%, $p < 0.01$) surfaces suggesting that SN is associated with increases in both endosteal and periosteal bone formation rate in response to loading (Figure 56).

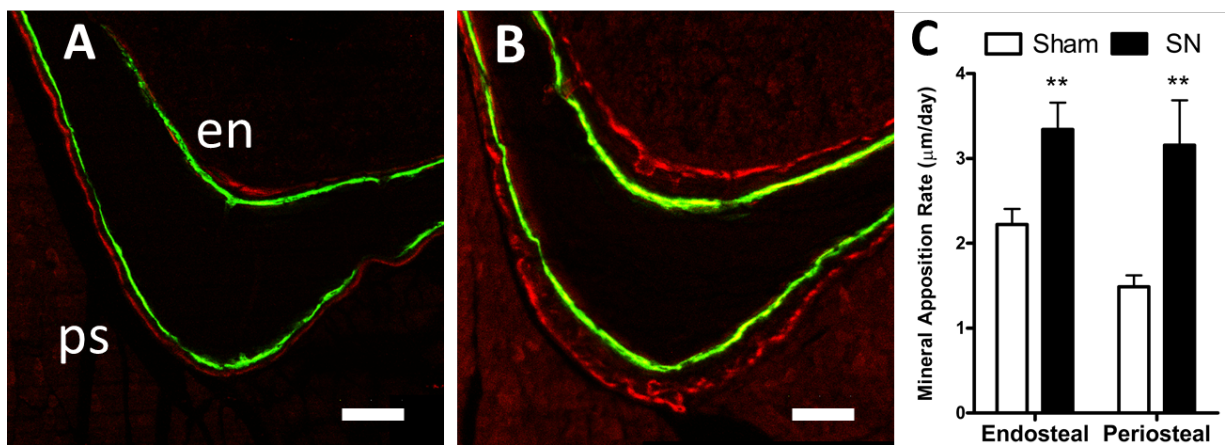


Figure 56 – Effect of a background of disuse engendered by SN on the loading-associated periosteal and endosteal bone formation in aged mice.

Confocal images of representative transverse sections of the posteriolateral cortex of the tibia taken at the 37% site illustrating calcein and alizarin fluorocholesterol labels administered at day 6 and day 18 of loading. The scale bars indicate 50µm. Endosteal surface = en, Periosteal surface = ps. (A) Loaded without prior SN; (B) Loaded with prior SN. (C) Mineral Apposition Rate at the posteriolateral cortex. Un-paired t-tests were used to compare sham and SN groups. ** = $p < 0.01$. This figure is modified from the figure published in [9].

5.4.6 Objective 5: Determine the effect of prior SN on the response to mechanical loading of the entire cortical bone in old female mice, using SSA.

Mixed model analysis of the data for this objective was performed and the p-values of main effects and interactions from the mixed model are reported in Table 6.

Periosteally-enclosed area (Tt.Ar)

Tt.Ar was significantly increased by loading, and this effect was site-specific, with a greater increase due to loading in the distal cortical bone (distal to 75% site) than in the proximal region of the bone. Prior SN resulted in a significantly greater loading related increase in Tt.Ar than in the sham surgery group (SN*Loading interaction = $p < 0.001$) (Figure 57A, B). Interestingly, this SN-associated increase in the response to loading appeared to focus around the 37% site, where single-site analysis identified a response, and also in the cortical bone distal to ~78% site, a region which is normally minimally responsive to loading in aged mice.

Cortical bone area (Ct.Ar)

Ct.Ar was significantly increased by loading and this effect was site-specific, with greater loading-related increase proximally and distally, compared to the mid-shaft (~50-70%). Prior SN resulted in a significantly greater loading-related increase in Ct.Ar than in the sham surgery group (Figure 57C, D).

Medullary Area (Ma.Ar)

Loading resulted in overall significant reductions in Ma.Ar and this effect was site specific, with loading related decreases in Ma.Ar confined to the proximal cortical bone and loading related increases in Ma.Ar observed distally. Prior SN resulted in a significantly greater loading related increase in Ma.Ar than Sham surgery, particularly in the cortex distal to the 60% site (Figure 57E, F)

Polar Moment of Inertia (PMI)

Loading resulted in a significant increase in PMI and this effect was site specific, with greater loading-related increase in PMI proximally, compared with distal sites. Prior SN resulted in a significantly greater loading-related increase in PMI than in the sham surgery group (Figure 57G, H).

Effect	Tt.Ar	Ct.Ar	Ma.Ar	PMI	Ct.Po
SN	p=0.461	p=0.634	p=0.547	p=0.546	p=0.383
Loading	p<0.001	p<0.001	p<0.001	p<0.001	p=0.523
SN*Loading	p<0.001	p=0.009	p<0.001	p=0.001	p<0.001
Site*SN	p=0.857	p=0.431	p=0.980	p=0.956	p<0.001
Site*Loading	p<0.001	p<0.001	p<0.001	p=0.041	p<0.001

Table 6 - The effect of a background of disuse engendered by SN on the response to loading in old female mice.

Significance (p) values following mixed model analysis of SSA data exploring cortical bone parameters following unilateral loading with or without ipsilateral SN in old mice. n= 7-9.

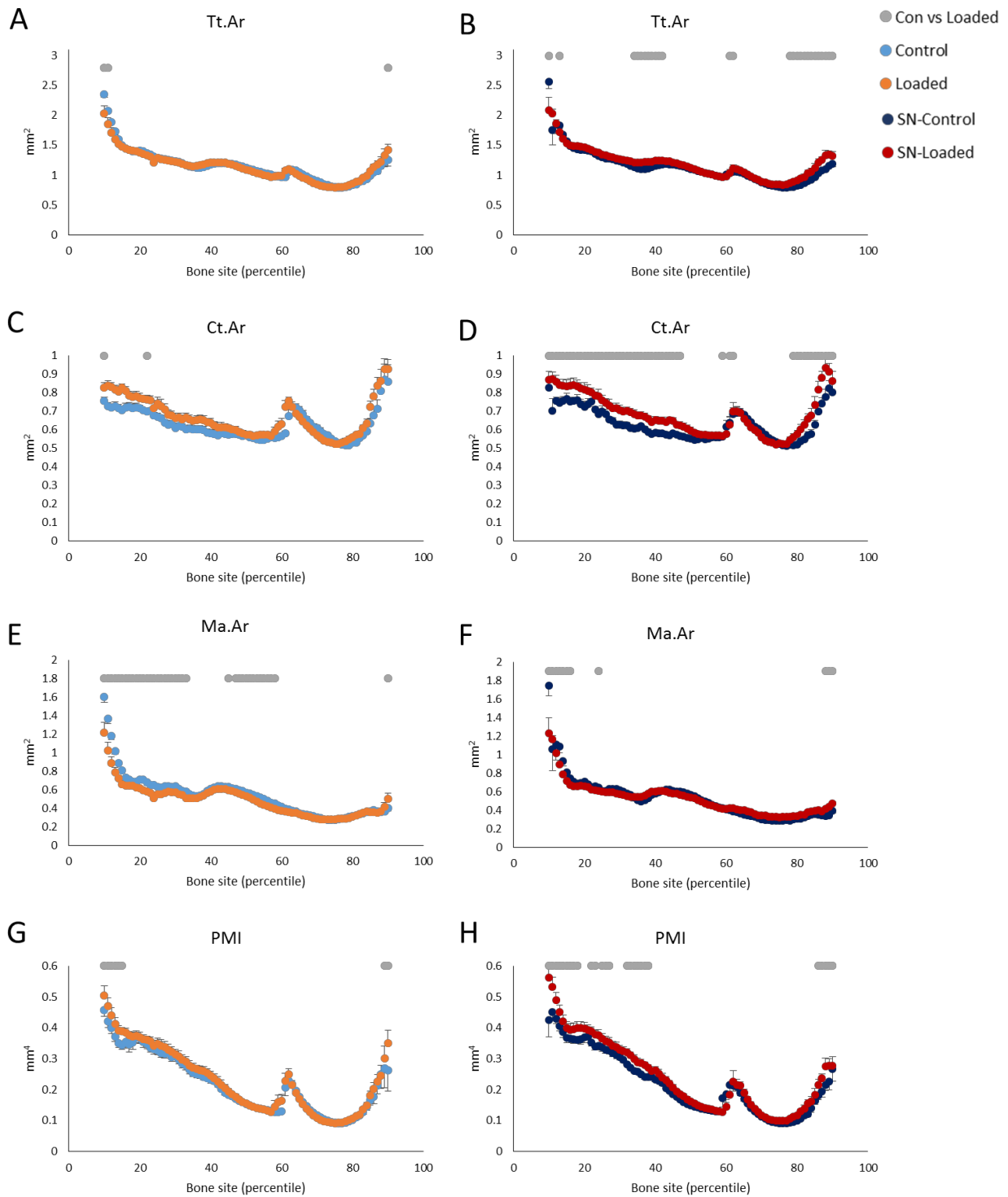


Figure 57 – Effect of a background of disuse engendered by SN on the adaptive response to loading in cortical bone of old female mice.

SSA was undertaken on μ CT data of tibias from 19m-old female C57BL/6 mice following sham surgery (A,C,E,G) or SN (B,D,F,H) and subsequent right axial tibial loading for 3 weeks. (A, B) Tt.Ar, (C, D) Ct.Ar, (E, F) Ma.Ar and (G, H) PMI were analysed using SSA. Grey spots represent a significant difference ($p < 0.05$) between control and loaded limbs at that site following mixed model analysis. Values represent Mean \pm SEM ($n = 7-9$)

Cortical Porosity (Ct.Po)

Ct.Po in the proximal cortical bone was significantly reduced with loading (Figure 58A). Prior SN resulted in a significantly different response to loading for Ct.Po, and this interaction demonstrated a site-specific effect. The proximal cortex showed *decreases* in Ct.Po with loading and the distal cortex, where the loading related increase in Tt.Ar is greatest, demonstrated a loading-related *increase* in Ct.Po (Figure 58B). This appeared to be due to increased woven bone formation in response to loading. Figure 59 shows representative images at the 85% site of loaded limbs from sham and SN mice, illustrating the increase in cortical porosity and apparent woven bone formation.

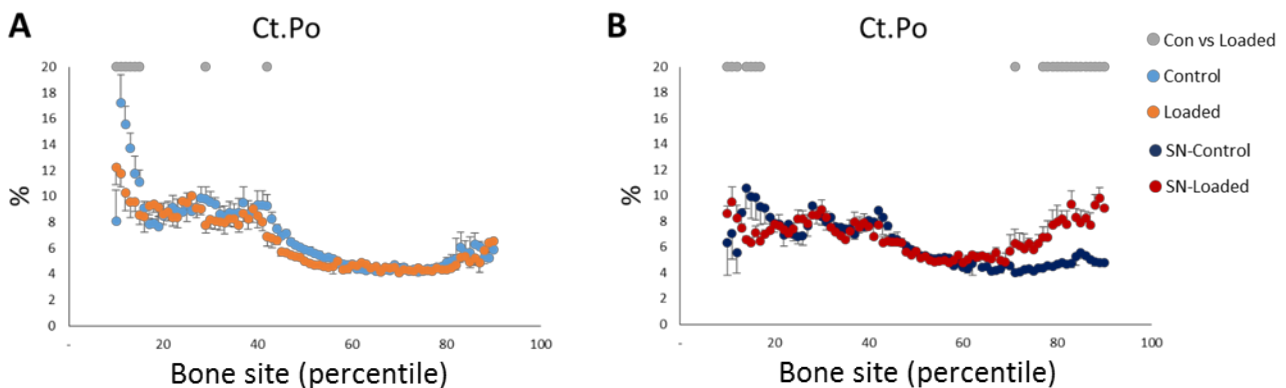


Figure 58 – The effect on cortical porosity of a background of disuse engendered by SN and/or mechanical loading of the tibia in old female mice.

SSA was undertaken on μ CT data of tibias from 19m-old female C57BL/6 mice following sham surgery (A) or SN (B) and subsequent right axial tibial loading for 3 weeks. Ct.Po was analysed using SSA. Grey spots represent a significant difference ($p < 0.05$) between control and loaded limbs at that site following mixed model analysis. Values represent Mean \pm SEM ($n=7-9$)

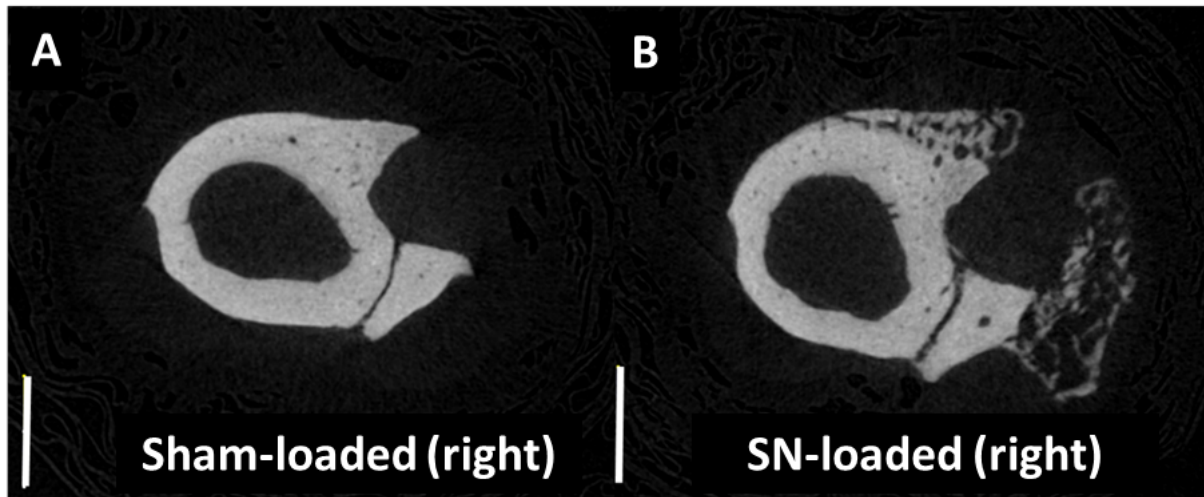


Figure 59 – The effect of a background of disuse engendered by SN on the ipsilaterally loaded limb of old female mice.

Representative μ CT transverse reconstructed slices from loaded bones at 85% site in (A) sham operated and (B) SN operated mice, demonstrating the increased periosteal woven bone formation in neurectomised limbs, resulting in greater porosity distally. Scale bars represent 500 μ m.

5.4.7 Results summary

Objective 1

- SN in old female mice resulted in significant reductions in Ct.Ar, primarily in the proximal tibia, associated with an increase in Ct.Po.

Objective 2

- SN had no effect on the cortical bone structure of the contralateral limb of old female mice.

Objective 3

- The adaptive response to loading in trabecular bone of old mice was unaffected by prior SN.
- The adaptive response to loading in cortical bone at the 37% site was increased following prior SN, compared with sham operated animals, with increased

periosteal apposition. A load-related medullary expansion was also seen in SN-operated mice.

Objective 4

- Loading-associated bone formation was increased periosteally and endosteally at the posteriolateral cortex in mice with prior SN, as demonstrated by DH.

Objective 5

- SSA confirmed that prior disuse resulted in a greater load-related increase in total area, cortical bone area and PMI compared to sham-operated controls, despite decreased load-associated medullary contraction in mice that experienced prior disuse.
- Prior SN resulted in a significantly greater load-associated decrease in Ct.Po in proximal cortical bone, but a significantly greater load-associated increase in Ct.Po in distal cortical bone associated with periosteal woven bone formation distally.

5.5 Discussion

In the experiments described in this chapter, we demonstrate that 3 weeks of SN reduces bone mass in old female mice, with a concurrent increase in porosity proximally. A short duration of reduced loading, engendered by SN, improved the periosteal osteogenic response to loading; a finding consistent with previous data from both young and old mice [4, 35]. Concurrent SN also resulted in overall load-related endosteal expansion, despite an observed focal increase in endosteal bone formation engendered by loading at the posteriolateral tibial cortex.

Several previous studies have reported a lower response to mechanical loading in old rodents [25, 29, 389]. A previous study which demonstrated adult mice have a diminished response to loading compared to young, growing animals, also showed that increasing strain magnitude can restore the age-impaired loading response [453]. Taken together with our current study, these results suggest that the age-related impairment of the mechanostat is not consequent to an intrinsic failure of the mechanisms whereby bone

mass increases, but to a reduction in the efficacy of these mechanisms to respond to strain-related stimuli to which they respond effectively in the young, healthy skeleton.

5.5.1 Sciatic neurectomy in old mice results in endosteal and intracortical bone loss.

In this part of the study we were able to confirm, through use of the recently published SSA software [7], that SN of 3 weeks duration is sufficient to result in significant bone loss in old mice, primarily due to a reduction in cortical area, which was greater proximally than distally. SSA did not, however, demonstrate a significant effect of SN on total area or medullary area in the proximal cortex. This may have been due to limitations of the SSA programme to analyse these parameters effectively in this extremely porous old bone. Single-site μ CT analysis from the same mice confirmed this lack of effect of SN on medullary area and total area at the 37% site [4] suggesting the single-site μ CT analysis may also have similar limitations. These limitations were acknowledged in the original SSA publication describing application of this software [7].

The interpretation of the data from the proximal region in this study should be made with some caution. The variable results for the regions proximal to the ~45% site are likely in part due to the limitations of the SSA programme in dealing with breaches in the cortical bone resultant from the increased level of porosity engendered by SN in several of the mice analysed (Figure 52). The increase in porosity may partly explain the significant reduction in cortical area without a concurrent significant reduction in medullary area. A previous study using tail suspension demonstrated unloading-associated reduction in BMD with concurrent increases in intracortical porosity in aged (32-month) rats which were not present in young rats [184]. An earlier study also demonstrated an increase in porosity after unilateral hindlimb immobilisation by strapping the limb to the body [654].

Our original study using the site specificity approach demonstrated in young mice that endosteal expansion is greater in the proximal tibia following SN compared with distally [7]. The presence of endosteal expansion over a greater region of the distal tibia in old mice, which was not as apparent in young mice neurectomised for the same duration is

likely due to the increased basal resorption evident in aged vs young animals [30, 443]. Increased resorption with disuse can be mitigated with antiresorptive therapies, such as bisphosphonates. Several rodent studies have demonstrated that BPs are able to abrogate deterioration of bone parameters in disuse back to levels seen in ambulatory animals [458-461]. Chapter 6 of this thesis explores the effects of the bisphosphonate risedronate on bone's adaptive response to loading in the context of prior disuse.

5.5.2 A short period of prior disuse enhances the periosteal response to loading in old female mice.

We next confirmed that short periods of dynamic loading in aged mice stimulate a greater periosteal osteogenic formation response when applied over a background of disuse than against a background of habitual loading through normal ambulation. This finding supported a previous finding by our lab that imposing a background of disuse, rather than habitual loading, abrogates any age-related difference in the osteogenic response to external loading over the full physiological range of peak strains from 500 to 2500 $\mu\epsilon$ [4, 9](Figure 53). The nature of this “rescue” appears to be related to an activation of bone formation on the periosteal surface where it has previously been reported to be impaired [29, 455].

The data from the present study also support findings from a previous study in young adult mice which demonstrated that SN-induced disuse can increase the osteogenic response to loading [35]. The authors of this study proposed that the nature of the rescue was due to a degree of averaging of the total strain-related stimulus – ie. that mice performing normal habitual loading activity have a higher average strain stimulus due to the habitual loading. Thus, given the smaller difference between habitual loading strains and the strains experienced when greater abnormal loads are applied, ambulatory mice are less likely to respond to a given exogenous strain input than those mice who have a low average strain stimulus through disuse engendered by SN. Background strains engendered by ambulation during habitual cage activity measured *in vivo* at the medial surface of the

tibia were halved following SN from approximately $600\mu\epsilon$ in intact mice to approximately $300\mu\epsilon$ [11]. The strain averaging hypothesis is illustrated diagrammatically in Figure 60.

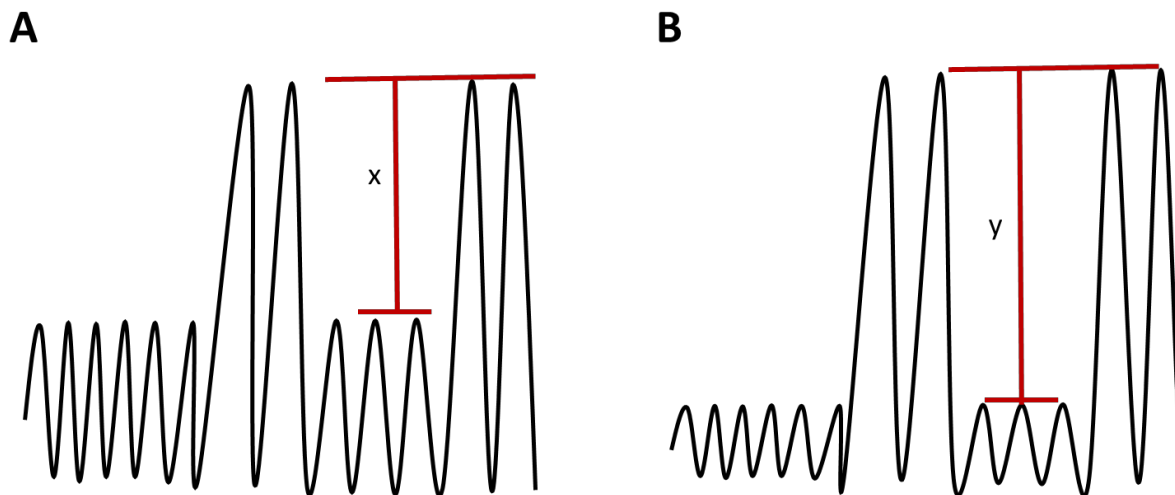


Figure 60 – Diagrammatic representation of the strain averaging hypothesis.

(A) normal habitual loading results in a smaller change in peak strain (x) following application of a set peak strain than the change in peak strain (y) seen after loading in mice with reduced habitual loading due to sciatic neurectomy (B)

Lanyon [655, 656] first proposed the response to functional strains as being “error driven” by suggesting it is abnormally large strains experienced which are the controlling stimulus for the mechanically adaptive response to loading, and not the strains that are being experienced habitually. This theory is supported by the finding that insertion of a 10s gap between load impulses in loading protocols was able to promote a greater osteogenic response in old mice when compared to sinusoidal loading [27].

This is also consistent with our previous observation that the osteogenic response to loading in group housed male mice was lower than that in individually housed males and in females because regular fighting between group-housed males engenders a habitual strain environment little different from that engendered by artificial loading [285]. Another study compared the historical loading environment in mice by incrementally increasing loading to a high peak load over several weeks in one group and decrementally reduced loading from an initially high peak load to low loads in another group, and demonstrated significantly greater bone formation in the latter group [590]. Our results

are also supported by the findings of a very recent study exploring the effect of prolonging the duration of disuse prior to loading in aged mice, which confirmed the “rescue” of age-impaired loading response, and that a longer duration of disuse (100d vs 5d) resulted in more robust increases in load induced cortical bone formation in old mice [657]. Furthermore, the trabecular bone response was not rescued by prior disuse of any duration.

Whether the observed rescue phenomenon is part of an “averaging” mechanism, as previously proposed [35], remains to be determined, although the results of these studies certainly suggest that the historical loading context is important in determining the response to a given strain stimulus.

In the study by de Souza *et al* [35], loading-related increase in both endosteal and periosteal mineral apposition rates were greater in young mice following SN than those which continued to load their limbs through normal ambulation between episodes of loading. In contrast, in the neurectomised limbs of old mice used in the present study, the increase in bone formation appears predominantly periosteal, as demonstrated by the μ CT and dynamic histomorphometric imaging. Interestingly, the periosteal surface is the area where the loading response is reported to be most impaired by age [29, 455]. Structurally, periosteal bone formation is ideally placed to most appropriately improve bone’s resistance to bending and reduce strains and likely fracture risk [443]. Periosteal expansion in long bones improves the resistance to bending/torsion, approximated as the moments of inertia. Using SSA, there was a significant effect of SN on the loading-related increase in PMI.

Prior disuse significantly altered the response to loading when considering the endosteal compartment. Load-related endosteal formation (indicated by medullary area reduction evident in sham-operated tibias using SSA) was partially abrogated in SN-operated tibias (Figure 57E, F). This appears to contradict the dynamic histomorphometry analysis which suggests that endosteal, as well as periosteal, load-related bone formation was increased in mice loaded on a background of disuse. Our interpretation of this apparent discrepancy is that the endosteal formation was focally discrete and primarily located at the load-

responsive posteriolateral cortex. Unfortunately, it is very difficult to quantify the amount of bone resorption using dynamic histomorphometry alone. Use of *in vivo* μ CT is a more versatile technique to evaluate the volumetric degree of bone resorption. Bone resorption rates have recently been reported to correlate with maximum principal strain magnitude, calculated based on FEM on the endosteal surface, but not on the periosteal surface [529]. This further supports the suggestion that the two compartments differ in their response to changes in mechanical strain.

Interestingly, spatially separate sites of formation and resorption endosteally within the same cross-section were found following loading of greater than 3 weeks in young adult mice (Chapter 3, Figure 28). This finding, combined with the SSA results from this chapter, suggests a site-specific component to the cross-sectional and proximo-distal location of bone formation following loading, in young and aged mice. The endosteal new bone formation was lamellar in appearance and was observed in the posteriolateral tibial cortex at the 37% site, which is the same site previously demonstrated by our group to display the greatest amount of formation following axial loading [1, 8].

An alternate hypothesis for the observed improvement in the osteogenic response to loading on a background of disuse is an increase in remodelling-based bone formation following initiation of a “pro-resorptive” state induced by SN. SN has been shown to increase osteoclast numbers very rapidly after surgery [106]. Anti-resorptive treatments such as bisphosphonates inhibit osteoclast function and if the increased presence of osteoclasts following disuse is involved in the augmented adaptive response to loading following SN, through osteoclast:osteoblast cell “coupling”, then impairing osteoclast activity would likely also impair the SN-associated improvement of bone formation. The studies described in chapter 6 of this thesis aim to determine if this potential mechanism underlies the observations made in this chapter.

Skeletal muscle’s potential control of bone homeostasis has been garnering significant attention in recent years [658]. The crosstalk between bone and the surrounding skeletal muscle has been demonstrated to have some effect over bone metabolism; for example the feed forward loop between interleukin-6 and osteocalcin secreted by muscles and

bone respectively is one mechanism which may facilitate control of bone mass through muscle activity [658]. Loss of muscle mass is a well-established consequence of SN and disuse in young mice. In the present study, SN resulted in significant reduction in muscle size compared to sham-operated controls. The enhanced osteogenic loading response on a background of disuse occurred despite this ongoing muscle loss, arguing against muscle/bone crosstalk as an important factor in the observed rescue of the osteogenic response to loading.

The experiments described in this chapter are not able to provide any explanation of the cellular mechanisms underlying the reported differences in the adaptive response to loading following SN. A previous study undertaken by our laboratory showed that loading in the context of disuse engendered by SN increased the number of genes differentially regulated by mechanical loading [86]. The cellular mechanisms underlying cellular mechanosensitivity remain incompletely understood, but recent work has demonstrated that mice deficient in Connexin 43 (Cx43) are resistant to bone loss seen with disuse [606] and have an improved osteogenic response to mechanical loading at the periosteal surface [659]. Cx43 is a gap junction protein. The authors of the study postulated that Cx43 affects bone cells' response to mechanical loading through altering levels of cellular Wnt/ β -catenin signalling. Alterations in Wnt signalling at endosteal and periosteal surfaces in aged mice following disuse could underlie the primary observation noted in this study that a background of disuse was associated with a greater osteogenic response to short periods of loading than loading on a background of habitual loading.

The observations in the present study may also be explained in part by transient adaptive cellular stiffness changes. It has recently been suggested that reversible and transient cell stiffness changes engendered by mechanical stimulation may act as an intrinsic "brake" to further mechanical responses by diminishing the strain a cell experiences when equivalent stress is applied [660]. This suggests that the intracellular cytoskeletal accommodation that occurs due to loading eventually impairs the ability for a cell to respond to the mechanical stress applied. These *in vitro* findings are consistent with the well-established finding that inserting rest periods between periods of loading increases the osteogenic

response to loading [27] and our present finding that “habitual” strains also blunt the loading response in old mice.

Our present study has also done nothing to establish the cellular mechanisms involved in the apparent site-specific differences in the loading response between sham and SN animals. In the study by Moustafa *et al* [8], the location of bone formation due to loading was found to correlate to the degree of relative osteocytic sclerostin down-regulation, rather than the local load-induced peak strain magnitude, estimated through finite element modelling. In the tibia, formation is greatest proximally, with a minimal response to loading distally, despite apparently osteogenic levels of strain according to FEM. This suggests that sclerostin regulation throughout the tibia may also be involved in the site-specific nature of the endosteal bone formation and resorption response in these mice following SN. Interestingly, the down regulation of sclerostin expression following loading does not appear affected in old mice despite the impaired osteogenic response to loading [29]. Periostin has been shown to be necessary for inhibition of sclerostin and to be involved in the bone loss associated with unloading. Periostin knockout mice showed no bone loss following hindlimb unloading, which corresponded with a lack of upregulation in sclerostin with unloading [630, 661].

Periostin is also reported to be involved in the periosteal expansion typically seen with ageing; it is impaired in periostin KO mice, with these mice demonstrating a smaller Tt.Ar and reduced periosteal formation with ageing, compared with wild-type controls [662]. Furthermore, qRT-PCR expression of periostin in cortical bone has been demonstrated to be lower in aged mice compared with young adult mice. Interestingly, expression of periostin did not increase with loading in aged mice, whereas it did increase in young mice in a microarray time course experiment [4]. Periostin expression also increased with loading in an earlier microarray study, and in that study, the regulation of periostin was different following loading on a background of SN compared to ambulatory mice [86]. Combining the results of the present study with those above implicating periostin in modulation of age-, loading- and site-specific bone formation suggests that changes in periostin expression could be involved in a potential mechanistic pathway for the

apparent rescue of periosteal formation following loading of old mice on a background of disuse. Further investigation into the mechanisms of the observations reported in this chapter would benefit from considering investigation of the relationship of periostin and sclerostin to the bone formation and loss demonstrated.

Regardless of the cellular mechanisms behind the SN-mediated improvement in load-related bone formation, the improvement in bone architecture by periosteal expansion will typically improve mechanical resistance to fracture better than that achieved by endosteal bone formation alone. When considering the clinical relevance of the current findings, to the extent that data from old mice can be extrapolated to old humans, it appears that modification of the pattern of mechanical loading in the elderly, with lower frequency, higher magnitude loading may be sufficient to improve the diminished osteogenic response to loading and improve structurally appropriate bone formation and possibly reduce fracture risk. This is consistent with exercise trials in post-menopausal women where unilateral strength exercises produced significant improvements in hip and radial bone mass, where endurance exercises did not [26]. Exercise interventions in the elderly do, however, have far smaller clinical benefits for bone mass than the same interventions in young people [663], so preventative exercise to develop bone mass is of greater benefit. Indeed, physical activity that benefits bone mass in youth provides lifelong benefits in cortical bone strength [664]. Nonetheless, in older people, modification of their physical loading/exercise regimens could provide non-pharmaceutical treatment options to improve bone mass in a structurally appropriate manner. Similarly, mechanical loading techniques/exercises in people with inherently low habitual loading levels, such as those confined to a bed, or in spinal injury patients, could be more osteogenic than in ambulatory people. These potential clinical benefits need to be confirmed and would need to be weighed against the potential detrimental and other general health effects of changes to exercise/loading patterns in people, such as cardiovascular health and increased fracture risk of over-loading osteoporotic and potentially weaker bone.

5.6 Conclusions

- Reducing habitual loading of the tibia in aged mice induced by SN increases the periosteal osteogenic response to short periods of dynamic artificial loading suggesting that strain-related stimulus arising from ongoing normal ambulatory loading may reduce the magnitude of response to short periods of more osteogenic stimulation.
- These results suggest that there is no inherent age-related impediment, either to the accurate assessment of strain and subsequent perception of strain, or to loading-related periosteal expansion in response to appropriate loading.
- As far as the data from old mice can be extrapolated to old humans, modification of the therapeutic regime of loading of bone may be able to improve the osteogenic response to loading and thus bone mass, although further studies are necessary.

Parts of this chapter contributed to a peer-reviewed publication (joint-first author). A copy of the published paper is included in Appendix 4 of this thesis:

Delisser, P. J.*, Meakin, L. B.*, Galea, G. L., Lanyon, L. E., & Price, J. S. (2015). **Disuse rescues the age-impaired adaptive response to external loading in mice**. *Osteoporosis International*, 26(11), 2703–2708.

*These authors contributed equally.

Chapter 6

The effect of Risedronate on the osteogenic response to loading in ambulatory and sciatic neurectomised old mice.

Chapter 6 - The effect of risedronate and loading in old mice

6.1 Introduction

The primary determinant of bone mass and architecture is mechanical loading and its influence is probably exerted by the effects of loading-induced strains on the cells resident in bone tissue, thus regulating bone modelling and remodelling. The adaptive (re)modelling response in young animals ensures sufficient bone is strategically placed to prevent excessive damage to the bone tissue and reduce the risk of undue damage and bone failure during functional loading. Failure in this regulatory mechanism, called the “mechanostat”, is hypothesised to be a major factor that underlies the increased incidence of fragility fractures in the elderly [23].

The bone loss associated with old age has many features in common with the bone loss that is the consequence of unloading (disuse) and is inevitably more severe when the two are combined, as is often the case in elderly patients who may be bed-bound or have increased sedentary behaviour [456, 665]. In the previous chapter of this thesis we showed that old female mice lose bone following disuse (by SN), and this bone loss involved increased intracortical porosity not seen following SN in young mice. The loss of bone observed in old mice [31] can be countered by the use of anti-resorptive drugs such as bisphosphonates (BPs) as their mechanism of action is to reduce resorption by inhibiting the activity and survival of osteoclasts [302] and interrupt the remodeling cycle. BPs are mainstay treatments for osteoporosis in humans; in 2012, 14.7 million prescriptions were dispensed in the USA alone [319]. However, the use of BPs as front-line drugs has decreased in the last decade as newer anti-resorptive therapies have become available and because of some concerns regarding their safety, namely their association with osteonecrosis of the jaw and atypical femoral fractures, particularly after prolonged use [666-668].

In addition to their use for treating age-related bone loss, BPs can also attenuate the bone loss seen with reduced loading in humans and experimental animals. Pamidronate reduced bone loss following extended bed rest in young men [456] and alendronate administration abrogated bone loss in astronauts treated with alendronate and exercise, compared to exercise-only controls [457]. Several rodent studies have demonstrated that BPs are able to completely abrogate deterioration of bone parameters in disuse back to levels seen in ambulatory animals [458-461].

Whilst BPs all inhibit the activity and/or survival of osteoclasts, different molecular variants of BPs have varied clinical efficacy for inhibiting bone resorption. These varied types and mechanisms are discussed in more detail in the general introduction (Chapter 1) of this thesis. Most newer generation bisphosphonates, such as risedronate (RIS), are termed nitrogen-containing bisphosphonates and act on the mevalonate pathway, by inhibiting the enzyme farnesyl pyrophosphate synthase (FPPS) in osteoclasts. This, in turn, causes an increase in the intracellular accumulation of prenylated proteins, which impairs osteoclast function and resorption, and eventually leads to apoptosis. Impairment of osteoclast function may in turn affect the subsequent activity of osteoblasts by interrupting the bone cell “coupling” of osteoclast to osteoblast function in the bone multicellular unit. While BPs are clearly very effective at preventing the bone loss associated with aging and with unloading, questions have been raised as to whether BPs may compromise the effect of concurrent anabolic therapies because they reduce remodelling activity; i.e. there is a body of literature to show that the positive effects of PTH may be reduced by prior BP treatment [380, 669-671]. The use of combination therapies remains controversial, although recent evidence suggests that PTH primarily stimulates new bone through modelling-based formation and can still produce new bone even when bone resorption is suppressed with BPs, and as such, concurrent anti-resorptive therapies should not diminish PTH’s anabolic effect [672]. Chapter 7 of this thesis investigates the combined effect of PTH and risedronate in old mice in more depth.

Several studies have previously investigated the combined use of BPs and anabolic levels of loading in young adult rodents. We have shown in young adult female mice (17-weeks-

old) that RIS has no effect on the magnitude of the osteogenic response to mechanical loading [34]. This suggests that the loading response primarily involves osteogenic modelling without requiring “coupling” of osteoblast and osteoclast activity in mice [34]. This study showed strong positive effects of RIS on trabecular bone, which were additive to the anabolic effects of loading. However, RIS had no independent effect on cortical bone parameters. In a similar study in young rats, Feher *et al* [462] showed the periosteal bone modelling response seen following axial ulnar loading was unaffected by treatment with a variety of BPs, including RIS. In the study by Feher *et al* [462], bisphosphonate treatment following concurrent ovariectomy, an additional resorptive stimulus, also had no effect on the degree of the loading-related response. Furthermore, whole body vibration-related changes in bone mass were unaffected by alendronate treatment [463]. Some human clinical trials have also shown that the response to exercise in humans is unaffected by BPs. While two studies from the same author have found additive increases in bone mass with exercise and BPs [464, 465], others have found no additional effect of exercise/loading on BMD above the effect of BPs [446, 466]. The section modulus (surrogate measure of bone strength) increased with jumping exercises in one study and this was unaffected by treatment with BPs [446].

Patients with osteoporosis, those most likely to be prescribed BPs, are usually elderly (and/or postmenopausal), and the effect of BPs on the loading response in old animals has, to the authors’ knowledge, not been investigated. **The first aim of this chapter was to determine the effect, in old female mice, of RIS treatment on bone’s response to axial tibial mechanical loading.** We did this initially using the artificial axial tibial loading model against a background of normal ambient loading.

We hypothesised that the osteogenic response to mechanical loading in old female mice, as in young mice, although inherently diminished due to age [29], would not be impaired by RIS.

In the previous chapter (and associated peer-reviewed publication [9]), we demonstrated that a short period of prior and concurrent disuse engendered by sciatic neurectomy was sufficient to “rescue” the impaired osteogenic response to loading in old female mice; an

observation which could have significant clinical implications. Improvement in the osteogenic loading response has previously been reported following prior and concurrent disuse in young mice [35]. As discussed in Chapter 5, these authors hypothesised that the improved response following SN was due to a depressive modulatory effect of habitual loading on the response to externally applied exogenous loading in ambulatory animals, which is removed in neurectomised animals. An alternate hypothesis for this observation is that prior disuse in old mice “primes” the osteogenic response through an increase in resorptive action, increasing the possibility of remodeling-based bone formation through “coupling” of osteoclast and osteoblast activity. If this alternate hypothesis were true, then treatment with BPs would inhibit the apparent “rescue” of the loading response. The loading response in old mice following RIS treatment has not been studied, nor has the effect of RIS on the response to loading on a background of disuse, in young or old animals. **The second aim of this chapter was to determine the effect of RIS treatment on the modulation by disuse of bone’s response to axial tibial mechanical loading.** We did this by applying the axial tibial loading model on a background of disuse engendered by SN.

We hypothesised that treatment with RIS would not impair the augmented loading response seen following loading preceded by prior disuse. We postulated that if RIS treatment does not affect the loading response, or the disuse-associated improvement of the loading response seen in old female mice, that these processes do not involve the coupling of osteoclasts and osteoblasts to any significant degree.

6.2 Objectives

1. Determine, using single-site μ CT analysis, the effect of RIS treatment on the response to axial tibial mechanical loading in old (19-months-old) female C57BL/6J mice.
2. Determine, using single site μ CT analysis, the effect of RIS treatment on the disuse-modulated osteogenic response to loading in old (19-month-old) female C57BL/6J mice.

3. Use Site-specificity analysis (SSA) to evaluate the bone-wide effects of RIS on the osteogenic response to axial tibial mechanical loading, with or without prior disuse, engendered by SN, in old female mice.

6.3 Materials and Methods

6.3.1 Effects of risedronate and disuse on tibial loading responses in aged female mice

Animals

Nineteen-month-old female C57BL/6 mice (n=60) were purchased from Charles River Laboratories Inc. (Margate, UK). Housing and nutritional management is described in Chapter 2. Mice were weight matched into four equal sized groups of n=15 then allowed 1 week of acclimatisation.

Experimental design

On day 0, mice underwent right SN (n=30) or right sham surgery (n=30). Also starting on day 0, mice were treated with daily subcutaneous injections of vehicle (0.9% NaCl; n = 30) or risedronate (RIS) [Sigma-Aldrich, Gillingham, Dorset, UK] at a dose of 15µg/kg/day for 21 days (days 0–20). Starting on day 4, the right tibiae were subjected to external loading under isoflurane-induced anaesthesia on alternate days for 8 treatments, on day 4, 6, 8, 10, 12, 14, 16 and 18. The loading treatments lasted approximately 7-8 minutes. Normal activity within the cages was allowed between loading episodes. The non-loaded contra-lateral (left) bones were used as internal controls, as has been previously validated in chapter 3 of this thesis and by Sugiyama *et al* [1] and confirmed by others in the rat ulna axial loading model [525]. Mice were killed on day 21. The experimental timeline is illustrated in Figure 61.

As loading has been demonstrated to abrogate disuse associated bone loss [9, 673, 674], a SN control group without additional loading was not included in the present study to

minimize the number of animals used in experimental procedures. For the same reason, we also chose not to include a group of mice treated with RIS and subjected to SN without additional loading as BPs have been demonstrated to completely abrogate deterioration of bone parameters in disuse back to levels seen in ambulatory animals [458-461].

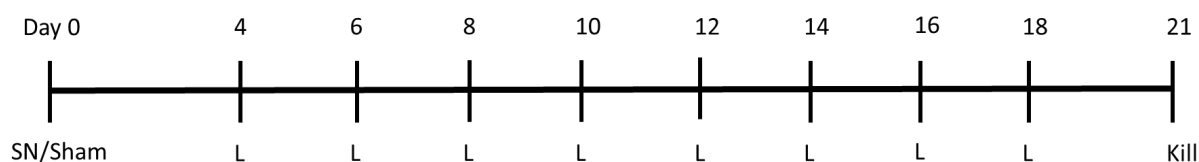


Figure 61 – Experimental timetable for loading/SN and Risedronate (RIS) experiment in old female mice.

Mice were operated in day 0 and killed on day 21. All mice received either 15 μ g/kg RIS or Saline vehicle via daily subcutaneous injection. Loading started on day 4 and was performed every second day for 8 sessions. L = Loading, SN – Sciatic Neurectomy.

Strain gauges attached *ex vivo* to the medial aspect of the tibia at 37% of the bone's length measured from the proximal end of 19-month-old female C57BL/6 mice showed that a peak load of 11.77N engendered approximately 2500 μ e in that region [9].

Experimental groups were divided as follows: VEH-Sham (n=15), VEH-SN (n=15), RIS-Sham (n=15) and RIS-SN (n=15). Due to animal losses, final mouse numbers for the respective groups above, were n=15, 14, 15, 13.

High-resolution micro-computed tomography (μ CT) analysis

Following humane culling and sample collection as described in Chapter 2, fixed tibias were scanned by μ CT (SkyScan 1172; Bruker, Kontich, Belgium) with a voxel size of 4.78 μ m. Trabecular bone (secondary spongiosa; 0.25–0.75 mm distal to the proximal growth plate) and proximal cortical bone (0.5 mm long region of interest centered at 37% of the bone's length from its proximal end) were assessed using single-site μ CT analysis as described in Chapter 2. The trabecular bone parameters evaluated included bone mass parameters; (Bone volume fraction (BV/TV), trabecular number (Tb.N), trabecular separation (Tb.Sp) and trabecular thickness (Tb.Th)) and architectural parameters

(Structure Model Index (SMI) and Trabecular Pattern Factor (Tb.Pf)). In the cortical region of interest, cortical bone area (Ct.Ar), periosteally enclosed area (Tt.Ar), medullary area (Ma.Ar), cortical area fraction (Ct.Ar/Tt.Ar), cortical thickness (Ct.Th), cortical porosity (Ct.Po) and polar moment of inertia (PMI) were evaluated. These parameters were assessed as recommended [570]. Additionally, muscle area (Mu.Ar) was measured as the cross-sectional area of the soft-tissue envelope at the mid-tibia (50% of the length of the bone), excluding the periosteally enclosed area. This measure was calculated from the μ CT images and was performed to confirm the efficacy of the disuse induced by SN.

Site Specificity Analysis (SSA)

Following single-site μ CT analysis methods for Objectives 1 and 2, the μ CT data was further analysed using SSA to evaluate the “global” changes generated by the treatments. The procedure for SSA is further detailed in Chapter 2.

Statistical analysis

All data are shown as mean \pm SEM. Body weight and lengths of the left control and right loaded tibiae were compared by mixed-design repeated measures ANOVA. Percentage change in bodyweight $[(\text{End weight} - \text{Start Weight})/\text{Start Weight} * 100]$ was compared using two-way ANOVA (Table 1). Percentage change in Mu.Ar $[(\text{Right Mu.Ar} - \text{Left Mu.Ar})/\text{Left Mu.Ar} * 100]$ was compared using two-way ANOVA. Control (left) and loaded (right) limbs of vehicle and RIS mice were compared using mixed-design repeated measures ANOVA, with loading and RIS as the main effects (Fig 1 and 2, Table 2). Percentage change with loading $[(\text{right limb} - \text{left limb})/\text{left limb} * 100]$ values between sham and SN mice were compared using Two-way ANOVA to assess the effect of SN +/- RIS on the loading response. The main effects (SN and RIS) and any interactions on the adaptive loading response were considered (Fig 3). Post-hoc comparisons were carried out for all ANOVAs using the least significant differences (LSD) method. Statistical analysis was performed using SPSS for Windows (version 23.0; SPSS Inc., Chicago, USA) and $p < 0.05$ was considered to be significant for all analyses.

Analysis of SSA data was performed using a linear mixed model approach, with bone site as a fixed categorical parameter and intervention (surgery, loading, RIS) as a fixed effect. Intervention by site interaction was also assessed to identify any site-specific responses. Mouse ID was included as a random effect. If effects were significant, post-hoc Sidak correction was applied to identify individual sites where the effect was significant ($p < 0.05$).

6.4 Results

Animal body weight, tibial lengths and Mu.Ar are reported in Table 7. All groups lost a small amount of weight over the duration of the experiment ($p < 0.001$, Table 7). The percentage of weight loss during the experiment was smaller in RIS treated mice compared with vehicle treated mice ($-6.19 \pm 0.58\%$ vs $-8.53 \pm 0.65\%$ respectively, $n = 28-29$, $p = 0.009$), and greater in SN mice compared with Sham-operated mice ($-8.56 \pm 0.76\%$ vs $-6.33 \pm 0.48\%$ respectively, $n = 27-30$, $p = 0.011$). There was no interaction between RIS treatment and surgery on bodyweight ($p > 0.05$). When compared using mixed-design ANOVA, tibial length was not affected by loading ($p = 0.7$), surgery ($p = 0.37$) or RIS treatment ($p = 0.14$). The decrease in muscle area was significantly greater following SN, compared with Sham operated mice, and the decrease in each SN mouse was greater than the maximal decrease in any individual sham mouse, confirming the efficacy of SN. RIS treatment did not affect the change in muscle area (Table 7).

SN did not result in greater weight loss following a similar duration of loading and experimental protocol in the previous chapter of this thesis. Sciatic neurectomy resulted in significant reduction in muscle size compared to sham-operated controls. As there were more mice neurectomised in the present study ($n = 27$, vs $n = 7$ in the previous study), the increased weight loss in SN mice may be due to a small, but statistically significant disuse-associated muscle mass loss that the previous study was insufficiently powered to detect. The clear effects of RIS treatment we report, particularly in cortical bone, confirm that the treatment regime used was effective and would have been expected to abrogate bone loss caused by disuse alone, supporting our decision not to include a non-loaded RIS+SN group.

Treatment		Vehicle		Risedronate	
		Sham (n=15)	SN (n=14)	Sham (n=15)	SN (n=13)
Tibial length (mm)	Left (Control)	18.71±0.07	18.61±0.08	18.79±0.06	18.74±0.08
	Right (Loaded)	18.68±0.05	18.65±0.06	18.77±0.05	18.72±0.09
Bodyweight (g)	Start	28.3±0.4	27.8±0.7	28.0±0.4	27.9±0.4
	End	26.1±0.4 §	25.1±0.5 §	26.6±0.3 §	25.8±0.4 §
	% change	-7.6±0.6%	-9.6±1.2%	-5.1±0.7% ‡	-7.5±0.9% *
Mu.Ar (%)	% change with loading	-2.58±2.62%	-23.04±1.41% ***	1.61±2.42%	-26.79±1.94% ***

Table 7 – Effect of RIS treatment, loading and/or sciatic neurectomy on tibial length, bodyweight and muscle area in aged mice.

Tibial length of left (control) and right (loaded) tibias and bodyweight in mice treated with vehicle or RIS with right sham or SN. Percentage change in weight for each mouse = (Weight@end-Weight@start)/Weight@start * 100. Percentage change with loading of muscle area (Mu.Ar) = (Right Mu.Ar – Left Mu.Ar)/Left Mu.Ar * 100. Values are Mean ± SEM (n=13-15). Tibial length was unaffected by any main effect. § = p<0.001 weight at end of experiment vs experiment start (Mixed design ANOVA). * = p<0.05 – main effect of SN; ‡ = p<0.05 – main effect of RIS (Two-way ANOVA on percentage weight change values). *** = p<0.001 versus sham operated group (Two-way ANOVA on % change Mu.Ar with loading).

6.4.1 Effect of RIS on the response to mechanical loading in old female mice

6.4.1.1 Effect of risedronate.

The effect of RIS treatment was determined by comparing effect of RIS between the control (non-loaded) limbs of vehicle-treated mice and RIS-treated mice using a mixed-design ANOVA and post-hoc adjustments. In trabecular bone, RIS alone resulted in a decrease in SMI (-20.2%, p<0.01) and Tb.Pf (-38.1%, p<0.01) (Figure 62A, B, Table 8). This suggests a change from rod to plate-like trabeculae and an increase in trabecular connectivity respectively. Tb.Th was also greater following treatment, when RIS was considered as a main effect in the ANOVA (p<0.05), however, differences between individual groups did not reach significance following post-hoc adjustments (Figure 62C). RIS treatment did not affect BV/TV, Tb.Sp or Tb.N (Table 8). In cortical bone, Ct.Ar was greater following RIS treatment, when RIS was considered as a main effect in the ANOVA

All values represent Mean \pm SEM		Vehicle		Risedronate	
		n=15 (sham), n=14 (SN)		n=15 (sham), n=13 (SN)	
		Non-loaded	Loaded	Non-loaded	Loaded
Trabecular					
BV/TV (%)	Sham	5.64 \pm 0.40	7.40 \pm 1.50	7.08 \pm 0.83	7.00 \pm 0.75
	SN	6.70 \pm 0.90	6.42 \pm 0.52	6.10 \pm 0.51	6.51 \pm 0.75
Tb.N. (/mm)	Sham	1.16 \pm 0.10	1.38 \pm 0.37	1.34 \pm 0.18	1.14 \pm 0.14
	SN	1.42 \pm 0.23	1.13 \pm 0.14	1.22 \pm 0.13	1.13 \pm 0.12
Tb.Th. (mm)	Sham	0.050 \pm 0.002	0.058 \pm 0.002 §§	0.054 \pm 0.001	0.064 \pm 0.002 §§§ ^a
	SN	0.049 \pm 0.001	0.059 \pm 0.003	0.052 \pm 0.001	0.059 \pm 0.002
Tb.Sp (mm)	Sham	0.381 \pm 0.007	0.369 \pm 0.018	0.382 \pm 0.010	0.392 \pm 0.007
	SN	0.371 \pm 0.013	0.373 \pm 0.010	0.393 \pm 0.005	0.395 \pm 0.005
SMI	Sham	1.79 \pm 0.05	1.95 \pm 0.10	1.43 \pm 0.11 ###	1.66 \pm 0.12 §
	SN	1.83 \pm 0.07	2.13 \pm 0.06	1.66 \pm 0.04	1.66 \pm 0.09
Tb.Pf	Sham	21.50 \pm 1.12	21.54 \pm 1.76	13.31 \pm 2.07 ###	14.31 \pm 1.59 ###
	SN	22.45 \pm 1.55	24.37 \pm 1.28	18.3 \pm 0.52	16.55 \pm 1.71
Cortical (37%)					
Tt.Ar. (mm ²)	Sham	1.100 \pm 0.015	1.188 \pm 0.015 §§§	1.127 \pm 0.016	1.192 \pm 0.019 §§§
	SN	1.129 \pm 0.016	1.233 \pm 0.022	1.110 \pm 0.016	1.202 \pm 0.015
Ct.Ar. (mm ²)	Sham	0.520 \pm 0.018	0.564 \pm 0.015 §§§ ‡	0.520 \pm 0.015	0.522 \pm 0.018 §§§
	SN	0.566 \pm 0.017	0.580 \pm 0.019	0.521 \pm 0.015	0.527 \pm 0.012 ‡
Ma.Ar. (mm ²)	Sham	0.578 \pm 0.013	0.625 \pm 0.010 §§	0.606 \pm 0.009	0.670 \pm 0.011
	SN	0.563 \pm 0.016	0.653 \pm 0.015	0.589 \pm 0.009	0.674 \pm 0.008
Ct.Ar/Tt.Ar. (%)	Sham	52.71 \pm 1.27	52.64 \pm 0.89	53.9 \pm 0.86	56.31 \pm 1.01
	SN	49.89 \pm 1.23	53.08 \pm 1.09	53.16 \pm 0.96	56.16 \pm 0.64
Ct.Th. (mm)	Sham	0.229 \pm 0.005	0.258 \pm 0.005 §	0.247 \pm 0.006 #	0.278 \pm 0.007 §§ ###
	SN	0.234 \pm 0.007	0.275 \pm 0.008	0.237 \pm 0.006	0.278 \pm 0.006
PMI (mm ⁴)	Sham	0.108 \pm 0.004	0.117 \pm 0.003 §§§	0.12 \pm 0.002 #	0.129 \pm 0.002 §§§ #
	SN	0.105 \pm 0.002	0.112 \pm 0.003 ‡	0.117 \pm 0.002	0.127 \pm 0.002
Ct.Po (%)	Sham	11.73 \pm 1.12	10.72 \pm 0.26	10.89 \pm 0.26	10.83 \pm 0.41
	SN	10.88 \pm 0.72	14.17 \pm 0.79 ‡‡‡	10.21 \pm 0.42	12.69 \pm 0.70 ‡‡

Table 8 - Trabecular and cortical μ CT parameters in the left (non-loaded) and right (loaded) tibiae of old mice.

19m-old female C57BL/6J mice underwent right SN or sham surgery then were treated with daily vehicle (saline) or risedronate (RIS) (15 μ g/kg/day) and alternate day axial tibial loading for 8 episodes. Mice were killed 21d after surgery. Mean \pm SEM are shown. n = 13-15. § = p<0.05, §§ = p<0.01, §§§ = p<0.001 - effect of loading vs control limbs; # = p<0.05, ## = p<0.01, ### = p<0.001 vs vehicle-treated mice (mixed-design ANOVA). ^a = p<0.05 - main effect of RIS following mixed-design, repeated-measures ANOVA - post-hoc tests do not reach significance. ‡ = p<0.05, ‡‡ = p<0.01, ‡‡‡ = p<0.001 - effect of SN on the magnitude of the loading response (Two-way ANOVA from percentage change with loading values ((Right-left)/left * 100)). There were no significant effects of RIS treatment on the magnitude of the response to loading or interactions of RIS with SN (Two-way ANOVA).

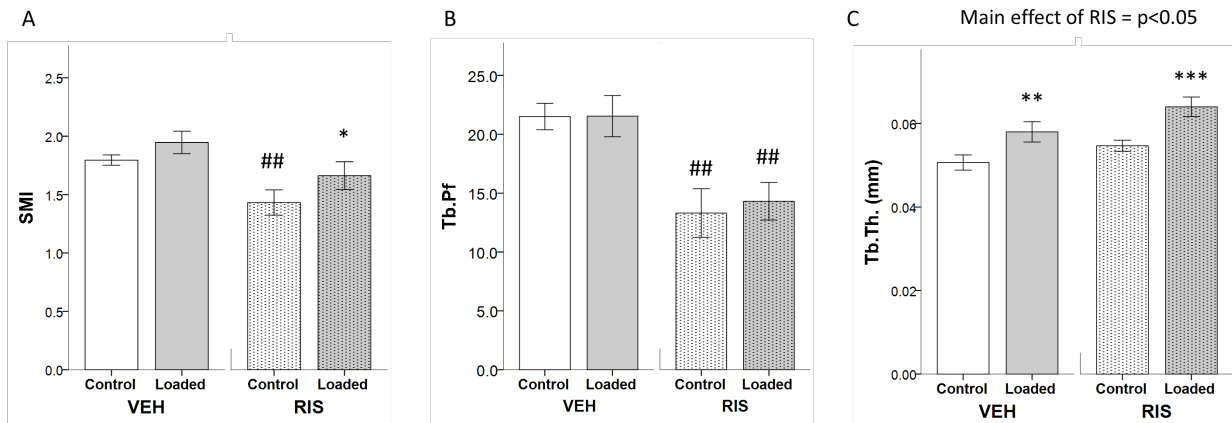


Figure 62 – The effect of axial compressive tibial loading and Risedronate (RIS) treatment on trabecular bone parameters of old mice.

19m-old female C57BL/6J mice underwent treatment with daily injections of subcutaneous 15µg/kg RIS, or vehicle solution for 21 days. The right tibia also underwent axial tibial loading on alternate days for 8 treatments from day 4. Mixed-design repeated measures ANOVA with LSD post-hoc adjustment was performed. * = p<0.05, ** = p<0.01, *** = p<0.001 vs control (non-loaded) limb. # = p<0.05, ## = p<0.01 vs Vehicle (VEH) limb. Bars indicate Mean ± SEM, n = 14-15.

(p<0.05), but differences between control limbs did not reach significance following post-hoc adjustments (Figure 63A). RIS increased Ct.Th (p<0.05) and PMI (p<0.05) (Figure 63B-C, Table 8), but did not affect Tt.Ar, Ct.Ar/Tt.Ar, Ma.Ar and Ct.Po (Table 8).

6.4.1.2 Effect of loading

The effect of loading was determined by comparing between the left (non-loaded) and right (loaded) limbs of vehicle-treated mice using a mixed-design ANOVA and post-hoc adjustments. In the proximal tibial trabecular bone of vehicle-treated mice, loading increased Tb.Th (+18.4 ±4.65% p<0.01) (Figure 62C, Table 8) but did not affect BV/TV, Tb.Sp, Tb.N, or Tb.Pf (Table 8). When considered as a main effect in the ANOVA, SMI was significantly greater in loaded limbs, but this was not significant in vehicle-treated mice following post-hoc adjustments (Figure 62A).

In cortical bone, there were significant loading-related increases in Tt.Ar (8.3±1.1%, p<0.001), Ct.Ar (+8.5±1.8%, p<0.001), Ct.Th (+11.03±5.26%, p<0.05) and PMI

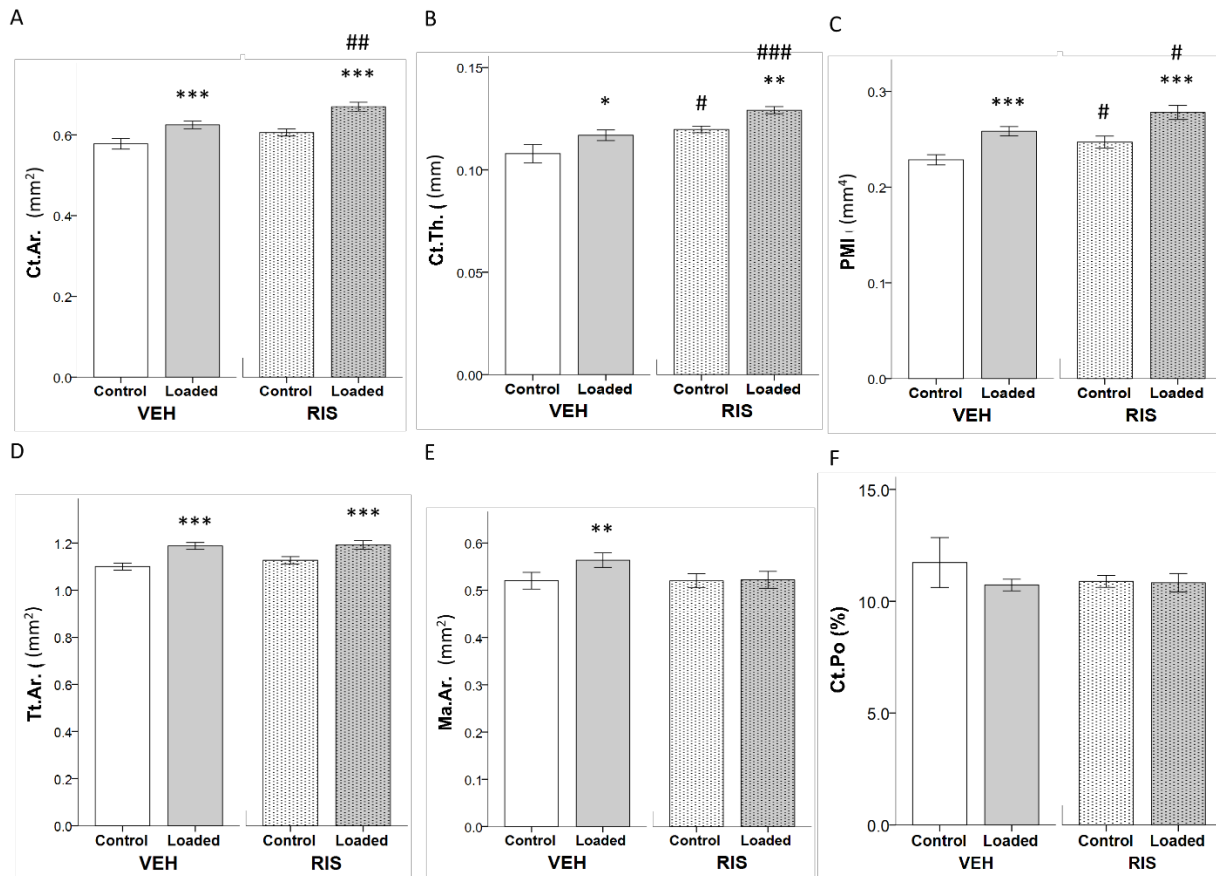


Figure 63 — The effect of axial compressive tibial loading and Risedronate (RIS) treatment on proximal cortical bone parameters of old mice.

19m-old female C57BL/6J mice underwent daily treatment with daily injections of subcutaneous 15µg/kg RIS, or vehicle solution for 21 days. The right tibia also underwent axial tibial loading on alternate days for 8 treatments from day 4. Mixed-design repeated measures ANOVA with LSD post-hoc adjustment was performed. * = $p < 0.05$, ** = $p < 0.01$, *** = $p < 0.001$ vs control (non-loaded) limb. # = $p < 0.05$, ## = $p < 0.01$, ### = $p < 0.001$ vs Vehicle (VEH) limb. Bars indicate Mean ± SEM. $n = 14-15$

(+13.55±2.48, $p < 0.001$) indicating an overall increase in bone mass following loading, primarily due to periosteal expansion (Figure 63A-D, Table 8). This increase in bone mass occurred despite a loading-associated concurrent increase in Ma.Ar (+9.22±2.99%, $p < 0.01$) (Figure 63E). Ct.Po (Figure 63F) and Ct.Ar/Tt.Ar were unaffected by loading ($p > 0.05$)

6.4.1.3 Combined effect of risedronate and loading

When considered together using ANOVA, the main effects of loading ($p < 0.001$) and RIS ($p < 0.05$) on Tb.Th were positive and additive (Figure 62C), but the RIS associated

decreases in Tb.Pf and SMI were not affected by loading ($p>0.05$). Although SMI did not increase following loading alone, it was increased following loading in the RIS-treated group ($p<0.05$)(Figure 62A). In cortical bone, the effects of RIS treatment and loading were additive for Ct.Ar, Ct.Th and PMI. in the proximal cortical bone site (Figure 63A-C). RIS treatment did not affect the loading-related increase in Tt.Ar but abrogated the loading-related increase in Ma.Ar seen in vehicle-treated mice (Figure 63D, E).

6.4.2 Effect of RIS on the disuse-mediated rescue of the impaired loading response in old mice

6.4.2.1 Effect of disuse on the osteogenic response to loading

Analysis of the effect of SN on the loading response at the cortical site showed that vehicle-treated mice subjected to SN demonstrated a greater loading-related increase than sham mice in Ct.Ar ($+8.51\pm 1.84\%$ vs $+16.4\pm 1.82\%$ respectively, $p<0.01$) and PMI ($+13.6\pm 2.5\%$ vs $+18.1\pm 2.7\%$ respectively, $p<0.05$) (Figure 64A, B; Table 8). Ct.Ar/Tt.Ar also showed a tendency towards a greater increase with loading in the SN group, relative to sham operated mice ($p=0.055$) (Figure 64C). Although RIS inhibited the loading-induced increase in Ma.Ar in sham operated mice, Ma.Ar was unaffected with loading in the SN group. In the loaded limbs of vehicle-treated mice that had been neurectomised, Ct.Po increased compared to the sham group (SN: $+33.96\pm 7.28\%$, Sham: $-0.78\pm 6.68\%$, $p<0.001$)(Figure 64D). There was no observed effect of SN on loading-related changes in Tt.Ar, Ma.Ar, or Ct.Th in cortical bone, or with any trabecular bone parameter ($p>0.05$) (Table 8).

6.4.2.2 Effect of RIS on the modulation of responses to loading by disuse

RIS treatment did not affect the response to prior disuse engendered by SN for any parameter examined in either cortical or trabecular bone ($p>0.05$) (Figure 64, Table 8). This confirms what we observed in chapter 5; prior and concurrent disuse enhanced the osteogenic response to loading in cortical bone in these aged mice and that this response was not significantly altered by treatment with RIS.

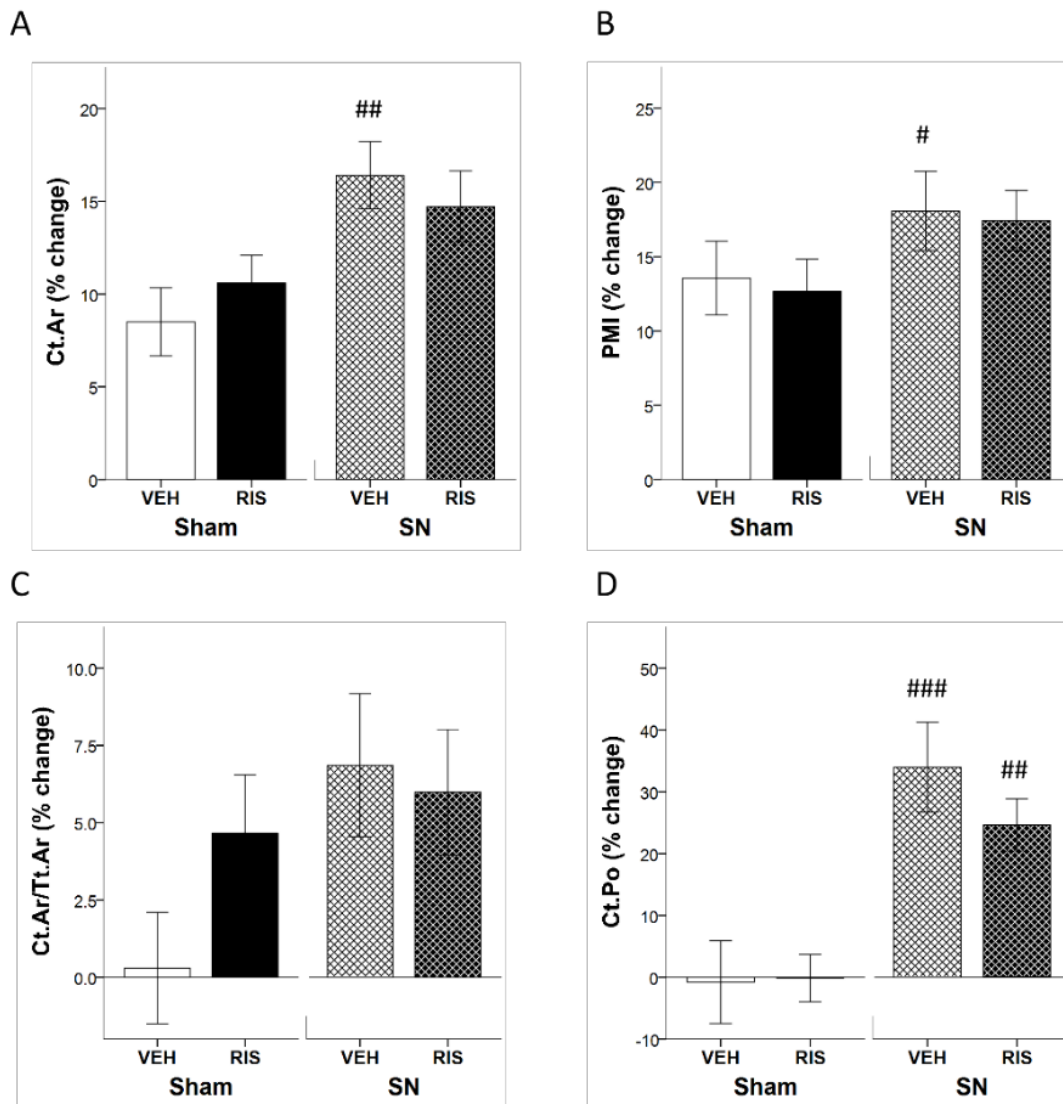


Figure 64 - Effect of Risedronate (RIS) and Sciatic Neurectomy (SN) on the adaptive response to axial tibial mechanical loading in cortical bone.

Percentage change in response to loading ($(\text{right} - \text{left}) / \text{left} * 100$) for cortical bone μ CT parameters of mice following initial right SN or Sham surgery on day 0, and daily treatment for 21 days with 15 μ g/kg RIS or saline vehicle solution then alternate-day unilateral axial right tibial loading for 8 episodes starting from day 4. MicroCT analysis data for (A) Ct.Ar, (B) PMI, (C) Ct.Ar/Tt.Ar and (D) Ct.Po are shown. Two-way ANOVA with LSD post-hoc adjustment was used to compare the effects of SN and RIS on the % change due to loading. For the effect of SN vs sham operated mice, # = $p < 0.05$; ## = $p < 0.01$, ### = $p < 0.001$, following post-hoc adjustments. RIS did not affect the magnitude of response for any measure examined when compared with VEH. There were no significant SN*RIS interactions. Error bars indicate Mean \pm SEM. n = 13-15

6.4.3 Site Specificity Analysis

Mixed model results definitions:

If a given interaction is significant (i.e. $p < 0.05$) for:

- Bone-site*loading (or RIS) interaction – effect of loading (or RIS) is significantly different at different sites.
- RIS*loading interaction – percentage change due to loading is significantly different in RIS treated compared to vehicle-treated mice which was interpreted as a synergistic interaction (or an inhibitory interaction if the effects were opposite).
 - If the interaction is not significant, yet the independent variables are significant, this indicates an additive effect.
- SN*loading interaction – percentage change due to loading is significantly different in SN mice compared with sham mice.
- SN*RIS interaction – percentage difference due to SN is significantly different in RIS-treated mice compared to Vehicle-treated mice.
 - A non-significant interaction indicates that RIS had no effect on the osteogenic response to loading following SN.

6.4.3.1 Effect of RIS on the loading response in old mice.

To explore the effect of RIS on the bones' loading response in old mice, we performed a within-treatment comparison of sham operated mice with RIS treatment, Loading and Bone site as fixed effects. Tt.Ar ($p < 0.001$) and Ct.Ar ($p < 0.05$) demonstrated significant RIS*Bone-site interactions, indicating they demonstrated a site-specific response to treatment with RIS (Figure 65A, Figure 66A). However, the magnitude of any effect is quite small, with a few sites proximally and distally bone demonstrating significant changes. Ma.Ar was not significantly affected by RIS treatment ($p > 0.05$) (Figure 67A). RIS treatment demonstrated significant main effects only for Ct.Th ($p < 0.05$), with RIS demonstrating a trend towards a significant main effect for Ct.Ar ($p = 0.075$). In vehicle treated mice, RIS treatment resulted in a significant increase in Ct.Th, primarily around the 37% and 60%

sites, according to SSA although the treatment effect was not significantly site-specific (Treatment*Bone-site interaction $p=0.986$)(Figure 68A). These increases in bone mass indicate a small but significant effect of RIS on the entire cortical bone of aged mice.

We next mapped the effect of loading in vehicle-treated mice. Axial tibial loading significantly increased Tt.Ar, primarily at the region surrounding the 37% site (Figure 65B) and this change was site-specific ($p<0.001$ for Bone-site*Loading interaction). Ct.Ar increased with loading around the 37% site as expected, but this effect extended over most of the proximal tibia (10-45%) and also reached significance distally (80-85%) (Figure 66B). The changes in Ct.Ar with loading were site-specific ($p<0.001$ for Bone-site*Loading interaction). Loading resulted in a regional increase in Ma.Ar at the 37% site (Figure 67B) and this effect was site-specific ($p<0.001$ for Bone-site*Loading interaction) suggesting slight loading associated endosteal expansion, consistent with the single-site CT analysis. Loading also significantly and site-specifically affected Ct.Th, primarily increasing in thickness in the proximal half of the cortical bone (10-50%), but also distally (75-80% sites)(Figure 68B).

To demonstrate any combined effects of RIS treatment and mechanical loading on bone mass, the loaded limb of vehicle-treated mice was compared to the loaded limb of RIS-treated mice. There were minimal further RIS-associated increases in Tt.Ar of loaded limbs (Figure 65C) although 3 single, non-continuous sites of significance were present at the bone extremities after post-hoc adjustments. RIS treatment resulted in additive increases in Ct.Ar (Load*RIS interaction $p=0.130$) (Figure 66C). RIS treatment resulted in additive increases in Ct.Th (Figure 68D) where the thickness increased compared to vehicle treated loaded limbs in both the 37% region and also in the distal cortical bone. The RIS-associated increase in Ma.Ar identified at 37% site appeared abrogated following treatment with RIS, consistent with the findings of single-site μ CT analysis at this site, although Ma.Ar at this site was not significantly different from the vehicle-loaded limb following post hoc adjustments (Figure 67B, C). According to the mixed model analysis, a significant Loading*RIS interaction for Ma.Ar ($p<0.05$) was present, suggesting that RIS abrogated the loading-related increase in Ma.Ar seen in vehicle treated mice.

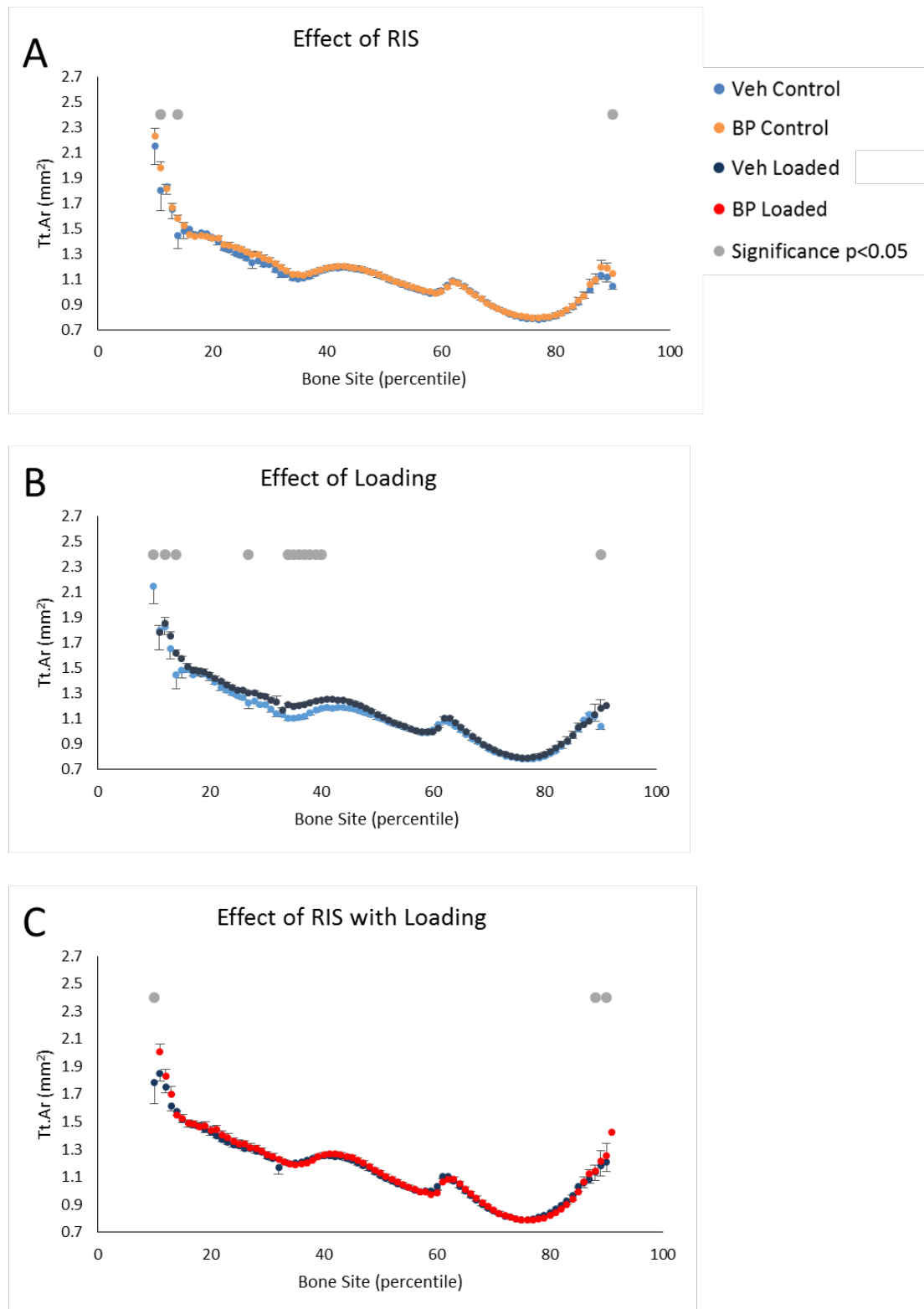


Figure 65 – The effect of risedronate (RIS) and/or loading on Tt.Ar of whole tibia in old female mice.

SSA was performed on tibias from 19month old female C57BL/6 mice after 21 days of daily injections of RIS or vehicle (Veh). Loading was performed on alternate days from day 4 for 8 episodes. Mice were killed on day 21. (A) Effect of RIS on control limbs, (B) Effect of unilateral loading on vehicle-treated mice and (C) Effect of loading on RIS treated mice. Analysis was performed via Mixed Model analysis using Sidak post-hoc correction for multiple comparisons. Grey spots indicate $p < 0.05$ for that bone site after post-hoc comparisons. $n = 15$. Values and error bars represent Mean \pm SEM.

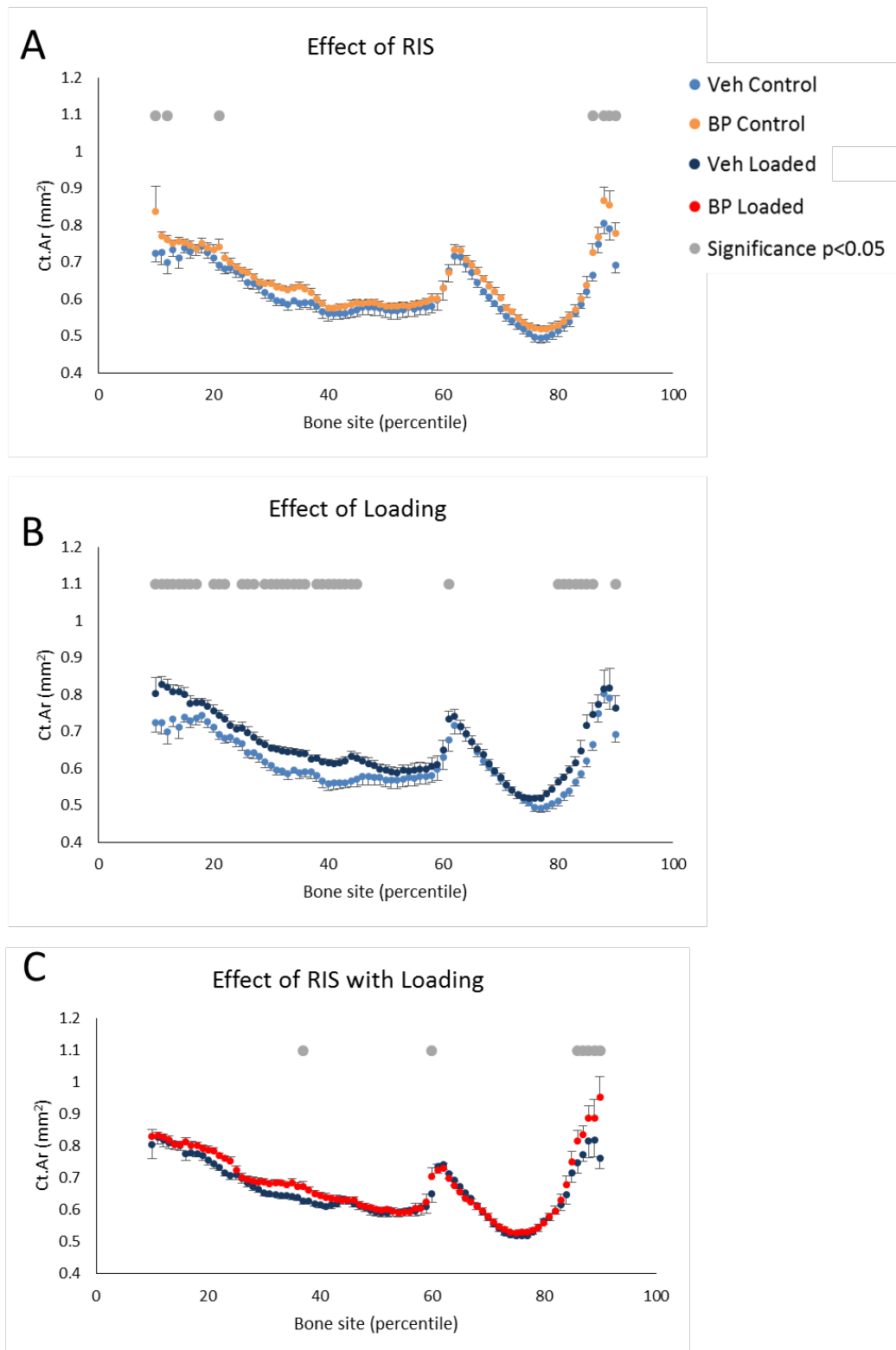


Figure 66 – The effect of risedronate (RIS) and/or loading on Ct.Ar of whole tibia in old female mice.

SSA was performed on tibias from 19month old female C57BL/6 mice after 21 days of daily injections of RIS or vehicle (Veh). Loading was performed on alternate days from day 4 for 8 episodes. Mice were killed on day 21. (A) Effect of RIS on control limbs, (B) Effect of unilateral loading on vehicle-treated mice and (C) Effect of loading on RIS-treated mice. Analysis was performed via Mixed Model analysis using Sidak post-hoc-correction for multiple comparisons. Grey spots indicate p<0.05 for that bone site after post-hoc comparisons. n=15. Values and error bars represent Mean \pm SEM.

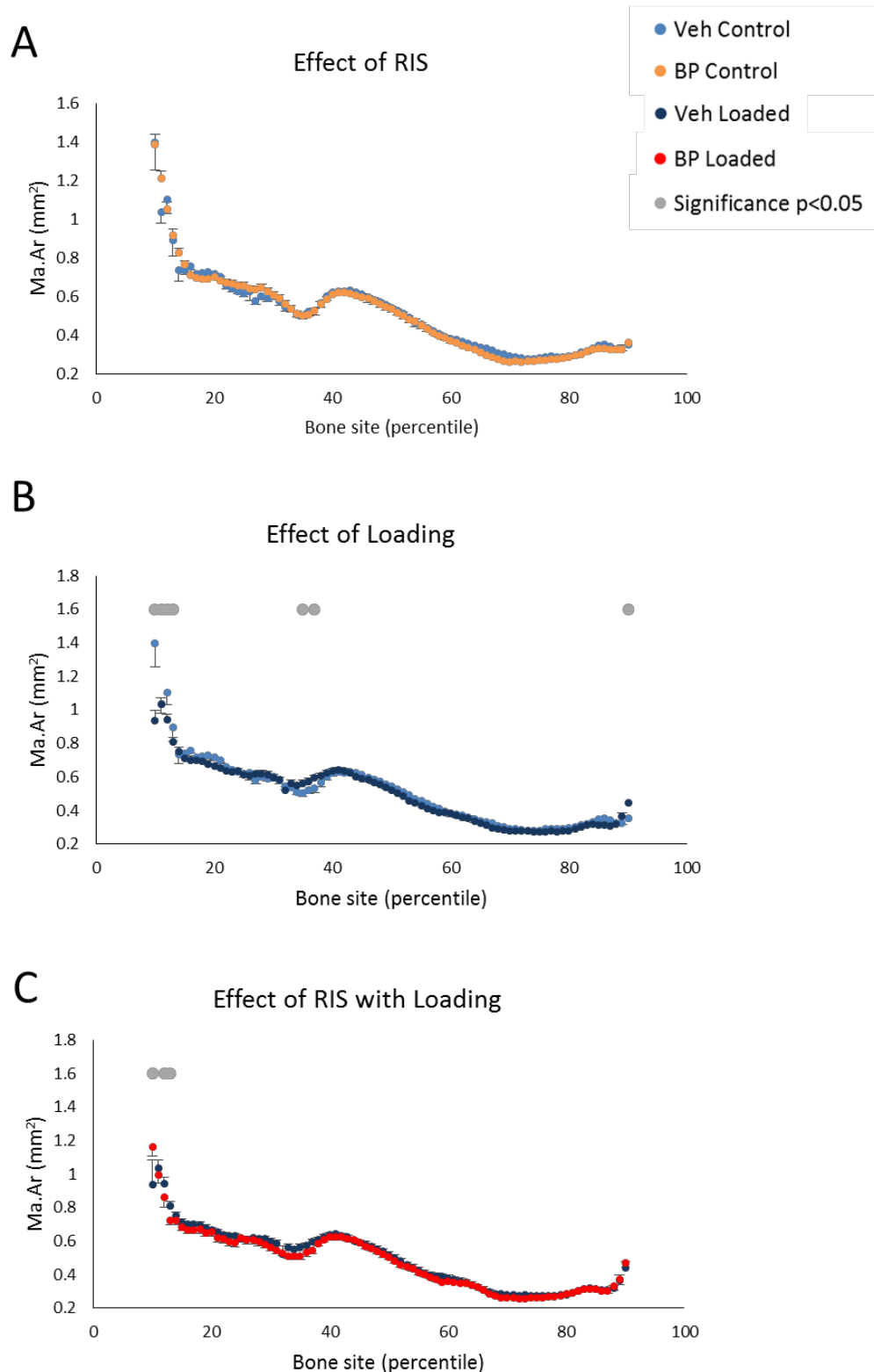


Figure 67 – The effect of risedronate (RIS) and/or loading on Ma.Ar of whole tibia in old female mice.

SSA was performed on tibias from 19month old female C57BL/6 mice after 21 days of daily injections of RIS or vehicle (Veh). Loading was performed on alternate days from day 4 for 8 episodes. Mice were killed on day 21. (A) Effect of RIS on control limbs, (B) Effect of unilateral loading on vehicle-treated mice and (C) Effect of loading on RIS treated mice. Analysis was performed via Mixed Model analysis using Sidak post-hoc correction for multiple comparisons. Grey spots indicate $p < 0.05$ for that bone site after post-hoc comparisons. $n=15$. Values and error bars represent Mean \pm SEM.

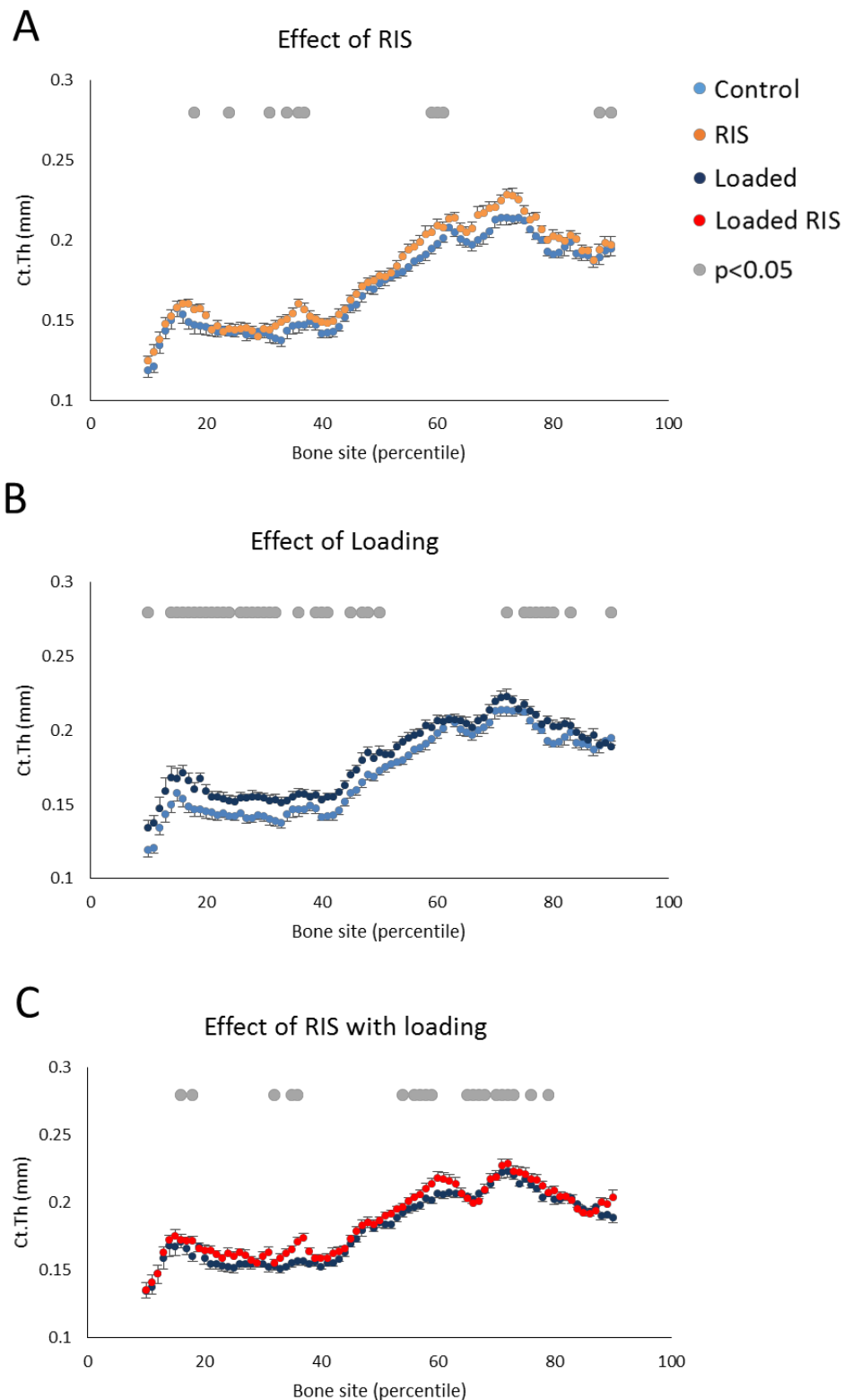


Figure 68 - The effect of risedronate (RIS) and/or loading on Ct.Th of whole tibia in old female mice.

SSA was performed on tibias from 19month old female C57BL/6 mice after 21 days of daily injections of RIS or vehicle (Veh). Loading was performed on alternate days from day 4 for 8 episodes. Mice were killed on day 21. (A) Effect of RIS on control limbs, (B) Effect of unilateral loading on vehicle-treated mice and (C) Effect of loading on RIS_____ treated mice. Analysis was performed via Mixed Model analysis using Sidak post-hoc correction for multiple comparisons. Grey spots indicate p<0.05 for that bone site after post-hoc comparisons. n=15. Values and error bars represent Mean \pm SEM.

6.4.3.2 Effect of disuse on the response to loading in old mice

To explore the effect of disuse on the bones' response to loading in old mice using SSA, we calculated the percentage change with loading for each site and used these values to perform a within-treatment comparison of vehicle-treated mice, with SN and Bone site as fixed effects. SN significantly increased the loading-related change in Tt.Ar ($p < 0.001$) in a site-specific manner ($p < 0.001$), predominantly limited to the distal tibia (83-90%) (Figure 69A). There was no apparent effect in the normally load responsive area surrounding the 37% site. SN also significantly increased the loading related change in Ct.Ar ($p < 0.001$) in a site specific manner ($p < 0.001$), again predominantly in the distal tibia, but also at the 37% and 60% sites (Figure 69B). SN did not affect the loading-related change in Ma.Ar, nor was

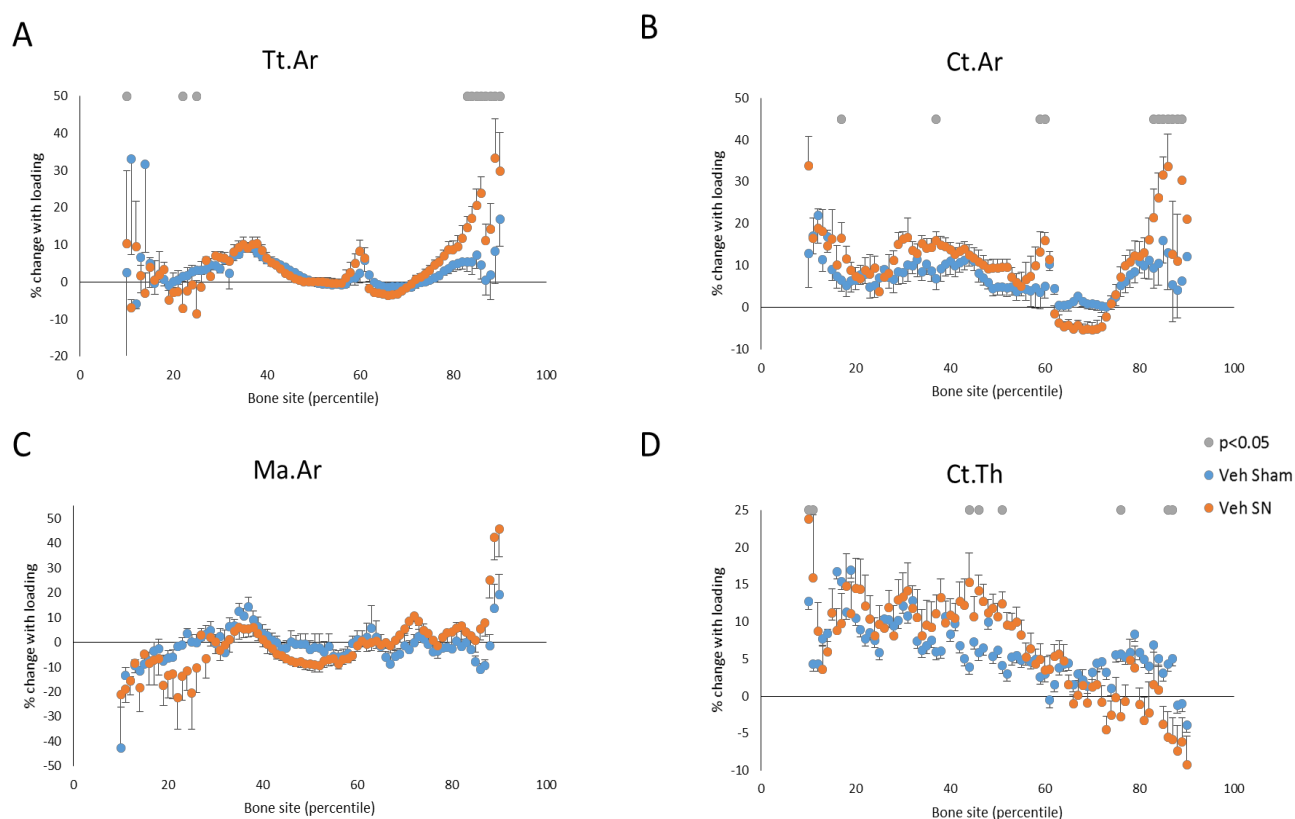


Figure 69 – The effect of SN on the loading response in old female mice.

SSA was performed on tibias from mice that had undergone right SN or Sham surgery on day 0 and right tibial loading on alternate days from day 4 for 8 episodes. Mice were killed on day 21. Analysis for (A) Tt.Ar, (B) Ct.Ar, (C) Ma.Ar, and (D) Ct.Th was performed via Mixed Model analysis using Sidak post-hoc correction for multiple comparisons. Grey spots indicate $p < 0.05$ for that bone site after post-hoc comparisons. $n = 13-15$. Values and error bars represent Mean \pm SEM.

there any site-specific effect ($p > 0.05$) (Figure 69C). SN did not significantly increase the loading related change in Ct.Th overall ($p > 0.05$), but the effect of SN was site-specific ($p < 0.05$) (Figure 69D). In effect, SN resulted in a greater change with loading for Ct.Th in the mid-shaft tibia, but a smaller change with loading in the distal cortical bone.

6.4.3.3 Effect of RIS on the loading response in old female mice

Following confirmation of the disuse-associated “rescue” of adaptive bone formation, we assessed the effect of RIS on the adaptive loading response in sham operated female mice. RIS treatment did not alter the loading-related changes in Tt.Ar, Ct.Ar, Ma.Ar or Ct.Th (Figure 70).

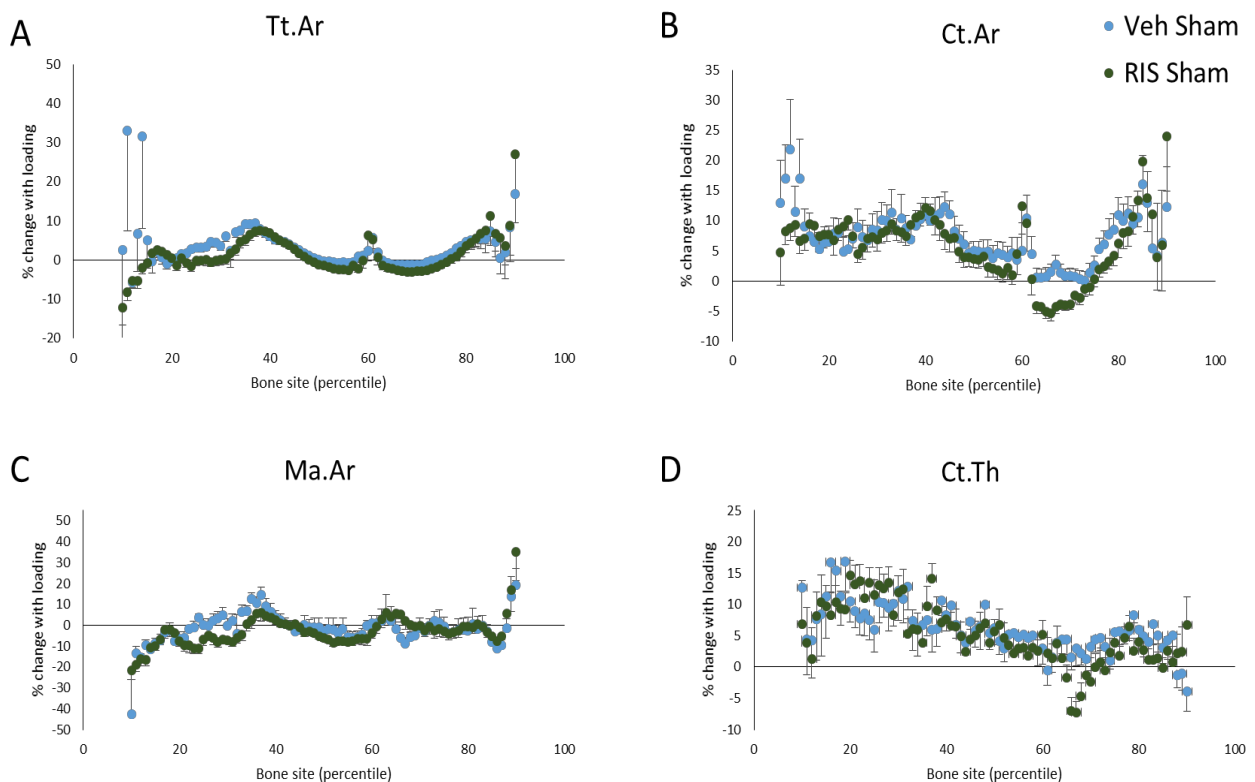


Figure 70 - The effect of RIS on the loading response in old female mice.

SSA was performed on tibias from mice that had been administered RIS or vehicle daily from day 0 and administered right tibial loading on alternate days from day 4 for 8 episodes. Mice were killed on day 21. Analysis for (A) Tt.Ar, (B) Ct.Ar, (C) Ma.Ar, and (D) Ct.Th was performed via Mixed Model analysis. None of the parameters were found to be significantly different so no post-hoc tests were performed. $n = 15$. Values and error bars represent Mean \pm SEM.

6.4.3.4 Effect of RIS on the modulation of responses to loading by disuse

Next, we examined the effect of RIS on the loading response in SN mice. RIS treatment did not significantly affect the loading response in SN mice for any parameter ($p > 0.05$) suggesting that RIS had no effect on the magnitude of the increased loading response in SN mice (Figure 71A-D).

Finally, we evaluated the effect of SN on the loading response in RIS treated mice. SN resulted in a significantly greater response to loading in RIS treated mice for both Tt.Ar and Ct.Ar ($p < 0.001$) with significant site-specific effects for both Tt.Ar and Ct.Ar

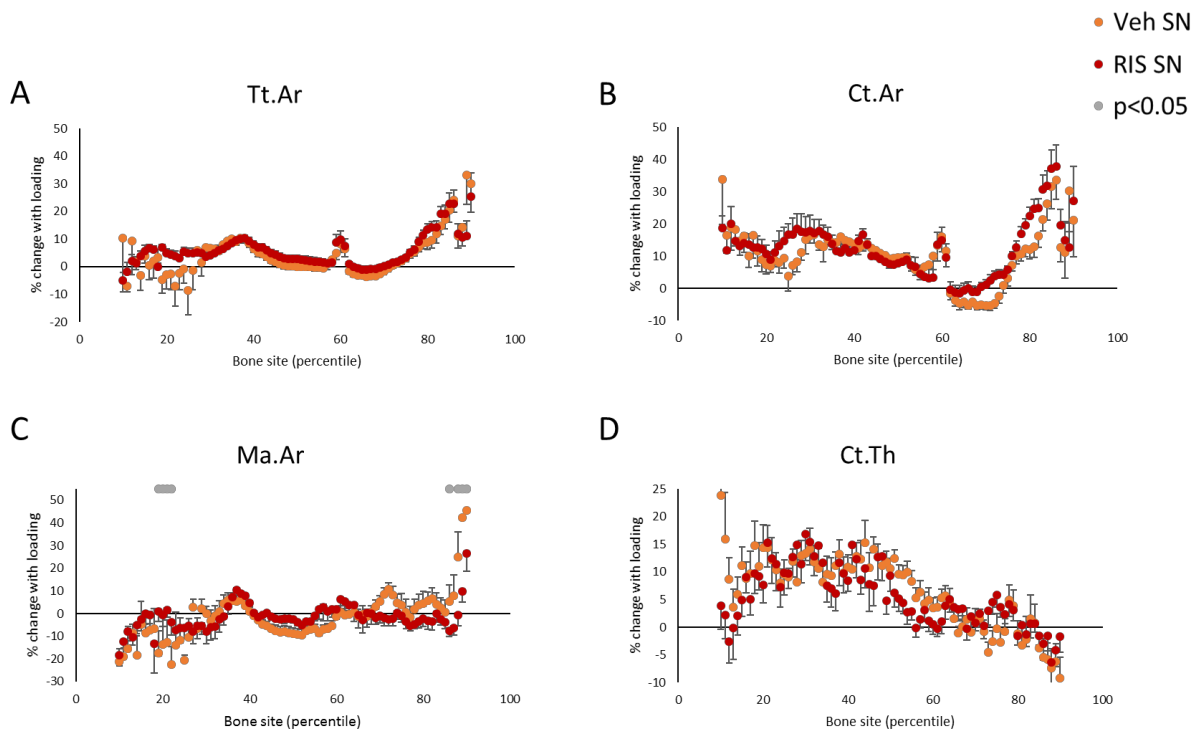


Figure 71 Effect of Risedronate (RIS) on the response to loading following prior disuse in old female mice.

SSA was performed on tibias from mice that had undergone right SN or Sham surgery on day 0 and daily RIS or vehicle injections for 21 days including right tibial loading on alternate days from day 4 for 8 episodes. Mice were killed on day 21. Analysis for (A) Tt.Ar, (B) Ct.Ar, (C) Ma.Ar, and (D) Ct.Th was performed via Mixed Model analysis. The effect of RIS on the percentage change with loading was evaluated. Sidak post hoc corrections were performed where main effects or interactions were significant in the mixed model. $n = 13-15$. Values and error bars represent Mean \pm SEM. Grey spots indicate significantly different responses to mechanical loading ($p < 0.05$) at a given site.

($p < 0.001$) (Figure 72 A, B). SN did not significantly affect the loading response for Ma.Ar or Ct.Th in RIS treated mice ($p > 0.05$) (Figure 72 C, D). SN however, did demonstrate a site-specific effect of SN on the loading response for Ct.Th in RIS treated animals ($p < 0.001$), although following post hoc comparisons, this was only significant at two adjacent sites (66-67%). These two sites no longer demonstrated a reduction in Ct.Th with loading following SN, compared to Sham operated mice. There were no interactions between RIS treatment and SN for any measure, further supporting the suggestion that RIS treatment did not affect the augmentation of the loading response by SN.

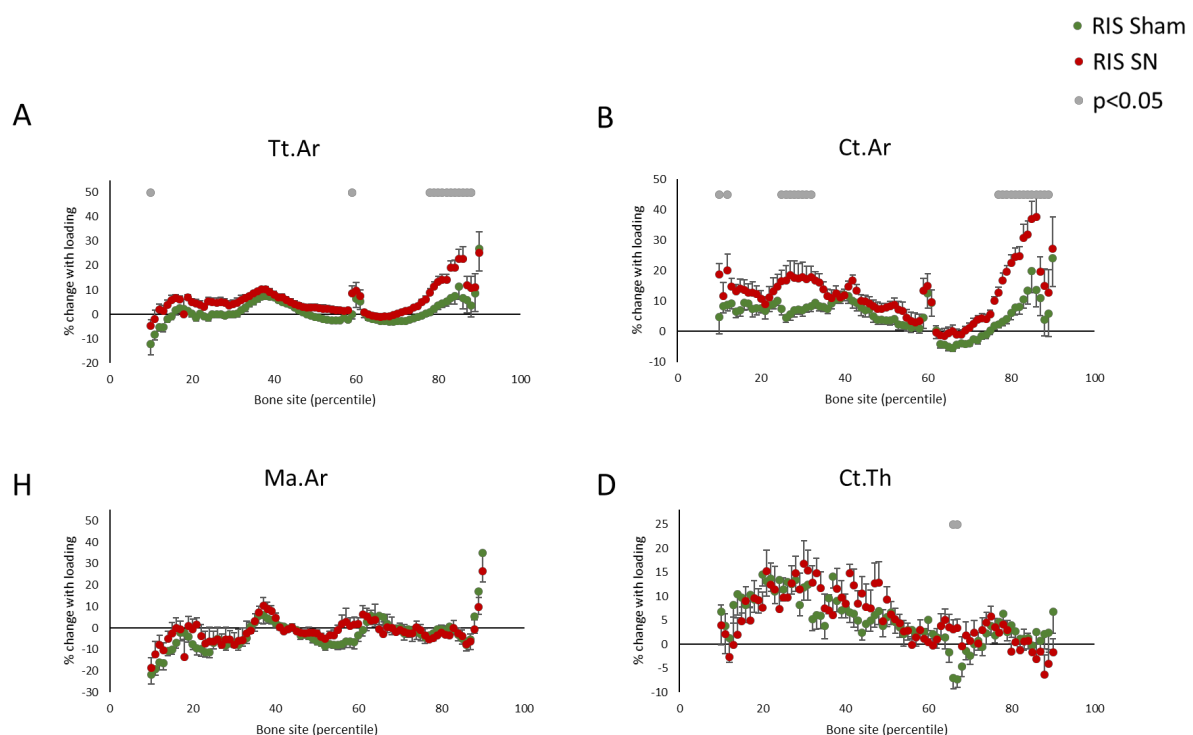


Figure 72 Effect of SN on the response to loading following Risedronate (RIS) treatment in old female mice.

SSA was performed on tibias from mice that had undergone right SN or Sham surgery on day 0 and daily RIS or vehicle injections for 21 days including right tibial loading on alternate days from day 4 for 8 episodes. Mice were killed on day 21. Analysis for (A) Tt.Ar, (B) Ct.Ar, (C) Ma.Ar, and (D) Ct.Th was performed via Mixed Model analysis. The effect of SN on the percentage change with loading was evaluated. Sidak post hoc corrections were performed where main effects or interactions were significant in the mixed model. $n = 13-15$. Values and error bars represent Mean \pm SEM. Grey spots indicate significantly different responses to mechanical loading ($p < 0.05$) at a given site.

6.5 Discussion

In this thesis chapter, we have demonstrated that RIS treatment in old female mice has small but significant effects on cortical bone mass, and that the response to mechanical loading is unaffected by RIS. We have also demonstrated that the “rescue” of loading-related bone formation seen following disuse engendered by SN is similarly unaffected by co-treatment with RIS.

6.5.1 Response to risedronate treatment is site- and age-specific

In a previous study in young mice we observed that RIS had a positive effect on trabecular bone mass and no effect on any cortical bone parameters [34]. In the old mice used in the current study, the response to treatment was different; we observed a positive effect of RIS treatment on cortical bone mass which was not noted in young mice. This age-related difference in the cortical bone response to RIS is likely to reflect the ongoing endocortical resorption in aged mice which is greater than in young mice [530]. RIS increased Ct.Ar and Ct.Th without affecting Tt.Ar and also abrogated the loading-associated increase in Ma.Ar. One study has demonstrated a small but significant increase in Ct.Th in 4-month-old mice following alendronate treatment, which was also sufficient to mitigate bone loss seen following tail suspension [461]. Other studies in young, growing rodents have detected a slightly reduced periosteal bone formation following bisphosphonate treatment [675, 676], whereas studies in skeletally mature rats and dogs show no effect on periosteal apposition following use of RIS [462, 677].

Although cortical bone was more responsive to RIS treatment in old mice compared to young, surprisingly, trabecular BV/TV did not increase following RIS treatment in the old mice in this study. The lack of response to RIS treatment in trabecular bone was surprising considering it is a site of higher osteoclast numbers and remodeling activity, and the result may reflect the very small amount of trabecular bone remaining in the bones of 19-month-old female mice, with only a few trabeculae per bone. This restricts the available bone on which to exert anti-resorptive effects and additionally restricts the available bone on which formation can continue. However, RIS was associated with alterations in

architectural parameters - decreased Tb.Pf and SMI. This suggests RIS results in increased trabecular connectivity (reduced Tb.Pf), and formation of plate-like rather than rod-like trabeculae (reduced SMI), without a significant increase in overall bone volume. One recent study [678] concluded that although SMI was developed to represent a quantifiable measure of surface shape (sphericity) of a given structure, due to the high degree of concavity presented in highly connected trabecular bone, SMI was more representative of changes in BV/TV rather than changes in plate:rod architecture. However, as BV/TV was unaffected by any treatment in this experiment, and there was limited connectivity in the trabeculae, it is arguable that the SMI values attained in the present experiment are representative of changes in plate:rod architecture.

Greater trabecular connectivity and wider plate-like trabeculae are likely to increase mechanical strength, even without increased BV/TV. BP treatment in young adult mice and rats has been shown to result in similar reductions in SMI [679, 680]. The effect of BP treatment on Tb.Pf in young adult bone has only been reported in the context of ovariectomy, where BPs were protective of the ovariectomy-induced increase in Tb.Pf. [681]. Osteoporotic humans also have been shown to improve trabecular microarchitecture following treatment with BPs, particularly with respect to SMI [682, 683]. To the author's knowledge, there are no studies which report the effect of BPs on Tb.Pf. in human subjects.

When considering the results of our study and those discussed above, it appears that the type of response seen following treatment with BPs is age-specific. Care should therefore be taken when extrapolating data from young animals to old animals, and indeed to old humans. To the authors' knowledge this is the only study currently available which documents the trabecular bone response (or lack thereof) to treatment with RIS in old mice. RIS has also been demonstrated to have a different effect between long bones and mandibular bones in young mice, further suggesting that a differential, site-specific response to treatment between bone sites exists [667].

In addition to our single-site μ CT analysis at the 37%, load-responsive site, site-specific changes in the tibial cortical bone were examined following RIS treatment alone and this

demonstrated only a small but still statistically significant response to treatment, primarily through a general increase in Ct.Th. This finding is consistent with the single-site μ CT analysis. Ct.Ar, Tt.Ar and Ma.Ar were not affected by RIS independently of loading. This may be due to inherently low levels of basal resorption in cortical bone of control limbs. Resorption rates are still relatively low in old mice [530], so it may be that a longer treatment course than 3 weeks of RIS would result in clearer benefits to bone mass beyond increases in Ct.Th quantifiable by μ CT. Longer-term treatment with RIS would be expected to result in smaller Ma.Ar due to inhibited endosteal resorption in aged mice as the endocortical resorption rate is significantly higher than in young animals [530]. To the author's knowledge, there are no longer term studies exploring the effect of prolonged BP use on bone mass and architecture in old mice. However, the next chapter of this thesis describes the results of an experiment where old female mice were treated with RIS for 6 weeks. A study in adult rats (6m-old) treated with pamidronate for 5 months was unable to identify changes in Tt.Ar, Ct.Ar or Ct.Th according to histomorphometry [684], further supporting the lack of response to BP treatment in cortical bone of young mice. This study in rats only explored the proximal tibial metaphyseal cortical bone, so site-specific effects could not be evaluated as in the present study.

The positive effects noted with RIS treatment in this study could be partly explained by the ability of some bisphosphonates to have anti-apoptotic effects on osteocytes and osteoblasts. This may contribute to the age-related difference in responses to RIS given bones from old mice have a greater proportion of empty osteocyte lacunae [29] and higher rates of osteocyte apoptosis [685]. Future studies could investigate this by undertaking TUNEL or cleaved caspase-3 staining of bone sections from mice treated with RIS or vehicle. Interestingly, in a recently-published study, a selective analogue of alendronate, IG9402, which does not impair resorption, but retains the anti-apoptotic effects on osteocytes and osteoblasts, was unable to mitigate the bone loss seen following unloading [461]. However, it is not known whether IG9402 would have the same effects in old mice and whether it would mitigate the bone loss associated with aging.

In addition to an age-dependent difference in the response between trabecular and cortical bone in mice, the cortical bone response to RIS in this study (10-90% site) demonstrates site-specific effects, primarily at the bones' extremities (metaphyseal) rather than in the diaphyseal region. This tendency for effects in the metaphyseal region due to RIS could be due to the greater proximity of these areas to the trabecular bone, where more osteoclasts typically reside. When designing future experiments including use of bisphosphonates in mice, use of techniques to assess a larger range of sites will increase the chance that any effect of treatment is identified. The lack of cortical bone response to RIS in young mice in our previous study [34] and presence of a significant response in old mice in this study emphasize the importance of considering the age and bone site assessed when investigating the effect of interventions in experimental mouse models.

6.5.2 Risedronate treatment does not impair the loading response in aged mice.

We, and others, have previously reported that the adaptive response to loading in old mice is diminished compared with young mice [25, 29, 389]. In the present study, the magnitude of the loading response in cortical bone was similar to that previously reported [9, 29, 455]. Interestingly, in this cohort of animals, loading unexpectedly resulted in focally increased Ma.Ar at around 37%, suggesting that axial tibial compressive loading can potentially stimulate increased endosteal resorption. Endosteal resorption was demonstrated at the 37% site in the face of ongoing loading in young mice in Chapter 4 of this thesis. A regionally-confined increase in Ma.Ar could be explained by continued bone resorption without adequate adaptive bone formation, due to age-related deficiencies in endosteal bone formation. Holguin *et al* [455] have also reported a greater increase in medullary volume associated with loading in young mice, although they did not see this response in aged mice in the same study. Other loading studies in old mice have demonstrated no change in Ma.Ar with loading, or even a reduction with loading in some cases at higher strain [9, 29, 530]. The focal endosteal expansion response seen at the 37% site in our study is, therefore, not fully consistent with that reported in other studies. This difference could be explained by different operators, different loading protocols and

machines, and different selected cortical regions of interest. Regardless of these differences between studies, the increased levels of resorption in old mice could help explain the positive response of cortical bone to treatment with RIS, via increases in Ct.Th and PMI. In young mice, RIS treatment has no measurable effect on the endosteum of cortical bone and the loading response is unaffected by RIS treatment [34].

Combined treatment with RIS and loading showed additive increases in Ct.Ar, Ct.Th and PMI; this could be attributed to the loading-related increase in Tt.Ar combined with abrogation of the loading-related increase in Ma.Ar by RIS. RIS treatment did not adversely affect any of the loading-related gains achieved in this experiment. This supports the conclusions of Sugiyama *et al* [34] that the osteogenic loading response is primarily mediated by bone osteogenic modelling involving de novo bone formation, and not bone remodeling where formation is preceded by, and coupled to, resorption.

6.5.3 The SN-associated rescue of age-impaired adaptive bone formation is not affected by treatment with risedronate

We hypothesised that coupling of osteoclast and osteoblast activity is not responsible for increased loading-related bone formation when loading is superimposed on disuse. In the previous chapter of this thesis, we demonstrated that a short period of disuse preceding axial mechanical loading of the tibia was sufficient to “rescue” the age-impaired osteogenic response to loading. In this chapter, we confirmed that the improvement in the adaptive loading response in old female mice following prior SN is reproducible. However, the pattern of formation was slightly different to that reported by us previously [9], with increases in Ct.Ar, and no further increase in Tt.Ar, indicating that the augmented adaptive response in this experiment was not primarily periosteal, as was seen in the earlier report. Nevertheless, the increase in Ct.Ar still resulted in a concomitant improvement in PMI, a surrogate measure of bone torsional strength, suggesting that the improvement in the adaptive response following SN still led to structural improvements in the cortical bone. An explanation for this observation is provided in Chapter 5. Briefly, the strain context on which loading is applied may affect a given bone’s response to

additional mechanical loading. Bones' response to short periods of artificial loading superimposed on disuse have been previously investigated in young [35, 673, 674], and old rodents [9, 657]. In these studies, axial tibial loading or simulated resistance training abrogated bone loss due to disuse. Only the studies by De Souza *et al* [35, 657] and Meakin *et al* [9] effectively compared the loading response when superimposed on normal loading with that where it was superimposed on disuse. In these studies, the osteogenic response to loading was greater in disuse animals than it was in ambulatory animals. Furthermore, extending the length of preceding disuse further augmented the improvement in the osteogenic response [657]. Combining the results of these three studies together with the present study's results, suggests that the impaired adaptive loading response in old mice can be rescued by a period of disuse starting shortly before mechanical loading. Dynamic histomorphometry would have allowed better characterization of the formative and resorptive responses in this experiment, and was originally planned, but not performed due to financial and time restrictions

Notwithstanding the age-related differences in the effect of RIS noted in the present study, our findings that RIS did not impair the osteogenic adaptive loading response are consistent with the modeling-based adaptive response to loading seen in young mice [34]. The lack of effect of RIS on the loading response in SN mice also suggests that an increase in basal remodeling is not involved in the observed "rescue" of the osteogenic response to loading seen in these old animals and that the likely mechanism involved in the observed rescue does not involve the processes of osteoclast:osteoblast coupling.

Bisphosphonates are effective in preventing disuse-related bone loss in humans, such as in patients subjected to bed-rest or spaceflight [456, 457], but it remains to be determined whether the adaptive loading response in humans is augmented following disuse, as it is in mice. The effect of RIS on the adaptive loading response in human patients with reduced bone loading also remains to be examined. However, to the extent that results in old animals can be extrapolated to old humans, our data suggest concurrent RIS treatment should not adversely affect the ability for the aged skeleton to respond to mechanical loading.

6.6 Conclusions

- In old mice, RIS treatment increased cortical bone mass but had no effect on trabecular bone mass. This response to RIS treatment in old mice differs from that observed in young mice. This is further evidence that caution should be exercised when extrapolating results between age groups.
- RIS treatment in old mice, sufficient by itself to result in greater cortical bone mass, did not alter the osteogenic loading response relative to vehicle-treated mice. This suggests that loading related bone gain in old mice, as in young mice, is unaffected by processes involved in bone remodelling.
- The observed “rescue” of the age-impaired osteogenic response to loading by prior disuse was unaffected by RIS, and thus our hypothesis was supported.
- To the extent that the situation in old mice can be extrapolated to old humans, the benefits of RIS treatment in maintaining bone mass are achieved without any impairment on the bone gain potentially conferred by increased loading.

Parts of the experiments reported in this chapter were presented as an abstract to the 2015 annual meeting of the ASBMR in Seattle, Washington where it received a Plenary Poster Prize, leading to a Young Investigator Travel Grant being awarded [686]. A copy of the poster abstract is included in Appendix 4. A manuscript is being prepared for submission to the journal *Osteoporosis International*.

Chapter 7

The effect of risedronate on the anabolic effect of PTH and loading on bone in old mice.

Chapter 7 – RIS+PTH and the loading response in old mice

7.1 Introduction

In the previous chapter of this thesis, we demonstrated that risedronate (RIS) treatment did not affect the anabolic response to loading in old female mice, nor did it affect the improvement in the anabolic response to loading brought about by a short period of prior disuse induced with sciatic neurectomy. These findings both suggest that functional adaptation in old mice, and its enhancement by disuse, are primarily bone modelling responses that can work independently of the need for resorption.

As described previously, bone mass, as well as basal bone formation rates are inherently reduced in old mice [29-31, 389], and reduced bone mass and deteriorations in bone architecture are a major underlying factor for the development of fragility fractures in the elderly [656]. As antiresorptive medications alone typically only limit further loss of bone mass, finding potent anabolic stimuli for bone formation and restoration of bone mass that work in the bone of old people is of paramount importance to improving successful management of osteoporosis in the future.

While loading has been shown to be osteogenic in old mice and humans [687], there is a risk of fracture and low patient compliance [688]. Furthermore, the scope for pharmaceutical anabolism of bone mass is currently limited. The only licenced anabolic treatments for osteoporosis is parathyroid hormone (PTH) (including truncated analogues of the hormone). Sclerostin antibody is another promising anabolic therapy which is in the final regulatory phases prior to licensing for treatment of low bone mass and reductions in vertebral fracture risk, however, this is still unavailable as a licensed treatment for people. PTH treatment is a potent anabolic therapy, although it does promote bone resorption as well as formation, with the anabolic effects initially exceeding the resorptive effects [379]. The cellular effects of PTH treatment are described in more detail in the general introduction of this thesis.

PTH therapy is well described in young adult rodents, with the effects well characterised [32, 672, 689, 690]. PTH has effects in both trabecular and cortical bone; it typically results in increased bone mass in the trabecular compartment through increases in Tb.Th and Tb.N., whilst cortical bone mass is primarily augmented by periosteal proliferation and increased Tt.Ar. Significantly, the anabolic response to loading in young mice is synergistically improved following prior pre-treatment with PTH [32], suggesting that PTH treatment sensitises the mechanostat to respond with a greater formation response to the same loading stimulus. Concurrent to undertaking the experiments for the present chapter, our lab performed a related experiment exploring the combined effect of PTH treatment and loading in old mice. The combined effects of PTH and loading were different when loading was applied to old mice treated with PTH; although additive, the response to loading is no longer synergised by PTH treatment as observed in young mice [388]. Furthermore, in this study, PTH treatment showed an inhibitory effect on the positive effects of 2 of weeks loading in trabecular bone. In another study directly comparing the response to PTH treatment in young (8w) and old (12 months) mice in a fracture healing model, PTH treatment increased osteoblast proliferation and subsequent bone formation, but the old mice demonstrated significantly reduced PTH-related effects compared with young mice [691]. Notwithstanding, despite the differences in response between old and young mice in the above studies, PTH still demonstrated a dose and time dependent effect on the increase in bone mass in old mice, but interestingly, also an increase in porosity was observed, associated with PTH treatment [388]. This increase in porosity demonstrates the additional resorptive effects that treatment with PTH engenders. This porosity was not noted in young mice treated with PTH [32].

For obvious reasons, there is substantial clinical interest in the potential to combine anabolic PTH treatment with anti-resorptive bisphosphonates [374, 375, 692-696]. The key question is whether the remodelling induced by PTH is necessary for its anabolic effects to work. Inhibition of resorption is a potential concern when treating with any medications which could, at least in part, rely on the osteoclast:osteoblast “coupling” which is inherent in bone remodelling. There is a body of literature which has suggested that pretreating people with anti-resorptive medications before treatment with PTH may

actually impair the magnitude of the anabolic effect of PTH, consistent with the suggestion that significant proportions of PTH's anabolic effect may be linked with concurrent resorption and remodelling-based bone formation [379, 697, 698]. One study demonstrated that remodelling-based formation made up 70% of bone formation sites in iliac biopsies of PTH-treated people compared with only 30% associated with *de novo* modelling-based formation, although this assessment was based on visually determining the appearance of formation sites according to dynamic histomorphometry, and didn't determine if concurrent resorption was a prerequisite for the formation observed [699].

Further rodent studies have also demonstrated the importance of the presence of osteoclasts for an optimal PTH effect. Mice treated with anti-RANKL antibody, which greatly reduced osteoclast numbers, demonstrated a reduced PTH effect, whereas mice in the same study treated with Alendronate, a bisphosphonate which reduced osteoclast activity, but not osteoclast number still demonstrated a normal PTH anabolic response [700] suggesting that osteoclast presence, but not necessarily resorptive activity was necessary for PTH's anabolic effect. A separate study demonstrated a ~50% decrease in osteoclast numbers with alendronate treatment whilst still demonstrating additive positive effects on bone mass and architecture with combined PTH-alendronate therapy compared to monotherapy [701]. A further study in mice with constitutively increased PTH-R signalling demonstrated that impairing resorption with alendronate, sufficient to reduce osteoclast numbers, resulted in reduced bone formation on the endocortical surface, but had no effect on the periosteal surface, and that bone mass was additively increased in the trabecular bone compartment, demonstrating a site-specific effect of the actions of PTH on the relative balance between modelling- and remodelling-driven bone formation [702].

The bisphosphonate RIS has age-specific effects on bone in mice. In young adult mice, RIS increases trabecular bone of the proximal tibia with increases in BV/TV primarily through increases in Tb.N, whilst having minimal effects in the cortical bone [34]. Conversely, in old mice studied in the previous chapter of this thesis, cortical bone mass increased following RIS treatment using the same treatment protocol as previously employed in

young adult mice. Additionally, we did not observe a significant effect of RIS on the trabecular bone mass, although it did alter some architectural parameters. Despite these age-related differences in response to RIS, the response to loading in mice of both ages was still unaffected by concurrent treatment suggesting that loading-induced formation in mice was likely via bone modelling-based mechanisms in both old and young mice. Furthermore, the rescued bone formation seen following disuse in old mice was unaffected by RIS treatment, further supporting the modelling-based nature of bone formation in response to loading in old mice. The augmented anabolic response of loading brought about by prior disuse is also not likely related to the increased basal resorption stimulated by disuse. Whether the effect of remodelling-based bone formation has a significant effect on the overall anabolic effect of other anabolic treatments remains a contentious issue.

Despite several studies in both rodents and humans demonstrating that cellular activity can be impaired by co-treatment with anti-resorptives and PTH, multiple studies in humans have suggested that concurrent or sequential use of PTH and antiresorptives still results in an additive and clinically significant positive effect on overall bone mass [350, 378]. In a recent meta-analysis of studies assessing the effect of combined therapy with alendronate and PTH, the authors observed a reduction in the anabolic effect of PTH in bone sites made of largely trabecular bone (lumbar spine, femoral neck) when combined with BPs. The distal radius site however, experiences a greater increase in BMD with combination therapy [671]. A systematic review evaluating the effect of PTH monotherapy vs combination therapy on peripheral cortical bone sites has actually demonstrated a reduction in bone mineral density following PTH monotherapy, which is typically attenuated when PTH is combined with an antiresorptive treatment [703].

Rodent studies have demonstrated mixed findings with regards to the combined effects of BPs and PTH on bone mass, with some suggesting inhibitory effects of BPs with PTH treatment, some demonstrating no additional effect of BPs over PTH, and others demonstrating additive effects of PTH and BPs [696, 700, 704, 705]. These rodent studies have all used young or adult mice. One study has suggested that the difference in response

may be to do with the remodelling status of the bone that is studied [706]. They found that alendronate blunted the anabolic effect of PTH in bone that was undergoing remodelling (secondary spongiosa) but not bone that was non-remodelling (primary spongiosa). Interestingly, this study also compared co-treatment with a Cathepsin K inhibitor (another anti-resorptive treatment), which demonstrated additive effects in both remodelling and non-remodelling bone. Considering the differences reported between the responses to risedronate and PTH in old versus young mice demonstrated in chapter 6 of this thesis and in other studies [32, 34, 388], and the potential for greater amounts of remodelling occurring in old mouse cortical bone, **the aim of this chapter was to evaluate the effect of inhibiting resorption with RIS on the anabolic stimuli of PTH and/or loading in old female mice.**

We did this by administering RIS and PTH concurrently then applying the axial tibial loading model to old mice and assessed the outcome with μ CT. We hypothesised that impairing the resorptive response by administering RIS would not affect the anabolic effects of PTH in the tibias of old mice and that the anabolic response to combined PTH and loading would also not be affected as the primary mechanism for bone gain for each of these anabolic stimuli is via bone modelling.

7.2 Objectives:

Using μ CT analysis, to:

1. Establish the effect of treatment with RIS on the response to concurrent treatment with PTH in the tibias of old female mice.
2. Establish the effect of RIS treatment on the adaptive response to mechanical loading in the tibias of old female mice treated with PTH.

7.2 Materials and Methods

Old (18-month-old) female C57BL/6 mice (n=84) were obtained from Charles River Laboratories (Margate, UK). Originally these mice were planned to begin the experiment after 1 week of acclimatisation, however the author's personal circumstances resulted in

a significant delay in the commencement of the experiment. A 3-month period of premature paternity leave meant the mice began the experiment at 21-months of age, rather than the planned 18 months.

7.2.1 Experiment 1: load strain relationship of old mice treated with RIS and/or PTH

At 21 months of age, 24 mice (n=6/group) were divided into 4 groups. Group one (VEH) was administered saline vehicle injections, group 2 (RIS) was administered RIS 15µg/kg SC three times weekly, group 3 (PTH) was administered PTH (1-34) 50µg/kg daily, SC, and group 4 (RIS+PTH) was administered RIS 15µg/kg three times weekly and PTH 50µg/kg daily. Injections were administered for 4 weeks. At this point, mice were killed and their right pelvic limbs were harvested for strain gauge application to determine the load strain relationship for each treatment group, to ensure application of similar strains between groups. Full details of the protocol used to perform *ex vivo* strain gauging can be found in chapter 2 of this thesis. The experimental timeline is illustrated in Figure 73.

7.2.2 Experiment 2: The effect of concurrent RIS treatment on the anabolic effect of PTH and axial tibial loading.

In vivo procedures

Using identical group assignment and treatments to those described in objective 1 of this chapter, 21-month old mice (n=60) were weight matched and divided into 4 equal groups (n=15). Following 4 weeks of injections, mice underwent loading to achieve 1800µε measured at the medial tibial cortex, according to the calculated forces measured using strain gauging from Objective 1. The forces applied to each group are shown in Table 9. This strain was selected to allow further positive treatment responses to be detected following treatment with both PTH and RIS. The strain for each group was achieved by adapting the peak load applied as: Peak load = target load + 0.5N pre-load.

Loading was performed three times weekly (M, W, F) for 2 weeks as described in Chapter 2 of this thesis, then mice were killed on day 42, 3 days following the final loading episode

and both hind limbs were dissected and fixed for μ CT scanning as described in Chapter 2. The experimental time line is illustrated in Figure 73.

μ CT scanning and single-site analysis

Left (control) and right (loaded) tibiae underwent μ CT scanning and image reconstruction as described in Chapter 2. Initially, our single-site regions of interest (ROIs) at the proximal trabecular bone (0.25-0.75mm distal to the proximal tibial physis) and the maximally load responsive cortical site (37% of the length of the bone measured from proximal) were examined for changes in the standard trabecular and cortical measures, as described in Chapter 2 and recommended by Bouxsein *et al* [570]. Parameters assessed included BV/TV, Tb.Th, Tb.N, Tb.Sp, Tb.Pf and SMI for the trabecular bone, and Tt.Ar, Ct.Ar, Ma.Ar, Ct.Th and PMI for the cortical bone.

Due to obvious and significant increases in cortical porosity in mice treated with 6 weeks of PTH, a new task list was developed to more accurately assess the degree of porosity of the cortical bone envelope, without including the vacant space in the medullary cavity. This customised task list was developed following communication with, and advice from Kjell Laperre, product specialist for Bruker microCT (Kontich, Belgium). The full detailed task list for the μ CT analysis programme CTAn (Skyscan, Bruker, Kontich, Belgium) is included in the Materials and Methods chapter. Briefly, the task list allows isolation of a region of interest (ROI) including all of the cortical bone, and any pores up to a pre-determined size, but excluding the large volume medullary cavity. The porosity calculations are then made on this newly formed ROI, rather than the entire area inside the periosteal envelope. The Ct.Po tasklist was also run in the trabecular region of interest after initial manual selection of the tibia only (and subsequent exclusion of the fibula)

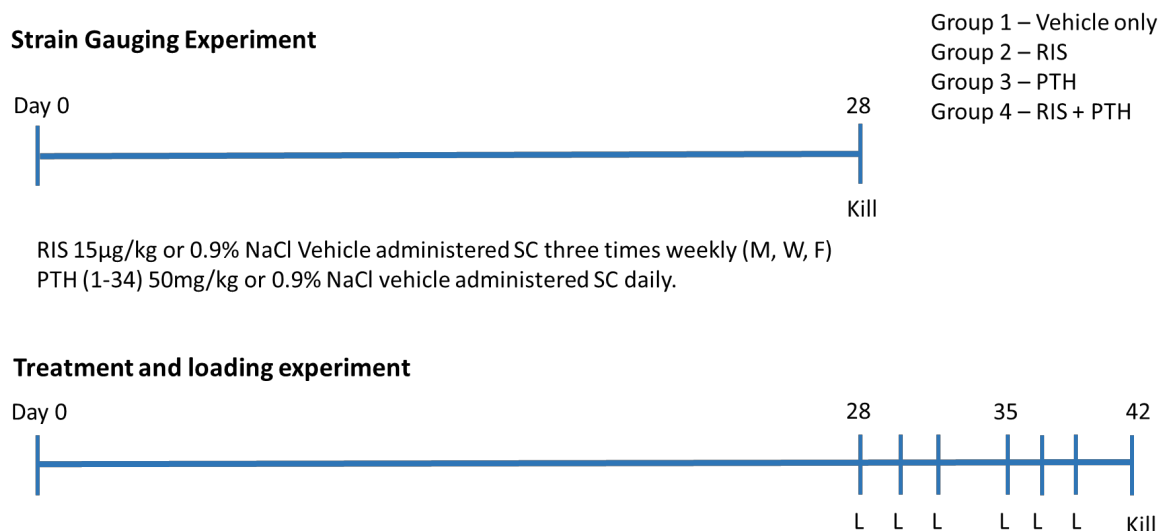


Figure 73 – Experimental plan for the Strain gauging and RIS-PTH treatment response study.

Mice were treated with daily PTH or vehicle and/or thrice-weekly RIS or vehicle subcutaneously for four weeks, then either killed ($n=24$) for strain gauging (Experiment 1), or had their right tibia loaded three-times weekly for two weeks ($n=60$) then were killed for μ CT assessment of their tibias on day 42 (Experiment 2).

SSA analysis

Following initial examination using single-site μ CT analysis of trabecular and 37% cortical ROIs, we also performed site-specificity analysis (SSA) to evaluate the tibia-wide changes in cortical bone due to the different treatments. SSA technique is described in detail in Chapter 2 of this thesis. The results from this analysis demonstrated increased variability in the most proximal bone sites (10-14%) in this batch of mice, primarily due to cortical breaches preventing automatic segmentation of the entire cortex, so all analyses for this experiment were performed only on the sites between 15% and 90%, rather than the normal 10-90%.

7.2.3 Statistical Analysis

Analyses were carried out using SPSS (version 23) or GraphPad Prism (Version 5). Analysis of the effect of RIS and/or PTH treatment was performed using a two-way ANOVA. The effect of treatments on the loading response was assessed using the % change with

loading $[(\text{Right-Left})/\text{Left} * 100]$ values and then similarly compared using two-way ANOVA. Post-hoc tests were performed using the Least Significant Differences (LSD) (equivalent to no correction for multiple comparisons) as there were only 2 treatment groups in each of the 2 main effects.

Analysis of SSA data was performed using a linear mixed model approach, with bone site as a fixed categorical parameter and intervention (RIS, PTH) as a fixed effect. Intervention by site interaction was also assessed to identify any site-specific responses. Mouse ID was included as a random effect. If effects were significant, post-hoc Sidak correction was applied to identify individual sites where the effect was significant ($p < 0.05$).

Mixed model results interaction definitions:

If a given interaction is significant (i.e. $p < 0.05$) for:

- Bone-site*RIS (or PTH) interaction – effect of RIS (or PTH) is significantly different at different sites.
- RIS*PTH interaction – change due to RIS is significantly different in PTH treated, compared to vehicle-treated mice which was interpreted as a synergistic interaction (or an inhibitory interaction if the effects were opposite).
 - If the interaction is not significant, yet the independent variables are significant, this indicates an additive effect.
- RIS (or PTH)*loading interaction – percentage change due to loading is significantly different in RIS (or PTH) treated mice compared with sham mice.

7.4 Results

7.4.1 Strain gauge experiment

The relative load:strain relationships for mice following treatment with VEH, RIS, PTH or RIS+PTH are demonstrated in Figure 74 and Table 9. After 4 weeks of treatment the load strain relationship showed no significant difference between the load:strain relationship of different groups ($p=0.28$), although the slope of the RIS+PTH group tended to be lower than the slope for RIS treated mice on post-hoc comparisons ($p=0.06$). Considering these apparent differences, the decision was made to apply load to each group according to their individual regression line calculations, rather than apply the same load to all mice.

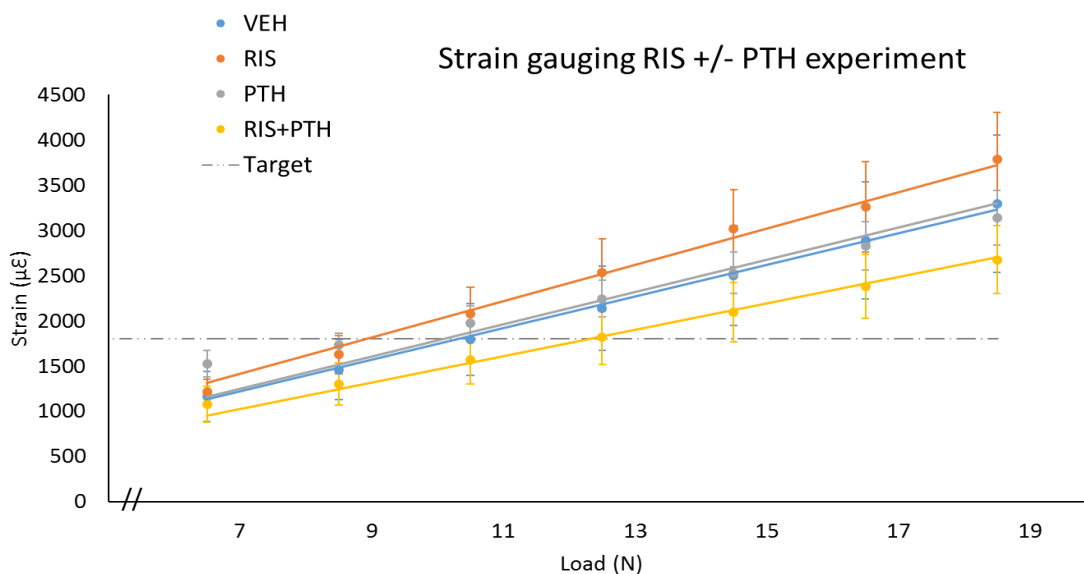


Figure 74 – The effect of 28 days of RIS and/or PTH treatment on the load:strain relationship in the tibia of old female mice.

Statistical analysis was via linear regression. Strains were determined via *ex vivo* strain gauging as described in Chapter 2. Data points represent the mean \pm SEM. Lines indicate linear regression line. The regression lines were constrained to pass through zero. The reference line is placed to indicate the load required to engender 1800 $\mu\epsilon$ at the medial tibial diaphysis.

Group	VEH	RIS	PTH	RIS+PTH
R²	0.9971	0.9929	0.8849	0.9889
Slope	174.49	201.4	178.19	146.25
Load at 1800 $\mu\epsilon$	10.32N	8.94N	10.10N	12.31N
Peak load applied (+0.5N)	10.83N	9.44N	10.6N	12.81N

Table 9 - Load:Strain relationship from tibiae of old female mice treated with RIS, PTH or both.

R² represents the closeness of fit of the regression line. The slope is the gradient of the line. All regression lines were constrained to pass through zero. The load required to achieve 1800 $\mu\epsilon$ was used for each respective group in the loading experiment following the addition of the 0.5N preload required to hold the limb within the cups of the loading device.

7.4.2 The effect of RIS and/or PTH on the tibial trabecular and cortical bone.

Trabecular bone

We first assessed the effect of RIS and PTH treatment on the trabecular and proximal (37% site) cortical bone by using a within treatment comparison of the control limb in these old mice. When considering the trabecular region of interest, PTH treatment had no effect on trabecular bone in control treated bones for any measure ($p>0.05$) (Figure 75, Figure 76). PTH did result in a significant increase in Tb.Ct.Po of the cortical shell at the level of the trabecular ROI ($p<0.001$) (Figure 76C). RIS also had no effect on control treated bones in trabecular bone.

BV/TV was significantly increased in bones treated with PTH and RIS. The RIS*PTH interaction was significant ($p<0.05$) suggesting that concurrent treatment enabled a gain in bone mass that was not observed in mice treated with RIS alone. In mice treated with RIS, the Tb.Pf and SMI significantly decreased following treatment with PTH ($p<0.05$), where they did not decrease in mice not treated with RIS, however this interaction between RIS and PTH was not significant ($p>0.05$) (Figure 76). Table 10 reports the significance (p -values) following Two-way ANOVA for both the main effects (RIS and PTH) and their interaction (RIS*PTH).

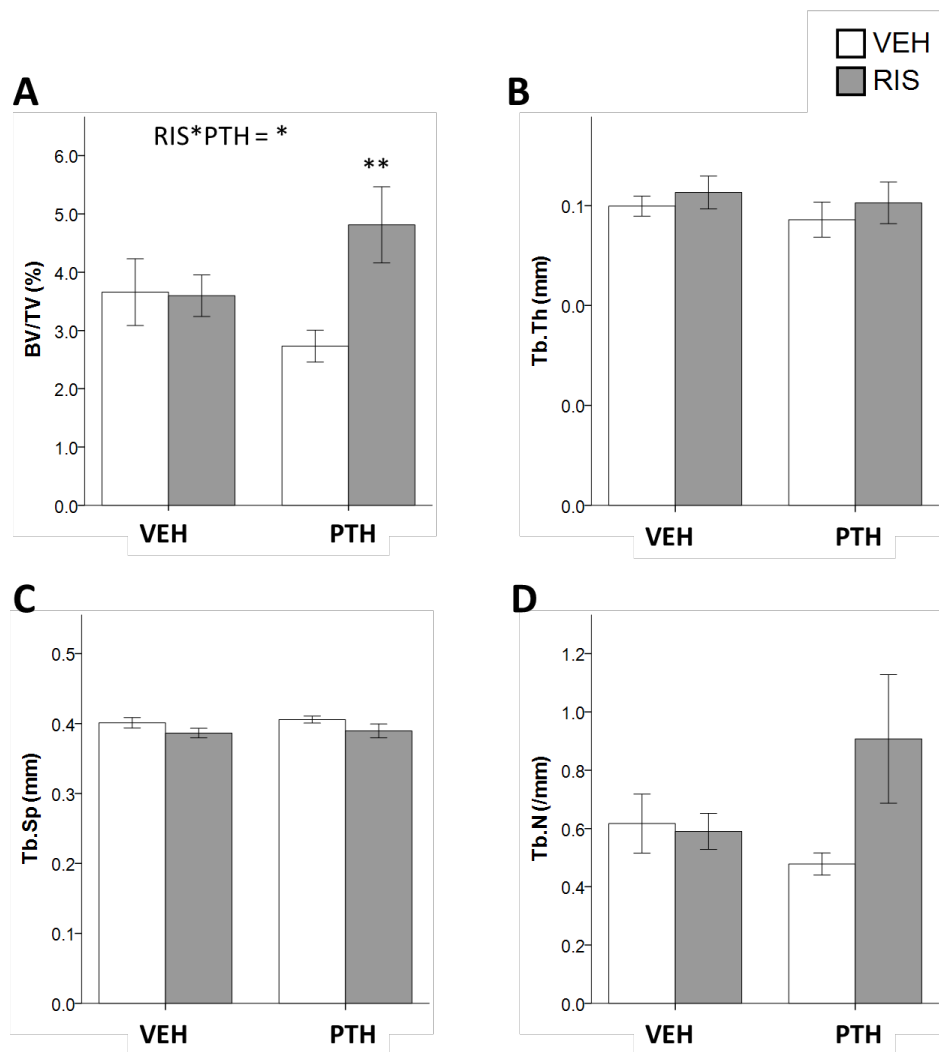


Figure 75 – The effect of 6 weeks of RIS and/or PTH treatment on bone mass μ CT parameters of the proximal trabecular region of the tibia of old female mice.

22-month-old female C57BL/6 mice (n=60) underwent daily PTH injections and three-times weekly RIS injections for 6 weeks. μ CT assessment of (A) BV/TV, (B) Tb.Th, (C) Tb.Sp, (D) Tb.N of a region of interest 0.25-0.755 distal to the proximal tibial physis. Comparisons were performed with a two-way ANOVA with LSD post hoc comparisons. Values displayed are mean \pm SEM. ** = $p < 0.01$ RIS vs VEH of same PTH group. # = $p < 0.05$, ### - $p < 0.001$ PTH vs VEH for same RIS group.

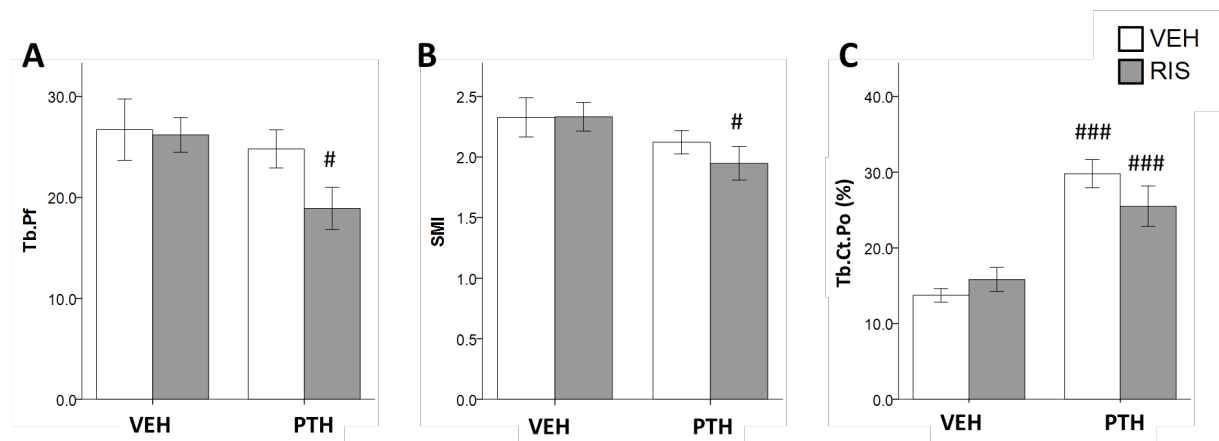


Figure 76 – The effect of RIS on the anabolic response to PTH treatment on tibial trabecular bone microarchitectural parameters in old female mice.

22-month-old female C57BL/6 mice (n=60) underwent daily PTH injections and three-times weekly RIS injections for 6 weeks. μ CT assessment of (A) Tb.Pf, (B) SMI and (c) Tb.Ct.Po of a region of interest 0.25–0.755 distal to the proximal tibial physis. Comparisons were performed with a two-way ANOVA with LSD post hoc comparisons. Values displayed are mean \pm SEM. # = $p < 0.05$, ### - $p < 0.001$ PTH vs VEH for same RIS group.

PARAMETER	BV/TV	Tb.Th	Tb.Sp	Tb.N	Tb.Pf	SMI	Tb.Ct.Po
RIS	0.043	0.361	0.042	0.110	0.162	0.522	0.549
PTH	0.767	0.470	0.608	0.474	0.048	0.029	<0.001
RIS*PTH	0.033	0.927	0.922	0.071	0.241	4.990	0.088

Table 10 – Effect of RIS and PTH treatment on the trabecular bone of old female mice.

P-values following tests of between subjects effects following Two-way ANOVA on control (unloaded) limbs of 22month old female mice following 6 weeks of treatment with RIS and/or PTH. RIS and PTH were included as between-subjects effects. Main effects or their interactions were considered significant if $p < 0.05$.

Cortical bone

PTH treatment also resulted in significant increases in Tt.Ar ($p < 0.01$) and Ct.Ar ($p < 0.001$) but had no effect on Ma.Ar ($p > 0.05$). Ct.Th also did not change with PTH treatment alone ($p > 0.05$) (Figure

77). Cortical Area Fraction (Ct.Ar/Tt.Ar) also increased significantly with PTH treatment, along with PMI ($p < 0.001$). Ct.Po was also significantly greater in PTH treated mice ($p < 0.01$) (Figure 78). RIS treatment alone resulted in decreased Ma.Ar ($p < 0.05$) and increased Ct.Th ($p < 0.05$) (Figure 77) and Ct.Ar/Tt.Ar ($p < 0.01$) (Figure 78). RIS treatment did not affect any other μ CT parameter measured ($p > 0.05$).

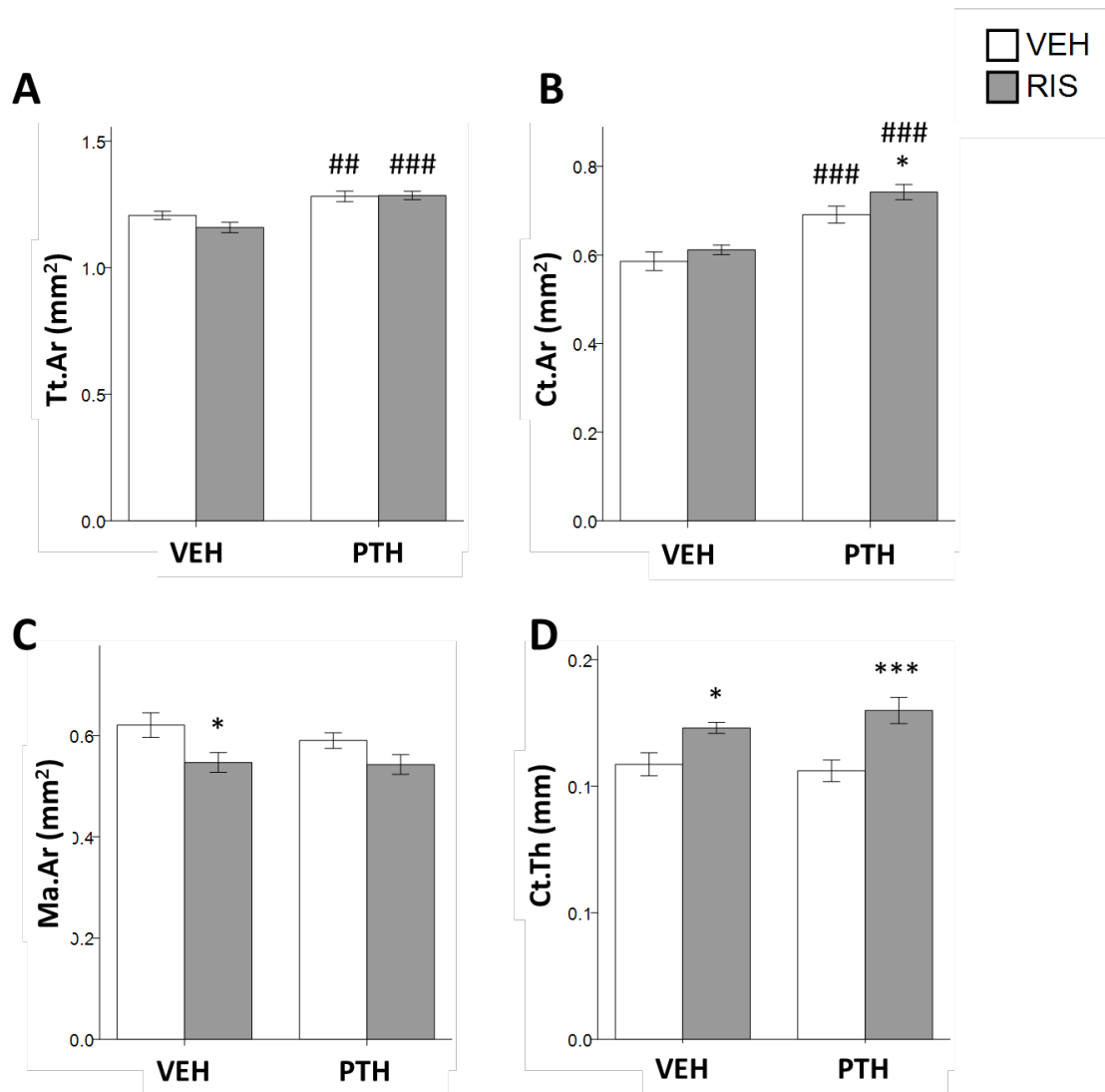


Figure 77 – The effect of 6 weeks of RIS and/or PTH treatment on bone mass μ CT parameters of the 37% site cortical bone of the tibia of old female mice.

22-month-old female C57BL/6 mice ($n=60$) underwent daily PTH injections and thrice weekly RIS injections for 6 weeks. μ CT assessment of (A) Tt.Ar, (B) Ct.Ar, (C) Ma.Ar, (D) Ct.Th, (E) Ct.Ar/Tt.Ar, (F) PMI and (G) Ct.Po of the cortical bone centred around 37% of the length of the bone measured from proximal. Comparisons were performed with a two-way ANOVA with LSDpost hoc comparisons. Values displayed are mean \pm SEM. * = $p < 0.05$, *** = $p < 0.01$ RIS vs VEH of same PTH group. ## = $p < 0.01$, ### = $p < 0.001$ PTH vs VEH for same RIS group.

In mice treated with RIS and PTH we observed increased Tt.Ar, Ct.Ar, PMI ($p < 0.001$) and Ct.Ar/Tt.Ar ($p < 0.01$) and increases in Ct.Ar ($p < 0.05$) that were not present in mice treated RIS alone, although this interaction was not significant. Ct.Th ($p < 0.001$) and Ct.Ar/Tt.Ar ($p < 0.05$) were also increased in PTH/RIS treated mice. A decrease in porosity was observed in PTH/RIS mice which was not present in mice treated with RIS alone. The effects of PTH and RIS were additive for Ct.Ar and

PARAMETER	Tt.Ar	Ct.Ar	Ma.Ar	Ct.Th	PMI	Ct.Ar/Tt.Ar	Ct.Po
RIS	0.232	0.033	0.004	<0.001	0.223	0.003	0.013
PTH	<0.001	<0.001	0.396	0.611	<0.001	<0.001	0.002
RIS*PTH	0.169	0.486	0.511	0.270	0.336	0.872	0.317

Table 11 – Effect of RIS and PTH treatment on the cortical bone of old female mice.

P-values following tests of between subjects effects following Two-way ANOVA on control (unloaded) limbs of 22month old female mice following 6 weeks of treatment with RIS and/or PTH. RIS and PTH were included as between-subjects effects. Main effects or their interactions were considered significant if $p < 0.05$.

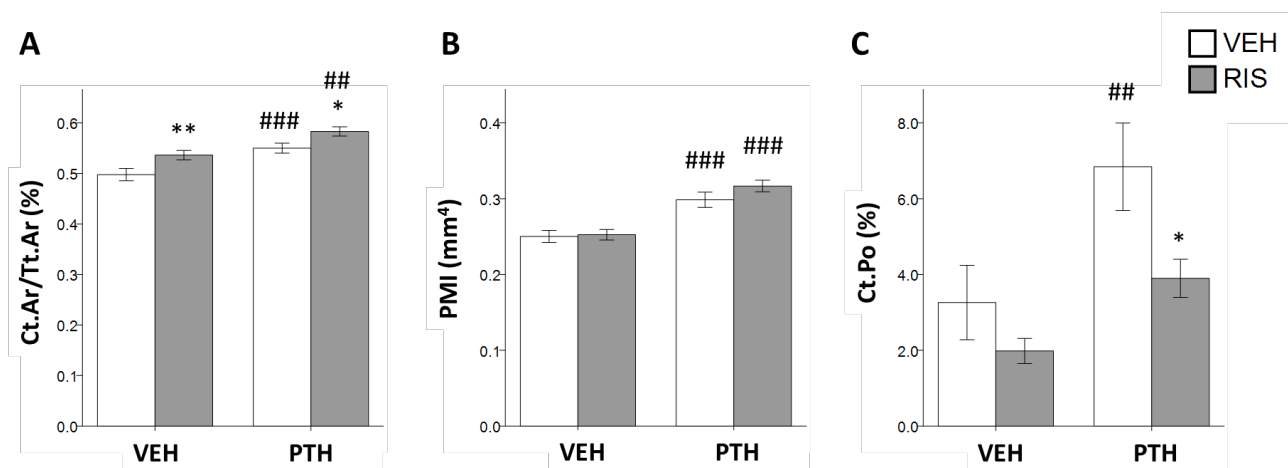


Figure 78 – The effect of 6 weeks of RIS and/or PTH treatment on micro-architectural μ CT parameters of the 37% site cortical bone of the tibia of old female mice.

22-month-old female C57BL/6 mice ($n=60$) underwent daily PTH injections and thrice weekly RIS injections for 6 weeks. μ CT assessment of (A) Ct.Ar/Tt.Ar, (B) PMI and (C) Ct.Po of the cortical bone centred around 37% of the length of the bone measured from proximal. Comparisons were performed with a two-way ANOVA with LSD post hoc comparisons. Values displayed are mean \pm SEM. * = $p < 0.05$, ** = $p < 0.01$ RIS vs VEH of same PTH group. ## = $p < 0.01$, ### = $p < 0.001$ PTH vs VEH for same RIS group

Ct.Ar/Tt.Ar. The magnitude of effect seen with PTH treatment alone was not affected for any measure in RIS/PTH treated mice, except that the PTH-associated increase in Ct.Po was abrogated by RIS treatment, although this interaction was not statistically significant. Table 11 reports the significance (p-values) following Two-way ANOVA for both the main effects (RIS and PTH) and their interaction (RIS*PTH)

Site-specificity analysis (SSA)

Following single-site μ CT analysis, SSA was used to evaluate the cortical bone changes over the length of the tibia. Table 12 reports the significance (p-values) following mixed-model analysis for both the main effects (RIS, PTH and loading) and their interactions.

	RIS	PTH	SITE*RIS	SITE*PTH	RIS*PTH	SITE*RIS*PTH
Tt.Ar	0.206	<0.001	0.928	<0.001	0.592	0.256
Ct.Ar	0.120	<0.001	0.825	<0.001	0.929	0.991
Ma.Ar	0.001	0.039	<0.001	0.463	0.491	0.202
Ct.Th	<0.001	<0.001	0.931	<0.001	0.200	1.000
PMI	0.608	<0.001	0.311	<0.001	0.558	0.019
I_{max}	0.543	<0.001	0.360	<0.001	0.712	0.247
I_{min}	0.964	<0.001	0.647	<0.001	0.570	0.025
Ct.Po	0.005	0.219	<0.001	<0.001	0.700	0.993

Table 12 – Effect of RIS and PTH and their interactions on the cortical bone of old female mice.

SSA was performed and values represent p-values of fixed effects and interactions following Type III tests of fixed effects in tibias of 22month old female mice following 6 weeks of treatment with RIS and/or PTH, and loading three-times weekly for the final two weeks. Main effects or their interactions were considered significant if $p < 0.05$.

Periosteally Enclosed area (Tt.Ar)

PTH resulted in a significant increase in Tt.Ar and this effect was site specific with the bone sites proximal to the 40% site being most significantly increased. RIS treatment did not significantly affect Tt.Ar. RIS treatment did not significantly affect the response to PTH treatment (Figure 79A).

Cortical bone Area (Ct.Ar)

PTH treatment resulted in a significant increase in Ct.Ar and this effect was site specific, with greater increases in Ct.Ar seen in the proximal bone compared with the distal bone, although significant increases in Ct.Ar following PTH treatment were identified at the majority of bone sites. RIS treatment did not significantly affect Ct.Ar. RIS treatment did not significantly affect the response to PTH treatment (Figure 79B).

Medullary Area (Ma.Ar)

PTH treatment resulted in significant decreases in Ma.Ar, at both the proximal and distal extremities of the bone, although this effect was not site-specific. RIS treatment resulted in significant decreases in Ma.Ar in the proximal cortical bone (proximal to 45% site), and this effect was site-specific. RIS treatment did not significantly affect the response to PTH treatment (Figure 79C).

Cortical Thickness (Ct.Th)

PTH treatment resulted in significant increases in Ct.Th and this effect was site specific, with the bone distal to ~50% site demonstrating the most significant increases, while the proximal bone was mostly unaffected. RIS treatment also resulted in a significant increase in the Ct.Th, with a site-specific effect where the distal bone was also more significantly affected than the proximal cortex. RIS treatment did not significantly affect the response to PTH treatment (Figure 79D).

Polar Moment of Inertia (PMI)

PTH resulted in a significant increase in PMI and this effect was site specific, with the bone proximal to the ~70% site responsive and the distal bone unaffected. RIS treatment alone

did not result in a significant increase in PMI. There was a significant site-specific RIS*PTH interaction, with RIS treatment resulting in a greater increase in PMI in the proximal bone of PTH treated mice, compared with vehicle treated mice (Figure 80A).

Maximum moment of inertia (I_{max})

PTH treatment resulted in significant improvements in I_{max} and this effect was site-specific, with the proximal cortical bone significantly affected, whilst the distal cortex was unaffected. RIS treatment did not affect I_{max} nor did it significantly affect the response to PTH (Figure 80B).

Minimum moment of inertia (I_{min})

PTH treatment resulted in significant increases in I_{min} and this effect was site specific, with the bone proximal to the 70% site significantly greater following treatment compared with vehicle treated bones. RIS treatment alone did not result in significant increases in I_{min} . There was a significant site-specific RIS*PTH interaction, with RIS treatment resulting in an increase in I_{min} in the proximal bone of PTH treated mice, compared with a significant decrease associated with RIS treatment in vehicle treated mice (Figure 80C).

Cortical Porosity (Ct.Po)

PTH treatment resulted in significant site-specific increases in Ct.Po, with bone sites proximal to the ~20% site were most affected by PTH treatment. RIS treatment resulted in significant decreases in Ct.Po of the cortical bone, and this effect was site-specific, with significant effects demonstrated in the regions between 20-60%. RIS treatment did not significantly affect the response to PTH treatment (Figure 80D).

Figure 79 – Legend on following page

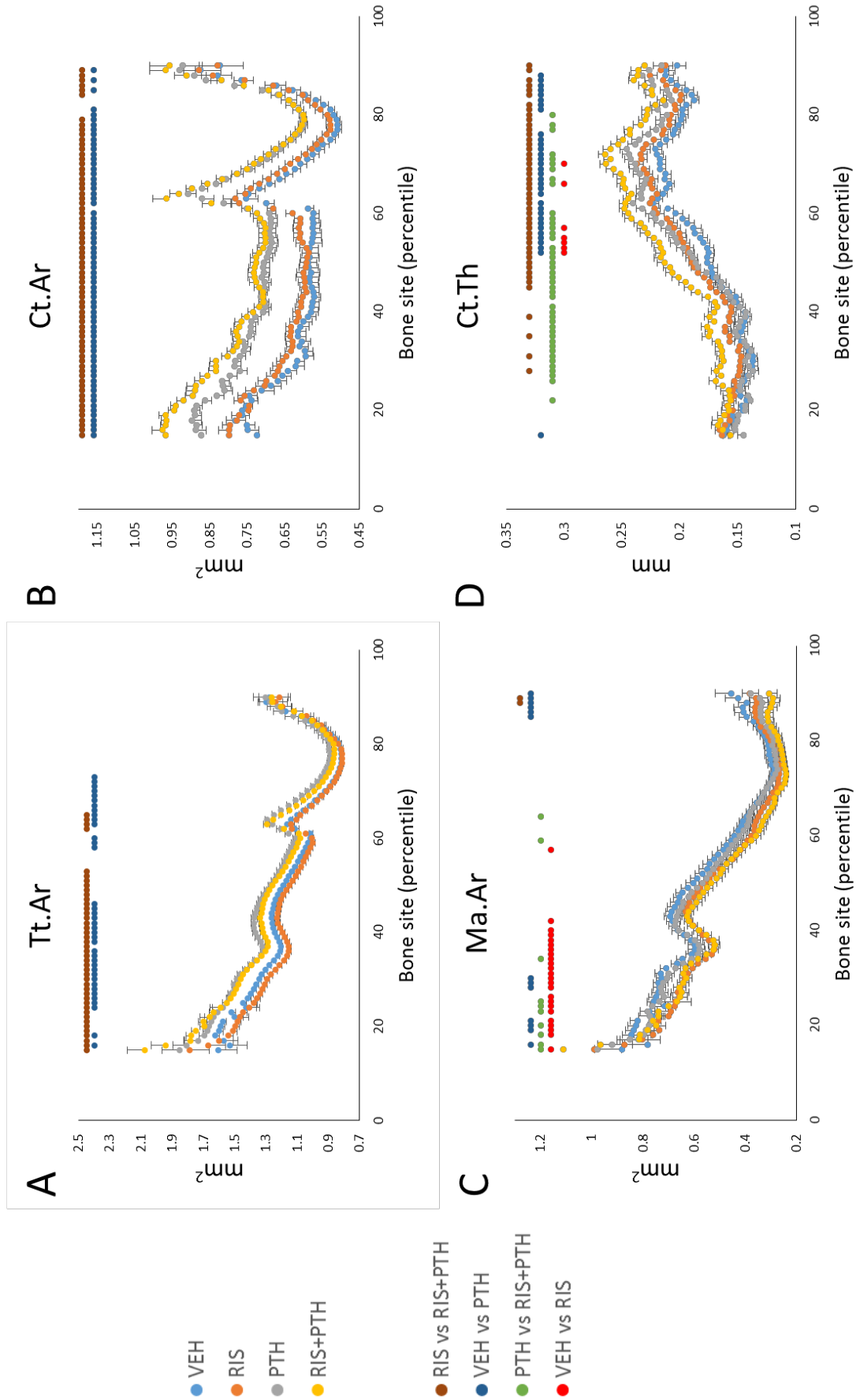


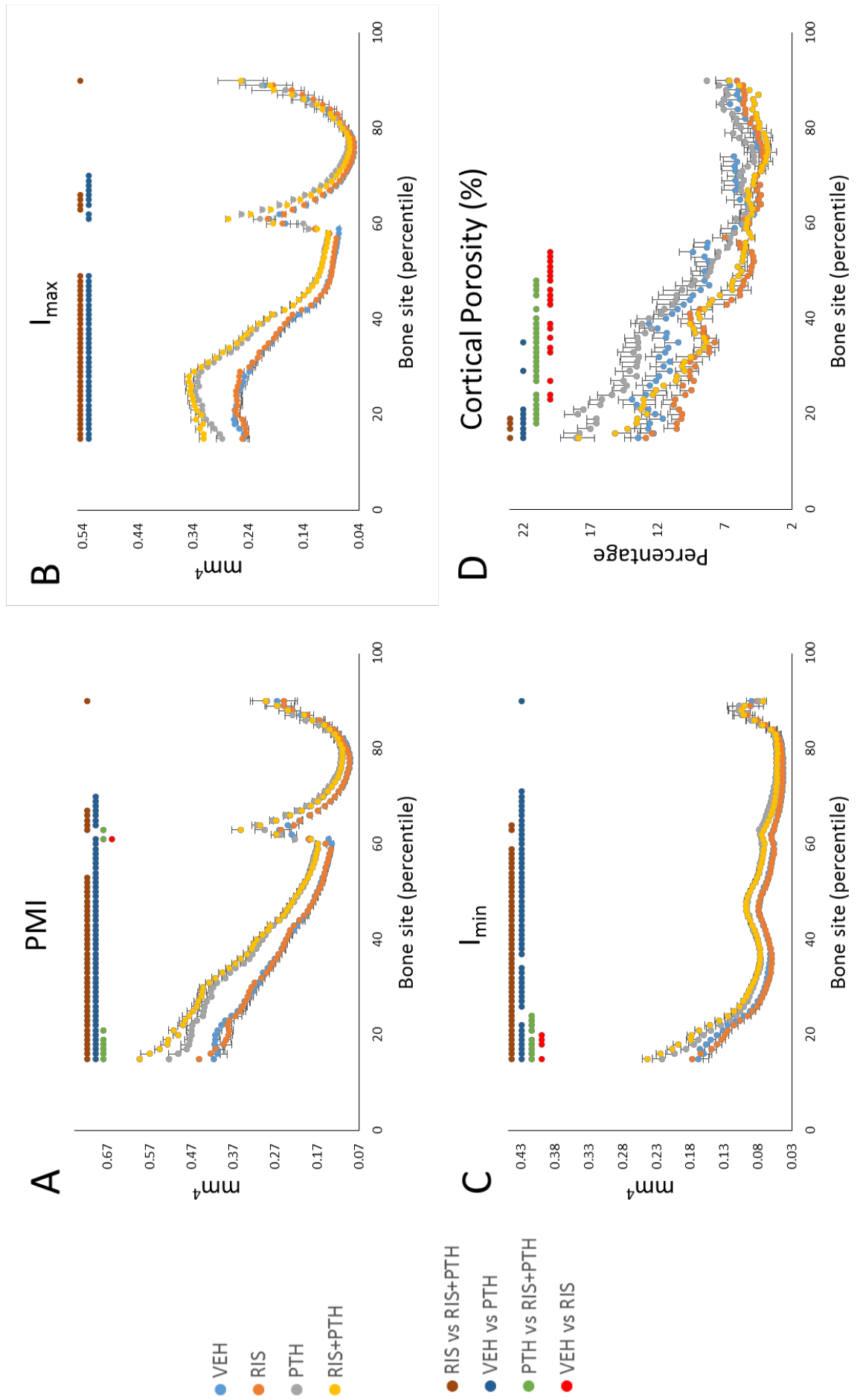
Figure 79 – Effect of RIS treatment on the anabolic response to PTH treatment in old female mice.

FIGURE ON PREVIOUS PAGE. Site-specificity analysis was performed on the tibias of 22-month-old female mice following 6 weeks of treatment with 15µg/kg RIS three times weekly and 50µg/kg PTH (1-34) daily. Sites between 15% and 90% were analysed – 10-14% sites were excluded from analysis due to high variability in this old cohort of mice. (A) Periosteally enclosed area (Tt.Ar), (B) Cortical bone area (Ct.Ar), (C) Medullary area (Ma.Ar) and (D) Cortical Thickness (Ct.Th) were analysed using a mixed model approach with Sidak post-hoc adjustments. The coloured spots above each graph represent the post-hoc comparisons between individual groups, as described by the key at the bottom of the figure and represent sites where $p < 0.05$. (n=13).

Figure 80 - Effect of RIS treatment on the anabolic response to PTH treatment in old female mice.

FIGURE ON FOLLOWING PAGE. Site-specificity analysis was performed on the tibias of 22 month-old female mice following 6 weeks of treatment with 15µg/kg RIS three times weekly and 50µg/kg PTH (1-34) daily. Sites between 15% and 90% were analysed – 10-14% sites were excluded from analysis due to high variability in this old cohort of mice. (A) Polar moment of inertia (PMI), (B) Maximum moment of inertia (I_{max}), (C) Minimum moment of inertia (I_{min}) and (D) Cortical porosity (Ct.Po) were analysed using a mixed model approach with Sidak post-hoc adjustments. The coloured spots above each graph represent the post-hoc comparisons between individual groups, as described by the key at the bottom of the figure and represent sites where $p < 0.05$. (n=13).

Figure 80 – Legend on previous page



7.4.3 The effect of RIS and/or PTH on the adaptive response to loading in old female mice

7.4.3.1 The effect of loading on vehicle treated mice

Single-site analysis

Following our demonstration that RIS and PTH have largely additive effects on cortical bone and possibly a synergistic effect in proximal cortical bone, with regards to moments of inertia, we next evaluated the effect of axial loading on the tibia of vehicle treated, old mice. Results are presented in Table 13.

μ CT parameter	Control (n=14)	Loaded (n=14)	p-value (paired t-test)
Cortical bone			
Tt.Ar (mm ²)	1.21 ± 0.02	1.22 ± 0.02	.479
Ct.Ar (mm ²)r	0.59 ± 0.02	0.62 ± 0.01	.073
Ma.Ar (mm ²)	0.62 ± 0.02	0.60 ± 0.03	.397
Ct.Th (mm)	0.109 ± 0.005	0.115 ± 0.004	.129
PMI (mm ⁴)	0.25 ± 0.01	0.27 ± 0.01	.180
Ct.Ar/Tt.Ar (%)	0.49 ± 0.02	0.51 ± 0.02	.087
Ct.Po (%)	3.26 ± 0.98	2.87 ± 0.75	.674
Trabecular bone			
BV/TV (%)	3.66 ± 0.57	5.00 ± 0.76	.020
Tb.Th (mm)	0.06 ± 0.002	0.067 ± 0.003	.101
Tb.Sp (mm)	0.40 ± 0.01	0.39 ± 0.01	.157
Tb.N (mm ⁻¹)	0.62 ± 0.1	0.77 ± 0.13	.085
Tb.Pf	26.72 ± 3.04	20.53 ± 1.93	.083
SMI	2.33 ± 0.16	2.13 ± 0.13	.341
Tb.Ct.Po	13.74 ± 0.89	14.36 ± 1.4	.658

Table 13 – The effect of two weeks of axial tibial loading on bone in vehicle (control) 22-month-old female mice using single-site μ CT analysis.

μ CT parameters of cortical (37% site, measured from proximal end) and trabecular bone in vehicle-treated mice were compared using a paired t-test. Significance values are reported in the table – values <0.05 are highlighted in bold. Values reported are Mean ± SEM.

When assessing the cortical bone loading response in vehicle treated mice, there was no significant response to mechanical loading for any of the cortical bone parameters evaluated. There was a tendency for Ct.Ar ($p=0.073$) and Ct.Ar/Tt.Ar ($p=0.087$) to increase with loading, but these increases were not significant.

Loading resulted in a significant increase in BV/TV ($+68.5 \pm 32.6\%$, $p<0.05$) and also resulted in a trend towards increase in Tb.N ($p=0.085$) and Tb.Pf (0.083), although these changes were not significant (Table 13). Loading did not result in changes in any other trabecular bone parameter.

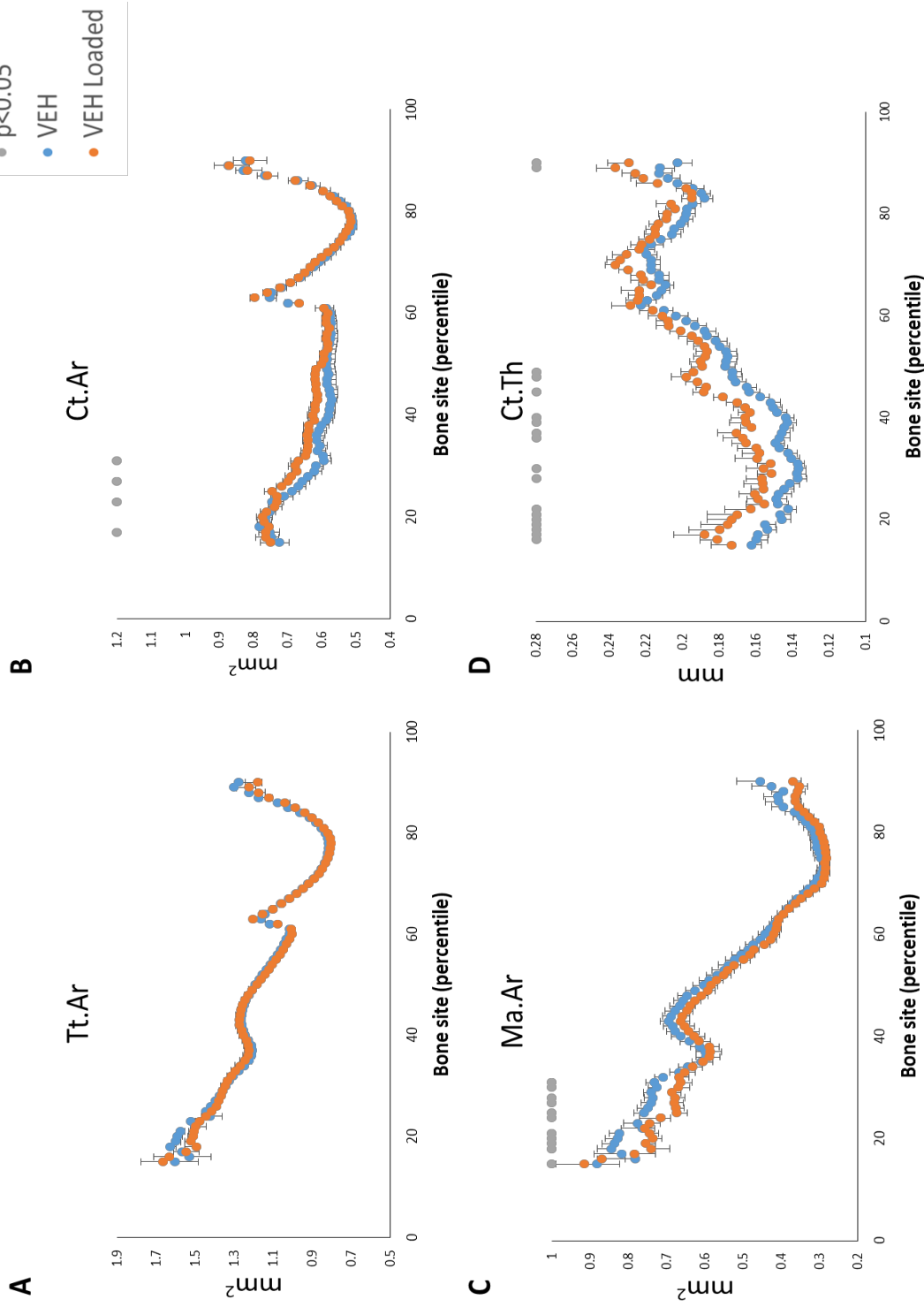
Site specificity analysis

In addition to evaluation using single-site analysis, SSA was also performed on the vehicle-treated mice to explore the effect of loading in these old mice. It is important to note when interpreting these results that the mice in this study were older than used in previous studies in earlier chapters, due to operational and technical reasons explained in the Methods and Materials section of this chapter. Loading resulted in no significant change in Tt.Ar ($p>0.05$), (Figure 81A), but increased Ct.Ar in cortical bone ($p<0.001$). However, this effect was not site-specific ($p>0.05$), with the increase only significant in the proximal bone, although not specifically at the normally load responsive 37% site (Figure 81B). Loading also resulted in a significant reduction in Ma.Ar in the proximal cortical bone ($p<0.001$), although this site-specific response was not statistically significant ($p>0.05$) (Figure 81C). Loading also increased the Ct.Th ($p<0.001$) but this effect was also not site-specific ($p>0.05$). Ct.Th also appeared to demonstrate the largest magnitude of change in response to loading, compared to other parameters examined (Figure 81D).

Loading did not cause an increase in PMI ($p>0.05$)(Figure 82A). Loading increased I_{max} ($p<0.05$) but not I_{min} ($p>0.05$)(Figure 82B, C). Loading resulted in a significant decrease in Ct.Po with sites around 20% and sites around 50% demonstrating significant decreases, although this site-specific effect was not statistically significant (Figure 82D).

Figure 81 – Effect of two weeks of axial tibial loading on the tibia of old female mice using SSA.

22mo female C57BL/6 mice were loaded M,W,F for two weeks and their tibias scanned with μ CT. SSA was performed on CT data and (A) Periosteally enclosed area (Tt.Ar), (B) Cortical bone area (Ct.Ar), (C) Medullary area and (D) Cortical bone thickness (Ct.Th) were evaluated for the effect of loading on the tibias of vehicle-treated mice. Analysis was performed via Mixed Model analysis using Sidak post-hoc correction for multiple



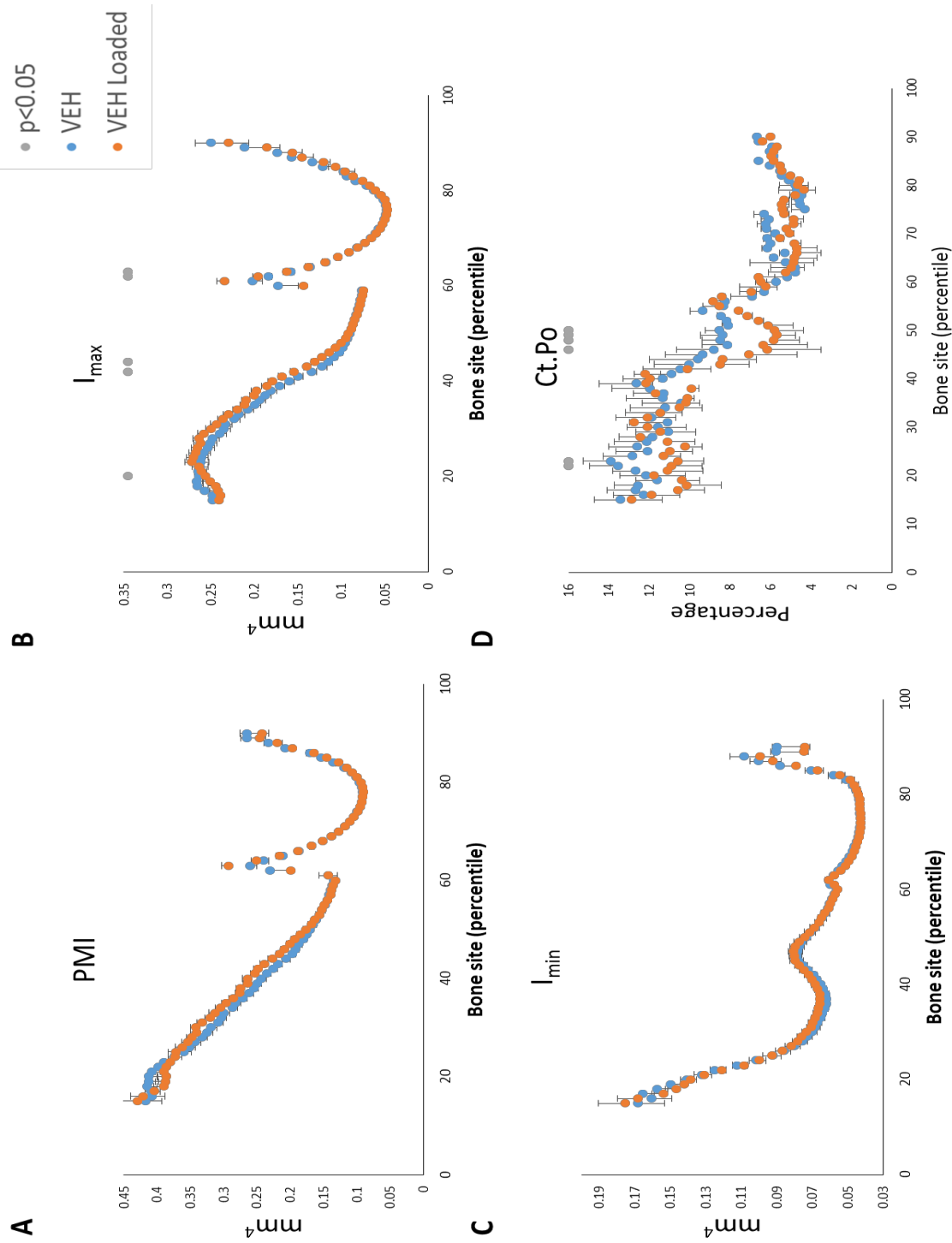


Figure 82 - Effect of two weeks of axial tibial loading on the tibia of old female mice using SSA.

22mo female C57BL/6 mice were loaded M,W,F for two weeks and their tibias scanned with μ CT. SSA was performed on CT data and (A) Polar moment of inertia (PMI), (B) Maximum moment of inertia (I_{max}), (C) Minimum moment of inertia (I_{min}) and (D) Cortical porosity (Ct.Po) were evaluated for the effect of loading on the tibias of vehicle-treated mice. Analysis was performed via Mixed Model analysis using Sidak post-hoc correction for multiple comparisons. Grey spots indicate $p < 0.05$ for that bone site after

7.4.3.2 Effect of RIS and PTH on the response to loading in old female mice

Single-site analysis

Although there was limited osteogenic response to loading in the vehicle-treated 22-month-old mice, we proceeded to evaluate if there was any significant effect of PTH on the loading response and the effect of concurrent RIS treatment. The percentage change in response to loading for each parameter for each treatment group is reported in Table 14 and Figure 83. At the 37% site, using single-site analysis, the response to mechanical loading was not significantly affected by RIS treatment or PTH treatment, nor was there any significant interaction between them when compared using a two-way ANOVA. This suggests that treatment with RIS and/or PTH had no effect on the response to loading in these 22-month-old female mice at the load-responsive 37% site (Table 14, Figure 83).

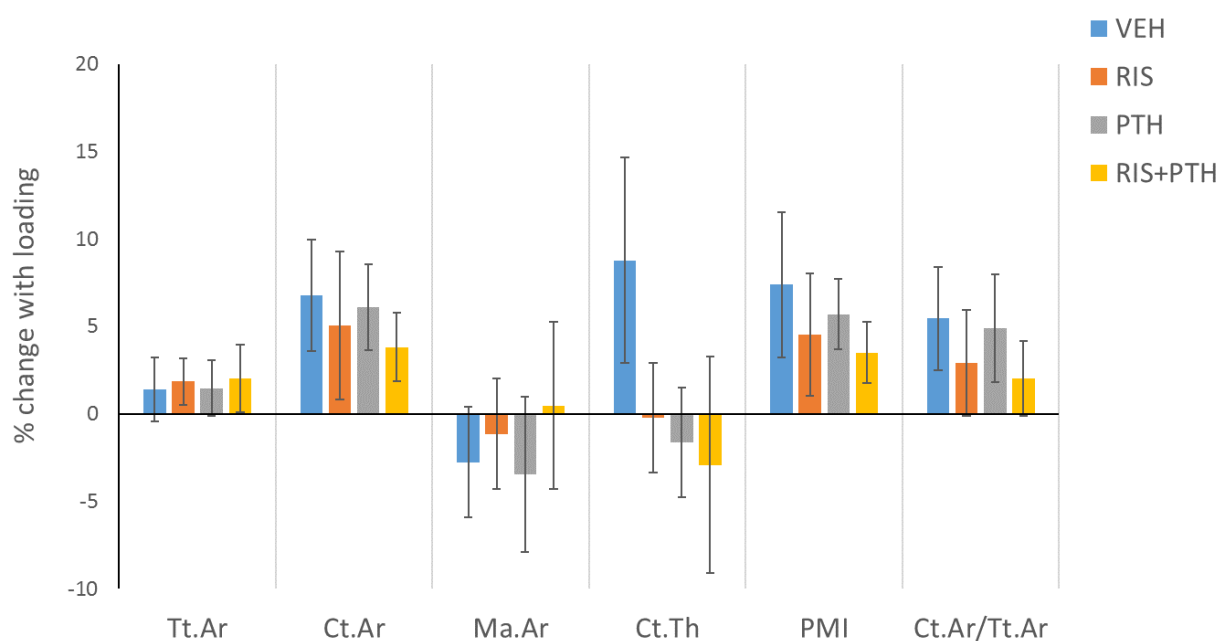


Figure 83 – The effect of RIS and PTH on the response to axial tibial loading in cortical bone of old female mice using single-site analysis at the 37% site.

22-month-old female C57BL/6 mice were treated with subcutaneous injections (three-times weekly of RIS and daily of PTH) for 6 weeks. Mice had their right tibia loading three times weekly for the final two weeks. The tibia was scanned using μ CT and single-site analysis was performed on the 37% site (measured from the proximal end). The percentage change due to loading was calculated $((\text{Right-Left})/\text{Left} * 100)$. Values were compared using a two-way ANOVA and post-hoc adjustments were made with the least squares difference test (equivalent to no adjustment). Bars represent mean \pm SEM. n=13-14

Considering the response to mechanical loading in the trabecular bone, concurrent PTH treatment demonstrated no significant effects in all parameters evaluated. However, the decrease in Ct.Po in the trabecular region (Tb.Ct.Po) following loading tended to be lower following treatment with PTH ($p=0.056$), compared to vehicle-treated mice. Neither RIS alone, nor the RIS*PTH interaction affected the change seen with loading for any of the parameters measured ($p>0.05$)(Figure 84, Table 14, Table 15).

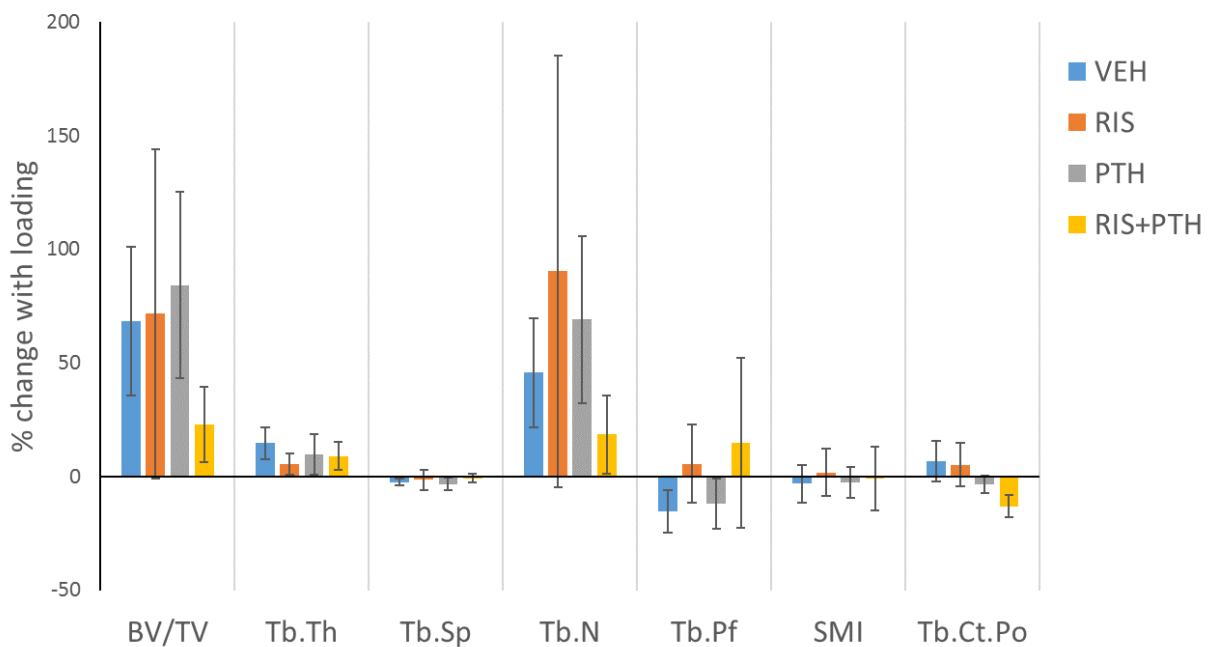


Figure 84 - The effect of RIS and PTH on the response to axial tibial loading in trabecular bone of old female mice using single-site analysis.

22-month-old female C57BL/6 mice were treated with subcutaneous injections (three-times weekly of RIS and daily of PTH) for 6 weeks. Mice had their right tibia loading three times weekly for the final two weeks and were killed 3 days after the final loading session. The tibia was scanned using μ CT and single-site analysis was performed on the 37% site (measured from the proximal end). The percentage change due to loading was calculated $((\text{Right-Left})/\text{Left} * 100)$. Values were compared using a two-way ANOVA and post-hoc adjustments were made with the least squares difference test (equivalent to no adjustment). Bars represent mean \pm SEM. $n=13-14$.

Parameter	VEH (n=14)	RIS (n=13)	PTH (n=14)	RIS + PTH (n=13)
Cortical Bone (37% site)				
Tt.Ar	1.39 ± 1.84	1.84 ± 1.32	1.47 ± 1.61	2.03 ± 1.92
Ct.Ar	6.79 ± 3.19	5.06 ± 4.23	6.09 ± 2.46	3.81 ± 1.96
Ma.Ar	-2.77 ± 3.16	-1.14 ± 3.15	-3.48 ± 4.44	0.48 ± 4.77
Ct.Th	8.78 ± 5.87	-0.22 ± 3.12	-1.62 ± 3.13	-2.93 ± 6.19
PMI	7.38 ± 4.15	4.51 ± 3.5	5.7 ± 2.03	3.5 ± 1.76
Ct.Ar/Tt.Ar	5.45 ± 2.94	2.9 ± 3.03	4.9 ± 3.09	2.02 ± 2.16
Ct.Po	6.79 ± 19.19	6.77 ± 27.15	42.89 ± 18.24	10.86 ± 15.34
Trabecular Bone				
BV/TV	68.47 ± 32.59	71.69 ± 72.53	84.24 ± 41.01	22.89 ± 16.63
Tb.Th	14.79 ± 7.07	5.52 ± 4.58	9.64 ± 8.9	9.12 ± 6.14
Tb.Sp	-2.38 ± 1.57	-1.42 ± 4.46	-3.22 ± 2.87	-0.71 ± 1.9
Tb.N	45.75 ± 24.06	90.31 ± 94.93	69.1 ± 36.76	18.63 ± 17.2
Tb.Pf	-15.28 ± 9.41	5.71 ± 17.28	-11.92 ± 11.2	14.91 ± 37.54
SMI	-3.14 ± 8.28	1.86 ± 10.27	-2.6 ± 6.84	-0.85 ± 13.9
Tb.Ct.Po	6.83 ± 9.03	5.24 ± 9.68	-3.37 ± 3.87	-12.99 ± 4.76

Table 14 – The effect of RIS and/or PTH treatment on the osteogenic response to loading in 22-month-old female mice.

Percentage change with loading was calculated for each mouse ((Right-left)/left * 100) and values reported are Mean ± SEM.

	Cortical (37% site)			Trabecular			
	RIS	PTH	RIS*PTH	RIS	PTH	RIS*PTH	
Tt.Ar	0.708	0.862	0.887	BV/TV	0.521	0.715	0.476
Ct.Ar	0.142	0.936	0.540	Tb.Th	0.485	0.912	0.532
Ma.Ar	0.499	0.570	0.636	Tb.Sp	0.551	0.984	0.790
Ct.Th	0.744	0.129	0.152	Tb.N	0.955	0.642	0.363
PMI	0.200	0.960	0.483	Tb.Pf	0.267	0.769	0.891
Ct.Ar/Tt.Ar	0.182	0.814	0.503	SMI	0.737	0.914	0.871
Ct.Po	0.434	0.328	0.435	Tb.Ct.Po	0.445	0.056	0.584

Table 15 - The effect of RIS and/or PTH treatment on the response to axial tibial loading in 22-month-old female mice.

Two-way ANOVA was used to analyse the percentage change with loading of cortical and trabecular bone sites in old (22m-old) female mice following 6 weeks of treatment with RIS and/or PTH and 2 weeks of loading in the final two weeks of treatment. Values reported are p-values following tests of between-subjects effects. p<0.05 for RIS*PTH indicates a significant difference in the response to loading in the presence of PTH as a result of concurrent RIS treatment. (n=13-14).

Site Specificity analysis

Further to our demonstration that neither PTH, nor RIS affected the response to loading in these 22-month-old mice at the 37% cortical or trabecular site, the lack of any significant RIS*PTH interaction for the response to loading for any parameter measured indicates that the response to loading following PTH is not significantly different from the response to loading following RIS+PTH.

As we had demonstrated site-specific effects of PTH and RIS treatment earlier in this chapter, we also performed SSA to evaluate the effects of RIS and/or PTH on the response to loading throughout the whole tibia. Table 16 illustrates the results following mixed model analysis.

	RIS	PTH	Site*RIS	Site*PTH	RIS*PTH	Site*RIS*PTH
TT.AR	0.228	0.709	0.478	0.001	0.518	0.455
CT.AR	0.850	0.890	0.780	0.006	0.356	0.876
MA.AR	0.378	0.826	0.120	0.106	0.161	0.080
CT.TH	0.107	0.085	0.171	0.166	0.195	0.882
PMI	0.393	0.563	0.332	<0.001	0.506	0.382
I_{MAX}	0.387	0.289	0.134	<0.001	0.422	0.968
I_{MIN}	0.303	0.601	0.992	0.001	0.666	0.687
CT.PO	0.361	0.176	0.035	0.823	0.417	0.835

Table 16 – The effect of PTH and RIS on the loading response of 22-month-old female mice by SSA.

Results shown are p-values from the Type III tests of fixed effects for the main effects and interactions following analysis of percentage change with loading values ((Right-left)/left)*100) using a mixed model approach. This analysis was performed using site as a fixed categorical variable, and RIS and PTH as fixed effects. p<0.05 for Site*RIS (or PTH) indicates significantly different responses to RIS (or PTH) at different sites of the bone. p<0.05 for RIS*PTH indicates a significant difference in the response to loading in the presence of PTH as a result of concurrent RIS treatment. p<0.05 for Site*RIS*PTH indicates that the effect of RIS on the PTH+loading response is significantly different at different sites. Values of p<0.05 are highlighted in bold type.

Effect of PTH on the response to loading

PTH treatment alone resulted in a site-specific increase ($p < 0.01$ for Site*PTH) for the change with loading for Tt.Ar and Ct.Ar, although after post-hoc comparisons, there was only 1-2 individual bone-sites proximally which demonstrated significantly greater response to loading following PTH treatment compared with vehicle treatment (Figure 85). PTH treatment did not significantly affect the response to loading for Ma.Ar and Ct.Th, although PTH-treated mice showed a tendency ($p = 0.085$) to increase Ct.Th less than vehicle treated mice (Figure 85). PTH treatment resulted in a site-specific increase in loading-related changes in PMI, I_{max} and I_{min} (Figure 85). For these measures, the metaphyseal bone sites appeared to tend towards an increase in loading-related improvement, however, following post-hoc testing, no individual bone sites were significantly different. PTH treatment did not affect the response to loading with respect to Ct.Po (Figure 85).

Effect of RIS on the response to loading

RIS treatment had no effect on the response to loading when considering Tt.Ar, Ct.Ar, Ma.Ar, Ct.Th, PMI, I_{max} and I_{min} (Figure 85 –, Figure 86), RIS treatment resulted in a site-specific response to loading for Ct.Po. RIS “protected” against the loading-related increase in Ct.Po in the mid-shaft tibia (56-59%), but resulted in a slight load-related increase in Ct.Po in the distal bone (data not shown).

Combined effect of RIS and PTH on the response to loading.

Similar to the single-site analysis performed earlier in this chapter, RIS treatment did not have any significant effect on the loading response seen following PTH treatment for any measure examined (Figure 85 –, Figure 86). However, in the distal sites, the response to mechanical loading was apparently greater following combined treatment with RIS+PTH than with either RIS or PTH alone. This response was most evident when examining Tt.Ar, Ct.Ar, PMI, I_{max} and I_{min} . (Figure 85 –, Figure 86). These changes were typically due to woven bone formation at the periosteum formed at the distal bone sites (Figure 87).

Figure 85 – legend on following page

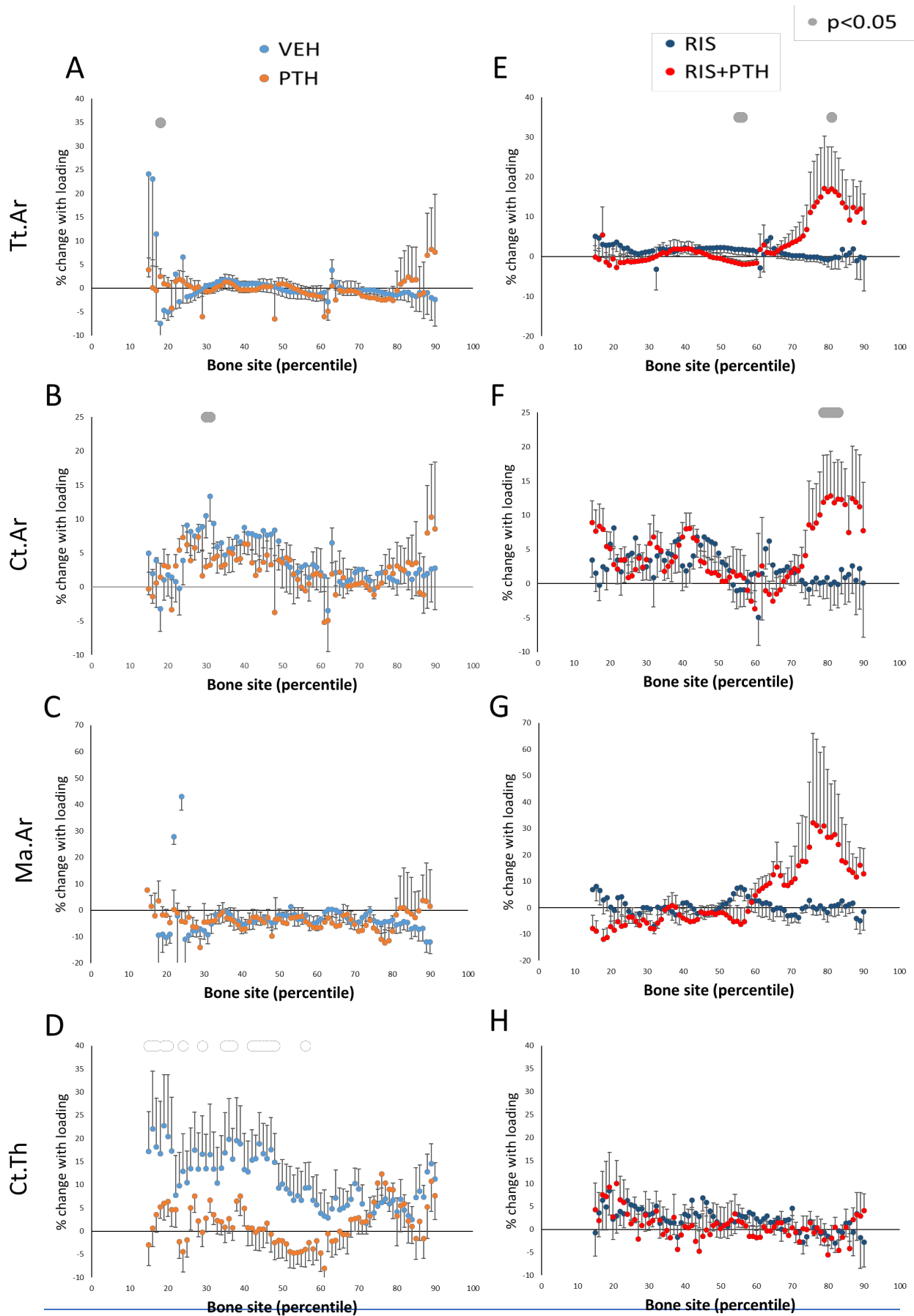


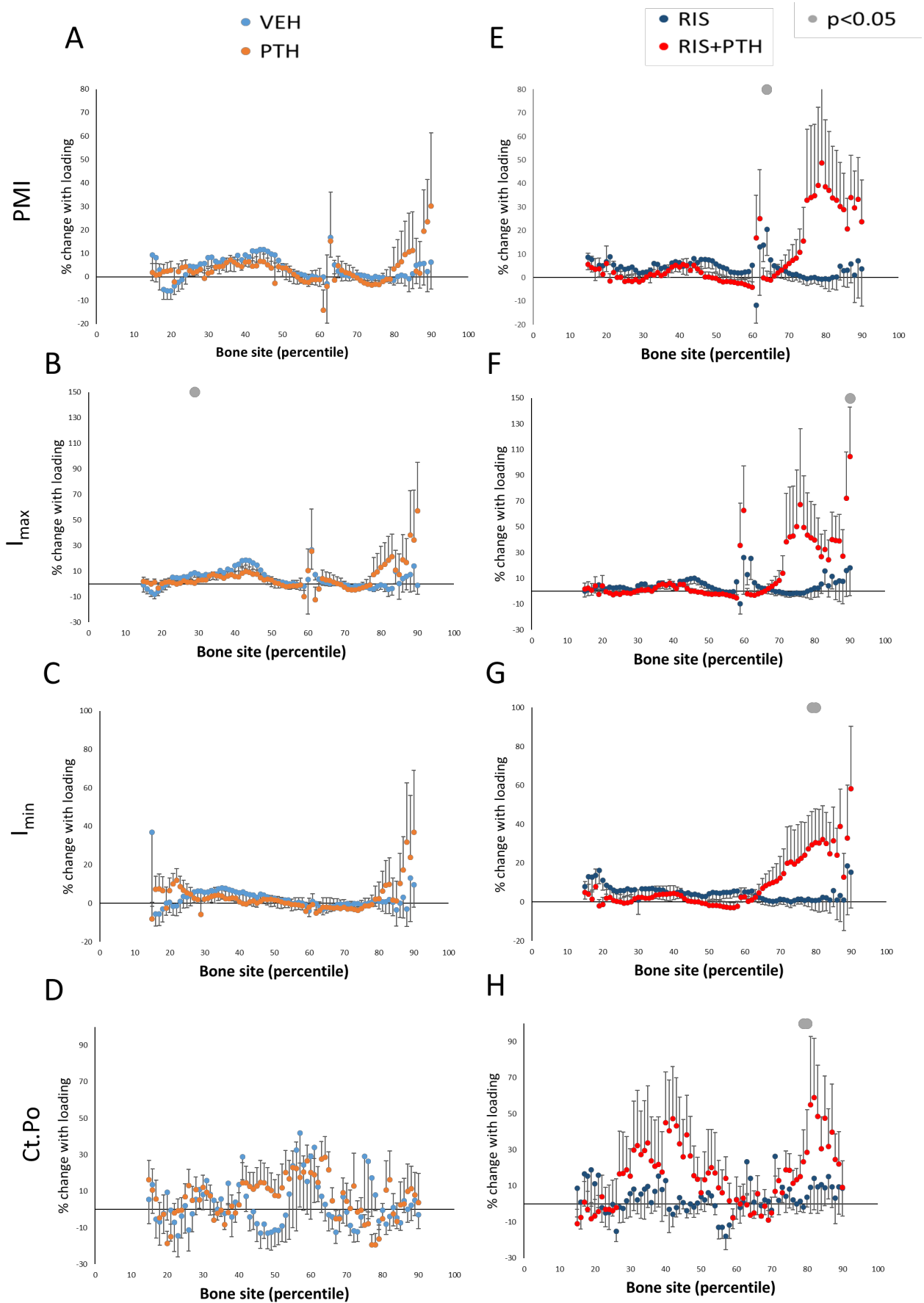
Figure 85 – The effect of PTH and combined RIS+PTH on the osteogenic response to loading in old female mice.

FIGURE ON PREVIOUS PAGE. SSA was performed on mice following 6 weeks of treatment with Vehicle or RIS and/or PTH and three-times weekly loading for the final two weeks. (A, E) Periosteally enclosed area (Tt.Ar), (B, F) Cortical bone area (Ct.Ar), (C, G) Medullary area (Ma.Ar), (D, H) Cortical thickness (Ct.Th) were compared between vehicle and PTH treated mice (A-D) and RIS and RIS+PTH mice (E-H). A mixed model approach was used to compare groups and Sidak post-hoc adjustments performed where effects were significant. Grey spots indicate individual sites that are significantly different ($p < 0.05$). Values indicate Mean \pm SEM. (n=13-14)

Figure 86 – The effect of PTH and combined RIS+PTH on the osteogenic response to loading in old female mice.

FIGURE ON FOLLOWING PAGE. SSA was performed on mice following 6 weeks of treatment with Vehicle or RIS and/or PTH and three-times weekly loading for the final two weeks. (A, E) Polar moment of inertia (PMI), (B, F) Maximum moment of inertia (I_{max}), (C, G) Minimum moment of inertia (I_{min}) and (D, H) Cortical porosity (Ct.Po) were compared between vehicle and PTH treated mice (A-D) and RIS and RIS+PTH mice (E-H). A mixed model approach was used to compare groups and Sidak post-hoc adjustments performed where effects were significant. Grey spots indicate individual sites that are significantly different ($p < 0.05$). Values indicate Mean \pm SEM. (n=13-14)

Figure 86 – legend on previous page



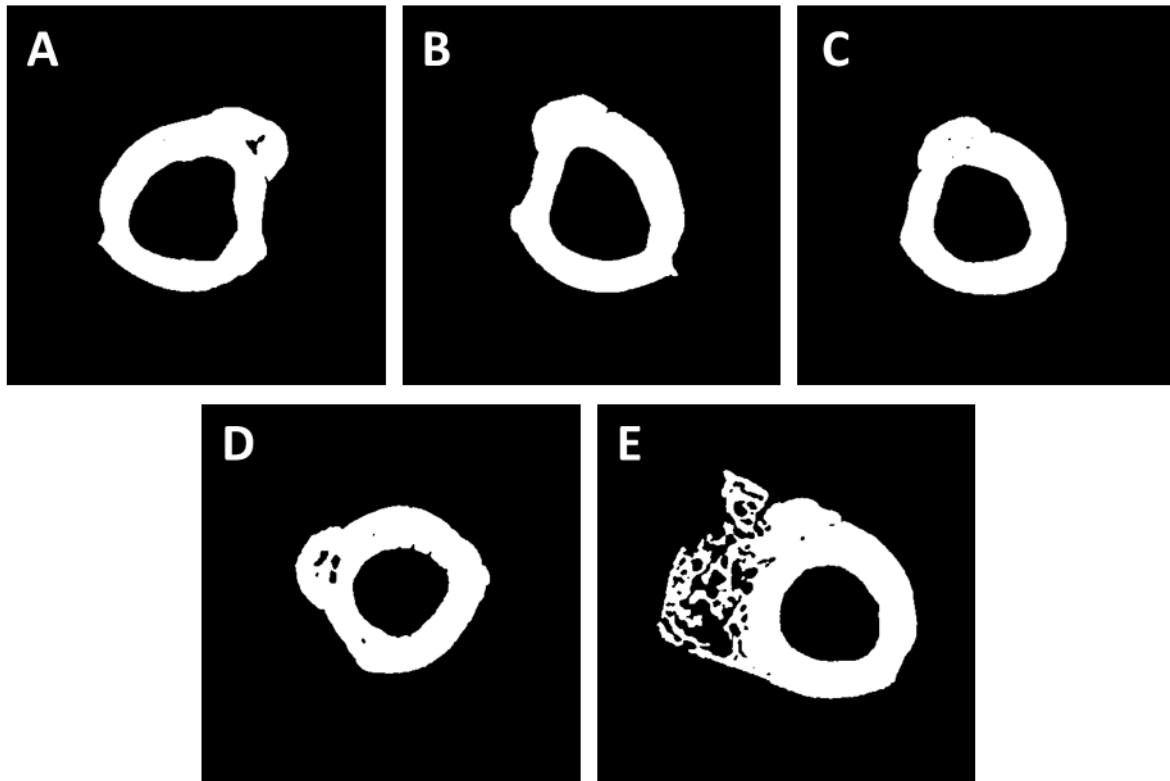


Figure 87 – The effect of RIS and/or PTH on the loading response in the distal tibia of 22-month-old female mice.

Binarised μ CT images following SSA, taken from the 82% bone site of (A) unloaded left tibia of vehicle (control) mouse, (B) loaded right tibia of vehicle (control) mouse, (C) loaded right tibia of RIS treated mouse, (D) loaded right tibia of PTH-treated mouse and (E) right loaded tibia of RIS+PTH treated mouse. Combined treatment appears to result in an exaggerated woven bone response to loading in the distal bone.

7.4.4 Results summary

1. The effect of PTH on the tibia of old female mice

- a. In trabecular bone, PTH treatment had no effect. However, a significant increase in the Ct.Po of the cortical shell at this specific level was observed.
- b. In the 37% cortical region, PTH treatment resulted in significant increases in periosteal expansion and subsequent increases in bone mass (Ct.Ar), but concurrent increases in cortical porosity.
- c. Following SSA, PTH treatment resulted in significant increases in Tt.Ar with concurrent decreases in Ma.Ar, resulting in increases in Ct.Ar and Ct.Th. These increases in periosteal expansion resulted in subsequent increases in measures of moment of inertia, particularly in the proximal bone, due to periosteal expansion. Ct.Po also increased following PTH treatment, primarily in the proximal bone.

2. The effect of RIS on the tibia of old female mice

- a. In trabecular bone, RIS treatment permitted an increase in BV/TV and an increase in trabecular connectivity (Tb.Pf) and a change from rod- to plate-like trabeculae (SMI).
- b. In the 37% cortical region, RIS treatment generated increases in Ct.Th which resulted in additive increases in Ct.Ar and Ct.Ar/Tt.Ar.
- c. Following SSA, RIS treatment resulted in decreased Ma.Ar and Ct.Po in the proximal bone, with increased Ct.Th in the distal bone.

3. The combined effect of PTH and RIS on the tibia of old female mice

- a. In trabecular bone, an increase in BV/TV and Tb.Pf, and a decrease in SMI was seen in mice treated with RIS+PTH that was not observed in mice treated with PTH alone.
- b. At the 37% cortical region, there were additive increases in Ct.Ar and Ct.Ar/Tt.Ar in mice treated with both PTH and RIS. There was no difference in Ct.Po between mice treated with RIS+PTH and those treated with PTH alone.

- c. Following SSA, a small but significant improvement in the response to PTH treatment for PMI and I_{\min} was seen following concurrent RIS treatment in the proximal cortical bone site. Furthermore, there were additive increases in Ct.Th, and additive decreases in Ma.Ar following combined PTH+RIS treatment.

4. The effect of RIS and PTH on the adaptive response to loading in old female mice

- a. Effect of Loading alone
 - i. Loading did not result in significant increases in bone mass at the 37% cortical bone site, although did result in a significant increase in BV/TV in the trabecular region. The mice used in this study were older than previously examined (22-month-old vs 19-month-old).
 - ii. SSA demonstrated that loading resulted in small but significant increases in bone mass, with decreases in Ma.Ar and increases in Ct.Ar and subsequent increases in bending strength (I_{\max}). These changes were only significant in the proximal regions of the bone. Loading also significantly reduced cortical porosity in the proximal cortical bone.
- b. Effect of PTH/RIS on the response to mechanical loading
 - i. At the 37% cortical site, using the single-site analysis technique and at the trabecular bone site, there was no significant effect of treatment with either PTH or RIS on the response to loading.
 - ii. Using SSA, PTH treatment resulted in a site-specific improvement in the response to loading for periosteal expansion and bone area, and subsequent increases in moments of inertia. RIS treatment alone resulted in a marginally lower change in Ct.Po, but did not affect the response to loading for any other parameter.
 - iii. There did appear to be an exaggerated periosteal woven bone response to loading evident in the distal cortical bone of mice treated with RIS+PTH which was not evident in the mice treated

with either agent alone, although this effect was not significant ($p>0.05$).

7.5 Discussion

In this chapter, we have demonstrated that PTH and RIS have additive effects on cortical bone mass and moments of inertia when administered concurrently in old female mice, and that inhibiting resorption through use of risedronate does not appear to impair the anabolic effect achieved by intermittent administration of PTH in old mice. Furthermore, despite observing a limited loading response in these very old mice, we have also demonstrated that neither PTH, nor risedronate, negatively affected the magnitude of the loading response, and in fact, PTH treatment resulted in a mild improvement load-related change in Tt.Ar in the proximal bone of 22-month-old mice, supporting the findings previously that both PTH and Risedronate act additively to the anabolic stimulus of loading to further improve cortical bone mass. This suggests that active resorption is not necessary to permit the anabolic activity of PTH to proceed.

7.5.1 PTH treatment increases bone mass, but concurrently increases porosity in old mice.

PTH treatment was anabolic in cortical bone in the present study, with increases in Ct.Ar and Tt.Ar, resulting in subsequent increases in calculated moments of inertia (indicators of likely bending/torsional strength). These changes are similar to other published responses to treatment with marked bone formation and subsequent increases in bone mass in both old and young mice [32, 388, 707, 708]. These changes were seen primarily in the proximal bone, but did demonstrate changes in Ct.Ar throughout the length of the cortical bone, suggesting a more generalised effect that that seen with mechanical loading [7, 11]. The response to PTH treatment has actually been demonstrated to be more effective in old mice, compared to young mice [707] which, these authors proposed, is due to additional anti-oxidant effects of PTH beyond those of the recognised anabolic effects demonstrated in young animals. Although there was no reported effect of PTH on

trabecular bone in these aged mice, similar findings to a recently published study by our laboratory [388], this may be due to the very low numbers of trabeculae in aged mice bone in the proximal tibia. This lack of response differs to the profuse anabolic response of trabecular bone seen in young mice treated with PTH [32].

The increase in intracortical porosity following PTH treatment in these mice mirrors that in our earlier study [388], and also that seen in mice with constitutively active PTH receptors [702, 708]. This increase in porosity was primarily identified in the proximal cortical bone, according to the SSA, similar to the findings in our earlier study [388]. The PTH-associated “pore” formation has been demonstrated to be associated with an influx of osteoclasts, demonstrated by increased cathepsin K staining and osteoclast localisation within the “pores” [388], suggesting these resorption events are mediated by osteoclasts, rather than by any other intracortical resorption event, such as that reported with osteocytic osteolysis reported in situations of lactation [83]. Our earlier study also demonstrated periostin-positive cells and concurrent bone formation (using fluorescent labelling) within these pores, suggesting that bone remodelling-based formation is occurring following PTH treatment as resorption and formation are spatially occurring in adjacent sites [388]. Contrary to the suggestion that all PTH-associated resorption is osteoclast mediated, however, PTH/PTHrP has been demonstrated to be associated with osteocytic osteolysis and perilacunar/pericanalicular demineralisation [709, 710] and this appears mediated via osteocytic production of Cathepsin K and TRAP [214]. Furthermore, genetically-modified mice lacking osteoclasts still showed evidence of pericanalicular resorption, indicating that osteoclasts are unnecessary for osteocytic osteolysis to occur [710]. Regardless of whether osteocytic osteolysis is involved in PTH-mediated resorption, the apparent increase in bone remodelling-based formation in mice following PTH treatment is supported by the finding that the anabolic effect of PTH in mice was impaired in the absence of osteoclasts promoted by RANKL antibody treatment (Denosumab)[700]. Although significant amounts of *de novo* bone formation without preceding resorption occur following PTH treatment, the coupling of bone formation to osteoclastic activity, stimulated by PTH still likely plays some role in its anabolic effect, although the

proportional contributions of modelling-based and remodelling-based bone formation following PTH treatment remains unclear.

7.5.2 RIS treatment has no effect on the anabolic effect of PTH in old mice

Due to the likelihood of remodelling playing a significant role in the anabolic effects of PTH in mice, we next explored the effect of the anti-resorptive RIS on the PTH response in old mice. Similar to the reports by Pierroz *et al* [700] and de Bakker *et al* [672], we did not observe any impairment of the anabolic effect of PTH following co-treatment with a bisphosphonate in these old female mice. Conversely, the study by Pierroz *et al* [700] has shown that reducing the number of osteoclasts with RANKL antibody (Denosumab) did impair the anabolic effect of PTH, however reducing their activity alone, without decreasing osteoclast numbers through treatment with the bisphosphonate alendronate, did not impair the anabolic response to PTH treatment. This suggests that the presence of osteoclasts, and not necessarily the active resorption of bone may be important for promoting the anabolic effect of PTH associated with “remodelling”. Alendronate treatment in a study by de Bakker *et al* [672] was associated with a significant reduction in osteoclast numbers. Although we did not quantify osteoclast numbers following RIS treatment in the present study, our earlier study demonstrated an increase in osteoclast numbers within the cortical pores generated following 4 weeks of PTH treatment [388]. Inhibition of resorption with both alendronate and risedronate does not require osteoclast apoptosis [711], so, given the PTH anabolic effect was not apparently affected by RIS treatment, it would appear plausible that the majority of the anabolic effect of PTH in the present study was not dependent on the active resorption of bone for its effect.

RIS treatment significantly reduced Ct.Po in the control limbs of mice in this study. Given the clear evidence of increased Ct.Po shown in this study, and increased Ct.Po and osteoclast activity within the intracortical pores in our previous study [388], it is perhaps surprising that treatment with RIS did not result in greater reduction in Ct.Po in PTH-treated mice than in Vehicle-treated mice. This could suggest that a proportion of the intracortical resorption seen following PTH treatment could be mediated by processes separate to those generated by osteoclasts, such as osteocytic osteolysis, as discussed

earlier. Mice lacking osteocytic cathepsin K and/or TRAP could help dissect the contribution of osteocytic osteolysis to the PTH-associated increase in Ct.Po in old mice.

Our study also demonstrated additive effects on the cortical bone mass of old female mice treated with combined PTH and RIS. This finding is mirrored by a study in young mice which similarly demonstrated additive effects on BV/TV following combined PTH and alendronate treatment by increasing formation and decreasing resorption respectively. Although these findings were only reported in trabecular bone of young adult mice [672], this study used longitudinal *in vivo* μ CT scanning to perform volumetric dynamic histomorphometry to evaluate both formation and resorption indices and the results suggested that the early anabolic responses to PTH are independent of resorption. Another study has demonstrated additive positive effects of PTH and alendronate in cortical bone using μ CT and histomorphometry [701].

Although molecular evidence suggests that use of antiresorptive treatments such as RIS may impair some of the cellular anabolic effects of PTH in bone, clinical and experimental evaluation of the effects of combination therapy appears to support their use together as beneficial to bone mass beyond the effects of therapy with either alone. Our study demonstrates that, even in old mice with lower bone mass and increased basal resorption, combined therapy with PTH and RIS can act additively to improve bone mass in mice. This is supported by several clinical studies demonstrating a positive clinical effect in combination therapy [350, 378, 703]. Another meta-analysis has demonstrated that alendronate has additive effects to PTH in cortical sites but can impair the anabolic effect of PTH in trabecular sites [671]. As the trabecular bone stock in aged female mice tibias is so small, it is difficult to draw conclusions in this study based on the combined effects of RIS and PTH. Future studies in aged mice looking to explore the effect of combination therapy on trabecular bone in aged female mice should examine bone sites with greater trabecular bone stock, such as the vertebrae, or the distal femur. This was outside the scope of the present study.

7.5.3 Mechanical loading is not affected by PTH and/or RIS treatment in old female mice

Previous studies have examined the effect of mechanical loading in mice following pre-treatment with RIS [34] and PTH [32] in young adult mice, and RIS (Chapter 6) and PTH [388] in old mice. These studies have all demonstrated additive or synergistic positive effects on bone mass when combining loading with RIS or PTH. We sought to determine if the loading response in old mice was affected following pretreatment with both PTH and RIS concurrently. The bone mass in vehicle-treated mice in this study was only mildly increased following loading, with BV/TV increased with loading in trabecular bone, and a small increase in Ct.Ar through a decrease in Ma.Ar, according to SSA. This response was reduced in magnitude to that reported in old mice by our laboratory previously, however this is possibly because the mice used in this study were 3 months older (22-months vs 19-months) than those previously reported (Chapters 5 & 6)[9, 29, 388, 396]. We also reduced the applied peak strain from 2500 $\mu\epsilon$ to 1800 $\mu\epsilon$ in this experiment to allow the potential additive effects on bone mass of both PTH and RIS to be observed (ie. we did not want the bones' adaptive capacity to be "maxed" out). It is therefore possible this applied strain was not sufficient to reach the minimum effective strain needed to stimulate bone formation in these older mice. 1800 $\mu\epsilon$ was sufficient to generate an osteogenic response in previous studies in 19-month-old mice [286, 388]. Despite the diminished response to mechanical loading in this study, comparison of the percentage changes with loading of μ CT parameters still enabled us to determine if the addition of PTH and/or RIS was able to alter the osteogenic effect of mechanical loading. The response to loading was unaffected by treatment with PTH or RIS individually in the old mice used in this study. This is consistent with the findings reported by Meakin *et al* [388] and those in chapter 6. Furthermore, treatment with RIS did not impair the osteogenic response achieved by combining loading and PTH.

Interestingly, when exploring the effect of combined therapy on the response to loading, the distal tibia demonstrated an apparent synergistic effect of RIS+PTH on the periosteal bone formation (Figure 85E-F, Figure 87) which subsequently affected the calculated

measures of moments of inertia (Figure 85 –E-G). Examination of the μ CT images from the tibia demonstrated that mechanical loading stimulated an apparent woven bone proliferative response in the periosteal distal tibia of mice following combined RIS/PTH treatment that was not present in vehicle treated mice, or those treated with either RIS or PTH alone. This finding is difficult to explain simply but could be due to regional changes in bone stiffness that were not accounted for by the single-site strain-gauging experiment measured at the ~37% site. For example, it may be possible for the distal tibia in RIS+PTH-treated mice to experience greater peak strains with loading calibrated to achieve a certain strain at the 37% site, compared to strains distally in monotherapy or vehicle treated mice, which could lead to the observed woven bone formation. Site-specific changes in the expression of sclerostin could also affect the loading response. PTH-mediated decrease in osteocytic sclerostin expression has been demonstrated to relate to the modelling-related bone formation response on the periosteal surface [702]. The distal tibial cortical bone does not normally respond to axial compressive mechanical loading [7, 8, 11], despite finite element modelling suggesting sufficient strains exist to permit formation. Interestingly, in addition to minimal bone formation, expression of sclerostin in the distal tibia does not change with loading [8]. This suggests that it could be the down-regulation of sclerostin mediated by PTH treatment combined with the reduced resorptive drive seen with RIS treatment which facilitates the observed periosteal woven bone response seen with loading in these aged mice. Furthermore, control of sclerostin expression has also recently been implicated in the osteogenic response to mechanical loading. Two separate studies have demonstrated an improved response to mechanical loading following either genetic deletion of sclerostin, or inhibition of sclerostin using an anti-sclerostin antibody [33, 372]. This further supports the suggestion that sclerostin could be involved in the site-specific differences in the loading response in mouse tibias.

In summary, treatment with PTH promoted an anabolic response in old female mice, which was additively improved by concurrent treatment with RIS. The loading response, despite being diminished by aging, was similarly not negatively affected by treatment with PTH and/or RIS. Combined treatment with PTH and RIS may have site-specifically improved the response to loading in the distal tibia, with increases in Tt.Ar suggesting an

improved periosteal response to loading. To the extent that these findings in experimental animals can be extrapolated to humans, from this study combined treatment with RIS and PTH appears to be beneficial for bone mass and the effects of concurrent physical activity should remain unaffected in the face of pharmaceutical management with combined anabolic and anti-resorptive therapy.

7.6 Conclusions

1. In very old (22-month-old) mice, PTH increased bone mass, as did RIS. The effects of PTH and RIS on Ct.Ar and Ct.Ar/Tt.Ar (following single site analysis) and PMI and I_{min} (following SSA) were additive. This suggests that osteoclastic resorption is not required for the anabolic effects of PTH, although this requires further investigation.
2. The osteogenic response to loading in these very old mice was lower than in 19-month-old mice. Neither PTH nor RIS alone, or in combination impaired the magnitude of the observed loading response. This is consistent with several earlier studies which have shown that bisphosphonate treatment does not impair bone's anabolic response to PTH or loading.
3. There may be some synergistic effect of combined treatment on bone's osteogenic response to loading in a site-specific manner, with the distal cortical bone demonstrating a greater periosteal woven bone response to loading following combined treatment that was not evident following monotherapy with either agent. This observation needs further investigation to confirm the finding, and if repeatable, to establish the mechanisms behind it.
4. Site-specificity analysis provides an added tool to explore the adaptive loading response in murine cortical bone which allowed detection of subtle, but significant changes in bone mass/architecture that were not identified by traditional single-site analysis.
5. The clinical implication of this finding is that any potential beneficial effects of exercise in the elderly will not be abrogated by PTH, RIS or a combination of both therapies.

Chapter 8

General Discussion

Chapter 8 - General Discussion

Studies described in this thesis have aimed to address the general hypothesis that altering the context within which mechanical loading is applied, either physically and/or pharmacologically, may affect the magnitude of the impaired adaptive response to mechanical loading in the aged skeleton, that normally provides a site-specific, and structurally appropriate, controlling influence on bone mass and architecture.

8.1 Optimising murine tibial loading models to study the effect of altering the loading context in old mice.

Since the primary goal of this thesis was to determine if altering the context on which loading was provided would alter the adaptive response to loading in old mice, we first needed to determine the optimal time points at which to examine the peak response to loading, both with respect to the “complete” adaptive loading response using μ CT and also the optimal time point to examine peak cellular activity for bone formation, using dynamic histomorphometry. Most commonly, loading experiments load mouse bones for two weeks, as significant bone formation is present at this time point [1, 8, 29, 34, 285, 287, 531, 582, 606, 608, 609]. We sought to determine at which point the adaptive response to loading reached a plateau in cortical bone, suggesting it had “habituated” to the newly applied load. Despite the reported study being a pilot study, we demonstrated that examining bone mass and architecture changes with μ CT 3 weeks after the onset of loading provided no less bone mass change than that reported after 4 weeks, suggesting that exploring the loading response after 3 weeks loading establishes the level of adaptive response once it has “plateaued” or “habituated”. Although a previous report determined that the adaptive response for trabecular bone following tail vertebral loading was significantly longer (10 weeks) than for our findings in cortical bone [586], our primary endpoint was to assess the cortical bone adaptive changes. For this reason, we selected 14-16 days of loading for the experiments included in the latter parts of this thesis, to permit a robust loading response which allowed for some further osteogenic response to be stimulated by the additional interventions planned in these studies.

Our study also demonstrated delayed onset bone resorption endosteally in response to continued mechanical loading, in a site-specific manner, with bone at the neutral axis of the cortical bone cross-section displaying evidence of bone resorption, despite a concurrent robust formation response in regions of increased strain according to FEM. Recent work using *in vivo* μ CT has demonstrated that the endosteal surface in mice tibias is more mechano-responsive than the periosteal surface and confirmed that resorption sites are associated with areas of low strain [529] supporting our conclusion. Ongoing collaborations with Professor Pivonka at the Queensland University of Technology aim to help identify if the adaptive response to loading can be predicted by modelling the expected strain and strain energy density. This new analysis tool may then help identify if the age-associated deficiency in the loading response is associated with reduced responsiveness to strain, without the need for *in vivo* μ CT. Recent *in vivo* μ CT evidence suggests that the mechanosensitivity of bone becomes dysregulated with age, with reduced ability to inhibit resorption or initiate formation [30].

The rate of bone formation in our study peaked in the second week of loading (between 7 and 14 days) periosteally, but was consistent throughout the experiment on the endosteal surface despite medullary area decreasing only after 2 weeks, then normalising back to control limb levels again at 3 weeks. It must be borne in mind that we only examined the most load responsive region of the cortical bone cross section in this experiment (posteriolateral cortex at 37% of the length of the bone measured from the proximal end). Notwithstanding, in experiments where the osteogenic cellular response is assessed, it appears that the optimal timepoint to assess the cellular proliferative/formation response to continued loading is in the second week of loading. We initially planned to explore mechanistic cellular responses to loading using DH in latter experiments of the thesis, however due to the negative results yielded from Chapter 4, we did not pursue these mechanistic endpoints.

Although still able to provide valuable information on the appropriate timing of sampling following the onset of loading in mice, this pilot study was not sufficiently powered to permit robust evaluation of the temporal response of the murine tibia to repeated

loading. It was also unable to absolutely confirm that formation had plateaued by 4 weeks following loading. Greater group size and a further, later time point after onset of loading would have helped mitigate these experimental limitations. Furthermore, the use of serial imaging via *in vivo* μ CT for this experiment could potentially have provided a further mechanism to provide measures of dynamic indices of bone formation and could have provided accurate and site-specific indices of resorption as seen in recent publications from the Julius Wolff Institute [33, 529, 612].

As we induce disuse in mice using a surgical procedure to transect the sciatic nerve, we wanted to ensure that a surgical insult alone was not sufficient to result in altered Receptor Activator for Nuclear Factor κ B Ligand (RANKL) expression. We did this because, as well as being an essential signalling factor for osteoclasts, and an apparently important factor in the bone loss associated with disuse [21], RANKL is also involved in several other pathways involved in inflammation [140]. Therefore, we performed a contralateral sham surgery in mice that underwent unilateral sciatic neurectomy to control for any potential effect surgery alone would have on RANKL expression. Before we examined this, we first needed to ensure that the act of sham surgery did not affect the degree of unilateral bone loss. Our further experiment exploring the effect of unilateral SN and contralateral sham surgery confirmed unilateral bone loss of similar magnitude to that previously reported [8, 11, 613]. The changes were also similar to the losses reported following tail suspension [614] and Botox injection [467]. Based on the results of this experiment, contralateral sham surgery performed concurrently to unilateral SN is unlikely to affect the contralateral limb's bone mass or architecture. For subsequent experiments in this thesis we therefore included sham surgery in our experimental design.

8.2 RANKL expression is unaffected in murine cortical bone following increased or decreased loading.

In addition to experiments aimed at determining if altering the context on which loading is provided can affect the adaptive loading response in old mice, we also sought to determine if the immediate cellular response to mechanical loading and disuse could be

used to help provide mechanistic insights to the deficient adaptive response in old mice and if these responses were affected once the loading context was changed. Work published at the time of conception of the experiments for this thesis demonstrated for the first time, that it is osteocytes, and not osteoblasts, as previously thought, that produce the RANKL necessary for the bone loss associated with disuse [21, 22]. This led us to hypothesise that the osteocytic expression of RANKL would be increased following disuse and decreased following loading, and that RANKL may be involved in the age-related impairment of the loading response. To explore this, we first developed a new protocol for the immunolocalisation of osteocytic RANKL in collaboration with Professor Larry Suva at the University of Arkansas for Medical Sciences and were able to identify multiple different suitable positive control cell populations in bone sections. Despite significant reductions in bone mass and the concurrent increase in the expression of sclerostin, disuse was not associated with changes in osteocytic RANKL protein expression in tibial cortical bone of young mice.

The original hypothesis that changes in loading may alter RANKL expression is supported by other studies published after this project was started. Pichler *et al* [645] demonstrated a decrease in RANKL expression in tibial trabecular osteoblasts following whole body vibration, whilst Plotkin *et al* [461] demonstrated an increase in RANKL positive osteocytes in vertebral bone following tail suspension (disuse). Both evaluations were, however, performed in primarily trabecular bone of young mice. We evaluated changes in diaphyseal cortical bone following SN or axial tibial loading as we were interested in the cortical bone adaptive response. This shows that there can be compartment specific (trabecular vs cortical) responses to the mechanical environment.

RANKL mRNA expression was also unaffected following both disuse and loading, despite changes in the expression of sclerostin. Other reports have demonstrated increases in RANKL mRNA expression following disuse [21, 614, 630] but these studies have examined the response in trabecular bone following tail suspension. The findings of the experiments described in Chapter 4, combined with existing studies suggest that regulation of RANKL expression in trabecular bone appears more important to the remodelling response than

changes in diaphyseal cortical bone. Further work exploring the effect of disuse on RANKL expression between several different sites will help elucidate any site-specificity to the changes seen following unloading.

However, as the expression of RANKL, in cortical bone at least, using the experimental techniques reported in this chapter, did not change in response to either increased or decreased levels of mechanical loading, we chose not to pursue RANKL as an endpoint for analysing the cellular response to loading and unloading in cortical bone for further studies described in this thesis. The investigation of mechanisms involved in bone biology has been dominated in recent years by cell-specific conditional mutation of certain genes to help prise apart the details of the pathways concerned. Further studies on the mechanical-load associated regulation of formation and resorption particularly focused on RANKL expression will be best pursued using genetically manipulated mice, and in particular, conditional knockout strains to help dissect the mechanisms involved in the regulation of the mechanostat.

8.3 Disuse “rescues” the age-impaired osteogenic response to loading in old mice.

Prior to evaluating the effect of prior disuse on the loading response in old female mice, we used the recently developed Site-Specificity Analysis (SSA) software [7] to describe the bone-wide effects of 3 weeks of SN on the tibiae of old female mice. This novel tool helped define an increase in bone loss, with subsequent increase in cortical porosity, primarily in the proximal cortical bone, demonstrating the usefulness of SSA in defining the response to treatment in old mice although some limitations were evident in particularly porous bone, as discussed in the original publication [7].

Our finding that prior and concurrent disuse improves the magnitude of the loading response in mice is not novel [35], however, our demonstration that the age-impaired loading response can be rescued by preceding loading with a short period of disuse engendered by SN is both novel and important. It suggests that the impairment of the loading response is not due to an intrinsic failure of the mechanisms involved in bone

formation seen following mechanical loading, but rather a rescuable reduction in the efficacy of these mechanisms that are effective in the young, healthy skeleton. Additionally, the rescue response is primarily due to an increase in the periosteal formative response, which directly improves the resistance to bending force better than the endosteal formation which is primarily stimulated in loading of normally ambulatory old mice [29].

Our results are supported by the findings of a recent study exploring the effect of prolonging the duration of disuse prior to loading in aged mice, which confirmed prior SN resulted in the “rescue” of age-impaired loading response, and that a longer duration of disuse (100d vs 5d) resulted in more robust increases in load-induced cortical bone formation in old mice [657]. Furthermore, in this study the trabecular bone loading-response was not rescued by prior disuse of any duration, similar to our findings.

The results of our study were limited by statistical power due to low experimental numbers, high experimental variability and experimental losses. However, our findings are supported by those of Meakin [4]. These experimental findings have been subsequently combined to yield the publication included in Appendix 4 [9], in which the author was joint primary author. Furthermore, the rescue phenomenon reported was also evident in the results of the experiment included in Chapter 6.

That reducing habitual loading of the tibia in aged mice by SN increases the periosteal osteogenic response to short periods of dynamic artificial loading suggests that the strain-related stimulus arising from ongoing normal ambulatory loading may modify the magnitude of the response to short periods of abnormal osteogenic stimulation. These results also suggest that there is no absolute inherent age-related impediment, either to the accurate assessment of strain and subsequent perception of strain, or to loading-related periosteal expansion in response to appropriate loading. As far as the data from old mice can be extrapolated to old humans, modification of the pattern of loading of bone may be able to improve the osteogenic response to loading and thus bone mass, although further studies which modify the pattern of loading applied to the bones of the elderly, to determine the effect on the adaptive loading response are necessary. Whilst

intentionally promoting disuse as an amplifier of the mechanostat cannot be advocated for human activity programmes, modified exercise programmes which alter the pattern of experimental loading to take advantage of the proposed strain-averaging mechanisms underlying the observed rescue should be considered.

8.4 Disuse-mediated “rescue” of the age-impaired adaptive loading response is not mediated by remodelling associated with prior disuse

The bisphosphonate, risedronate was shown to result in increased cortical bone mass and thickness, but to have no effect on trabecular bone. This was different to the effects reported in young mice [34]. This suggests that caution should be exercised in extrapolating age-sensitive results from experiments in young animals. Despite the age-specific differences in risedronate effects on control bones, the response to mechanical loading in old mice, as in young mice, was not affected by concurrent treatment with the anti-resorptive treatment, risedronate. This suggests that the anabolic response to loading, although diminished in old mice, is probably mediated by a bone modelling response, as in young mice [34].

The lack of effect of risedronate on the loading response in SN mice also suggests that an increase in basal remodeling associated with prior disuse is not involved in the observed “rescue” of the osteogenic response to loading seen in these old animals and that the likely mechanism involved in the observed rescue does not involve the processes of osteoclast:osteoblast coupling. This is consistent with our primary hypothesis that the observed rescue is mediated by a reduction in the strain-related stimulus normally associated with habitual loading permitting a more robust response to exogenously applied load and is inconsistent with the remodelling-based hypothesis.

Although this experiment has helped better define the mechanisms involved in the observed “rescue” seen following prior disuse in mice, quantification of osteoclast activity, using histochemical techniques, such as TRAP staining, and dynamic histomorphometric parameters, using fluorochrome labelling or *in vivo* μ CT scanning, could have provided further mechanistic insight into this phenomenon. Our original intent was to evaluate the

relationship of RANKL expression to the observed effect, but due to our lack of observed response in chapter 4, this objective was not pursued.

To the extent that the situation in old mice can be extrapolated to old humans, the benefits of risedronate treatment in maintaining bone mass are achieved without any impairment on the bone gain potentially conferred by increased loading. As remodeling is a more prevalent part of the adaptive response in humans, compared to that in mice, it is possible that the response in humans could be different to that in mice. As an extension of the proposed exercise programmes mentioned at the end of section 8.3, including humans who are treated with either bisphosphonates, or a placebo could help distinguish if any effect on the loading-related adaptive response engendered by the pattern of mechanical load applied is mediated by bone remodeling.

8.5 The anabolic response to PTH treatment is maintained following impairment of resorption in old mice.

In addition to mechanical loading in mice, parathyroid hormone (PTH) is one of the few stimuli which has been shown to reliably act as an anabolic treatment for bone. As we had demonstrated that mechanical loading and the associated rescue of the age-impaired loading response in old mice was mediated through a modelling-based bone formation, we next chose to investigate the effect of another potentially anabolic treatment, PTH, on bone mass in old mice, and the effect of concurrent treatment with the anti-resorptive drug, risedronate. PTH resulted in potent anabolism with periosteal bone apposition, but marked increase in cortical porosity, consistent with the findings of our recent publication [388]. When combined with risedronate, bone mass was additively increased with consequent increases in moments of inertia. Inhibiting resorption through use of risedronate does not appear to impair the anabolic effect achieved by intermittent administration of PTH in old mice. Furthermore, despite observing a limited loading response in these very old mice, we have also demonstrated that neither PTH, nor risedronate, negatively affected the magnitude of the loading response, and in fact, PTH treatment resulted in a mild improvement load-related change in periosteal area in the

proximal bone of very old (22-month-old) mice, supporting the findings previously that both PTH and Risedronate act additively to the anabolic stimulus of loading to further improve cortical bone mass [34, 388]. This suggests that active resorption is not necessary to permit the anabolic activity of PTH to proceed.

The present study was performed in very old (22m old) mice, older than the mice used in the previous experiments involving old female mice in this thesis, and also older than the mice used in other experiments performed by our laboratory using old mice, which were all 19-months-old [7, 9, 29, 285, 388, 396, 413, 686]. This increase in age was due to an unavoidable operational complication which delayed the start of the planned experiment by 3 months, but unfortunately limits the ability to compare to previous studies in this thesis and also in our other studies. Regardless, it demonstrates the further deterioration in the integrity of the loading response with advancing age. Additionally, we reduced the loading target strain to 1800 $\mu\epsilon$, from 2500 $\mu\epsilon$ in prior experiments, although this was to ensure that we did not saturate the anabolic response, given we were also administering the potently anabolic PTH. Furthermore, the study by Meakin *et al* [388] used a target strain of 1800 $\mu\epsilon$ and still achieved a significant loading response in 19m-old mice. To further confirm the anti-resorptive effect of risedronate, evaluation of osteoclast activity using TRAP staining to evaluate osteoclast numbers and serum evaluation of Collagen type 1 cross-linked N-telopeptide to evaluate bone resorption. This would help increase confidence in the findings of the experiment.

There has been increasing clinical interest in the combined use of drugs licensed for treatment of osteoporosis in recent years. The prospect of both improving bone formation, and reducing bone resorption through subsequent uncoupling of the remodelling pathway holds promise. Combined use of anti-resorptives and anabolic therapies has, however, demonstrated variable success. Recent meta-analysis of clinical trials exploring combined treatment of PTH with bisphosphonates has demonstrated that the sequence of treatment is important in the observed effect. Although there may be some degree of impairment in the anabolic effect of PTH in certain trabecular skeletal locations if its use is preceded by bisphosphonate treatment, in general PTH treatment

used prior to, or concurrently to bisphosphonates (or other anti-resorptives) generally results in additive positive effects to bone mass – particularly in the hip and spine [382]. Therefore, pursuit of strategies that combine individual treatment to maximise the net benefit to bone mass, and more importantly, fracture risk will become increasingly more important as the average age of the population of the developed world increases.

There may be some synergistic effect of combined treatment with PTH and risedronate on bone's osteogenic response to loading in a site-specific manner, with the distal cortical bone demonstrating a greater periosteal woven bone response to loading following combined treatment that was not evident following monotherapy with either agent. This observation needs further investigation to confirm the finding, and if repeatable, to establish the mechanisms behind it. Use of site-specific cellular histomorphometry, such as immunohistochemistry of key osteoregulatory proteins such as sclerostin Connexin 43 and periostin to determine the cellular mechanisms behind this periosteal proliferative response could help delineate the pathways involved in this apparent synergism of loading with combined PTH/risedronate treatment.

The clinical implication of the findings of this experiment are that any potential beneficial effects of exercise in the elderly should not be abrogated by PTH, risedronate or a combination of both therapies, however human trials exploring the effects of combined treatment with exercise/loading are lacking.

8.6 Conclusions and implications

The studies described in this thesis explored the effect of altering the context on which mechanical loading was applied to determine their effects on the age-impaired adaptive loading response in old mice.

1. Loading for between 2 and 3 weeks provides the optimal duration of loading to evaluate both histomorphometric and μ CT parameters in murine bone. The magnitude of unilateral bone loss associated with disuse engendered by SN is not affected by concurrent contralateral sham surgery.

2. RANKL expression is unchanged following both disuse and increased loading in female mice, suggesting changes in its expression are not necessary for the adaptive changes associated with altered mechanical loading. Secondly, as changes in its expression were not identifiable, its use as an experimental endpoint to evaluate response to mechanical loading is not recommended.
3. Prior disuse “rescued” the impaired response to mechanical loading in old female mice, suggesting that recent mechanical loading history modulates the response to loading and can restore the deficient response evident in old mice.
4. Risedronate treatment provided additive effects to mechanical loading in cortical bone of old female mice and concurrent risedronate treatment with disuse induced by SN did not impair the observed “rescue” phenomenon, suggesting that the mechanism behind the observed “rescue” is not based on an increase in the basal rate of remodelling promoted by disuse, but rather is associated with the nature of the existent strain environment.
5. Risedronate treatment does not impair the anabolic effect of PTH, nor does it affect the magnitude of the (already age-impaired) loading response in old female mice. This suggests that the anabolic effect of PTH on bone in old mice is not dependent on the increased bone remodelling activity promoted by its use.

Implications and further work

Although apparently essential for the bone loss associated with disuse, due to our failure to identify any detectable change in its expression following either disuse or increased loading, use of RANKL expression as an endpoint in later chapters was abandoned for this thesis. It appears, however, that the response of RANKL expression to mechanical loading may be different between the trabecular bone, and cortical bone, although no direct studies exist comparing the response to loading of both regions with the relative expression of RANKL. Combining longitudinal *in vivo* μ CT of both trabecular and cortical bone with histomorphometry and RANKL immunostaining may help determine if there is a site-specific difference in the response to changes in mechanical loading.

With respect to the potential clinical relevance of the pre-clinical findings in old mice from chapters 5-7, modifying the activity regimen of patients to incorporate reduced frequency but higher impact activity, instead of frequent low-impact activity may provide a non-pharmaceutical strategy to increase bone mass in a structurally appropriate manner. Bisphosphonates are commonly used as a frontline treatment for patients with low bone mass and increased risk of fragility fractures. As far as the results of experiments in old mice can be extrapolated to old people, use of risedronate should not affect the beneficial effects of mechanical loading, and if used in conjunction with PTH, should provide additive effects on cortical bone mass, without affecting the response to mechanical loading.

As mechanical loading provides a structurally appropriate adaptive response by providing strength where it is most needed, further studies leading on from the work reported in this thesis should focus on strategies which rescue the impaired mechanical loading response, such as altering the habitual strain environment with prior disuse, and the molecular mechanisms which underpin these phenomena. By exploring the molecular mechanisms underlying these observed “rescue” phenomena, further detail may be gleaned which aids the understanding of the loading-responsive pathways affected by aging.

Technically, use of *in vivo* longitudinal μ CT techniques, and other global bone assessment techniques such as SSA should be used to give a “whole-bone” assessment of the effects of given interventions which will permit a better global assessment of the effect of interventions and allow their correlation to computed endpoints, such as finite element modelling. Furthermore, following identification of potential candidate genes involved in these “rescue” strategies, the use of conditional cell-specific knockout strains of mice will help further dissect the complex cellular mechanisms involved in the age-related impairment of loading response. Further appreciation of these cellular mechanisms will also help identify selected strategies which could further augment the age-impaired response.

In addition to PTH, another anabolic therapy of particular interest to our laboratory is sclerostin antibody, which will hopefully be available for clinical use shortly, although it is

currently still in Phase III clinical trials with the US and European regulatory authorities. It appears there is a repeatable benefit to the magnitude of the loading response following reduction in sclerostin. Genetic deletion of osteocytic sclerostin, and its inhibition with antibodies alone have both been shown to be anabolic in mice but have also been shown to augment the adaptive response to mechanical loading in young mice [33, 372]. To confirm that the mechanostat in old animals can also be stimulated to improve the magnitude of its response to loading, future studies should explore the effect of sclerostin inhibition on the age-related impairment of the adaptive loading response in old mice as this could provide another avenue to “rescue” the impaired loading response. These studies, in addition to having strong clinical implications for patients with low bone mass, would also provide strong evidence that sclerostin is important in the pathways involved in the mechanostat and could be, at least in part, responsible for the impaired response to mechanical loading in old mice. Further human clinical trials should explore the effect of sclerostin antibody on the response to exercise/mechanical loading in osteoporotic people to see if the diminished response can be rescued.

Considering their reported involvement in bone’s response to mechanical loading, further investigation of Periostin [630, 662] and Connexin 43 [606, 659] as potential mechanistic signalling steps involved in the age-impaired loading response may help provide further targets and potential strategies to “rescue” the impaired loading response should also be considered. Pursuing these strategies to improve the loading response by combining treatments in old mice could provide “smart” anabolic strategies which improve bone mass and strength in areas where it is needed to effectively and efficiently combat age-related osteoporosis and other age-related bone disease.

References

1. Sugiyama, T., J.S. Price, and L.E. Lanyon, *Functional adaptation to mechanical loading in both cortical and cancellous bone is controlled locally and is confined to the loaded bones*. Bone, 2010. **46**(2): p. 314-21.
2. De Souza, R.L., M. Matsuura, F. Eckstein, S.C. Rawlinson, L.E. Lanyon, and A.A. Pitsillides, *Non-invasive axial loading of mouse tibiae increases cortical bone formation and modifies trabecular organization: a new model to study cortical and cancellous compartments in a single loaded element*. Bone, 2005. **37**(6): p. 810-8.
3. Zebaze, R.M., A. Ghasem-Zadeh, A. Bohte, S. Iuliano-Burns, M. Mirams, R.I. Price, E.J. Mackie, and E. Seeman, *Intracortical remodelling and porosity in the distal radius and post-mortem femurs of women: a cross-sectional study*. Lancet, 2010. **375**(9727): p. 1729-36.
4. Meakin, L.B., *The effect of ageing on bone's adaptive response to mechanical loading*, in *Faculty of Medical and Veterinary Sciences 2013*, University of Bristol: Bristol, UK. p. 392.
5. Lanyon, L.E., T. Sugiyama, and J.S. Price, *Regulation of bone mass: Local control or systemic influence or both?* IBMS BoneKEy, 2009. **6**(6): p. 218-226.
6. Galea, G., *The regulation in bone cells of Sost/sclerostin by mechanical strain*, in *Faculty of Medical and Veterinary Science*. 2012, University of Bristol: Bristol. p. 363.
7. Galea, G.L., S. Hannuna, L.B. Meakin, P.J. Delisser, L.E. Lanyon, and J.S. Price, *Quantification of alterations in cortical bone geometry using Site Specificity Software in mouse models of aging and the responses to ovariectomy and altered loading*. Frontiers in endocrinology, 2015. **6**.
8. Moustafa, A., T. Sugiyama, J. Prasad, G. Zaman, T.S. Gross, L.E. Lanyon, and J.S. Price, *Mechanical loading-related changes in osteocyte sclerostin expression in mice are more closely associated with the subsequent osteogenic response than the peak strains engendered*. Osteoporos Int, 2012. **23**(4): p. 1225-34.
9. Meakin, L.B., P.J. Delisser, G.L. Galea, L.E. Lanyon, and J.S. Price, *Disuse rescues the age-impaired adaptive response to external loading in mice*. Osteoporosis International, 2015: p. 1-6.
10. Lanyon, L.E., *Control of bone architecture by functional load bearing*. J Bone Miner Res, 1992. **7 Suppl 2**: p. S369-75.
11. Sugiyama, T., L.B. Meakin, W.J. Browne, G.L. Galea, J.S. Price, and L.E. Lanyon, *Bones' adaptive response to mechanical loading is essentially linear between the low strains associated with disuse and the high strains associated with the lamellar/woven bone transition*. J Bone Miner Res, 2012.
12. Frost, H.M., *Bone "mass" and the "mechanostat": a proposal*. Anat Rec, 1987. **219**(1): p. 1-9.
13. Frost, H.M., *Bone's mechanostat: a 2003 update*. Anat Rec A Discov Mol Cell Evol Biol, 2003. **275**(2): p. 1081-101.
14. Frost, H.M., *Utah Paradigm of Skeletal Physiology*. Vol. 1. 1960: International Society of Musculoskeletal and Neuronal Interactions.
15. Seeman, E., *Age- and menopause-related bone loss compromise cortical and trabecular microstructure*. J Gerontol A Biol Sci Med Sci, 2013. **68**(10): p. 1218-25.

16. Manolagas, S.C., *From estrogen-centric to aging and oxidative stress: a revised perspective of the pathogenesis of osteoporosis*. *Endocr Rev*, 2010. **31**(3): p. 266-300.
17. van Staa, T.P., E.M. Dennison, H.G. Leufkens, and C. Cooper, *Epidemiology of fractures in England and Wales*. *Bone*, 2001. **29**(6): p. 517-22.
18. Bonewald, L.F., *The Amazing Osteocyte*. *J Bone Miner Res*, 2011. **26**(2): p. 229-238.
19. Hemmatian, H., A.D. Bakker, J. Klein-Nulend, and G.H. van Lenthe, *Aging, Osteocytes, and Mechanotransduction*. *Curr Osteoporos Rep*, 2017. **15**(5): p. 401-411.
20. Robling, A.G., P.J. Niziolek, L.A. Baldridge, K.W. Condon, M.R. Allen, I. Alam, S.M. Mantila, J. Gluhak-Heinrich, T.M. Bellido, S.E. Harris, and C.H. Turner, *Mechanical stimulation of bone in vivo reduces osteocyte expression of Sost/sclerostin*. *Journal of Biological Chemistry*, 2008. **283**(9): p. 5866-5875.
21. Xiong, J., M. Onal, R.L. Jilka, R.S. Weinstein, S.C. Manolagas, and C.A. O'Brien, *Matrix-embedded cells control osteoclast formation*. *Nat Med*, 2011. **17**(10): p. 1235-41.
22. Nakashima, T., M. Hayashi, T. Fukunaga, K. Kurata, M. Oh-Hora, J.Q. Feng, L.F. Bonewald, T. Kodama, A. Wutz, E.F. Wagner, J.M. Penninger, and H. Takayanagi, *Evidence for osteocyte regulation of bone homeostasis through RANKL expression*. *Nat Med*, 2011. **17**(10): p. 1231-4.
23. Lanyon, L. and T. Skerry, *Postmenopausal osteoporosis as a failure of bone's adaptation to functional loading: a hypothesis*. *J Bone Miner Res*, 2001. **16**(11): p. 1937-47.
24. Rubin, C.T., S.D. Bain, and K.J. McLeod, *Suppression of the osteogenic response in the aging skeleton*. *Calcif Tissue Int*, 1992. **50**(4): p. 306-13.
25. Turner, C.H., Y. Takano, and I. Owan, *Aging changes mechanical loading thresholds for bone formation in rats*. *J Bone Miner Res*, 1995. **10**(10): p. 1544-9.
26. Kerr, D., A. Morton, I. Dick, and R. Prince, *Exercise effects on bone mass in postmenopausal women are site-specific and load-dependent*. *J Bone Miner Res*, 1996. **11**(2): p. 218-25.
27. Srinivasan, S., S.C. Agans, K.A. King, N.Y. Moy, S.L. Poliachik, and T.S. Gross, *Enabling bone formation in the aged skeleton via rest-inserted mechanical loading*. *Bone*, 2003. **33**(6): p. 946-55.
28. Prince, R., A. Devine, I. Dick, A. Criddle, D. Kerr, N. Kent, R. Price, and A. Randell, *The effects of calcium supplementation (milk powder or tablets) and exercise on bone density in postmenopausal women*. *J Bone Miner Res*, 1995. **10**(7): p. 1068-75.
29. Meakin, L.B., G.L. Galea, T. Sugiyama, L.E. Lanyon, and J.S. Price, *Age-related impairment of bones' adaptive response to loading in mice is associated with sex-related deficiencies in osteoblasts but no change in osteocytes*. *J Bone Miner Res*, 2014. **29**(8): p. 1859-71.
30. Razi, H., A.I. Birkhold, R. Weinkamer, G.N. Duda, B.M. Willie, and S. Checa, *Aging Leads to a Dysregulation in Mechanically Driven Bone Formation and Resorption*. *J Bone Miner Res*, 2015. **30**(10): p. 1864-73.
31. Birkhold, A.I., H. Razi, G.N. Duda, R. Weinkamer, S. Checa, and B.M. Willie, *The influence of age on adaptive bone formation and bone resorption*. *Biomaterials*, 2014. **35**(34): p. 9290-301.

32. Sugiyama, T., L.K. Saxon, G. Zaman, A. Moustafa, A. Sunters, J.S. Price, and L.E. Lanyon, *Mechanical loading enhances the anabolic effects of intermittent parathyroid hormone (1-34) on trabecular and cortical bone in mice*. Bone, 2008. **43**(2): p. 238-48.
33. Pflanz, D., A.I. Birkhold, L. Albiol, T. Thiele, C. Julien, A. Seliger, E. Thomson, I. Kramer, M. Kneissel, G.N. Duda, U. Kornak, S. Checa, and B.M. Willie, *Sost deficiency led to a greater cortical bone formation response to mechanical loading and altered gene expression*. Scientific Reports, 2017. **7**(1): p. 9435.
34. Sugiyama, T., L.B. Meakin, G.L. Galea, B.F. Jackson, L.E. Lanyon, F.H. Ebetino, R.G. Russell, and J.S. Price, *Risedronate does not reduce mechanical loading-related increases in cortical and trabecular bone mass in mice*. Bone, 2011.
35. de Souza, R.L., A.A. Pitsillides, L.E. Lanyon, T.M. Skerry, and C. Chenu, *Sympathetic nervous system does not mediate the load-induced cortical new bone formation*. J Bone Miner Res, 2005. **20**(12): p. 2159-68.
36. Xu, J., G. Lombardi, W. Jiao, and G. Banfi, *Effects of Exercise on Bone Status in Female Subjects, from Young Girls to Postmenopausal Women: An Overview of Systematic Reviews and Meta-Analyses*. Sports Med, 2016. **46**(8): p. 1165-82.
37. Quarles, L.D., *Skeletal secretion of FGF-23 regulates phosphate and vitamin D metabolism*. Nat Rev Endocrinol, 2012. **8**(5): p. 276-86.
38. Price, J.S., T. Sugiyama, G.L. Galea, L.B. Meakin, A. Sunters, and L.E. Lanyon, *Role of Endocrine and Paracrine Factors in the Adaptation of Bone to Mechanical Loading*. Curr Osteoporos Rep, 2011.
39. Wehrli, F.W., *Structural and functional assessment of trabecular and cortical bone by micro magnetic resonance imaging*. J Magn Reson Imaging, 2007. **25**(2): p. 390-409.
40. Muiznieks, L.D. and F.W. Keeley, *Molecular assembly and mechanical properties of the extracellular matrix: A fibrous protein perspective*. Biochimica et Biophysica Acta (BBA) - Molecular Basis of Disease, 2013. **1832**(7): p. 866-875.
41. Messina, C., G. Maffi, J.A. Vitale, F.M. Olivieri, G. Guglielmi, and L.M. Sconfienza, *Diagnostic imaging of osteoporosis and sarcopenia: a narrative review*. Quantitative Imaging in Medicine and Surgery, 2018. **8**(1): p. 86-99.
42. Kanis, J.A., E.V. McCloskey, H. Johansson, C. Cooper, R. Rizzoli, and J.-Y. Reginster, *European guidance for the diagnosis and management of osteoporosis in postmenopausal women*. Osteoporosis International, 2013. **24**(1): p. 23-57.
43. Wright, N.C., K.G. Saag, B. Dawson-Hughes, S. Khosla, and E.S. Siris, *The impact of the new National Bone Health Alliance (NBHA) diagnostic criteria on the prevalence of osteoporosis in the United States: supplementary presentation*. Osteoporos Int, 2017. **28**(11): p. 3283-3284.
44. Riggs, B.L., H.W. Wahner, L.J. Melton, 3rd, L.S. Richelson, H.L. Judd, and K.P. Offord, *Rates of bone loss in the appendicular and axial skeletons of women. Evidence of substantial vertebral bone loss before menopause*. J Clin Invest, 1986. **77**(5): p. 1487-91.
45. Riggs, B.L., L.J. Melton 3rd, R.A. Robb, J.J. Camp, E.J. Atkinson, J.M. Peterson, P.A. Rouleau, C.H. McCollough, M.L. Bouxsein, and S. Khosla, *Population-based study of age and sex differences in bone volumetric density, size, geometry, and structure at different skeletal sites*. J Bone Miner Res, 2004. **19**(12): p. 1945-54.

-
46. Khosla, S., B.L. Riggs, E.J. Atkinson, A.L. Oberg, L.J. McDaniel, M. Holets, J.M. Peterson, and L.J. Melton, 3rd, *Effects of sex and age on bone microstructure at the ultradistal radius: a population-based noninvasive in vivo assessment*. *J Bone Miner Res*, 2006. **21**(1): p. 124-31.
 47. Riggs, B.L., L.J. Melton, R.A. Robb, J.J. Camp, E.J. Atkinson, L. McDaniel, S. Amin, P.A. Rouleau, and S. Khosla, *A population-based assessment of rates of bone loss at multiple skeletal sites: evidence for substantial trabecular bone loss in young adult women and men*. *J Bone Miner Res*, 2008. **23**(2): p. 205-14.
 48. Uebelhart, D., F. Duboeuf, P.J. Meunier, and P.D. Delmas, *Lateral dual-photon absorptiometry: a new technique to measure the bone mineral density at the lumbar spine*. *J Bone Miner Res*, 1990. **5**(5): p. 525-31.
 49. Lian, J.B., G.S. Stein, J.L. Stein, and A.J. van Wijnen, *Regulated expression of the bone-specific osteocalcin gene by vitamins and hormones*. *Vitam Horm*, 1999. **55**: p. 443-509.
 50. Biver, E., F. Chopin, G. Coiffier, T.F. Brentano, B. Bouvard, P. Garnero, and B. Cortet, *Bone turnover markers for osteoporotic status assessment? A systematic review of their diagnosis value at baseline in osteoporosis*. *Joint Bone Spine*, 2012. **79**(1): p. 20-5.
 51. Wahner, H.W., W.L. Dunn, M.L. Brown, R.L. Morin, and B.L. Riggs, *Comparison of dual-energy x-ray absorptiometry and dual photon absorptiometry for bone mineral measurements of the lumbar spine*. *Mayo Clin Proc*, 1988. **63**(11): p. 1075-84.
 52. Miller, P.D., G. Hattersley, B. Riis, and et al., *Effect of abaloparatide vs placebo on new vertebral fractures in postmenopausal women with osteoporosis: A randomized clinical trial*. *JAMA*, 2016. **316**(7): p. 722-733.
 53. Body, J.-J., G.A. Gaich, W.H. Scheele, P.M. Kulkarni, P.D. Miller, A. Peretz, R.K. Dore, R. Correa-Rotter, A. Papaioannou, D.C. Cumming, and A.B. Hodsman, *A Randomized Double-Blind Trial to Compare the Efficacy of Teriparatide [Recombinant Human Parathyroid Hormone (1–34)] with Alendronate in Postmenopausal Women with Osteoporosis*. *The Journal of Clinical Endocrinology & Metabolism*, 2002. **87**(10): p. 4528-4535.
 54. Reginster, J.-Y., H.W. Minne, O.H. Sorensen, M. Hooper, C. Roux, M.L. Brandi, B. Lund, D. Ethgen, S. Pack, I. Roumagnac, and R. Eastell, *Randomized Trial of the Effects of Risedronate on Vertebral Fractures in Women with Established Postmenopausal Osteoporosis*. *Osteoporosis International*, 2000. **11**(1): p. 83-91.
 55. Black, D.M., S.R. Cummings, D.B. Karpf, J.A. Cauley, D.E. Thompson, M.C. Nevitt, D.C. Bauer, H.K. Genant, W.L. Haskell, R. Marcus, S.M. Ott, J.C. Torner, S.A. Quandt, T.F. Reiss, and K.E. Ensrud, *Randomised trial of effect of alendronate on risk of fracture in women with existing vertebral fractures*. *The Lancet*, 1996. **348**(9041): p. 1535-1541.
 56. Watts, N.B., S.T. Harris, H.K. Genant, R.D. Wasnich, P.D. Miller, R.D. Jackson, A.A. Licata, P. Ross, G.C.I. Woodson, M.J. Yanover, W.J. Mysiw, L. Kohse, M.B. Rao, P. Steiger, B. Richmond, and C.H.I. Chesnut *Intermittent Cyclical Etidronate Treatment of Postmenopausal Osteoporosis*. *New England Journal of Medicine*, 1990. **323**(2): p. 73-79.
 57. Carey, J.J. and M.F. Delaney, *Utility of DXA for monitoring, technical aspects of DXA BMD measurement and precision testing*. *Bone*, 2017.
 58. Cosman, F., S.J. de Beur, M.S. LeBoff, E.M. Lewiecki, B. Tanner, S. Randall, and R. Lindsay, *Clinician's Guide to Prevention and Treatment of Osteoporosis*. *Osteoporosis International*, 2014. **25**(10): p. 2359-2381.
-

59. Papaioannou, A., S. Morin, A.M. Cheung, S. Atkinson, J.P. Brown, S. Feldman, D.A. Hanley, A. Hodsman, S.A. Jamal, S.M. Kaiser, B. Kvern, K. Siminoski, W.D. Leslie, and f.t.S.A.C.o.O. Canada, *2010 clinical practice guidelines for the diagnosis and management of osteoporosis in Canada: summary*. Canadian Medical Association Journal, 2010. **182**(17): p. 1864-1873.
60. Knapp, K.M., J.R. Welsman, S.J. Hopkins, I. Fogelman, and G.M. Blake, *Obesity Increases Precision Errors in Dual-Energy X-Ray Absorptiometry Measurements*. Journal of Clinical Densitometry, 2012. **15**(3): p. 315-319.
61. Wang, J., B. Zhou, X.S. Liu, A.J. Fields, A. Sanyal, X. Shi, M. Adams, T.M. Keaveny, and X.E. Guo, *Trabecular plates and rods determine elastic modulus and yield strength of human trabecular bone*. Bone, 2015. **72**: p. 71-80.
62. Liu, X.S., J. Wang, B. Zhou, E. Stein, X. Shi, M. Adams, E. Shane, and X.E. Guo, *Fast trabecular bone strength predictions of HR-pQCT and individual trabeculae segmentation-based plate and rod finite element model discriminate postmenopausal vertebral fractures*. J Bone Miner Res, 2013. **28**(7): p. 1666-78.
63. Liu, X.S., A. Cohen, E. Shane, E. Stein, H. Rogers, S.L. Kokolus, P.T. Yin, D.J. McMahon, J.M. Lappe, R.R. Recker, and X.E. Guo, *Individual trabeculae segmentation (ITS)-based morphological analysis of high-resolution peripheral quantitative computed tomography images detects abnormal trabecular plate and rod microarchitecture in premenopausal women with idiopathic osteoporosis*. J Bone Miner Res, 2010. **25**(7): p. 1496-505.
64. Lespessailles, E., R. Hambli, and S. Ferrari, *Osteoporosis drug effects on cortical and trabecular bone microstructure: a review of HR-pQCT analyses*. Bonekey Rep, 2016. **5**: p. 836.
65. Bousson, V., A. Meunier, C. Bergot, É. Vicaut, M.A. Rocha, M.H. Morais, A.-M. Laval-Jeantet, and J.-D. Laredo, *Distribution of Intracortical Porosity in Human Midfemoral Cortex by Age and Gender*. Journal of Bone and Mineral Research, 2001. **16**(7): p. 1308-1317.
66. Nicks, K.M., S. Amin, E.J. Atkinson, B.L. Riggs, L.J. Melton, 3rd, and S. Khosla, *Relationship of age to bone microstructure independent of areal bone mineral density*. J Bone Miner Res, 2012. **27**(3): p. 637-44.
67. Gabet, Y. and I. Bab, *Microarchitectural changes in the aging skeleton*. Curr Osteoporos Rep, 2011. **9**(4): p. 177-83.
68. Silva, M.J., *Biomechanics of osteoporotic fractures*. Injury, 2007. **38 Suppl 3**: p. S69-76.
69. Mathieu, P.S. and E.G. Lobo, *Cytoskeletal and Focal Adhesion Influences on Mesenchymal Stem Cell Shape, Mechanical Properties, and Differentiation Down Osteogenic, Adipogenic, and Chondrogenic Pathways*. Tissue Eng Part B Rev, 2012.
70. Komori, T., *Runx2, a multifunctional transcription factor in skeletal development*. J Cell Biochem, 2002. **87**(1): p. 1-8.
71. Nakashima, K., X. Zhou, G. Kunkel, Z. Zhang, J.M. Deng, R.R. Behringer, and B. de Crombrughe, *The novel zinc finger-containing transcription factor osterix is required for osteoblast differentiation and bone formation*. Cell, 2002. **108**(1): p. 17-29.
72. Marie, P.J., *Transcription factors controlling osteoblastogenesis*. Arch Biochem Biophys, 2008. **473**(2): p. 98-105.

-
73. Chen, D., M. Zhao, and G.R. Mundy, *Bone morphogenetic proteins*. Growth Factors, 2004. **22**(4): p. 233-41.
 74. Wu, M., G. Chen, and Y.-P. Li, *TGF- β and BMP signaling in osteoblast, skeletal development, and bone formation, homeostasis and disease*. 2016. **4**: p. 16009.
 75. Dallas, S.L. and L.F. Bonewald, *Dynamics of the transition from osteoblast to osteocyte*. Ann N Y Acad Sci, 2010. **1192**: p. 437-43.
 76. Kalajzic, I., B.G. Matthews, E. Torreggiani, M.A. Harris, P. Divieti Pajevic, and S.E. Harris, *In vitro and in vivo approaches to study osteocyte biology*. Bone, 2013. **54**(2): p. 296-306.
 77. Zhang, J. and D.C. Link, *Targeting of Mesenchymal Stromal Cells by Cre-Recombinase Transgenes Commonly Used to Target Osteoblast Lineage Cells*. J Bone Miner Res, 2016. **31**(11): p. 2001-2007.
 78. Jilka, R.L., R.S. Weinstein, T. Bellido, A.M. Parfitt, and S.C. Manolagas, *Osteoblast programmed cell death (apoptosis): modulation by growth factors and cytokines*. J Bone Miner Res, 1998. **13**(5): p. 793-802.
 79. Franz-Odenaal, T.A., B.K. Hall, and P.E. Witten, *Buried alive: how osteoblasts become osteocytes*. Dev Dyn, 2006. **235**(1): p. 176-90.
 80. Holmbeck, K., P. Bianco, I. Pidoux, S. Inoue, R.C. Billingham, W. Wu, K. Chrysovergis, S. Yamada, H. Birkedal-Hansen, and A.R. Poole, *The metalloproteinase MT1-MMP is required for normal development and maintenance of osteocyte processes in bone*. J Cell Sci, 2005. **118**(Pt 1): p. 147-56.
 81. Okada, S., S. Yoshida, S.H. Ashrafi, and D.E. Schraufnagel, *The canalicular structure of compact bone in the rat at different ages*. Microsc Microanal, 2002. **8**(2): p. 104-15.
 82. Milovanovic, P., E.A. Zimmermann, M. Hahn, D. Djonic, K. Puschel, M. Djuric, M. Amling, and B. Busse, *Osteocytic canalicular networks: morphological implications for altered mechanosensitivity*. ACS Nano, 2013. **7**(9): p. 7542-51.
 83. Wysolmerski, J.J., *Osteocytes remove and replace perilacunar mineral during reproductive cycles*. Bone, 2013. **54**(2): p. 230-6.
 84. Tang, S.Y., R.P. Herber, S.P. Ho, and T. Alliston, *Matrix metalloproteinase-13 is required for osteocytic perilacunar remodeling and maintains bone fracture resistance*. J Bone Miner Res, 2012. **27**(9): p. 1936-50.
 85. Skerry, T.M., L. Bitensky, J. Chayen, and L.E. Lanyon, *Early strain-related changes in enzyme activity in osteocytes following bone loading in vivo*. J Bone Miner Res, 1989. **4**(5): p. 783-8.
 86. Zaman, G., L.K. Saxon, A. Sunters, H. Hilton, P. Underhill, D. Williams, J.S. Price, and L.E. Lanyon, *Loading-related regulation of gene expression in bone in the contexts of estrogen deficiency, lack of estrogen receptor alpha and disuse*. Bone, 2010. **46**(3): p. 628-42.
 87. Guo, D., A. Keightley, J. Guthrie, P.A. Veno, S.E. Harris, and L.F. Bonewald, *Identification of osteocyte-selective proteins*. Proteomics, 2010. **10**(20): p. 3688-98.
 88. Bonewald, L.F., *The Osteocyte Network as a Source and Reservoir of Signaling Factors*. Endocrinol Metab, 2010. **25**(3): p. 161-165.
 89. Xiong, J. and C.A. O'Brien, *Osteocyte RANKL: new insights into the control of bone remodeling*. J Bone Miner Res, 2012. **27**(3): p. 499-505.
-

90. Udagawa, N., N. Takahashi, T. Akatsu, H. Tanaka, T. Sasaki, T. Nishihara, T. Koga, T.J. Martin, and T. Suda, *Origin of osteoclasts: mature monocytes and macrophages are capable of differentiating into osteoclasts under a suitable microenvironment prepared by bone marrow-derived stromal cells*. Proc Natl Acad Sci U S A, 1990. **87**(18): p. 7260-4.
91. Boyce, B.F., Z. Yao, and L. Xing, *Osteoclasts have multiple roles in bone in addition to bone resorption*. Crit Rev Eukaryot Gene Expr, 2009. **19**(3): p. 171-80.
92. Wojtowicz, A., A. Dziedzic-Goclawska, A. Kaminski, W. Stachowicz, K. Wojtowicz, S.C. Marks, Jr., and M. Yamauchi, *Alteration of mineral crystallinity and collagen cross-linking of bones in osteopetrotic toothless (tl/tl) rats and their improvement after treatment with colony stimulating factor-1*. Bone, 1997. **20**(2): p. 127-32.
93. Felix, R., M.G. Cecchini, and H. Fleisch, *Macrophage colony stimulating factor restores in vivo bone resorption in the op/op osteopetrotic mouse*. Endocrinology, 1990. **127**(5): p. 2592-4.
94. Yoshida, H., S. Hayashi, T. Kunisada, M. Ogawa, S. Nishikawa, H. Okamura, T. Sudo, and L.D. Shultz, *The murine mutation osteopetrosis is in the coding region of the macrophage colony stimulating factor gene*. Nature, 1990. **345**(6274): p. 442-4.
95. Lacey, D.L., E. Timms, H.L. Tan, M.J. Kelley, C.R. Dunstan, T. Burgess, R. Elliott, A. Colombero, G. Elliott, S. Scully, H. Hsu, J. Sullivan, N. Hawkins, E. Davy, C. Capparelli, A. Eli, Y.X. Qian, S. Kaufman, I. Sarosi, V. Shalhoub, G. Senaldi, J. Guo, J. Delaney, and W.J. Boyle, *Osteoprotegerin ligand is a cytokine that regulates osteoclast differentiation and activation*. Cell, 1998. **93**(2): p. 165-76.
96. Yasuda, H., N. Shima, N. Nakagawa, K. Yamaguchi, M. Kinosaki, S. Mochizuki, A. Tomoyasu, K. Yano, M. Goto, A. Murakami, E. Tsuda, T. Morinaga, K. Higashio, N. Udagawa, N. Takahashi, and T. Suda, *Osteoclast differentiation factor is a ligand for osteoprotegerin/osteoclastogenesis-inhibitory factor and is identical to TRANCE/RANKL*. Proc Natl Acad Sci U S A, 1998. **95**(7): p. 3597-602.
97. Oursler, M.J., *Osteoclast synthesis and secretion and activation of latent transforming growth factor beta*. J Bone Miner Res, 1994. **9**(4): p. 443-52.
98. Erlebacher, A., E.H. Filvaroff, J.Q. Ye, and R. Derynck, *Osteoblastic responses to TGF-beta during bone remodeling*. Mol Biol Cell, 1998. **9**(7): p. 1903-18.
99. Lassen, N.E., T.L. Andersen, G.G. Pløen, K. Sjøe, E.M. Hauge, S. Harving, G.E.T. Eschen, and J.-M. Delaisse, *Coupling of Bone Resorption and Formation in Real Time: New Knowledge Gained From Human Haversian BMUs*. Journal of Bone and Mineral Research, 2017. **32**(7): p. 1395-1405.
100. Matsuo, K., *Cross-talk among bone cells*. Curr Opin Nephrol Hypertens, 2009. **18**(4): p. 292-7.
101. Kaunitz, J.D. and D.T. Yamaguchi, *TNAP, TrAP, ecto-purinergic signaling, and bone remodeling*. J Cell Biochem, 2008. **105**(3): p. 655-62.
102. Hauge, E.M., D. Qvesel, E.F. Eriksen, L. Mosekilde, and F. Melsen, *Cancellous bone remodeling occurs in specialized compartments lined by cells expressing osteoblastic markers*. J Bone Miner Res, 2001. **16**(9): p. 1575-82.
103. Andersen, T.L., T.E. Sondergaard, K.E. Skorzynska, F. Dagnaes-Hansen, T.L. Plesner, E.M. Hauge, T. Plesner, and J.M. Delaisse, *A physical mechanism for coupling bone resorption and formation in adult human bone*. Am J Pathol, 2009. **174**(1): p. 239-47.

-
104. Uda, Y., E. Azab, N. Sun, C. Shi, and P.D. Pajevic, *Osteocyte Mechanobiology*. Current Osteoporosis Reports, 2017. **15**(4): p. 318-325.
 105. Burger, E.H., J. Klein-Nulend, and T.H. Smit, *Strain-derived canalicular fluid flow regulates osteoclast activity in a remodelling osteon--a proposal*. J Biomech, 2003. **36**(10): p. 1453-9.
 106. Weinreb, M., G.A. Rodan, and D.D. Thompson, *Osteopenia in the immobilized rat hind limb is associated with increased bone resorption and decreased bone formation*. Bone, 1989. **10**(3): p. 187-94.
 107. Manolagas, S.C., *Birth and death of bone cells: basic regulatory mechanisms and implications for the pathogenesis and treatment of osteoporosis*. Endocr Rev, 2000. **21**(2): p. 115-37.
 108. Hadjidakis, D.J. and Androulakis, II, *Bone remodeling*. Ann N Y Acad Sci, 2006. **1092**: p. 385-96.
 109. Burr, D.B., R.B. Martin, M.B. Schaffler, and E.L. Radin, *Bone remodeling in response to in vivo fatigue microdamage*. J Biomech, 1985. **18**(3): p. 189-200.
 110. Mori, S. and D.B. Burr, *Increased intracortical remodeling following fatigue damage*. Bone, 1993. **14**(2): p. 103-109.
 111. Martin, R.B., *Targeted bone remodeling involves BMU steering as well as activation*. Bone, 2007. **40**(6): p. 1574-80.
 112. Kennedy, O.D., B.C. Herman, D.M. Laudier, R.J. Majeska, H.B. Sun, and M.B. Schaffler, *Activation of resorption in fatigue-loaded bone involves both apoptosis and active pro-osteoclastogenic signaling by distinct osteocyte populations*. Bone, 2012. **50**(5): p. 1115-22.
 113. Honma, M., Y. Ikebuchi, Y. Kariya, M. Hayashi, N. Hayashi, S. Aoki, and H. Suzuki, *RANKL subcellular trafficking and regulatory mechanisms in osteocytes*. Journal of Bone and Mineral Research, 2013: p. n/a-n/a.
 114. Udagawa, N., N. Takahashi, T. Akatsu, T. Sasaki, A. Yamaguchi, H. Kodama, T.J. Martin, and T. Suda, *The bone marrow-derived stromal cell lines MC3T3-G2/PA6 and ST2 support osteoclast-like cell differentiation in cocultures with mouse spleen cells*. Endocrinology, 1989. **125**(4): p. 1805-13.
 115. Takahashi, N., T. Akatsu, N. Udagawa, T. Sasaki, A. Yamaguchi, J.M. Moseley, T.J. Martin, and T. Suda, *Osteoblastic cells are involved in osteoclast formation*. Endocrinology, 1988. **123**(5): p. 2600-2.
 116. Xiong, J., M. Piemontese, M. Onal, J. Campbell, J.J. Goellner, V. Dusevich, L. Bonewald, S.C. Manolagas, and C.A. O'Brien, *Osteocytes, not Osteoblasts or Lining Cells, are the Main Source of the RANKL Required for Osteoclast Formation in Remodeling Bone*. PLoS One, 2015. **10**(9): p. e0138189.
 117. Dougall, W.C., M. Glaccum, K. Charrier, K. Rohrbach, K. Brasel, T. De Smedt, E. Daro, J. Smith, M.E. Tometsko, C.R. Maliszewski, A. Armstrong, V. Shen, S. Bain, D. Cosman, D. Anderson, P.J. Morrissey, J.J. Peschon, and J. Schuh, *RANK is essential for osteoclast and lymph node development*. Genes Dev, 1999. **13**(18): p. 2412-24.
 118. Kong, Y.Y., H. Yoshida, I. Sarosi, H.L. Tan, E. Timms, C. Capparelli, S. Morony, A.J. Oliveiras-Santos, G. Van, A. Itie, W. Khoo, A. Wakeham, C.R. Dunstan, D.L. Lacey, T.W. Mak, W.J.
-

- Boyle, and J.M. Penninger, *OPGL is a key regulator of osteoclastogenesis, lymphocyte development and lymph-node organogenesis*. *Nature*, 1999. **397**(6717): p. 315-23.
119. Bucay, N., I. Sarosi, C.R. Dunstan, S. Morony, J. Tarpley, C. Capparelli, S. Scully, H.L. Tan, W. Xu, D.L. Lacey, W.J. Boyle, and W.S. Simonet, *osteoprotegerin-deficient mice develop early onset osteoporosis and arterial calcification*. *Genes Dev*, 1998. **12**(9): p. 1260-8.
120. Mizuno, A., N. Amizuka, K. Irie, A. Murakami, N. Fujise, T. Kanno, Y. Sato, N. Nakagawa, H. Yasuda, S. Mochizuki, T. Gomibuchi, K. Yano, N. Shima, N. Washida, E. Tsuda, T. Morinaga, K. Higashio, and H. Ozawa, *Severe osteoporosis in mice lacking osteoclastogenesis inhibitory factor/osteoprotegerin*. *Biochem Biophys Res Commun*, 1998. **247**(3): p. 610-5.
121. Mizuno, A., T. Kanno, M. Hoshi, O. Shibata, K. Yano, N. Fujise, M. Kinoshita, K. Yamaguchi, E. Tsuda, A. Murakami, H. Yasuda, and K. Higashio, *Transgenic mice overexpressing soluble osteoclast differentiation factor (sODF) exhibit severe osteoporosis*. *J Bone Miner Metab*, 2002. **20**(6): p. 337-44.
122. Min, H., S. Morony, I. Sarosi, C.R. Dunstan, C. Capparelli, S. Scully, G. Van, S. Kaufman, P.J. Kostenuik, D.L. Lacey, W.J. Boyle, and W.S. Simonet, *Osteoprotegerin reverses osteoporosis by inhibiting endosteal osteoclasts and prevents vascular calcification by blocking a process resembling osteoclastogenesis*. *Journal of Experimental Medicine*, 2000. **192**(4): p. 463-74.
123. Hikita, A., I. Yana, H. Wakeyama, M. Nakamura, Y. Kadono, Y. Oshima, K. Nakamura, M. Seiki, and S. Tanaka, *Negative regulation of osteoclastogenesis by ectodomain shedding of receptor activator of NF-kappaB ligand*. *Journal of Biological Chemistry*, 2006. **281**(48): p. 36846-55.
124. Miyamoto, T., F. Arai, O. Ohneda, K. Takagi, D.M. Anderson, and T. Suda, *An adherent condition is required for formation of multinuclear osteoclasts in the presence of macrophage colony-stimulating factor and receptor activator of nuclear factor kappa B ligand*. *Blood*, 2000. **96**(13): p. 4335-43.
125. Suda, T., N. Takahashi, N. Udagawa, E. Jimi, M.T. Gillespie, and T.J. Martin, *Modulation of osteoclast differentiation and function by the new members of the tumor necrosis factor receptor and ligand families*. *Endocr Rev*, 1999. **20**(3): p. 345-57.
126. Nakashima, T., Y. Kobayashi, S. Yamasaki, A. Kawakami, K. Eguchi, H. Sasaki, and H. Sakai, *Protein expression and functional difference of membrane-bound and soluble receptor activator of NF-kappaB ligand: modulation of the expression by osteotropic factors and cytokines*. *Biochem Biophys Res Commun*, 2000. **275**(3): p. 768-75.
127. Singh, P.P., A.G. van der Kraan, J. Xu, M.T. Gillespie, and J.M. Quinn, *Membrane-bound receptor activator of NFkappaB ligand (RANKL) activity displayed by osteoblasts is differentially regulated by osteolytic factors*. *Biochem Biophys Res Commun*, 2012. **422**(1): p. 48-53.
128. Takai, H., M. Kanematsu, K. Yano, E. Tsuda, K. Higashio, K. Ikeda, K. Watanabe, and Y. Yamada, *Transforming growth factor-beta stimulates the production of osteoprotegerin/osteoclastogenesis inhibitory factor by bone marrow stromal cells*. *J Biol Chem*, 1998. **273**(42): p. 27091-6.
129. Kreja, L., A. Liedert, S. Hasni, L. Claes, and A. Ignatius, *Mechanical regulation of osteoclastic genes in human osteoblasts*. *Biochem Biophys Res Commun*, 2008. **368**(3): p. 582-7.

-
130. Mulcahy, L.E., D. Taylor, T.C. Lee, and G.P. Duffy, *RANKL and OPG activity is regulated by injury size in networks of osteocyte-like cells*. Bone, 2011. **48**(2): p. 182-8.
 131. Xu, X.Y., C. Guo, Y.X. Yan, Y. Guo, R.X. Li, M. Song, and X.Z. Zhang, *Differential effects of mechanical strain on osteoclastogenesis and osteoclast-related gene expression in RAW264.7 cells*. Mol Med Report, 2012. **6**(2): p. 409-15.
 132. Kulkarni, R.N., A.D. Bakker, V. Everts, and J. Klein-Nulend, *Mechanical loading prevents the stimulating effect of IL-1 β on osteocyte-modulated osteoclastogenesis*. Biochemical and Biophysical Research Communications, 2012. **420**(1): p. 11-16.
 133. Rubin, J., T.C. Murphy, J. Rahnert, H. Song, M.S. Nanes, E.M. Greenfield, H. Jo, and X. Fan, *Mechanical inhibition of RANKL expression is regulated by H-Ras-GTPase*. Journal of Biological Chemistry, 2006. **281**(3): p. 1412-8.
 134. Li, J., E. Rose, D. Frances, Y. Sun, and L. You, *Effect of oscillating fluid flow stimulation on osteocyte mRNA expression*. J Biomech, 2012. **45**(2): p. 247-51.
 135. Liu, C., Y. Zhao, W.Y. Cheung, R. Gandhi, L. Wang, and L. You, *Effects of cyclic hydraulic pressure on osteocytes*. Bone, 2010. **46**(5): p. 1449-56.
 136. Moriishi, T., R. Fukuyama, M. Ito, T. Miyazaki, T. Maeno, Y. Kawai, H. Komori, and T. Komori, *Osteocyte network; a negative regulatory system for bone mass augmented by the induction of Rankl in osteoblasts and Sost in osteocytes at unloading*. PLoS One, 2012. **7**(6): p. e40143.
 137. Sakai, A., T. Mori, M. Sakuma-Zenke, T. Takeda, K. Nakai, Y. Katae, H. Hirasawa, and T. Nakamura, *Osteoclast development in immobilized bone is suppressed by parathyroidectomy in mice*. J Bone Miner Metab, 2005. **23**(1): p. 8-14.
 138. Onal, M., J. Xiong, X. Chen, J.D. Thostenson, M. Almeida, S.C. Manolagas, and C.A. O'Brien, *Receptor Activator of Nuclear Factor kappaB Ligand (RANKL) Protein Expression by B Lymphocytes Contributes to Ovariectomy-induced Bone Loss*. J Biol Chem, 2012. **287**(35): p. 29851-60.
 139. Rossi, S.W., M.Y. Kim, A. Leibbrandt, S.M. Parnell, W.E. Jenkinson, S.H. Glanville, F.M. McConnell, H.S. Scott, J.M. Penninger, E.J. Jenkinson, P.J. Lane, and G. Anderson, *RANK signals from CD4(+) β 2-microglobulin(-) inducer cells regulate development of Aire-expressing epithelial cells in the thymic medulla*. Journal of Experimental Medicine, 2007. **204**(6): p. 1267-72.
 140. Hanada, R., T. Hanada, V. Sigl, D. Schramek, and J.M. Penninger, *RANKL/RANK-beyond bones*. J Mol Med (Berl), 2011. **89**(7): p. 647-56.
 141. Kartsogiannis, V., H. Zhou, N.J. Horwood, R.J. Thomas, D.K. Hards, J.M. Quinn, P. Niforas, K.W. Ng, T.J. Martin, and M.T. Gillespie, *Localization of RANKL (receptor activator of NF kappa B ligand) mRNA and protein in skeletal and extraskelatal tissues*. Bone, 1999. **25**(5): p. 525-34.
 142. Palafox, M., I. Ferrer, P. Pellegrini, S. Vila, S. Hernandez-Ortega, A. Urruticoechea, F. Climent, M.T. Soler, P. Munoz, F. Vinals, M. Tometsko, D. Branstetter, W.C. Dougall, and E. Gonzalez-Suarez, *RANK induces epithelial-mesenchymal transition and stemness in human mammary epithelial cells and promotes tumorigenesis and metastasis*. Cancer Res, 2012. **72**(11): p. 2879-88.
 143. Lipton, A., K. Fizazi, A.T. Stopeck, D.H. Henry, J.E. Brown, D.A. Yardley, G.E. Richardson, S. Siena, P. Maroto, M. Clemens, B. Bilynskyy, V. Charu, P. Beuzeboc, M. Rader, M. Viniegra, F. Saad, C. Ke, A. Braun, and S. Jun, *Superiority of denosumab to zoledronic acid for*
-

- prevention of skeletal-related events: A combined analysis of 3 pivotal, randomised, phase 3 trials.* Eur J Cancer, 2012. **48**(16): p. 3082-92.
144. Paller, C.J., M.A. Carducci, and G.K. Philips, *Management of bone metastases in refractory prostate cancer - role of denosumab.* Clin Interv Aging, 2012. **7**: p. 363-72.
145. Adami, S., C. Libanati, S. Boonen, S.R. Cummings, P.R. Ho, A. Wang, E. Siris, and J. Lane, *Denosumab Treatment in Postmenopausal Women with Osteoporosis Does Not Interfere with Fracture-Healing: Results from the FREEDOM Trial.* J Bone Joint Surg Am, 2012.
146. McClung, M.R., E.M. Lewiecki, M.L. Geller, M.A. Bolognese, M. Peacock, R.L. Weinstein, B. Ding, E. Rockabrand, R.B. Wagman, and P.D. Miller, *Effect of denosumab on bone mineral density and biochemical markers of bone turnover: 8-year results of a phase 2 clinical trial.* Osteoporos Int, 2012.
147. Andersen, T.L., M.E. Abdelgawad, H.B. Kristensen, E.M. Hauge, L. Rolighed, J. Bollerslev, P. Kjaersgaard-Andersen, and J.M. Delaisse, *Understanding coupling between bone resorption and formation: are reversal cells the missing link?* Am J Pathol, 2013. **183**(1): p. 235-46.
148. Abdelgawad, M.E., J.M. Delaisse, M. Hinge, P.R. Jensen, R.W. Alnaimi, L. Rolighed, L.H. Engelholm, N. Marcussen, and T.L. Andersen, *Early reversal cells in adult human bone remodeling: osteoblastic nature, catabolic functions and interactions with osteoclasts.* Histochem Cell Biol, 2016. **145**(6): p. 603-15.
149. Kristensen, H.B., T.L. Andersen, N. Marcussen, L. Rolighed, and J.M. Delaisse, *Osteoblast recruitment routes in human cancellous bone remodeling.* Am J Pathol, 2014. **184**(3): p. 778-89.
150. Sims, N.A. and T.J. Martin, *Coupling the activities of bone formation and resorption: a multitude of signals within the basic multicellular unit.* Bonekey Rep, 2014. **3**: p. 481.
151. Langdahl, B., S. Ferrari, and D.W. Dempster, *Bone modeling and remodeling: potential as therapeutic targets for the treatment of osteoporosis.* Therapeutic Advances in Musculoskeletal Disease, 2016. **8**(6): p. 225-235.
152. Delaisse, J.-M., *The reversal phase of the bone-remodeling cycle: cellular prerequisites for coupling resorption and formation.* BoneKEy Reports, 2014. **3**: p. 561.
153. Matic, I., B.G. Matthews, X. Wang, N.A. Dymont, D.L. Worthley, D.W. Rowe, D. Grcevic, and I. Kalajzic, *Quiescent Bone Lining Cells Are a Major Source of Osteoblasts During Adulthood.* Stem Cells, 2016. **34**(12): p. 2930-2942.
154. Matthews, B.G., E. Torreggiani, E. Roeder, I. Matic, D. Grcevic, and I. Kalajzic, *Osteogenic potential of alpha smooth muscle actin expressing muscle resident progenitor cells.* Bone, 2016. **84**: p. 69-77.
155. Grcevic, D., S. Pejda, B.G. Matthews, D. Repic, L. Wang, H. Li, M.S. Kronenberg, X. Jiang, P. Maye, D.J. Adams, D.W. Rowe, H.L. Aguila, and I. Kalajzic, *In vivo fate mapping identifies mesenchymal progenitor cells.* Stem Cells, 2012. **30**(2): p. 187-96.
156. Day, T.F. and Y. Yang, *Wnt and hedgehog signaling pathways in bone development.* J Bone Joint Surg Am, 2008. **90 Suppl 1**: p. 19-24.
157. Baron, R. and M. Kneissel, *WNT signaling in bone homeostasis and disease: from human mutations to treatments.* Nat Med, 2013. **19**(2): p. 179-92.

-
158. Duan, P. and L.F. Bonewald, *The role of the wnt/ β -catenin signaling pathway in formation and maintenance of bone and teeth*. The International Journal of Biochemistry & Cell Biology, 2016. **77**: p. 23-29.
159. Galea, G.L., L.E. Lanyon, and J.S. Price, *Sclerostin's role in bone's adaptive response to mechanical loading*. Bone, 2017. **96**: p. 38-44.
160. Moustafa, A., T. Sugiyama, L.K. Saxon, G. Zaman, A. Sunters, V.J. Armstrong, B. Javaheri, L.E. Lanyon, and J.S. Price, *The mouse fibula as a suitable bone for the study of functional adaptation to mechanical loading*. Bone, 2009. **44**(5): p. 930-5.
161. Glass, D.A., 2nd, P. Bialek, J.D. Ahn, M. Starbuck, M.S. Patel, H. Clevers, M.M. Taketo, F. Long, A.P. McMahon, R.A. Lang, and G. Karsenty, *Canonical Wnt signaling in differentiated osteoblasts controls osteoclast differentiation*. Dev Cell, 2005. **8**(5): p. 751-64.
162. Atkins, G.J., P.S. Rowe, H.P. Lim, K.J. Welldon, R. Ormsby, A.R. Wijenayaka, L. Zelenchuk, A. Evdokiou, and D.M. Findlay, *Sclerostin is a locally acting regulator of late-osteoblast/preosteocyte differentiation and regulates mineralization through a MEPE-ASARM-dependent mechanism*. J Bone Miner Res, 2011. **26**(7): p. 1425-36.
163. Marcellini, S., J.P. Henriquez, and A. Bertin, *Control of osteogenesis by the canonical Wnt and BMP pathways in vivo: cooperation and antagonism between the canonical Wnt and BMP pathways as cells differentiate from osteochondroprogenitors to osteoblasts and osteocytes*. Bioessays, 2012. **34**(11): p. 953-62.
164. Atkins, G.J. and D.M. Findlay, *Osteocyte regulation of bone mineral: a little give and take*. Osteoporos Int, 2012. **23**(8): p. 2067-79.
165. Kim, S.W., Y. Lu, E.A. Williams, F. Lai, J.Y. Lee, T. Enishi, D.H. Balani, M.S. Ominsky, H.Z. Ke, H.M. Kronenberg, and M.N. Wein, *Sclerostin Antibody Administration Converts Bone Lining Cells Into Active Osteoblasts*. J Bone Miner Res, 2017. **32**(5): p. 892-901.
166. McClung, M.R., A. Grauer, S. Boonen, M.A. Bolognese, J.P. Brown, A. Diez-Perez, B.L. Langdahl, J.Y. Reginster, J.R. Zanchetta, S.M. Wasserman, L. Katz, J. Maddox, Y.C. Yang, C. Libanati, and H.G. Bone, *Romozosumab in postmenopausal women with low bone mineral density*. N Engl J Med, 2014. **370**(5): p. 412-20.
167. Recker, R.R., C.T. Benson, T. Matsumoto, M.A. Bolognese, D.A. Robins, J. Alam, A.Y. Chiang, L. Hu, J.H. Krege, H. Sowa, B.H. Mitlak, and S.L. Myers, *A randomized, double-blind phase 2 clinical trial of blosozumab, a sclerostin antibody, in postmenopausal women with low bone mineral density*. J Bone Miner Res, 2015. **30**(2): p. 216-24.
168. Recknor, C.P., R.R. Recker, C.T. Benson, D.A. Robins, A.Y. Chiang, J. Alam, L. Hu, T. Matsumoto, H. Sowa, J.H. Sloan, R.J. Konrad, B.H. Mitlak, and A.A. Sipos, *The Effect of Discontinuing Treatment With Blosozumab: Follow-up Results of a Phase 2 Randomized Clinical Trial in Postmenopausal Women With Low Bone Mineral Density*. J Bone Miner Res, 2015. **30**(9): p. 1717-25.
169. Parfitt, A.M., *Age-related structural changes in trabecular and cortical bone: cellular mechanisms and biomechanical consequences*. Calcif Tissue Int, 1984. **36 Suppl 1**: p. S123-8.
170. Dunstan, C.R., N.M. Somers, and R.A. Evans, *Osteocyte death and hip fracture*. Calcif Tissue Int, 1993. **53 Suppl 1**: p. S113-6; discussion S116-7.
171. Weinstein, R.S., C. Wan, Q. Liu, Y. Wang, M. Almeida, C.A. O'Brien, J. Thostenson, P.K. Roberson, A.L. Boskey, T.L. Clemens, and S.C. Manolagas, *Endogenous glucocorticoids*
-

- decrease skeletal angiogenesis, vascularity, hydration, and strength in aged mice. Aging Cell*, 2010. **9**(2): p. 147-61.
172. Manolagas, S.C. and A.M. Parfitt, *What old means to bone*. *Trends Endocrinol Metab*, 2010. **21**(6): p. 369-74.
173. Weinstein, R.S., R.W. Nicholas, and S.C. Manolagas, *Apoptosis of osteocytes in glucocorticoid-induced osteonecrosis of the hip*. *J Clin Endocrinol Metab*, 2000. **85**(8): p. 2907-12.
174. Dodd, J.S., J.A. Raleigh, and T.S. Gross, *Osteocyte hypoxia: a novel mechanotransduction pathway*. *Am J Physiol*, 1999. **277**(3 Pt 1): p. C598-602.
175. Bakker, A., J. Klein-Nulend, and E. Burger, *Shear stress inhibits while disuse promotes osteocyte apoptosis*. *Biochem Biophys Res Commun*, 2004. **320**(4): p. 1163-8.
176. Yang, Y., X. Zheng, B. Li, S. Jiang, and L. Jiang, *Increased activity of osteocyte autophagy in ovariectomized rats and its correlation with oxidative stress status and bone loss*. *Biochem Biophys Res Commun*, 2014. **451**(1): p. 86-92.
177. Tomkinson, A., E.F. Gevers, J.M. Wit, J. Reeve, and B.S. Noble, *The role of estrogen in the control of rat osteocyte apoptosis*. *J Bone Miner Res*, 1998. **13**(8): p. 1243-50.
178. Emerton, K.B., B. Hu, A.A. Woo, A. Sinofsky, C. Hernandez, R.J. Majeska, K.J. Jepsen, and M.B. Schaffler, *Osteocyte apoptosis and control of bone resorption following ovariectomy in mice*. *Bone*, 2010. **46**(3): p. 577-83.
179. Noble, B.S., N. Peet, H.Y. Stevens, A. Brabbs, J.R. Mosley, G.C. Reilly, J. Reeve, T.M. Skerry, and L.E. Lanyon, *Mechanical loading: biphasic osteocyte survival and targeting of osteoclasts for bone destruction in rat cortical bone*. *Am J Physiol Cell Physiol*, 2003. **284**(4): p. C934-43.
180. Komori, T., *Cell Death in Chondrocytes, Osteoblasts, and Osteocytes*. *Int J Mol Sci*, 2016. **17**(12).
181. Shahnazari, M., D. Dwyer, V. Chu, F. Asuncion, M. Stolina, M. Ominsky, P. Kostenuik, and B. Halloran, *Bone turnover markers in peripheral blood and marrow plasma reflect trabecular bone loss but not endocortical expansion in aging mice*. *Bone*, 2012. **50**(3): p. 628-37.
182. Henriksen, K., D.J. Leeming, I. Byrjalsen, R.H. Nielsen, M.G. Sorensen, M.H. Dziegiel, T.J. Martin, C. Christiansen, P. Qvist, and M.A. Karsdal, *Osteoclasts prefer aged bone*. *Osteoporos Int*, 2007. **18**(6): p. 751-9.
183. Fan, W., R. Crawford, and Y. Xiao, *Structural and cellular differences between metaphyseal and diaphyseal periosteum in different aged rats*. *Bone*, 2008. **42**(1): p. 81-9.
184. Perrien, D.S., N.S. Akel, E.E. Dupont-Versteegden, R.A. Skinner, E.R. Siegel, L.J. Suva, and D. Gaddy, *Aging alters the skeletal response to disuse in the rat*. *Am J Physiol Regul Integr Comp Physiol*, 2007. **292**(2): p. R988-96.
185. Ota, K., P. Quint, M. Ruan, L. Pederson, J.J. Westendorf, S. Khosla, and M.J. Oursler, *Sclerostin is expressed in osteoclasts from aged mice and reduces osteoclast-mediated stimulation of mineralization*. *J Cell Biochem*, 2013. **114**(8): p. 1901-1907.
186. Liu, H., X. Xia, and B. Li, *Mesenchymal stem cell aging: Mechanisms and influences on skeletal and non-skeletal tissues*. *Exp Biol Med (Maywood)*, 2015. **240**(8): p. 1099-106.

-
187. Almeida, M. and C.A. O'Brien, *Basic biology of skeletal aging: role of stress response pathways*. J Gerontol A Biol Sci Med Sci, 2013. **68**(10): p. 1197-208.
 188. Kassem, M. and P.J. Marie, *Senescence-associated intrinsic mechanisms of osteoblast dysfunctions*. Aging Cell, 2011. **10**(2): p. 191-7.
 189. Bethel, M., B.R. Chitteti, E.F. Srouf, and M.A. Kacena, *The Changing Balance Between Osteoblastogenesis and Adipogenesis in Aging and its Impact on Hematopoiesis*. Current osteoporosis reports, 2013. **11**(2): p. 99-106.
 190. Abuna, R.P.F., C.T. Stringhetti-Garcia, L.P. Fiori, R.C.M. Dornelles, A.L. Rosa, and M.M. Beloti, *Aging impairs osteoblast differentiation of mesenchymal stem cells grown on titanium by favoring adipogenesis*. Journal of Applied Oral Science, 2016. **24**(4): p. 376-382.
 191. Ambrosi, T.H., A. Scialdone, A. Graja, S. Gohlke, A.M. Jank, C. Bocian, L. Woelk, H. Fan, D.W. Logan, A. Schurmann, L.R. Saraiva, and T.J. Schulz, *Adipocyte Accumulation in the Bone Marrow during Obesity and Aging Impairs Stem Cell-Based Hematopoietic and Bone Regeneration*. Cell Stem Cell, 2017. **20**(6): p. 771-784.e6.
 192. Zhang, W., G. Ou, M. Hamrick, W. Hill, J. Borke, K. Wenger, N. Chutkan, J. Yu, Q.S. Mi, C.M. Isales, and X.M. Shi, *Age-related changes in the osteogenic differentiation potential of mouse bone marrow stromal cells*. J Bone Miner Res, 2008. **23**(7): p. 1118-28.
 193. Sadie-Van Gijzen, H., F.S. Hough, and W.F. Ferris, *Determinants of bone marrow adiposity: The modulation of peroxisome proliferator-activated receptor- γ 2 activity as a central mechanism*. Bone, 2013. **56**(2): p. 255-265.
 194. Moerman, E.J., K. Teng, D.A. Lipschitz, and B. Lecka-Czernik, *Aging activates adipogenic and suppresses osteogenic programs in mesenchymal marrow stroma/stem cells: the role of PPAR-gamma2 transcription factor and TGF-beta/BMP signaling pathways*. Aging Cell, 2004. **3**(6): p. 379-89.
 195. Roholl, P.J., E. Blauw, C. Zurcher, J.A. Dormans, and H.M. Theuns, *Evidence for a diminished maturation of preosteoblasts into osteoblasts during aging in rats: an ultrastructural analysis*. J Bone Miner Res, 1994. **9**(3): p. 355-66.
 196. Almeida, M., L. Han, M. Martin-Millan, L.I. Plotkin, S.A. Stewart, P.K. Roberson, S. Kousteni, C.A. O'Brien, T. Bellido, A.M. Parfitt, R.S. Weinstein, R.L. Jilka, and S.C. Manolagas, *Skeletal involution by age-associated oxidative stress and its acceleration by loss of sex steroids*. J Biol Chem, 2007. **282**(37): p. 27285-97.
 197. Zhou, S., J.S. Greenberger, M.W. Epperly, J.P. Goff, C. Adler, M.S. Leboff, and J. Glowacki, *Age-related intrinsic changes in human bone-marrow-derived mesenchymal stem cells and their differentiation to osteoblasts*. Aging Cell, 2008. **7**(3): p. 335-43.
 198. Jiang, Y., H. Mishima, S. Sakai, Y.K. Liu, Y. Ohyabu, and T. Uemura, *Gene expression analysis of major lineage-defining factors in human bone marrow cells: effect of aging, gender, and age-related disorders*. J Orthop Res, 2008. **26**(7): p. 910-7.
 199. Stenderup, K., J. Justesen, C. Clausen, and M. Kassem, *Aging is associated with decreased maximal life span and accelerated senescence of bone marrow stromal cells*. Bone, 2003. **33**(6): p. 919-26.
 200. Baxter, M.A., R.F. Wynn, S.N. Jowitt, J.E. Wraith, L.J. Fairbairn, and I. Bellantuono, *Study of telomere length reveals rapid aging of human marrow stromal cells following in vitro expansion*. Stem Cells, 2004. **22**(5): p. 675-82.
-

201. Khosla, S. and D.G. Monroe, *Regulation of Bone Metabolism by Sex Steroids*. Cold Spring Harb Perspect Med, 2017.
202. Syed, F. and S. Khosla, *Mechanisms of sex steroid effects on bone*. Biochem Biophys Res Commun, 2005. **328**(3): p. 688-96.
203. Sinnesael, M., F. Claessens, S. Boonen, and D. Vanderschueren, *Novel insights in the regulation and mechanism of androgen action on bone*. Curr Opin Endocrinol Diabetes Obes, 2013. **20**(3): p. 240-4.
204. D'Amour, P., *Acute and chronic regulation of circulating PTH: significance in health and in disease*. Clin Biochem, 2012. **45**(12): p. 964-9.
205. Govoni, K.E., *Insulin-like growth factor-I molecular pathways in osteoblasts: potential targets for pharmacological manipulation*. Curr Mol Pharmacol, 2012. **5**(2): p. 143-52.
206. Fei, Y. and M.M. Hurley, *Role of fibroblast growth factor 2 and Wnt signaling in anabolic effects of parathyroid hormone on bone formation*. J Cell Physiol, 2012. **227**(11): p. 3539-45.
207. Perrini, S., L. Laviola, M.C. Carreira, A. Cignarelli, A. Natalicchio, and F. Giorgino, *The GH/IGF1 axis and signaling pathways in the muscle and bone: mechanisms underlying age-related skeletal muscle wasting and osteoporosis*. J Endocrinol, 2010. **205**(3): p. 201-10.
208. Bhattacharyya, N., W.H. Chong, R.I. Gafni, and M.T. Collins, *Fibroblast growth factor 23: state of the field and future directions*. Trends Endocrinol Metab, 2012. **23**(12): p. 610-8.
209. de Paula, F.J. and C.J. Rosen, *Back to the future: revisiting parathyroid hormone and calcitonin control of bone remodeling*. Horm Metab Res, 2010. **42**(5): p. 299-306.
210. Seki, K., N. Makimura, C. Mitsui, J. Hirata, and I. Nagata, *Calcium-regulating hormones and osteocalcin levels during pregnancy: a longitudinal study*. Am J Obstet Gynecol, 1991. **164**(5 Pt 1): p. 1248-52.
211. Cross, B.M., G.E. Breitwieser, T.A. Reinhardt, and R. Rao, *Cellular calcium dynamics in lactation and breast cancer: from physiology to pathology*. American Journal of Physiology - Cell Physiology, 2014. **306**(6): p. C515-C526.
212. Kovacs, C.S., *Calcium and bone metabolism during pregnancy and lactation*. J Mammary Gland Biol Neoplasia, 2005. **10**(2): p. 105-18.
213. Lee, D.B., L.L. Hardwick, M.S. Hu, and N. Jamgotchian, *Vitamin D-independent regulation of calcium and phosphate absorption*. Miner Electrolyte Metab, 1990. **16**(2-3): p. 167-73.
214. Qing, H., L. Ardeshirpour, P.D. Pajevic, V. Dusevich, K. Jahn, S. Kato, J. Wysolmerski, and L.F. Bonewald, *Demonstration of osteocytic perilacunar/canalicular remodeling in mice during lactation*. J Bone Miner Res, 2012. **27**(5): p. 1018-29.
215. Kogawa, M., A.R. Wijenayaka, R.T. Ormsby, G.P. Thomas, P.H. Anderson, L.F. Bonewald, D.M. Findlay, and G.J. Atkins, *Sclerostin regulates release of bone mineral by osteocytes by induction of carbonic anhydrase 2*. J Bone Miner Res, 2013. **28**(12): p. 2436-48.
216. VanHouten, J.N. and J.J. Wysolmerski, *Low estrogen and high parathyroid hormone-related peptide levels contribute to accelerated bone resorption and bone loss in lactating mice*. Endocrinology, 2003. **144**(12): p. 5521-9.

-
217. Sowers, M.F., B.W. Hollis, B. Shapiro, J. Randolph, C.A. Janney, D. Zhang, A. Schork, M. Crutchfield, F. Stanczyk, and M. Russell-Aulet, *Elevated parathyroid hormone-related peptide associated with lactation and bone density loss*. *Jama*, 1996. **276**(7): p. 549-54.
218. Kirby, B.J., Y. Ma, H.M. Martin, K.L. Buckle Favaro, A.C. Karaplis, and C.S. Kovacs, *Upregulation of calcitriol during pregnancy and skeletal recovery after lactation do not require parathyroid hormone*. *J Bone Miner Res*, 2013. **28**(9): p. 1987-2000.
219. Ma, Y.L., R.L. Cain, D.L. Halladay, X. Yang, Q. Zeng, R.R. Miles, S. Chandrasekhar, T.J. Martin, and J.E. Onyia, *Catabolic effects of continuous human PTH (1--38) in vivo is associated with sustained stimulation of RANKL and inhibition of osteoprotegerin and gene-associated bone formation*. *Endocrinology*, 2001. **142**(9): p. 4047-54.
220. Locklin, R.M., S. Khosla, R.T. Turner, and B.L. Riggs, *Mediators of the biphasic responses of bone to intermittent and continuously administered parathyroid hormone*. *J Cell Biochem*, 2003. **89**(1): p. 180-90.
221. Gardella, T., *Interactions of PTH with receptors and signaling*. *The Parathyroids: Basic and Clinical Concepts*. Third ed. Elsevier Inc, 2015: p. 65-80.
222. Leder, B.Z., *Parathyroid Hormone and Parathyroid Hormone-Related Protein Analogs in Osteoporosis Therapy*. *Current Osteoporosis Reports*, 2017. **15**(2): p. 110-119.
223. Hansen, S., E.M. Hauge, J.E. Beck Jensen, and K. Brixen, *Differing effects of PTH 1-34, PTH 1-84, and zoledronic acid on bone microarchitecture and estimated strength in postmenopausal women with osteoporosis: An 18-month open-labeled observational study using HR-pQCT*. *Journal of Bone and Mineral Research*, 2013. **28**(4): p. 736-745.
224. Macdonald, H.M., K.K. Nishiyama, D.A. Hanley, and S.K. Boyd, *Changes in trabecular and cortical bone microarchitecture at peripheral sites associated with 18 months of teriparatide therapy in postmenopausal women with osteoporosis*. *Osteoporos Int*, 2011. **22**(1): p. 357-62.
225. Ballane, G., J.A. Cauley, M.M. Luckey, and G. El-Hajj Fuleihan, *Worldwide prevalence and incidence of osteoporotic vertebral fractures*. *Osteoporos Int*, 2017. **28**(5): p. 1531-1542.
226. Almeida, M., M.R. Laurent, V. Dubois, F. Claessens, C.A. O'Brien, R. Bouillon, D. Vanderschueren, and S.C. Manolagas, *Estrogens and Androgens in Skeletal Physiology and Pathophysiology*. *Physiol Rev*, 2017. **97**(1): p. 135-187.
227. Sapir-Koren, R. and G. Livshits, *Osteocyte control of bone remodeling: is sclerostin a key molecular coordinator of the balanced bone resorption-formation cycles?* *Osteoporosis International*, 2014. **25**(12): p. 2685-2700.
228. Khalid, A.B. and S.A. Krum, *Estrogen receptors alpha and beta in bone*. *Bone*, 2016. **87**: p. 130-5.
229. Windahl, S.H., G. Andersson, and J.A. Gustafsson, *Elucidation of estrogen receptor function in bone with the use of mouse models*. *Trends Endocrinol Metab*, 2002. **13**(5): p. 195-200.
230. Borjesson, A.E., M.K. Lagerquist, S.H. Windahl, and C. Ohlsson, *The role of estrogen receptor alpha in the regulation of bone and growth plate cartilage*. *Cell Mol Life Sci*, 2013. **70**(21): p. 4023-37.
231. Karimian, E. and L. Savendahl, *Estrogen signaling in growth plate cartilage*. *Endocr Dev*, 2011. **21**: p. 42-51.
-

232. Lee, K., H. Jessop, R. Suswillo, G. Zaman, and L. Lanyon, *Endocrinology: bone adaptation requires oestrogen receptor-alpha*. *Nature*, 2003. **424**(6947): p. 389.
233. Frenkel, B., A. Hong, S.K. Baniwal, G.A. Coetzee, C. Ohlsson, O. Khalid, and Y. Gabet, *Regulation of adult bone turnover by sex steroids*. *J Cell Physiol*, 2010. **224**(2): p. 305-10.
234. Riggs, B.L., S. Khosla, and L.J. Melton, 3rd, *Sex steroids and the construction and conservation of the adult skeleton*. *Endocr Rev*, 2002. **23**(3): p. 279-302.
235. Bouxsein, M.L., K.S. Myers, K.L. Shultz, L.R. Donahue, C.J. Rosen, and W.G. Beamer, *Ovariectomy-induced bone loss varies among inbred strains of mice*. *J Bone Miner Res*, 2005. **20**(7): p. 1085-92.
236. Fitzpatrick, L.A., E. Buzas, T.J. Gagne, A. Nagy, C. Horvath, V. Ferencz, A. Mester, B. Kari, M. Ruan, A. Falus, and J. Barsony, *Targeted deletion of histidine decarboxylase gene in mice increases bone formation and protects against ovariectomy-induced bone loss*. *Proc Natl Acad Sci U S A*, 2003. **100**(10): p. 6027-32.
237. Garnero, P., E. Sornay-Rendu, M.C. Chapuy, and P.D. Delmas, *Increased bone turnover in late postmenopausal women is a major determinant of osteoporosis*. *J Bone Miner Res*, 1996. **11**(3): p. 337-49.
238. Watkins, M.P., J.Y. Norris, S.K. Grimston, X. Zhang, R.J. Phipps, F.H. Ebetino, and R. Civitelli, *Bisphosphonates improve trabecular bone mass and normalize cortical thickness in ovariectomized, osteoblast connexin43 deficient mice*. *Bone*, 2012. **51**(4): p. 787-94.
239. Falahati-Nini, A., B.L. Riggs, E.J. Atkinson, W.M. O'Fallon, R. Eastell, and S. Khosla, *Relative contributions of testosterone and estrogen in regulating bone resorption and formation in normal elderly men*. *J Clin Invest*, 2000. **106**(12): p. 1553-60.
240. Zirilli, L., V. Rochira, C. Diazi, G. Caffagni, and C. Carani, *Human models of aromatase deficiency*. *J Steroid Biochem Mol Biol*, 2008. **109**(3-5): p. 212-8.
241. Lanfranco, F., L. Zirilli, M. Baldi, E. Pignatti, G. Corneli, E. Ghigo, G. Aimaretti, C. Carani, and V. Rochira, *A novel mutation in the human aromatase gene: insights on the relationship among serum estradiol, longitudinal growth and bone mineral density in an adult man under estrogen replacement treatment*. *Bone*, 2008. **43**(3): p. 628-35.
242. Venken, K., S. Moverare-Skrtic, J.J. Kopchick, K.T. Coschigano, C. Ohlsson, S. Boonen, R. Bouillon, and D. Vanderschueren, *Impact of androgens, growth hormone, and IGF-I on bone and muscle in male mice during puberty*. *J Bone Miner Res*, 2007. **22**(1): p. 72-82.
243. Stepan, J.J., M. Lachman, J. Zverina, V. Pacovsky, and D.J. Baylink, *Castrated men exhibit bone loss: effect of calcitonin treatment on biochemical indices of bone remodeling*. *J Clin Endocrinol Metab*, 1989. **69**(3): p. 523-7.
244. Laurent, M., E. Gielen, F. Claessens, S. Boonen, and D. Vanderschueren, *Osteoporosis in older men: recent advances in pathophysiology and treatment*. *Best Pract Res Clin Endocrinol Metab*, 2013. **27**(4): p. 527-39.
245. Fink, H.A., S.K. Ewing, K.E. Ensrud, E. Barrett-Connor, B.C. Taylor, J.A. Cauley, and E.S. Orwoll, *Association of testosterone and estradiol deficiency with osteoporosis and rapid bone loss in older men*. *J Clin Endocrinol Metab*, 2006. **91**(10): p. 3908-15.
246. Almeida, M., L. Han, E. Ambrogini, R.S. Weinstein, and S.C. Manolagas, *Glucocorticoids and tumor necrosis factor alpha increase oxidative stress and suppress Wnt protein signaling in osteoblasts*. *J Biol Chem*, 2011. **286**(52): p. 44326-35.

-
247. Kondo, H., S. Takeuchi, and A. Togari, *beta-Adrenergic signaling stimulates osteoclastogenesis via reactive oxygen species*. *Am J Physiol Endocrinol Metab*, 2013. **304**(5): p. E507-15.
248. Callaway, D.A. and J.X. Jiang, *Reactive oxygen species and oxidative stress in osteoclastogenesis, skeletal aging and bone diseases*. *J Bone Miner Metab*, 2015. **33**(4): p. 359-70.
249. Ambrogini, E., M. Almeida, M. Martin-Millan, J.H. Paik, R.A. Depinho, L. Han, J. Goellner, R.S. Weinstein, R.L. Jilka, C.A. O'Brien, and S.C. Manolagas, *FoxO-mediated defense against oxidative stress in osteoblasts is indispensable for skeletal homeostasis in mice*. *Cell Metab*, 2010. **11**(2): p. 136-46.
250. Almeida, M., L. Han, M. Martin-Millan, C.A. O'Brien, and S.C. Manolagas, *Oxidative stress antagonizes Wnt signaling in osteoblast precursors by diverting beta-catenin from T cell factor- to forkhead box O-mediated transcription*. *J Biol Chem*, 2007. **282**(37): p. 27298-305.
251. Li, X., Y. Han, Y. Guan, L. Zhang, C. Bai, and Y. Li, *Aluminum induces osteoblast apoptosis through the oxidative stress-mediated JNK signaling pathway*. *Biol Trace Elem Res*, 2012. **150**(1-3): p. 502-8.
252. De Martinis, M., M.C. Di Benedetto, L.P. Mengoli, and L. Ginaldi, *Senile osteoporosis: is it an immune-mediated disease?* *Inflamm Res*, 2006. **55**(10): p. 399-404.
253. Montecino-Rodriguez, E., B. Berent-Maoz, and K. Dorshkind, *Causes, consequences, and reversal of immune system aging*. *J Clin Invest*, 2013. **123**(3): p. 958-65.
254. Giustina, A., G. Mazziotti, and E. Canalis, *Growth hormone, insulin-like growth factors, and the skeleton*. *Endocr Rev*, 2008. **29**(5): p. 535-59.
255. Marie, P.J., *Bone cell senescence: mechanisms and perspectives*. *J Bone Miner Res*, 2014. **29**(6): p. 1311-21.
256. Fleming, T.H., P.M. Humpert, P.P. Nawroth, and A. Bierhaus, *Reactive metabolites and AGE/RAGE-mediated cellular dysfunction affect the aging process: a mini-review*. *Gerontology*, 2011. **57**(5): p. 435-43.
257. Sethe, S., A. Scutt, and A. Stolzing, *Aging of mesenchymal stem cells*. *Ageing Res Rev*, 2006. **5**(1): p. 91-116.
258. Armanios, M., *Telomeres and age-related disease: how telomere biology informs clinical paradigms*. *J Clin Invest*, 2013. **123**(3): p. 996-1002.
259. Jee, W.S., S. Mori, X.J. Li, and S. Chan, *Prostaglandin E2 enhances cortical bone mass and activates intracortical bone remodeling in intact and ovariectomized female rats*. *Bone*, 1990. **11**(4): p. 253-66.
260. Syed, F.A. and K.A. Hoey, *Integrative physiology of the aging bone: insights from animal and cellular models*. *Ann N Y Acad Sci*, 2010. **1211**: p. 95-106.
261. Lees, C.J. and H. Ramsay, *Histomorphometry and bone biomarkers in cynomolgus females: a study in young, mature, and old monkeys*. *Bone*, 1999. **24**(1): p. 25-8.
262. Jerome, C.P., C.S. Carlson, T.C. Register, F.T. Bain, M.J. Jayo, D.S. Weaver, and M.R. Adams, *Bone functional changes in intact, ovariectomized, and ovariectomized, hormone-supplemented adult cynomolgus monkeys (Macaca fascicularis) evaluated by serum markers and dynamic histomorphometry*. *J Bone Miner Res*, 1994. **9**(4): p. 527-40.
-

263. Black, A. and M.A. Lane, *Nonhuman primate models of skeletal and reproductive aging*. Gerontology, 2002. **48**(2): p. 72-80.
264. Gilardi, K.V., S.E. Shideler, C.R. Valverde, J.A. Roberts, and B.L. Lasley, *Characterization of the onset of menopause in the rhesus macaque*. Biol Reprod, 1997. **57**(2): p. 335-40.
265. Champ, J.E., N. Binkley, T. Havighurst, R.J. Colman, J.W. Kemnitz, and E.B. Roecker, *The effect of advancing age on bone mineral content of female rhesus monkeys*. Bone, 1996. **19**(5): p. 485-92.
266. Black, A., E.M. Tilmont, A.M. Handy, W.W. Scott, S.A. Shapses, D.K. Ingram, G.S. Roth, and M.A. Lane, *A nonhuman primate model of age-related bone loss: a longitudinal study in male and premenopausal female rhesus monkeys*. Bone, 2001. **28**(3): p. 295-302.
267. Chavassieux, P., P. Pastoureau, M.C. Chapuy, P.D. Delmas, and P.J. Meunier, *Glucocorticoid-induced inhibition of osteoblastic bone formation in ewes: a biochemical and histomorphometric study*. Osteoporos Int, 1993. **3**(2): p. 97-102.
268. Carbone, A., D.W. Howie, M. McGee, J. Field, M. Pearcy, N. Smith, and E. Jones, *Aging performance of a compliant layer bearing acetabular prosthesis in an ovine hip arthroplasty model*. J Arthroplasty, 2006. **21**(6): p. 899-906.
269. Sachse, A., A. Wagner, M. Keller, O. Wagner, W.D. Wetzels, F. Layher, R.A. Venbrocks, P. Hortschansky, M. Pietraszczyk, B. Wiederanders, H.J. Hempel, J. Bossert, J. Horn, K. Schmuck, and J. Mollenhauer, *Osteointegration of hydroxyapatite-titanium implants coated with nonglycosylated recombinant human bone morphogenetic protein-2 (BMP-2) in aged sheep*. Bone, 2005. **37**(5): p. 699-710.
270. O'Connor, J.A., L.E. Lanyon, and H. MacFie, *The influence of strain rate on adaptive bone remodelling*. J Biomech, 1982. **15**(10): p. 767-81.
271. Sumner, D.R., T.M. Turner, M. Cohen, P. Losavio, R.M. Urban, E.H. Nichols, and J.M. McPherson, *Aging does not lessen the effectiveness of TGFbeta2-enhanced bone regeneration*. J Bone Miner Res, 2003. **18**(4): p. 730-6.
272. Kettler, A., L. Liakos, B. Haegele, and H.J. Wilke, *Are the spines of calf, pig and sheep suitable models for pre-clinical implant tests?* Eur Spine J, 2007. **16**(12): p. 2186-92.
273. Huja, S.S., A.M. Rummel, and F.M. Beck, *Changes in mechanical properties of bone within the mandibular condyle with age*. J Morphol, 2008. **269**(2): p. 138-43.
274. Mosekilde, L., *Assessing bone quality--animal models in preclinical osteoporosis research*. Bone, 1995. **17**(4 Suppl): p. 343s-352s.
275. Takeda, T., M. Hosokawa, S. Takeshita, M. Irino, K. Higuchi, T. Matsushita, Y. Tomita, K. Yasuhira, H. Hamamoto, K. Shimizu, M. Ishii, and T. Yamamuro, *A new murine model of accelerated senescence*. Mech Ageing Dev, 1981. **17**(2): p. 183-94.
276. Matsushita, M., T. Tsuboyama, R. Kasai, H. Okumura, T. Yamamuro, K. Higuchi, K. Higuchi, A. Kohno, T. Yonezu, A. Utani, and et al., *Age-related changes in bone mass in the senescence-accelerated mouse (SAM). SAM-R/3 and SAM-P/6 as new murine models for senile osteoporosis*. Am J Pathol, 1986. **125**(2): p. 276-83.
277. Chen, H. and K.Y. Kubo, *Segmental variations in trabecular bone density and microstructure of the spine in senescence-accelerated mouse (SAMP6): a murine model for senile osteoporosis*. Exp Gerontol, 2012. **47**(4): p. 317-22.

-
278. Silva, M.J. and M.D. Brodt, *Mechanical stimulation of bone formation is normal in the SAMP6 mouse*. *Calcif Tissue Int*, 2008. **82**(6): p. 489-97.
279. Fukuda, S. and H. Iida, *Age-related changes in bone mineral density, cross-sectional area and the strength of long bones in the hind limbs and first lumbar vertebra in female Wistar rats*. *J Vet Med Sci*, 2004. **66**(7): p. 755-60.
280. Jilka, R.L. and C.A. O'Brien, *The Role of Osteocytes in Age-Related Bone Loss*. *Current Osteoporosis Reports*, 2016. **14**(1): p. 16-25.
281. Ferguson, V.L., R.A. Ayers, T.A. Bateman, and S.J. Simske, *Bone development and age-related bone loss in male C57BL/6J mice*. *Bone*, 2003. **33**(3): p. 387-98.
282. Willingham, M.D., M.D. Brodt, K.L. Lee, A.L. Stephens, J. Ye, and M.J. Silva, *Age-related changes in bone structure and strength in female and male BALB/c mice*. *Calcif Tissue Int*, 2010. **86**(6): p. 470-83.
283. Skarnes, W.C., B. Rosen, A.P. West, M. Koutsourakis, W. Bushell, V. Iyer, A.O. Mujica, M. Thomas, J. Harrow, T. Cox, D. Jackson, J. Severin, P. Biggs, J. Fu, M. Nefedov, P.J. de Jong, A.F. Stewart, and A. Bradley, *A conditional knockout resource for the genome-wide study of mouse gene function*. *Nature*, 2011. **474**(7351): p. 337-42.
284. Akhter, M.P., D.M. Cullen, E.A. Pedersen, D.B. Kimmel, and R.R. Recker, *Bone response to in vivo mechanical loading in two breeds of mice*. *Calcif Tissue Int*, 1998. **63**(5): p. 442-9.
285. Meakin, L.B., T. Sugiyama, G.L. Galea, W.J. Browne, L.E. Lanyon, and J.S. Price, *Male mice housed in groups engage in frequent fighting and show a lower response to additional bone loading than females or individually housed males that do not fight*. *Bone*, 2013. **54**(1): p. 113-7.
286. Todd, H., G.L. Galea, L.B. Meakin, P.J. Delisser, L.E. Lanyon, S.H. Windahl, and J.S. Price, *Wnt16 Is Associated with Age-Related Bone Loss and Estrogen Withdrawal in Murine Bone*. *PLoS ONE*, 2015. **10**(10): p. e0140260.
287. Sugiyama, T., G.L. Galea, L.E. Lanyon, and J.S. Price, *Mechanical loading-related bone gain is enhanced by tamoxifen but unaffected by fulvestrant in female mice*. *Endocrinology*, 2010. **151**(12): p. 5582-90.
288. MacLaughlin, J. and M.F. Holick, *Aging decreases the capacity of human skin to produce vitamin D₃*. *J Clin Invest*, 1985. **76**(4): p. 1536-8.
289. Holick, M.F., L.Y. Matsuoka, and J. Wortsman, *Age, vitamin D, and solar ultraviolet*. *Lancet*, 1989. **2**(8671): p. 1104-5.
290. Boonen, S., P. Lips, R. Bouillon, H.A. Bischoff-Ferrari, D. Vanderschueren, and P. Haentjens, *Need for additional calcium to reduce the risk of hip fracture with vitamin d supplementation: evidence from a comparative metaanalysis of randomized controlled trials*. *J Clin Endocrinol Metab*, 2007. **92**(4): p. 1415-23.
291. Weaver, C.M., D.D. Alexander, C.J. Boushey, B. Dawson-Hughes, J.M. Lappe, M.S. LeBoff, S. Liu, A.C. Looker, T.C. Wallace, and D.D. Wang, *Calcium plus vitamin D supplementation and risk of fractures: an updated meta-analysis from the National Osteoporosis Foundation*. *Osteoporos Int*, 2016. **27**(1): p. 367-76.
292. Tankeu, A.T., V. Ndip Agbor, and J.J. Noubiap, *Calcium supplementation and cardiovascular risk: A rising concern*. *J Clin Hypertens (Greenwich)*, 2017. **19**(6): p. 640-646.
-

293. Bjornerem, A., N. Emaus, G.K. Berntsen, R.M. Joakimsen, V. Fonnebo, T. Wilsgaard, P. Oian, E. Seeman, and B. Straume, *Circulating sex steroids, sex hormone-binding globulin, and longitudinal changes in forearm bone mineral density in postmenopausal women and men: the Tromso study*. *Calcif Tissue Int*, 2007. **81**(2): p. 65-72.
294. Khosla, S., *Update on estrogens and the skeleton*. *J Clin Endocrinol Metab*, 2010. **95**(8): p. 3569-77.
295. Quigley, M.E., P.L. Martin, A.M. Burnier, and P. Brooks, *Estrogen therapy arrests bone loss in elderly women*. *Am J Obstet Gynecol*, 1987. **156**(6): p. 1516-23.
296. Eriksen, E.F., *Hormone replacement therapy or SERMS in the long term treatment of osteoporosis*. *Minerva Ginecol*, 2012. **64**(3): p. 207-21.
297. Rossouw, J.E., G.L. Anderson, R.L. Prentice, A.Z. LaCroix, C. Kooperberg, M.L. Stefanick, R.D. Jackson, S.A. Beresford, B.V. Howard, K.C. Johnson, J.M. Kotchen, and J. Ockene, *Risks and benefits of estrogen plus progestin in healthy postmenopausal women: principal results From the Women's Health Initiative randomized controlled trial*. *Jama*, 2002. **288**(3): p. 321-33.
298. Seeman, E., G.G. Crans, A. Diez-Perez, K.V. Pinette, and P.D. Delmas, *Anti-vertebral fracture efficacy of raloxifene: a meta-analysis*. *Osteoporos Int*, 2006. **17**(2): p. 313-6.
299. Maximov, P.Y., T.M. Lee, and V.C. Jordan, *The discovery and development of selective estrogen receptor modulators (SERMs) for clinical practice*. *Curr Clin Pharmacol*, 2013. **8**(2): p. 135-55.
300. Cummings, S.R., K. Ensrud, P.D. Delmas, A.Z. LaCroix, S. Vukicevic, D.M. Reid, S. Goldstein, U. Sriram, A. Lee, J. Thompson, R.A. Armstrong, D.D. Thompson, T. Powles, J. Zanchetta, D. Kendler, P. Neven, and R. Eastell, *Lasofixifene in postmenopausal women with osteoporosis*. *N Engl J Med*, 2010. **362**(8): p. 686-96.
301. Cummings, S.R., M. McClung, J.Y. Reginster, D. Cox, B. Mitlak, J. Stock, M. Amewou-Atisso, T. Powles, P. Miller, J. Zanchetta, and C. Christiansen, *Arzoxifene for prevention of fractures and invasive breast cancer in postmenopausal women*. *J Bone Miner Res*, 2011. **26**(2): p. 397-404.
302. Russell, R.G.G., N.B. Watts, F.H. Ebetino, and M.J. Rogers, *Mechanisms of action of bisphosphonates: similarities and differences and their potential influence on clinical efficacy*. *Osteoporosis International*, 2008. **19**(6): p. 733-759.
303. Siu, W.S., C.H. Ko, L.K. Hung, C.P. Lau, C.B. Lau, K.P. Fung, and P.C. Leung, *Effect of anti-osteoporotic agents on the prevention of bone loss in unloaded bone*. *Mol Med Rep*, 2013. **8**(4): p. 1188-94.
304. Khosla, S. and L.C. Hofbauer, *Osteoporosis treatment: recent developments and ongoing challenges*. *Lancet Diabetes Endocrinol*, 2017. **5**(11): p. 898-907.
305. Ebetino, F., M. Francis, M. Rogers, and R. Russell, *Mechanisms of action of etidronate and other bisphosphonates*. *Reviews in Contemporary Pharmacotherapy*, 1998. **9**(4): p. 233-243.
306. Nancollas, G.H., R. Tang, R.J. Phipps, Z. Henneman, S. Gulde, W. Wu, A. Mangood, R.G. Russell, and F.H. Ebetino, *Novel insights into actions of bisphosphonates on bone: differences in interactions with hydroxyapatite*. *Bone*, 2006. **38**(5): p. 617-27.

-
307. Ebetino, R., P. Emmerling, B. Barnett, and G. Nancollas. *Differentiation of hydroxyapatite affinity of bisphosphonate analogs for mechanism of action studies*. in *JOURNAL OF BONE AND MINERAL RESEARCH*. 2004. AMER SOC BONE & MINERAL RES 2025 M ST, NW, STE 800, WASHINGTON, DC 20036-3309 USA.
308. Thompson, K., M.J. Rogers, F.P. Coxon, and J.C. Crockett, *Cytosolic entry of bisphosphonate drugs requires acidification of vesicles after fluid-phase endocytosis*. *Mol Pharmacol*, 2006. **69**(5): p. 1624-32.
309. Luckman, S.P., D.E. Hughes, F.P. Coxon, R. Graham, G. Russell, and M.J. Rogers, *Nitrogen-containing bisphosphonates inhibit the mevalonate pathway and prevent post-translational prenylation of GTP-binding proteins, including Ras*. *J Bone Miner Res*, 1998. **13**(4): p. 581-9.
310. van Beek, E., E. Pieterman, L. Cohen, C. Lowik, and S. Papapoulos, *Farnesyl pyrophosphate synthase is the molecular target of nitrogen-containing bisphosphonates*. *Biochem Biophys Res Commun*, 1999. **264**(1): p. 108-11.
311. Kogianni, G., V. Mann, F. Ebetino, M. Nuttall, P. Nijweide, H. Simpson, and B. Noble, *Fas/CD95 is associated with glucocorticoid-induced osteocyte apoptosis*. *Life Sci*, 2004. **75**(24): p. 2879-95.
312. Plotkin, L.I., R.S. Weinstein, A.M. Parfitt, P.K. Roberson, S.C. Manolagas, and T. Bellido, *Prevention of osteocyte and osteoblast apoptosis by bisphosphonates and calcitonin*. *J Clin Invest*, 1999. **104**(10): p. 1363-74.
313. Lezcano, V., T. Bellido, L.I. Plotkin, R. Boland, and S. Morelli, *Role of connexin 43 in the mechanism of action of alendronate: dissociation of anti-apoptotic and proliferative signaling pathways*. *Arch Biochem Biophys*, 2012. **518**(2): p. 95-102.
314. Plotkin, L.I., S.C. Manolagas, and T. Bellido, *Dissociation of the pro-apoptotic effects of bisphosphonates on osteoclasts from their anti-apoptotic effects on osteoblasts/osteocytes with novel analogs*. *Bone*, 2006. **39**(3): p. 443-52.
315. Plotkin, L.I., N. Bivi, and T. Bellido, *A bisphosphonate that does not affect osteoclasts prevents osteoblast and osteocyte apoptosis and the loss of bone strength induced by glucocorticoids in mice*. *Bone*, 2011. **49**(1): p. 122-7.
316. Black, D.M., P.D. Delmas, R. Eastell, I.R. Reid, S. Boonen, J.A. Cauley, F. Cosman, P. Lakatos, P.C. Leung, Z. Man, C. Mautalen, P. Mesenbrink, H. Hu, J. Caminis, K. Tong, T. Rosario-Jansen, J. Krasnow, T.F. Hue, D. Sellmeyer, E.F. Eriksen, and S.R. Cummings, *Once-yearly zoledronic acid for treatment of postmenopausal osteoporosis*. *N Engl J Med*, 2007. **356**(18): p. 1809-22.
317. Cummings, S.R., D.M. Black, D.E. Thompson, W.B. Applegate, E. Barrett-Connor, T.A. Musliner, L. Palermo, R. Prineas, S.M. Rubin, J.C. Scott, T. Vogt, R. Wallace, A.J. Yates, and A.Z. LaCroix, *Effect of alendronate on risk of fracture in women with low bone density but without vertebral fractures: results from the Fracture Intervention Trial*. *Jama*, 1998. **280**(24): p. 2077-82.
318. Jha, S., Z. Wang, N. Laucis, and T. Bhattacharyya, *Trends in Media Reports, Oral Bisphosphonate Prescriptions, and Hip Fractures 1996-2012: An Ecological Analysis*. *J Bone Miner Res*, 2015. **30**(12): p. 2179-87.
319. Wysowski, D.K. and P. Greene, *Trends in osteoporosis treatment with oral and intravenous bisphosphonates in the United States, 2002–2012*. *Bone*, 2013. **57**(2): p. 423-428.
-

320. Ruggiero, S.L., B. Mehrotra, T.J. Rosenberg, and S.L. Engroff, *Osteonecrosis of the jaws associated with the use of bisphosphonates: a review of 63 cases*. J Oral Maxillofac Surg, 2004. **62**(5): p. 527-34.
321. Mucke, T., C.R. Krestan, D.A. Mitchell, J.S. Kirschke, and A. Wutzl, *Bisphosphonate and Medication-Related Osteonecrosis of the Jaw: A Review*. Semin Musculoskelet Radiol, 2016. **20**(3): p. 305-314.
322. Marx, R.E., *Pamidronate (Aredia) and zoledronate (Zometa) induced avascular necrosis of the jaws: a growing epidemic*. Journal of Oral and Maxillofacial Surgery, 2003. **61**(9): p. 1115-1117.
323. Patel, R.N., A. Ashraf, and M. Sundaram, *Atypical Fractures Following Bisphosphonate Therapy*. Semin Musculoskelet Radiol, 2016. **20**(4): p. 376-381.
324. Lee, S., R.V. Yin, H. Hirpara, N.C. Lee, A. Lee, S. Llanos, and O.J. Phung, *Increased risk for atypical fractures associated with bisphosphonate use*. Fam Pract, 2015. **32**(3): p. 276-81.
325. Bronson, W.H., I.D. Kaye, and K.A. Egol, *Atypical femur fractures: a review*. Curr Osteoporos Rep, 2014. **12**(4): p. 446-53.
326. Russell, R.G., *Bisphosphonates: the first 40 years*. Bone, 2011. **49**(1): p. 2-19.
327. Russell, R.G., *Bisphosphonates: from bench to bedside*. Ann N Y Acad Sci, 2006. **1068**: p. 367-401.
328. Bekker, P.J., D. Holloway, A. Nakanishi, M. Arrighi, P.T. Leese, and C.R. Dunstan, *The effect of a single dose of osteoprotegerin in postmenopausal women*. J Bone Miner Res, 2001. **16**(2): p. 348-60.
329. Kostenuik, P.J., H.Q. Nguyen, J. McCabe, K.S. Warmington, C. Kurahara, N. Sun, C. Chen, L. Li, R.C. Cattley, G. Van, S. Scully, R. Elliott, M. Grisanti, S. Morony, H.L. Tan, F. Asuncion, X. Li, M.S. Ominsky, M. Stolina, D. Dwyer, W.C. Dougall, N. Hawkins, W.J. Boyle, W.S. Simonet, and J.K. Sullivan, *Denosumab, a fully human monoclonal antibody to RANKL, inhibits bone resorption and increases BMD in knock-in mice that express chimeric (murine/human) RANKL*. J Bone Miner Res, 2009. **24**(2): p. 182-95.
330. Kostenuik, P.J., S.Y. Smith, J. Jolette, J. Schroeder, I. Pyrah, and M.S. Ominsky, *Decreased bone remodeling and porosity are associated with improved bone strength in ovariectomized cynomolgus monkeys treated with denosumab, a fully human RANKL antibody*. Bone, 2011. **49**(2): p. 151-61.
331. Bekker, P.J., D.L. Holloway, A.S. Rasmussen, R. Murphy, S.W. Martin, P.T. Leese, G.B. Holmes, C.R. Dunstan, and A.M. DePaoli, *A single-dose placebo-controlled study of AMG 162, a fully human monoclonal antibody to RANKL, in postmenopausal women*. J Bone Miner Res, 2004. **19**(7): p. 1059-66.
332. McClung, M.R., E.M. Lewiecki, S.B. Cohen, M.A. Bolognese, G.C. Woodson, A.H. Moffett, M. Peacock, P.D. Miller, S.N. Lederman, C.H. Chesnut, D. Lain, A.J. Kivitz, D.L. Holloway, C. Zhang, M.C. Peterson, and P.J. Bekker, *Denosumab in postmenopausal women with low bone mineral density*. N Engl J Med, 2006. **354**(8): p. 821-31.
333. Lewiecki, E.M., P.D. Miller, M.R. McClung, S.B. Cohen, M.A. Bolognese, Y. Liu, A. Wang, S. Siddhanti, and L.A. Fitzpatrick, *Two-year treatment with denosumab (AMG 162) in a randomized phase 2 study of postmenopausal women with low BMD*. J Bone Miner Res, 2007. **22**(12): p. 1832-41.

-
334. Miller, P.D., M.A. Bolognese, E.M. Lewiecki, M.R. McClung, B. Ding, M. Austin, Y. Liu, and J. San Martin, *Effect of denosumab on bone density and turnover in postmenopausal women with low bone mass after long-term continued, discontinued, and restarting of therapy: a randomized blinded phase 2 clinical trial*. *Bone*, 2008. **43**(2): p. 222-9.
335. Bone, H.G., M.A. Bolognese, C.K. Yuen, D.L. Kendler, P.D. Miller, Y.C. Yang, L. Grazette, J. San Martin, and J.C. Gallagher, *Effects of denosumab treatment and discontinuation on bone mineral density and bone turnover markers in postmenopausal women with low bone mass*. *J Clin Endocrinol Metab*, 2011. **96**(4): p. 972-80.
336. Cummings, S.R., J. San Martin, M.R. McClung, E.S. Siris, R. Eastell, I.R. Reid, P. Delmas, H.B. Zoog, M. Austin, A. Wang, S. Kutilek, S. Adami, J. Zanchetta, C. Libanati, S. Siddhanti, and C. Christiansen, *Denosumab for prevention of fractures in postmenopausal women with osteoporosis*. *N Engl J Med*, 2009. **361**(8): p. 756-65.
337. Reid, I.R., P.D. Miller, J.P. Brown, D.L. Kendler, A. Fahrleitner-Pammer, I. Valter, K. Maasalu, M.A. Bolognese, G. Woodson, H. Bone, B. Ding, R.B. Wagman, J. San Martin, M.S. Ominsky, and D.W. Dempster, *Effects of denosumab on bone histomorphometry: the FREEDOM and STAND studies*. *J Bone Miner Res*, 2010. **25**(10): p. 2256-65.
338. Brown, J.P., D.W. Dempster, B. Ding, R. Dent-Acosta, J. San Martin, A. Grauer, R.B. Wagman, and J. Zanchetta, *Bone remodeling in postmenopausal women who discontinued denosumab treatment: off-treatment biopsy study*. *J Bone Miner Res*, 2011. **26**(11): p. 2737-44.
339. McClung, M.R., E.M. Lewiecki, M.L. Geller, M.A. Bolognese, M. Peacock, R.L. Weinstein, B. Ding, E. Rockabrand, R.B. Wagman, and P.D. Miller, *Effect of denosumab on bone mineral density and biochemical markers of bone turnover: 8-year results of a phase 2 clinical trial*. *Osteoporos Int*, 2013. **24**(1): p. 227-35.
340. von Keyserlingk, C., R. Hopkins, A. Anastasilakis, K. Toulis, R. Goeree, J.E. Tarride, and F. Xie, *Clinical efficacy and safety of denosumab in postmenopausal women with low bone mineral density and osteoporosis: a meta-analysis*. *Semin Arthritis Rheum*, 2011. **41**(2): p. 178-86.
341. Bone, H.G., R.B. Wagman, M.L. Brandi, J.P. Brown, R. Chapurlat, S.R. Cummings, E. Czerwinski, A. Fahrleitner-Pammer, D.L. Kendler, K. Lippuner, J.Y. Reginster, C. Roux, J. Malouf, M.N. Bradley, N.S. Daizadeh, A. Wang, P. Dakin, N. Pannaciuoli, D.W. Dempster, and S. Papapoulos, *10 years of denosumab treatment in postmenopausal women with osteoporosis: results from the phase 3 randomised FREEDOM trial and open-label extension*. *Lancet Diabetes Endocrinol*, 2017. **5**(7): p. 513-523.
342. Miyazaki, T., F. Tokimura, and S. Tanaka, *A review of denosumab for the treatment of osteoporosis*. *Patient Prefer Adherence*, 2014. **8**: p. 463-71.
343. Narayanan, P., *Denosumab: A comprehensive review*. *South Asian J Cancer*, 2013. **2**(4): p. 272-7.
344. Duong, L.T., *Therapeutic inhibition of cathepsin K—reducing bone resorption while maintaining bone formation*. *BoneKEy reports*, 2012. **1**: p. 67.
345. Cusick, T., C.M. Chen, B.L. Pennypacker, M. Pickarski, D.B. Kimmel, B.B. Scott, and L.T. Duong, *Odanacatib treatment increases hip bone mass and cortical thickness by preserving endocortical bone formation and stimulating periosteal bone formation in the ovariectomized adult rhesus monkey*. *J Bone Miner Res*, 2012. **27**(3): p. 524-37.
-

346. Masarachia, P.J., B.L. Pennypacker, M. Pickarski, K.R. Scott, G.A. Wesolowski, S.Y. Smith, R. Samadfam, J.E. Goetzmann, B.B. Scott, D.B. Kimmel, and L.T. Duong, *Odanacatib reduces bone turnover and increases bone mass in the lumbar spine of skeletally mature ovariectomized rhesus monkeys*. J Bone Miner Res, 2012. **27**(3): p. 509-23.
347. Pennypacker, B.L., C.M. Chen, H. Zheng, M.S. Shih, M. Belfast, R. Samadfam, and L.T. Duong, *Inhibition of cathepsin K increases modeling-based bone formation, and improves cortical dimension and strength in adult ovariectomized monkeys*. J Bone Miner Res, 2014. **29**(8): p. 1847-58.
348. Bone, H.G., D.W. Dempster, J.A. Eisman, S.L. Greenspan, M.R. McClung, T. Nakamura, S. Papapoulos, W.J. Shih, A. Rybak-Feiglin, A.C. Santora, N. Verbruggen, A.T. Leung, and A. Lombardi, *Odanacatib for the treatment of postmenopausal osteoporosis: development history and design and participant characteristics of LOFT, the Long-Term Odanacatib Fracture Trial*. Osteoporos Int, 2015. **26**(2): p. 699-712.
349. O'Donoghue, M., I. Cavallari, S. Wiviott, A. Cange, L. Grip, N. Deenadayalu, K. Im, S. Murphy, and M. Sabatine, *The Long-Term Odanacatib Fracture Trial (LOFT): Cardiovascular Safety Results*, in *ASBMR Annual Congress*, ASBMR, Editor. 2016, ASBMR: Georgia, Atlanta USA.
350. Leder, B.Z., J.N. Tsai, A.V. Uihlein, S.-A.M. Burnett-Bowie, Y. Zhu, K. Foley, H. Lee, and R.M. Neer, *Two Years of Denosumab and Teriparatide Administration in Postmenopausal Women With Osteoporosis (The DATA Extension Study): A Randomized Controlled Trial*. The Journal of Clinical Endocrinology & Metabolism, 2014. **99**(5): p. 1694-1700.
351. Tice, J.A., R. Chapman, V. Kumar, P. Synnott, M. Seidner, D.A. Ollendorf, D.M. Rind, and S.D. Pearson, *Anabolic Therapies for Osteoporosis in Postmenopausal Women: Effectiveness and Value*, in *California Technology Assessment Forum*, I.f.C.a.E. Review., Editor. 2017, Institute for Clinical and Economic Review.
352. Lindsay, R., J.H. Krege, F. Marin, L. Jin, and J.J. Stepan, *Teriparatide for osteoporosis: importance of the full course*. Osteoporos Int, 2016. **27**: p. 2395-410.
353. Dempster, D.W., H. Zhou, R.R. Recker, J.P. Brown, M.A. Bolognese, C.P. Recknor, D.L. Kendler, E.M. Lewiecki, D.A. Hanley, D.S. Rao, P.D. Miller, G.C. Woodson, 3rd, R. Lindsay, N. Binkley, X. Wan, V.A. Ruff, B. Janos, and K.A. Taylor, *Skeletal histomorphometry in subjects on teriparatide or zoledronic acid therapy (SHOTZ) study: a randomized controlled trial*. J Clin Endocrinol Metab, 2012. **97**(8): p. 2799-808.
354. Vahle, J.L., M. Sato, G.G. Long, J.K. Young, P.C. Francis, J.A. Engelhardt, M.S. Westmore, Y. Linda, and J.B. Nold, *Skeletal changes in rats given daily subcutaneous injections of recombinant human parathyroid hormone (1-34) for 2 years and relevance to human safety*. Toxicol Pathol, 2002. **30**(3): p. 312-21.
355. Pavone, V., G. Testa, S.M.C. Giardina, A. Vescio, D.A. Restivo, and G. Sessa, *Pharmacological Therapy of Osteoporosis: A Systematic Current Review of Literature*. Front Pharmacol, 2017. **8**: p. 803.
356. Jolette, J., B. Attalla, A. Varela, G.G. Long, N. Mellal, S. Trimm, S.Y. Smith, M.S. Ominsky, and G. Hattersley, *Comparing the incidence of bone tumors in rats chronically exposed to the selective PTH type 1 receptor agonist abaloparatide or PTH(1-34)*. Regulatory Toxicology and Pharmacology, 2017. **86**(Supplement C): p. 356-365.
357. Miller, P.D., *Safety of parathyroid hormone for the treatment of osteoporosis*. Current Osteoporosis Reports, 2008. **6**(1): p. 12-16.

-
358. Damron, T.A., W.G. Ward, and A. Stewart, *Osteosarcoma, chondrosarcoma, and Ewing's sarcoma: National Cancer Data Base Report*. Clin Orthop Relat Res, 2007. **459**: p. 40-7.
359. Cosman, F., N. Gilchrist, M. McClung, J. Foldes, T. de Villiers, A. Santora, A. Leung, S. Samanta, N. Heyden, J.P. McGinnis, 2nd, E. Rosenberg, and A.E. Denker, *A phase 2 study of MK-5442, a calcium-sensing receptor antagonist, in postmenopausal women with osteoporosis after long-term use of oral bisphosphonates*. Osteoporos Int, 2016. **27**(1): p. 377-86.
360. Fitzpatrick, L.A., C.E. Dabrowski, G. Cicconetti, D.N. Gordon, S. Papapoulos, H.G. Bone, 3rd, and J.P. Bilezikian, *The effects of ronacaleret, a calcium-sensing receptor antagonist, on bone mineral density and biochemical markers of bone turnover in postmenopausal women with low bone mineral density*. J Clin Endocrinol Metab, 2011. **96**(8): p. 2441-9.
361. Seeman, E., S. Boonen, F. Borgström, B. Vellas, J.-P. Aquino, J. Semler, C.-L. Benhamou, J.-M. Kaufman, and J.-Y. Reginster, *Five years treatment with strontium ranelate reduces vertebral and nonvertebral fractures and increases the number and quality of remaining life-years in women over 80 years of age*. Bone, 2010. **46**(4): p. 1038-1042.
362. Kaufman, J.M., M. Audran, G. Bianchi, V. Braga, M. Diaz-Curiel, R.M. Francis, S. Goemaere, R. Josse, S. Palacios, J.D. Ringe, D. Felsenberg, and S. Boonen, *Efficacy and Safety of Strontium Ranelate in the Treatment of Osteoporosis in Men*. The Journal of Clinical Endocrinology & Metabolism, 2013. **98**(2): p. 592-601.
363. Reginster, J.Y., D. Felsenberg, S. Boonen, A. Diez-Perez, R. Rizzoli, M.L. Brandi, T.D. Spector, K. Brixen, S. Goemaere, C. Cormier, A. Balogh, P.D. Delmas, and P.J. Meunier, *Effects of long-term strontium ranelate treatment on the risk of nonvertebral and vertebral fractures in postmenopausal osteoporosis: Results of a five-year, randomized, placebo-controlled trial*. Arthritis Rheum, 2008. **58**(6): p. 1687-95.
364. Meunier, P.J., C. Roux, E. Seeman, S. Ortolani, J.E. Badurski, T.D. Spector, J. Cannata, A. Balogh, E.M. Lemmel, S. Pors-Nielsen, R. Rizzoli, H.K. Genant, and J.Y. Reginster, *The effects of strontium ranelate on the risk of vertebral fracture in women with postmenopausal osteoporosis*. N Engl J Med, 2004. **350**(5): p. 459-68.
365. Bolland, M.J. and A. Grey, *Ten years too long: strontium ranelate, cardiac events, and the European Medicines Agency*. BMJ, 2016. **354**.
366. Baron, R. and G. Rawadi, *Targeting the Wnt/beta-catenin pathway to regulate bone formation in the adult skeleton*. Endocrinology, 2007. **148**(6): p. 2635-43.
367. Cosman, F., D.B. Crittenden, J.D. Adachi, N. Binkley, E. Czerwinski, S. Ferrari, L.C. Hofbauer, E. Lau, E.M. Lewiecki, A. Miyauchi, C.A. Zerbin, C.E. Milmont, L. Chen, J. Maddox, P.D. Meisner, C. Libanati, and A. Grauer, *Romsozumab Treatment in Postmenopausal Women with Osteoporosis*. N Engl J Med, 2016. **375**(16): p. 1532-1543.
368. Saag, K.G., J. Petersen, M.L. Brandi, A.C. Karaplis, M. Lorentzon, T. Thomas, J. Maddox, M. Fan, P.D. Meisner, and A. Grauer, *Romsozumab or Alendronate for Fracture Prevention in Women with Osteoporosis*. N Engl J Med, 2017. **377**(15): p. 1417-1427.
369. Kang, J.-H., J.J. Keller, and H.-C. Lin, *Bisphosphonates reduced the risk of acute myocardial infarction: a 2-year follow-up study*. Osteoporosis International, 2013. **24**(1): p. 271-277.
370. Amgen and UCB. *Amgen And UCB Provide Update On Regulatory Status Of EVENITY™ (romosozumab) In The US*. 2017 [cited 2017 08/12/2017]; Available from:
-

<https://www.amgen.com/media/news-releases/2017/07/amgen-and-ucb-provide-update-on-regulatory-status-of-evenity-romosozumab-in-the-us/>.

371. Sugiyama, T., T. Torio, T. Miyajima, Y.T. Kim, and H. Oda, *Romosozumab and Blosozumab: Alternative Drugs of Mechanical Strain-Related Stimulus Toward a Cure for Osteoporosis*. *Frontiers in Endocrinology*, 2015. **6**: p. 54.
372. Morse, A., A. Schindeler, M.M. McDonald, M. Kneissel, I. Kramer, and D.G. Little, *Sclerostin Antibody Augments the Anabolic Bone Formation Response in a Mouse Model of Mechanical Tibial Loading*. *J Bone Miner Res*, 2017.
373. Chouinard, L., M. Felx, N. Mellal, A. Varela, P. Mann, J. Jolette, R. Samadfam, S.Y. Smith, K. Locher, S. Buntich, M.S. Ominsky, I. Pyrah, and R.W. Boyce, *Carcinogenicity risk assessment of romosozumab: A review of scientific weight-of-evidence and findings in a rat lifetime pharmacology study*. *Regul Toxicol Pharmacol*, 2016. **81**: p. 212-222.
374. Cosman, F., *Anabolic and antiresorptive therapy for osteoporosis: combination and sequential approaches*. *Curr Osteoporos Rep*, 2014. **12**(4): p. 385-95.
375. Cosman, F., *Combination therapy for osteoporosis: a reappraisal*. *BoneKEy Rep*, 2014. **3**.
376. Li, W., W. Chen, and Y. Lin, *The Efficacy of Parathyroid Hormone Analogues in Combination With Bisphosphonates for the Treatment of Osteoporosis: A Meta-Analysis of Randomized Controlled Trials*. *Medicine (Baltimore)*, 2015. **94**(38): p. e1156.
377. Tsai, J.N., A.V. Uihlein, H. Lee, R. Kumbhani, E. Siwila-Sackman, E.A. McKay, S.A.M. Burnett-Bowie, R.M. Neer, and B.Z. Leder, *Teriparatide and denosumab, alone or combined, in women with postmenopausal osteoporosis: The DATA study randomised trial*. *The Lancet*, 2013. **382**(9886): p. 50-56.
378. Tsai, J.N., A.V. Uihlein, S.M. Burnett-Bowie, R.M. Neer, N.P. Derrico, H. Lee, M.L. Bouxsein, and B.Z. Leder, *Effects of Two Years of Teriparatide, Denosumab, or Both on Bone Microarchitecture and Strength (DATA-HRpQCT study)*. *The Journal of Clinical Endocrinology & Metabolism*, 2016. **101**(5): p. 2023-2030.
379. Black, D.M., S.L. Greenspan, K.E. Ensrud, L. Palermo, J.A. McGowan, T.F. Lang, P. Garnero, M.L. Bouxsein, J.P. Bilezikian, and C.J. Rosen *The Effects of Parathyroid Hormone and Alendronate Alone or in Combination in Postmenopausal Osteoporosis*. *New England Journal of Medicine*, 2003. **349**(13): p. 1207-1215.
380. Finkelstein, J.S., J.J. Wyland, H. Lee, and R.M. Neer, *Effects of teriparatide, alendronate, or both in women with postmenopausal osteoporosis*. *Journal of Clinical Endocrinology and Metabolism*, 2010. **95**(4): p. 1838-1845.
381. Ma, Y.L., Q.Q. Zeng, A.Y. Chiang, D. Burr, J. Li, H. Dobnig, A. Fahrleitner-Pammer, D. Michalska, F. Marin, I. Pavo, and J.J. Stepan, *Effects of teriparatide on cortical histomorphometric variables in postmenopausal women with or without prior alendronate treatment*. *Bone*, 2014. **59**: p. 139-47.
382. Cosman, F., J.W. Nieves, and D.W. Dempster, *Treatment Sequence Matters: Anabolic and Antiresorptive Therapy for Osteoporosis*. *J Bone Miner Res*, 2017. **32**(2): p. 198-202.
383. McClung, M.R., *Using Osteoporosis Therapies in Combination*. *Curr Osteoporos Rep*, 2017. **15**(4): p. 343-352.
384. Khan, M.P., A.K. Singh, A.K. Singh, P. Shrivastava, M.C. Tiwari, G.K. Nagar, H.K. Bora, V. Parameswaran, S. Sanyal, J.R. Bellare, and N. Chattopadhyay, *Odanacatib Restores*

-
- Trabecular Bone of Skeletally Mature Female Rabbits With Osteopenia but Induces Brittleness of Cortical Bone: A Comparative Study of the Investigational Drug With PTH, Estrogen, and Alendronate.* J Bone Miner Res, 2016. **31**(3): p. 615-29.
385. Ochi, Y., H. Yamada, H. Mori, N. Kawada, M. Tanaka, A. Imagawa, K. Ohmoto, and K. Kawabata, *Combination therapy with ONO-KK1-300-01, a cathepsin K inhibitor, and parathyroid hormone results in additive beneficial effect on bone mineral density in ovariectomized rats.* J Bone Miner Metab, 2016. **34**(1): p. 33-40.
386. Cosman, F., G. Hattersley, M.Y. Hu, G.C. Williams, L.A. Fitzpatrick, and D.M. Black, *Effects of Abaloparatide-SC on Fractures and Bone Mineral Density in Subgroups of Postmenopausal Women With Osteoporosis and Varying Baseline Risk Factors.* J Bone Miner Res, 2017. **32**(1): p. 17-23.
387. Roberts, M.D., T.J. Santner, and R.T. Hart, *Local bone formation due to combined mechanical loading and intermittent hPTH-(1-34) treatment and its correlation to mechanical signal distributions.* J Biomech, 2009. **42**(15): p. 2431-8.
388. Meakin, L.B., H. Todd, P.J. Delisser, G.L. Galea, A. Moustafa, L.E. Lanyon, S.H. Windahl, and J.S. Price, *Parathyroid hormone's enhancement of bones' osteogenic response to loading is affected by ageing in a dose- and time-dependent manner.* Bone, 2017. **98**: p. 59-67.
389. Srinivasan, S., B.J. Ausk, J. Prasad, D. Threet, S.D. Bain, T.S. Richardson, and T.S. Gross, *Rescuing loading induced bone formation at senescence.* PLoS Comput Biol, 2010. **6**(9).
390. Frost, H.M., *The mechanostat: a proposed pathogenic mechanism of osteoporoses and the bone mass effects of mechanical and nonmechanical agents.* Bone Miner, 1987. **2**(2): p. 73-85.
391. Jones, H.H., J.D. Priest, W.C. Hayes, C.C. Tichenor, and D.A. Nagel, *Humeral hypertrophy in response to exercise.* J Bone Joint Surg Am, 1977. **59**(2): p. 204-8.
392. Huddleston, A.L., D. Rockwell, D.N. Kulund, and R.B. Harrison, *Bone mass in lifetime tennis athletes.* Jama, 1980. **244**(10): p. 1107-9.
393. Heinonen, A., P. Oja, P. Kannus, H. Sievanen, H. Haapasalo, A. Manttari, and I. Vuori, *Bone mineral density in female athletes representing sports with different loading characteristics of the skeleton.* Bone, 1995. **17**(3): p. 197-203.
394. Wittich, A., C.A. Mautalen, M.B. Oliveri, A. Bagur, F. Somoza, and E. Rotemberg, *Professional football (soccer) players have a markedly greater skeletal mineral content, density and size than age- and BMI-matched controls.* Calcif Tissue Int, 1998. **63**(2): p. 112-7.
395. Siu, P.M., *Muscle apoptotic response to denervation, disuse, and aging.* Med Sci Sports Exerc, 2009. **41**(10): p. 1876-86.
396. Meakin, L.B., C. Udeh, G.L. Galea, L.E. Lanyon, and J.S. Price, *Exercise does not enhance aged bone's impaired response to artificial loading in C57Bl/6 mice.* Bone, 2015. **81**: p. 47-52.
397. Alexandre, C. and L. Vico, *Pathophysiology of bone loss in disuse osteoporosis.* Joint Bone Spine, 2011. **78**(6): p. 572-576.
398. Iwamoto, J., T. Takeda, and Y. Sato, *Interventions to prevent bone loss in astronauts during space flight.* Keio J Med, 2005. **54**(2): p. 55-9.
-

399. Carmeliet, G., L. Vico, and R. Bouillon, *Space flight: a challenge for normal bone homeostasis*. Crit Rev Eukaryot Gene Expr, 2001. **11**(1-3): p. 131-44.
400. Lang, T.F., A.D. Leblanc, H.J. Evans, and Y. Lu, *Adaptation of the proximal femur to skeletal reloading after long-duration spaceflight*. J Bone Miner Res, 2006. **21**(8): p. 1224-30.
401. Vico, L., B. van Rietbergen, N. Vilayphiou, M.T. Linossier, H. Locrelle, M. Normand, M. Zouch, M. Gerbaix, N. Bonnet, V. Novikov, T. Thomas, and G. Vassilieva, *Cortical and Trabecular Bone Microstructure Did Not Recover at Weight-Bearing Skeletal Sites and Progressively Deteriorated at Non-Weight-Bearing Sites During the Year Following International Space Station Missions*. J Bone Miner Res, 2017. **32**(10): p. 2010-2021.
402. Whedon, G.D., *Disuse osteoporosis: physiological aspects*. Calcif Tissue Int, 1984. **36 Suppl 1**: p. S146-50.
403. Bikle, D.D. and B.P. Halloran, *The response of bone to unloading*. J Bone Miner Metab, 1999. **17**(4): p. 233-44.
404. Takata, S. and N. Yasui, *Disuse osteoporosis*. J Med Invest, 2001. **48**(3-4): p. 147-56.
405. LeBlanc, A.D., E.R. Spector, H.J. Evans, and J.D. Sibonga, *Skeletal responses to space flight and the bed rest analog: a review*. J Musculoskelet Neuronal Interact, 2007. **7**(1): p. 33-47.
406. Garland, D.E., R.H. Adkins, C.A. Stewart, R. Ashford, and D. Vigil, *Regional osteoporosis in women who have a complete spinal cord injury*. J Bone Joint Surg Am, 2001. **83-a**(8): p. 1195-200.
407. Vico, L., P. Collet, A. Guignandon, M.-H. Lafage-Proust, T. Thomas, M. Rehalia, and C. Alexandre, *Effects of long-term microgravity exposure on cancellous and cortical weight-bearing bones of cosmonauts*. The Lancet, 2000. **355**(9215): p. 1607-1611.
408. Malone, A.M.D., C.T. Anderson, P. Tummala, R.Y. Kwon, T.R. Johnston, T. Stearns, and C.R. Jacobs, *Primary cilia mediate mechanosensing in bone cells by a calcium-independent mechanism*. Proceedings of the National Academy of Sciences, 2007. **104**(33): p. 13325-13330.
409. Yu, K., D.P. Sellman, A. Bahraini, M.L. Hagan, A. Elsherbini, K.T. Vanpelt, P.L. Marshall, M.W. Hamrick, A. McNeil, P.L. McNeil, and M.E. McGee-Lawrence, *Mechanical loading disrupts osteocyte plasma membranes which initiates mechanosensation events in bone*. J Orthop Res, 2018. **36**(2): p. 653-662.
410. Jiang, J.X. and P.P. Cherian, *Hemichannels formed by connexin 43 play an important role in the release of prostaglandin E(2) by osteocytes in response to mechanical strain*. Cell Commun Adhes, 2003. **10**(4-6): p. 259-64.
411. Genetos, D.C., C.J. Kephart, Y. Zhang, C.E. Yellowley, and H.J. Donahue, *Oscillating fluid flow activation of gap junction hemichannels induces ATP release from MLO-Y4 osteocytes*. J Cell Physiol, 2007. **212**(1): p. 207-14.
412. Zhang, Y., E.M. Paul, V. Sathyendra, A. Davison, N. Sharkey, S. Bronson, S. Srinivasan, T.S. Gross, and H.J. Donahue, *Enhanced osteoclastic resorption and responsiveness to mechanical load in gap junction deficient bone*. PLoS One, 2011. **6**(8): p. e23516.
413. Galea, G.L., L.B. Meakin, M.A. Harris, P.J. Delisser, L.E. Lanyon, S.E. Harris, and J.S. Price, *Old age and the associated impairment of bones' adaptation to loading are associated with transcriptomic changes in cellular metabolism, cell-matrix interactions and the cell cycle*. Gene, 2017. **599**: p. 36-52.

-
414. Galea, G.L., A. Sunters, L.B. Meakin, G. Zaman, T. Sugiyama, L.E. Lanyon, and J.S. Price, *Sost down-regulation by mechanical strain in human osteoblastic cells involves PGE2 signaling via EP4*. FEBS Lett, 2011. **585**(15): p. 2450-4.
415. Armstrong, V.J., M. Muzylak, A. Sunters, G. Zaman, L.K. Saxon, J.S. Price, and L.E. Lanyon, *Wnt/beta-catenin signaling is a component of osteoblastic bone cell early responses to load-bearing and requires estrogen receptor alpha*. J Biol Chem, 2007. **282**(28): p. 20715-27.
416. Damien, E., J.S. Price, and L.E. Lanyon, *The estrogen receptor's involvement in osteoblasts' adaptive response to mechanical strain*. J Bone Miner Res, 1998. **13**(8): p. 1275-82.
417. Damien, E., J.S. Price, and L.E. Lanyon, *Mechanical strain stimulates osteoblast proliferation through the estrogen receptor in males as well as females*. J Bone Miner Res, 2000. **15**(11): p. 2169-77.
418. Saxon, L.K., G. Galea, L. Meakin, J. Price, and L.E. Lanyon, *Estrogen Receptors alpha and beta Have Different Gender-Dependent Effects on the Adaptive Responses to Load Bearing in Cancellous and Cortical Bone*. Endocrinology, 2012. ;**153**(5):**2254-66**.
419. Galea, G.L., L.B. Meakin, T. Sugiyama, N. Zebda, A. Sunters, H. Taipaleenmaki, G.S. Stein, A.J. van Wijnen, L.E. Lanyon, and J.S. Price, *Estrogen receptor alpha mediates proliferation of osteoblastic cells stimulated by estrogen and mechanical strain, but their acute down-regulation of the Wnt antagonist Sost is mediated by estrogen receptor beta*. J Biol Chem, 2013. **288**(13): p. 9035-48.
420. Sunters, A., V.J. Armstrong, G. Zaman, R.M. Kypta, Y. Kawano, L.E. Lanyon, and J.S. Price, *Mechano-transduction in osteoblastic cells involves strain-regulated estrogen receptor alpha-mediated control of insulin-like growth factor (IGF) I receptor sensitivity to Ambient IGF, leading to phosphatidylinositol 3-kinase/AKT-dependent Wnt/LRP5 receptor-independent activation of beta-catenin signaling*. J Biol Chem, 2010. **285**(12): p. 8743-58.
421. Windahl, S.H., A.E. Borjesson, H.H. Farman, C. Engdahl, S. Moverare-Skrtic, K. Sjogren, M.K. Lagerquist, J.M. Kindblom, A. Koskela, J. Tuukkanen, P. Divieti Pajevic, J.Q. Feng, K. Dahlman-Wright, P. Antonson, J.A. Gustafsson, and C. Ohlsson, *Estrogen receptor-alpha in osteocytes is important for trabecular bone formation in male mice*. Proc Natl Acad Sci U S A, 2013. **110**(6): p. 2294-9.
422. Lee, K.C. and L.E. Lanyon, *Mechanical loading influences bone mass through estrogen receptor alpha*. Exerc Sport Sci Rev, 2004. **32**(2): p. 64-8.
423. Ajubi, N.E., J. Klein-Nulend, M.J. Alblas, E.H. Burger, and P.J. Nijweide, *Signal transduction pathways involved in fluid flow-induced PGE2 production by cultured osteocytes*. American Journal of Physiology - Endocrinology And Metabolism, 1999. **276**(1): p. E171-E178.
424. Lean, J.M., C.J. Jagger, T.J. Chambers, and J.W. Chow, *Increased insulin-like growth factor I mRNA expression in rat osteocytes in response to mechanical stimulation*. American Journal of Physiology - Endocrinology And Metabolism, 1995. **268**(2): p. E318-E327.
425. Sterck, J.G., J. Klein-Nulend, P. Lips, and E.H. Burger, *Response of normal and osteoporotic human bone cells to mechanical stress in vitro*. Am J Physiol, 1998. **274**(6 Pt 1): p. E1113-20.
426. Mullender, M.G., D.D. van der Meer, R. Huiskes, and P. Lips, *Osteocyte density changes in aging and osteoporosis*. Bone, 1996. **18**(2): p. 109-13.
-

427. Joiner, D.M., R.J. Tayim, J.D. McElderry, M.D. Morris, and S.A. Goldstein, *Aged male rats regenerate cortical bone with reduced osteocyte density and reduced secretion of nitric oxide after mechanical stimulation*. *Calcif Tissue Int*, 2014. **94**(5): p. 484-94.
428. Holguin, N., M.D. Brodt, and M.J. Silva, *Activation of Wnt Signaling By Mechanical Loading Is Impaired in the Bone of Old Mice*. *J Bone Miner Res*, 2016.
429. Plotkin, L.I., *Apoptotic osteocytes and the control of targeted bone resorption*. *Curr Osteoporos Rep*, 2014. **12**(1): p. 121-6.
430. Pead, M.J., T.M. Skerry, and L.E. Lanyon, *Direct transformation from quiescence to bone formation in the adult periosteum following a single brief period of bone loading*. *J Bone Miner Res*, 1988. **3**(6): p. 647-56.
431. Turner, C.H., I. Owan, T. Alvey, J. Hulman, and J.M. Hock, *Recruitment and proliferative responses of osteoblasts after mechanical loading in vivo determined using sustained-release bromodeoxyuridine*. *Bone*, 1998. **22**(5): p. 463-9.
432. Rooney, A.M. and M.C.H. van der Meulen, *Mouse models to evaluate the role of estrogen receptor α in skeletal maintenance and adaptation*. *Annals of the New York Academy of Sciences*, 2017. **1410**(1): p. 85-92.
433. Melville, K.M., N.H. Kelly, G. Surita, D.B. Buchalter, J.C. Schimenti, R.P. Main, F.P. Ross, and M.C. van der Meulen, *Effects of Deletion of ERalpha in Osteoblast-Lineage Cells on Bone Mass and Adaptation to Mechanical Loading Differ in Female and Male Mice*. *J Bone Miner Res*, 2015. **30**(8): p. 1468-80.
434. Kohrt, W.M., *Aging and the osteogenic response to mechanical loading*. *Int J Sport Nutr Exerc Metab*, 2001. **11 Suppl**: p. S137-42.
435. Skerry, T.M., *The response of bone to mechanical loading and disuse: fundamental principles and influences on osteoblast/osteocyte homeostasis*. *Arch Biochem Biophys*, 2008. **473**(2): p. 117-23.
436. Guo, Y., Y. Wang, Y. Liu, H. Wang, C. Guo, and X. Zhang, *Effect of the same mechanical loading on osteogenesis and osteoclastogenesis in vitro*. *Chin J Traumatol*, 2015. **18**(3): p. 150-6.
437. Zhang, P., K. Hamamura, and H. Yokota, *A Brief Review of Bone Adaptation to Unloading*. *Genomics, Proteomics & Bioinformatics*, 2008. **6**(1): p. 4-7.
438. Basse, E.J., M.C. Rothwell, J.J. Littlewood, and D.W. Pye, *Pre- and postmenopausal women have different bone mineral density responses to the same high-impact exercise*. *J Bone Miner Res*, 1998. **13**(12): p. 1805-13.
439. Kohrt, W.M., A.A. Ehsani, and S.J. Birge, Jr., *Effects of exercise involving predominantly either joint-reaction or ground-reaction forces on bone mineral density in older women*. *J Bone Miner Res*, 1997. **12**(8): p. 1253-61.
440. Kanis, J.A., O. Johnell, A. Oden, A. Dawson, C. De Laet, and B. Jonsson, *Ten year probabilities of osteoporotic fractures according to BMD and diagnostic thresholds*. *Osteoporos Int*, 2001. **12**(12): p. 989-95.
441. Johnell, O. and J. Kanis, *Epidemiology of osteoporotic fractures*. *Osteoporos Int*, 2005. **16 Suppl 2**: p. S3-7.

-
442. Bleibler, F., K. Rapp, A. Jaensch, C. Becker, and H.H. Konig, *Expected lifetime numbers and costs of fractures in postmenopausal women with and without osteoporosis in Germany: a discrete event simulation model*. BMC Health Serv Res, 2014. **14**: p. 284.
443. Srinivasan, S., T.S. Gross, and S.D. Bain, *Bone mechanotransduction may require augmentation in order to strengthen the senescent skeleton*. Ageing Res Rev, 2012. **11**(3): p. 353-60.
444. Specker, B. and T. Binkley, *Randomized trial of physical activity and calcium supplementation on bone mineral content in 3- to 5-year-old children*. J Bone Miner Res, 2003. **18**(5): p. 885-92.
445. MacKelvie, K.J., M.A. Petit, K.M. Khan, T.J. Beck, and H.A. McKay, *Bone mass and structure are enhanced following a 2-year randomized controlled trial of exercise in prepubertal boys*. Bone, 2004. **34**(4): p. 755-64.
446. Uusi-Rasi, K., P. Kannus, S. Cheng, H. Sievanen, M. Pasanen, A. Heinonen, A. Nenonen, J. Halleen, T. Fuerst, H. Genant, and I. Vuori, *Effect of alendronate and exercise on bone and physical performance of postmenopausal women: a randomized controlled trial*. Bone, 2003. **33**(1): p. 132-43.
447. Karinkanta, S., A. Heinonen, H. Sievanen, K. Uusi-Rasi, M. Pasanen, K. Ojala, M. Fogelholm, and P. Kannus, *A multi-component exercise regimen to prevent functional decline and bone fragility in home-dwelling elderly women: randomized, controlled trial*. Osteoporos Int, 2007. **18**(4): p. 453-62.
448. Kukuljan, S., C.A. Nowson, K.M. Sanders, G.C. Nicholson, M.J. Seibel, J. Salmon, and R.M. Daly, *Independent and combined effects of calcium-vitamin D3 and exercise on bone structure and strength in older men: an 18-month factorial design randomized controlled trial*. J Clin Endocrinol Metab, 2011. **96**(4): p. 955-63.
449. Nilsson, M., D. Sundh, C. Ohlsson, M. Karlsson, D. Mellstrom, and M. Lorentzon, *Exercise during growth and young adulthood is independently associated with cortical bone size and strength in old Swedish men*. J Bone Miner Res, 2014. **29**(8): p. 1795-804.
450. Prior, J.C., S.I. Barr, R. Chow, and R.A. Faulkner, *Prevention and management of osteoporosis: consensus statements from the Scientific Advisory Board of the Osteoporosis Society of Canada. 5. Physical activity as therapy for osteoporosis*. Cmaj, 1996. **155**(7): p. 940-4.
451. Thorsen, K., A. Kristoffersson, and R. Lorentzon, *The effects of brisk walking on markers of bone and calcium metabolism in postmenopausal women*. Calcif Tissue Int, 1996. **58**(4): p. 221-5.
452. Marques, E.A., J. Mota, and J. Carvalho, *Exercise effects on bone mineral density in older adults: a meta-analysis of randomized controlled trials*. Age (Dordr), 2012. **34**(6): p. 1493-515.
453. Lynch, M.E., R.P. Main, Q. Xu, T.L. Schmicker, M.B. Schaffler, T.M. Wright, and M.C. van der Meulen, *Tibial compression is anabolic in the adult mouse skeleton despite reduced responsiveness with aging*. Bone, 2011. **49**(3): p. 439-46.
454. Willie, B.M., A.I. Birkhold, H. Razi, T. Thiele, M. Aido, B. Kruck, A. Schill, S. Checa, R.P. Main, and G.N. Duda, *Diminished response to in vivo mechanical loading in trabecular and not cortical bone in adulthood of female C57Bl/6 mice coincides with a reduction in deformation to load*. Bone, 2013. **55**(2): p. 335-46.
-

455. Holguin, N., M.D. Brodt, M.E. Sanchez, and M.J. Silva, *Aging diminishes lamellar and woven bone formation induced by tibial compression in adult C57BL/6*. Bone, 2014. **65**: p. 83-91.
456. Rittweger, J., H.M. Frost, H. Schiessl, H. Ohshima, B. Alkner, P. Tesch, and D. Felsenberg, *Muscle atrophy and bone loss after 90 days' bed rest and the effects of flywheel resistive exercise and pamidronate: Results from the LTBR study*. Bone, 2005. **36**(6): p. 1019-1029.
457. Leblanc, A., T. Matsumoto, J. Jones, J. Shapiro, T. Lang, L. Shackelford, S.M. Smith, H. Evans, E. Spector, R. Ploutz-Snyder, J. Sibonga, J. Keyak, T. Nakamura, K. Kohri, and H. Ohshima, *Bisphosphonates as a supplement to exercise to protect bone during long-duration spaceflight*. Osteoporos Int, 2013. **24**(7): p. 2105-14.
458. Tarvainen, R., I. Arnala, H. Olkkonen, R. Lappalainen, T. Nevalainen, and E. Alhava, *Clodronate prevents immobilization osteopenia in rats*. Acta Orthop Scand, 1994. **65**(6): p. 643-6.
459. Iwamoto, J., T. Takeda, T. Katsumata, T. Tanaka, S. Ichimura, and Y. Toyama, *Effect of etidronate on bone in orchidectomized and sciatic neurectomized adult rats*. Bone, 2002. **30**(2): p. 360-7.
460. Iwamoto, J., A. Seki, T. Takeda, Y. Sato, and H. Yamada, *Effects of risedronate on femoral bone mineral density and bone strength in sciatic neurectomized young rats*. J Bone Miner Metab, 2005. **23**(6): p. 456-62.
461. Plotkin, L.I., A.R. Gortazar, H.M. Davis, K.W. Condon, H. Gabilondo, M. Maycas, M.R. Allen, and T. Bellido, *Inhibition of osteocyte apoptosis prevents the increase in osteocytic receptor activator of nuclear factor kappaB ligand (RANKL) but does not stop bone resorption or the loss of bone induced by unloading*. J Biol Chem, 2015. **290**(31): p. 18934-42.
462. Feher, A., A. Koivunemi, M. Koivunemi, R.K. Fuchs, D.B. Burr, R.J. Phipps, S. Reinwald, and M.R. Allen, *Bisphosphonates do not inhibit periosteal bone formation in estrogen deficient animals and allow enhanced bone modeling in response to mechanical loading*. Bone, 2010. **46**(1): p. 203-7.
463. Hatori, K., G.V. Camargos, M. Chatterjee, F. Faot, K. Sasaki, J. Duyck, and K. Vandamme, *Single and combined effect of high-frequency loading and bisphosphonate treatment on the bone micro-architecture of ovariectomized rats*. Osteoporos Int, 2015. **26**(1): p. 303-13.
464. Braith, R.W., J.A. Conner, M.N. Fulton, C.F. Lisor, D.P. Casey, K.S. Howe, and M.A. Baz, *Comparison of Alendronate vs Alendronate Plus Mechanical Loading as Prophylaxis for Osteoporosis in Lung Transplant Recipients: a Pilot Study*. The Journal of Heart and Lung Transplantation, 2007. **26**(2): p. 132-137.
465. Braith, R.W., P.M. Magyari, M.N. Fulton, J. Aranda Jr, T. Walker, and J.A. Hill, *Resistance exercise training and alendronate reverse Glucocorticoid-Induced osteoporosis in heart transplant recipients*. The Journal of Heart and Lung Transplantation, 2003. **22**(10): p. 1082-1090.
466. Chilibeck, P.D., K.S. Davison, S.J. Whiting, Y. Suzuki, C.L. Janzen, and P. Peloso, *The effect of strength training combined with bisphosphonate (etidronate) therapy on bone mineral, lean tissue, and fat mass in postmenopausal women*. Canadian Journal of Physiology and Pharmacology, 2002. **80**(10): p. 941-950.

-
467. Vegger, J.B., E.S. Nielsen, A. Brüel, and J.S. Thomsen, *Additive effect of PTH (1–34) and zoledronate in the prevention of disuse osteopenia in rats*. *Bone*, 2014. **66**: p. 287-295.
468. Turner, R.T., G.L. Evans, S. Lotinun, P.D. Lapke, U.T. Iwaniec, and E. Morey-Holton, *Dose-response effects of intermittent PTH on cancellous bone in hindlimb unloaded rats*. *J Bone Miner Res*, 2007. **22**(1): p. 64-71.
469. Bruel, A., J.B. Vegger, A.C. Raffalt, J.E. Andersen, and J.S. Thomsen, *PTH (1-34), but not strontium ranelate counteract loss of trabecular thickness and bone strength in disuse osteopenic rats*. *Bone*, 2013. **53**(1): p. 51-8.
470. Brent, M.B., A. Bruel, and J.S. Thomsen, *PTH (1-34) and growth hormone in prevention of disuse osteopenia and sarcopenia in rats*. *Bone*, 2018.
471. Ma, Y., W.S. Jee, Z. Yuan, W. Wei, H. Chen, S. Pun, H. Liang, and C. Lin, *Parathyroid hormone and mechanical usage have a synergistic effect in rat tibial diaphyseal cortical bone*. *J Bone Miner Res*, 1999. **14**(3): p. 439-48.
472. Delgado-Calle, J., X. Tu, R. Pacheco-Costa, K. McAndrews, R. Edwards, G.G. Pellegrini, K. Kuhlenschmidt, N. Olivos, A. Robling, M. Peacock, L.I. Plotkin, and T. Bellido, *Control of Bone Anabolism in Response to Mechanical Loading and PTH by Distinct Mechanisms Downstream of the PTH Receptor*. *J Bone Miner Res*, 2017. **32**(3): p. 522-535.
473. Grosso, M.J., H.W. Courtland, X. Yang, J.P. Sutherland, K. Stoner, J. Nguyen, A. Fahlgren, F.P. Ross, M.C. van der Meulen, and M.P. Bostrom, *Intermittent PTH administration and mechanical loading are anabolic for periprosthetic cancellous bone*. *J Orthop Res*, 2015. **33**(2): p. 163-73.
474. Zhao, R., Z. Xu, and M. Zhao, *Effects of Oestrogen Treatment on Skeletal Response to Exercise in the Hips and Spine in Postmenopausal Women: A Meta-Analysis*. *Sports Med*, 2015. **45**(8): p. 1163-73.
475. Brooke-Wavell, K., G.M. Prelevic, C. Bartram, and J. Ginsburg, *The influence of physical activity on the response of bone mineral density to 5 years tibolone*. *Maturitas*, 2000. **35**(3): p. 229-35.
476. Saxon, L.K. and C.H. Turner, *Low-dose estrogen treatment suppresses periosteal bone formation in response to mechanical loading*. *Bone*, 2006. **39**(6): p. 1261-7.
477. Wakley, G.K., B.L. Baum, K.S. Hannon, and R.T. Turner, *The effects of tamoxifen on the osteopenia induced by sciatic neurotomy in the rat: a histomorphometric study*. *Calcif Tissue Int*, 1988. **43**(6): p. 383-8.
478. Waters, D.J., D.D. Caywood, and R.T. Turner, *Effect of tamoxifen citrate on canine immobilization (disuse) osteoporosis*. *Vet Surg*, 1991. **20**(6): p. 392-6.
479. Tian, X., W.S. Jee, X. Li, C. Paszty, and H.Z. Ke, *Sclerostin antibody increases bone mass by stimulating bone formation and inhibiting bone resorption in a hindlimb-immobilization rat model*. *Bone*, 2011. **48**(2): p. 197-201.
480. Spatz, J.M., R. Ellman, A.M. Cloutier, L. Louis, M. van Vliet, L.J. Suva, D. Dwyer, M. Stolina, H.Z. Ke, and M.L. Bouxsein, *Sclerostin antibody inhibits skeletal deterioration due to reduced mechanical loading*. *J Bone Miner Res*, 2013. **28**(4): p. 865-74.
481. Shahnazari, M., T. Wronski, V. Chu, A. Williams, A. Leeper, M. Stolina, H.Z. Ke, and B. Halloran, *Early response of bone marrow osteoprogenitors to skeletal unloading and sclerostin antibody*. *Calcif Tissue Int*, 2012. **91**(1): p. 50-8.
-

482. Qin, W., X. Li, Y. Peng, L.M. Harlow, Y. Ren, Y. Wu, J. Li, Y. Qin, J. Sun, S. Zheng, T. Brown, J.Q. Feng, H.Z. Ke, W.A. Bauman, and C.C. Cardozo, *Sclerostin antibody preserves the morphology and structure of osteocytes and blocks the severe skeletal deterioration after motor-complete spinal cord injury in rats*. *J Bone Miner Res*, 2015. **30**(11): p. 1994-2004.
483. Zhang, D., M. Hu, T. Chu, L. Lin, J. Wang, X. Li, H.Z. Ke, and Y.X. Qin, *Sclerostin antibody prevented progressive bone loss in combined ovariectomized and concurrent functional disuse*. *Bone*, 2016. **87**: p. 161-8.
484. Meakin, L.B., J.S. Price, and L.E. Lanyon, *The Contribution of Experimental in vivo Models to Understanding the Mechanisms of Adaptation to Mechanical Loading in Bone*. *Front Endocrinol (Lausanne)*, 2014. **5**: p. 154.
485. Woo, S.L., S.C. Kuei, D. Amiel, M.A. Gomez, W.C. Hayes, F.C. White, and W.H. Akeson, *The effect of prolonged physical training on the properties of long bone: a study of Wolff's Law*. *J Bone Joint Surg Am*, 1981. **63**(5): p. 780-7.
486. Yeh, J.K., J.F. Aloia, M.M. Chen, J.M. Tierney, and S. Sprintz, *Influence of exercise on cancellous bone of the aged female rat*. *J Bone Miner Res*, 1993. **8**(9): p. 1117-25.
487. Bourrin, S., S. Palle, R. Pupier, L. Vico, and C. Alexandre, *Effect of physical training on bone adaptation in three zones of the rat tibia*. *J Bone Miner Res*, 1995. **10**(11): p. 1745-52.
488. Rubin, C.T. and L.E. Lanyon, *Limb mechanics as a function of speed and gait: a study of functional strains in the radius and tibia of horse and dog*. *J Exp Biol*, 1982. **101**: p. 187-211.
489. Konieczynski, D.D., M.J. Truty, and A.A. Biewener, *Evaluation of a bone's in vivo 24-hour loading history for physical exercise compared with background loading*. *J Orthop Res*, 1998. **16**(1): p. 29-37.
490. Umemura, Y., D.J. Baylink, J.E. Wergedal, S. Mohan, and A.K. Srivastava, *A time course of bone response to jump exercise in C57BL/6J mice*. *J Bone Miner Metab*, 2002. **20**(4): p. 209-15.
491. Kodama, Y., Y. Umemura, S. Nagasawa, W.G. Beamer, L.R. Donahue, C.R. Rosen, D.J. Baylink, and J.R. Farley, *Exercise and mechanical loading increase periosteal bone formation and whole bone strength in C57BL/6J mice but not in C3H/HeJ mice*. *Calcif Tissue Int*, 2000. **66**(4): p. 298-306.
492. Hoshi, A., H. Watanabe, M. Chiba, and Y. Inaba, *Effects of swimming and weight loading on bone density and mechanical properties of the mouse femoral bone*. *Environ Health Prev Med*, 1996. **1**(3): p. 128-32.
493. Buhl, K.M., C.R. Jacobs, R.T. Turner, G.L. Evans, P.A. Farrell, and H.J. Donahue, *Aged bone displays an increased responsiveness to low-intensity resistance exercise*. *J Appl Physiol* (1985), 2001. **90**(4): p. 1359-64.
494. Snyder, A., J.R. Zierath, J.A. Hawley, M.D. Sleeper, and B.W. Craig, *The effects of exercise mode, swimming vs. running, upon bone growth in the rapidly growing female rat*. *Mech Ageing Dev*, 1992. **66**(1): p. 59-69.
495. Okubo, R., L.S. Sanada, V.A. Castania, M.J. Louzada, F.J. de Paula, N. Maffulli, and A.C. Shimano, *Jumping exercise preserves bone mineral density and mechanical properties in osteopenic ovariectomized rats even following established osteopenia*. *Osteoporos Int*, 2017. **28**(4): p. 1461-1471.

-
496. Falcai, M.J., A. Zamarioli, R. Okubo, F.J. de Paula, and J.B. Volpon, *The osteogenic effects of swimming, jumping, and vibration on the protection of bone quality from disuse bone loss*. Scand J Med Sci Sports, 2015. **25**(3): p. 390-7.
497. Umemura, Y., T. Ishiko, T. Yamauchi, M. Kurono, and S. Mashiko, *Five jumps per day increase bone mass and breaking force in rats*. J Bone Miner Res, 1997. **12**(9): p. 1480-5.
498. Chamay, A. and P. Tschantz, *Mechanical influences in bone remodeling. Experimental research on Wolff's law*. Journal of Biomechanics, 1972. **5**(2): p. 173-180.
499. Goodship, A.E., L.E. Lanyon, and H. McFie, *Functional adaptation of bone to increased stress. An experimental study*. J Bone Joint Surg Am, 1979. **61**(4): p. 539-46.
500. Lanyon, L.E., A.E. Goodship, C.J. Pye, and J.H. MacFie, *Mechanically adaptive bone remodelling*. J Biomech, 1982. **15**(3): p. 141-54.
501. Burr, D.B., M.B. Schaffler, K.H. Yang, D.D. Wu, M. Lukoschek, D. Kandzari, N. Sivaneri, J.D. Blaha, and E.L. Radin, *The effects of altered strain environments on bone tissue kinetics*. Bone, 1989. **10**(3): p. 215-21.
502. Burr, D.B., M.B. Schaffler, K.H. Yang, M. Lukoschek, N. Sivaneri, J.D. Blaha, and E.L. Radin, *Skeletal change in response to altered strain environments: is woven bone a response to elevated strain?* Bone, 1989. **10**(3): p. 223-33.
503. Hille, E., K.P. Schulitz, J. Gipperich, and B. Dettmann, *Experimental stress-induced changes in growing long bones*. Int Orthop, 1988. **12**(4): p. 309-15.
504. Liskova, M. and J. Hert, *Reaction of bone to mechanical stimuli. 2. Periosteal and endosteal reaction of tibial diaphysis in rabbit to intermittent loading*. Folia Morphol (Praha), 1971. **19**(3): p. 301-17.
505. Hert, J., M. Liskova, and J. Landa, *Reaction of bone to mechanical stimuli. 1. Continuous and intermittent loading of tibia in rabbit*. Folia Morphol (Praha), 1971. **19**(3): p. 290-300.
506. Churches, A.E. and C.R. Howlett, *Functional adaptation of bone in response to sinusoidally varying controlled compressive loading of the ovine metacarpus*. Clin Orthop Relat Res, 1982(168): p. 265-80.
507. Meade, J.B., S.C. Cowin, J.J. Klawitter, W.C. Van Buskirk, and H.B. Skinner, *Bone remodeling due to continuously applied loads*. Calcif Tissue Int, 1984. **36 Suppl 1**: p. S25-30.
508. Rubin, C.T. and L.E. Lanyon, *Kappa Delta Award paper. Osteoregulatory nature of mechanical stimuli: function as a determinant for adaptive remodeling in bone*. J Orthop Res, 1987. **5**(2): p. 300-10.
509. Rubin, C.T. and L.E. Lanyon, *Regulation of bone mass by mechanical strain magnitude*. Calcif Tissue Int, 1985. **37**(4): p. 411-7.
510. Lanyon, L.E., C.T. Rubin, and G. Baust, *Modulation of bone loss during calcium insufficiency by controlled dynamic loading*. Calcif Tissue Int, 1986. **38**(4): p. 209-16.
511. Lanyon, L.E. and C.T. Rubin, *Static vs dynamic loads as an influence on bone remodelling*. J Biomech, 1984. **17**(12): p. 897-905.
512. Chambers, T.J., M. Evans, T.N. Gardner, A. Turner-Smith, and J.W. Chow, *Induction of bone formation in rat tail vertebrae by mechanical loading*. Bone Miner, 1993. **20**(2): p. 167-78.
-

513. Webster, D., F.A. Schulte, F.M. Lambers, G. Kuhn, and R. Muller, *Strain energy density gradients in bone marrow predict osteoblast and osteoclast activity: a finite element study*. J Biomech, 2015. **48**(5): p. 866-74.
514. Lambers, F.M., F. Stuker, C. Weigt, G. Kuhn, K. Koch, F.A. Schulte, J. Ripoll, M. Rudin, and R. Muller, *Longitudinal in vivo imaging of bone formation and resorption using fluorescence molecular tomography*. Bone, 2013. **52**(2): p. 587-95.
515. Lambers, F.M., F.A. Schulte, G. Kuhn, D.J. Webster, and R. Muller, *Mouse tail vertebrae adapt to cyclic mechanical loading by increasing bone formation rate and decreasing bone resorption rate as shown by time-lapsed in vivo imaging of dynamic bone morphometry*. Bone, 2011. **49**(6): p. 1340-50.
516. Lambers, F.M., G. Kuhn, F.A. Schulte, K. Koch, and R. Muller, *Longitudinal assessment of in vivo bone dynamics in a mouse tail model of postmenopausal osteoporosis*. Calcif Tissue Int, 2012. **90**(2): p. 108-19.
517. Turner, C.H., M.P. Akhter, D.M. Raab, D.B. Kimmel, and R.R. Recker, *A noninvasive, in vivo model for studying strain adaptive bone modeling*. Bone, 1991. **12**(2): p. 73-9.
518. Akhter, M.P., D.M. Raab, C.H. Turner, D.B. Kimmel, and R.R. Recker, *Characterization of in vivo strain in the rat tibia during external application of a four-point bending load*. J Biomech, 1992. **25**(10): p. 1241-6.
519. Gross, T.S., S. Srinivasan, C.C. Liu, T.L. Clemens, and S.D. Bain, *Noninvasive loading of the murine tibia: an in vivo model for the study of mechanotransduction*. J Bone Miner Res, 2002. **17**(3): p. 493-501.
520. Torrance, A.G., J.R. Mosley, R.F. Suswillo, and L.E. Lanyon, *Noninvasive loading of the rat ulna in vivo induces a strain-related modeling response uncomplicated by trauma or periosteal pressure*. Calcif Tissue Int, 1994. **54**(3): p. 241-7.
521. Lee, K.C., A. Maxwell, and L.E. Lanyon, *Validation of a technique for studying functional adaptation of the mouse ulna in response to mechanical loading*. Bone, 2002. **31**(3): p. 407-12.
522. Mosley, J.R., B.M. March, J. Lynch, and L.E. Lanyon, *Strain magnitude related changes in whole bone architecture in growing rats*. Bone, 1997. **20**(3): p. 191-8.
523. Robling, A.G., K.M. Duijvelaar, J.V. Geever, N. Ohashi, and C.H. Turner, *Modulation of appositional and longitudinal bone growth in the rat ulna by applied static and dynamic force*. Bone, 2001. **29**(2): p. 105-13.
524. Sample, S.J., M. Behan, L. Smith, W.E. Oldenhoff, M.D. Markel, V.L. Kalscheur, Z. Hao, V. Miletic, and P. Muir, *Functional adaptation to loading of a single bone is neuronally regulated and involves multiple bones*. J Bone Miner Res, 2008. **23**(9): p. 1372-81.
525. McKenzie, J.A. and M.J. Silva, *Comparing histological, vascular and molecular responses associated with woven and lamellar bone formation induced by mechanical loading in the rat ulna*. Bone, 2011. **48**(2): p. 250-8.
526. de Souza, R.L. and L. Saxon, *In vivo mechanical loading*. Methods Mol Biol, 2012. **816**: p. 621-36.
527. Pierroz, D.D., N. Bonnet, E.N. Bianchi, M.L. Boussein, P.A. Baldock, R. Rizzoli, and S.L. Ferrari, *Deletion of beta-adrenergic receptor 1, 2, or both leads to different bone*

- phenotypes and response to mechanical stimulation*. J Bone Miner Res, 2012. **27**(6): p. 1252-62.
528. Tu, X., Y. Rhee, K.W. Condon, N. Bivi, M.R. Allen, D. Dwyer, M. Stolina, C.H. Turner, A.G. Robling, L.I. Plotkin, and T. Bellido, *Sost downregulation and local Wnt signaling are required for the osteogenic response to mechanical loading*. Bone, 2012. **50**(1): p. 209-17.
529. Birkhold, A.I., H. Razi, G.N. Duda, S. Checa, and B.M. Willie, *Tomography-Based Quantification of Regional Differences in Cortical Bone Surface Remodeling and Mechano-Response*. Calcif Tissue Int, 2017. **100**(3): p. 255-270.
530. Birkhold, A.I., H. Razi, G.N. Duda, R. Weinkamer, S. Checa, and B.M. Willie, *The Periosteal Bone Surface is Less Mechano-Responsive than the Endocortical*. Scientific Reports, 2016. **6**: p. 23480.
531. Bergstrom, I., J.G. Kerns, A.E. Tornqvist, C. Perdikouri, N. Mathavan, A. Koskela, H.B. Henriksson, J. Tuukkanen, G. Andersson, H. Isaksson, A.E. Goodship, and S.H. Windahl, *Compressive loading of the murine tibia reveals site-specific micro-scale differences in adaptation and maturation rates of bone*. Osteoporos Int, 2017. **28**(3): p. 1121-1131.
532. Brodt, M.D. and M.J. Silva, *Aged mice have enhanced endocortical response and normal periosteal response compared with young-adult mice following 1 week of axial tibial compression*. J Bone Miner Res, 2010. **25**(9): p. 2006-15.
533. Rubin, C.T. and L.E. Lanyon, *Regulation of bone formation by applied dynamic loads*. J Bone Joint Surg Am, 1984. **66**(3): p. 397-402.
534. Mosley, J.R. and L.E. Lanyon, *Strain rate as a controlling influence on adaptive modeling in response to dynamic loading of the ulna in growing male rats*. Bone, 1998. **23**(4): p. 313-8.
535. Turner, C.H., I. Owan, and Y. Takano, *Mechanotransduction in bone: role of strain rate*. Am J Physiol, 1995. **269**(3 Pt 1): p. E438-42.
536. Fritton, S.P. and C.T. Rubin, *In vivo measurement of bone deformations using strain gauges*, in *Bone Biomechanics Handbook*, S.C. Cowin, Editor. 2001, CRC Press: Boca Raton, FL. p. 1-41.
537. Robling, A.G., D.B. Burr, and C.H. Turner, *Partitioning a daily mechanical stimulus into discrete loading bouts improves the osteogenic response to loading*. J Bone Miner Res, 2000. **15**(8): p. 1596-602.
538. Robling, A.G., D.B. Burr, and C.H. Turner, *Recovery periods restore mechanosensitivity to dynamically loaded bone*. J Exp Biol, 2001. **204**(Pt 19): p. 3389-99.
539. Srinivasan, S., D.A. Weimer, S.C. Agans, S.D. Bain, and T.S. Gross, *Low-magnitude mechanical loading becomes osteogenic when rest is inserted between each load cycle*. J Bone Miner Res, 2002. **17**(9): p. 1613-20.
540. Srinivasan, S., B.J. Ausk, S.L. Poliachik, S.E. Warner, T.S. Richardson, and T.S. Gross, *Rest-inserted loading rapidly amplifies the response of bone to small increases in strain and load cycles*. J Appl Physiol (1985), 2007. **102**(5): p. 1945-52.
541. Ilyin, E.A. and V.S. Oganov, *Microgravity and musculoskeletal system of mammals*. Adv Space Res, 1989. **9**(11): p. 11-9.

542. Vico, L., D. Chappard, C. Alexandre, S. Palle, P. Minaire, G. Riffat, V.E. Novikov, and A.V. Bakulin, *Effects of weightlessness on bone mass and osteoclast number in pregnant rats after a five-day spaceflight (COSMOS 1514)*. *Bone*, 1987. **8**(2): p. 95-103.
543. Vico, L., V.E. Novikov, J.M. Very, and C. Alexandre, *Bone histomorphometric comparison of rat tibial metaphysis after 7-day tail suspension vs. 7-day spaceflight*. *Aviat Space Environ Med*, 1991. **62**(1): p. 26-31.
544. Vico, L. and C. Alexandre, *Microgravity and bone adaptation at the tissue level*. *J Bone Miner Res*, 1992. **7 Suppl 2**: p. S445-7.
545. Zerath, E., D. Godet, X. Holy, C. Andre, S. Renault, M. Hott, and P.J. Marie, *Effects of spaceflight and recovery on rat humeri and vertebrae: histological and cell culture studies*. *J Appl Physiol* (1985), 1996. **81**(1): p. 164-71.
546. Foldes, I., M. Rapcsak, T. Szilagy, and V.S. Oganov, *Effects of space flight on bone formation and resorption*. *Acta Physiol Hung*, 1990. **75**(4): p. 271-85.
547. Gerbaix, M., V. Gnyubkin, D. Farlay, C. Olivier, P. Ammann, G. Courbon, N. Laroche, R. Genthial, H. Follet, F. Peyrin, B. Shenkman, G. Gauquelin-Koch, and L. Vico, *One-month spaceflight compromises the bone microstructure, tissue-level mechanical properties, osteocyte survival and lacunae volume in mature mice skeletons*. *Sci Rep*, 2017. **7**(1): p. 2659.
548. Morey-Holton, E.R., B.P. Halloran, L.P. Garetto, and S.B. Doty, *Animal housing influences the response of bone to spaceflight in juvenile rats*. *J Appl Physiol* (1985), 2000. **88**(4): p. 1303-9.
549. Willey, J.S., S.A.J. Lloyd, M.E. Robbins, J.D. Bourland, H. Smith-Sielicki, L.C. Bowman, R.W. Norrdin, and T.A. Bateman, *Early Increase in Osteoclast Number in Mice after Whole-Body Irradiation with 2 Gy X Rays*. *Radiation Research*, 2008. **170**(3): p. 388-392.
550. Wright, L.E., J.T. Buijs, H.-S. Kim, L.E. Coats, A.M. Scheidler, S.K. John, Y. She, S. Murthy, N. Ma, H.J. Chin-Sinex, T.M. Bellido, T.A. Bateman, M.S. Mendonca, K.S. Mohammad, and T.A. Guise, *Single-Limb Irradiation Induces Local and Systemic Bone Loss in a Murine Model*. *Journal of Bone and Mineral Research*, 2015. **30**(7): p. 1268-1279.
551. Shirazi-Fard, Y., J.S. Alwood, A.S. Schreurs, A.B. Castillo, and R.K. Globus, *Mechanical loading causes site-specific anabolic effects on bone following exposure to ionizing radiation*. *Bone*, 2015. **81**: p. 260-9.
552. Uhthoff, H.K. and Z.F. Jaworski, *Bone loss in response to long-term immobilisation*. *J Bone Joint Surg Br*, 1978. **60-b**(3): p. 420-9.
553. Turner, R.T. and N.H. Bell, *The effects of immobilization on bone histomorphometry in rats*. *J Bone Miner Res*, 1986. **1**(5): p. 399-407.
554. Rubin, C.T., G.W. Pratt, Jr., A.L. Porter, L.E. Lanyon, and R. Poss, *Ultrasonic measurement of immobilization-induced osteopenia: an experimental study in sheep*. *Calcif Tissue Int*, 1988. **42**(5): p. 309-12.
555. Li, X.J., W.S. Jee, S.Y. Chow, and D.M. Woodbury, *Adaptation of cancellous bone to aging and immobilization in the rat: a single photon absorptiometry and histomorphometry study*. *Anat Rec*, 1990. **227**(1): p. 12-24.
556. Skerry, T.M. and L.E. Lanyon, *Immobilisation induced bone loss in the sheep is not modulated by calcitonin treatment*. *Bone*, 1993. **14**(3): p. 511-6.

-
557. Thomas, T., L. Vico, T.M. Skerry, F. Caulin, L.E. Lanyon, C. Alexandre, and M.H. Lafage, *Architectural modifications and cellular response during disuse-related bone loss in calcaneus of the sheep*. J Appl Physiol (1985), 1996. **80**(1): p. 198-202.
558. Globus, R.K., D.D. Bikle, and E. Morey-Holton, *The temporal response of bone to unloading*. Endocrinology, 1986. **118**(2): p. 733-42.
559. Globus, R.K., D.D. Bikle, B. Halloran, and E. Morey-Holton, *Skeletal response to dietary calcium in a rat model simulating weightlessness*. J Bone Miner Res, 1986. **1**(2): p. 191-7.
560. Tanaka, S., A. Sakai, M. Tanaka, H. Otomo, N. Okimoto, T. Sakata, and T. Nakamura, *Skeletal Unloading Alleviates the Anabolic Action of Intermittent PTH(1–34) in Mouse Tibia in Association With Inhibition of PTH-Induced Increase in c-fos mRNA in Bone Marrow Cells*. Journal of Bone and Mineral Research, 2004. **19**(11): p. 1813-1820.
561. Dufour, C., X. Holy, and P.J. Marie, *Skeletal unloading induces osteoblast apoptosis and targets alpha5beta1-PI3K-Bcl-2 signaling in rat bone*. Exp Cell Res, 2007. **313**(2): p. 394-403.
562. Plotkin, L.I., A.R. Gortazar, H.M. Davis, K.W. Condon, H. Gabilondo, M. Maycas, M.R. Allen, and T. Bellido, *Inhibition of Osteocyte Apoptosis Prevents the Increase in Osteocytic Receptor Activator of Nuclear Factor κ B Ligand (RANKL) but Does Not Stop Bone Resorption or the Loss of Bone Induced by Unloading*. The Journal of Biological Chemistry, 2015. **290**(31): p. 18934-18942.
563. Can, A., D.T. Dao, C.E. Terrillion, S.C. Piantadosi, S. Bhat, and T.D. Gould, *The tail suspension test*. J Vis Exp, 2012(59): p. e3769.
564. Barkus, C., *Genetic mouse models of depression*. Curr Top Behav Neurosci, 2013. **14**: p. 55-78.
565. Warner, S.E., D.A. Sanford, B.A. Becker, S.D. Bain, S. Srinivasan, and T.S. Gross, *Botox induced muscle paralysis rapidly degrades bone*. Bone, 2006. **38**(2): p. 257-64.
566. Ausk, B.J., P. Huber, S.L. Poliachik, S.D. Bain, S. Srinivasan, and T.S. Gross, *Cortical bone resorption following muscle paralysis is spatially heterogeneous*. Bone, 2012. **50**(1): p. 14-22.
567. Warden, S.J., M.R. Galley, J.S. Richard, L.A. George, R.C. Dirks, E.A. Guildenbecher, A.M. Judd, A.G. Robling, and R.K. Fuchs, *Reduced gravitational loading does not account for the skeletal effect of botulinum toxin-induced muscle inhibition suggesting a direct effect of muscle on bone*. Bone, 2013. **54**(1): p. 98-105.
568. Pautke, C., S. Vogt, T. Tischer, G. Wexel, H. Deppe, S. Milz, M. Schieker, and A. Kolk, *Polychrome labeling of bone with seven different fluorochromes: enhancing fluorochrome discrimination by spectral image analysis*. Bone, 2005. **37**(4): p. 441-5.
569. Saxon, L.K., B.F. Jackson, T. Sugiyama, L.E. Lanyon, and J.S. Price, *Analysis of multiple bone responses to graded strains above functional levels, and to disuse, in mice in vivo show that the human Lrp5 G171V High Bone Mass mutation increases the osteogenic response to loading but that lack of Lrp5 activity reduces it*. Bone, 2011. **49**(2): p. 184-93.
570. Bouxsein, M.L., S.K. Boyd, B.A. Christiansen, R.E. Guldberg, K.J. Jepsen, and R. Muller, *Guidelines for assessment of bone microstructure in rodents using micro-computed tomography*. J Bone Miner Res, 2010. **25**(7): p. 1468-86.
-

571. Doube, M., M.M. Klosowski, I. Arganda-Carreras, F.P. Cordelieres, R.P. Dougherty, J.S. Jackson, B. Schmid, J.R. Hutchinson, and S.J. Shefelbine, *BoneJ: Free and extensible bone image analysis in ImageJ*. Bone, 2010. **47**(6): p. 1076-9.
572. Schneider, C.A., W.S. Rasband, and K.W. Eliceiri, *NIH Image to ImageJ: 25 years of image analysis*. Nat Methods, 2012. **9**(7): p. 671-5.
573. Dobson, K.R., L. Reading, M. Haberey, X. Marine, and A. Scutt, *Centrifugal isolation of bone marrow from bone: an improved method for the recovery and quantitation of bone marrow osteoprogenitor cells from rat tibiae and femurae*. Calcif Tissue Int, 1999. **65**(5): p. 411-3.
574. Windahl, S.H., L. Saxon, A.E. Borjesson, M.K. Lagerquist, B. Frenkel, P. Henning, U.H. Lerner, G.L. Galea, L.B. Meakin, C. Engdahl, K. Sjogren, M.C. Antal, A. Krust, P. Chambon, L.E. Lanyon, J.S. Price, and C. Ohlsson, *Estrogen receptor-alpha is required for the osteogenic response to mechanical loading in a ligand-independent manner involving its activation function 1 but not 2*. J Bone Miner Res, 2013. **28**(2): p. 291-301.
575. Sugiyama, T., L.B. Meakin, G.L. Galea, L.E. Lanyon, and J.S. Price, *The cyclooxygenase-2 selective inhibitor NS-398 does not influence trabecular or cortical bone gain resulting from repeated mechanical loading in female mice*. Osteoporos Int, 2012.
576. Sugiyama, T., L.B. Meakin, G.L. Galea, L.E. Lanyon, and J.S. Price, *The cyclooxygenase-2 selective inhibitor NS-398 does not influence trabecular or cortical bone gain resulting from repeated mechanical loading in female mice*. Osteoporos Int, 2013. **24**(1): p. 383-8.
577. Zaman, G., A. Sunters, G.L. Galea, B. Javaheri, L.K. Saxon, A. Moustafa, V.J. Armstrong, J.S. Price, and L.E. Lanyon, *Loading-related regulation of transcription factor EGR2/Krox-20 in bone cells is ERK1/2 protein-mediated and prostaglandin, Wnt signaling pathway-, and insulin-like growth factor-I axis-dependent*. J Biol Chem, 2012. **287**(6): p. 3946-62.
578. Moriya, S., Y. Izu, S. Arayal, M. Kawasaki, K. Hata, C. Pawaputanon Na Mahasarakham, Y. Izumi, P. Saftig, K. Kaneko, M. Noda, and Y. Ezura, *Cathepsin K Deficiency Suppresses Disuse-Induced Bone Loss*. J Cell Physiol, 2016. **231**(5): p. 1163-70.
579. Pead, M.J., R. Suswillo, T.M. Skerry, S. Vedi, and L.E. Lanyon, *Increased 3H-uridine levels in osteocytes following a single short period of dynamic bone loading in vivo*. Calcif Tissue Int, 1988. **43**(2): p. 92-6.
580. Forwood, M.R., I. Owan, Y. Takano, and C.H. Turner, *Increased bone formation in rat tibiae after a single short period of dynamic loading in vivo*. American Journal of Physiology - Endocrinology And Metabolism, 1996. **270**(3): p. E419-E423.
581. Javaheri, B., A.R. Stern, N. Lara, M. Dallas, H. Zhao, Y. Liu, L.F. Bonewald, and M.L. Johnson, *Deletion of a single beta-catenin allele in osteocytes abolishes the bone anabolic response to loading*. J Bone Miner Res, 2014. **29**(3): p. 705-15.
582. Main, R.P., M.E. Lynch, and M.C. van der Meulen, *Load-induced changes in bone stiffness and cancellous and cortical bone mass following tibial compression diminish with age in female mice*. J Exp Biol, 2014. **217**(Pt 10): p. 1775-83.
583. Weatherholt, A.M., R.K. Fuchs, and S.J. Warden, *Cortical and trabecular bone adaptation to incremental load magnitudes using the mouse tibial axial compression loading model*. Bone, 2013. **52**(1): p. 372-9.
584. Warden, S.J., M.R. Galley, A.L. Hurd, J.S. Richard, L.A. George, E.A. Guildenbecher, R.G. Barker, and R.K. Fuchs, *Cortical and trabecular bone benefits of mechanical loading are*

- maintained long term in mice independent of ovariectomy.* J Bone Miner Res, 2014. **29**(5): p. 1131-40.
585. Schulte, F.A., F.M. Lambers, G. Kuhn, and R. Muller, *In vivo micro-computed tomography allows direct three-dimensional quantification of both bone formation and bone resorption parameters using time-lapsed imaging.* Bone, 2011. **48**(3): p. 433-42.
586. Lambers, F.M., K. Koch, G. Kuhn, D. Ruffoni, C. Weigt, F.A. Schulte, and R. Müller, *Trabecular bone adapts to long-term cyclic loading by increasing stiffness and normalization of dynamic morphometric rates.* Bone, 2013. **55**(2): p. 325-334.
587. Kim, C.H., E. Takai, H. Zhou, D. Von Stechow, R. Müller, D.W. Dempster, and X.E. Guo, *Trabecular Bone Response to Mechanical and Parathyroid Hormone Stimulation: The Role of Mechanical Microenvironment.* Journal of Bone and Mineral Research, 2003. **18**(12): p. 2116-2125.
588. Turner, C.H., T.A. Woltman, and D.A. Belongia, *Structural changes in rat bone subjected to long-term, in vivo mechanical loading.* Bone, 1992. **13**(6): p. 417-22.
589. Cullen, D.M., R.T. Smith, and M.P. Akhter, *Time course for bone formation with long-term external mechanical loading.* Journal of Applied Physiology, 2000. **88**(6): p. 1943-1948.
590. Schriefer, J.L., S.J. Warden, L.K. Saxon, A.G. Robling, and C.H. Turner, *Cellular accommodation and the response of bone to mechanical loading.* J Biomech, 2005. **38**(9): p. 1838-45.
591. Abderhalden, L., F.M. Weaver, M. Bethel, H. Demirtas, S. Burns, J. Svircev, H. Hoenig, K. Lyles, S. Miskevics, and L.D. Carbone, *Dual-energy X-ray absorptiometry and fracture prediction in patients with spinal cord injuries and disorders.* Osteoporos Int, 2017. **28**(3): p. 925-934.
592. Ceroni, D., X. Martin, O. Kherad, D. Salvo, and V. Dubois-Ferriere, *Factors affecting bone mineral mass loss after lower-limb fractures in a pediatric population.* J Pediatr Orthop, 2015. **35**(4): p. 345-51.
593. Kingery, W.S., S.C. Offley, T.Z. Guo, M.F. Davies, J.D. Clark, and C.R. Jacobs, *A substance P receptor (NK1) antagonist enhances the widespread osteoporotic effects of sciatic nerve section.* Bone, 2003. **33**(6): p. 927-36.
594. Weinstein, R.S., C. Wan, Q. Liu, Y. Wang, M. Almeida, C.A. O'Brien, J. Thostenson, P.K. Roberson, A.L. Boskey, T.L. Clemens, and S.C. Manolagas, *Endogenous glucocorticoids decrease skeletal angiogenesis, vascularity, hydration, and strength in aged mice.* Aging Cell, 2010. **9**(2): p. 147-161.
595. Van Staa, T.P., H.G.M. Leufkens, L. Abenhaim, B. Zhang, and C. Cooper, *Use of Oral Corticosteroids and Risk of Fractures.* Journal of Bone and Mineral Research, 2000. **15**(6): p. 993-1000.
596. Humphrey, E.L., J.H.H. Williams, M.W.J. Davie, and M.J. Marshall, *Effects of dissociated glucocorticoids on OPG and RANKL in osteoblastic cells.* Bone, 2006. **38**(5): p. 652-661.
597. Hofbauer, L.C., F. Gori, B.L. Riggs, D.L. Lacey, C.R. Dunstan, T.C. Spelsberg, and S. Khosla, *Stimulation of Osteoprotegerin Ligand and Inhibition of Osteoprotegerin Production by Glucocorticoids in Human Osteoblastic Lineage Cells: Potential Paracrine Mechanisms of Glucocorticoid-Induced Osteoporosis.* Endocrinology, 1999. **140**(10): p. 4382-4389.

598. Brouwers, J.E., F.M. Lambers, B. van Rietbergen, K. Ito, and R. Huiskes, *Comparison of bone loss induced by ovariectomy and neurectomy in rats analyzed by in vivo micro-CT*. J Orthop Res, 2009. **27**(11): p. 1521-7.
599. Marenzana, M., R.L. De Souza, and C. Chenu, *Blockade of beta-adrenergic signaling does not influence the bone mechano-adaptive response in mice*. Bone, 2007. **41**(2): p. 206-15.
600. Hert, J., A. Sklenska, and M. Liskova, *Reaction of bone to mechanical stimuli. 5. Effect of intermittent stress on the rabbit tibia after resection of the peripheral nerves*. Folia Morphol (Praha), 1971. **19**(4): p. 378-87.
601. Pietschmann, P., D. Mechtcheriakova, A. Meshcheryakova, U. Föger-Samwald, and I. Ellinger, *Immunology of Osteoporosis: A Mini-Review*. Gerontology, 2016. **62**(2): p. 128-137.
602. Lee, Y., *The role of interleukin-17 in bone metabolism and inflammatory skeletal diseases*. BMB Rep, 2013. **46**(10): p. 479-83.
603. Ishimi, Y., C. Miyaura, C.H. Jin, T. Akatsu, E. Abe, Y. Nakamura, A. Yamaguchi, S. Yoshiki, T. Matsuda, T. Hirano, and et al., *IL-6 is produced by osteoblasts and induces bone resorption*. J Immunol, 1990. **145**(10): p. 3297-303.
604. Raisz, L.G., *Potential impact of selective cyclooxygenase-2 inhibitors on bone metabolism in health and disease*. Am J Med, 2001. **110 Suppl 3A**: p. 43s-5s.
605. Agas, D., L. Marchetti, M. Capitani, and M.G. Sabbieti, *The dual face of parathyroid hormone and prostaglandins in the osteoimmune system*. Am J Physiol Endocrinol Metab, 2013. **305**(10): p. E1185-94.
606. Lloyd, S.A., A.E. Loisel, Y. Zhang, and H.J. Donahue, *Connexin 43 deficiency desensitizes bone to the effects of mechanical unloading through modulation of both arms of bone remodeling*. Bone, 2013. **57**(1): p. 76-83.
607. Callewaert, F., A. Bakker, J. Schrooten, B. Van Meerbeek, G. Verhoeven, S. Boonen, and D. Vanderschueren, *Androgen receptor disruption increases the osteogenic response to mechanical loading in male mice*. J Bone Miner Res, 2010. **25**(1): p. 124-31.
608. Aido, M., M. Kerschnitzki, R. Hoerth, S. Checa, L. Spevak, A.L. Boskey, P. Fratzl, G.N. Duda, W. Wagermaier, and B.M. Willie, *Effect of in vivo loading on bone composition varies with animal age*. Exp Gerontol, 2015. **63**: p. 48-58.
609. Silva, M.J., M.D. Brodt, M.A. Lynch, A.L. Stephens, D.J. Wood, and R. Civitelli, *Tibial loading increases osteogenic gene expression and cortical bone volume in mature and middle-aged mice*. PLoS One, 2012. **7**(4): p. e34980.
610. Trichilo, S., R. Blanchard, S. Martelli, P.J. Delisser, L.B. Meakin, J.S. Price, L.E. Lanyon, and P. Pivonka, *Cortical bone's adaptive response to mechanical loading is regulated locally: A combined bone imaging – micro-finite element analysis*, in *Australasian Biomechanics Conference 10*. 2016, University of Melbourne: Melbourne.
611. Mantila Roosa, S.M., Y. Liu, and C.H. Turner, *Gene expression patterns in bone following mechanical loading*. J Bone Miner Res, 2011. **26**(1): p. 100-12.
612. Razi, H., A.I. Birkhold, P. Zaslansky, R. Weinkamer, G.N. Duda, B.M. Willie, and S. Checa, *Skeletal maturity leads to a reduction in the strain magnitudes induced within the bone: A murine tibia study*. Acta Biomaterialia, 2015. **13**(0): p. 301-310.

-
613. Matsumoto, T., K. Nishikawa, M. Tanaka, and K. Uesugi, *In Vivo CT Quantification of Trabecular Bone Dynamics in Mice after Sciatic Neurectomy Using Monochromatic Synchrotron Radiation*. *Calcified Tissue International*, 2011. **88**(5): p. 432-441.
614. Nakamura, H., K. Aoki, W. Masuda, N. Alles, K. Nagano, H. Fukushima, K. Osawa, H. Yasuda, I. Nakamura, Y. Mikuni-Takagaki, K. Ohya, K. Maki, and E. Jimi, *Disruption of NF- κ B1 prevents bone loss caused by mechanical unloading*. *Journal of Bone and Mineral Research*, 2013. **28**(6): p. 1457-1467.
615. Kemp, J.P., A. Sayers, L. Paternoster, D.M. Evans, K. Deere, B. St Pourcain, N.J. Timpson, S.M. Ring, M. Lorentzon, T. Lehtimäki, J. Eriksson, M. Kähönen, O. Raitakari, M. Laaksonen, H. Sievänen, J. Viikari, L.P. Lyytikäinen, G.D. Smith, W.D. Fraser, L. Vandenput, C. Ohlsson, and J.H. Tobias, *Does Bone Resorption Stimulate Periosteal Expansion? A Cross-Sectional Analysis of β -C-telopeptides of Type I Collagen (CTX), Genetic Markers of the RANKL Pathway, and Periosteal Circumference as Measured by pQCT*. *Journal of Bone and Mineral Research*, 2014. **29**(4): p. 1015-1024.
616. Manske, S.L., C.A. Good, R.F. Zernicke, and S.K. Boyd, *High-frequency, low-magnitude vibration does not prevent bone loss resulting from muscle disuse in mice following botulinum toxin injection*. *PLoS One*, 2012. **7**(5): p. e36486.
617. Dimitri, P. and C. Rosen, *The Central Nervous System and Bone Metabolism: An Evolving Story*. *Calcif Tissue Int*, 2016.
618. Sherman, B.E. and R.A. Chole, *Sympathectomy, Which Induces Membranous Bone Remodeling, Has No Effect on Endochondral Long Bone Remodeling In Vivo*. *Journal of Bone and Mineral Research*, 2000. **15**(7): p. 1354-1360.
619. Cherruau, M., P. Facchinetti, B. Baroukh, and J.L. Saffar, *Chemical sympathectomy impairs bone resorption in rats: a role for the sympathetic system on bone metabolism*. *Bone*, 1999. **25**(5): p. 545-551.
620. Takeda, S., F. Eleftheriou, R. Levasseur, X. Liu, L. Zhao, K.L. Parker, D. Armstrong, P. Ducy, and G. Karsenty, *Leptin regulates bone formation via the sympathetic nervous system*. *Cell*, 2002. **111**(3): p. 305-17.
621. Shaker, J.L., M.D. Fallon, S. Goldfarb, J. Farber, and M.F. Attie, *WR-2721 reduces bone loss after hindlimb tenotomy in rats*. *J Bone Miner Res*, 1989. **4**(6): p. 885-90.
622. Datta, H.K., J.J. Wu, S. Tuck, and J. Walker, *Emerging Evidence of Osteocytes as Mechanosensors and Regulators of Mineralisation*. *European Musculoskeletal Review*, 2008. **3**(2): p. 48-52.
623. Spatz, J.M., M.N. Wein, J.H. Gooi, Y. Qu, J.L. Garr, S. Liu, K.J. Barry, Y. Uda, F. Lai, C. Dedic, M. Balcells-Camps, H.M. Kronenberg, P. Babij, and P.D. Pajevic, *The Wnt Inhibitor Sclerostin Is Up-regulated by Mechanical Unloading in Osteocytes in Vitro*. *J Biol Chem*, 2015. **290**(27): p. 16744-58.
624. Tatsumi, S., K. Ishii, N. Amizuka, M. Li, T. Kobayashi, K. Kohno, M. Ito, S. Takeshita, and K. Ikeda, *Targeted ablation of osteocytes induces osteoporosis with defective mechanotransduction*. *Cell Metab*, 2007. **5**(6): p. 464-75.
625. Hughes, J.M. and M.A. Petit, *Biological underpinnings of Frost's mechanostat thresholds: the important role of osteocytes*. *J Musculoskelet Neuronal Interact*, 2010. **10**(2): p. 128-35.
-

626. Lin, C.W., X. Jiang, Z.Q. Dai, X.Z. Guo, T.J. Weng, J. Wang, Y.H. Li, G.Y. Feng, X. Gao, and L. He, *Sclerostin Mediates Bone Response to Mechanical Unloading Through Antagonizing Wnt/beta-Catenin Signaling*. Journal of Bone and Mineral Research, 2009. **24**(10): p. 1651-1661.
627. Ott, C.-E., S. Bauer, T. Manke, S. Ahrens, C. Rödelsperger, J. Grünhagen, U. Kornak, G. Duda, S. Mundlos, and P.N. Robinson, *Promiscuous and Depolarization-Induced Immediate-Early Response Genes Are Induced by Mechanical Strain of Osteoblasts*. Journal of Bone and Mineral Research, 2009. **24**(7): p. 1247-1262.
628. Franzoso, G., L. Carlson, L. Xing, L. Poljak, E.W. Shores, K.D. Brown, A. Leonardi, T. Tran, B.F. Boyce, and U. Siebenlist, *Requirement for NF-kappaB in osteoclast and B-cell development*. Genes Dev, 1997. **11**(24): p. 3482-96.
629. Martin, A., R. de Vittoris, V. David, R. Moraes, M. Begeot, M.H. Lafage-Proust, C. Alexandre, L. Vico, and T. Thomas, *Leptin modulates both resorption and formation while preventing disuse-induced bone loss in tail-suspended female rats*. Endocrinology, 2005. **146**(8): p. 3652-9.
630. Gerbaix, M., L. Vico, S.L. Ferrari, and N. Bonnet, *Periostin expression contributes to cortical bone loss during unloading*. Bone, 2015. **71**: p. 94-100.
631. Yoo, Y.M., J.H. Kwag, K.H. Kim, and C.H. Kim, *Effects of neuropeptides and mechanical loading on bone cell resorption in vitro*. Int J Mol Sci, 2014. **15**(4): p. 5874-83.
632. Wang, T., X. Zhang, and S. Li, *[Effect of different types of jumps on the expressions of IL-6, OPG and RANKL in rat tibia]*. Xi Bao Yu Fen Zi Mian Yi Xue Za Zhi, 2014. **30**(9): p. 909-12.
633. Grosso, M.J., H.-W. Courtland, X. Yang, J.P. Sutherland, K. Stoner, J. Nguyen, A. Fahlgren, F.P. Ross, M.C.H. van der Meulen, and M.P. Bostrom, *Intermittent PTH administration and mechanical loading are anabolic for periprosthetic cancellous bone*. Journal of orthopaedic research : official publication of the Orthopaedic Research Society, 2015. **33**(2): p. 163-173.
634. Bhatia, P., M.M. Sanders, and M.F. Hansen, *Expression of receptor activator of nuclear factor-kappaB is inversely correlated with metastatic phenotype in breast carcinoma*. Clin Cancer Res, 2005. **11**(1): p. 162-5.
635. Van Poznak, C., S.S. Cross, M. Saggese, C. Hudis, K.S. Panageas, L. Norton, R.E. Coleman, and I. Holen, *Expression of osteoprotegerin (OPG), TNF related apoptosis inducing ligand (TRAIL), and receptor activator of nuclear factor kappaB ligand (RANKL) in human breast tumours*. J Clin Pathol, 2006. **59**(1): p. 56-63.
636. Uhlén, M., L. Fagerberg, B.M. Hallström, C. Lindskog, P. Oksvold, A. Mardinoglu, Å. Sivertsson, C. Kampf, E. Sjöstedt, A. Asplund, I. Olsson, K. Edlund, E. Lundberg, S. Navani, C.A.-K. Szgyarto, J. Odeberg, D. Djureinovic, J.O. Takanen, S. Hober, T. Alm, P.-H. Edqvist, H. Berling, H. Tegel, J. Mulder, J. Rockberg, P. Nilsson, J.M. Schwenk, M. Hamsten, K. von Feilitzen, M. Forsberg, L. Persson, F. Johansson, M. Zwahlen, G. von Heijne, J. Nielsen, and F. Pontén, *Tissue-based map of the human proteome*. Science, 2015. **347**(6220).
637. Duheron, V., E. Hess, M. Duval, M. Decossas, B. Castaneda, J.E. Klopper, L. Amoasii, J.B. Barbaroux, I.R. Williams, H. Yagita, J. Penninger, Y. Choi, F. Lezot, R. Groves, R. Paus, and C.G. Mueller, *Receptor activator of NF-kappaB (RANK) stimulates the proliferation of epithelial cells of the epidermo-pilosebaceous unit*. Proc Natl Acad Sci U S A, 2011. **108**(13): p. 5342-7.

-
638. Pettit, A.R., N.C. Walsh, C. Manning, S.R. Goldring, and E.M. Gravallese, *RANKL protein is expressed at the pannus-bone interface at sites of articular bone erosion in rheumatoid arthritis*. *Rheumatology (Oxford)*, 2006. **45**(9): p. 1068-76.
639. Branstetter, D., K. Rohrbach, L.Y. Huang, R. Soriano, M. Tometsko, M. Blake, A.P. Jacob, and W.C. Dougall, *RANK and RANK ligand expression in primary human osteosarcoma*. *J Bone Oncol*, 2015. **4**(3): p. 59-68.
640. Fata, J.E., Y.Y. Kong, J. Li, T. Sasaki, J. Irie-Sasaki, R.A. Moorehead, R. Elliott, S. Scully, E.B. Voura, D.L. Lacey, W.J. Boyle, R. Khokha, and J.M. Penninger, *The osteoclast differentiation factor osteoprotegerin-ligand is essential for mammary gland development*. *Cell*, 2000. **103**(1): p. 41-50.
641. Liu, W. and X. Zhang, *Receptor activator of nuclear factor-kappaB ligand (RANKL)/RANK/osteoprotegerin system in bone and other tissues (review)*. *Mol Med Rep*, 2015. **11**(5): p. 3212-8.
642. Perrien, D.S., K.M. Nicks, L. Liu, N.S. Akel, A.W. Bacon, R.A. Skinner, F.L. Swain, J. Aronson, L.J. Suva, and D. Gaddy, *Inhibin A enhances bone formation during distraction osteogenesis*. *J Orthop Res*, 2012. **30**(2): p. 288-95.
643. Pereira, A.F., B. Javaheri, A.A. Pitsillides, and S.J. Shefelbine, *Predicting cortical bone adaptation to axial loading in the mouse tibia*. *J R Soc Interface*, 2015. **12**(110): p. 0590.
644. Wijenayaka, A.R., M. Kogawa, H.P. Lim, L.F. Bonewald, D.M. Findlay, and G.J. Atkins, *Sclerostin stimulates osteocyte support of osteoclast activity by a RANKL-dependent pathway*. *PLoS One*, 2011. **6**(10): p. e25900.
645. Pichler, K., C. Loreto, R. Leonardi, T. Reuber, A.M. Weinberg, and G. Musumeci, *RANKL is downregulated in bone cells by physical activity (treadmill and vibration stimulation training) in rat with glucocorticoid-induced osteoporosis*. *Histol Histopathol*, 2013. **28**(9): p. 1185-96.
646. Martin, T.J. and N.A. Sims, *RANKL/OPG; Critical role in bone physiology*. *Rev Endocr Metab Disord*, 2015. **16**(2): p. 131-9.
647. Sun, X., K. Yang, C. Wang, S. Cao, M. Merritt, Y. Hu, and X. Xu, *Paradoxical response to mechanical unloading in bone loss, microarchitecture, and bone turnover markers*. *Int J Med Sci*, 2015. **12**(3): p. 270-9.
648. Armstrong, J.W., K.A. Nelson, S.J. Simske, M.W. Luttges, J.J. Landolo, and S.K. Chapes, *Skeletal unloading causes organ-specific changes in immune cell responses*. *Journal of Applied Physiology*, 1993. **75**(6): p. 2734-2739.
649. Cabahug-Zuckerman, P., D. Frikha-Benayed, R.J. Majeska, A. Tuthill, S. Yakar, S. Judex, and M.B. Schaffler, *Osteocyte Apoptosis Caused by Hindlimb Unloading is Required to Trigger Osteocyte RANKL Production and Subsequent Resorption of Cortical and Trabecular Bone in Mice Femurs*. *J Bone Miner Res*, 2016. **31**(7): p. 1356-65.
650. Onal, M., H.C. St John, A.L. Danielson, and J.W. Pike, *Deletion of the Distal Tnfrsf11 RL-D2 Enhancer That Contributes to PTH-Mediated RANKL Expression in Osteoblast Lineage Cells Results in a High Bone Mass Phenotype in Mice*. *J Bone Miner Res*, 2016. **31**(2): p. 416-29.
651. Kamiya, N., L. Shuxian, R. Yamaguchi, M. Phipps, O. Aruwajoye, N.S. Adapala, H. Yuan, H.K. Kim, and J.Q. Feng, *Targeted disruption of BMP signaling through type IA receptor (BMPRI1A) in osteocyte suppresses SOST and RANKL, leading to dramatic increase in bone mass, bone mineral density and mechanical strength*. *Bone*, 2016. **91**: p. 53-63.
-

652. Delisser, P., L. Meakin, G. Galea, L. Lanyon, L. Suva, and J. Price. *Disuse sufficient to cause bone loss increases osteocytes' expression of sclerostin but has no effect on osteocyte RANKL*. in *JOURNAL OF BONE AND MINERAL RESEARCH*. 2013. Baltimore: WILEY-BLACKWELL 111 RIVER ST, HOBOKEN 07030-5774, NJ USA.
653. Li, X.J. and W.S.S. Jee, *Adaptation of diaphyseal structure to aging and decreased mechanical loading in the adult rat: A densitometric and histomorphometric study*. *The Anatomical Record*, 1991. **229**(3): p. 291-297.
654. Ijiri, K., Y.F. Ma, W.S. Jee, T. Akamine, and X. Liang, *Adaptation of non-growing former epiphysis and metaphyseal trabecular bones to aging and immobilization in rat*. *Bone*, 1995. **17**(4 Suppl): p. 207s-212s.
655. Lanyon, L.E., *Functional strain in bone tissue as an objective, and controlling stimulus for adaptive bone remodelling*. *Journal of Biomechanics*, 1987. **20**(11): p. 1083-1093.
656. Lanyon, L.E., *The success and failure of the adaptive response to functional load-bearing in averting bone fracture*. *Bone*, 1992. **13 Suppl 2**: p. S17-21.
657. de Souza, R., B. Javaheri, R. Collinson, C. Chenu, S. Shefelbine, P. Lee, and A. Pitsillides, *Prolonging disuse in aged mice amplifies cortical but not trabecular bones' response to mechanical loading*. *J Musculoskelet Neuronal Interact*, 2017. **17**(3): p. 218-25.
658. Karsenty, G. and P. Mera, *Molecular bases of the crosstalk between bone and muscle*. *Bone*, 2017.
659. Lloyd, S.A., A.E. Loisel, Y. Zhang, and H.J. Donahue, *Shifting paradigms on the role of connexin43 in the skeletal response to mechanical load*. *J Bone Miner Res*, 2014. **29**(2): p. 275-86.
660. Yang, Z., S. Tan, Y. Shen, R. Chen, C. Wu, Y. Xu, Z. Song, and Q. Fu, *Inhibition of FSS-induced actin cytoskeleton reorganization by silencing LIMK2 gene increases the mechanosensitivity of primary osteoblasts*. *Bone*, 2015. **74**: p. 182-90.
661. Bonnet, N., K.N. Standley, E.N. Bianchi, V. Stadelmann, M. Foti, S.J. Conway, and S.L. Ferrari, *The matricellular protein periostin is required for sost inhibition and the anabolic response to mechanical loading and physical activity*. *J Biol Chem*, 2009. **284**(51): p. 35939-50.
662. Bonnet, N., P. Garnero, and S. Ferrari, *Periostin action in bone*. *Molecular and Cellular Endocrinology*, 2016. **432**: p. 75-82.
663. Nikander, R., H. Sievanen, A. Heinonen, R.M. Daly, K. Uusi-Rasi, and P. Kannus, *Targeted exercise against osteoporosis: A systematic review and meta-analysis for optimising bone strength throughout life*. *BMC Med*, 2010. **8**: p. 47.
664. Warden, S.J., S.M. Mantila Roosa, M.E. Kersh, A.L. Hurd, G.S. Fleisig, M.G. Pandy, and R.K. Fuchs, *Physical activity when young provides lifelong benefits to cortical bone size and strength in men*. *Proceedings of the National Academy of Sciences*, 2014. **111**(14): p. 5337-5342.
665. Chastin, S.F.M., O. Mandrichenko, J.L. Helbostadt, and D.A. Skelton, *Associations between objectively-measured sedentary behaviour and physical activity with bone mineral density in adults and older adults, the NHANES study*. *Bone*, 2014. **64**: p. 254-262.

-
666. Black, J.D., V.K. Kancherla, and W.G. De Long, Jr., *A Review of Atypical Femoral Fractures From a Tertiary Care Teaching Hospital: An Alarming Trend?* J Orthop Trauma, 2016. **30**(4): p. 182-8.
667. Vermeer, J.A., G.A. Renders, and V. Everts, *Osteonecrosis of the Jaw-a Bone Site-Specific Effect of Bisphosphonates*. Curr Osteoporos Rep, 2016. **14**(5): p. 219-25.
668. Watts, N.B. and D.L. Diab, *Long-term use of bisphosphonates in osteoporosis*. J Clin Endocrinol Metab, 2010. **95**(4): p. 1555-65.
669. Ettinger, B., J. San Martin, G. Crans, and I. Pavo, *Differential effects of teriparatide on BMD after treatment with raloxifene or alendronate*. J Bone Miner Res, 2004. **19**(5): p. 745-51.
670. Miller, P.D., P.D. Delmas, R. Lindsay, N.B. Watts, M. Luckey, J. Adachi, K. Saag, S.L. Greenspan, E. Seeman, S. Boonen, S. Meeves, T.F. Lang, and J.P. Bilezikian, *Early responsiveness of women with osteoporosis to teriparatide after therapy with alendronate or risedronate*. J Clin Endocrinol Metab, 2008. **93**(10): p. 3785-93.
671. Wang, C., G. Zhang, M. Gu, J. Fan, J. Chen, G. Zhang, and B. Li, *Parathyroid Hormone Plus Alendronate in Osteoporosis: A Meta-Analysis of Randomized Controlled Trials*. J Invest Surg, 2015. **28**(6): p. 309-16.
672. de Bakker, C.M., A.R. Altman, W.J. Tseng, M.B. Tribble, C. Li, A. Chandra, L. Qin, and X.S. Liu, *muCT-based, in vivo dynamic bone histomorphometry allows 3D evaluation of the early responses of bone resorption and formation to PTH and alendronate combination therapy*. Bone, 2015. **73**: p. 198-207.
673. Macias, B.R., J.M. Swift, M.I. Nilsson, H.A. Hogan, S.D. Bouse, and S.A. Bloomfield, *Simulated resistance training, but not alendronate, increases cortical bone formation and suppresses sclerostin during disuse*. J Appl Physiol (1985), 2012. **112**(5): p. 918-25.
674. Swift, J.M., M.I. Nilsson, H.A. Hogan, L.R. Sumner, and S.A. Bloomfield, *Simulated resistance training during hindlimb unloading abolishes disuse bone loss and maintains muscle strength*. Journal of Bone and Mineral Research, 2010. **25**(3): p. 564-574.
675. Iwata, K., J. Li, H. Follet, R.J. Phipps, and D.B. Burr, *Bisphosphonates suppress periosteal osteoblast activity independently of resorption in rat femur and tibia*. Bone, 2006. **39**(5): p. 1053-8.
676. Nakamura, M., N. Udagawa, S. Matsuura, M. Mogi, H. Nakamura, H. Horiuchi, N. Saito, B.Y. Hiraoka, Y. Kobayashi, K. Takaoka, H. Ozawa, H. Miyazawa, and N. Takahashi, *Osteoprotegerin regulates bone formation through a coupling mechanism with bone resorption*. Endocrinology, 2003. **144**(12): p. 5441-9.
677. Fuchs, R.K., R.J. Phipps, and D.B. Burr, *Recovery of trabecular and cortical bone turnover after discontinuation of risedronate and alendronate therapy in ovariectomized rats*. J Bone Miner Res, 2008. **23**(10): p. 1689-97.
678. Salmon, P.L., C. Ohlsson, S.J. Shefelbine, and M. Doube, *Structure Model Index Does Not Measure Rods and Plates in Trabecular Bone*. Frontiers in Endocrinology, 2015. **6**(162).
679. Brouwers, J.E., B. van Rietbergen, and M.L. Bouxsein, *Influence of early and late zoledronic acid administration on vertebral structure and strength in ovariectomized rats*. Calcif Tissue Int, 2008. **83**(3): p. 186-91.
-

680. Ito, M., A. Nishida, K. Aoyagi, M. Uetani, K. Hayashi, and M. Kawase, *Effects of risedronate on trabecular microstructure and biomechanical properties in ovariectomized rat tibia*. *Osteoporos Int*, 2005. **16**(9): p. 1042-8.
681. Kippo, K., R. Hannuniemi, P. Isaksson, L. Lauren, T. Osterman, Z. Peng, J. Tuukkanen, P. Kuurtamo, H.K. Vaananen, and R. Sellman, *Clodronate prevents osteopenia and loss of trabecular connectivity in estrogen-deficient rats*. *J Bone Miner Res*, 1998. **13**(2): p. 287-96.
682. Borah, B., T.E. Dufresne, P.A. Chmielewski, T.D. Johnson, A. Chines, and M.D. Manhart, *Risedronate preserves bone architecture in postmenopausal women with osteoporosis as measured by three-dimensional microcomputed tomography*. *Bone*, 2004. **34**(4): p. 736-46.
683. Recker, R.R., L.G. Ste-Marie, B. Langdahl, D. Masanouskaite, D. Ethgen, and P.D. Delmas, *Oral ibandronate preserves trabecular microarchitecture: micro-computed tomography findings from the oral iBandronate Osteoporosis vertebral fracture trial in North America and Europe study*. *J Clin Densitom*, 2009. **12**(1): p. 71-6.
684. Bourrin, S., P. Ammann, J.P. Bonjour, and R. Rizzoli, *Recovery of proximal tibia bone mineral density and strength, but not cancellous bone architecture, after long-term bisphosphonate or selective estrogen receptor modulator therapy in aged rats*. *Bone*, 2002. **30**(1): p. 195-200.
685. Davis, H.M., R. Pacheco-Costa, E.G. Atkinson, L.R. Brun, A.R. Gortazar, J. Harris, M. Hiasa, S.A. Bolarinwa, T. Yoneda, M. Ivan, A. Bruzzaniti, T. Bellido, and L.I. Plotkin, *Disruption of the Cx43/miR21 pathway leads to osteocyte apoptosis and increased osteoclastogenesis with aging*. *Aging Cell*, 2017. **16**(3): p. 551-563.
686. Delisser, P., H. Todd, L. Meakin, G. Galea, L. Lanyon, S.H. Windahl, and J. Price. *Risedronate has no effect on the adaptive response to loading in aged mice*. in *JOURNAL OF BONE AND MINERAL RESEARCH*. 2015. Seattle: WILEY-BLACKWELL 111 RIVER ST, HOBOKEN 07030-5774, NJ USA.
687. Watson, S.L., B.K. Weeks, L.J. Weis, S.A. Horan, and B.R. Beck, *Heavy resistance training is safe and improves bone, function, and stature in postmenopausal women with low to very low bone mass: novel early findings from the LIFTMOR trial*. *Osteoporos Int*, 2015. **26**(12): p. 2889-94.
688. Beck, B.R., R.M. Daly, M.A.F. Singh, and D.R. Taaffe, *Exercise and Sports Science Australia (ESSA) position statement on exercise prescription for the prevention and management of osteoporosis*. *Journal of Science and Medicine in Sport*, 2017. **20**(5): p. 438-445.
689. Qi, H., M. Li, and T.J. Wronski, *A comparison of the anabolic effects of parathyroid hormone at skeletal sites with moderate and severe osteopenia in aged ovariectomized rats*. *Journal of Bone and Mineral Research*, 1995. **10**(6): p. 948-955.
690. Kramer, I., G.G. Loots, A. Studer, H. Keller, and M. Kneissel, *Parathyroid hormone (PTH)-induced bone gain is blunted in SOST overexpressing and deficient mice*. *J Bone Miner Res*, 2010. **25**(2): p. 178-89.
691. Yukata, K., C. Xie, T.F. Li, M. Takahata, D. Hoak, S. Kondabolu, X. Zhang, H.A. Awad, E.M. Schwarz, C.A. Beck, J.H. Jonason, and R.J. O'Keefe, *Aging periosteal progenitor cells have reduced regenerative responsiveness to bone injury and to the anabolic actions of PTH 1-34 treatment*. *Bone*, 2014. **62**: p. 79-89.

-
692. Meier, C., O. Lamy, M.A. Krieg, H.U. Mellinshoff, M. Felder, S. Ferrari, and R. Rizzoli, *The role of teriparatide in sequential and combination therapy of osteoporosis*. Swiss Med Wkly, 2014. **144**: p. w13952.
693. Ishtiaq, S., I. Fogelman, and G. Hampson, *Treatment of post-menopausal osteoporosis: beyond bisphosphonates*. J Endocrinol Invest, 2015. **38**(1): p. 13-29.
694. Gennari, L., S. Rotatori, S. Bianciardi, R. Nuti, and D. Merlotti, *Treatment needs and current options for postmenopausal osteoporosis*. Expert Opin Pharmacother, 2016. **17**(8): p. 1141-52.
695. Cosman, F., E.F. Eriksen, C. Recknor, P.D. Miller, N. Guañabens, C. Kasperk, P. Papanastasiou, A. Readie, H. Rao, J.A. Gasser, C. Bucci-Rechtweg, and S. Boonen, *Effects of intravenous zoledronic acid plus subcutaneous teriparatide [rhPTH(1-34)] in postmenopausal osteoporosis*. Journal of Bone and Mineral Research, 2011. **26**(3): p. 503-511.
696. Johnston, S., S. Andrews, V. Shen, F. Cosman, R. Lindsay, D.W. Dempster, and A. Iida-Klein, *The effects of combination of alendronate and human parathyroid hormone(1-34) on bone strength are synergistic in the lumbar vertebra and additive in the femur of C57BL/6J mice*. Endocrinology, 2007. **148**(9): p. 4466-74.
697. Finkelstein, J.S., A. Hayes, J.L. Hunzelman, J.J. Wyland, H. Lee, and R.M. Neer *The Effects of Parathyroid Hormone, Alendronate, or Both in Men with Osteoporosis*. New England Journal of Medicine, 2003. **349**(13): p. 1216-1226.
698. Finkelstein, J.S., B.Z. Leder, S.M. Burnett, J.J. Wyland, H. Lee, A.V. de la Paz, K. Gibson, and R.M. Neer, *Effects of teriparatide, alendronate, or both on bone turnover in osteoporotic men*. J Clin Endocrinol Metab, 2006. **91**(8): p. 2882-7.
699. Lindsay, R., F. Cosman, H. Zhou, M.P. Bostrom, V.W. Shen, J.D. Cruz, J.W. Nieves, and D.W. Dempster, *A Novel Tetracycline Labeling Schedule for Longitudinal Evaluation of the Short-Term Effects of Anabolic Therapy With a Single Iliac Crest Bone Biopsy: Early Actions of Teriparatide*. Journal of Bone and Mineral Research, 2006. **21**(3): p. 366-373.
700. Pierroz, D.D., N. Bonnet, P.A. Baldock, M.S. Ominsky, M. Stolina, P.J. Kostenuik, and S.L. Ferrari, *Are Osteoclasts Needed for the Bone Anabolic Response to Parathyroid Hormone?: A STUDY OF INTERMITTENT PARATHYROID HORMONE WITH DENOSUMAB OR ALENDRONATE IN KNOCK-IN MICE EXPRESSING HUMANIZED RANKL*. Journal of Biological Chemistry, 2010. **285**(36): p. 28164-28173.
701. Campbell, G.M., R. Bernhardt, D. Scharnweber, and S.K. Boyd, *The bone architecture is enhanced with combined PTH and alendronate treatment compared to monotherapy while maintaining the state of surface mineralization in the OVX rat*. Bone, 2011. **49**(2): p. 225-32.
702. Rhee, Y., E.Y. Lee, V. Lezcano, A.C. Ronda, K.W. Condon, M.R. Allen, L.I. Plotkin, and T. Bellido, *Resorption controls bone anabolism driven by parathyroid hormone (PTH) receptor signaling in osteocytes*. J Biol Chem, 2013. **288**(41): p. 29809-20.
703. Metcalf, L.M., T.J. Aspray, and E.V. McCloskey, *The effects of parathyroid hormone peptides on the peripheral skeleton of postmenopausal women. A systematic review*. Bone, 2017. **99**: p. 39-46.
-

704. Pettway, G.J., J.A. Meganck, A.J. Koh, E.T. Keller, S.A. Goldstein, and L.K. McCauley, *Parathyroid hormone mediates bone growth through the regulation of osteoblast proliferation and differentiation*. *Bone*, 2008. **42**(4): p. 806-18.
705. Samadfam, R., Q. Xia, and D. Goltzman, *Co-treatment of PTH with osteoprotegerin or alendronate increases its anabolic effect on the skeleton of oophorectomized mice*. *J Bone Miner Res*, 2007. **22**(1): p. 55-63.
706. Yamane, H., A. Sakai, T. Mori, S. Tanaka, K. Moridera, and T. Nakamura, *The anabolic action of intermittent PTH in combination with cathepsin K Inhibitor or alendronate differs depending on the remodeling status in bone in ovariectomized mice*. *Bone*, 2009. **44**(6): p. 1055-1062.
707. Jilka, R.L., M. Almeida, E. Ambrogini, L. Han, P.K. Roberson, R.S. Weinstein, and S.C. Manolagas, *Decreased oxidative stress and greater bone anabolism in the aged, when compared to the young, murine skeleton with parathyroid hormone administration*. *Aging Cell*, 2010. **9**(5): p. 851-67.
708. Rhee, Y., M.R. Allen, K. Condon, V. Lezcano, A.C. Ronda, C. Galli, N. Olivos, G. Passeri, C.A. O'Brien, N. Bivi, L.I. Plotkin, and T. Bellido, *PTH receptor signaling in osteocytes governs periosteal bone formation and intracortical remodeling*. *J Bone Miner Res*, 2011. **26**(5): p. 1035-46.
709. Tazawa, K., K. Hoshi, S. Kawamoto, M. Tanaka, S. Ejiri, and H. Ozawa, *Osteocytic osteolysis observed in rats to which parathyroid hormone was continuously administered*. *J Bone Miner Metab*, 2004. **22**(6): p. 524-9.
710. Nango, N., S. Kubota, T. Hasegawa, W. Yashiro, A. Momose, and K. Matsuo, *Osteocyte-directed bone demineralization along canaliculi*. *Bone*, 2016. **84**: p. 279-88.
711. Halasy-Nagy, J.M., G.A. Rodan, and A.A. Reszka, *Inhibition of bone resorption by alendronate and risedronate does not require osteoclast apoptosis*. *Bone*, 2001. **29**(6): p. 553-9.

Appendices

Appendix 1

CTAn μ CT analysis task lists

Step number	Procedure
1	Thresholding – Binarising images Mode,Global Lower grey threshold: 100 Upper grey threshold: 255
2	Despeckle Type: Remove white speckles (2D space) Area: less than 100 pixels Apply to: Image
3	Despeckle Type: Remove black speckles (3D space) Volume : less than 20 voxels Apply to: Image
4	ROI shrink-wrap Mode : Shrink-wrap (2D space) Stretch over holes with a diameter in 10 pixels
5	2D analysis

Table A1. 1 - CTAn tasklist for analysis of cortical bone parameters in young mice tibias

Step number	Procedure
1	Thresholding – Binarising images Mode,Global Lower grey threshold: 100 Upper grey threshold: 255
2	Despeckle Type: Remove white speckles (3D space) Area: less than 20 voxels Apply to: Image
3	Despeckle Type: Remove black speckles (3D space) Volume : less than 10 voxels Apply to: Image
4	ROI shrink-wrap Mode : Shrink-wrap (2D space) Stretch over holes with a diameter in 26 pixels
5	2D analysis

Table A1. 2 - CTAn tasklist for analysis of cortical bone parameters in old mice tibias

Step number	Procedure
1	Thresholding – Binarising images Mode,Global Lower grey threshold: 100 Upper grey threshold: 255
2	Despeckle Type: Sweep (3D space) Remove: all but the largest object Apply to: Image
3	Bitwise operations <Clipboard> = COPY <Image>
4	Morphological operations Type: Closing (2D space) Kernel: Round Radius: 7 Apply to: Image
5	Despeckle Type: Remove black speckles (2D space) Area: less than 400 pixels Apply to: Image
6	Despeckle Type: Sweep (3D space) Remove: all except the largest object Apply to: Image
7	Bitwise operations <Region of Interest> = COPY <Image>
8	Bitwise operations <Image> = COPY <Clipboard>
9	3D Analysis

Table A1. 3 - – CTAn tasklist for analysis of cortical bone porosity

Table A1.4

Step number	Procedure
1	Thresholding – Binarising images Mode, Global Lower grey threshold: 100 Upper grey threshold: 255
2	Despeckle Type: Sweep (3D space) Remove: all but the largest object Apply to: Image
3	Bitwise operations <Clipboard> = COPY <Image>
4	Morphological operations Type: Closing (2D space) Kernel: Round Radius: 7 Apply to: Image
5	Despeckle Type: Remove black speckles (2D space) Area: less than 1000 pixels Apply to: Image
6	Despeckle Type: Sweep (3D space) Remove: all except the largest object Apply to: Image
7	Bitwise operations <Region of Interest> = COPY <Image>
8	Bitwise operations <Image> = COPY <Clipboard>
9	3D Analysis

Table A1. 4 – CTAn tasklist for analysis of trabecular and cortical bone porosity in proximal tibial metaphyseal bone of mice

Table A1.5

Step number	Procedure
1	Thresholding – Binarising images Mode,Global Lower grey threshold: 100 Upper grey threshold: 255
2	Despeckle Type: Remove white speckles (3D space) Area: less than 10 voxels Apply to: Image
3	Despeckle Type: Remove black speckles (3D space) Volume : less than 10 voxels Apply to: Image
4	3D analysis

Table A1. 5 – CTAn tasklist for analysis of trabecular bone parameters in old mice tibias

Appendix 2

Immunohistochemistry Protocols

IHC Staining protocol for mouse RANKL on paraffin-embedded bone					
Step	Procedure	Location	Time	Temp	Done
1	XYLENE	In slide rack	5 min	room temp	
2	XYLENE	In slide rack	5 min	room temp	
4	100% EtOH	In slide rack	5 min	room temp	
5	100% EtOH	In slide rack	5 min	room temp	
6	80% EtOH	In slide rack	5 min	room temp	
7	70% EtOH	In slide rack	3 min	room temp	
8	DISTILLED WATER	In slide rack	10 min	room temp	
9	PBS pH 7.6	Hellendahl Jar	5 min	room temp	
11	Citrate Buffer 10mM pH 6.0 (Place slides in when hot then leave at room temp to cool)	Coplin Jar	2 hours	Microwave (~90°C)	
12	PBS pH 7.6	Hellendahl Jar	5 min	room temp	
13	Peroxidase Blocking Solution (keep in dark)	Hellendahl Jar	5 min	room temp	
14	PBS pH 7.6	Hellendahl Jar	5 min	room temp	
14	PBS pH 7.6	Hellendahl Jar	5 min	room temp	
15	Apply PAP pen (control sections on each slide)				
16	BLOCKING SERUM 1.5%	on slides in box	1 Hour	room temp	
	Shake excess from slides			room temp	
17	primary antibody/negative(diluent) RANKL ab (Santa Cruz 1:50)	on slides in box	overnight	@ 4°C	
	while slides are coming to room temperature prepare the secondary antibody				
	in accordance with preparation sheet.				
18	PBS pH 7.6	Hellendahl Jar	5 min	room temp	
19	PBS pH 7.6	Hellendahl Jar	5 min	room temp	
20	PBS pH 7.6	Hellendahl Jar	5 min	room temp	
	Prepare ABC solution as per prep sheet;let stand at RT			room temp	
	for 30 minutes before using.				
21	Apply Biotinylated Secondary Ab (Kit)	on slides in box	30 min	room temp	
22	PBS pH 7.6	Hellendahl Jar	5 min	room temp	
23	PBS pH 7.6	Hellendahl Jar	5 min	room temp	
24	PBS pH 7.6	Hellendahl Jar	5 min	room temp	
25	Apply ABC to sections and incubate	on slides in box	30 min	room temp	
26	prepare DAB in accordance with solution preparation sheet.				
27	PBS pH 7.6	Hellendahl Jar	5 min	room temp	
28	PBS pH 7.6	Hellendahl Jar	5 min	room temp	
29	PBS pH 7.6	Hellendahl Jar	5 min	room temp	
30	Apply DAB and incubate for	on slides in box	30 sec-10 min	room temp	
31	Distilled Water	Hellendahl Jar	5 min	room temp	
32	Distilled Water	Hellendahl Jar	5 min	room temp	

33	Dako DAB Enhancer (Optional)	on slides in box	2 min	room temp	
34	Distilled Water	Hellendahl Jar	5 min	room temp	
35	Distilled Water	Hellendahl Jar	3 min	room temp	
36	Mayers Hematoxylin	on slides in box	45 sec	room temp	
37	RTW	In slide rack	2 min	room temp	
38	Scott's Water	In slide rack	45 sec	room temp	
39	RTW	In slide rack	5 min	room temp	
40	80% EtOH	In slide rack	30 sec	room temp	
41	95% EtOH	In slide rack	30 sec	room temp	
42	100% EtOH	In slide rack	30 sec	room temp	
43	100% EtOH	In slide rack	1 min	room temp	
44	Xylene	In slide rack	3 min	room temp	
45	Xylene	In slide rack	3 min	room temp	
46	Xylene	In slide rack	3 min	room temp	
47	Mount with Permount				
SOLUTION PREPARATION FOR PROCEDURE.					
Solution				Amt Needed	
Phosphate Buffered Saline (Sigma) Mix Distilled Water 800 ml with 1 pck of				1-2 Liters	
Phosphate Buffered Saline (Sigma) packet. QS to 1000 ml with distilled water.					
10.0 mM Citric Acid pH 6.0 (Dako Antigen Retrieval Solution)				100ml/8 slides	
Peroxidase Solution : 10 ml of 30% Hydrogen Peroxide and 90 ml of Methanol				100ml/8 slides	
Blocking Serum Solution 1.5%: In mixing bottle 1 (blue cap), combine					
75ul normal blocking serum stock with 5 ml PBS				800ul/slide	
Primary Antibody: Santa Cruz RANKL Antibody (N-19): sc-7628 - Dilute 1 in 50 with				200ul/slide	
dilute blocking serum solution initially. May need higher dilution.					
for negative control use blocking serum 1.5%. Could add 1:50 goat IgG					
Biotinylated Secondary Antibody: In mixing bottle 2(green cap) combine 75ul					
normal blocking serum stock, 5 ml PBS and 25ul biotinylated secondary anti-				200ul/slide	
body stock					
ABC reagent: In AB mixing bottle (purple cap) combine 50ul reagent A				200ul/slide	
(avidin),					
50ul reagent B (biotinylated HRP and 2.5 ml PBS. Mix and let stand for 30					
minutes					
Use after 30 minutes of standing.					
Peroxidase substrate:(substrate mixing bottle yellow cap) combine 1.6 ml					
distilled water, 5 drops 10x substrate buffer, 1 drop 50x DAB chromagen and					
1 drop 50X peroxidate substrate (sufficient for 15-20 slides)				1-5 drops per section	
Mayer's Hematoxylin				300 ml	
Scott's Water				300 ml	

Table A2. 1 – Immunostaining protocol for RANKL

IHC Staining protocol for mouse RANKL on paraffin-embedded bone				
Step	Procedure	Time	Temp	Done
1	XYLENE	5 min	room temp	
2	XYLENE	5 min	room temp	
3	XYLENE	5 min	room temp	
4	100% EtOH	5 min	room temp	
5	100% EtOH	5 min	room temp	
6	95% EtOH	5 min	room temp	
7	80% EtOH	3 min	room temp	
8	70% EtOH	3 min	room temp	
9	Distilled Water	3 min	room temp	
10	PBS pH 7.6	5 min	room temp	
11	Peroxidase Blocking Solution	5-10min	Room Temp	
12	PBS pH 7.6	5 min	room temp	
13	PBS pH 7.6	5 min	room temp	
14	PBS pH 7.6	5 min	room temp	
15	APPLY PAP PEN			
16	10% Rabbit Serum	1 Hour	room temp	
17	Blot excess from slides		room temp	
18	primary antibody/negative(diluent)Sclerostin ab(R&D Goat Anti Mouse SOST 1:200)	overnight	@ 4°C	
19	while slides are coming to room temperature prepare the secondary antibody in accordance with preparation sheet			
20	PBS pH 7.6	5 min	room temp	
21	PBS pH 7.6	5 min	room temp	
22	PBS pH 7.6	5 min	room temp	
23	Prepare ABC solution as per prep sheet;let stand at RT		room temp	
24	for 30 minutes before using.			
25	Apply Biotinylated Secondary Ab (Dako Rabbit anti Goat 1:400)	30 min	room temp	
26	PBS Triton	5 min	room temp	
27	PBS Triton	5 min	room temp	
28	PBS Triton	5 min	room temp	
29	Apply ABC to sections and incubate	30 min	room temp	
30	prepare DAB in accordance with solution preparation sheet.			
31	PBS Triton	5 min	room temp	
32	PBS Triton	5 min	room temp	
33	PBS Triton	5 min	room temp	
34	Apply DAB and incubate for	30 sec-10 min	room temp	
35	Distilled Water	5 min	room temp	
36	Distilled Water	5 min	room temp	
37	1% Light Green Solution	45 sec	room temp	
38	Running tap water	5 min	room temp	
39	80% EtOH	30 sec	room temp	
40	95% EtOH	30 sec	room temp	
41	100% EtOH	30 sec	room temp	
42	100% EtOH	1 min	room temp	
43	Xylene	3 min	room temp	

44	Xylene	3 min	room temp	
45	Mount with Permount			
SOLUTION PREPARATION FROM R & D USING R& D GOAT HRP-DAB KIT.				
Solution				Amt Needed
Phosphate Buffered Saline (Sigma) Mix Distilled Water 800 ml with 1 pck of				1-2 Liters
Phosphate Buffered Saline (Sigma) packet. QS to 1000 ml with distilled water.				
PBS/Triton mix - 2.5ml Triton 100 to 500ml PBS				
Citrate Buffer pH 6.0 10mM				
1.47g in 500ml PBS with 0.5ml TWEEN 20 - adjusted to pH 6.0				
Peroxidase Solution : 10 ml of 30% Hydrogen Peroxide and 90 ml of Methanol				100 -200 ul / section
Rabbit Serum 10%				
75ul normal blocking serum stock with 5 ml PBS				1-3 drops/section
PRIMARY ANTIBODY DILUTION: R&D Sclerostin 1:200				
1.0ul Sclerostin Ab	X _____	=total amt. _____		
199.0ul Blocking Serum Solution	X _____	=total amt. _____		
mix well keep on ice.				
Biotinylated Secondary Antibody: Dako Polyclonal Rabbit Anti Goat- E0466				
1.0ul 2ry Ab	X _____	=total amt. _____		1-3 drops/section
399ul Blocking Serum Solution	X _____	=total amt. _____		
ABC reagent:				
Add 2 drops Reagent A to 5ml Buffer then add 2 drops of reagent B.				100-200ul/section
Mix well and let stand for 30 minutes before use.				
Peroxidase substrate: Vector DAB - 2 drops Buffer stock to 5 ml distilled H₂O - Mix Well				
4 drops of DAB Stock Solution - Mix Well				4ml/10 slides
2 drops Hydrogen peroxide solution - Mix well.				
1% Light Green solution -				300 ml
for negative control use blocking serum 1.5%.				
RANKL Antibody diluted with blocking serum as per protocol.				

Table A2. 2 – Immunostaining protocol for Sclerostin

Appendix 3

Experimental data tables

Chapter 3

Loading group		2 weeks	3 weeks	4 weeks
Mouse weight (g)		22.4 ± 0.93	21.92 ± 0.67	22 ± 0.45
Tibial length (mm)	Control	17.86 ± 0.17	17.62 ± 0.25	17.95 ± 0.11
	Loaded	17.98 ± 0.22	17.67 ± 0.3	18.1 ± 0.1
Cortical bone (37% site)				
Tt.Ar (mm ²)	Control	1.07 ± 0.01	1.07 ± 0.04	1.13 ± 0.02
	Loaded	1.17 ± 0.02	1.34 ± 0.06	1.39 ± 0.05
Ct.Ar (mm ²)	Control	0.63 ± 0.01	0.64 ± 0.02	0.68 ± 0.02
	Loaded	0.8 ± 0.02	0.92 ± 0.05	0.93 ± 0.04
Ma.Ar	Control	0.44 ± 0.01	0.43 ± 0.02	0.45 ± 0.01
	Loaded	0.38 ± 0.01	0.42 ± 0.02	0.46 ± 0.03
Ct.Th (mm)	Control	0.14 ± 0.005	0.149 ± 0.007	0.147 ± 0.004
	Loaded	0.15 ± 0.001	0.161 ± 0.004	0.174 ± 0.004
PMI	Control	0.23 ± 0.01	0.22 ± 0.03	0.26 ± 0.01
	Loaded	0.31 ± 0.01	0.34 ± 0.03	0.39 ± 0.02
Trabecular bone site				
BV/TV	Control	6.76 ± 1.24	8.55 ± 1	8.32 ± 0.66
	Loaded	10.25 ± 1.68	15.12 ± 1.01	13.07 ± 0.99
Tb.Th (mm)	Control	0.048 ± 0.002	0.047 ± 0.002	0.05 ± 0.002
	Loaded	0.057 ± 0.002	0.066 ± 0.003	0.06 ± 0.005
Tb.Sp (mm)	Control	0.28 ± 0.04	0.23 ± 0.01	0.26 ± 0.01
	Loaded	0.26 ± 0.04	0.22 ± 0.01	0.24 ± 0.01
Tb.N (/mm)	Control	1.4 ± 0.22	1.82 ± 0.17	1.68 ± 0.14
	Loaded	1.78 ± 0.23	2.3 ± 0.15	2.18 ± 0.09
Tb.Pf	Control	28.4 ± 3.15	28.02 ± 2.25	27.92 ± 1.4
	Loaded	22.44 ± 2.8	19.11 ± 0.95	20.11 ± 0.46
SMI	Control	2.04 ± 0.18	2.02 ± 0.06	2.17 ± 0.07
	Loaded	2.11 ± 0.23	2.06 ± 0.1	2 ± 0.11

Table A3. 1 – The effect of loading duration on μ CT parameters in tibial bone of young adult female mice following axial tibial loading.

Values represent mean ± SEM

		2 weeks	3 weeks	4 weeks
Ct.Ar	Control	0.23 ± 0.01	0.24 ± 0.01	0.24 ± 0.01
	Loaded	0.32 ± 0.01	0.38 ± 0.03	0.4 ± 0.03
Ct.Th	Control	162.4 ± 5.4	166.7 ± 5.5	169.5 ± 5.9
	Loaded	202 ± 6.1	249.7 ± 24.8	283.7 ± 20.9
Ec.Ir.L.Th	Control	8.02 ± 0.91	15.06 ± 8.61	17.02 ± 3.22
	Loaded	25.57 ± 1.6	37.63 ± 6.58	45.31 ± 7.25
Ec.MAR	Control	0.73 ± 0.08	0.84 ± 0.48	0.68 ± 0.13
	Loaded	2.78 ± 0.5	2.09 ± 0.37	1.81 ± 0.29
Ec.BFR.Bs	Control	0.67 ± 0.08	0.73 ± 0.46	0.67 ± 0.14
	Loaded	2.68 ± 0.32	2.05 ± 0.43	1.77 ± 0.29
Ps.Ir.L.Th	Control	3.83 ± 2.94	1.81 ± 1.81	0 ± 0
	Loaded	45.22 ± 2.53	67.32 ± 9.79	80.63 ± 15.07
Ps.MAR	Control	0.35 ± 0.27	0.1 ± 0.1	0 ± 0
	Loaded	4.97 ± 1.06	3.74 ± 0.54	3.23 ± 0.6
Ps.BFR.Bs	Control	0.16 ± 0.15	0.03 ± 0.03	0 ± 0
	Loaded	3.99 ± 0.94	3.11 ± 0.45	2.79 ± 0.46

Table A3. 2 Dynamic histomorphometry indices following axial tibial loading in young adult female mice for 2, 3 or four weeks.

17w female mice were loaded for three time weekly for 2, 3 or 4 weeks. Fluorochromes were administered as specified in

Table 1. The first and last fluorochrome administered for each group were used to calculate the overall value for each parameter for each group. Values represent mean ± SEM

	0-7 DAYS (n=11)	7-14 DAYS (n=8)	14-21 DAYS (n=4)
Ec.Ir.L.Th	12.87 ± 0.75	17.55 ± 1.96	10.4 ± 3.31
Ps.Ir.L.Th	14.84 ± 0.85	36.14 ± 3.21	17.43 ± 5.81
Ec.MAR	1.84 ± 0.11	2.51 ± 0.28	1.49 ± 0.47
Ps.MAR	2.12 ± 0.12	5.16 ± 0.46	2.49 ± 0.83
Ec.BFR.Bs	1.66 ± 0.07	2.4 ± 0.3	1.39 ± 0.51
Ps.BFR.Bs	1.82 ± 0.07	4.93 ± 0.65	2.78 ± 1.12

Table A3. 3 - Dynamic histomorphometric indices for the first, second and third week following induction of axial tibial loading in young adult female mice.

17w old female C57BL/6 mice were loaded 3 times weekly for up to 28 days. Fluorochromes were administered on day 0, 7, 14, 21 and histomorphometric indices calculated for each 7 day interval. Values represent mean ± SEM

		25% site	37% site	50% site	75% site
T.Ar	Left Sham	1.36 ± 0.02	1.11 ± 0.03	0.96 ± 0.01	0.74 ± 0.01
	Right SN	1.3 ± 0.03	1.14 ± 0.03	0.95 ± 0.02	0.72 ± 0.01
B.Ar	Left Sham	0.78 ± 0.01	0.63 ± 0.01	0.58 ± 0.01	0.54 ± 0.01
	Right SN	0.66 ± 0.02	0.53 ± 0.01	0.5 ± 0.01	0.49 ± 0.01
M.Ar	Left Sham	0.58 ± 0.02	0.69 ± 0.02	0.38 ± 0.01	0.2 ± 0.01
	Right SN	0.64 ± 0.02	0.61 ± 0.01	0.45 ± 0.01	0.22 ± 0.01
PMI	Left Sham	0.346 ± 0.008	9.189 ± 0.085	0.13 ± 0.003	0.081 ± 0.003
	Right SN	0.296 ± 0.012	9.709 ± 0.176	0.115 ± 0.004	0.075 ± 0.002
Cs.Th	Left Sham	0.145 ± 0.003	0.846 ± 0.006	0.18 ± 0.003	0.21 ± 0.003
	Right SN	0.121 ± 0.002	0.821 ± 0.007	0.154 ± 0.004	0.192 ± 0.005

Table A3. 4 – Effect of 3 weeks of right unilateral SN and left sham on cortical μ CT parameters in 20w old female mice.

17w-old female mice underwent SN and were killed 3 weeks later then tibias were scanned using μ CT. Values represent mean \pm SEM (n=6).

Chapter 4

	Sclerostin (n=4)		RANKL (n=4)	
	Control	Disuse	Control	Disuse
SN only	64.67 ± 3.29	85.02 ± 3.05**	62.83 ± 3.64	65.53 ± 1.71
Sham+SN	63.24 ± 5.25	85.9 ± 2.31**	61.5 ± 4.49	61.36 ± 0.69

Table A3. 5 - The effect of SN and contralateral sham surgery on sclerostin and RANKL expression in osteocytes of the mouse tibia.

** = $p < 0.01$ versus control limb. Comparisons were made using mixed design two-way ANOVA with LSD post-hoc corrections for multiple comparisons. N=4. Values represent mean \pm SEM

Time point	6h		12h		24h	
	Control	Loaded	Control	Loaded	Control	Loaded
RNA Concentration	93.14 ± 8.82	110.68 ± 9.86	98.1 ± 14.88	114.38 ± 22.67	121.74 ± 19.24	123.27 ± 12.15
Relative RANKL Expression	0.0064 ± 0.0007	0.0057 ± 0.0008	0.0042 ± 0.0004	0.0035 ± 0.0003	0.0051 ± 0.0008	0.0054 ± 0.0009
Relative OPG Expression	0.0412 ± 0.0045	0.0577 ± 0.0112	0.0342 ± 0.0089	0.0382 ± 0.0045	0.0308 ± 0.0043	0.0345 ± 0.0045
RANKL:OPG	0.1658 ± 0.0244	0.1116 ± 0.0172	0.162 ± 0.0318	0.0972 ± 0.0098	0.1752 ± 0.0238	0.1767 ± 0.0351
Relative SOST expression	0.0898 ± 0.0087	0.0557 ± 0.0077	0.0665 ± 0.009	0.047 ± 0.0082	0.0526 ± 0.0066	0.0429 ± 0.0039

Table A3. 6 – Experiment 1 - The temporal effect of unilateral tibial loading on expression of cortical bone RANKL, OPG and SOST.

Values represent mean ± SEM

Appendix 4

Peer-reviewed papers/conference abstracts.

Site Specificity Analysis Paper – Frontiers in Endocrinology

ORIGINAL RESEARCH
published: 23 April 2015
doi: 10.3389/fendo.2015.00052

Quantification of alterations in cortical bone geometry using site specificity software in mouse models of aging and the responses to ovariectomy and altered loading

Gabriel L. Galea^{1*}, Sion Hannuna², Lee B. Meakin¹, Peter J. Delisser¹, Lance E. Lanyon¹ and Joanna S. Price¹

¹ School of Veterinary Sciences, University of Bristol, Bristol, UK, ² Faculty of Engineering, University of Bristol, Bristol, UK

OPEN ACCESS

Edited by:
Phil Salmon,
Bruker-microCT, Belgium

Reviewed by:
Slatan Alexander Jackowski,
University of Saskatchewan, Canada
David M. L. Cooper,
University of Saskatchewan, Canada

***Correspondence:**
Gabriel L. Galea,
School of Veterinary Sciences,
University of Bristol, Southwell Street,
Bristol BS2 8EJ, UK
gabriel.galea@bristol.ac.uk

Specialty section:
This article was submitted to Bone
Research, a section of the journal
Frontiers in Endocrinology

Received: 26 January 2015

Paper pending published:
23 February 2015

Accepted: 03 April 2015

Published: 23 April 2015

Citation:
Galea GL, Hannuna S, Meakin LB,
Delisser PJ, Lanyon LE and Price JS
(2015) Quantification of alterations in
cortical bone geometry using site
specificity software in mouse models
of aging and the responses to
ovariectomy and altered loading.
Front. Endocrinol. 6:52.
doi: 10.3389/fendo.2015.00052

Investigations into the effect of (re)modeling stimuli on cortical bone in rodents normally rely on analysis of changes in bone mass and architecture at a narrow cross-sectional site. However, it is well established that the effects of axial loading produce site-specific changes throughout bones' structure. Non-mechanical influences (e.g., hormones) can be additional to or oppose locally controlled adaptive responses and may have more generalized effects. Tools currently available to study site-specific cortical bone adaptation are limited. Here, we applied novel site specificity software to measure bone mass and architecture at each 1% site along the length of the mouse tibia from standard micro-computed tomography (μ CT) images. Resulting measures are directly comparable to those obtained through μ CT analysis ($R^2 > 0.96$). Site Specificity analysis was used to compare a number of parameters in tibiae from young adult (19-week-old) versus aged (19-month-old) mice; ovariectomized and entire mice; limbs subjected to short periods of axial loading or disuse induced by sciatic neurectomy. Age was associated with uniformly reduced cortical thickness and site-specific decreases in cortical area most apparent in the proximal tibia. Mechanical loading site-specifically increased cortical area and thickness in the proximal tibia. Disuse uniformly decreased cortical thickness and decreased cortical area in the proximal tibia. Ovariectomy uniformly reduced cortical area without altering cortical thickness. Differences in polar moment of inertia between experimental groups were only observed in the proximal tibia. Aging and ovariectomy also altered eccentricity in the distal tibia. In summary, site specificity analysis provides a valuable tool for measuring changes in cortical bone mass and architecture along the entire length of a bone. Changes in the (re)modeling response determined at a single site may not reflect the response at different locations within the same bone.

Keywords: bone, mechanical loading, neurectomy, ovariectomy, aging

Introduction

Mechanical loading is the primary functional determinant of bone mass and architecture. Resident bone cells' responses to local changes in loading-engendered strains site-specifically

fine tune architectural features including curvature (1–3), eccentricity (4), cross-sectional thickness (5, 6), and polar moment of inertia, which is a measurement of bone strength (6, 7). In the young, healthy skeleton, this functional adaptation to loading matches bone's form to its load-bearing function through a homeostatic feedback loop commonly referred to as the "mechanostat" (8, 9). This feedback loop maintains bone strains within a tolerated range during habitual levels of loading. However, the mechanostat appears to fail in humans with age, correlating with reduced availability of estrogen leading to the bone fragility characteristic of osteoporosis (10, 11). Thinning of the load-bearing cortices predisposes to fractures, which in long bones occur preferentially at specific sites including the hip and wrist. It is now well documented that the overall geometry of these high-risk sites, particularly of the femoral neck, determines bone resistance to fracture independently of the absolute mass of bone present (12–14).

Despite regional differences in mass and architecture along their length, long bones must locally fine tune their structure to withstand load-bearing as functional units. At the cellular level, this is achieved through modeling (in which the activity of bone forming osteoblasts is independent of resorbing osteoclasts) and re-modeling (in which osteoblast activity follows osteoclastic resorption). Bone mass and architecture in one region influence the mechanical strain environment in other regions (15), such that structural properties at different sites within the same bone are inter-related. For example, the angle of articulation between the femur and tibia predicts the location of bisphosphonate-associated atypical fractures in the femoral diaphysis in humans (16). Experimental studies in rodents using micro-computed tomography (μ CT) and histomorphometry analyses have documented the bone formation response following physiological axial loading and demonstrated that it is site specific. For example, in the ulna loading model, an adaptive response is observed distally but not proximally (17) and axial loading in the mouse tibia elicits a response at 37% of the bone's length from the proximal end, but not distally at 75% of the bone's length (6, 18, 19). Consequently, deductions on the effect of loading based on measurements at a single cortical site cannot be generalized to the rest of the bone. This is particularly relevant given the increasing use of *in vivo* μ CT scanning of short sections of bone to provide longitudinal data within the same bone.

Unlike the site-specific targeting of bone (re)modeling following loading, systemic and genetic interventions may have indiscriminate, uniform effects on bone mass and architecture and where load-bearing remains constant may intrinsically alter the strain environment. The long-term (re)modeling outcomes of osteogenic or catabolic interventions will therefore be influenced by their interactions with the mechanostat, either suppressing bone's adaptation to loading such that net bone loss occurs or enhancing the sensitivity/responsiveness of the mechanisms involved in the mechanostat such that a lower level of habitual strain is tolerated (18, 20). Since systemic interventions are additive, synergistic, or oppose the site-specific effects of loading, their outcome is expected to have a degree of regional-ity. This is clearly demonstrated in our recent report that deletion of *Prkca* in mice leads to age-, gender-, and site-specific alterations in bone structure under the influence of mechanical

load-bearing (21). Documentation of these findings in *Prkca*^{-/-} mice required systematic analyses of bone mass and architecture at numerous sites. However, there are limited tools available for analyzing changes in whole-bone cortical architecture following altered loading or systemic interventions such as ovariectomy.

The primary aim of this study was to generate, validate, apply, and freely disseminate a new site specificity software tool, which allows bias-free and convenient quantification of standard measures of bone mass and architecture at multiple cortical bone sites in the mouse tibia. To demonstrate the efficacy of this software, we produced global maps of changes in bone geometry along the length of the mouse tibia in a number of routinely investigated experimental interventions in bone biology research (aging, axial loading, ovariectomy, and disuse).

Materials and Methods

Site Specificity Software for the Analysis of μ CT Data

Mouse tibiae were scanned with high resolution μ CT (Bruker, Kontich, Belgium) with a voxel size of 4.8 μ m as previously reported (6, 19). Images were reconstructed in NRecon (Bruker, Kontich, Belgium) with the following settings: threshold 1.000–1.160, ring artifacts correction 5, beam hardening correction 25%, smoothing 0. Folders containing all the sequentially labeled cross-sectional images from a single bone are defined as the "in path" for site specificity analysis. A new, empty folder labeled "output" is created inside each "in path" folder. The newly developed site specificity program (Data Sheet 1 in Supplementary Material) is then opened for editing in MatLab (R2012a). The site specificity software "in path" (line 13) is set to the folder containing the cross-sectional μ CT images of the bone to be analyzed following the format in the example provided (Table S1 in Supplementary Material, Excel file containing a worked out example and a blank sheet into which raw values generated below can be entered). This program is then run as a standard script in MatLab to identify and analyze the μ CT slices corresponding to each 1% of the bone's length.

Measures of area given are in pixels, with each pixel representing the scanning voxel size (in our system each pixel represents 4.8 μ m). Site specificity isolates the tibia and calculates the area of bone (cortical area, Ct.Ar) and the enclosed non-bone area (marrow area, Ma.Ar, Figure 1A) by segmenting the pixel values using the *k*-means algorithm applied to pixel intensity values where *k* is equal to 2. For pixels representing a mixture of tissue types (partial volume effect), their initial classification depends solely on their similarity to the mean of the two clusters. However, in a subsequent processing stage, pixels disconnected from the main bony component are classified as background using connected component analysis. Summation of Ct.Ar and Ma.Ar provides tissue area within the periosteum (Tt.Ar). In cases in which the cortex is breached such that there is no enclosed space, neither Ma.Ar nor Tt.Ar can be calculated for that individual slice but Ct.Ar is still reliable. This is relatively rare in normal mouse tibiae given vessels and cortical defects rarely run directly through the entire cortex in a single cross-section. Errors increase toward the proximal (trabecular bone) and distal (calcaneus) extremes of the bone such

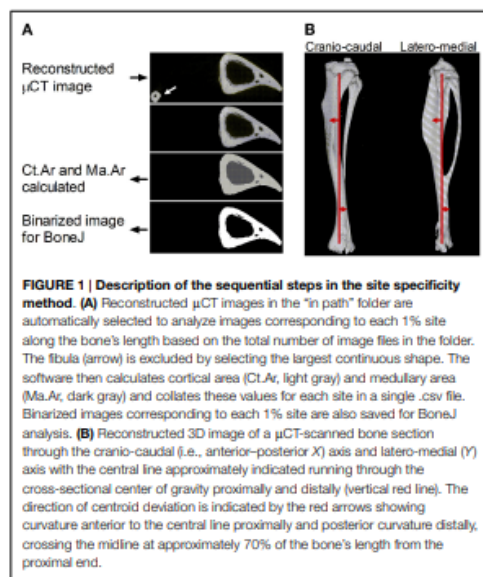


FIGURE 1 | Description of the sequential steps in the site specificity method. (A) Reconstructed μ CT images in the “in path” folder are automatically selected to analyze images corresponding to each 1% site along the bone’s length based on the total number of image files in the folder. The fibula (arrow) is excluded by selecting the largest continuous shape. The software then calculates cortical area (Ct.Ar, light gray) and medullary area (Ma.Ar, dark gray) and collates these values for each site in a single .csv file. Binarized images corresponding to each 1% site are also saved for BoneJ analysis. **(B)** Reconstructed 3D image of a μ CT-scanned bone section through the crano-caudal (i.e., anterior–posterior X) axis and latero-medial (Y) axis with the central line approximately indicated running through the cross-sectional center of gravity proximally and distally (vertical red line). The direction of centroid deviation is indicated by the red arrows showing curvature anterior to the central line proximally and posterior curvature distally, crossing the midline at approximately 70% of the bone’s length from the proximal end.

that only the 81 individual slices $4.8 \mu\text{m}$ thick at each 1% site between 10 and 90% of the bones length were analyzed.

The site specificity program collates all the measures in an Excel (.csv) file within the “output” folder. In addition, it saves binarized images of the tibia without the fibula in the “output” folder as .gif files, which retain the same pixel size (Figure 1A) but have a much smaller file size, facilitating subsequent analysis and storage. These .gif files can be exported to the previously validated and freely available BoneJ program in ImageJ (22, 23) to obtain cross-sectional thickness (Cs.Th), moments of inertia (minimum moment of inertia IMin, maximum moment of inertia IMax, and polar moment of inertia PMI through the summation of IMin and IMax), cross-sectional centroid in the X and Y direction. BoneJ also calculates Feret’s maximum diameter, minimum diameter, and angle by rotating the cross-sectional images to identify the maximum and minimum caliper dimensions. Eccentricity was obtained from the maximum and minimum diameters essentially as calculated by Bruker software (24) based on the length of the major axis (Feret Max from BoneJ) and minor axis (Feret Min from BoneJ).

All bones were oriented such that Feret’s angle at the 37% site (arbitrarily chosen) was 0° , i.e., parallel to the x -axis such that the x -axis is anterior–posterior while the y -axis is medial–lateral. Centroid was then used to calculate absolute center of mass deviation from the bone’s central axis as a measure of curvature. The central axis was defined as an extrapolated straight line running between 5 and 95% of the bone’s length (Figure 1B). Calculating the absolute deviation from this line defined within the bone itself accounts for any differences in bone position while being scanned, producing values, which were highly consistent

between similar mice in a semi-automated manner but which lose information on the direction of curvature along the axis being investigated.

The outputs of the site specificity program are: Ct.Ar, Ma.Ar, Tl.Ar, and binarized images, which can then be analyzed with BoneJ in ImageJ to provide Cs.Th, PMI, eccentricity, and curvature in the anterior–posterior (x) or medial–lateral (y) directions. Only cortical bone can be analyzed using site specificity. The site specificity and BoneJ analyses for an entire tibia with the data entry form provided (Table S1 in Supplementary Material) take <10 min on a standard laptop computer.

Site Specificity Validation

In order to ensure that bone structural measurements obtained through site specificity analysis are directly comparable with “conventional” μ CT analyses, cortical parameters were calculated at four sites in each of six mice using conventional μ CT or site specificity analysis. Conventional μ CT analysis was performed using CTan (Bruker, Kontich, Belgium) as previously reported by our group (6, 19). In brief, bones were imaged with an X-ray tube voltage of 49 kV and current 200 μA , with a 0.5 mm aluminum filter. The scanning angular rotation was 180° and the angular increment was 0.6° . The voxel size was $4.8 \mu\text{m}$ isotropically. Images were reconstructed using a modified Feldkamp algorithm in NRecon and opened for analysis in CTan. The regions of interest calculated based on the length of each bone. A region of 100 μ CT slices around each region of interest was selected and the fibula manually excluded (versus automatic exclusion using site specificity). Reconstructed cross-sectional gray scale images were segmented into binary images using adaptive local thresholding with a threshold window of 100–255. The images then underwent sequential modifications to reduce noise and improve continuity and then image series underwent removal of white speckles (<100 pixels area) and black speckles (<20 voxels). The outer periosteal border was isolated by a shrink wrap function stretching over holes with a diameter greater than 10 pixels. The resulting standard cortical bone measures averaged over 100 slices were compared with the Ct.Ar, Tl.Ar, and Ma.Ar values automatically generated by the site specificity software at the single cross-sectional slice at the desired percentage site.

To test the reproducibility of site specificity analysis, a bone was analyzed five times with complete system restarts between analyses. In addition, Ct.Ar calculated by site specificity was compared to the same parameter calculated by BoneJ.

Animal Studies

To investigate the effect of aging, young adult 18-week-old and aged 19-month-old C57B/16 mice were obtained from Charles River ($n = 6$ in each age group).

To study the effect of loading and disuse, C57B/16 mice were also obtained from Charles River. For loading experiments, 17-week-old female mice ($n = 15$) were subjected to axial tibial loading of the right limb three times a week for 2 weeks as previously described (6, 19). In brief, the flexed knee and ankle joints are positioned in concave cups; the upper cup containing the knee is attached to an actuator arm of a loading device and the lower cup to a dynamic load cell. The tibia is held in place by a 0.5 N continuous static pre-load. Forty cycles of dynamic load are superimposed

with 10 s rest intervals between each cycle. The protocol for one cycle consists of loading to the target peak load, hold for 0.05 s at the peak load, and unloading back to the 0.5 N pre-load at a load of 13.5 N to engender a peak strain of 2,250 μe on the medial surface of the tibia 37% of its length from the proximal end. The left limbs served as normally loaded internal controls. Disuse was induced as previously described (6, 25) through unilateral sciatic neurectomy (SN) ($n = 6$) of the right limb of 17-week-old female mice. Bones were collected 3 weeks following SN. The left limbs served as normally loaded internal controls.

To investigate the effect of estrogen withdrawal, ovariectomy (OVX) was performed as previously described (18, 21) in 8-week-old mice C57Bl/6 mice bred in house. Bones were collected 10 weeks after ovariectomy and compared to non-ovariectomized littermate controls ($n = 6$).

All procedures complied with the UK Animals (Scientific Procedures) Act 1986 undertaken under project license PPL 30-2829 and were reviewed and approved by the University of Bristol ethics committee (Bristol, UK). All mice were allowed free access to water and a maintenance diet containing 0.75% calcium (EU-Rodent Diet 22%; PMI Nutrition International, LLC, Brentwood, MO, USA) in a 12-h light/dark cycle, with room temperature at $21 \pm 2^\circ\text{C}$. Mice were housed in groups of up to five animals and all cages contained wood shavings, bedding, and a cardboard tube for environmental enrichment.

Statistics

Statistical comparison was by mixed model analysis in SPSS (PASW Statistics, v.18) with bone site as a fixed categorical parameter, the intervention (aging, loading, disuse, OVX, or control) as a fixed effect, and an intervention by site interaction to determine whether the effect of the intervention was site-specific (i.e., significantly different at different sites) or uniform. For loading and disuse analyses, mouse ID was included as a random effect to account for left and right limbs originating from the same mouse. When the effect of the intervention was significant overall, a *post hoc* Bonferroni correction was applied to identify the individual sites at which the effect was significant at $p < 0.05$.

In order to test the ability to detect differences at $p < 0.05$, a simulated 10% global changes in Ct.Ar were statistically analyzed using mixed models. This magnitude of change was selected because OVX caused a $-10.0 \pm 0.03\%$ change in Ct.Ar averaged across all sites (range -4 to -20%), described in the Section "Results." To do this, Ct.Ar values from six mice were increased by 10% across all sites (the "Intervention") and analyzed by mixed model analysis with *post hoc* Bonferroni. The overall p value associated with the intervention fixed effect and the p values comparing each site were then obtained.

Results are presented as the mean \pm SEM.

Results

Validation of the Site Specificity Program

Ct.Ar, Ma.Ar, and Tl.Ar measures obtained from site specificity and conventional μCT analysis were highly correlated ($R^2 = 0.99$ for each parameter, Figure 2A), with slight differences between the two likely due to conventional μCT analysis taking the

average of 100 CT slices, whereas site specificity analysis analyses individual slices corresponding to each 1% site. Within each site tested, the site specificity value obtained from a single slice will always be different from that generated by conventional μCT analysis if the parameter in question changes rapidly over the 100 lines analyzed. In areas of rapid change, such as at the tibia–fibula junction, the site specificity represents the actual value for the cross-sectional image corresponding to that level rather than an average of slices around the level of interest. Using the statistical approach described, a simulated intervention effect causing 10% change in Ct.Ar could be detected as significant ($p < 0.05$) with $n = 4$ bones. With a sample size of $n = 6$ (the smallest group size used in the studies presented here), a 10% change was detected as significant in 98.8% of sites analyzed.

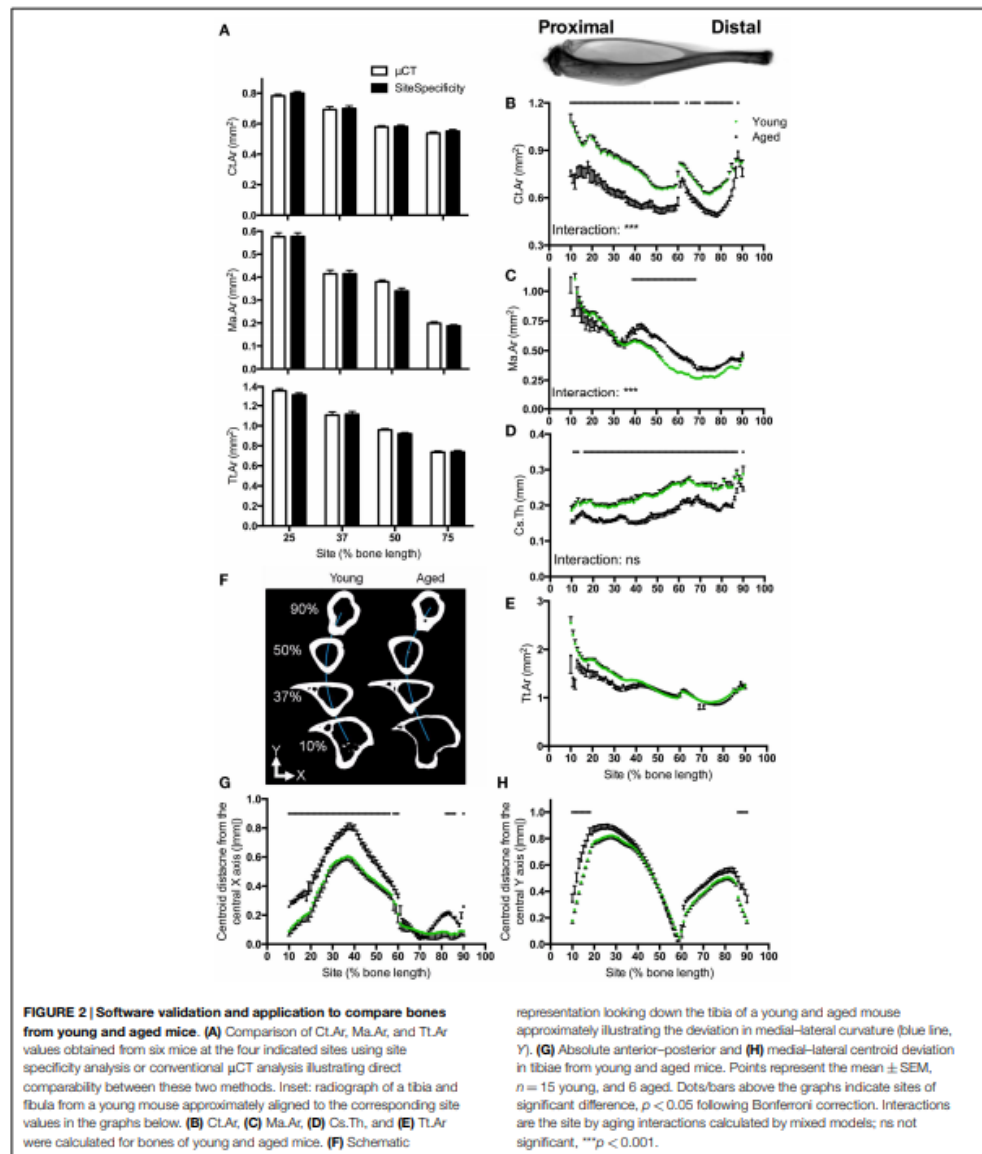
Parameters obtained from BoneJ were as previously validated (22) and the eccentricity parameter calculated from these was also highly correlated to values obtained from conventional μCT analysis ($R^2 = 0.96$, not shown). Results obtained using this software can therefore be directly compared to data obtained through conventional μCT analysis. Re-analysis of the same bone produced identical results each time ($R^2 = 1$, t -test $p = 1$, not shown). Ct.Ar calculated by site specificity and BoneJ were identical ($R^2 = 1$, t -test $p = 1$, not shown).

Site specificity analyses illustrate differences in structural parameters along the length of the bone functional unit. The proximal tibia of young mice has a greater cortical area surrounding a larger medullary area, but a narrower cortical thickness as compared with distal regions of the same bone, such that total tissue area is smaller distally than proximally (Figures 2B–E). Absolute centroid deviation from the central axis, as a measure of bone curvature, in the anterior–posterior direction is more marked in the proximal to middle region of the bone corresponding to the tibial crest (Figures 2F,G). Curvature in the medial–lateral direction is also most marked in the proximal half of the bone, curving back to the midline by 60% of the bone's length from the proximal end (Figure 2H). All patterns of curvature and structural parameters were highly consistent between different mice: for example, the tibia–fibula junction occurred within 2% of the bone's length in all young mice analyzed.

Effect of Aging

Aging was associated with smaller cortical area and larger medullary area, but these differences were site-specific such that the greatest differences were observed in the proximal regions of the bone (Figures 2B,C). Conversely, bones from aged mice had lower cortical thickness than those from young mice, but this difference was uniform along the length of the bone (Figure 2D). Differences in total tissue area between young and aged were not significant (Figure 2E).

Aging was associated with significant differences in deviation in centroid from the central axis. Centroid deviation was greater in aged than young adult bones in the anterior–posterior axis, particularly in the proximal half of the bone (Figure 2G). Centroid deviation along the medial–lateral axis was greater in aged bones in both the proximal and distal extremes of the region analyzed (Figure 2H).



Effect of Additional Loading

We have previously reported that the region of the mouse tibia, which undergoes the greatest osteogenic response following non-invasive axial loading, is localized to 37% of the bone's length

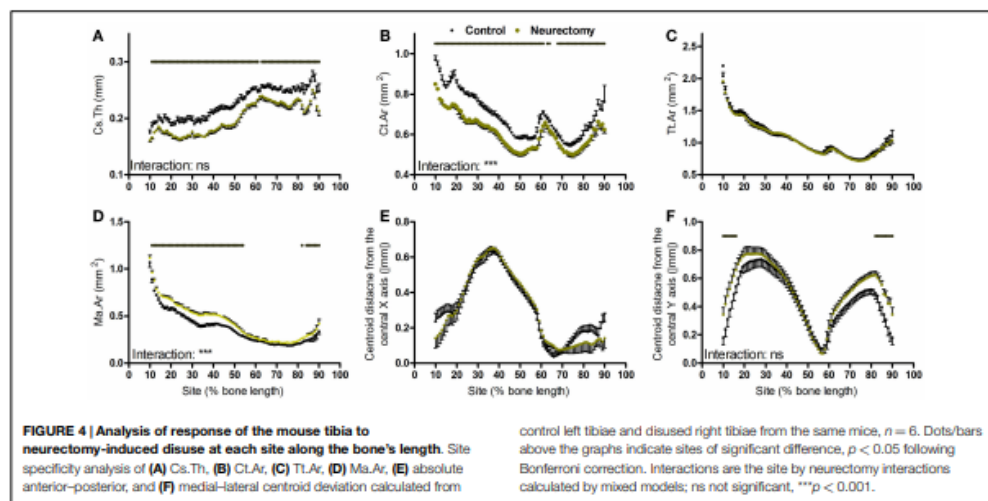
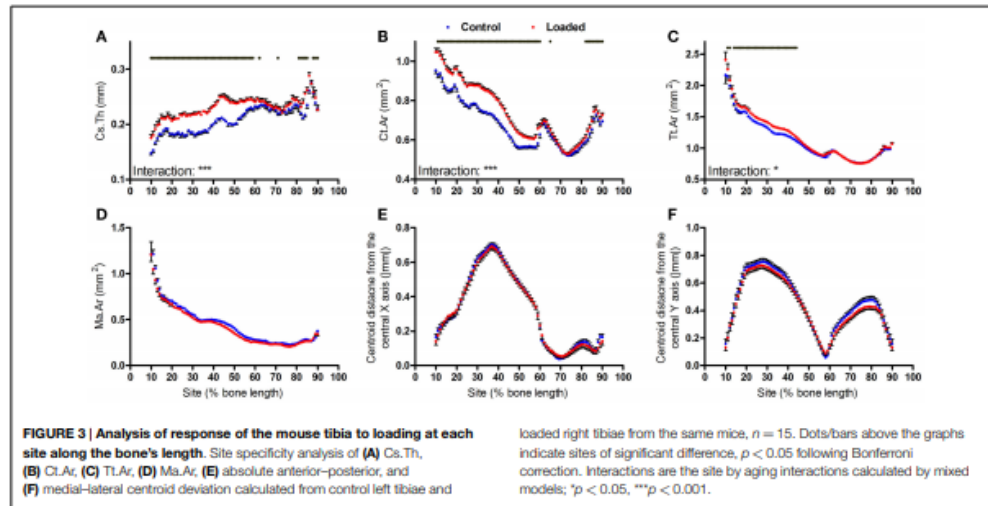
from the proximal end, whereas other studies using similar models have analyzed responses at the mid-diaphysis (26–30). Loading increased cortical thickness and cortical area at both sites, whereas total tissue area was only significantly increased more

proximally (Figures 3A–C). Although the effect of loading on medullary area was significant overall (mixed model $p = 0.01$), and left versus right comparisons were significant ($p < 0.05$) by *t*-test at all sites between 40 and 70% of the bone's length, none of these differences were statistically significant following Bonferroni correction for multiple comparisons (Figure 3D). Thus, a study analyzing the effect of loading on medullary area would conclude this as reduced if the 50% site is analyzed, but that it is unchanged if the 37% site is analyzed (Figure S1 in Supplementary Material).

Two weeks of loading did not significantly alter bone centroid deviation in either the anterior–posterior or medial–lateral directions (Figures 3E,F).

Effect of Disuse

Bones' response to changes in loading follows a linear continuum between the low strains associated with the bone loss and the higher strains associated with bone gain (6). However, unlike loading, SN-induced disuse resulted in uniform loss of cortical thickness throughout the tibial cortex (Figure 4A). The reduction



in bone area due to disuse was site specific; greater in the more proximal than distal regions of the bone (Figure 4B). Disuse did not alter total tissue area but significantly increased marrow area in a site-specific manner (Figures 4C,D). Curvature in the anterior-posterior axis was not significantly altered by disuse whereas medial-lateral curvature was significantly increased at the proximal and distal extremes of the region analyzed, but the site by neuroectomy interaction was not statistically significant (Figures 4E,F).

Effect of Ovariectomy

Ovariectomy during growth did not alter average cortical thickness achieved in adulthood (Figure 5A) but resulted in smaller cortical bone area in a uniform manner (Figure 5B). This involved smaller total tissue area and larger medullar cavity in a non-site-specific manner (Figures 5C,D). Ovariectomy did not alter the absolute centroid deviation in the anterior-posterior axis (Figure 5E), but significantly increased medial-lateral centroid deviation between approximately 30 and 60% of the bone's length while decreasing it between approximately 65 and 80% of the bone's length from the proximal end (Figure 5F). This pattern of change in bone curvature is distinct from that observed following aging or disuse.

Site-Specific Influences on Polar Moment of Inertia and Eccentricity

Aging, axial loading, and ovariectomy all influence overall strength of the bone functional unit. Moments of inertia are structural parameters related to bone strength, which can be calculated from CT images (31). Within each tibia, the polar moment of inertia was greater in the proximal region of the bone than the distal regions beyond the tibia-fibula junction (Figures 6A-C). Loading increased polar moment of inertia in a site-specific manner, with significant changes proximally but not distally (Figures 6A-F).

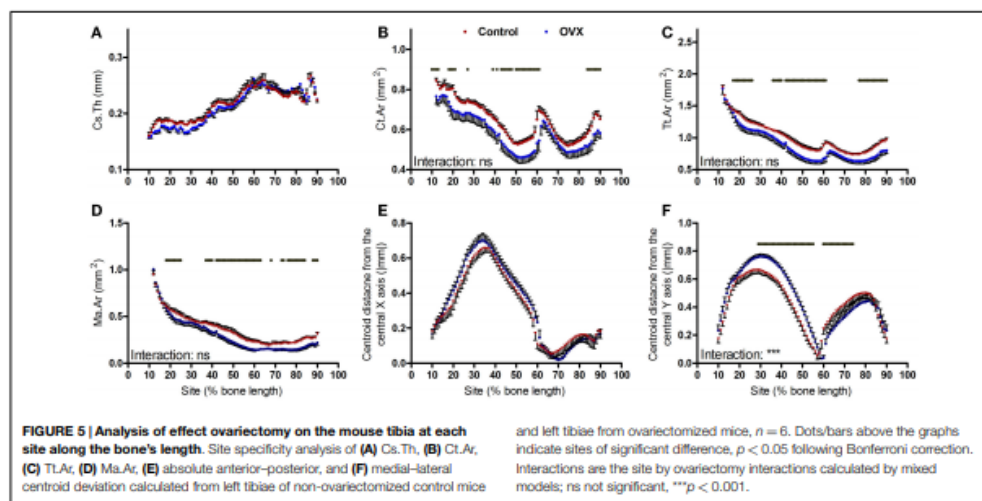
Tibiae from aged mice followed a similar pattern, with smaller polar moment of inertia in the proximal but not distal regions of the bone relative to young mice (Figures 6G-I).

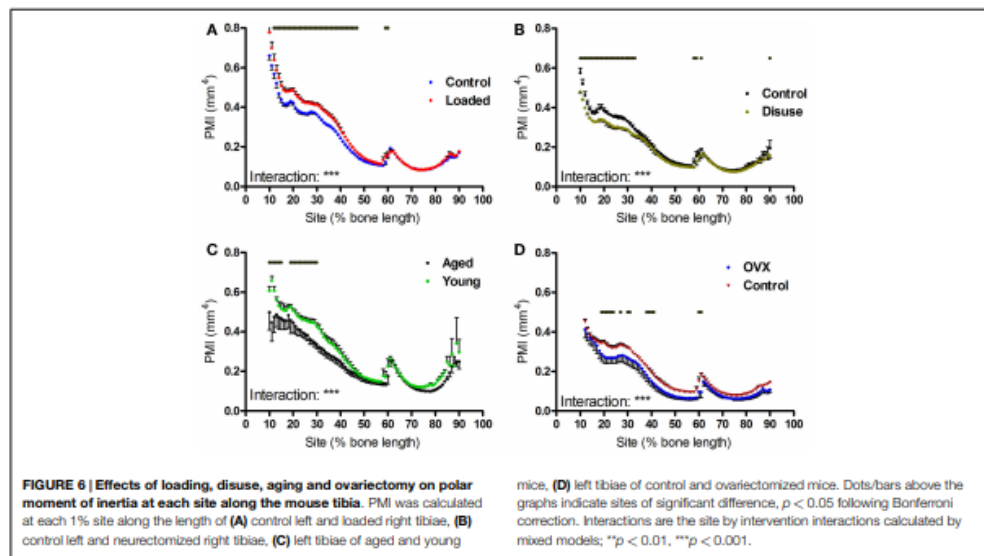
Unexpectedly, ovariectomy also decreased polar moment of inertia in a site-specific manner (Figures 6J-L), despite having caused a uniform loss in bone area. We hypothesized that the site-specific effects on polar moment may be due to uniform bone loss from different baselines along the length of the bone functional unit. Simulated reductions in bone mass at the periosteal or endosteal surface cause relatively greater reductions in polar moment of inertia at the proximal 37% site than at the distal 75% site (Figure S2 in Supplementary Material), indicating that the polar moment of inertia in the distal tibia is relatively unaffected by changes in cortical area compared with the less circular proximal tibia. This suggests that the uniform reduction in bone area caused by ovariectomy would reduce PMI in the proximal tibia to a greater extent than in the distal tibia.

Given moments of inertia influenced by shape, we also investigated whether the interventions tested altered bone shape by calculating the eccentricity parameter, which is a load-bearing responsive geometric parameter (4). Eccentricity was not significantly altered by loading or disuse (not shown), but was significantly affected by both ovariectomy and aging in a site-specific manner predominantly in the distal regions of the bone (Figures 7A-C).

Discussion

Bone mass and architecture are the outcome of bone's functional adaptation to local load-bearing occurring on a background of systemic and genetic influences. The effect of these influences can be additive, synergistic, or to oppose those of functional adaptation. The study that we report here describes alterations in bone mass and architecture resulting from aging,



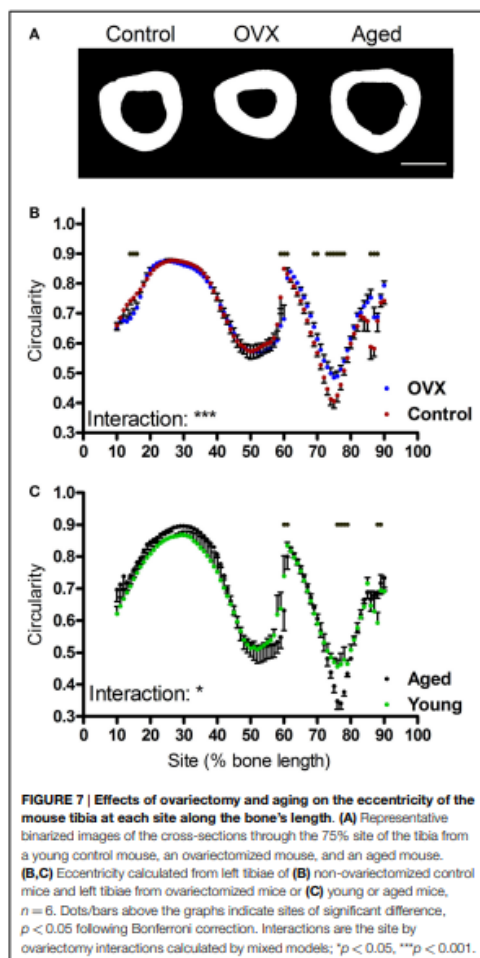


changing the mechanical environment, or ovariectomy. It shows that analysis of cortical bone at multiple sites provides more meaningful information than that obtained from analysis of candidate sites because several parameters are altered in a site-specific manner and so conclusions made about changes in one site may not be meaningfully extrapolated to the remainder of the bone functional unit. This is particularly true in relation to the moments of inertia and curvature, which can only be appreciated when the entire bone is analyzed. These analyses have shown that site specificity analysis provides additional information over conventional approaches and have demonstrated that several physiological contexts, not only mechanical loading, can induce significant site-specific changes in cortical bone mass and architecture. Site specificity analysis quantifies standard cortical parameters precisely and reproducibly. It provides measures, which are directly comparable to those obtained using conventional μ CT analysis. Furthermore, using mixed model statistical approaches, it allows comparisons at numerous sites along the bone's length with adequate statistical power.

Most published studies investigating the effects of altered mechanical loading, systemic or genetic interventions on bone only investigate differences at pre-determined sites along the bone's length. This may begin to explain discrepancies in reported responses. For example, the present study using a relatively large sample of 15 mice suggests that axial loading of the mouse tibia tends to reduce marrow area if the 50% site is analyzed, but does not significantly alter marrow area at the 37% site in the same mice. This is consistent with previous studies analyzing the 50% site concluding that axial loading alters the endosteal surface (26–28), whereas studies focused on the 37% site observed

no such change (29, 30, 32). It is now widely accepted that changes in local mechanical loading have site-specific effects and it is common practice to compare responsive and less responsive sites along the bone's length (6, 20, 25, 33). The novel methodology described here eliminates the intrinsic bias in selecting candidate sites irrespective of potential inter-group differences in properties such as curvature, and facilitates comparisons by allowing automated determination of cross-sectional parameters at each 1% of the bone's length. Curvature and eccentricity are likely to be influenced by poorly understood interactions between the mechanical, genetic, and hormonal contexts, which ultimately determine bone architecture. For example, in humans, the buckling ratio of the femoral neck is a macro-architectural feature, which deteriorates with age (34, 35) and is influenced by genetic polymorphisms including variants in the paracrine signaling molecule Wnt16 (36–38). Understanding how the magnitude and direction of mechanical cues informs overall bone structure is likely to require integration of biomechanical and mechanistic studies. However, characterization of site-specific and macro-architectural bone phenotypes in transgenic mouse models may begin to elucidate the genetic determinants of bone architecture beyond simply quantifying bone mass at individual sites.

To this end, a few groups have developed systems to map differences in bone mass between wild-type and transgenic mice to specific locations (33, 39, 40). In addition, commercially available software is also able to analyze serial 2D μ CT images, as we have previously reported (21). A key advantage of site specificity over currently available software is the ability to automatically analyze images based on percentages of bone length (represented by the absolute number of cross-sectional images for that bone)



rather than analyzing specific lengths. The percentage-based approach accounts for differences in bone length and thereby facilitates alignment between different mice. Another advantage of site specificity is the free availability of the program code provided with this publication, such that it can be adapted to novel approaches. In addition, automated site specificity analysis is very rapid: in our hands, an entire bone can be analyzed on a laptop computer in 4 min (Bone) analyses being additional) as compared with analysis of a single 100-line section using commercially available software taking 5–6 min. Irrespective of the software used, the general method of analyzing μ CT data at multiple sites may begin to inform the mechanisms by which bones achieve and maintain their geometry.

Biological regulation of macro-architectural features is suggested by consistency in properties such as the position of the tibia–fibula junction between different mice. The genetically determined baseline toward which the diaphyses of long bones are programmed to develop in the absence of mechanical stimulation is effectively cylindrical (41, 42). Although cylindrical bones would be ideally suited to withstand loading applied in a predictably axial direction, this design is inefficient when the direction of loading cannot be reliably predicted as in the case of footfall. Consequently, bone (re)models toward a compromise between energetically unfavorable increases in mass and functionally integral resistance to fracture. This compromise has been suggested to explain the tendency of bones to be curved; although curvature is inefficient in that it increases strains experienced, it may be beneficial by providing predictability of strain direction (15, 43).

The biomechanical significance of changes in curvature observed following disuse, ovariectomy, and aging, but not following loading in the accustomed axial direction, is poorly understood. As curvature of the mouse tibiae provides a damping effect (15), increased curvature may be an adaptive process in situations of sub-optimal bone mass. This hypothesis is consistent with the observation that the proximal region of the mouse tibia, which has the greatest deviation from the central axis, also has greater mass and is less cylindrical than the distal tibia. The greater polar moment of inertia in the proximal than distal tibia suggests greater resistance to torsional forces (31). Similar regional differences in polar moment of inertia have been reported in the human tibia (44). Finite element modeling may be able to further clarify whether proximal tibial architecture increases distal strain predictability and thereby favors a more cylindrical shape. Given simulated periosteal or endocortical expansion has a greater absolute effect on the calculated polar moment of inertia in the proximal than distal tibia, it is possible that the apparent “unresponsiveness” of polar moments of inertia in the distal tibia following any of the interventions tested may be due to these changes being too small to detect as statistically significant. When effect sizes are small, performing multiple comparisons followed by a Bonferroni *post hoc* test results in Type II errors (at a rate of 1.2% in our simulated 10% change in Ct.Ar with $n = 6$). Future studies aimed at detecting smaller differences may require an increase in sample size to maintain their statistical power. Alternatively less stringent *post hoc* tests (e.g., Tukey’s HSD) could be used while accepting a greater proportion of false positive results. Another approach would be to analyze a smaller subset of the data; for example, by only statistically comparing each 5% site to reduce multiple comparisons. Whatever approach is used, graphical representation of site specificity outputs provides a visual representation of the magnitude of differences in different sites, permitting more targeted investigation of sites of potential interest; e.g., by histomorphometry.

Notwithstanding, the distal tibia below the tibia–fibula junction is not “architecturally inert.” In a recent study, electrical stimulation of the rat common peroneal nerve resulting in muscle contraction was found to cause bone formation in this distal region of the tibia, correlating with the highest localized strain levels predicted by finite element modeling (45). In the present study, significant differences were observed in distal tibial eccentricity

following ovariectomy and aging. Although 2 weeks of disuse has previously been reported to decrease bone eccentricity in growing mice (4), 3 weeks of disuse did not result in significant changes in eccentricity in skeletally mature mice in the present study. Also in growing mice, 10 weeks of ovariectomy significantly increased eccentricity in the distal tibia, potentially reflecting altered loading due to impoverished architecture proximal to the tibia-fibula junction. Aging had the opposite effect, decreasing eccentricity as the distal tibial cortex thinned into a more uniformly circular shape with age.

Aging is associated with reduced bone strength, thinning of the load-bearing cortices, and impoverished bone architecture in mice (19, 26) as in humans (12, 13, 34, 46). Why it is that functionally adapted bones undergo seemingly maladaptive age-related structural changes remains incompletely understood. At the cellular level, age-related deficiencies in the responses of osteoblasts to mechanical strain have been identified (19). At the tissue level, we describe in this study the site-specific reduction in cortical area and increase in medullary area as well as uniform reduction in cortical thickness in the mouse tibia, a pattern of change, which is similar to that seen following neurectomy. These similarities between the effects of aging and neurectomy-induced disuse are consistent with our group's hypothesis that aging reflects a failure of bone's adaptation to mechanical loading such that (re)modeling occurs as in a state of disuse (10).

In summary, automated site specificity analysis of bone structure at multiple sites along a bone's length provides the opportunity to study local and systemic influences on site-specific responses, which alter bone architecture. Application of this system of analysis to the mouse tibia demonstrates that increased

or decreased loading, ovariectomy, and aging all cause site-specific changes in bone, such that the structural alterations achieved by these changes, be they strategic or maladaptive, remain preferentially targeted to specific locations. Even when the imposed (re)modeling stimulus is apparently systemic, as in the case of ovariectomy, alteration in bone structural properties including polar moment of inertia remains site specific. Elucidating the interactions between systemic and mechano-adaptive (re)modeling stimuli, which determine bone architecture, and therefore fracture resistance is expected to be facilitated by integrated analysis of structural responses along the length of the bone functional unit. Site specificity analysis may help refine experimental design by selectively targeting optimally responsive or unresponsive cortical regions. It is anticipated that application of site specificity analysis will begin to identify mechanisms by which genetic or systemic cues enhance or suppress the local, site-specific mechanisms underlying the mechanostat to determine the overall mechanical suitability of the bone functional unit.

Acknowledgments

LM is a recipient of an Integrated Training Fellowships for Veterinarians from the Wellcome Trust. GG and PD were supported by the Wellcome Trust when this work was undertaken.

Supplementary Material

The Supplementary Material for this article can be found online at <http://www.frontiersin.org/article/10.3389/fendo.2015.00052/abstract>

References

- Lanyon LE, Baggott DG. Mechanical function as an influence on the structure and form of bone. *J Bone Joint Surg Br* (1976) **58-B**:436–43.
- Biewener AA, Bertram JE. Structural response of growing bone to exercise and disuse. *J Appl Physiol* (1985) (1994) **76**:946–55.
- Iwaniec UT, Wronski TJ, Amblard D, Nishimura Y, Van der Meulen MC, et al. Effects of disrupted beta1-integrin function on the skeletal response to short-term hindlimb unloading in mice. *J Appl Physiol* (1985) (2005) **98**:690–6. doi:10.1152/japplphysiol.00689.2004
- Marenzana M, De Souza RL, Chenu C. Blockade of beta-adrenergic signaling does not influence the bone mechano-adaptive response in mice. *Bone* (2007) **41**:206–15. doi:10.1016/j.bone.2007.04.184
- Stadelmann VA, Bonnet N, Pioletti DP. Combined effects of zoledronate and mechanical stimulation on bone adaptation in an axially loaded mouse tibia. *Clin Biomech (Bristol, Avon)* (2011) **26**:101–5. doi:10.1016/j.clinbiomech.2010.08.014
- Sugiyama T, Meakin LB, Browne WJ, Galea GL, Price JS, Lanyon LE. Bone's adaptive response to mechanical loading is essentially linear between the low strains associated with disuse and the high strains associated with the lamellar/woven bone transition. *J Bone Miner Res* (2012) **27**(8):1784–93. doi:10.1002/jbmr.1599
- Warden SJ, Mantilla Roosa SM, Kersh ME, Hurd AL, Fleisig GS, Pandy MG, et al. Physical activity when young provides lifelong benefits to cortical bone size and strength in men. *Proc Natl Acad Sci U S A* (2014) **111**:5337–42. doi:10.1073/pnas.1321605111
- Frost HM. Bone's mechanostat: a 2003 update. *Anat Rec A Discov Mol Cell Evol Biol* (2003) **275**:1081–101. doi:10.1002/ar.a.10119
- Frost HM. Bone "mass" and the "mechanostat": a proposal. *Anat Rec* (1987) **219**:1–9. doi:10.1002/ar.1092190104
- Lanyon L, Skerry T. Postmenopausal osteoporosis as a failure of bone's adaptation to functional loading: a hypothesis. *J Bone Miner Res* (2001) **16**:1937–47. doi:10.1359/jbmr.2001.16.11.1937
- Sapir-Koren R, Livshits G. Is interaction between age-dependent decline in mechanical stimulation and osteocyte-estrogen receptor levels the culprit for postmenopausal-impaired bone formation? *Osteoporos Int* (2013) **24**:1771–89. doi:10.1007/s00198-012-2208-2
- LaCroix AZ, Beck TJ, Cauley JA, Lewis CE, Bassford T, Jackson R, et al. Hip structural geometry and incidence of hip fracture in postmenopausal women: what does it add to conventional bone mineral density? *Osteoporos Int* (2010) **21**:919–29. doi:10.1007/s00198-009-1056-1
- Nicks KM, Amin S, Melton LJ III, Atkinson EJ, McCready LK, Riggs BL, et al. Three-dimensional structural analysis of the proximal femur in an age-stratified sample of women. *Bone* (2013) **55**:179–88. doi:10.1016/j.bone.2013.02.009
- Bredbenner TL, Mason RL, Havill LM, Orwoll ES, Nicolella DP. Osteoporotic Fractures in Men (MrOS) Study: Fracture risk predictions based on statistical shape and density modeling of the proximal femur. *J Bone Miner Res* (2014) **29**(9):2090–100. doi:10.1002/jbmr.2241
- Dodge T, Wanis M, Ayoub R, Zhao L, Watts NB, Bhattacharya A, et al. Mechanical loading, damping, and load-driven bone formation in mouse tibiae. *Bone* (2012) **51**:810–8. doi:10.1016/j.bone.2012.07.021
- Saita Y, Ishijima M, Mogami A, Kubota M, Baba T, Kaketa T, et al. The fracture sites of atypical femoral fractures are associated with the weight-bearing lower limb alignment. *Bone* (2014) **66**:105–10. doi:10.1016/j.bone.2014.06.008
- Lee KCL, Maxwell A, Lanyon LE. Validation of a technique for studying functional adaptation of the mouse ulna in response to mechanical loading. *Bone* (2002) **31**(3):407–12. doi:10.1016/S8756-3282(02)00842-6
- Sugiyama T, Galea GL, Lanyon LE, Price JS. Mechanical loading-related bone gain is enhanced by tamoxifen but unaffected by fulvestrant in female mice. *Endocrinology* (2010) **151**:5582–90. doi:10.1210/en.2010-0645

19. Meakin LB, Galea GL, Sugiyama T, Lanyon LE, Price JS. Age-related impairment of bones' adaptive response to loading in mice is associated with gender-related deficiencies in osteoblasts but no change in osteocytes. *J Bone Miner Res* (2014) **29**(8):1859–71. doi:10.1002/jbmr.2222
20. Sugiyama T, Saxon LK, Zaman G, Moustafa A, Sunters A, Price JS, et al. Mechanical loading enhances the anabolic effects of intermittent parathyroid hormone (1–34) on trabecular and cortical bone in mice. *Bone* (2008) **43**:238–48. doi:10.1016/j.bone.2008.04.012
21. Galea GL, Meakin LB, Williams CM, Hulin-Curtis SL, Lanyon LE, Poole AW, et al. Protein kinase C α (PKC α) regulates bone architecture and osteoblast activity. *J Biol Chem* (2014) **289**(37):25509–22. doi:10.1074/jbc.M114.580365
22. Doube M, Klosowski MM, Arganda-Carreras I, Cordelières FP, Dougherty RP, Jackson JS, et al. BoneJ: free and extensible bone image analysis in imageJ. *Bone* (2010) **47**:1076–9. doi:10.1016/j.bone.2010.08.023
23. Schneider CA, Rasband WS, Eliceiri KW. NIH image to imageJ: 25 years of image analysis. *Nat Methods* (2012) **9**:671–5. doi:10.1038/nmeth.2089
24. Bruker. *Structural Parameters Measured by the Skyscan™ CT-Analyser Software*. Available from: <http://www.skyscan.be/next/ctan03.pdf>
25. Moustafa A, Sugiyama T, Prasad J, Zaman G, Gross TS, Lanyon LE, et al. Mechanical loading-related changes in osteocyte sclerostin expression in mice are more closely associated with the subsequent osteogenic response than the peak strains engendered. *Osteoporos Int* (2012) **23**(4):1225–34. doi:10.1007/s00198-011-1656-4
26. Willie BM, Birkhøld AI, Razi H, Thiele T, Aido M, Kruck B, et al. Diminished response to in vivo mechanical loading in trabecular and not cortical bone in adulthood of female C57BL/6 mice coincides with a reduction in deformation to load. *Bone* (2013) **55**:335–46. doi:10.1016/j.bone.2013.04.023
27. Niziolek PJ, Warman ML, Robling AG. Mechanotransduction in bone tissue: the A214V and G171V mutations in Lrp5 enhance load-induced osteogenesis in a surface-selective manner. *Bone* (2012) **51**:459–65. doi:10.1016/j.bone.2012.05.023
28. Holguin N, Brodt MD, Sanchez ME, Kotiya AA, Silva MJ. Adaptation of tibial structure and strength to axial compression depends on loading history in both C57BL/6 and BALB/c mice. *Calcif Tissue Int* (2013) **93**:211–21. doi:10.1007/s00223-013-9744-4
29. Saxon LK, Galea G, Meakin L, Price J, Lanyon LE. Estrogen receptors alpha and beta have different gender-dependent effects on the adaptive responses to load bearing in cancellous and cortical bone. *Endocrinology* (2012) **153**(5):2254–66. doi:10.1210/en.2011-1977
30. Meakin LB, Sugiyama T, Galea GL, Browne WJ, Lanyon LE, Price JS. Male mice housed in groups engage in frequent fighting and show a lower response to additional bone loading than females or individually housed males that do not fight. *Bone* (2013) **54**:113–7. doi:10.1016/j.bone.2013.01.029
31. Bagi CM, Hanson N, Andresen C, Pero R, Larivière R, Turner CH, et al. The use of micro-CT to evaluate cortical bone geometry and strength in nude rats: correlation with mechanical testing, pQCT and DXA. *Bone* (2006) **38**:136–44. doi:10.1016/j.bone.2005.07.028
32. Brodt MD, Silva MJ. Aged mice have enhanced endocortical response and normal periosteal response compared with young-adult mice following 1 week of axial tibial compression. *J Bone Miner Res* (2010) **25**:2006–15. doi:10.1002/jbmr.96
33. Morse A, McDonald M, Kelly N, Melville K, Schindeler A, Kramer I, et al. Mechanical load increases in bone formation via a sclerostin-independent pathway. *J Bone Miner Res* (2014) **29**(11):2456–67. doi:10.1002/jbmr.2278
34. Duan Y, Beck TJ, Wang XF, Seeman E. Structural and biomechanical basis of sexual dimorphism in femoral neck fragility has its origins in growth and aging. *J Bone Miner Res* (2003) **18**:1766–74. doi:10.1359/jbmr.2003.18.10.1766
35. Djonic D, Milovanovic P, Nikolic S, Ivovic M, Marinkovic J, Beck T, et al. Intersex differences in structural properties of aging femora: implications on differential bone fragility: a cadaver study. *J Bone Miner Metab* (2011) **29**:449–57. doi:10.1007/s00774-010-0240-x
36. Garcia-Ibarbia C, Perez-Nunez MI, Olmos JM, Valero C, Perez-Aguilar MD, Hernandez JL, et al. Missense polymorphisms of the WNT16 gene are associated with bone mass, hip geometry and fractures. *Osteoporos Int* (2013) **24**:2449–54. doi:10.1007/s00198-013-2302-0
37. Zhao LJ, Liu XG, Liu YZ, Liu YJ, Papisian CJ, Sha BY, et al. Genome-wide association study for femoral neck bone geometry. *J Bone Miner Res* (2010) **25**:320–9. doi:10.1359/jbmr.090726
38. Shen H, Long JR, Xiong DH, Liu YJ, Liu YZ, Xiao P, et al. Mapping quantitative trait loci for cross-sectional geometry at the femoral neck. *J Bone Miner Res* (2005) **20**:1973–82. doi:10.1359/JBMR.050715
39. Yamamoto Y, Yoshizawa T, Fukuda T, Shirode-Fukuda Y, Yu T, Sekine K, et al. Vitamin D receptor in osteoblasts is a negative regulator of bone mass control. *Endocrinology* (2013) **154**:1008–20. doi:10.1210/en.2012-1542
40. Nakamura T, Imai Y, Matsumoto T, Sato S, Takeuchi K, Igarashi K, et al. Estrogen prevents bone loss via estrogen receptor alpha and induction of Fas ligand in osteoclasts. *Cell* (2007) **130**:811–23. doi:10.1016/j.cell.2007.07.025
41. Gomez C, David V, Peet NM, Vico L, Chenu C, Malaval L, et al. Absence of mechanical loading in utero influences bone mass and architecture but not innervation in Myod-Myf5-deficient mice. *J Anat* (2007) **210**:259–71. doi:10.1111/j.1469-7580.2007.00698.x
42. Rot-Nikcevic I, Reddy T, Downing KJ, Belliveau AC, Hallgrímsson B, Hall BK, et al. Myf5^{-/-}:MyoD^{-/-} amyogenic fetuses reveal the importance of early contraction and static loading by striated muscle in mouse skeletogenesis. *Dev Genes Evol* (2006) **216**:1–9. doi:10.1007/s00427-005-0024-9
43. Bertram JE, Biewener AA. Bone curvature: sacrificing strength for load predictability? *J Theor Biol* (1988) **131**:75–92. doi:10.1016/S0022-5193(88)80122-X
44. Sherk VD, Bemben DA. Age and sex differences in estimated tibia strength: influence of measurement site. *J Clin Densitom* (2013) **16**:196–203. doi:10.1016/j.jocd.2012.03.006
45. Vickerton P, Jarvis JC, Gallagher JA, Akhtar R, Sutherland H, Jeffery N. Morphological and histological adaptation of muscle and bone to loading induced by repetitive activation of muscle. *Proc Biol Sci* (2014) **281**(1788):20140786. doi:10.1098/rspb.2014.0786
46. Russo CR, Lauretani F, Seeman E, Bartali B, Bandinelli S, Di Iorio A, et al. Structural adaptations to bone loss in aging men and women. *Bone* (2006) **38**:112–8. doi:10.1016/j.bone.2005.07.025

Conflict of Interest Statement: The authors declare that the research was conducted in the absence of any commercial or financial relationships that could be construed as a potential conflict of interest.

Copyright © 2015 Galea, Hannuna, Meakin, Delisser, Lanyon and Price. This is an open-access article distributed under the terms of the Creative Commons Attribution License (CC BY). The use, distribution or reproduction in other forums is permitted, provided the original author(s) or licensor are credited and that the original publication in this journal is cited, in accordance with accepted academic practice. No use, distribution or reproduction is permitted which does not comply with these terms.

RANKL – Disuse ASBMR Abstract

Disuse sufficient to cause bone loss increases osteocytes' expression of sclerostin but has no effect on RANKL



LB-M005

Delisser, P.J. ¹, Meakin, L.B. ¹, Galea, G.L. ¹, Lanyon, L.E. ¹, Suva, L.J. ², Price, J.S. ¹

¹School of Veterinary Science, University of Bristol, Bristol, UK; ²Center for Orthopaedic Research, University of Arkansas for Medical Science, Little Rock, AR, USA

wellcome trust

Fellow

Introduction

- Disuse, induced by tail suspension, in mice whose osteocytes lack RANKL has been reported to lead to reduced bone loss compared to wild-type controls¹.
- This suggests that regulation of osteocytic RANKL expression is one of the key mechanisms by which mechanical loading regulates bone resorption.
- The aim of the present study was to establish disuse-related changes in RANKL expression in cortical bone osteocytes following unilateral limb paralysis induced by sciatic neurectomy (SN). Changes in RANKL expression were related to changes in sclerostin expression, which has previously been shown to increase following disuse induced by unilateral paralysis or by tail suspension^{2,3}.

Objectives

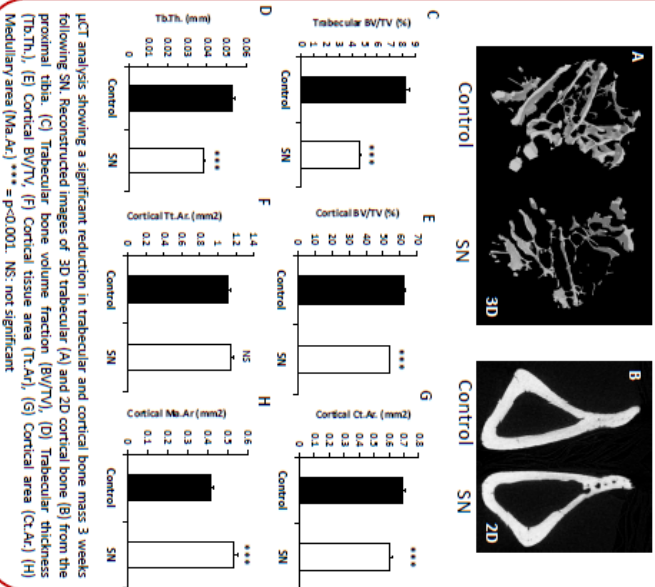
- To use IJCT to quantify the effect of 3 weeks of disuse induced by SN on cortical and trabecular bone loss in the mouse tibia.
- To establish the effect of SN-induced disuse on the expression of RANKL, OPG and SOST mRNA using quantitative reverse transcriptase PCR (qRT-PCR) and on sclerostin and RANKL protein expression using immunohistochemistry.

Materials and Methods

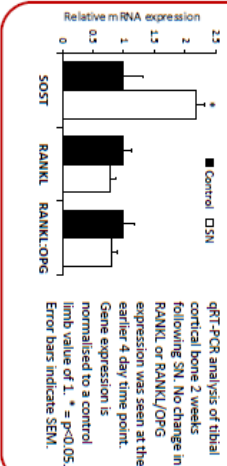
- The right limb of 17 week female C57BL/6J mice⁴ was subjected to sciatic neurectomy, the left limb underwent sham surgery. Left control limbs were compared with the right SN limb.
- IJCT analysis was performed 3 weeks following SN (n=6) and cortical and trabecular bone endpoints analysed as described previously⁵.
- qRT-PCR for RANKL, SOST and OPG was performed on cortical bone from the tibial diaphysis flushed free of marrow^{6,7} 3 days (not shown) and 2 weeks (n=8) following SN. β2MG was used as a reference gene.
- RANKL and sclerostin were immunolocalised in the posterolateral cortex of transverse sections of cortical bone from the proximal 37% site of the tibia 4 days following SN, a time point when sclerostin expression is known to be elevated in this model⁸. An indirect immunoperoxidase technique was used and the % positive osteocytes calculated as previously described⁹. IgG negative control sections did not show evidence of staining.

Results

Disuse leads to significant trabecular and cortical bone loss.



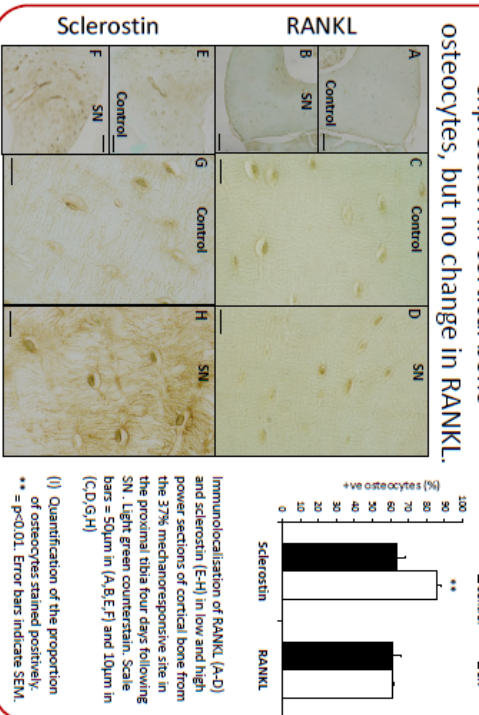
Disuse increases SOST mRNA expression in cortical bone, but no change in RANKL or the RANKL:OPG ratio.



Conclusions

This study demonstrates that disuse-related resorption associated with unilateral sciatic neurectomy does not require changes in RANKL expression in osteocytes.

Disuse increases sclerostin protein expression in cortical bone osteocytes, but no change in RANKL.



Acknowledgements

Peter Delisser, Lee Meakin and Gabriel Galea are Wellcome Trust Veterinary Training Fellows. The authors thank Frances Swain and Bob Skinner from UAMS for their assistance with histological processing and analysis

References

- Xiong J, et al. *Nat Med* 17:1235-1241, 2011.
- Moustafa A, et al. *Osteoporos Int* Apr;23(4):1225-34, 2012.
- Robling AG, et al. *Journal of Biological Chemistry* 283:5866-5875, 2008.
- Sugiyama T, et al. *J Bone Miner Res*, 2012.
- Sugiyama T, et al. *Bone* 46:314-321, 2010.
- Zaman G, et al. *Bone* 46:828-842, 2010.
- Galea GL, et al. *Journal of Biological Chemistry* 288:9035-9048, 2013.
- Sugiyama T, et al. *J Bone Miner Res*, 2012.

Osteoporos Int (2015) 26:2703–2708
 DOI 10.1007/s00198-015-3142-x

SHORT COMMUNICATION

Disuse rescues the age-impaired adaptive response to external loading in mice

L. B. Meakin¹ · P. J. Delisser¹ · G. L. Galea¹ · L. E. Lanyon¹ · J. S. Price¹

Received: 21 October 2014 / Accepted: 17 March 2015 / Published online: 29 April 2015
 © The Author(s) 2015. This article is published with open access at Springerlink.com

Abstract

Summary: We aimed to determine whether aged bone's diminished response to mechanical loading could be rescued by modulating habitual activity. By reducing background loading, aged bone's response to loading increased to a level no different to young mice. This suggests, given the right stimulus, that ageing bone can respond to mechanical loading.

Introduction: Age-related decline in bone mass has been suggested to represent an impaired ability of bone to adapt to its mechanical environment. In young mice, the tibia's response to external mechanical loading has been shown to increase when habitual activity is reduced by sciatic neurectomy. Here we investigate if neurectomy can rescue bone's response to loading in old mice.

Methods: The effect of tibial disuse, induced by unilateral sciatic neurectomy (SN), on the adaptive response to a single peak magnitude of dynamic load-engendered mechanical strain was assessed in 19-month-old (aged) mice. In a second experiment, a range of peak loads was used to assess the load magnitude-related effects of loading on a background of disuse in young adult and aged mice. Bone architecture was analysed using micro-computed tomography (μ CT) and dynamic histomorphometry.

Results: In the first experiment, SN in aged mice was associated with a significant periosteal osteogenic response to loading not observed in sham-operated mice (7.98 ± 1.7 vs 1.02 ± 2.2 % increase in periosteally enclosed area, $p < 0.05$). In the second experiment, SN abrogated the expected age-related difference in the bones' osteogenic response to peak strain magnitude ($p > 0.05$).

Conclusions: These data suggest that bones' age-related decline in osteogenic responsiveness to loading does not originate in bone cells to either assess, or appropriately respond to strain, but rather is likely to be due to inhibitory "averaging" effects derived from the habitual strains to which the bone is already adapted. If such "strain averaging" is applicable to humans, it suggests that gentle exercise may degrade the beneficially osteogenic effects of short periods of more vigorous activity.

Keywords: Bone · Habitual activity · Mechanical loading · Neurectomy

Introduction

Bones ensure that their structural strength is sufficient to withstand normal loading without fracture through a process of functional adaptation. This adaptation is thought to be controlled by a local negative feedback mechanism with "target" loading-engendered strain as its objective and "off target" strains as its controlling stimulus. This homeostatic mechanism is known as the mechanostat. In old age, the function of the mechanostat appears to be impaired since despite continued functional activity, sufficient bone tissue is lost that the incidence of fragility fracture increases [1]. Several previous experimental studies suggest an impaired response to mechanical loading in aged animals including rats and mice [2–7]. In regions of cortical bone at least, the mechanism of the failure

L. B. Meakin and P. J. Delisser contributed equally to this work.

Electronic supplementary material The online version of this article (doi:10.1007/s00198-015-3142-x) contains supplementary material, which is available to authorized users.

✉ L. B. Meakin
 lee.meakin@bristol.ac.uk

¹ School of Veterinary Science, University of Bristol, Langford, Bristol BS40 5DU, UK

appears to be a reduced periosteal osteogenic response to loading. It has been suggested that this may be due to impaired capability of periosteal osteoblasts to proliferate [2].

Interestingly, in loading experiments in young adult mice, artificially loading the tibia in limbs where normal loading is reduced by sciatic neurectomy (SN) engenders more new bone formation than when similar artificial loading is superimposed upon the loads of normal activity [8]. In the study reported here, we aimed to investigate whether sciatic neurectomy would increase the osteogenic response to artificial loading in aged animals and perhaps restore it to that seen in young adults.

Materials and methods

Animals

Young adult (17-week) and aged (19-month-old) female C57BL/6 mice were obtained from Charles River Laboratories (Margate, UK). Housing and diet were as previously reported [9]. All procedures complied with the UK Animals (Scientific Procedures) Act 1986 and were approved by the institutional ethics committee.

Ex vivo strain measurement

The strains produced by loading were calibrated in young adult and aged mice ($n=5$) by using bonded strain gauges attached ex vivo to the medial tibial cortex at a site 37 % of the bone's length from the proximal end [2]. Loads required to engender equivalent strains and strain rates in young and aged animals with different bone mass and architecture were calculated using linear regression as reported previously [2]. This information is presented in Supplementary Table S1. Although the load-strain relationship is affected by age, the strain distribution does not change substantially [10].

Surgical procedures

Sciatic neurectomy (SN) was performed on the right limb as previously described [11, 12]. An incision was made caudal to the right hip joint and the biceps femoris muscle elevated to expose the nerve. This was sharply transected and a 5–7-mm segment removed. Sham surgery was performed on the right limb of control group animals. In experiment 1, ($n=20$ aged mice) mice were weight-matched and divided evenly to sham or SN groups. In experiment 2, young and aged mice ($n=30$ young and $n=30$ aged mice, $n=5$ per strain magnitude) all received SN and groups were weight-matched into even sized groups for each strain magnitude.

In vivo external mechanical loading

Four days following SN surgery, right tibiae were subjected to external mechanical loading under isoflurane-induced anaesthesia on alternate days for eight sessions to investigate the effect of loading and SN on bone (re)modeling in young and aged mice. Left limbs were used as internal controls as previously validated [13]. The protocol for non-invasively loading the mouse tibia has been reported previously [9, 14]. A 0.5-N continuous static preload was applied in addition to which 40 cycles of dynamic load were superimposed with 10-s rest interval between each cycle. The protocol for one cycle consists of loading at a constant rate to the target peak load, hold for 0.05 s at the peak load and unloading back to the 0.5-N preload at the same rate. From the strain gage data, the peak loads required to engender strain magnitudes of 500, 1000, 1500, 2000 and 2500 $\mu\epsilon$ on the medial surface of the tibia at the 37 % site were calculated [2]. The strain rates during the application and release of load were 30,000 $\mu\epsilon$ s⁻¹.

High-resolution μ CT analysis

Mice were killed 2 days after the final episode of mechanical loading. Lower legs were dissected and stored in 70 % ethanol and whole tibiae imaged using the SkyScan 1172 (Bruker, Kontich, Belgium) with a voxel size of 4.8 μm (110 μm^3). The scanning, reconstruction and method of analysis have been previously reported [2, 9, 15]. We evaluated the effect of SN and age on changes [(right – left) / left]*100 due to loading in the trabecular region (0.25–0.75 mm distal to the proximal physis) and at the cortical site (37 % from the proximal end), according to the ASBMR guidelines [16]. The parameters measured included trabecular bone volume fraction (BV/TV), trabecular thickness (Tb.Th), trabecular number (Tb.N), trabecular pattern factor (Tb.Pf), cortical bone area (Ct.Ar), total cross-sectional area inside the periosteal envelope (Tt.Ar), medullary area (Ma.Ar), cortical thickness (Ct.Th) and bone area fraction (Ct.Ar/Tt.Ar).

Dynamic histomorphometry

Mice were injected with calcein (50 mg/kg) and alizarin (50 mg/kg) subcutaneously on day 6 and day 14 of the loading period respectively. Following sacrifice, fixation and μ CT scanning, tibiae were embedded in methylmethacrylate as reported previously [15]. Transverse sections were taken from the region in the tibia where we have previously demonstrated the response to axial loading to be maximal (37 % of the length measured from the proximal end) [13]. Images were captured using a confocal microscope with HeNe (563 nm) and diode (494 nm) lasers. Mineral apposition rates between the two labels on the endosteal and periosteal surfaces were

measured in the postero-lateral aspect of the right loaded tibiae only, where strains and bone formation engendered by loading have previously been shown to be maximal [11].

Statistical analysis

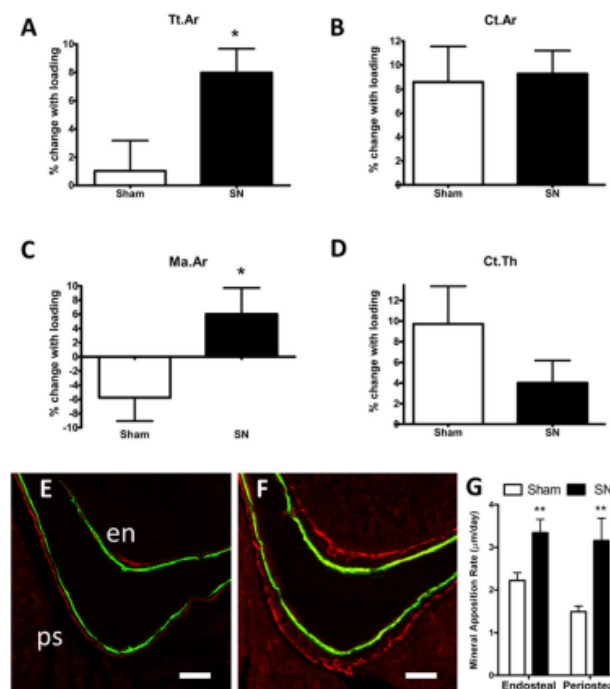
Repeated-measures ANOVA, with post hoc least squares difference testing, was used to evaluate the effect of loading between left control and right loaded samples (loading effect) and between sham and SN groups (surgery effect) in experiment 1. The interaction “loading*surgery” was also established. The effect of SN on the interlabel distance due to loading in aged mice of experiment 1 was evaluated using an unpaired *t* test on right loaded limbs only since insufficient double label was present on left control limbs of aged mice due to their high rates of resorption. In experiment 2, linear regression analysis was used to compare the effect of age on the response to loading over a range of strain stimuli, and each line separately was compared to a gradient of zero. Values are reported as mean±standard error of the mean (SEM).

Results

In the first experiment, the effect of SN ($n=7$) or sham surgery ($n=9$) on the response of cortical and trabecular bone mass and architecture to dynamic axial tibial loading in aged C57BL/6 mice was established using μ CT. There was no significant difference in body weight or tibial lengths between the groups (Supplementary Table S2), and as expected, right SN had no effect on measures of bone mass or architecture in the left control limbs between groups (Supplementary Table S2).

The means and SEM of the μ CT parameters are presented in Supplementary Table S2. Loading significantly altered Tt.Ar, Ct.Ar, Ct.Ar/Tt.Ar, Ct.Th ($p<0.01$ for loading as a main effect by repeated measures ANOVA) but had no effect on Ma.Ar. There was no significant main effect of surgery for any measure. Neurectomy significantly altered the effect of loading on Tt.Ar and Ma.Ar ($p<0.05$ for the loading*surgery interaction by repeated measures ANOVA). The increase in Tt.Ar associated with loading was significantly higher in mice subjected to SN ($7.98\pm 1.7\%$) than the sham group ($1.02\pm 2.2\%$, $p<0.05$) and the change in Ma.Ar was significantly greater in the SN group (6.02 ± 3.69) than in the sham group

Fig. 1 Sciatic neurectomy preceding axial tibial loading increases periosteal bone formation in aged mice. C57BL/6 female mice (19-months old) underwent right axial tibial loading sufficient to generate a strain magnitude of $2500\ \mu\epsilon$ following SN ($n=7$) or sham surgery ($n=9$). **a–d** μ CT analysis showing the percentage change between left control and right loaded limbs. Data represented as mean±SEM. **a** Total area within the periosteal envelope (Tt.Ar); **b** cortical bone area (Ct.Ar); **c** medullary area (Ma.Ar); **d** average cortical thickness (Ct.Th). **e–g** Confocal images of representative transverse sections of the postero-lateral cortex of the tibia taken at the 37% site illustrating calcein and alizarin fluoro-chrome labels administered at day 6 and day 15 of loading. The scale bars indicate 50 μ m. Endosteal surface=en, periosteal surface=ps. **e** Loaded without prior SN; **f** loaded with prior SN. **g** Mineral apposition rate at the postero-lateral cortex. * $p<0.05$; ** $p<0.01$



(-5.76 ± 3.30 , $p < 0.05$). Ct.Ar, Ct.Th and Ct.Ar/Tt.Ar did not show significantly different responses to loading between surgery groups (Fig. 1 and Supplementary Table S2). This indicates that SN was associated with greater overall endosteal resorption, but concurrently greater periosteal bone formation, following loading. Confocal microscopy of the posteriolateral tibial cortex revealed an increase in the interlabel distance in SN compared to sham loaded mice on both the endosteal ($+50.4\%$, $p < 0.01$) and periosteal ($+112.2\%$, $p < 0.01$) surfaces suggesting that neurectomy is associated with both endosteal and periosteal bone formation rate at the posteriolateral cortex in response to loading (Fig. 1).

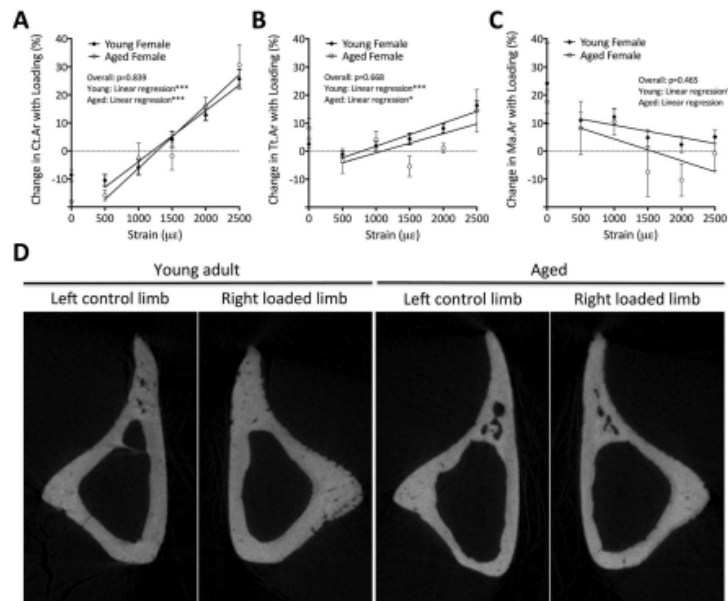
As we have recently published [2], aged female mice have a lower periosteal osteogenic response to loading over a range of mechanical strains than young adults. We therefore proceeded to determine whether SN could restore the response to mechanical loading in aged mice back to levels seen in young mice. Linear regression analysis was used to compare the response to loading in young and aged neurectomized mice over a range of peak strains. Increases in Ct.Ar and Tt.Ar showed no significant differences between the two ages of mouse ($p > 0.05$, Fig. 2). This suggests that SN in aged mice rescued the diminished response to loading in the periosteum over the full range of peak strains investigated to the same level as that seen in young adults.

Discussion

In this study, we first established that, as in young mice [8], the periosteal osteogenic response to short periods of dynamic loading in aged mice is greater when imposed against a background of disuse than against a background of habitual locomotor loading. We also establish that imposing a background of disuse, rather than habitual loading, eliminates any age-related difference in the osteogenic response to external loading over the full physiological range of peak strains from 500 to 2500 $\mu\epsilon$. The nature of this “rescue” appears to be related to an activation of bone formation on the periosteal surface where it has previously been reported to be impaired [2, 7].

These data build upon those from the previous study which reported that in young adult mice, SN-induced disuse can increase the osteogenic response to loading [8]. These authors suggested that the nature of the rescue was due to a degree of averaging of the total strain-related stimulus. This would be consistent with the finding that the background strain stimulus engendered by habitual cage activity at the medial surface of the tibia was halved following SN from approximately 600 $\mu\epsilon$ in intact mice to approximately 300 $\mu\epsilon$ [12]. In De Souza and others’ previous study, SN was associated with an increase in both endosteal and periosteal mineral apposition rates [8]. Interestingly, in neurectomized loaded limbs of aged mice, it appears, as demonstrated by the μ CT and dynamic

Fig. 2 Sciatic neurectomy preceding axial tibial loading restores the response to mechanical loading in aged mice back to levels seen in young mice. Seventeen-week-old and 19-month-old aged neurectomized (SN) C57BL/6 female mice underwent right axial tibial loading sufficient to generate a range of strain magnitudes (500, 1000, 1500, 2000 and 2500 $\mu\epsilon$). **a–c** μ CT analysis showing the percentage change between left control and right loaded limbs in young and aged SN mice. Data represented as mean \pm SEM. **a** Cortical bone area (Ct.Ar); **b** total area within the periosteal envelope (Tt.Ar); **c** medullary area (Ma.Ar). **d** Representative μ CT scans from left control and right loaded young and aged SN mice. * $p < 0.05$; *** $p < 0.001$



histomorphometric imaging, that the increase in bone formation is predominantly periosteal, the same surface where the response is reported to be impaired by age [2, 7]. μ CT also demonstrated an overall resorptive response endosteally (increased Ma.Ar) following SN, although this was not universal since there was a focally increased endosteal bone formation in the posteriolateral cortex. This suggests a site-specific component to the cross-sectional location of bone formation. This endosteal new bone was lamellar in appearance and occurs in the posteriolateral tibial cortex at the 37 % site, which is the same site previously identified by our group to display the greatest amount of formation following axial loading [11].

A number of previous studies have reported a lower response to mechanical loading in aged rodents [2–4, 17]. Here we show that it is possible to rescue this response by changing the character of the background strain-related environment against which the loading is imposed. Our results are consistent with those of a previous study showing that adult mice have a diminished response to loading than growing animals, but by increasing the magnitude of the strain stimulus, bone formation can be increased [5]. Taken together with our current study, these results suggest that the age-related impairment of the mechanostat is not consequent to an intrinsic failure of the mechanisms whereby bone mass increases, but a reduction in the sensitivity of these mechanisms to the strain-related stimuli to which they respond in the young, healthy skeleton. This would be consistent with our previous observation that the osteogenic response to loading in group-housed male mice was lower than that in individually housed males and in females because fighting engenders a habitual strain environment little different from that engendered by artificial loading [9]. Whether this is part of an “averaging” mechanism, as previously suggested [8], remains to be determined.

Our present study does nothing to establish the cellular mechanisms underlying the differences in the adaptive response to loading. However, it is interesting that a previous microarray study performed by our laboratory showed that loading the tibias of young adult mice in the context of disuse engendered by SN increased the number of genes differentially regulated by mechanical loading [18]. The cellular mechanisms underlying cellular mechanosensitivity remain incompletely understood, but recent work has demonstrated that mice deficient in Connexin 43 (Cx43) are resistant to bone loss seen with disuse [19] and have an improved osteogenic response to mechanical loading at the periosteal surface [20]. The authors of this study postulate that Cx43 affects regulation of bone cells’ response to mechanical loading through altering levels of cellular β -catenin signalling. Alterations in Wnt signalling at endosteal and periosteal surfaces in aged mice following disuse could underlie the primary observation noted in this study that a background of disuse is associated with a greater osteogenic response to short periods of loading than a background of habitual loading. Changes in cellular

stiffness could also play a role as it has recently been suggested that reversible increases in cell stiffness engendered by mechanical stimulation may act as an intrinsic “brake” to further mechanical responses by diminishing the strain a cell experiences when the same stress is applied [21]. These in vitro findings are consistent with the well-established finding that inserting rest periods between periods of loading increases the osteogenic response to loading [3] and our present finding that “habitual” strains also blunt this response in aged mice.

In summary, the data presented here demonstrate that reducing habitual loading of the tibia in aged mice by sciatic neurectomy increases the periosteal osteogenic response to short periods of dynamic artificial loading restoring it across the full range of physiological strains to that seen in young adults. These data are consistent with the idea that the strain-related stimulus arising from long periods of normal loading may reduce the response to short periods of more osteogenic stimulation. These results also suggest that there is no inherent age-related impediment either to the accurate assessment of strain or to loading-related periosteal expansion in response to appropriate loading.

Funding L. B. Meakin is supported by a Veterinary Training Fellowship provided by the Wellcome Trust. P. J. Delisser and G. L. Galea were supported by Veterinary Training Fellowships provided by the Wellcome Trust when the work was conducted.

Conflicts of interest None.

Open Access This article is distributed under the terms of the Creative Commons Attribution 4.0 International License (<http://creativecommons.org/licenses/by/4.0/>), which permits use, duplication, adaptation, distribution, and reproduction in any medium or format, as long as you give appropriate credit to the original author(s) and the source, provide a link to the Creative Commons license, and indicate if changes were made.

References

1. Lanyon L, Skerry T (2001) Postmenopausal osteoporosis as a failure of bone’s adaptation to functional loading: a hypothesis. *J Bone Miner Res* 16:1937–1947. doi:10.1359/jbmr.2001.16.11.1937
2. Meakin LB, Galea GL, Sugiyama T et al (2014) Age-Related impairment of bones’ adaptive response to loading in mice is associated with gender-related deficiencies in osteoblasts but no change in osteocytes. *J Bone Miner Res*. doi:10.1002/jbmr.2222
3. Srinivasan S, Agans SC, King KA et al (2003) Enabling bone formation in the aged skeleton via rest-inserted mechanical loading. *Bone* 33:946–955
4. Turner CH, Takano Y, Owan I (1995) Aging changes mechanical loading thresholds for bone formation in rats. *J Bone Miner Res* 10: 1544–1549. doi:10.1002/jbmr.5650101016

5. Lynch ME, Main RP, Xu Q et al (2011) Tibial compression is anabolic in the adult mouse skeleton despite reduced responsiveness with aging. *Bone* 49:439–446. doi:10.1016/j.bone.2011.05.017
6. Main RP, Lynch ME, van der Meulen MCH (2014) Load-induced changes in bone stiffness and cancellous and cortical bone mass following tibial compression diminish with age in female mice. *J Exp Biol* 217:1775–1783. doi:10.1242/jeb.085522
7. Holguin N, Brodt MD, Sanchez ME, Silva MJ (2014) Aging diminishes lamellar and woven bone formation induced by tibial compression in adult C57BL/6. *Bone* 65:83–91. doi:10.1016/j.bone.2014.05.006
8. De Souza RL, Pitsillides AA, Lanyon LE et al (2005) Sympathetic nervous system does not mediate the load-induced cortical new bone formation. *J Bone Miner Res* 20:2159–2168. doi:10.1359/JBMR.050812
9. Meakin LB, Sugiyama T, Galea GL et al (2013) Male mice housed in groups engage in frequent fighting and show a lower response to additional bone loading than females or individually housed males that do not fight. *Bone* 54:113–117. doi:10.1016/j.bone.2013.01.029
10. Patel TK, Brodt MD, Silva MJ (2014) Experimental and finite element analysis of strains induced by axial tibial compression in young-adult and old female C57Bl/6 mice. *J Biomech* 47:451–457. doi:10.1016/j.jbiomech.2013.10.052
11. Moustafa A, Sugiyama T, Prasad J et al (2011) Mechanical loading-related changes in osteocyte sclerostin expression in mice are more closely associated with the subsequent osteogenic response than the peak strains engendered. *Osteoporos Int*. doi:10.1007/s00198-011-1656-4
12. Sugiyama T, Meakin LB, Browne WJ et al (2012) Bones' adaptive response to mechanical loading is essentially linear between the low strains associated with disuse and the high strains associated with the lamellar/woven bone transition. *J Bone Miner Res* 27:1784–1793. doi:10.1002/jbmr.1599
13. Sugiyama T, Price JS, Lanyon LE (2010) Functional adaptation to mechanical loading in both cortical and cancellous bone is controlled locally and is confined to the loaded bones. *Bone* 46:314–321. doi:10.1016/j.bone.2009.08.054
14. De Souza RL, Matsuura M, Eckstein F et al (2005) Non-invasive axial loading of mouse tibiae increases cortical bone formation and modifies trabecular organization: a new model to study cortical and cancellous compartments in a single loaded element. *Bone* 37:810–818. doi:10.1016/j.bone.2005.07.022
15. Sugiyama T, Meakin LB, Galea GL et al (2011) Risedronate does not reduce mechanical loading-related increases in cortical and trabecular bone mass in mice. *Bone* 49:133–139. doi:10.1016/j.bone.2011.03.775
16. Bouxsein ML, Boyd SK, Christiansen BA et al (2010) Guidelines for assessment of bone microstructure in rodents using micro-computed tomography. *J Bone Miner Res* 25:1468–1486. doi:10.1002/jbmr.141
17. Rubin CT, Bain SD, McLeod KJ (1992) Suppression of the osteogenic response in the aging skeleton. *Calcif Tissue Int* 50:306–313
18. Zaman G, Saxon LK, Sunter A et al (2010) Loading-related regulation of gene expression in bone in the contexts of estrogen deficiency, lack of estrogen receptor alpha and disuse. *Bone* 46:628–642. doi:10.1016/j.bone.2009.10.021
19. Lloyd SA, Loisel AE, Zhang Y, Donahue HJ (2013) Connexin 43 deficiency desensitizes bone to the effects of mechanical unloading through modulation of both arms of bone remodeling. *Bone* 57:76–83. doi:10.1016/j.bone.2013.07.022
20. Lloyd SA, Loisel AE, Zhang Y, Donahue HJ (2014) Shifting paradigms on the role of connexin43 in the skeletal response to mechanical load. *J Bone Miner Res* 29:275–286
21. Yang Z, Shen Y, Tan S et al (2014) Inhibition of FSS-induced actin cytoskeleton reorganization by silencing LIMK2 gene increases the mechanosensitivity of primary osteoblasts. *Bone*. doi:10.1016/j.bone.2014.12.024

Risedronate and Mechanical Loading Have Additive Effects Increasing Bone Mass in Cortical, but not Cancellous, Bone in Aged Mice

Delisser, P.J.¹, Todd, H.E.¹, Meakin, L.B.¹, Galea, G.L.¹, Lanyon, L.E.¹, Windahl, S.H.^{1,2*}, Price, J.S.^{1*}

¹School of Veterinary Science, University of Bristol, Bristol, UK; ²Centre for Bone and Arthritis Research, Sahlgrenska Academy, University of Gothenburg, Sweden. *These authors contributed equally.

Email address: peterdelisser@bristol.ac.uk

Introduction

- Mechanical loading is the principal functional determinant of bone mass and architecture and we have hypothesised that the steady decline in bone mass and strength with ageing can be attributed to reduced physical activity/loading of the skeleton, as well as a reduced ability to respond to the loading placed upon it.¹
- In young mice, mechanical loading primarily increases bone mass via osteogenic modelling since inhibiting bone resorption with the bisphosphonate risedronate does not inhibit the osteogenic response to loading.²
- In aged mice there is an adaptive response to loading, but it is significantly reduced when compared to the response in young animals.³ It remains unknown whether this abrogated adaptive response is dependent on accompanying resorption. This is an important question to address since most therapeutic strategies for treating post-menopausal osteoporosis involve the use of anti-resorptives.

Aim

- To establish the effect of inhibiting bone resorption with risedronate on the adaptive response to mechanical loading in aged (19-20-month-old) female mice.

Materials and Methods

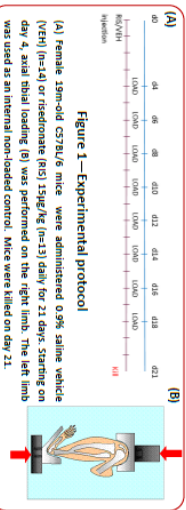


Figure 1—Experimental protocol

- µCT scanning was performed as previously described^{4,5} on dissected and fixed tibiae. Trabecular bone (proximal metaphysis) and cortical bone (75% site, measured from proximal end, and 75% site) regions of interest were analysed. Standard ASBMR µCT parameters were assessed.⁶
- Mixed model analysis was used to compare the main effects of risedronate and loading and any interactions. Post-hoc analysis was performed using pairwise comparisons with Bonferroni adjustments to determine differences between individual treatment groups. All data is presented as mean ± SEM.

Results

The effect of loading

- In trabecular bone, loading increased Trabecular Thickness (Tb.Th) (Fig 2).
- In cortical bone at the proximal site, loading increased Periosteal Enclosed Area (Tt.Ar), Cortical Area (Ct.Ar), Cortical Thickness (Ct.Th), and Polar Moment of Inertia (PMI), despite a concurrent increase in Medullary Area (Ma.Ar) (Fig 2). As expected, loading had no osteogenic effect at the distal (75%) site (data not shown).

The effect of risedronate

- In trabecular bone, risedronate decreased Structure Model Index (SMI) and Trabecular Pattern Factor (Tb.Pf), indicating a significant change from rod to plate-like trabeculae and an increase in trabecular connectivity (Fig 3). However, unlike in young mice², risedronate did not increase bone volume fraction (BV/TV) or Tb.Th. (Representative images – Fig 4).

Combination of loading and risedronate

- Risedronate treatment prevented the loading-related increase in Ma.Ar observed in the proximal cortical bone of the vehicle treated group (Fig 5).
- Loading had no effect on the increase in Ct.Th observed in the distal tibia of risedronate treated animals (data not shown).

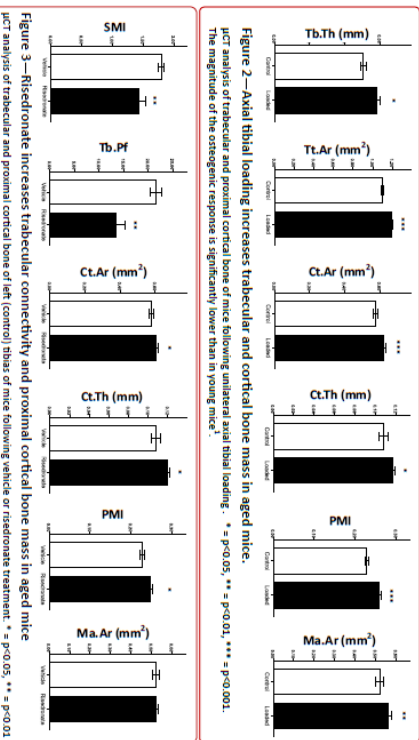


Figure 2—Axial tibial loading increases trabecular and cortical bone mass in aged mice. µCT analysis of trabecular and proximal cortical bone of mice following unilateral axial tibial loading. * $p < 0.05$, ** $p < 0.01$, *** $p < 0.001$. The magnitude of the osteogenic response is significantly lower than in young mice².

Figure 3—Risedronate increases trabecular connectivity and proximal cortical bone mass in aged mice. µCT analysis of trabecular and proximal cortical bone of left (control) tibiae of mice following vehicle or risedronate treatment. * $p < 0.05$, ** $p < 0.01$.

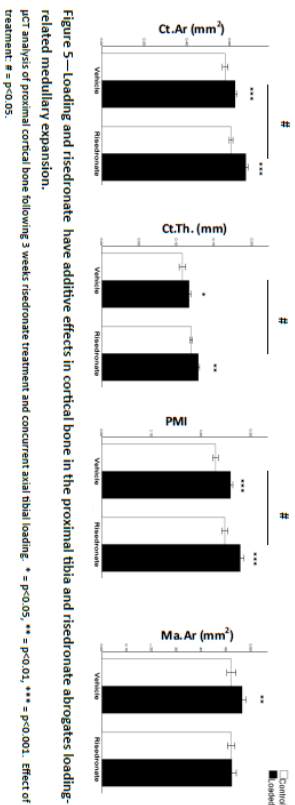


Figure 5—Loading and risedronate have additive effects in cortical bone in the proximal tibia and risedronate abrogates loading-related medullary expansion. µCT analysis of proximal cortical bone following 3 weeks risedronate treatment and concurrent axial tibial loading. * $p < 0.05$, ** $p < 0.01$, *** $p < 0.001$. Effect of treatment: # $p < 0.05$.

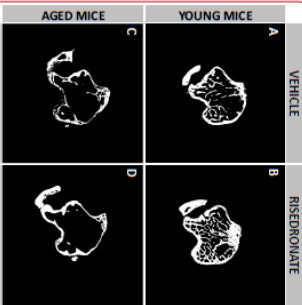


Figure 4—Risedronate increases trabecular bone mass in young but not aged mice. Representative binarized transverse µCT reconstructed images of trabecular bone of young (A,B) and (C,D) aged mice following treatment with vehicle or risedronate (15µg/kg). Images A & B are used with kind permission of Dr Toshiro Sugiyama.

Conclusions

- Mechanical loading of the tibia of aged mice increases trabecular thickness and cortical bone mass at the proximal site, replicating findings from previous studies.^{1,3}
- Unlike the situation in young mice², risedronate has no effect on trabecular bone mass but increases cortical bone mass in aged mice. This clearly demonstrates that observations made in young mice cannot necessarily be extrapolated to the old.
- Risedronate does not impair the loading response in old mice which suggests that the adaptive process primarily involves osteogenic modelling.
- The potential benefit of risedronate treatment on cortical bone is further augmented by mechanical loading because of increased periosteal formation unaccompanied by endosteal resorption.
- To the extent that the situation in mice can be extrapolated to old people, these results suggest that combining physical exercise with bisphosphonate treatment should confer the clinical benefit of increased bone mass.

References

- Mason et al. JBMR 29(9): 1859-71, 2014
- Seligson et al. Bone 49(11):1333-2011
- Mason et al. Osteopor Int. Feb-Mar 2013
- Bowden et al. JBMR 25(7): 1468-86, 2010

Acknowledgements

This work was performed with support from the University of Bristol, UK Medical and Dental Grants for Worldwide Trust Centre Research Training (Region 2010 research) and Wellcome Trust (097096) funding under the Academic Research Fellowship scheme (award number 105712).
Siddiqui@bristol.ac.uk grant reference 105712.

